

Lecture Notes in Production Engineering

Hans Kurt Toenshoff
Berend Denkena

Basics of Cutting and Abrasive Processes

 Springer

Lecture Notes in Production Engineering

For further volumes:
<http://www.springer.com/series/10642>

Hans Kurt Toenshoff · Berend Denkena

Basics of Cutting and Abrasive Processes

 Springer

Hans Kurt Toenshoff
Berend Denkena
Institute for Production Engineering and Machine Tools
Gottfried Wilhelm Leibniz Universität Hannover
Garbsen
Germany

ISSN 2194-0525 ISSN 2194-0533 (electronic)
ISBN 978-3-642-33256-2 ISBN 978-3-642-33257-9 (eBook)
DOI 10.1007/978-3-642-33257-9
Springer Heidelberg New York Dordrecht London

Library of Congress Control Number: 2013938164

© Springer-Verlag Berlin Heidelberg 2013

This work is subject to copyright. All rights are reserved by the Publisher, whether the whole or part of the material is concerned, specifically the rights of translation, reprinting, reuse of illustrations, recitation, broadcasting, reproduction on microfilms or in any other physical way, and transmission or information storage and retrieval, electronic adaptation, computer software, or by similar or dissimilar methodology now known or hereafter developed. Exempted from this legal reservation are brief excerpts in connection with reviews or scholarly analysis or material supplied specifically for the purpose of being entered and executed on a computer system, for exclusive use by the purchaser of the work. Duplication of this publication or parts thereof is permitted only under the provisions of the Copyright Law of the Publisher's location, in its current version, and permission for use must always be obtained from Springer. Permissions for use may be obtained through RightsLink at the Copyright Clearance Center. Violations are liable to prosecution under the respective Copyright Law. The use of general descriptive names, registered names, trademarks, service marks, etc. in this publication does not imply, even in the absence of a specific statement, that such names are exempt from the relevant protective laws and regulations and therefore free for general use.

While the advice and information in this book are believed to be true and accurate at the date of publication, neither the authors nor the editors nor the publisher can accept any legal responsibility for any errors or omissions that may be made. The publisher makes no warranty, express or implied, with respect to the material contained herein.

Printed on acid-free paper

Springer is part of Springer Science+Business Media (www.springer.com)

Preface

“The principal part of a chisel is the cutting edge. If there is a single principle on which our business rests—it is that.”, Henry Ford wrote in his memoirs “My life and work”. A contemporary of Henry Ford was Frederick Winslow Taylor. We know him as the first engineer, who worked scientifically in the field of cutting technology. His work “On the art of cutting metals”, published in 1907 was the first scientific contribution in the field of manufacturing which was able to describe parts of the cutting process qualitatively as well as quantitatively.

The significance of cutting and abrasive processes has grown substantially during the last century with the development of the automotive, aircraft and machine building industry. Therefore, the theory of these processes and knowledge about their application in industrial practice are a prerequisite for the studies of manufacturing science and an important part of the curriculum of the master study in German mechanical engineering.

The basis of this book is our lecture “Basics of cutting and abrasive processes” (4 semester hours/3 credit hours) at the Leibniz University Hannover, which we offer to the diploma and master students specializing in manufacturing science. We present the knowledge of modern manufacturing in these technologies. Comprehensive research in the laboratory of Production Engineering and Machine Tools of our institute introduces the newest results in the relevant fields.

The introductory chapter explains the significance of cutting and abrasive processes to manufacturing science using examples of industrial practice and gives criteria to evaluate cutting and abrasive processes with respect to economic and ecological issues. General material removal principles are presented in the next chapter. Large strains and strain rates and the moving of material with its instantaneously generated new surface over the tool faces under high load, are the specific characteristics of cutting in general. However, there is a broad variety of processes requiring a systematic taxonomy.

The following chapters discuss the four basic criteria, i.e. chip formation, forces and power, wear and surface generation. We see an important impetus on our work in a scientific and analytical approach to cutting and we have tried to describe the phenomena and their dependencies on input variables based on physical models and perceptions rather than presenting mere empirical equations. A particular chapter on modelling and simulation was written due to the fact that meanwhile,

there is a large variety of highly productive options to determine process and effective variables, not only in a momentary recording but also on the basis of kinematic or motion studies, which are adapted to actual machining processes, i. e. illustrate the ongoing process. It is the concern of this chapter to enable the reader to find his way around the various approaches and their limits. Dr.-Ing. Böß with his mathematical competence, took over the generation of this section to a large extent.

The progress of cutting and abrasive processes is strongly based on the development of cutting materials. Therefore, the different materials and their specific application domains described are followed consequently by new technologies, e.g. hard machining, high speed and high performance cutting.

New findings concerning the influence of the micro-geometry of the cutting wedge on the wear behavior of a tool, on the force and performance requirements in cutting and not least, on the surface influence have been included. The chapter “Surface and surface zone properties” contains the latest status of measurement possibilities, based on the work of Dr. rer. nat. habil. Breidenstein.

We owe some valuable information about new processes for the dressing of grinding wheels, which have just recently been put into practice, by Prof. Dr.-Ing. T. Lierse and the company Kaiser GmbH, Celle. Numerous co-workers of the institute have helped to accomplish this edition. Therefore, we would especially like to thank Dr.-Ing. V. Böß, Dr. rer. nat. habil. B. Breidenstein, Dipl.-Ing. J. Henjes, Dipl.-Math. A. Schindler and Dipl.-Ing. V. Sellmeier for their committed and competent co-operation. We would also sincerely like to thank Birte Fischer and Julia Körber, who carried out the translation.

Your suggestions and corrections will be appreciated.

Hannover, May 2013

Berend Denkena
Hans Kurt Toenshoff

Introductory Literature on Manufacturing Processes

There is a wide range of literature on manufacturing in general. For introductory purposes, the following books may be used:

Groover, M. P.: *Fundamentals of Modern Manufacturing*. 3rd edition (Wiley: New York 2009)

Kalpakjian, S.; Schmid, S.R.: *Manufacturing Engineering and Technology*. 6th edition in SI units (Prentice Hall: Singapore 2010)

Further Reading on Cutting and Abrasive Processes

The following books on the technology of cutting and abrasive processes may be used as accompanying literature to this book (references and specific additional literature for single chapters are given in the respective chapters):

Stephenson, D. A.; Agapiou, J. S.: *Metal Cutting Theory and Practice*. 2nd edition (Taylor & Francis: Boca Raton 2006)

Klocke, F.: *Manufacturing Processes 1: Cutting* (Springer: Berlin 2011)

Klocke, F.: *Manufacturing Processes 2: Grinding, Honing, Lapping* (Springer; Berlin 2009)

Shaw, M. C.: *Metal Cutting Principles*. 2nd edition (Oxford University Press: New York 2005)

Toenshoff, H. K.: *Cutting, Fundamentals*. CIRPedia, section Cutting (Springer 2012)

Trent, E. M.; Wright, P. K.: *Metal Cutting*. 4th edition (Butterworth Heinemann: Boston 2000)

Contents

1	Introduction to the Technology of Cutting and Abrasive Processes	1
1.1	Economic Relevance	1
1.2	Taxonomy	3
1.3	Motions, Angles at the Cutting Edge and Engagement Parameters	4
1.4	Cutting and Abrasive Processes as Black Box Systems	8
1.5	Process Types and Engagement Parameters in Drilling	9
1.6	Process Types and Engagement Parameters in Milling	15
1.7	Questions	18
	References	19
2	Chip Formation	21
2.1	Mechanisms of Chip Formation	21
2.2	Chip Root Analysis	25
2.3	Shear Plane Model	29
2.4	Questions	35
	References	36
3	Chip Control	37
3.1	Chip Volume Ratio and Chip Form Classification	37
3.2	Chip Guidance	38
3.3	Influence of the Workpiece Material	42
3.4	Influence of the Cutting Conditions	45
3.5	Questions	46
	References	48
4	Forces and Powers in Cutting and Abrasive Processes	49
4.1	Empirical Models	50
4.2	Modeling of the Feed Force and the Passive Force	59
4.3	Surface Forces at the Cutting Edge	60

4.4	Analytical Approaches in Plastomechanics	63
4.4.1	Theory by Ernst and Merchant	63
4.4.2	Hucks's Theory	64
4.5	Flow Curves and Constitutive Equations	66
4.6	Numerical Theory	68
4.7	Powers, Torques and Forces in Drilling	70
4.8	Power and Forces in Milling Processes	76
4.9	Questions	80
	References	81
5	Energy Conversion and Temperature	83
5.1	Conversion Effects	83
5.2	Heat Flow	86
5.3	Temperatures of Cutting Wedge and Workpiece	89
5.3.1	Temperature Measurement	89
5.3.2	Temperature Fields	96
5.4	Optimization of the Cutting Wedge	101
5.5	Questions	102
	References	103
6	Modeling and Simulation	105
6.1	Kinematic Simulation	106
6.1.1	Representation of the Workpiece	108
6.1.2	Tool Model	114
6.1.3	Determination of Process Values	115
6.2	Numerical Simulation by FEM	119
6.3	Molecular Dynamic Modeling	123
6.4	Questions	126
	References	126
7	Wear	129
7.1	Wear Forms	129
7.2	Loading	132
7.3	Wear Mechanisms	138
7.4	Tool Life	140
7.5	Tool Life Scatter and Process Reliability	146
7.6	Influence of Work Material on Wear	148
7.6.1	Work Material Composition	149
7.6.2	Melting Procedure	150
7.6.3	Heat Treatment	152
7.7	Rounding of the Cutting Edge	153
7.8	Questions	156
	References	157

8	Cutting Materials	159
8.1	Requirements on Cutting Materials	159
8.2	Tool Steels	163
8.3	High Speed Steels	163
8.4	Stellites	165
8.5	Cemented Carbides	166
8.6	Cermets	174
8.7	Ceramics	176
8.8	Diamond	181
8.8.1	Mono-Crystalline Diamond	181
8.8.2	Polycrystalline Diamond	181
8.9	Boron Nitride	183
8.10	Questions	186
	References	187
9	High Speed Cutting	189
9.1	Definition	189
9.2	Chip Formation	192
9.3	Application	193
9.4	High Power Cutting	196
9.5	High Power Drilling	196
9.6	Questions	198
	References	199
10	Hard Machining, Process Design	201
10.1	Hard Turning	201
10.2	Hard Drilling	207
10.3	Hard Milling	209
10.4	Materials	211
10.5	Chip Formation, Forces and Temperature	212
10.6	Cutting Materials and Tool Wear	217
10.7	Questions	218
	References	219
11	Hard Machining, Component Quality	221
11.1	Macro Geometrical Deviations	221
11.2	Micro Geometrical Properties	224
11.3	Physical Influence	226
11.4	Rolling Fatigue Strength	227
11.5	Fatigue Strength	228
11.6	Sealability	230
11.7	Post-treatment Processes	231
11.7.1	Hard Roller Burnishing	231
11.7.2	Water Peening	233

11.8	Questions	234
	References	235
12	Broaching	237
12.1	Broaching Process	237
12.2	Machine Development.	242
12.3	Questions.	246
	References	246
13	Grinding	247
13.1	Cutting with Geometrically Undefined Cutting Edges.	247
13.2	Grinding Materials	250
13.2.1	Corundum	251
13.2.2	Silicon Carbide	253
13.2.3	Cubic Crystalline Boron Nitride and Diamond.	254
13.2.4	Grain Sizes of Grinding Materials	255
13.3	Bonding	257
13.4	Grinding Wheels	258
13.5	Burst Safety of Grinding Wheels	261
13.6	Grinding Processes	265
13.6.1	Input Variables.	266
13.6.2	Process Variables	276
13.6.3	Output Variables	279
13.7	Conditioning of Grinding Tools	286
13.7.1	Basics	286
13.7.2	Conditioning of Conventional Grinding Wheels.	290
13.7.3	Conditioning of Super Hard Grinding Wheels	292
13.8	Grinding Costs	295
13.9	Questions.	296
	References	297
14	Gear Grinding	303
14.1	Introduction	303
14.2	Discontinuous Profile Grinding	308
14.3	Continuous Generating Grinding with Grinding Worms	312
14.4	Continuous Crossed Helical Grinding	316
14.5	Questions.	320
	References	321
15	Process Layout and Integration into the Process Chain	325
15.1	Basics of Process Chain Layout	325
15.1.1	Technological Interfaces	326
15.1.2	Process Chain Layout	327
15.2	Process Model Generation	328

- 15.3 Process Layout Using the Example of “Hard Finishing” 331
- 15.4 Process Chain Layout Using the Example
“Gear Production” 335
- 15.5 Process Supervision 341
- 15.6 Questions. 345
- References 346

- 16 Surface and Subsurface Properties 349**
 - 16.1 Surface Properties. 350
 - 16.1.1 Determination of Surface Properties 351
 - 16.2 Subsurface Properties 355
 - 16.2.1 Determination of Subsurface Properties. 356
 - 16.2.2 Effects of Cutting Processes. 362
 - 16.3 Questions. 368
 - References 369

- 17 Cooling Lubrication 371**
 - 17.1 Requirements 371
 - 17.2 Cooling Lubricating Fluids 373
 - 17.2.1 Not Water-Mixable Cooling Lubricating Fluids 373
 - 17.2.2 Water-Mixable Cooling Lubricating Fluids 375
 - 17.2.3 Additivation of Cooling Lubricating Fluids 378
 - 17.3 Use of Cooling Lubricating Fluids in Geometrically
Determined Cutting. 380
 - 17.4 Use of Cooling Lubricating Fluid in Grinding 383
 - 17.4.1 Methods to Determine the Cooling Lubricating
Fluid Effect in Grinding 385
 - 17.4.2 Applications and Effects 387
 - 17.5 Questions. 392
 - References 393

- 18 Appendix 397**
 - 18.1 Solution to the Exercise for Chap. 3, Question 9 397
 - 18.2 Solution to the Exercise for Chap. 4, Question 26 397
 - 18.3 Solution to the Exercise for Chap. 5, Question 17 398
 - 18.4 Solution to the Exercise for Chap. 6, Question 25 399

Chapter 1

Introduction to the Technology of Cutting and Abrasive Processes

1.1 Economic Relevance

It stands to reason that manufacturing and assembly play an essential role in the industrial production process: They represent the transfer of planned products into real products by the fabrication of components, units and aggregates. Manufacturing processes can be divided into six main groups [TÖN94, DIN8580]:

- primary shaping
- forming
- separating
- joining
- coating
- changing material properties.

Cutting and abrasive processes are part of the main group of separation processes. They are mainly used for metallic materials and are fundamental steps in the production processes in machine and vehicle manufacturing, in the aerospace industry, in equipment and drive technology, in biomedical engineering and in many other industrial sectors. They provide an unsurpassed range of options for adapting qualities and shapes as well as the productivity. Compared to related, partly competing manufacturing processes like casting and forging, they stand out due to the large range of producible designs and shapes as well as their high accuracy. However, they are inferior to these processes regarding efficiency and productivity, i.e., the number of parts produced per unit time, at least in the production of larger quantities. Furthermore, in cutting and abrasive processes chips are removed from a workpiece, which includes material loss; therefore, cutting and abrasive processes are also inferior regarding sustainability, i.e., stewardship of energy and material resources. Figure 1.1 shows a rough qualitative comparison of cutting and abrasive processes with casting and forging.

Cutting and abrasive processes provide accuracies within the ISO tolerance grades of IT2 to IT10. They are used for the individual production of single pieces or small numbers of pieces, e.g., for the production of customized endoprostheses;

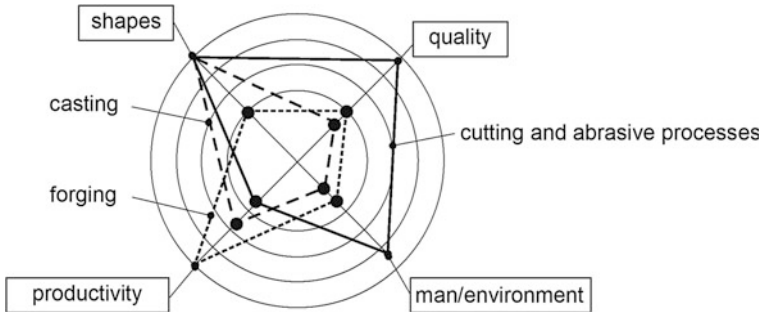


Fig. 1.1 Comparison of three manufacturing processes

for the production of small or medium series, e.g., for racing vehicle engine components and for mass production, e.g., in automotive engineering. Because they provide high accuracies, they are often placed at the end of a sequence of several manufacturing processes, which means that additional emphasis has to be put on the process reliability. As mentioned above, cutting and abrasive processes can be used to produce a nearly unlimited variety of shapes. This is mainly due to the fact that they are generating (in the sense of kinematically controlled) processes (in contrast to copying processes): the necessary tool geometry is independent from the final shape of the product. In other words, the product is not an image of the tool shape, but its shape is produced by a controlled movement and interaction between the tool and the workpiece (Fig. 1.2). This means that the movement of the tool can be directly computer-controlled using path variables.

This provides high flexibility: Different components can be produced within a continuous sequence or clamping and a lot size of 1 is feasible.

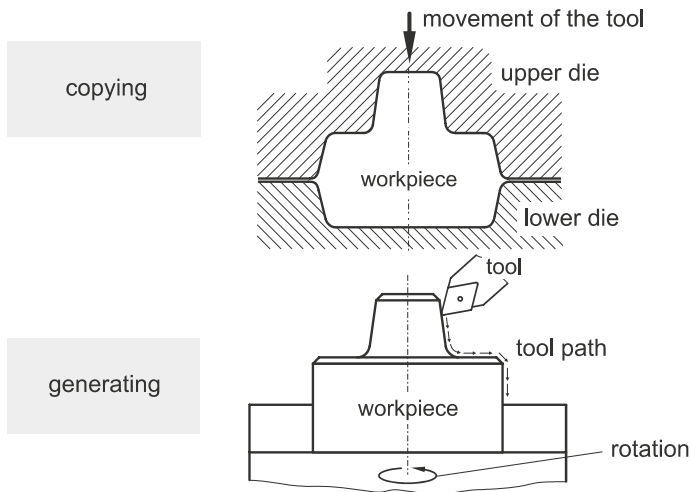


Fig. 1.2 The principles of copying and generating

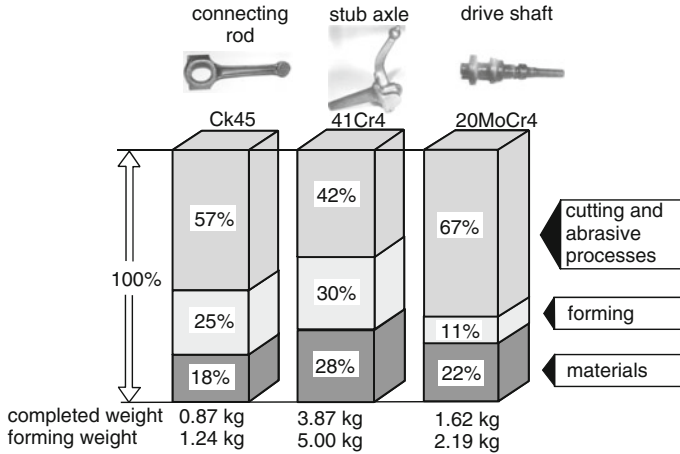


Fig. 1.3 Manufacturing cost structure of selected power train components [TÖN10]

Figure 1.3 shows that cutting and abrasive processes are of decisive relevance in serial production, e.g., in automotive engineering.

1.2 Taxonomy

Cutting and abrasive processes represent manufacturing by means of material separation, particularly of material removal. Material in the form of chips is mechanically removed from a raw part/workpiece by one cutting edge (in turning), several cutting edges (in milling) or numerous cutting edges (in grinding). In *cutting processes*, the number of cutting edges, the shape of the cutting edges and their position in relation to the workpiece are known and describable (Fig. 1.4). In contrast, in *abrasive processes*, only statistical parameters are known regarding the geometry and the number of the cutting edges in the abrasive material.

According to the most comprehensive taxonomy of cutting and abrasive processes [TÖN94b, CIRP04, DIN8589-0], the groups of cutting processes respectively abrasive processes can first be further divided regarding the specific process (1st digit: separation, 2nd digit: cutting, abrasive processes, 3rd digit: e.g., turning, milling), and then according to

- the geometry of the surface to be produced (4th digit: plain/slab, cylindrical/circular, thread/helical, hobbing, profile, form)¹
- the feed direction (5th: orthogonal, longitudinal) or tool characteristics
- the position of the surface to be produced (6th digit: external, internal)

Typical examples of turning processes are presented in Fig. 1.5.

¹ With the exceptions of tapping (for thread drilling) and hobbing (for gear milling).

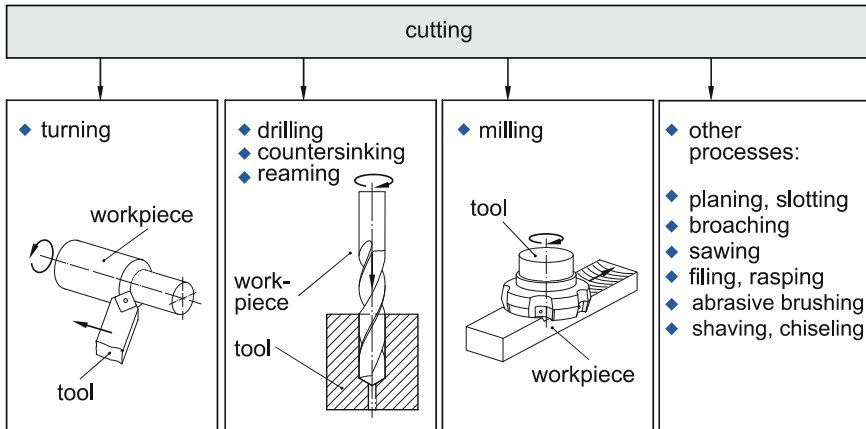


Fig. 1.4 Manufacturing processes: cutting [TÖN94b, CIRP04, DIN8589-0]

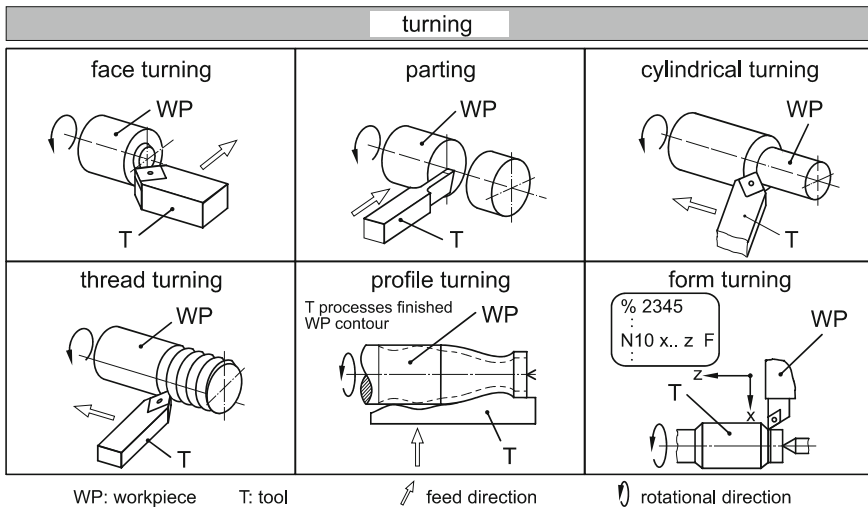


Fig. 1.5 Turning processes [TÖN94c, DIN8589-1]

1.3 Motions, Angles at the Cutting Edge and Engagement Parameters

In cutting processes, a cutting edge penetrates into the workpiece material. The relative movement between the tool and the workpiece can be described by means of the primary motion (cutting motion) with the cutting speed v_c and the feed motion with the feed speed v_f (Fig. 1.6). The depth of cut and the feed speed determine the cross-section of the undeformed chip A .

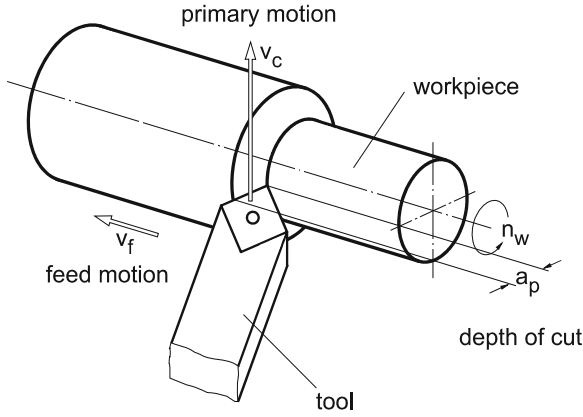
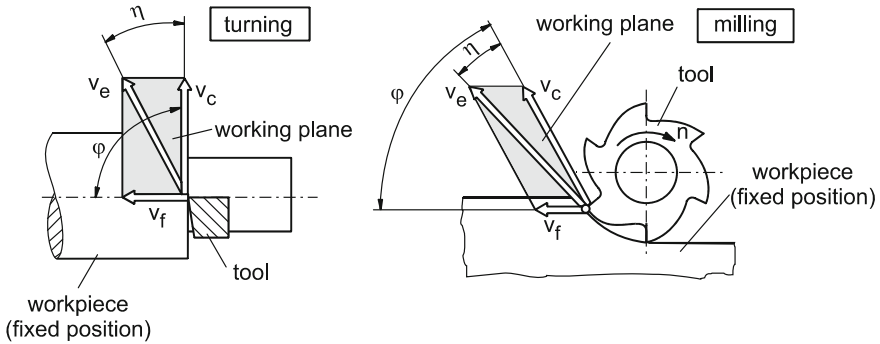


Fig. 1.6 Motions in cutting processes (In all presented figures, speed arrows are assigned to the tool (independently from the real actions in the process), thus pretending that the workpiece is fixed in position and that the tool performs all motions. In most real turning processes (but by no means all), the tool performs the feed motion while the workpiece performs the rotary motion)

The vectors of the feed speed and the cutting speed span the working plane (Fig. 1.7). The vectorial sum of the cutting speed and the feed speed is the effective cutting speed v_e . The cutting speed and the effective cutting speed form the effective cutting speed angle η . The cutting speed and the feed speed form the feed motion angle φ . In turning and drilling (in all processes with a helical or linear effective cutting motion) η and φ are constant ($\varphi = 90^\circ$), while in milling,



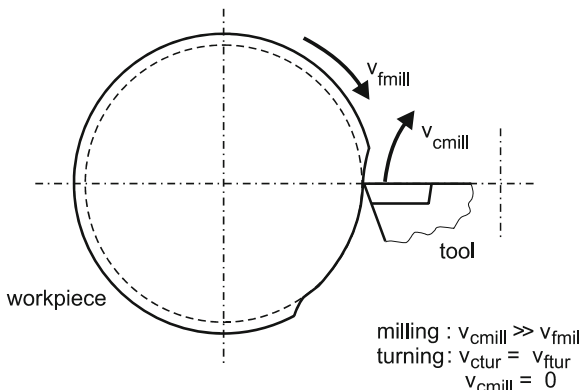
$$\tan \eta = \frac{\sin \varphi}{v_c / v_f + \cos \varphi}$$

v_c = cutting speed
 v_e = effective speed
 v_f = feed speed

η = effective cutting speed angle
 φ = feed motion angle

Fig. 1.7 Effective cutting direction in the working plane in cylindrical turning and peripheral milling

Fig. 1.8 Turning as a special case of milling (To illustrate this point, the speed arrows have for once been assigned to the workpiece)



circular sawing and grinding (in all processes with a cycloidal effective cutting motion) they are variable and time-dependent.

In all processes with a constant feed motion angle of $\varphi = 90^\circ$ (turning, drilling, broaching), i.e., all processes with a linear, helical or spiral effective cutting motion, the material removal rate Q_w (the volume of material removed per unit time) is

$$Q_w = a_p \cdot f \cdot v_c, \quad (1.1)$$

while in processes with a time-dependent feed motion angle (milling, grinding, circular sawing), it is

$$Q_w = a_p \cdot a_e \cdot v_f. \quad (1.2)$$

It might be surprising that (according to Eq. 1.1) the material removal rate for turning processes is calculated using the cutting speed, whereas according to Eq. 1.2, the feed speed is used for milling processes. Figure 1.8 illustrates that turning can be regarded as a special case of milling and consequently with a fixed tool, the primary motion actually is a feed motion.

The relevant angles at the cutting edge are located within different planes. In the tool orthogonal plane (i.e., the plane orthogonal to the tool reference plane and the cutting edge plane), these are the clearance α ($\alpha > 0$ in every case), the rake angle γ ($\gamma > 0$ if the tool tip is preceding) and the wedge angle $\beta = 90^\circ - (\alpha + \gamma)$. In the cutting edge plane the relevant angle is the tool cutting edge inclination λ ($\lambda > 0$ if the tool tip is preceding). The tool cutting angle κ and the tool included angle ε are located in the tool reference plane (Fig.1.9). The cutting edge itself is defined by the corner radius r_c , measured in the tool reference plane and by the cutting edge rounding, measured in the tool orthogonal plane using the cutting edge radius r_β .

The undeformed chip cross section A can be described using two different systems of parameters: either by coordinates derived from the relative movement between the tool and the workpiece, i.e., the engagement parameters a_p (depth of

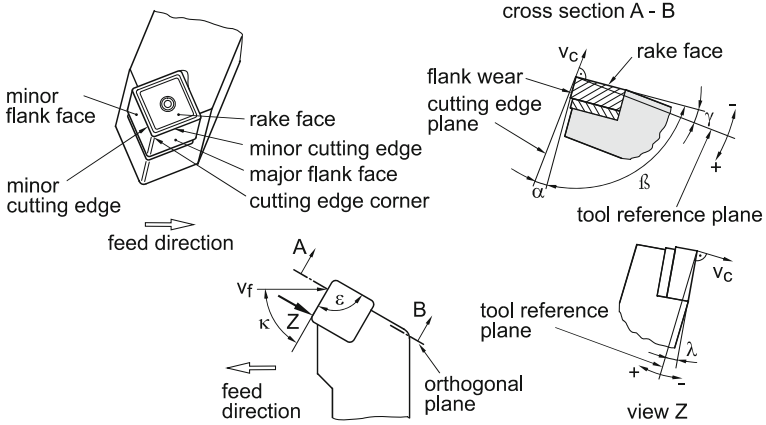


Fig. 1.9 Terminology for turning tools [ISO3002-1, ISO3002-3, DIN6581]

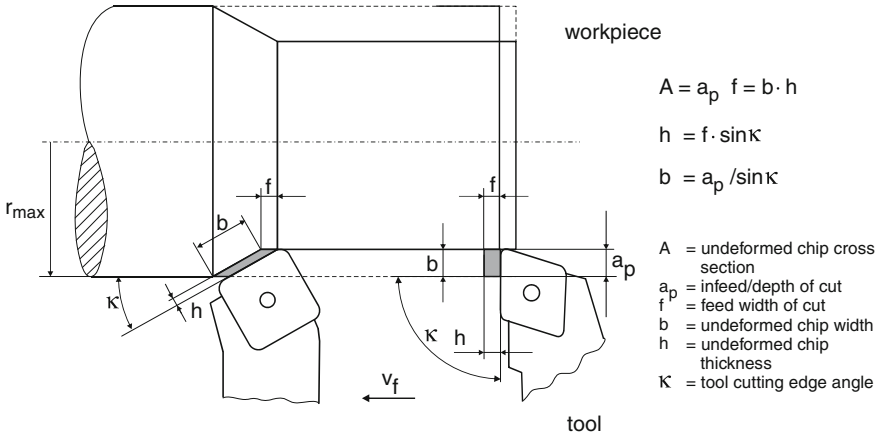


Fig. 1.10 Turning: engagement parameters and undeformed chip parameters

cut) and a_e (width of cut), in practice called the infeed a_p and the feed $f = a_e$, or by the essential parameters in the chip formation process, i.e., the undeformed chip parameters b and h (Fig. 1.10).

The feed is determined using the rotational speed of the workpiece n_w :

$$f = \frac{v_f}{n_w} \tag{1.3}$$

The cutting speed v_c is usually indicated for the maximum contact diameter $2 \cdot r_{\max}$:

$$v_c = 2\pi \cdot r_{\max} \cdot n_w \tag{1.4}$$

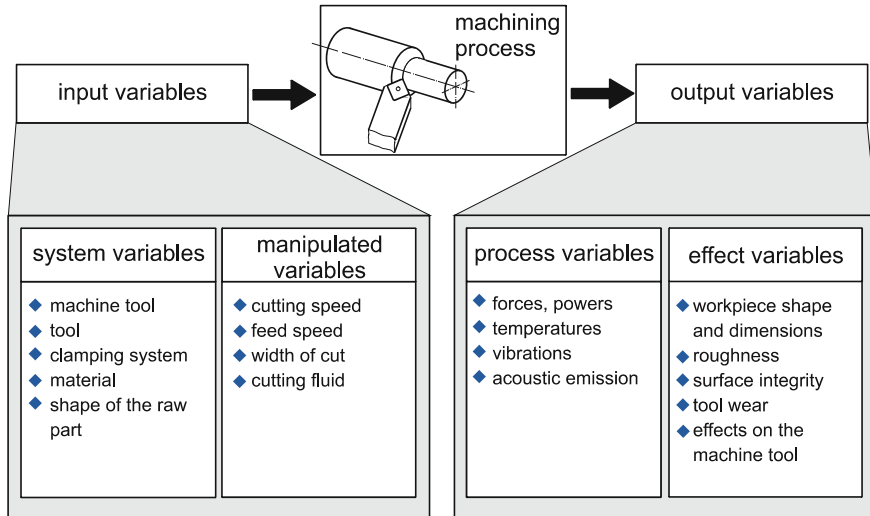


Fig. 1.11 Cutting and abrasive processes as a black box system

1.4 Cutting and Abrasive Processes as Black Box Systems

From a system-oriented point of view, cutting and abrasive processes can be described as black boxes with input variables and output variables (Fig. 1.11). The input variables can be divided into system variables and manipulated variables (set variables). System variables describe process conditions which are either completely fixed or at least constant over a relatively long period of time. They depend on the machine tool (static and dynamic stiffness, temperature response), the workpiece (strength, shape of the raw part, chemical composition, structure) and the tool (material, shape, mechanical properties) (Fig. 1.11).

The manipulated variables or set variables for each workpiece or job order are usually assessed and adjusted manually or using a program memory. They include the rotational speed or cutting speed, feed speed (depth of cut) and width of cut (infeed of the tool towards the workpiece). Furthermore, they can include the cutting liquid supply and the clamping force applied to fix the workpiece.

The output variables are divided into process and effect variables. Process variables like resultant forces, powers, temperatures in the chip formation zone, vibrations caused by the process and acoustic emissions are only perceivable during the actual process. They can be used for monitoring or diagnosing purposes [TÖN01]. Effect variables can be measured at the workpiece (deviations in dimension, shape and position, micro-geometry, influence on the external surface zone), at the tool (wear), at the machine tool (temperature rise, wear) and in the cutting fluids (temperature rise, contamination and chemical properties).

In the process the input variables are converted into output variables. The transmission behavior of the process can be characterized by a comparison of the

input and output variables. The following four criteria are used for evaluating a process and define the machinability:

- resultant force
- tool wear
- surface properties of the workpiece
- chip form.

It is assumed that the input variables are predetermined, because the main technology and the productivity (e.g., the material removal rate) are determined by the process, the machine tool and the corresponding movement control [TÖN94a].

The *resultant forces* influence

- the design of the machine tool drives
- the design of the machine tool frame, respectively the deformation of the machine tool frame
- the power requirement
- the elastic deformation of the workpiece and the tool
- the requirements on the clamping systems for the workpiece and the tool.

The *tool wear* has a crucial influence on the economic efficiency of the process. The deviation of the *surface properties* from the ideal target values (dimensions, shape, position, roughness, physical properties of the external zone) determines the workpiece quality. The *chip form* is important for the tool design (flutes or gullets for chip removal), for the design of the working space of the machine tool and for an disturbance-free process (process reliability).

1.5 Process Types and Engagement Parameters in Drilling

Drilling is a cutting process with a rotational primary motion. Common drilling processes are shown in Fig. 1.12. The tools usually have a complex design. The following general characteristics of drilling processes can make their use problematic:

- The cutting speed is dependent on the radius, i.e., it is proportional to the radius from the axis of rotation of the drill and has a value of zero at the axis itself. As a result, no material separation can take place at this part of the drill. This influences the necessary forces and torques.
- Chips have to be removed from the drilled hole. The respective travel distance increases with the drilling depth, which can cause problems in the chip removal.
- The supply of cutting liquid also becomes increasingly difficult with an increase in the drilling depth, which sometimes makes additional measures necessary (internal cutting liquid supply).
- Drilling tools can only produce holes of fixed dimensions, so that the drilling diameter cannot be adjusted by means of the process control.

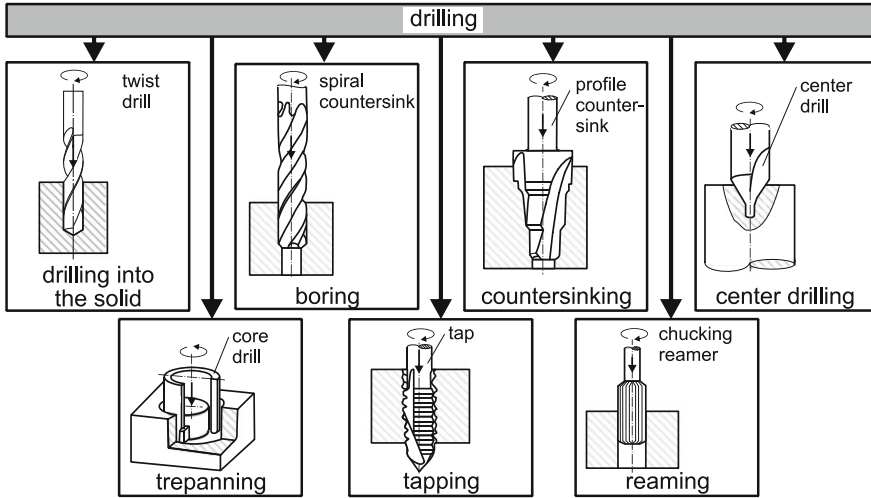


Fig. 1.12 Drilling processes [DIN8589-2]

In the following, two technological parameters that make up essential manipulated variables will be defined using the example of drilling processes: the cutting speed v_c and the feed per cutting edge f_z . They are each limited by a characteristic process limit. The cutting speed is limited due to the thermal load and thus by the wear behavior of the tool, while the feed per cutting edge is limited due to the mechanical load. The derived manipulated variables like the rotational speed n_t with the drilling radius r and the feed speed v_f with the cutting edge number z depend on these technological parameters as follows:

$$n_t = v_c / (2 \cdot \pi \cdot r) \quad (1.5)$$

$$v_f = z \cdot f_z \cdot n_t \quad (1.6)$$

In general, a twist drill with $z = 2$ is used for *drilling from the solid*. The material removal rate in drilling from the solid is

$$Q_w = \frac{1}{2} r \cdot f \cdot v_c \quad (1.7)$$

with the feed f of the drill:

$$f = z \cdot f_z \quad (1.8)$$

The twist drill consists of a shank (cylindrical or conical) and a cutting part. The terminology for drills, the engagement parameters and the angles at the cutting edges are illustrated in Fig. 1.13. The drill is clamped and guided by the shank. As a result the shank particularly serves the purpose of torque transmission. By means of the complex cutting edge geometries of the different drills, the tool can be adapted to each specific drilling task. On the one hand, the profile of the twist drill

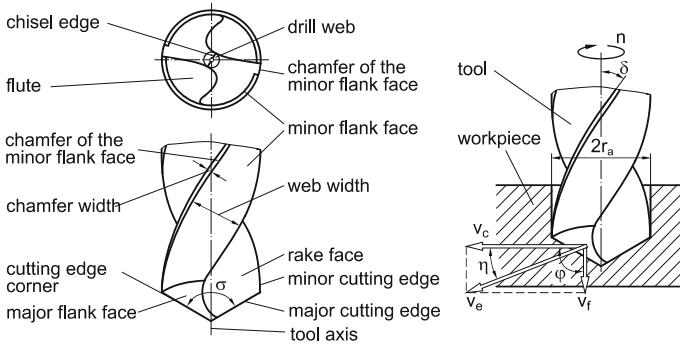


Fig. 1.13 Terminology and mode of the operation of a twist drill [DIN8589-2]

has to possess large flutes in order to provide sufficient space for chip removal; on the other hand, the drill must exhibit appropriate torsional rigidity (polar moment of inertia) and torsional strength (shear modulus). The helix angle δ of the flutes influences both the chip removal and the rake angle at the cutting edges.

The rake angle at the drill has an essential influence on the deformation and the forces at the cutting edges. We distinguish between the rake angle at the chisel edge γ_q , which can by all means be highly negative due to geometrical reasons and the rake angle at the major cutting edge γ_h (Fig. 1.14).

Near the center of the drill, γ_q is $-\sigma/2$. Further along the chisel edge it rises slightly but remains within the range of

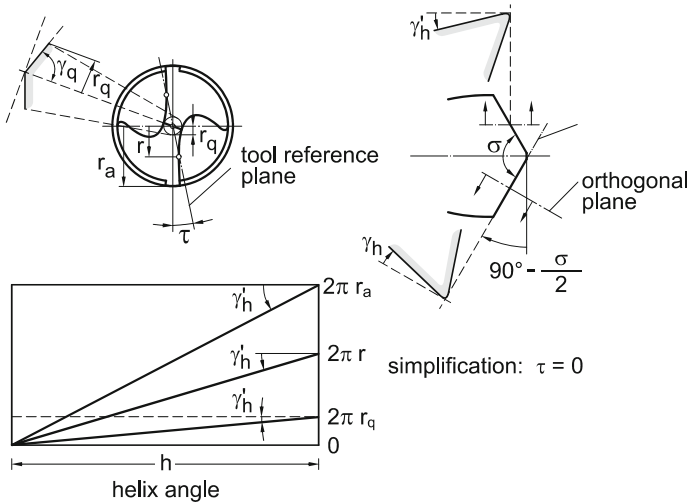


Fig. 1.14 Rake angle at the drill

$$-\frac{\sigma}{2} \leq \gamma_q \leq -\left(1 - \frac{r_q}{r_a}\right) \cdot \frac{\sigma}{2}. \quad (1.9)$$

At the outer perimeter of the drill ($r = r_a$), the rake angle at the major cutting edge is the helix angle corrected by the drill-point angle σ :

$$\gamma_h(r = r_a) = \arctan \frac{\tan \delta}{\sin \sigma/2}. \quad (1.10)$$

Towards the axis of rotation, it changes with the radius (Fig. 1.10):

$$\gamma_h = \arctan \left(\frac{r}{r_a} \frac{\tan \delta}{\sin \sigma/2} \right). \quad (1.11)$$

Figure 1.15 illustrates the significant change in the rake angle along the radius of the drill, by means of a cross-section through the chip formation zone in front of the cutting edges.

The drill-point shape of the twist drill has an essential influence on the cutting ability, because it determines the clearance angle. Attention has to be paid to the fact that the ratio of the feed speed to the cutting speed and thus the effective cutting speed angle η along the cutting edges, vary with the drill radius (Fig. 1.14).

Taking this speed ratio into account, the clearance angle has to be increased—if only for kinematic reasons—in order to avoid pressure generation (for a detailed derivation, see Sect. 7.1). Because the cutting edge is inclined by a lead angle of $\kappa = -\sigma/2$, the minimum clearance angle α_{\min} can be calculated regardless of elastic flattening as:

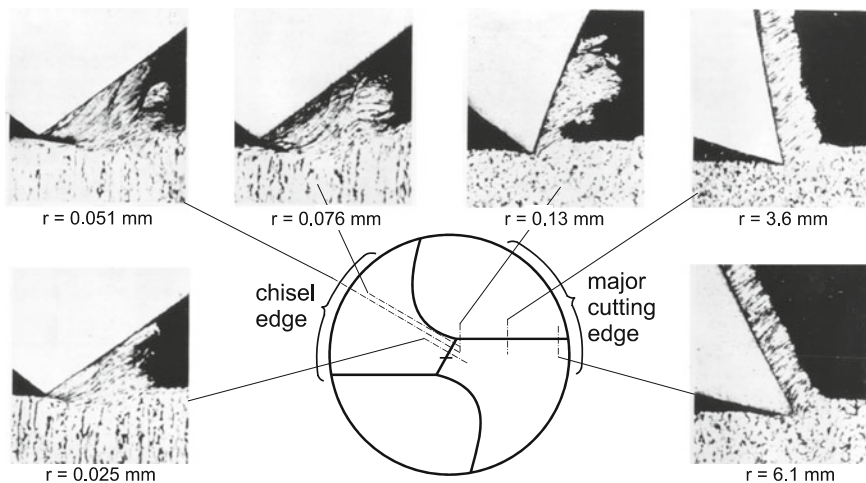


Fig. 1.15 Chip formation in drilling from the solid

$$\tan \alpha_{\min} = \frac{v_f}{v_c} \cdot \sin \frac{\sigma}{2} = \frac{f \cdot \sin \frac{\sigma}{2}}{2\pi \cdot r}, \quad (1.12)$$

assuming that the cutting edge is not preceding ($\tau = 0$).

Vice versa, if the minimum clearance angle at the outer radius of the web r_q is given, the maximum permitted feed across the radius $f_{\max}/2r_a$ can be calculated as

$$\frac{f_{\max}}{2r_a} = \frac{\pi \cdot \tan \alpha_{\min}}{\sin \frac{\sigma}{2}} \cdot \frac{r_q}{r_a}. \quad (1.13)$$

With common values ($\sigma = 118^\circ$, $r_q/r_a = 0.2$) and assuming a minimum clearance angle of $\alpha_{\min} = 2^\circ$, the maximum permitted feed related to the outer diameter is $f_{\max}/2r_a = 0.026$. Considering flattening and wear, the value used in the process should never exceed half this calculated value.

The drill-point is ground considering the following conditions:

- The drill should have appropriate centering properties.
- The clearance angle should be adequately large along the whole length of the cutting edge.
- However, the cutting edge should be as stable as possible.
- The chisel edge should be as short as possible because of the disadvantageous chip formation processes.

The most common drill-point shape for HSS twist drills is the conical point. It is produced by grinding the drill using a grinding face, revolving the drill around an axis that is inclined by a certain angle towards its center axis, e.g., with a tilt angle of 20° . The clearance angle is thus part of a cone surface. It increases towards the axis of rotation. The conical point can be ground using a simple kinematic process on a point grinding machine.

There is also a range of special drill-point shapes which are partly standardized (DIN1412) and partly manufacturer-specific. Depending on the specific application, particular significance is attached to one of the conditions mentioned above. Some special drill-point shapes are presented in Fig. 1.16.

To produce shape A the chisel edge is reduced to about half its initial length by web thinning, with the shape of the thinned chisel edge adjusted to the flute profile. The shortening of the chisel edge reduces the feed forces, while it has almost no influence on the torque.

To produce shape B out of shape A, the rake angle is corrected at the major cutting edges. Thus, the rake angle is no longer dependent on the helix angle of the flutes. Such corrections can increase the stability of the cutting edges and have a positive effect on the chip form.

The split point (shape C) can be regarded as a special kind of web thinned point. The length of the chisel edge is reduced to about 6 % of the outer radius. Hence, even positive rake angles can be produced at the chisel edge.

In *boring out and countersinking* processes, a previously produced hole is enlarged. It is difficult to guide the tool on a coaxial path, because there is no

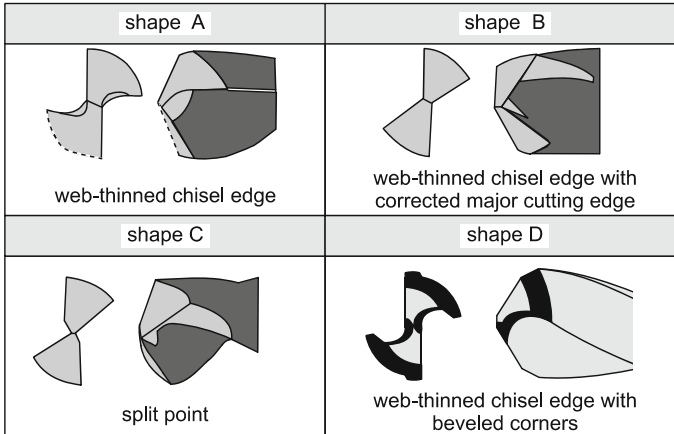


Fig. 1.16 Common drill-point shapes [DIN1412]

center point in the workpiece material, so the tools generally have three or multiple cutting edges. However, chip removal is easier than in drilling from the solid. Therefore, bore holes with a high diameter are often predrilled using a smaller twist drill and then enlarged within several steps, until they reach the nominal diameter. This procedure is also called for, if the maximum permitted feed force, respectively the maximum permitted torque of a machine are not sufficient to drill the hole within one stroke. The material removal rate in drill out processes with the inner radius r_i is

$$Q_w = \frac{1}{2} \left(r - \frac{r_i^2}{r} \right) \cdot f \cdot v_c \quad (1.14)$$

Center drilling is necessary, if the surface to be drilled is rough, uneven or inclined. It can be avoided by using a very stiff guidance for the drill (drill clamped with a short projecting length, stiff spindle) or by using drill bushings.

Trepanning is used for large bore hole diameters. An annular cut is produced instead of cutting the whole bore diameter. This reduces the required torque and power. However, trepanning can only be used for through holes.

Tapping is used to produce internal threads. The tap feed must be adjusted to the thread pitch. In machine production, this can be achieved by exact guidance using an NC machine tool or by first using a starting taper and then a tap holder. The rotational direction has to be reversed to remove the drill from the hole. If multi spindle bar machines are used, special devices are needed for this purpose (disconnecting the spindle and reversing the rotational direction or using a second spindle which is attached to the tool and outruns the workpiece spindle). To avoid having to reverse the rotational direction, large internal threads can be produced by thread chasing, which is profile turning within several strokes. This can also be done using controllable collapsible taps.

Reaming is a finishing process corresponding to a boring out process with a multiple edged tool and a small depth of cut. It is used for bore holes with high dimension and shape accuracy. The position accuracy cannot be influenced. Tolerance grades of IT 7—with an increased effort even IT 6—can be achieved. The surface roughness R_z is about $5 \mu\text{m}$. Conventional HSS reamers are used at low cutting speeds of 10–20 m/min and low feed rates of 0.08–1.25 mm. If clocked automated systems are used, this kind of reaming has a significant influence on the clock cycle. Therefore, alternative processes and tools have been developed.

1.6 Process Types and Engagement Parameters in Milling

In *milling*, the necessary relative movement between the tool and the workpiece is achieved by a rotational cutting motion of the tool and a feed motion orthogonal or at a certain angle to the rotational axis of the tool. The feed motion can be performed by the tool or the workpiece or by a combined movement of the two. The cutting edges are not permanently engaged. The feed motion angle and the effective cutting speed angle are time-dependent (see Sect. 1.3). The most important milling processes are shown in Fig. 1.17. They are classified according to the produced shapes, which are determined by the feed motion. In *face milling* the rotation axis of the tool is orthogonal to the produced surface, while in *peripheral milling* it is parallel to the surface. *Side milling* is a combination of these two processes and is used to produce two surfaces that are orthogonal to each other. *Helical milling* and *hobbing* produce helical or gear surfaces. In *profile*

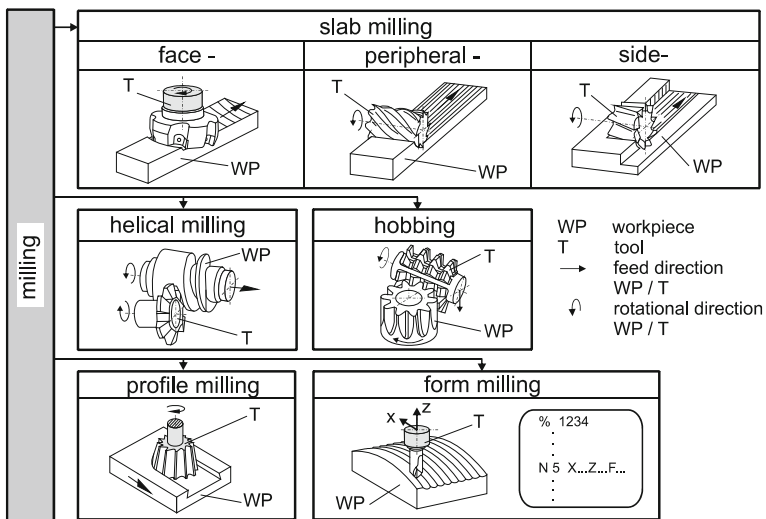


Fig. 1.17 Milling processes [DIN8589-3]

milling the tool shape is reproduced on the workpiece, making its shape and dimensions dependent on those of the tool. The largest variety of shapes can be produced by *form milling*, even though the range of producible shapes depends on the number of controllable feed axes on the milling machine. A milling machine usually possesses three linear feed axes, which can be controlled both simultaneously and independently (continuous path control), enabling the tool to follow any three-dimensional path. In special machines, two rotational axes are added to these three linear axes (five axes milling), so that the rotational axis of the milling cutter can be positioned in any direction at any point of the path.

If we focus on the productivity of the milling process in *roughing* processes, i.e., on removing large volumes of workpiece material as fast as possible, we have to determine the material removal rate Q_w :

$$Q_w = a_p \cdot a_e \cdot v_f \tag{1.15}$$

If we want to cut a large surface by a *finishing* process, the productivity is determined using the area cut per time unit \dot{A}_w (applicable for face milling; for peripheral milling, a_e is replaced by a_p):

$$\dot{A}_w = a_e \cdot v_f \tag{1.16}$$

At any point of time each cutting edge of the milling cutter is engaged by a maximum of 180° or less, leading to an interrupted cut. The chips produced in the process are comma-shaped. The engagement parameters are dependent on the penetration angle/feed motion angle φ (Fig. 1.18).

The milling process is often characterized using the mean chip thickness h_m . It is the average chip thickness across the engagement path.

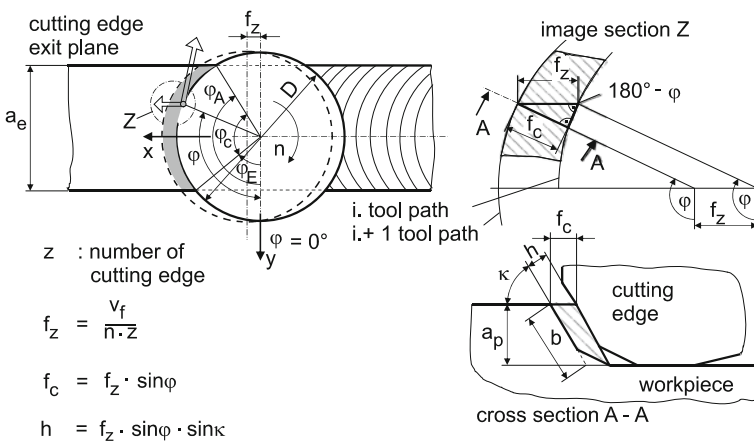


Fig. 1.18 Engagement parameters in face milling

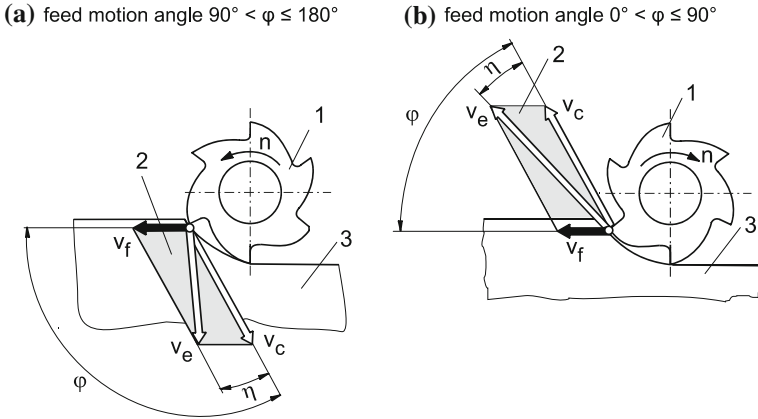


Fig. 1.19 Down milling **a** and up milling **b**

$$h_m = \frac{1}{\varphi_c} \cdot \int_{\varphi_E}^{\varphi_A} h(\varphi) d\varphi = \frac{1}{\varphi_c} \cdot f_z \sin \kappa (\cos \varphi_E - \cos \varphi_A) \quad (1.17)$$

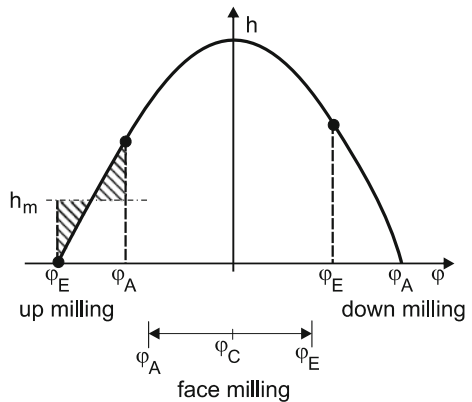
where

$$(\cos \varphi_A - \cos \varphi_E) = 2a_e/D \quad (1.18)$$

According to the approach type, we distinguish between down milling and up milling (Figs. 1.19, 1.20).

In the down milling process, the cutting edge enters the workpiece at the thicker end of the comma-shaped chip and builds up a shock-type resultant force. Therefore, the machine tool must exhibit appropriate dynamic stiffness (against vibrations). In the up milling process, the chip formation starts at the thinner end, thus pressure forming takes place at the beginning. This results in unfavorable chip

Fig. 1.20 Chip thickness in milling processes



formation conditions, because the chip thickness is below the minimum value in the beginning and instead of chip formation only high normal forces and friction forces occur, leading to an increased wear compared to that in the down milling process. If the machine tool and the workpiece allow for it, down milling should be used. In particular, the machine tool must not allow for any backlash in the feed drive—a condition which is met by all modern NC machine tools anyway. In down milling, one force component is orthogonal to the produced surface and thus the workpiece is automatically pressed against the supporting surface. This also makes down milling convenient for the cutting of long, slender workpieces, which, in up milling would be pulled away from the supporting surface. In face milling, the process mode changes between up and down milling, depending on the position of the rotation axis towards the workpiece, as illustrated in Fig. 1.18.

According to Eq. 1.17, the mean chip thickness is calculated as the average value of the chip thickness across the engagement path. In literature this is simplified by using the value of the chip thickness across the average value of the engagement path. Equation 1.17 shows that the relation between the path and the chip thickness is nonlinear. Thus these two definitions are not identical. However, there is only a slight difference in the calculated chip thickness for both up and down milling.

1.7 Questions

1. Give a taxonomy of all manufacturing processes and of the cutting and abrasive processes. Which classification criteria have been applied?
2. Assess the manufacturing processes of casting, forging and cutting/abrasive processes with regard to different aspects.
3. Which values can be used to determine the efficiency of the processes of roughing and finishing?
4. Why do we use different parameters for calculating the material removal rate in turning and in milling?
5. What are the process limits of finishing processes?
6. What are the process limits of roughing processes?
7. What is the difference between the effective cutting speed angle and the feed motion angle in turning and drilling on the one hand and milling on the other hand?
8. How can we determine the material removal rates of different drilling processes?
9. Give the definition of the terms “tool reference plane”, “cutting edge plane” and “tool orthogonal plane”.
10. Describe cutting and abrasive processes from a system-oriented point of view.
11. Which are the input variables of cutting and abrasive processes?

12. Which effect variables can be relevant? Which criteria are used for evaluating cutting and abrasive processes?
13. Which are the relevant process parameters in cutting and abrasive processes?
14. What are the technological parameters (i.e., largely predetermined manipulated variables) in drilling processes?
15. Compare the essential input variables in turning processes with those in drilling, broaching and milling.
16. How do we determine the mean chip thickness in peripheral face milling and in down milling?

References

- [CIRP04] CIRP (ed.): Trennende Verfahren/Material Removal Processes/Procédés d'Enlèvement de Matière. Wörterbuch der Fertigungstechnik/Dictionary of Production Engineering/Dictionnaire des Techniques de Production Mécanique, vol. II, Ch. 1.01. Springer, Berlin (2004)
- [DIN1412] Deutsches Institut für Normung/German Institute for Standardization (ed.): DIN 1412: Spiralbohrer aus HSS—Anschliffformen/Twist drills made of high-speed steel—Shapes of points. Beuth, Berlin (2001)
- [DIN6581] Deutsches Institut für Normung/German Institute for Standardization (ed.): DIN 6581: Begriffe der Zerspantechnik; Bezugssysteme und Winkel am Schneidkeil des Werkzeuges/Terminology of chip removing; reference systems and angles on the cutting part of the tool. Beuth, Berlin (1985)
- [DIN8580] Deutsches Institut für Normung/German Institute for Standardization (ed.): DIN 8580: Fertigungsverfahren—Begriffe, Einteilung /Manufacturing processes—Terms and definitions, division. Beuth, Berlin (2003)
- [DIN8589-0] Deutsches Institut für Normung/German Institute for Standardization (ed.): DIN 8589-0: Fertigungsverfahren Spanen—Teil 0: Allgemeines; Einordnung, Unterteilung, Begriffe/Manufacturing processes chip removal—Part 0: General; Classification, subdivision, terms and definitions. Beuth, Berlin (2003)
- [DIN8589-1] Deutsches Institut für Normung/German Institute for Standardization (ed.): DIN 8589-1: Fertigungsverfahren Spanen—Teil 1: Drehen; Einordnung, Unterteilung, Begriffe/Manufacturing processes chip removal—Part 1: Turning; Classification, subdivision, terms and definitions. Beuth, Berlin (2003)
- [DIN8589-2] Deutsches Institut für Normung/German Institute for Standardization (ed.): DIN 8589-2: Fertigungsverfahren Spanen—Teil 2: Bohren, Senken, Reiben; Einordnung, Unterteilung, Begriffe/Manufacturing processes chip removal—Part 2: Drilling, countersinking and Counterboring, Reaming; Classification, Subdivision, Terms and Definitions. Beuth, Berlin (2003)
- [DIN8589-3] Deutsches Institut für Normung/German Institute for Standardization (ed.): DIN 8589-3: Fertigungsverfahren Spanen—Teil 3: Fräsen; Einordnung, Unterteilung, Begriffe/Manufacturing Processes Chip Removal—Part 3: Milling; Classification, Subdivision, Terms and Definitions. Beuth, Berlin (2003)
- [ISO3002-1] International Standard Organisation (ed.): ISO 3002-1: Basic Quantities in Cutting and Grinding—Part 1: Geometry of the active part of cutting tools (1992)

- [ISO3002-3] International Standard Organisation (ed.): ISO 3002-3: Basic Quantities in Cutting and Grinding—Part 3: Geometric and Kinematic Quantities in Cutting (1984)
- [TÖN01] Tönshoff, H.K., Inasaki, I.: Sensors in Manufacturing. Sensors Applications, vol. 1. Wiley-VCH, Weinheim (2001)
- [TÖN10] Tönshoff, H.K.: Massivumformteile wirtschaftlich spanen [Machining solid forming components economically] Infostelle Industrieverband Massivumformung e.V., Hagen (2010)
- [TÖN94] Tönshoff, H.K.: Manufacturing Processes. Dubbel Handbook of Mechanical Engineering, K2. Springer, Berlin (1994)
- [TÖN94a] Tönshoff, H.K.: Survey of Manufacturing Processes. Dubbel Handbook of Manufacturing Engineering, K1/2. Springer, Berlin (1994)
- [TÖN94b] Tönshoff, H.K.: Cutting. Dubbel Handbook of Mechanical Engineering, K36. Springer, Berlin (1994)
- [TÖN94c] Tönshoff, H.K.: Cutting. Dubbel Handbook of Mechanical Engineering, K38. Springer, Berlin (1994)

Chapter 2

Chip Formation

In cutting and abrasive processes, the cutting edge penetrates into the workpiece material, which is thus plastically deformed and slides off along the rake face of the cutting edge. This is called chip formation. The processes in chip formation can be examined within the orthogonal plane (Fig. 1.9), because essential parts of the material flow take place within this plane (Fig. 2.1). We can assume that the deformation is two-dimensional. The two-dimensional deformation is only disturbed at the edges of the cross section of the undeformed chip, at the free surface and in front of the cutting edge corner, as there is material flow at an angle towards the orthogonal plane, which is caused by linkage to the undeformed material by the free surface respectively.

Depending on the deformation behavior of the workpiece material, there are different mechanisms of chip formation with either continuous or discontinuous chip flow.

2.1 Mechanisms of Chip Formation

Depending on the workpiece material and the cutting conditions, the following mechanisms of chip formation can be distinguished (Fig. 2.2):

- continuous chip formation
- lamellar chip formation
- segmented chip formation
- discontinuous chip formation.

In *continuous chip formation* the chip slides off along the rake face at a constant speed in a stationary flow. Continuous chip formation is promoted by a uniform, fine-grained structure and high ductility of the workpiece material, by high cutting speeds and low friction on the rake face, by positive rake angles and a low undeformed chip thickness (Fig 2.3).

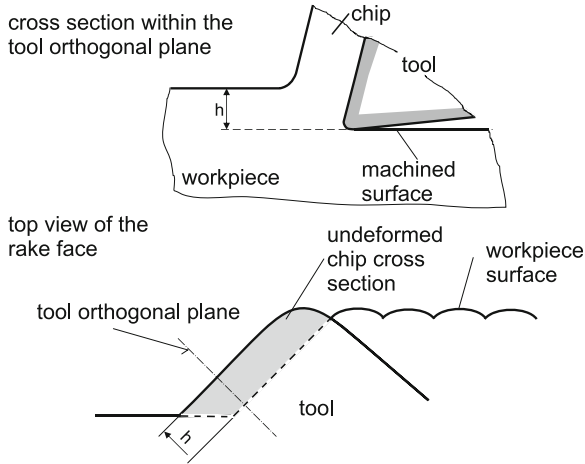


Fig. 2.1 Undeformed chip cross section and the cutting edge

Lamellar chip formation is a continuous, periodic chip formation process similar to pure continuous chip formation. However, there are variations in the deformation process that cause more or less significant cleavages or even concentrated shear bands. The lamellae are produced due to thermal or elastomechanical processes with a high formation frequency within the kHz range. Lamellar chips occur with highly ductile workpiece materials with an increased strength, especially at high cutting speeds (q. v. high speed cutting).

Segmented chip formation is the discontinuous formation of a chip with still more or less connected elements, yet with significant variations in the degree of

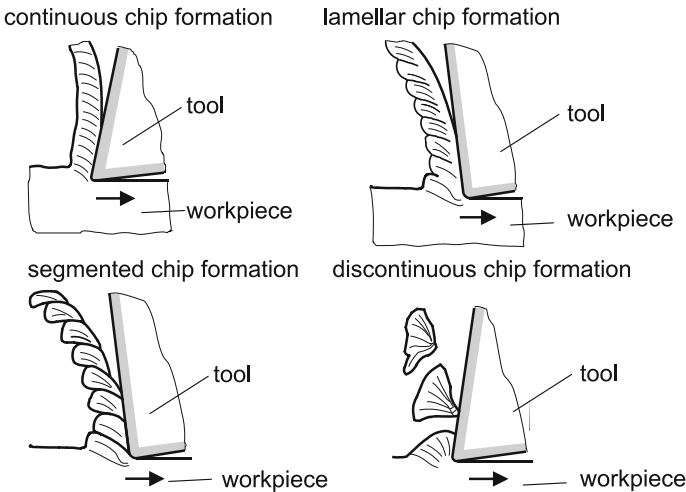


Fig. 2.2 Mechanisms of chip formation

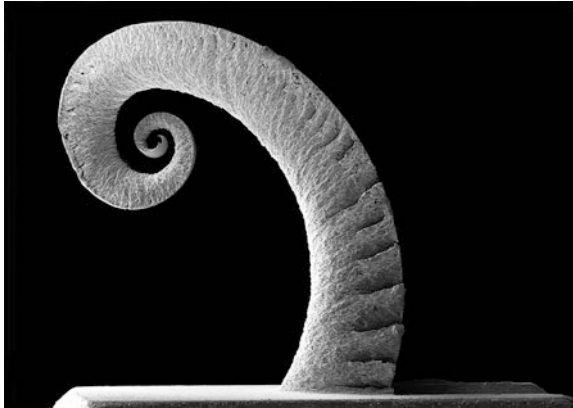


Fig. 2.3 Scanning electron micrographs of chip forms

deformation along the flow path. It primarily occurs with negative rake angles, lower cutting speeds and a higher chip thickness.

Discontinuous chip formation occurs if the plastic ductility of the workpiece material is very low or if predefined slide paths are formed due to high inhomogeneities (e. g. if cast iron with lamellar graphite is machined). Parts of the workpiece material are ripped out of the compound material without significant deformation. The workpiece surface is then rather produced by the ripping out process in the chip formation than by the tool traces.

With continuous chip formation, *built-up edges* can occur (Fig. 2.4). They are formed by particles of the workpiece material, which adhere to the rake face and to the cutting edge. These particles have been subject to high deformation and have

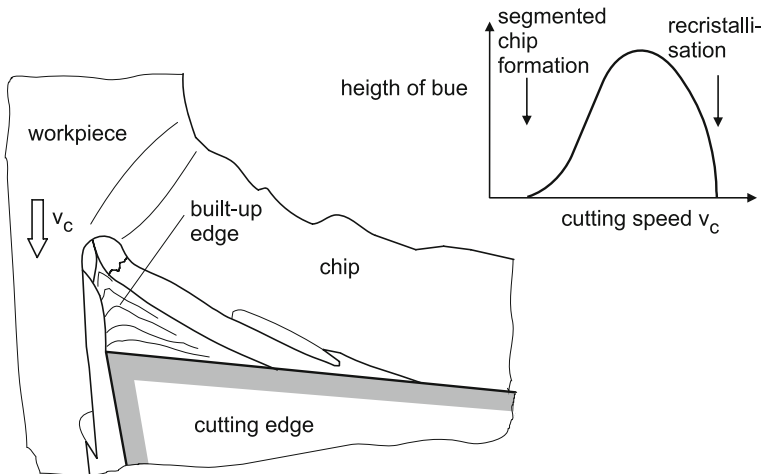


Fig. 2.4 Formation of built-up edges

been strain-hardened. They are much harder than the base workpiece material. Built-up edges only occur if

- the workpiece material promotes strain-hardening,
- the chip formation is stable and largely stationary,
- there is a stagnant zone in the material flow in front of the cutting edge,
- the temperatures in the chip formation zone are sufficiently low and do not allow for recrystallization.

Built-up edges influence the cutting edge geometry. They generally facilitate chip formation (lower forces). When they move off, they can drag along workpiece particles (adhesive wear). Sometimes strain-hardened parts of the built-up edges are integrated into the newly formed workpiece surface. Therefore, the formation of built-up edges is generally undesirable. However, it does not occur at higher cutting speeds and resulting higher temperatures in the chip formation zone, because there is no strain-hardening if the recrystallization temperature is exceeded during the deformation process.

The process for continuous chip formation can be described using a model of five *deformation zones* (Fig. 2.5). The main part of the plastic deformation takes place in the primary shear zone in the form of shear deformation. In the secondary shear zones in front of the rake face and the flank face, the workpiece material is additionally deformed under the influence of high friction forces. A stagnant zone (zone with high pressure from all sides) develops in front of the cutting edge. The actual separation of workpiece material also takes place in this zone. Furthermore,

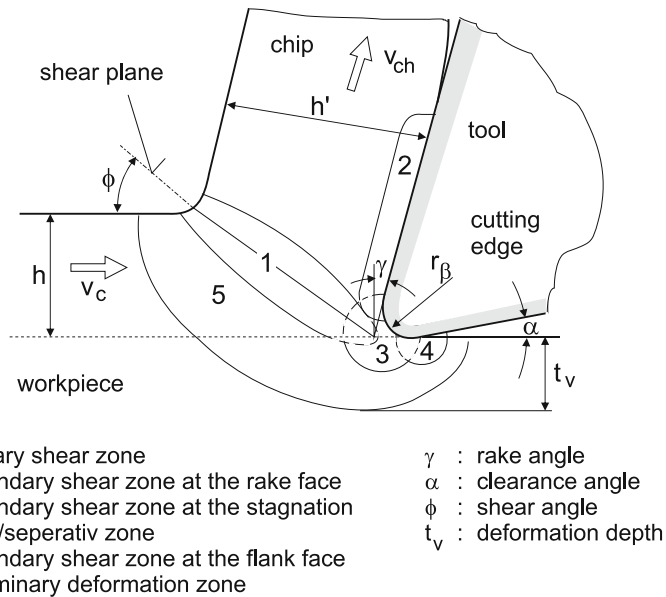


Fig. 2.5 Chip formation zones [WAR74]

minor plastic deformations occur in the preliminary deformation zone. This zone has an essential influence on the penetration depth of plastic deformations in the workpiece and so on the external workpiece zone.

2.2 Chip Root Analysis

Several methods have been developed to visualize the deformation process in front of the cutting edge and to analyze the chip formation process and the material behavior in the working zone. The most important methods are

- interrupted cut
- micro-cinematography
- the finite element method (FEM).

The analyses provide information on the mechanisms of chip formation, the plastic deformations in the chip formation zone and the position of the shear plane. They provide the basis for a calculation of the kinematic, mechanical and thermal conditions in the chip formation zone.

The basic principle of the interrupted cut is an abrupt separation of the tool from the workpiece. The current status in the deformation process is thus “frozen”, can be subject to metallographic preparation and analyzed under the microscope. Although the process is interrupted in an abrupt manner (quick-stop), the process has to be slowed down from the initial deformation speed until it actually comes to zero. Therefore, the cutting process is not frozen at the normal, stationary cutting speed, but at an unsteady phase while slowing down. In spite of this, the interrupted cut method is widely accepted. It should however be considered problematic for highly time-dependent processes, like thermally dominated processes or processes with fast, unsteady deformation.

The cutting speed at which the chip root is to be frozen determines the design of the devices used for the interrupted cut. Especially with high cutting speeds, the process has to be interrupted within a minimum time interval t_0 .

Figure 2.6 is a highly simplified illustration of the speed ratios for the interrupted cut method. We assume that the constant acceleration a is negative (deceleration), thus

$$v_{rel} = v_c - a_T \cdot t \quad (2.1)$$

With $v_{rel} = 0$ m/min after t_0 , the necessary braking distance Δx is

$$\Delta x = \frac{1}{2} v_c t_0 \quad (2.2)$$

These equations can be used to determine the necessary deceleration a for the maximum permitted braking distance:

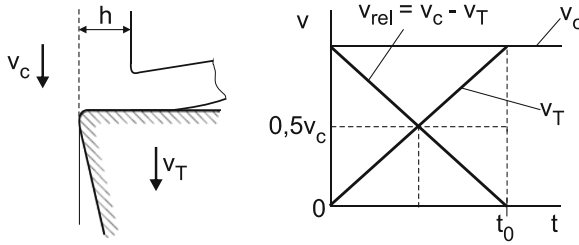


Fig. 2.6 Speed ratios for the interrupted cut method

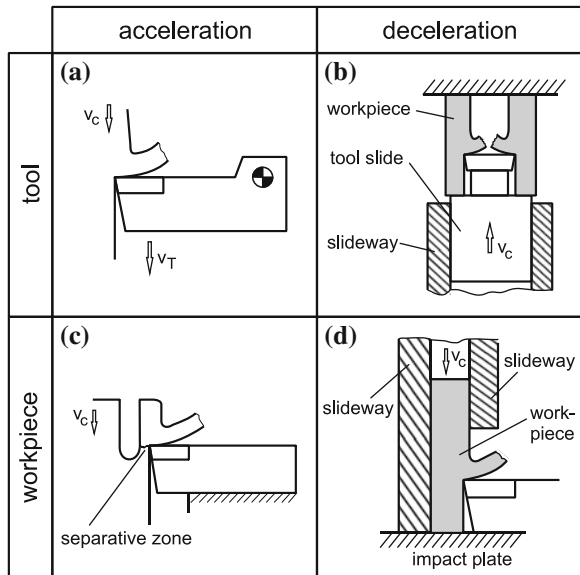
$$a_T = \frac{v_c^2}{2\Delta x} \tag{2.3}$$

This shows that the deceleration value has to be very high, even with low cutting speeds and a maximum permitted braking distance of up to 10 % of the undeformed chip thickness. Please note that the second order value of the cutting speed is used in Eq. 2.3. In order to keep the necessary deceleration forces within acceptable limits, especially with high cutting speeds, it is important to keep the decelerated masses at a minimum (Fig 2.6).

Different methods can be used to interrupt the cut (Abb. 2.7). Generally, either the tool or the workpiece can be accelerated or decelerated.

Part (a) of Fig. 2.7 illustrates the principle of interrupting the cut by accelerating the tool [KLO93]. Usually, the whole tool unit is accelerated via the tool holder. The necessary potential energy which has initially been stored is transferred into kinetic energy within a few milliseconds. The energy is stored using

Fig. 2.7 Methods used for the interrupted cut



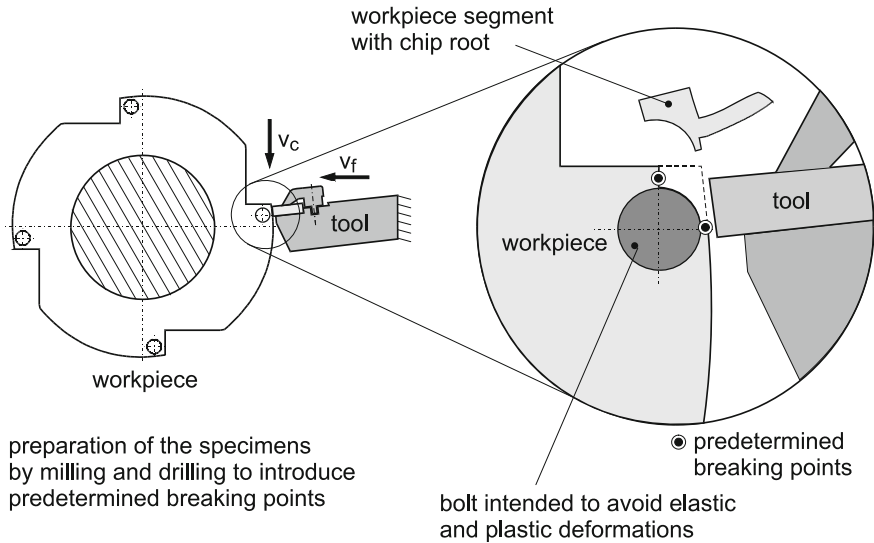


Fig. 2.8 Interrupted cut method according to Ben Amor

springs, compressed air or explosive materials. The tool can also be accelerated by means of mechanical cut-off devices [BAI88]. For this purpose, a mechanical barrier initially rotates with the tool and is then within one revolution, brought to a position where it accelerates the tool out of the workpiece.

In part (b), the tool (a double-sided cutting insert) is fixed on a low-mass slide. For example, the slide is accelerated using compressed air and hits the workpiece. A short length of material is cut (by planing), and the tool on the slide is decelerated by the workpiece, which works as an impact ring.

The method illustrated in part (c) relates to a set-up for high cutting speeds developed by Ben Amor [BEN03] based on an approach by Buda [BUD68]. This method can only be used for very low masses. Some details of this method are illustrated in Fig. 2.8. A predetermined breaking point is introduced into a bar, which is then cut by radial grooving. The remaining cross section at the predetermined breaking point is finally reduced to an extent where the break stress is exceeded and the segment breaks off from the workpiece. This segment including adhesive chips, is then accelerated away from the workpiece by means of the cutting force and is used as a chip root for the analysis of the chip formation process. The following exemplary values demonstrate that this method is very effective. The given parameters are as follows:

$$h \cdot b = 0.2 \cdot 3 \text{ mm}^2, v_c = 300 \text{ m/min}, \text{ C45 steel}, F_c = 1800 \text{ N}, m = 3 \text{ g}.$$

We assume that the initial accelerating force is applied throughout the whole separation process and that accordingly, the acceleration is constant. As a result,

$$a_T = F_c/m \quad (2.4)$$

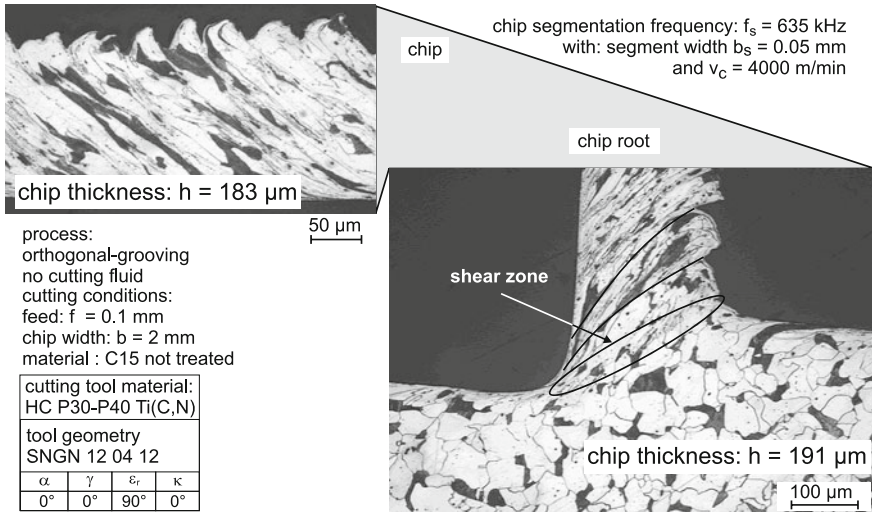


Fig. 2.9 C15 steel chip root obtained at a high cutting speed [TÖN05]

According to Eq. 2.3, the corresponding acceleration distance is 21 μm .

Figure 2.9 shows a chip root obtained by this method at a high cutting speed. Although the accelerating distance is higher than 10 % of the undeformed chip thickness, the image is well-suited for analyzing the deformation mechanisms in front of the cutting edge.

Part (d) of Fig. 2.7 illustrates the method of accelerating a low-mass workpiece in a slideway by means of compressed air and then, after a short length of material has been cut, rapidly decelerating it by making it hit an impact plate. The chip roots in Fig. 2.10 have been obtained using a similar method with an initial cutting speed of $2,400$ m/min and a braking distance of less than 20 μm [HOW05].

In contrast to the interrupted cut method, micro-cinematography allows for examining the chip formation while the process is still running [WAR74]. For this purpose, a polished and etched specimen (black-and-white structure) is pressed against a fused quartz glass plate (Fig. 2.11) and cut by orthogonal turning. The process can be observed through the fused quartz glass plate and magnified using a microscope. However, the image of the process is only an approximation because of the free surface of the workpiece. Images without motion blur can only be taken at cutting speeds of up to 1 m/min.

2.3 Shear Plane Model

Several theories for the calculation of parameters in cutting and abrasive processes make use of a shear plane model, assuming that all plastic deformations take place within the shear plane. Depending on the deformation behavior of the workpiece

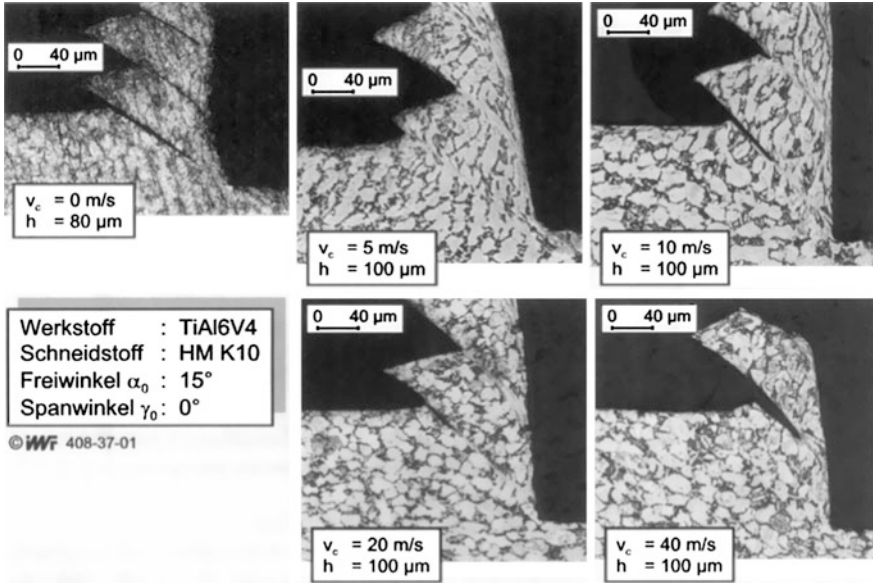


Fig. 2.10 TiAl6V4 chip roots [HOW05]

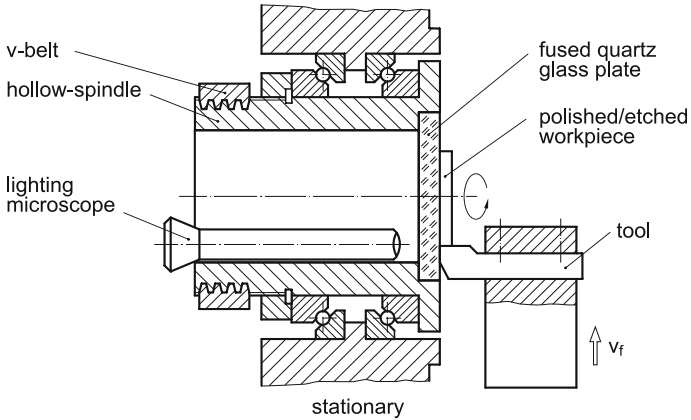


Fig. 2.11 Test stand for micro-machining processes [WAR74]

material and on the process conditions, this model can be adequately true to reality. If we assume that the shear plane model (Fig. 2.12) is applicable and that the deformation is two-dimensional (orthogonal cut), the shear velocity v_ϕ can be calculated as

$$v_\phi = v_c \frac{\sin(90^\circ - \gamma)}{\sin(90^\circ + \gamma - \phi)} = v_c \frac{\cos \gamma}{\cos(\phi - \gamma)} \tag{2.5}$$

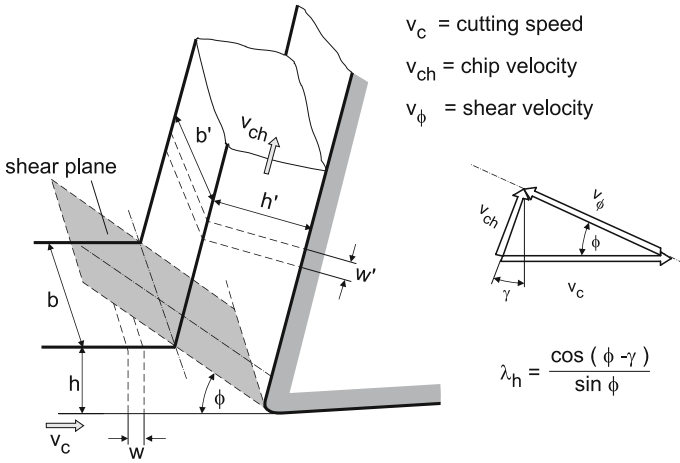


Fig. 2.12 Shear plane model and shear velocity

As major plastic deformations take place, the volume can be regarded as constant, thus¹

$$\frac{b'}{b} \cdot \frac{h'}{h} \cdot \frac{w'}{w} = 1 \text{ oder } \lambda_b \cdot \lambda_h \cdot \lambda_w = 1, \tag{2.6}$$

for the compressions λ . As we assume that the deformation is two-dimensional, the compression of the chip width (chip width ratio) is $\lambda_b = 1$; thus,

$$\lambda_h \cdot \lambda_w = 1. \tag{2.7}$$

Furthermore,

$$\lambda_w = \frac{w'}{w} = \frac{v_{ch}}{v_c} \tag{2.8}$$

And consequently,

$$\lambda_h = \frac{v_c}{v_{ch}} = \frac{1}{\lambda_w}. \tag{2.9}$$

From the velocity triangle (Fig. 2.12) follows

$$\lambda_h = \frac{\cos(\phi - \gamma)}{\sin \phi} \tag{2.10}$$

¹ In contrast to elastic deformations, the workpiece volume in the case of major plastic deformations is constant. In the elastic mode, the volume change can be determined by means of the dimensional changes in the transverse and axial direction (Poisson's ratio ν): $\Delta V/V = (1-2\nu)\epsilon$. But this only applies to elastic deformations!

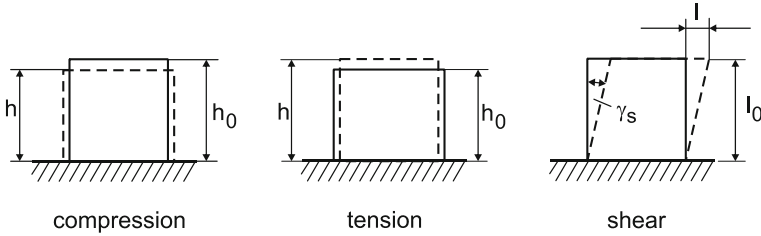


Fig. 2.13 Deformations

The compression of the chip thickness λ_h (chip thickness ratio) can be determined by measuring the chip thickness or the chip length (with an interrupted cut) and by means of the manipulated variables, so that the shear angle ϕ can be determined experimentally.

In plastomechanics (the mechanics of plastic deformations), deformations are treated as relative parameters. Figure 2.13 shows the mechanisms of compression, tension and shearing.

In literature, two different notations are used for the numerical description of plastic deformations of the overall shape. The notation used in English-speaking countries and in material science in general is based on the relative dimensional change or strain ε , with ε_C for compression and ε_T for tension.

$$\varepsilon_C = \frac{h_0 - h}{h_0} = 1 - \frac{h}{h_0} \quad (2.11)$$

and

$$\varepsilon_T = \frac{h - h_0}{h_0} = \frac{h}{h_0} - 1 \quad (2.12)$$

In the field of forming technology and in German-speaking countries, the logarithmic deformation φ is used²:

$$\varphi = \ln \frac{h}{h_0} \quad (2.13)$$

Please note that B.A. Behrens gives good reasons for using the notation of logarithmic deformation [DOB07, p. 56 et seq.]. It is easy to transform one notation into the other:

$$\varphi = \ln(1 - \varepsilon_C) \quad (2.14)$$

and

² The logarithmic deformation does not take into account elastic deformations, but only plastic ones. However, this can be neglected if major plastic deformations take place.

$$\varphi = \ln(\varepsilon_T - 1) \quad (2.15)$$

For small deformations below $\varphi = 0.1$, the calculated values are practically identical.

The notations for the deformation rate (compression and tension) are:

$$\varepsilon_C = 1 - e^\varphi \quad (2.14a)$$

and

$$\varepsilon_T = e^\varphi - 1 \quad (2.15a)$$

$$\dot{\varepsilon}_C = \frac{d}{d\varphi}(1 - e^\varphi) \cdot \frac{d\varphi}{dt} \quad (2.16)$$

and

$$\dot{\varepsilon}_T = \frac{d}{d\varphi}(e^\varphi - 1) \frac{d\varphi}{dt} \quad (2.17)$$

$$\dot{\varphi} = \frac{1}{1 - \varepsilon_C} \dot{\varepsilon}_C \quad (2.16a)$$

and

$$\dot{\varphi} = \frac{1}{\varepsilon_T - 1} \dot{\varepsilon}_T \quad (2.17a)$$

In plastomechanical calculations for cutting and abrasive processes, the focus is on the extent of the deformations within the workpiece material. If the following assumptions are valid, the shear γ_S can be calculated as the tangent of the deformation angle χ^3 (Fig. 2.14):

- shear plane model
- constant volume
- homogeneous workpiece material
- isotropic workpiece material
- two-dimensional deformation.

The deformation angle χ is measured at the normal to the shear plane. Thus

$$\tan \chi = \tan(\phi - \gamma) + \frac{1}{\tan \phi} \quad (2.18)$$

The volume segment in Fig. 2.14 is parallel to the shear plane, so that the shear deformation $\tan \chi$ is directly visible. To relate the deformation process to a reference deformation, we have to determine the relative deformations, the maximum

³ The term “shear angle” would be more suitable, but it is used for the angle ϕ between the cutting direction and the shear plane.

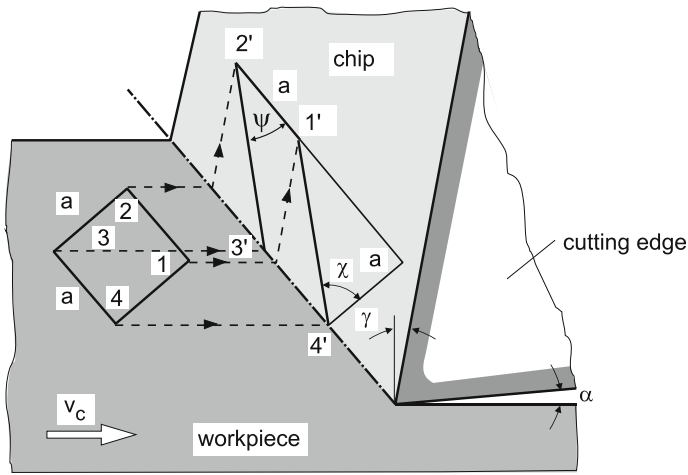
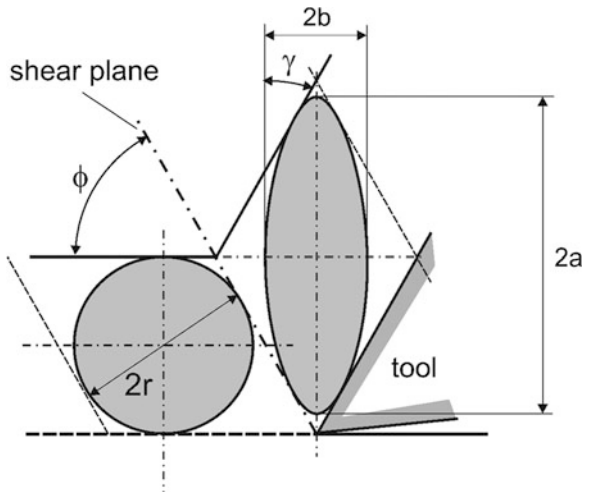


Fig. 2.14 Geometry of the deformations in an orthogonal cutting process

Fig. 2.15 Changes in the overall shape in cutting processes

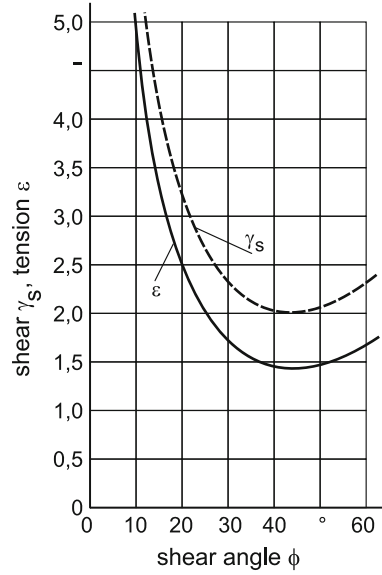


tension ε_T and the maximum compression ε_C of the workpiece material after it has passed through the shear plane. For this purpose, we use an unsigned volume element, i. e. a circular element, which is deformed into an ellipse behind the shear plane (Fig. 2.15).

The ratios of the long axis ($2a$) and the short axis ($2b$) to the diameter ($2r$) of the circular element correspond to the maximum tension and compression respectively. Thus, the tension and compression are

$$\varepsilon_T = \frac{2a}{d} - 1 \tag{2.19}$$

Fig. 2.16 Deformations and shear angles [KÖH68]



and

$$\epsilon_C = 1 - \frac{2b}{d} \quad (2.20)$$

$$\epsilon_T = \frac{1}{2} \left[\tan(\phi - \gamma) + \frac{1}{\tan \phi} \right] - 1 + \sqrt{\left[\tan(\phi - \gamma) + \frac{1}{\tan \phi} \right]^2 + 1} \quad (2.19a)$$

$$\epsilon_C = \frac{1}{2} \left[\tan(\phi - \gamma) + \frac{1}{\tan \phi} \right] + 1 + \sqrt{\left[\tan(\phi - \gamma) + \frac{1}{\tan \phi} \right]^2 + 1} \quad (2.20b)$$

We can conclude that

$$\epsilon_T + \epsilon_C = \tan \chi = \gamma_s \quad (2.21)$$

Figure 2.16 shows the progression of the tension ϵ_T and the shear γ_s across the shear angle ϕ for a rake angle of $\gamma = 0^\circ$. The shear angle, the tension and the shear decrease with higher rake angles.

The calculations of deformations and their conversion are only based on geometrical relations. Forming technology usually uses comparative hypotheses to convert multiaxial deformations and strains into uniaxial reference values [DOB07, S.153 f]. Tresca uses the shear stress hypothesis for his calculation, while von Mises uses the strain energy hypothesis. We can also deduce the reference deformations using an energy approach.

The shear γ_s in Eq. 2.21 can be converted into the uniaxial reference deformation ϕ . We obtain

$$\varphi = \frac{1}{2}\gamma_s \quad \text{according to Tresca} \quad (2.22)$$

$$\varphi = \frac{1}{\sqrt{3}}\gamma_s \quad \text{according to v. Mises} \quad (2.23)$$

2.4 Questions

1. What is “two-dimensional deformation” and what is “plane strain”?
2. Which processes can be used for orthogonal cutting?
3. How can we describe uniaxial deformations? Please give both notations.
4. How can the strain velocity be derived?
5. Which parameters must be known to determine the angle with which a segment in the shear plane is deformed by shear if the shear plane model is applicable?
6. How can these parameters be measured?
7. Which methods can be used to examine the chip root? These methods only provide an approximated image of the deformation process. Which restrictions apply?
8. Which are the different zones of deformation in chip formation processes?
9. Define the different types of chip formation. How are they distinct from the chip forms?
10. What is a lamellar chip? How can we determine the corresponding degree of uniformity?
11. Under which conditions might a shear cleavage be produced?
12. What are built-up edges?
13. Why do built-up edges only occur with continuous chips?
14. Which effect does a built-up edge have on the workpiece quality and on the tool?
15. Determine the shear velocity by means of the shear plane model.
16. Using Poisson’s ratio (which is usually applied for metallic materials), explain why the volume is not constant with elastic (non-plastic) deformations.
17. How can the shear angle be determined by means of the chip compression ratio?
18. How can the deformation angle χ be calculated?

References

- [BAI88] Baik, M.C.: Beitrag zur Zerspanbarkeit von Kobaltlegierungen [Contribution to the machinability of cobalt alloys]. Dr.-Ing. Diss., University of Dortmund, Dortmund (1988)
- [BEN03] Ben Amor, R.: Thermomechanische Wirkmechanismen und Spanbildung bei der Hochgeschwindigkeitszerspannung [Thermomechanical effect mechanisms and chip formation at high speed cutting]. Dr.-Ing. Diss., University of Hannover, Hannover (2003)

- [BUD68] Buda, J., Vasilko, K., Stranova, J.: Neue Methoden der Spanwurzelgewinnung zur Untersuchung des Schneidvorganges [New methods to gain chip roots for the investigation of the cutting process]. *Industrie Anzeiger* **90**(5), 78-81 (1968)
- [DOB07] Doege, E., Behrens, B.-A.: *Handbuch der Umformtechnik* [Handbook of forming technology]. Springer, Berlin (2007)
- [HOW05] Hoffmeister, H.-W., Wessels, T.: Thermomechanische Wirkmechanismen bei der Hochgeschwindigkeitszerspannung von Titan- und Nickelbasislegierungen [Thermo-mechanical effect mechanisms in high speed cutting of titanium- and nickel based alloys]. In [TÖN05], pp. 470–491
- [KLO93] Klose, H.-J.: Einfluss der Werkstofftechnologie auf die Zerspanbarkeit niedriglegierter Gusseisen [Influence of the material technology on the machinability of low alloyed cast iron]. Dr.-Ing. Diss., University of Hannover, Hannover (1993)
- [KÖH68] Koehler, G.: Modelltheoretische Betrachtungen und Untersuchungen mit Hilfe der Spanwurzel-Mikrografie als Beitrag zur Beschreibung der spanenden Bearbeitung metallischer Werkstoffe [Model based theoretical considerations and investigations with the chip root micrography as a contribution to the characterization of cutting of metals]. Dr.-Ing. Diss., TU Berlin (1968)
- [TÖN05] Tönshoff, H. K., Hollmann, F.: *Hochgeschwindigkeitsspanen* [High speed cutting]. Wiley-VCH, Weinheim (2005)
- [WAR74] Warnecke, G.: *Spanbildung bei metallischen Werkstoffen* [Chip formation at metallic materials]. Resch, Munich (1974)

Chapter 3

Chip Control

The chip form is one of the four criteria which determine the machinability (see [Sect. 1.4](#)). An undisturbed chip flow is especially important in automated processes in order to spare the human operator the tedious and often dangerous task of monitoring the chip flow (which would tie him to the machine tool and the process; man-environment criterion). The problem of chip control does not apply to processes in which an interrupted cut is inherent to the functional principle (milling, circular sawing, grinding). In continuous processes like turning and drilling, the chip control can be dominant compared to the other machinability criteria, because it has an essential influence on the process safety. The chip form is the final shape of the chip after the machining process. It is the result of the chip formation and the chip flow from the material separation zone. To quantify the chip control, a chip form classification and the chip volume ratio have been introduced [[STA90](#), [CIR04](#)].









3.1 Chip Volume Ratio and Chip form Classification

Depending on the chip form, the bulk chip volume can be much higher than the volume of the initial workpiece material. The ratio between the two volumes or volumetric flow rates is the chip volume ratio RZ

$$RZ = \frac{Q_{ch}}{Q_w} \quad (3.1)$$

It indicates the bulkiness of the chips and is used for the dimensioning of the machine tool working area, of the open space in the tool to accommodate chips (flutes in milling and drilling) and of the transport devices for the chips. Depending on the chip form, the values of the chip volume ratio can vary significantly ([Fig. 3.1](#)).

The maximum feasible and most economical cutting speed (see [Sect. 7.1](#)) and the maximum feasible material removal rate have been increased considerably thanks to enhanced cutting tool materials. On average, an increase by the factor 2

	chip volume ratio RZ	chip form classification	rating
ribbon chips 	≥ 90	1	<div style="display: flex; flex-direction: column; align-items: center; justify-content: center;"> <div style="border: 1px solid black; padding: 2px;">disadvantageous</div> <div style="border: 1px solid black; padding: 2px; margin: 2px;">favorable</div> <div style="border: 1px solid black; padding: 2px;">useable</div> </div>
snarled chips 	≥ 90	2	
flat helical chips 	≥ 50	3	
long, cylindrical helical chips 	≥ 50	4	
helical chip segments 	≥ 25	5	
spiral chips 	≥ 8	6	
spiral chip segments 	≥ 8	7	
discontinuous chips 	≥ 3	8	

source : Stahl-Eisen-Prüfblatt 1178-69 34/09700c © IFW

Fig. 3.1 Chip forms (steel test specification 1178–90) [CIR04]

has been achieved each decade. The chip volume ratio tends to decrease with increasing cutting speeds. For example, the material removal rate in turning processes has been increased to such an extent that the chip control can become a major limiting factor in the process. This is supported by the trend towards stronger and tougher workpiece materials.

Eight chip form classes have been introduced to characterize the different chip forms (Fig. 3.1) [STA90]. Each of them relates to different chip volume ratios. Long chips, like ribbon chips, snarled chips and flat helical chips, are disadvantageous and can endanger persons, tools, workpieces and the machine tool. Short chips, like discontinuous chips and spiral chip segments, can cause problems in the transport from the material separation zone (e.g., in drilling) or if the operator is not adequately protected (eye injuries). Spiral chips and helical chip segments are most favorable.

To obtain favorable chip forms, the chip has to be broken down to segments. This can be done by primary chip control or by secondary chip control.

Primary chip control is obtained by discontinuous chip formation. Workpiece materials which tend towards primary chip control are lamellar graphite cast iron, brass with a low copper content and eutectic or hypereutectic aluminum-silicon alloys, i.e., brittle materials with low plastic ductility which already break during the chip formation process. They are called short-chipping materials. With segmented or continuous chip formation, *secondary chip control* has to be enforced after the actual chip formation process. The corresponding materials are called long-chipping materials.

3.2 Chip Guidance

With long-chipping materials, i.e., with continuous or segmented chip formation and with an adequately high feed, favorable chip forms can be obtained by chip guidance. The chip is removed from the chip formation zone in its natural direction

of flow. There are two main flow directions, parallel or normal to the rake face; the flow direction of the chip is determined by the plastomechanical processes at the cutting edge and can lie between the two main directions (Fig. 3.2). To illustrate this, Okushima and Minato have developed a simple model which divides the cross-section of the undeformed chip into a series of increments and adds up the incremental flow vectors to form a resultant using a link polygon method [OKU59] (Fig. 3.3). For this purpose, each increment is weighted according to its surface area. This is a purely graphical method which can only provide an approximation of the plastomechanical processes. Methods that provide a more realistic image of the processes are based on FEM calculations [MÜL93]. A further disadvantage of the Okushima/Minato method is that the link polygon method does not account for chip guidance by the inclination of the rake face (by the rake angle γ and the wedge angle β). Due to developments in powder metallurgy, especially the rake face shape on indexable inserts is used to influence the chip flow direction. By means of an appropriate rake face shape, the moving chip can be guided towards the cut workpiece surface, the uncut workpiece surface or the tool flank face (Fig. 3.4). The consecutive flow of material bends open the chip which has been stopped by the obstacle. This subjects the chip to additional plastic deformation. The upper surface of the chip, which has mostly already been notched and jagged in the chip formation process, is tensioned and thus breaks when the chip is bent open.

Chips can be guided either by ground-in or sintered-in chip breakers or by attached breakers which have been integrated into the clamping system of the indexable insert (Fig. 3.5). Many shapes of sintered-in chip breakers have been developed. Their geometry has to be adapted to the setting conditions, especially to the feed, the cutting speed and the depth of cut (Fig. 3.6).

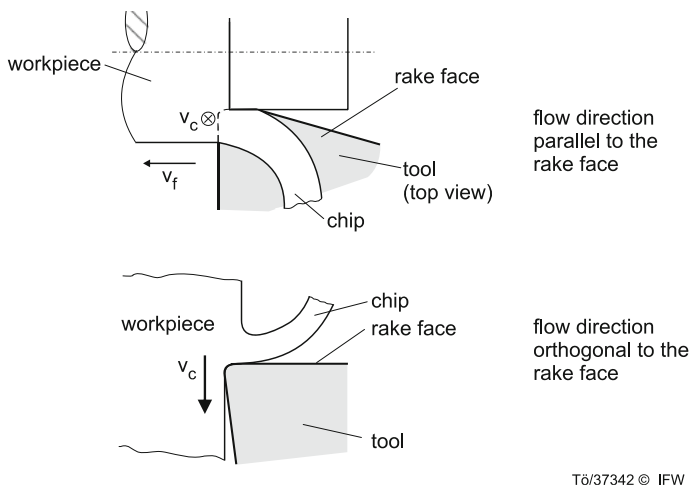


Fig. 3.2 Chip flow direction

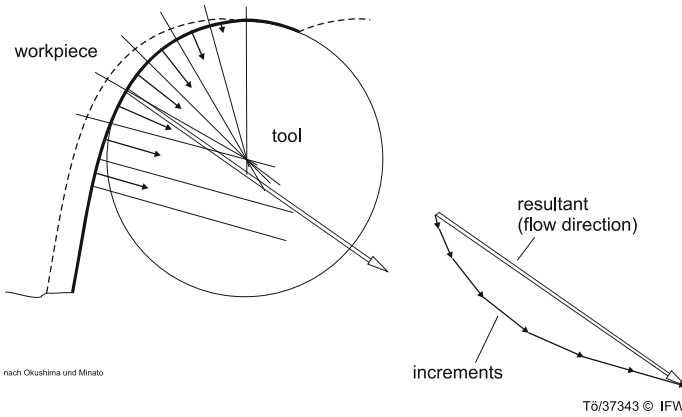


Fig. 3.3 Link polygon method for the determination of the flow direction

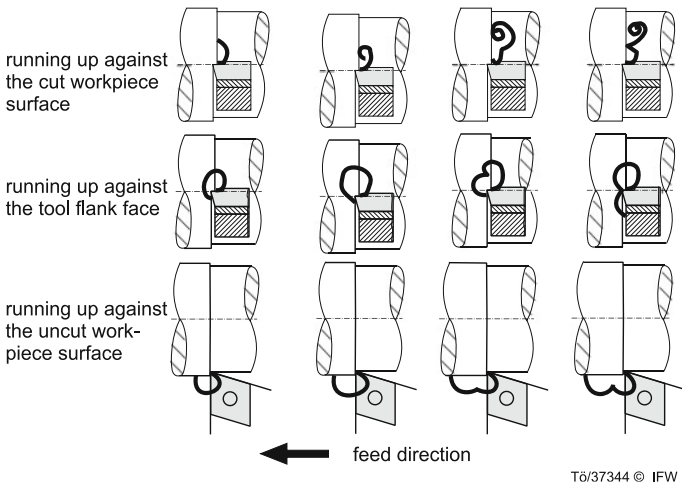


Fig. 3.4 Working principle of chip breakers

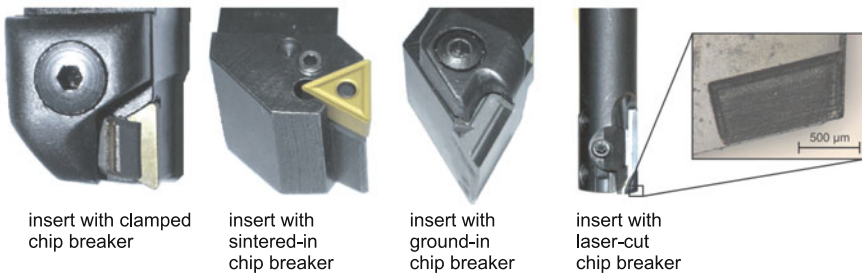


Fig. 3.5 Different types of chip breakers [HIN09]

Fig. 3.6 Zone of favorable chip forms achieved by tools with chip breakers (acc. Sandvik)

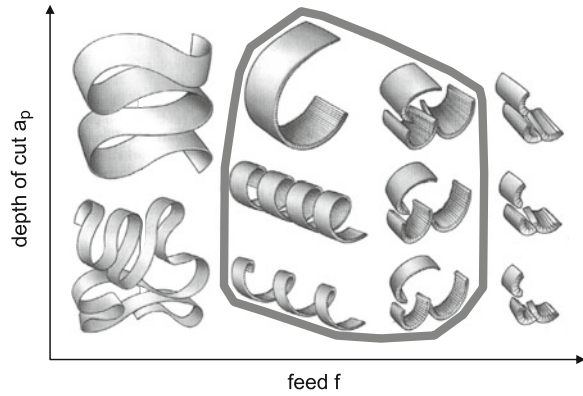
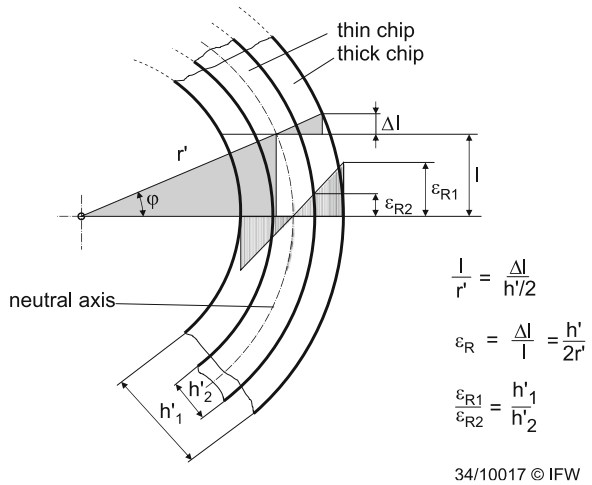


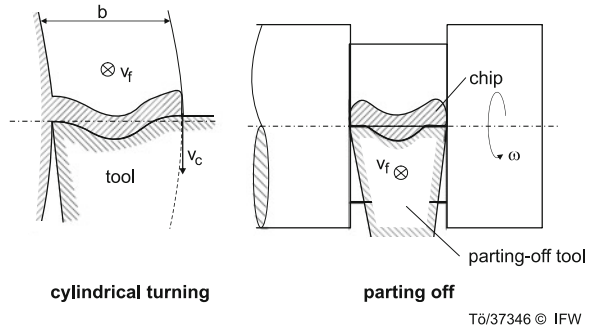
Fig. 3.7 Deformation of the chip edge



At low feeds, chip control by means of chip guidance is hardly feasible, because the plastic tension which can be achieved by bending the chip open is not high enough to break it. Figure 3.7 shows that the tension of the chip edge ϵ_R of a bent chip with a given bend radius r' is proportional to the chip thickness h' . Thus with thinner chips there are only minor plastic tensions, which the workpiece material can resist without breaking.

An effect similar to that of an increased chip thickness can be obtained by a curvature of the chip cross section along the cutting edge (Fig. 3.8). This increases the strain of the chip edge partially and the chip becomes stiffer, which increases its tendency to break. Parting-off tools and grooving tools also have bent rake faces to avoid the chips from being trapped in the groove between the cut faces.

Fig. 3.8 Curved rake face



T6/37346 © IFW

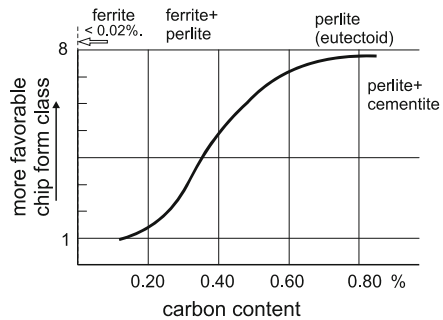
3.3 Influence of the Workpiece Material

In the chip formation process the workpiece material is subject to high plastic deformations. The deformability mainly depends on the composition of the workpiece material. Therefore, the chip control mode (primary or secondary) also mainly depends on the workpiece material. In general, we distinguish between short-chipping and long-chipping materials. Lamellar graphite cast iron (gray cast iron), brittle brass and cast aluminum alloys are examples of short-chipping materials, which tend towards discontinuous chip formation. Steels, coppers and wrought aluminum alloys are long-chipping materials.

With steels, the deformability can be influenced by means of alloying elements to achieve more favorable chip forms. However, these elements mostly have a negative effect on the toughness of the steel.

Carbon is the most important accompanying element to iron (Fig. 3.9). Carbon steels contain ferrite (α -solid solution) and perlite, which is a eutectoid consisting

Fig. 3.9 Chip forms and material structures



structural constituents	HV	
ferrite (α -solid solution)	90	<div style="display: flex; align-items: center; justify-content: center;"> <div style="writing-mode: vertical-rl; transform: rotate(180deg);">hardness ↓</div> <div style="writing-mode: vertical-rl; transform: rotate(180deg);">deformability ↑</div> </div>
perlite (ferrite + cementite)	200	
martensite	800	
cementite	>1000	

T6/37347

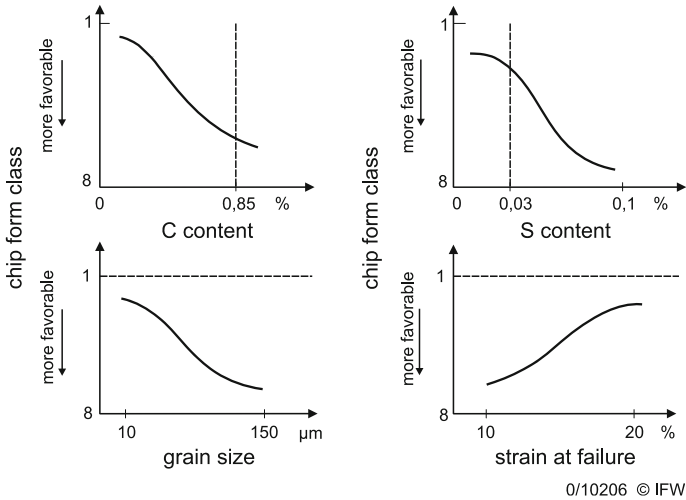






Fig. 3.10 Influence of the workpiece material on the chip form (for carbon steel)

of cementite (iron carbide Fe_3C) and ferrite. Ferrite is a soft material with good deformability, while cementite (orthorhombic crystalline) is hard, brittle and barely deformable. With an increase in the carbon content from $>0.2\%$ C up to the eutectoid composition (perlite) of 0.8% C, the deformability of the steel decreases. Case-hardened steels ($<0.2\%$ C) like C15, 16MnCr5 and 18CrNi8 tend towards forming ribbon chips and snarled chips. Steels with a higher perlite content produce more favorable chip forms (Fig. 3.10).

Sulfur is hardly soluble in iron. Depending on the other alloying elements, sulfides can be produced. Iron sulfide forms an eutectic (FeS). Within the temperature range of $800\text{--}1,000\text{ }^\circ\text{C}$, this makes the material red short. Oxygen decreases the temperatures of the sulfide eutectic and thus increases its tendency towards red shortness. With manganese, which has a higher chemical affinity to sulfur than iron, manganese sulfide is formed (MnS). Its melting point is higher than that of FeS . This eliminates the risk of red shortness. Subsequent to the rolling process, manganese sulfides are elongated and arranged in rows. They form discontinuities within the steel structure and so improve the chip form. However, this also decreases the transverse toughness of the steel. Free cutting steels are alloyed with high sulfur contents (9S20 or 45S20) of about 0.2% S. Besides providing other positive effects on the machinability (wear, forces), this consistently leads to favorable chip forms. Steels with especially low sulfur contents can be produced by newly developed steelmaking processes (blowing processes). They lead to unfavorable chip forms (Fig. 3.11).

Phosphor leads to significant phase separation (segregation) within the steel which can hardly be eliminated by heat treatments. Phosphor increases the tendency towards brittle fracture at room temperature as well as the temper brittleness. Therefore, it is considered as a steel parasite. Depending on the steel grade,

workpiece material : C 45 (\pm S) BY
 sulfur content : -S $\hat{=}$ 0.002 %, +S $\hat{=}$ 0.030 %
 cutting tool material : TiC / TiN coated tungsten carbide
 chip form geometry : A, F
 cutting speed : $v_c = 160 \text{ m} \cdot \text{min}^{-1}$
 feed : $f = 0.1 \text{ mm}, 0.25 \text{ mm}$
 depth of cut : $a_p = 2.5 \text{ mm}$
 cutting edge geometry : $\kappa = 75^\circ / \beta = 90^\circ / \alpha = 6^\circ / r_\xi = 0.8 \text{ mm}$

	- S : 0.002 %	+ S : 0.03 %
	chip form / chip form class	
roughing feed $f = 0.25 \text{ mm}$ chip form geometry A	 3,4	 8
finishing feed $f = 0.1 \text{ mm}$ chip form geometry F	 3,4	 5

34/09702 © IFW

Fig. 3.11 Influence of the sulfur content on the chip form

the content is limited down to 0.05 % P or less. However, due to ferrite embrittlement, phosphor leads to favorable chip forms.

Lead is practically insoluble in iron. The critical points of iron (in the iron-carbon system) are not affected by lead. Lead submicroscopically attaches itself to the grain boundaries, leading to short-brittle chips.

A *heat treatment* of the steel influences the deformability via the material structure and thus also has a significant effect on the chip formation and chip control [WIN82, PAT87]. In general, the chip form becomes more favorable with an increasingly inhomogeneous and coarse-grained workpiece material. With heat-treated steels (e.g., C45, 42CrMo4, 36CrNiMo4), controlled cooling from the forging temperature (Fig. 3.12) has a positive effect.¹ This treatment saves further heat treatments (heating for hardening and tempering, truing), in consequence reducing the costs for the rough part production by forging. It leads to a coarse-grained structure with perlite grains surrounded by a closed ferrite network structure. The chip forms are more favorable than those produced with a tempered or normalized structure. Other heat treatments influence specific physical properties and are not primarily used to enhance the chip control.

Soft annealing (A) of steels with an increased C content or of alloyed steels is used to decrease the high hardness in order to increase the machinability (forces, wear). The chip forms become less favorable due to an increase in the ferrite content.

Normalizing (N) of steels with C contents below 0.9 % leads to a crystalline transformation of the structure (normalizing temperature slightly above the GOS

¹ This procedure leads to a forged perlite structure. It is used for precipitation hardened perlite-ferritic steels (AFP steels).

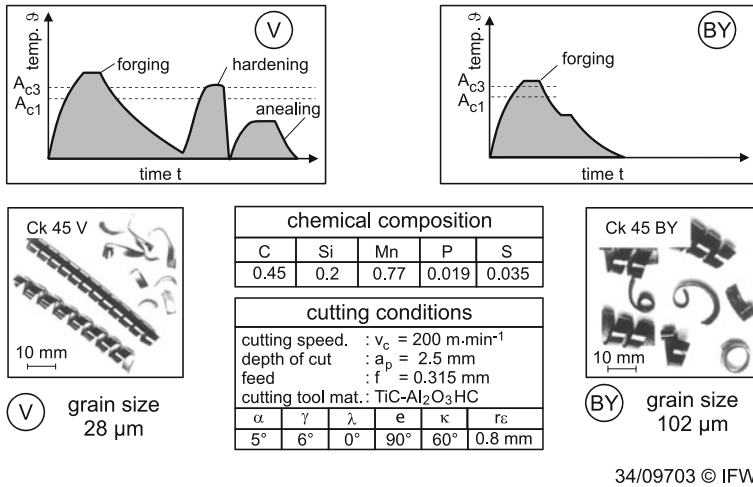


Fig. 3.12 Influence of heat treatment processes on the chip form

line of the iron carbon diagram), leading to finer, more evenly distributed grains. The process has hardly any influence on the chip control. If anything, the influence is negative.

Quenching (Q) increases the strength of steels by forming martensite in a hardening process. Subsequent tempering significantly decreases the hardness of the steel, but also makes it tougher. Quenched and tempered steels (high toughness) lead to generally favorable chip forms. With an increase in the tempering temperature, the strength decreases and the deformability rises. Correspondingly, the chip forms become less favorable.

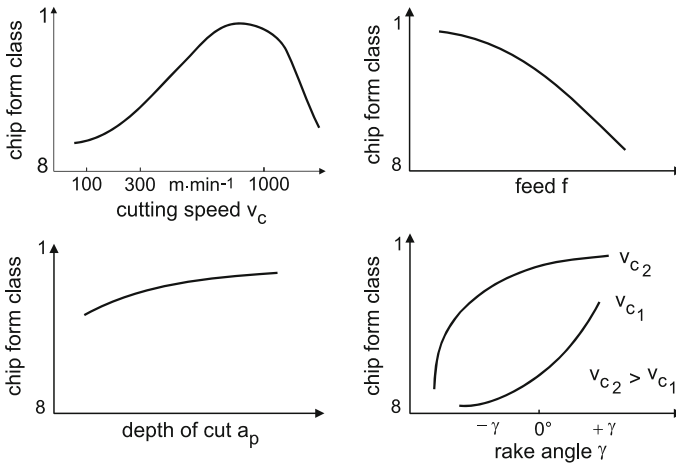
3.4 Influence of the Cutting Conditions

The cutting conditions influence the chip form through the chip formation (cutting speed and rake angle) and through secondary effects (secondary chip control: feed and depth of cut).

The *feed* influences the chip compression ratio, i.e., the chip thickness, and thus the chip deformability (see Sect. 3.2). Therefore, the chip forms highly depend on the feed (Fig. 3.13). With adequately designed chip breakers, favorable chip forms can be obtained at high feeds (roughing), but not at low feeds.

The *depth of cut* only has a minor influence on the chip form. With high depths of cut, the chip is less inclined to break when running up against an obstacle.

The *cutting speed* has an essential influence on the temperatures in the chip formation zone due to heat conduction and convection (see Chap. 5). Higher cutting speeds lead to higher chip formation temperatures. Most steels are more



nach Degner et al.

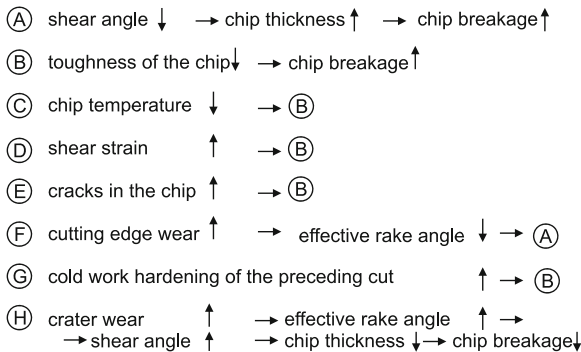
34/09701 © IFW

Fig. 3.13 Influence of the cutting conditions on the chip form [DEG93]

deformable at higher temperatures, so that they are less damaged in the chip formation process. Up to about $v_c = 400$ m/min, higher cutting speeds lead to less favorable chip forms. With heat-treated steels, the chip formation above this speed range is irregular, changing between periods of higher and lower plastic deformation. This can lead to significant lamellae as well as a fine segmentation of the chip (adiabatic shear).

The *rake angle* influences the shear in the chip formation process. Negative rake angles lead to high deformations, which cause prior damage to the chip and thus increase its tendency towards secondary breaking.

A comprehensive influence analysis (Fig. 3.14) has been conducted by Nakayama [NAK92]. He links the chip formation process with the chip control via



source : K. Nakayama

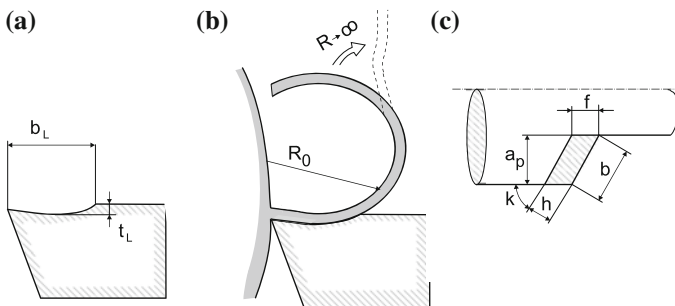
0/10019 © IFW

Fig. 3.14 Parameters influencing the chip form [NAK92]

the shear angle (A), the shear strain (D) and the cold work hardening (G). The influence of the workpiece material is represented by the toughness (B), the chip temperature (C) and the cracks in the chip (E). The shape of the cutting edge (F, H) and the influence of the tool wear are also included.

3.5 Questions

1. Define the terms “material removal rate” and “chip volume ratio”. How are the two terms connected?
2. Why is the chip volume ratio an important parameter?
3. Name and describe the most important chip forms. How favorable are they?
4. Which methods of influencing the chip form do you know? Explain their advantages and disadvantages.
5. Explain the functioning principle of chip breakers.
6. What effect do the most important accompanying elements to iron have on the chip control for steel workpieces?
7. Why is a high chip thickness linked with favorable chip forms?
8. What is the effect of crater wear respectively cutting edge wear on the chip form?
9. In practice, a common chip control method for turning processes is the use of chip breakers which guide the chip towards an obstacle in its flow direction and make it break due to the additional stress. In a turning process with the workpiece material C45, do sintered-in chip breakers (Fig. 3.15a) ensure the breaking of the chip if we assume that the chip is bent from an initial bending radius R to $R = \infty$ (Fig. 3.15b)? The tool cutting edge angle is $\kappa = 90^\circ$, the feed $f = 0.1$ mm, the rake angle $\gamma = 10^\circ$ and the shear angle $\phi = 35^\circ$ (Fig. 3.15c). The dimensions of the chip breaker are $b_L = 1.0$ mm,



34/09764c © IFW

Fig. 3.15 Use of chip breakers **a** sintered in chip breaker, **b** assumption: the chip is bent from a bending radius R to $R \rightarrow \infty$, and **c** undeformed chip parameters in turning

$t_L = 0.3$ mm. The tension at failure of C45, measured at the notched upper chip surface, is $\varepsilon_b = 7.1$ %.

10. How can the chip form be improved if the same tool is used?

References

- [CIR04] CIRP.: Dictionary of Production Engineering, vol. 2. Springer, Berlin (2004)
- [DEG93] Degner, W., Lutze, H., Smejkal, E.: Spanende Formung: Theorie, Berechnung, Richtwerte [Cutting: theory, calculation, recommended values], 13th edn. Carl Hanser, München, Wien (1993)
- [STA90] Eisenhüttenleute, V.D. (ed.): Stahl-Eisen-Liste [Steel-iron-list], 8th edn. Stahl Eisen, Düsseldorf (1990)
- [HIN09] Hintze, W.: Personal correspondence (2009)
- [MÜL93] Müller, M., Hintze, W.: Werkzeugentwicklung zur Spanbeherrschung beim Drehen und Bohren [Tool development to control the chip formation in turning and drilling], pp. 331–344. VDI-Berichte 988 (1993)
- [NAK92] Nakayama, K.: Personal correspondence (1992)
- [OKU59] Okushima, K., Minato, K.: On the behaviour of chip in steel cutting. Bull. Jpn. Soc. Mech. Eng. **2**(5), 58–64 (1959)
- [PAT87] Patzke, M.: Einfluss der Randzone auf die Zerspanbarkeit von Schmiedeteilen [Influence of surface zones on the machinability of forged components]. Dr.-Ing. Dissertation, University of Hannover (1987)
- [WIN82] Winkler, H.: Zerspanbarkeit von niedriglegierten Kohlenstoffstählen nach gesteuerter Abkühlung [Machinability of low alloyed carbon steels after controlled cooling]. Dr.-Ing. Dissertation, University of Hannover (1982)

Further Reading

- Crafoord, R., Kaminski, J., Lagerberg, S., Ljungkrona, O., Wretland, A.: Chip control in tube turning using a high-pressure water jet. Proc. Inst. Mech. Eng. [B], J. Eng. Manuf. **218**(8), 761–767 (1999)
- Jawahir, I.S., van Lutterfelt, C.A.: Recent developments in chip control research and applications. Ann. CIRP **42**(2), 659–693 (1993)
- Klocke, F.: Manufacturing Processes: Cutting. Springer, Berlin (2009)
- Klocke, F.: Manufacturing Processes 2: Grinding, Honing, Lapping. Springer, Berlin (2005)
- Nakayama, K., Arai, M.: Comprehensive Chip form classification based on the cutting mechanism. Ann. CIRP **41**(1), 71–74 (1992)
- Strenkowski, J.S., Athavale, S.M.: A partially constrained Eulerian orthogonal cutting model for chip control tools. J. Manuf. Sci. Eng. **119**(4B), 681–688 (1997)

Chapter 4

Forces and Powers in Cutting and Abrasive Processes

Knowledge of the forces and power involved in cutting and abrasive processes is essential for the design of machine tools, tools, clamping devices and the process in general. Therefore, several approaches have been developed to predict these process parameters. These are approaches using

- empirical models based on experimental results
- analytical models based on elementary plastomechanics
- the finite element method (FEM).

Empirical models can be used to predict forces and powers with adequate accuracy but within a limited range of validity. Although the determination of the validity limits generally causes some problems, the parameter calculation based on this method is largely common in practice because it is easy to handle. However, close attention must be paid to the question if the model is used within the range of validity.

Analytical models based on elementary plastomechanics can usually make no claim to provide exact results in individual cases. However, they express the relationships between the most important input parameters of a process by means of equations. These can be used to determine the overall conditions for the process control, i.e., to carry out a trend analysis.

The *finite element method* can be used for a largely exact prediction of forces and powers—and also of other parameters like displacements, path speeds, strains, stresses and even temperatures. However, the corresponding modeling of a process and—depending on the model—the computation can be very complex and time-consuming. Thanks to very efficient calculation software which reduces the modeling effort, and thanks to more efficient computers which also reduce the computation time, FEM is becoming more and more common in industrial development departments and in scientific research. However, the results are only reliable if the material behavior of the workpiece material and the contact conditions between the workpiece and the tool are modeled with adequate accuracy.

4.1 Empirical Models

The initial resistance of the workpiece material against the penetration of the cutting edge has to be overcome by means of the resultant force F_z . In general, this resultant force is oriented at a certain angle within the space (Fig. 4.1). Due to practical reasons, it is divided into several vectors within a rectangular coordinate system with one axis in the direction of the primary or cutting motion and one in the direction of the feed motion. Thus, the corresponding forces and powers can be directly related to the components and drives of the machine tool.

The active force F_a , i.e., the vectorial sum of the cutting force F_c and the feed force F_f , lies within the working plane (which is spanned between the vectors of the feed speed and the cutting speed):

$$\vec{F}_a = \vec{F}_c + \vec{F}_f \quad (4.1)$$

The passive force F_p is orthogonal to the active force, thus

$$\vec{F}_z = \vec{F}_a + \vec{F}_p \quad (4.2)$$

The passive force does not contribute to the process power, because there is no relative movement between the tool and the workpiece in its direction. However, depending on the stiffness of the components within the flow of forces, it can have an essential influence on the deflection of the tool and the workpiece and thus on dimension and form deviations.

The necessary power for the cutting process is the product of the speed components and the components of the resultant force in their direction. Thus we obtain:

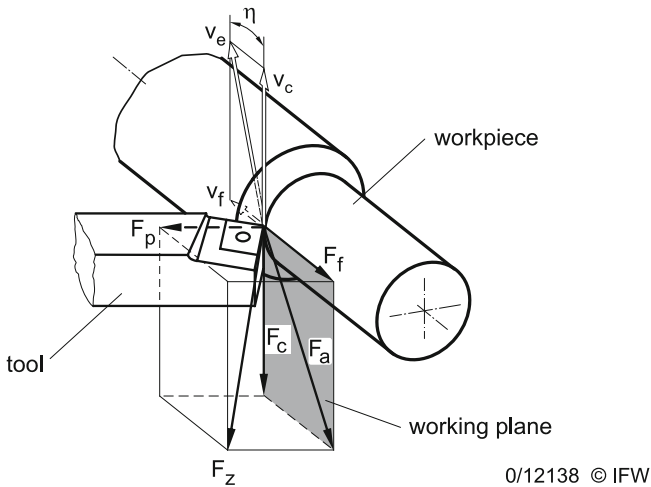


Fig. 4.1 Components of the resultant force in turning [ISO3002-4]

$$\text{cutting power: } P_c = F_c \cdot v_c \quad (4.3)$$

$$\text{feed power: } P_f = F_f \cdot v_f \quad (4.4)$$

In general: $F_c > F_f$ and $v_c \gg v_f$, thus $P_c \gg P_f$

This makes clear that the cutting power and the cutting force are important for the determination of the necessary drive power of the machine tool. The cutting force is usually higher than the feed force. As the cutting speed is also higher than the feed speed, the product of the cutting power and the cutting speed, i.e., the necessary cutting power, is significantly higher than the feed power.

However, the necessary cutting and feed power only play a minor role in the design of modern machine tools. Machine tool operators call for short downtimes and so for short acceleration times of the drives. Therefore, the installed acceleration power often exceeds the calculated powers P_c and P_f (Eqs. 4.3 and 4.4) many times over.

The cutting force is usually related to the cross section of the undeformed chip $A = a_p \cdot f$ (respectively $b \cdot h$) and is then called the specific cutting force k_c :

$$F_c = k_c \cdot A \quad (4.5)$$

The cutting force depends on numerous influences, including

- the workpiece material properties (strength, deformability, flow curve)
- the cutting speed
- the shape of the undeformed chip cross-section (ratio of a_p/f respectively b/h)
- the angles at the cutting edge
- the contact conditions between the workpiece and the cutting edge

There are also considerable interdependencies between several of these parameters and the cutting force. The general functional relationship between the specific cutting force and the influencing parameters is put down as

$$k_c = k_{c0} \cdot \Psi_0(k_{c0}; h; b; \gamma; v_c; \mu \dots) \quad (4.6)$$

where k_{c0} is the specific cutting force for predefined reference values of the influencing parameters h , b , γ , v_c , μ etc.; Ψ_0 is a dimensionless function used to include the effects of these influencing parameters and their interdependencies.

To separate a material volume unit V_w from the workpiece, the cutting energy W_c has to be performed. The corresponding specific cutting energy e_c is

$$e_c = \frac{W_c}{V_w} = \frac{P_c}{Q_w} = \frac{F_c \cdot v_c}{Q_w} = \frac{k_c \cdot b \cdot h \cdot v_c}{b \cdot h \cdot v_c} = k_c \quad (4.7)$$

This equation shows that the specific cutting force k_c is an energetic parameter, which corresponds with its physical definition. In fact, k_c is not a force acting on the cross section of the undeformed chip, i. e. a stress, but the energy per volume

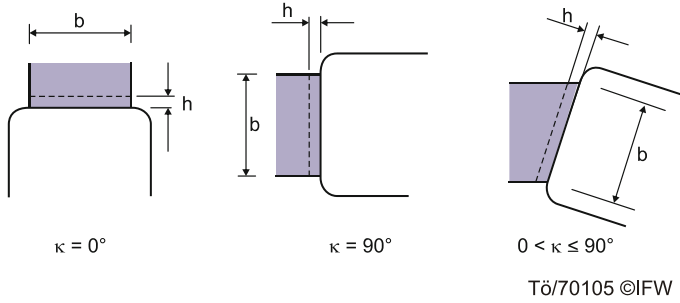


Fig. 4.2 Undeformed chip cross section with undeformed chip parameters

unit; respectively a power per material removal rate measured in J/mm^3 . Often, the dimension N/mm^2 is used, but this should not lead to the misinterpretation of e_c or k_c being a stress or even a pressure.

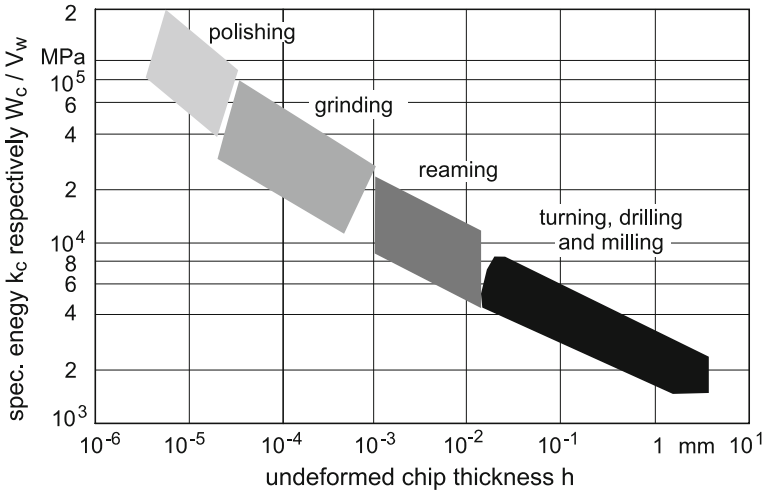
k_c depends on the shape of the undeformed chip cross section, which is determined by the undeformed chip parameters h and b respectively the cutting parameters a_p and f (for tools with multiple cutting edges: a_p and f_z). The fact that the tool cutting edge angle κ is not explicitly included in Eq. 4.6 goes down to an approach by Kienzle [KIE54] that bases cutting processes on idealized plasto-mechanical mechanisms.

Figure 4.2 illustrates the approach by O. Kienzle: It shows that the width of the undeformed chip b is in good approximation proportional to the cutting power, because the deformation processes in front of the cutting edge do not change with a change in b as long as $b \gg h$ and the effects of the chip formation on the external zone of the free workpiece surface and of the undeformed workpiece material are negligible. Accordingly, a change of the undeformed chip width b does not affect the specific energy. Thus, the undeformed chip width b can be treated as a proportional influencing parameter to the cutting force. The tool cutting edge angle is without influence as far as h and b are used to determine F_c , see Fig. 4.2.

In contrast, the undeformed chip thickness h has an immediate influence on the deformation processes. For example, the chip compression ratio changes with the undeformed chip thickness. This means that the curve of the undeformed chip thickness is not a straight proportional. In fact, experiments proved that the factor k_c is in good approximation independent from the undeformed chip width b , but non-linearly dependent to the undeformed chip thickness h , which has been proven for a wide range of values and for different cutting and abrasive processes (Fig. 4.3; with logarithmic axes).

The graph of the experimental results in the double logarithmic diagram (Fig. 4.4) can in good approximation be treated as a fitting straight line (at least for different sections), so that we can assume a power function¹:

¹ In the double logarithmic diagram, the linear equation is $\lg k_c - \lg k_{c1.1} = m_c (\lg h - \lg h_0)$; Eq. 4.6 is obtained by taking the antilogarithm.

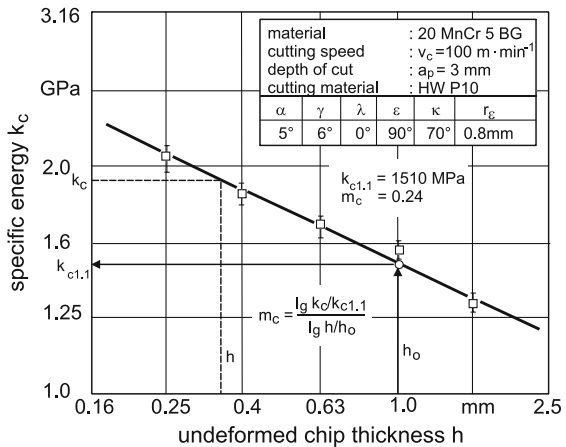


source : G. Vieregge

0/23576 © IFW

Fig. 4.3 Specific cutting energy and undeformed chip thickness for steel materials

Fig. 4.4 Specific energy across the undeformed chip thickness



0/21006 © IFW

$$k_{c0} = k_{c1.1} \cdot \left(\frac{h}{h_0}\right)^{-m_c} \tag{4.8}$$

where h_0 is a reference parameter, $k_{c1.1}$ is the base and $-m_c$ is the exponential increase in the specific cutting force. Based on Kienzle's notation, $k_{c1.1}$ ² is assumed as $h_0 = 1 \text{ mm}$. However, this means that $k_{c1.1}$ is generally unsuitable for

² Kienzle has chosen the notation $k_{c1.1}$ because it is the value of k_c for the reference values $b = 1 \text{ mm}$ and $h = 1 \text{ mm}$.

a direct calculation of the power by multiplying it with the material removal rate, because even in roughing processes, h is mostly considerably smaller than 1 mm. A more practice-oriented value for the undeformed chip thickness is calculated as follows:

$$k_{c1,x} = k_{c1,1} \cdot \left(\frac{h_0}{h_x}\right)^{-m_c} \tag{4.9}$$

e. g. with $h_x = 0,5$ mm, $k_{c1,0,5} = k_{c1,1} (1/0,5)^{-m_c}$

The specific cutting energies for the reference value $h = 1$ mm and the exponent $-m_c$ for common workpiece materials are presented in Table 4.1.

Based on the specific energy equation according to Kienzle, the basic equation for the calculation of the cutting power in cutting and abrasive processes can be put down as:

$$P_c = k_{c1,1} \cdot \left(\frac{h}{h_0}\right)^{-m_c} \cdot Q_w \cdot \Psi_0 \tag{4.10}$$

Using a multiplication approach for Ψ_0 , we can include further parameters:

$$\Psi_0 = \psi_\gamma \cdot \psi_{v_c} \cdot \psi_\mu \cdot \Psi_1(k_c; h; b; v_c; \dots) \tag{4.11}$$

The angle at the cutting edge with the most significant influence on the deformation is the rake angle γ respectively γ_r . This means that the power requirement also depends on the rake angle. For the cutting of steel and cast iron,

Table 4.1 Specific resultant forces in turning processes (according to Dubbel) [DIN6584, DUB94]

	α	γ	λ	ε	κ	r_ε
steel	5°	6°	0°	90°	70°	0.8mm
cast iron	5°	2°	0°	90°	70°	0.8mm

cutting speed : $v_c = 100$ m/min
depth of cut : $a_p = 3.0$ mm

workpiece material \ parameter	R_m MPa	specific forces $k_{i1,1}$ in MPa (i = c, n, p)						cutting tool material
		$k_{c1,1}$	$1-m_c$	$k_{f1,1}$	$1-m_f$	$k_{p1,1}$	$1-m_p$	
St 52-2	559	1499	0.71	351	0.30	274	0.51	P10
Ck 45 N	657	1659	0.79	521	0.51	309	0.60	P10
Ck 60	775	1686	0.78	285	0.28	259	0.59	P10
16 MnCr 5	500	1411	0.70	406	0.37	312	0.50	P10
100 Cr 6	624	1726	0.72	318	0.14	362	0.47	P10
GG-30	HB=206	899	0.59	170	0.09	164	0.30	K10
G-ALMg4SiMn*)	260	487	0.78					K10
X22CrNiMoNb1810**)	588	1397	0.76					K10

*) $v_c = 400$ m/min $\gamma = 15^\circ$

**) $v_c = 100$ m/min $\alpha = 8^\circ$

experiments proved that within the common range of rake angles, it can be assumed that the power is in good approximation linearly proportional to the rake angle (Fig. 4.5).

For Ck 45 steel, we can assume in good approximation:

$$\psi_\gamma = (1.11 - 0.11 \cdot \frac{\gamma}{\gamma_0}) \text{ with } \gamma_0 = 6^\circ \tag{4.12}$$

and for lamellar graphite cast iron:

$$\psi_\gamma = (1.03 - 0.03 \cdot \frac{\gamma}{\gamma_0}) \text{ with } \gamma_0 = 2^\circ \tag{4.13}$$

A comparison of the straight lines in Fig. 4.5 shows that the influence of the rake angle on the specific energy increases with the deformability or the expansion at failure.

Experiments have also been conducted on the influence of the cutting speed v_c . The studies on high-speed cutting [BEN03] showed that the power at high cutting speeds above a certain speed v_{cc} (see also Chap. 9) is in a first approximation proportional to the cutting speed, thus, Ψ_v is constant. With a decreasing cutting speed, Ψ_v rises. At $v_c = 0$, we assume $\Psi_v = \Psi_{v0}$. Figure 4.6 shows a simplified influencing parameter graph across the cutting speed.

These findings can be used to derive an approximation for the influence of the cutting speed:

$$\text{for } v_c < v_{cc}: \psi_v = (1 - \alpha) \cdot v_c / v_{cc} + \alpha \tag{4.14}$$

with the increase of the specific energy $\alpha = \frac{\psi_{v0}}{\psi_{vcc}}$;

$$\text{for } v_c \geq v_{cc}: \psi_v = 1 \tag{4.15}$$

The contact conditions can for instance be affected by different friction conditions. Experiments showed that the influence of the cutting liquid (emulsion or

Fig. 4.5 Influence of the rake angle

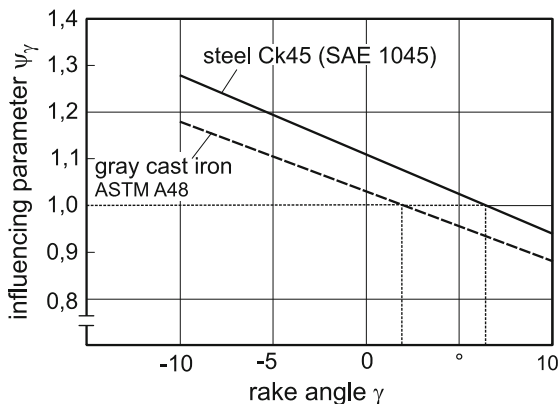
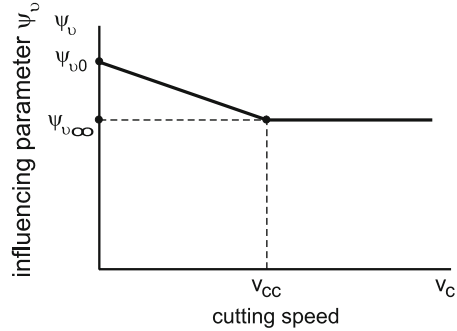


Fig. 4.6 Influence of the cutting speed



Tö/70107 ©IFW

mineral oil) is not significant, in contrast to the coating of the cutting edges. The friction coefficient of coated cemented carbide can be completely different from the coefficient μ_u of the uncoated material. There is frictional contact between the workpiece and the tool at the flank face and at the rake face. The predicted influence of the frictional contact is

$$\psi_\mu = \frac{1 + (\mu/\mu_u) \cdot R}{1 + R} \quad (4.16)$$

where $R = e_\gamma/e_\phi$ is the ratio of the friction energy to the deformation energy, μ_u is the friction coefficient for uncoated materials and μ is the lower friction coefficient for coated materials (see also [Chap. 7](#): cutting tool materials). In literature, the ratio values lie between $R = 0.15$ and 0.3 . With $R = 0.15$, ψ_μ reaches its maximum. The influence on the specific power is relatively low. It is in the order of ± 0.10 .

By approximation, Eq. 4.11 can be reduced to the factors ψ_γ , ψ_v and ψ_μ . The remaining factor Ψ_1 in Eq. 4.11 is negligible because the accuracy of the experimental results is limited anyway.

According to Eq. 4.3, the cutting force can be directly calculated using the power. It is

$$F_c = P_c/v_c \quad (4.17)$$

O. Kienzle initially aimed at determining the cutting force and not the necessary power for the process. k_c has been determined according to Eq. 4.5 as

$$F_c = k_c \cdot b \cdot h \quad (4.18)$$

Thus, according to Eq. 4.8:

$$F_c = k_{c1.1} \cdot b \cdot h_0 \cdot \left(\frac{h}{h_0}\right)^{1-m_c} \cdot \Psi_0 \quad (4.19)$$

Kienzle and Victor conducted experiments to evaluate the cutting force using the setup in Fig. 4.7. The torque is measured by strain gauges, and the cutting force

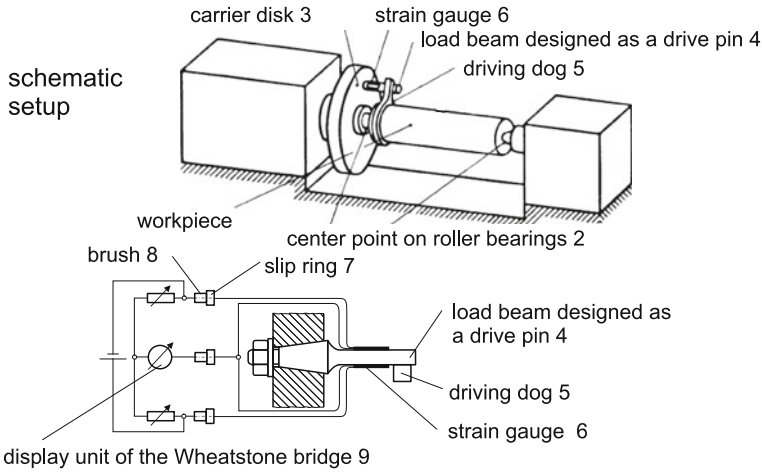


Fig. 4.7 Torque-measuring hub for cutting and abrasive processes (by Kienzle and Victor)

is derived from this torque. Today, the components of the resultant force are mostly measured by piezoelectric sensors.

When subjected to mechanical strain, piezoelectric materials like certain crystals—e.g., quartz (SiO_2)—or ceramics produce electric charge as a result of elastic deformation. This charge is converted into a voltage signal using appropriate amplifiers. Frequently used sensors are thin quartz crystal plates that are either pressure—sensitive or shear—sensitive, depending on their crystallographic orientation. If three correspondingly oriented plates are positioned and clamped on top of each other (to measure shear forces by means of friction contact and also tensile forces by means of the preload), they can be used to measure force components within three directions in space. These sensor units have a compact design, are very stiff and so have a high natural frequency, which is important for dynamic experiments. In Fig. 4.8, two shear—sensitive quartz plates are arranged above respectively and below a pressure—sensitive quartz plate. The Kistler Instrumente AG, Winterthur/Switzerland, which manufactures sensors of this type, states that the measuring errors due to crosstalk of its products are below 1 % [KIS09].

If four of the units described above are adequately connected (Fig. 4.9), three force components and up to three torques can be measured. If the presented type of circuitry is used, the forces can be measured largely independently from their effective direction, which significantly reduces the efforts for measurement and evaluation.

The circuitry of the four units S1 to S4 (which each measure three force components F_x , F_y and F_z) leads to the following equations for the global parameters [KIS09]:

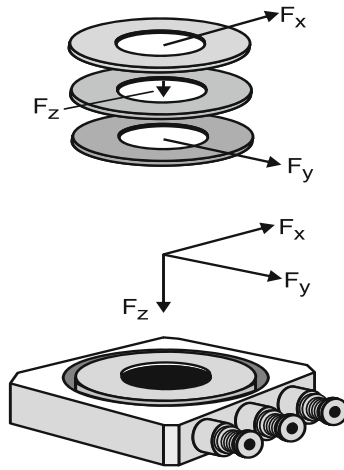
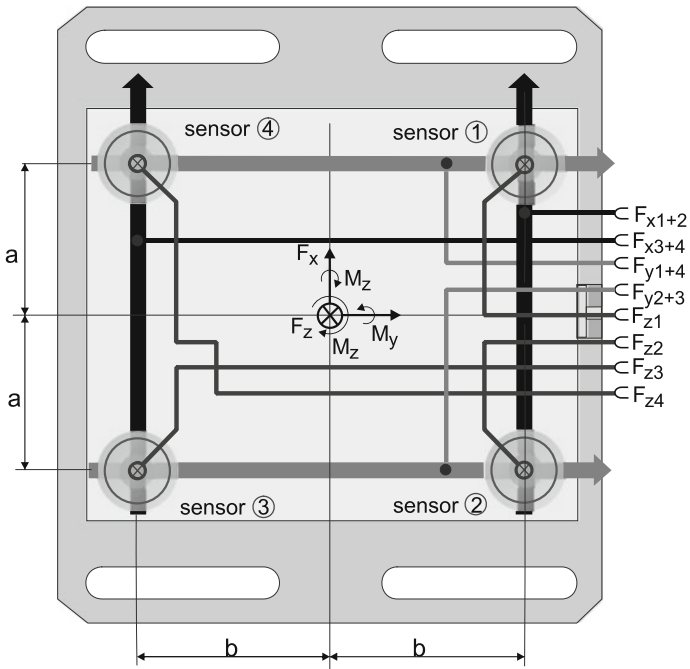


Fig. 4.8 Piezoelectric three-component force measurement (according to Kistler)



Tö/70108@IFW

Fig. 4.9 Setup for the three-component cutting force measurement (by Kistler)

$$F_x = F_{x1+2} + F_{x3+4} \quad (4.20)$$

$$F_y = F_{y1+4} + F_{y2+3} \quad (4.21)$$

$$F_z = F_{z1} + F_{z2} + F_{z3} + F_{z4} \quad (4.22)$$

$$\mathbf{M}_x = \mathbf{b} \times (F_{z1} + F_{z2} - F_{z3} - F_{z4}) \quad (4.23)$$

$$\mathbf{M}_y = \mathbf{a} \times (-F_{z1} + F_{z2} + F_{z3} - F_{z4}) \quad (4.24)$$

$$\mathbf{M}_z = \mathbf{b} \times (-F_{x1+2} + F_{x3+4}) + \mathbf{a} \times (F_{y1+4} - F_{y2+3}) \quad (4.25)$$

The values can be calculated using a sum calculator (analog) or a digital computer. Kistler states that the system has to be calibrated to achieve precise torque measurement [KIS09].

4.2 Modeling of the Feed Force and the Passive Force

The two remaining components of the resultant force are primarily relevant for the design of machine tool units. The feed force F_f can be relevant for the design of feed drives, although with modern automated machines, the necessarily high accelerations are mostly dominant compared to the feed forces required by the process. If we assume linear system performance, the elastic tool and workpiece deflections are proportional to the passive force F_p , which determines the dimension and shape deviations. While for instance in turning, the generally higher cutting force leads to second—order deviations,

$$\Delta d = \frac{2}{d} \cdot \left(\frac{F_c}{c_y} \right)^2 \quad (4.26)$$

the passive force leads to first—order deviations:

$$\Delta d = 2 \cdot \frac{F_p}{c_x} \quad (4.27)$$

The thrust force F_d is the vectorial sum of the passive force and the feed force:

$$\vec{F}_d = \vec{F}_f + \vec{F}_p. \quad (4.28)$$

With common setting conditions ($h \ll b$; the outer chip cross section does not influence the external workpiece zone), the thrust force is orthogonal to the major cutting edge due to reasons of symmetry. Thus, the ratio of the passive force to the feed force is

$$F_f = F_d \cdot \sin \kappa \quad (4.29)$$

$$F_p = F_d \cdot \cos \kappa \quad (4.30)$$

$$\frac{F_f}{F_p} = \tan \kappa \quad (4.31)$$

As a guide value for the thrust force, we can assume

$$F_d \approx 0.7 \cdot F_c (h \ll b) \quad (4.32)$$

Analogous to the modeling of the cutting force F_c , we can define power functions for the feed force and the passive force, however assuming that the undeformed chip width is also proportional to these parameters, which is less appropriate than in the case of the cutting force.

$$F_f = k_{f1.1} \cdot b \cdot h_0 \cdot \left(\frac{h}{h_0}\right)^{1-m_f} \quad (4.33)$$

$$F_p = k_{p1.1} \cdot b \cdot h_0 \cdot \left(\frac{h}{h_0}\right)^{1-m_p} \quad (4.34)$$

The principal values and the further progression of the specific feed forces and passive forces for some common metallic materials are included in Table 4.1.

As explained in Sect. 4.1, we can also use other reference values than $h_0 = 1 \text{ mm}$ and $b_0 = 1 \text{ mm}$. Eq. 4.8 is applicable in this case.

4.3 Surface Forces at the Cutting Edge

The presented measurement setups can only be used to determine the integral of the resultant forces. The measurements do not provide information on the surface forces, i.e., on the distribution of the forces across the contact surfaces. However, the resultant force is actually transmitted via the rake face and the flank face, and the forces are distributed across the surfaces. Figure 4.10 shows the distribution across the rake face and the flank face, assuming a quasiorthogonal cutting process. The following methods can be used to measure the surface forces:

- photoelastic study of stresses (cutting edge made of active material)
- variation of the contact surface areas
- separated cutting edges.

The characteristic distributions across the rake face for orthogonal grooving given in literature [ZOD67, KAT57, UST60] are presented in Fig. 4.11.

Ziebel uses a separated cutting edge, so that different components of the forces on the rake face can be measured at different contact lengths CL in the orthogonal cut [ZIE95]. He assumes that the cutting force is only transmitted via the rake face. Partial forces in the direction of the cutting force at the flank face are neglected. Figure 4.12 shows curves of normal stresses at different cutting speeds for an aluminum alloy.

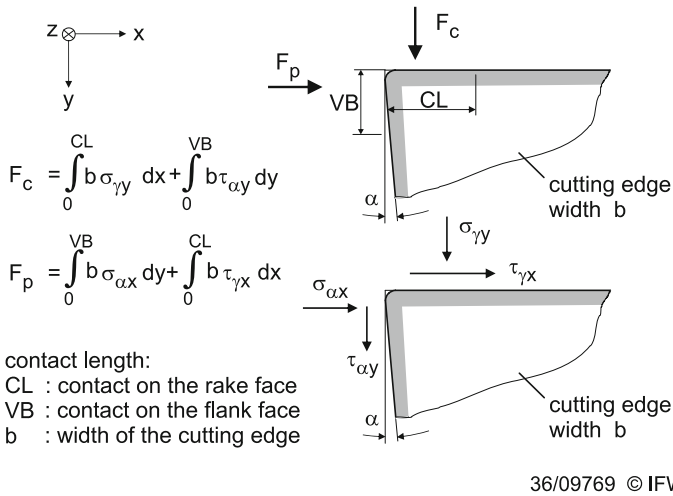


Fig. 4.10 Surface forces at the cutting edge

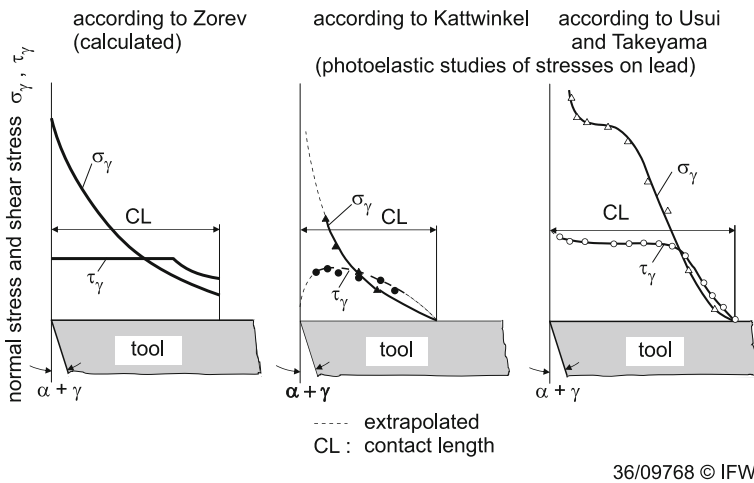


Fig. 4.11 Stress distribution on the rake face [ZIE95]

An alternative to this complex measurement method for the determination of partial forces at the rake and flank face is a simple consideration of discrete forces (Fig. 4.13). This method makes use of common friction laws (e.g., Amonton's friction law) which apply for both the flank face and the rake face:

$$F_{\alpha T} = \mu \cdot F_{\alpha N} \tag{4.35}$$

$$F_{\gamma T} = \mu \cdot F_{\gamma N} \tag{4.36}$$

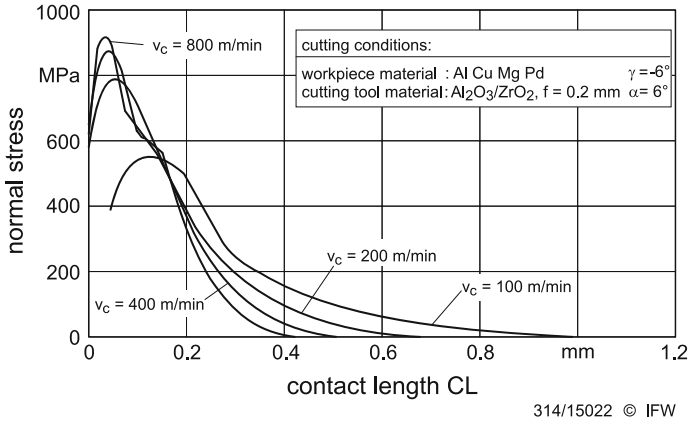
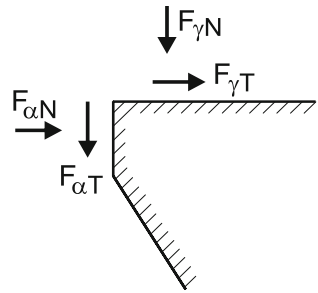


Fig. 4.12 Normal stress on the rake face [ZIE95]

Fig. 4.13 Discrete partial forces at the rake face and the flank face



From the sum of the forces follows

$$F_{\gamma N} + F_{\alpha T} = F_c \tag{4.37}$$

$$F_{\alpha N} + F_{\gamma T} = F_d \tag{4.38}$$

Using the measured forces F_c and F_t , the partial normal forces at the rake and flank face can be determined as

$$F_{\gamma N} = \frac{1}{1 - \mu^2} \times (F_c - \mu \times F_d) \tag{4.39}$$

and

$$F_{\alpha N} = \frac{1}{1 - \mu^2} \times (F_d - \mu \times F_c) \tag{4.40}$$

The tangential partial forces are calculated according to Amonton by inserting the values into Eqs. 4.35 and 4.36.

Example: for a roughing/finish turning process, the given values are

$$\mu = 0.3 \text{ and } F_t = 0.7 F_c$$

The corresponding partial forces are

$$F_{\gamma N} = 0.9 F_c, F_{\alpha N} = 0.33 F_c \text{ or } F_{\alpha N} = 0.56 F_t, F_{\gamma T} = 0.27 F_c \text{ or } F_{\gamma T} = F_t \text{ and } F_{\alpha T} = 0.1 F_c$$

These values are in good approximation equal to those given by Denkena [DEN92, SPA67].

4.4 Analytical Approaches in Plastomechanics

In plastomechanics, the determination of forces and powers is based on basic material properties and the general material behavior in plastic deformation processes. The basic theory, for which two examples will be presented in the following, uses highly simplified models from kinematics (deflections and deformations) and kinetics (stresses and force actions). These approaches do not actually provide exact descriptions of forces and powers, but are nonetheless of value because they describe relevant input and process parameters and their interdependencies.

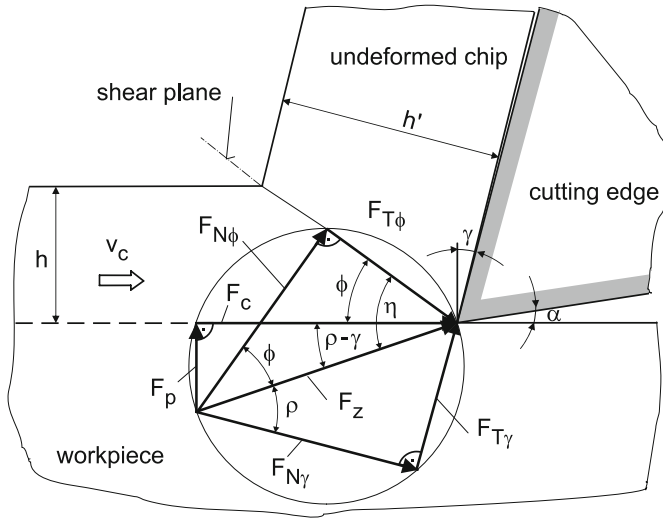
4.4.1 Theory by Ernst and Merchant

The theory by Ernst and Merchant [ERN41] is based on the following assumptions:

- the deformation is two-dimensional (orthogonal cutting)
- the resultant force is transmitted to the cutting edge on a linear contact orthogonal to the working plane
- Amonton's friction law applies
- the deformation only takes place in the shear plane (shear plane model)
- the stress on the shear plane is constant.

In Fig. 4.14, the resultant force acting between the tool and the workpiece is divided into orthogonal components in the form of three right triangles (circum-circle over F_z , Thales' theorem). These force components can be used to calculate the shear stress in the shear plane τ_ϕ :

$$\tau_\phi = \frac{F_z}{b \cdot h} \cdot \cos(\phi + \rho - \gamma) \cdot \sin \phi \quad (4.41)$$



36/10021 © IFW

Fig. 4.14 Force geometry in the orthogonal cut

The shear plane is located at the point of the maximum shear stress. The corresponding shear angle ϕ is calculated by setting the first derivation of the function $\tau_\phi(\phi)$ equal to zero:

$$\frac{d\tau_\phi}{d\phi} = 0 \quad (4.42)$$

After several conversions,

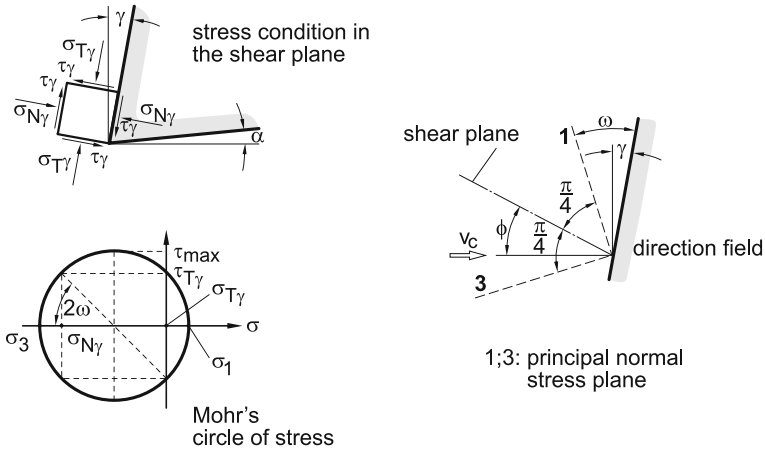
$$\cos(\phi + \rho - \gamma + \phi) = 0 \quad (4.43)$$

where only values of $\phi < 90^\circ$ are feasible. Accordingly, the shear angle relationship according to Ernst and Merchant is:

$$\phi = \frac{\pi}{4} - \frac{\rho}{2} + \frac{\gamma}{2} \quad (4.44)$$

4.4.2 Hucks's Theory

Hucks's theory also bases on the assumptions of orthogonal cutting, the shear model, Amonton's friction law (friction coefficient μ) and constant shear stress in the shear plane [HUC54]. Furthermore, he assumes that the chip flow across the rake face is undisturbed, i.e., that there is no normal stress at the rake face ($\sigma_{T\gamma} = 0$). Hucks's determination of the shear angle relationship is based on the relationships illustrated in Fig. 4.15.



0/11031 © IFW

Fig. 4.15 Shear angle relationship according to Hucks

From Mohr's circle of stress follows

$$\tan \omega = \frac{2\tau_\gamma}{\sigma_{N\gamma}} = 2\mu \tag{4.45}$$

and from the direction field follows

$$\frac{\pi}{2} = \phi + \frac{\pi}{4} + \omega - \gamma \tag{4.46}$$

Thus, we obtain the following equation:

$$\phi = \frac{\pi}{4} + \gamma - \frac{1}{2} \arctan 2\mu \tag{4.47}$$

Figure 4.16 is a graphic representation of the shear angle relationships according to Ernst/Merchant and Hucks. Besides these, about 20 further shear angle relationships have been defined. Their general form is

$$\phi = f(\rho, \gamma, \dots) \tag{4.48}$$

The shear angle can be used to determine the cross section after shear deformation $A\phi = b \cdot h / \sin\phi$. Using the shear stress $\tau\phi = \tau_{\max}$, we can calculate the shear force $F_{T\phi}$ whereas the known angles ϕ and ρ can be used to calculate the resultant force and its components. The shear stress can be determined by basic plastomechanical experiments [DOE86, ELM04].

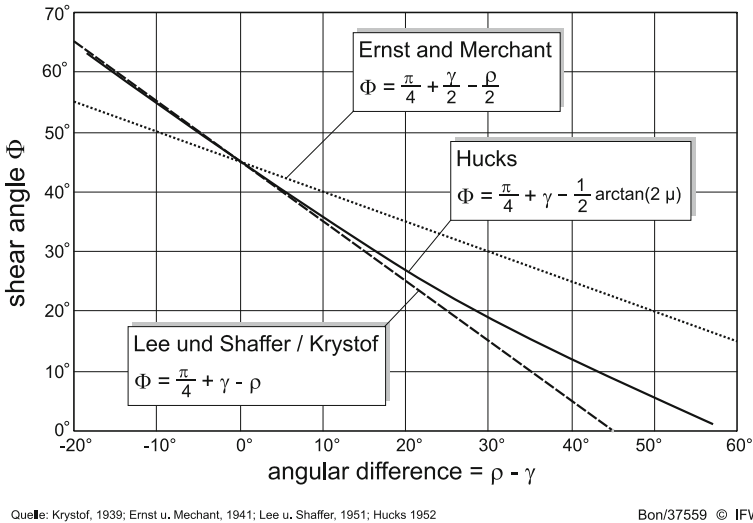


Fig. 4.16 Comparison of three shear angle relationships

4.5 Flow Curves and Constitutive Equations

The stresses required to achieve plastic deformation or flow of a workpiece material are mostly determined by basic uniaxial experiments (tensile tests or compression tests), less frequently by torsion tests or by experiments with technological conditions more similar to those of cutting and abrasive processes [ALS01]. The yield stress is primarily affected by the temperature, the strain (tension, compression or shear) and the strain rate. While in forming technology, e.g., in forging, extrusion or deep drawing processes, it is common to use quasi-stationary strain rates of up to $\dot{\varphi} = 50 \text{ s}^{-1}$, cutting and abrasive processes work with strain rates of up to 10^4 s^{-1} or even, in high-speed cutting, of up to 10^6 s^{-1} . Therefore, the flow curves designed for forming technology analyses cannot be transferred to cutting and abrasive processes. Flow curves for high speeds can be found in literature [e.g., TÖH05]. For CK45 N carbon steels, exemplary flow curves of up to $\dot{\varphi} = 5.000 \text{ s}^{-1}$, $\varphi_{\max} = 0.7$ and $\theta_{\max} = 1.000 \text{ }^\circ\text{C}$ are available. Figure 4.17 illustrates the influence of temperatures and strain rates on the yield stress. Due to dynamic strain hardening, the yield stress of the material increases significantly from 250 to 400 °C.

Figure 4.18 shows the yield stress across the strain at temperatures of 300 and 900 °C and a strain rate of $5,000 \text{ s}^{-1}$. Expectedly, the yield stress at 900 °C is lower than that at 300 °C. It decreases with an increasing strain as the temperature in the deformation zone rises due to the roughly adiabatic deformation.

For numerical calculations, the relationships between the yield stress, strain rate, strain and temperature are expressed by complex functions. This is an

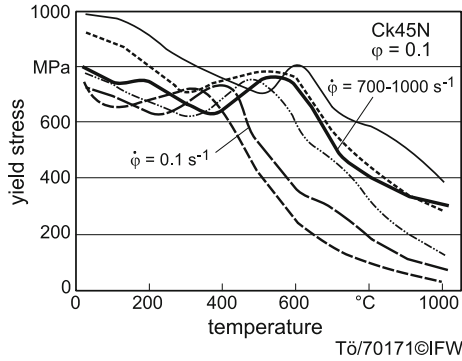


Fig. 4.17 Yield stress, temperature and strain rate

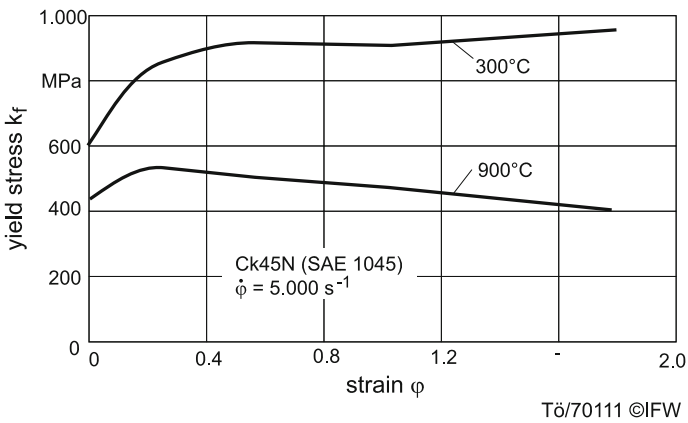


Fig. 4.18 Yield stress, temperature and strain

intricate task because of the interrelationships between the parameters and because of the irregular progression of the functions. These functions are called constitutive equations or flow laws. They are frequently integrated into commercial program systems for the numerical calculation of plastic deformations, like MARK or Deform. The most commonly used constitutive equation is the one by Johnson/Cook, particularly because it is relatively simple [JOC85]. El-Magd and Treppmann [ELM04] gives constitutive equations for cutting at high speeds with aluminum alloys, steels and titanium.

Flow curves/constitutive equations are used to determine the flow stress or yield stress k_f , i.e., the yield point under uniaxial stress. By means of a yield criterion, multiaxial normal stresses or shear stresses can be converted into the uniaxial reference stress k_f . Considering energies the findings can also be used to determine strains.

According to the flow criterion by Tresca (maximum shear stress theory), we have

$$\tau_{\max} = \frac{1}{2}k_f \quad (4.49)$$

$$\varphi = \frac{1}{2}\gamma_s \quad (4.50)$$

and according to the flow criterion by von Mises (distortion energy theory)

$$\tau_{\max} = \frac{1}{\sqrt{3}}k_f \quad (4.51)$$

$$\varphi = \frac{1}{\sqrt{3}}\gamma_s \quad (4.52)$$

These equations can be used to determine the forces $F_{T\phi}$, F_z and F_c in orthogonal cutting (see Sect. 4.4.1). The tangential force in the shear plane $F_{T\phi}$ is

$$F_{T\phi} = \tau_{\max} \cdot \frac{b \cdot h}{\sin \phi}. \quad (4.53)$$

From the force diagrams in Fig. 4.13 follows

$$F_z = F_{T\phi} \cdot \frac{1}{\cos(\phi + \rho - \gamma)} \quad (4.54)$$

and

$$F_c = F_z \cdot \sin 2\phi. \quad (4.55)$$

4.6 Numerical Theory

The finite elements method, which will be presented in Chap. 6, can be used to calculate stresses, forces and temperatures in cutting and abrasive processes. Because of the numerical approach, complex constitutive equations can be used, as indicated in Sect. 4.4. Two constitutive equations will be presented by way of example. The approach by Johnson/Cook already includes a dynamic component:

$$k_f(\varepsilon, \dot{\varepsilon}, \vartheta) = (A + B\varepsilon^n) \cdot (1 + C \cdot \ln(\dot{\varepsilon}/\dot{\varepsilon}_0)) \cdot (1 - (\vartheta^*)^m) \quad (4.56)$$

where

$$\vartheta^* = \frac{\vartheta - \vartheta_0}{\vartheta_m - \vartheta_0}. \quad (4.57)$$

The five parameters are material-specific and are determined by using a series of flow curves. ε and $\dot{\varepsilon}$ are plastic strain and strain rates; $\dot{\varepsilon}_0$ is the reference strain rate with $\dot{\varepsilon}_0 = 1\text{s}^{-1}$; ϑ^* is the specific temperature with a reference temperature of $\vartheta_0 = 293\text{ K}$ and the melting point of the workpiece material ϑ_m . For Ck45 N steel, we have $A = 500\text{ MPa}$, $B = 693\text{ MPa}$, $C = 0.0114$, $n = 0.36$, $m = 1$ and $\vartheta_m = 1808\text{ K}$ [JOC83].

The constitutive equation according to El-Magd [ELM04] has a similar structure. It is especially suitable for the numerical evaluation of cutting and abrasive processes, because it covers high ranges of strain rates, strains and temperatures. As mentioned above, the strain rates in cutting and abrasive processes are by two or three orders of magnitude higher than those in the mostly macroscopic forming processes in rolling, drawing, thermal cutting or deep drawing. The strains are within the same order of magnitude and the temperature range of a material particle throughout the chip formation process varies between room temperature and $500\text{ }^\circ\text{C}$ or can even, under special conditions, reach the melting point.

Numerical calculations using FEM are generally also based on the assumption of an isotropic continuum that is homogenous, at least towards the beginning of the process. We can also assume that the volume is constant because there is significant plastic deformation.

According to the constitutive equation, the flow stress k_f depends on the strain ε , the strain rate $\dot{\varepsilon}$ and the temperature ϑ . In El-Magd's equation, it is a product of an isothermal component σ_{iso} and a factor $\Psi(\vartheta)$ which accounts for the increasingly adiabatic behavior with an increase in the strain rate:

$$k_f(\varepsilon, \dot{\varepsilon}, \vartheta) = \sigma_{\text{iso}}(\varepsilon, \dot{\varepsilon}, \vartheta_0) \cdot \Psi(\vartheta). \quad (4.58)$$

The isothermal flow stress has to be indicated for a specific reference temperature. A frequently used value is $\vartheta_0 = 273\text{ K}$. By means of comprehensive experiments, it can be determined that, in good approximation,

$$\sigma_{\text{iso}}(\varepsilon, \dot{\varepsilon}) = K \cdot \varepsilon^n \cdot \dot{\varepsilon}^m + \eta \dot{\varepsilon}. \quad (4.59)$$

K [MPa] is the material strength; the exponents n and m represent the hardening dependent on the strain respectively on the strain rate. η [MPa · s] is a viscosity parameter that makes up the main part of the influence of the strain rate.

The energy imparted to the process, which is almost completely converted into heat, is restricted to the chip formation zone. The deformation process is nearly adiabatic and increasingly so with an increasing cutting speed and a decreasing thermal conductivity of the workpiece material. The deformation is variably far from the isothermal state. El-Magd includes this variation by means of the temperature function $\Psi(\vartheta)$:

$$\Psi(\vartheta) = \exp\left(-\frac{\vartheta}{\vartheta_1}\right) + A^x \exp\left(-\frac{\vartheta}{\vartheta_2}\right)^\mu \quad (4.60)$$

This exponential approach includes the two reference temperatures ϑ_1 [K] and ϑ_2 [K] as well as two dimensionless parameters, the weighting

factor A^x and the exponent μ . These parameters have to be determined by means of experiments for each workpiece material. However, tables with values for numerous workpiece materials are available [ELM04]. Admittedly, the total number of eight parameters in the presented constitutive equations leads to time-consuming and complex procedures, but this can be justified by the high range of validity. The parameters for Ck45N steel are $K = 1341 \text{ MPa}$, $n = 0.17$, $m = 0.01$, $\eta = 0.0242 \text{ MPa}\cdot\text{s}$, $\vartheta_1 = 1300\text{K}$, $\vartheta_2 = 700\text{K}$, $A_x = 0.33$ and $\mu = 7$. The flow curves determined by El-Magd are presented in Fig. 4.17.

The necessary data for the models by Johnson/Cook and El-Magd are determined by means of compression or shear tests. An interesting approach for the flow curve determination was developed by Altan. His basic idea is to adapt the data acquisition as closely as possible to the process for which the data will be needed. Therefore, he does not include conventional basic material tests, but uses a peripheral milling process and derives the parameters for the constitutive equation from resultant force components measured in a reverse simulation. The start values (A_0 , B_0 , C_0 , D_0 , E_0 , m_0 and n_0) are determined using the constitutive equation approach by Johnson/Cook,

$$\bar{k}_f = (A + B\varepsilon^n)(1 + C \ln \dot{\varepsilon})(D - E\vartheta^{xm}) \quad (4.61)$$

k_f is determined by means of the measured forces using Oxley's algorithm [OXL89]. The procedure is repeated iteratively until the measured forces and the forces determined by means of the model are in appropriate accordance [ALS01].

In connection with the constitutive equations, FEM can be used to determine forces and stresses in the chip formation zone. An example is presented in Fig. 4.19. The reference stresses at specific moments in the chip formation process according to von Mises are presented in the left upper part of the Figure. The nodal points on the continuous lines represent areas of equal stress. In the upper right part, the forces in the cutting direction are presented across the time or across the path length due to primary motion after the penetration of the cutting edge into the workpiece. The lower right part shows the forces at one nodal point across the time (using the example of the nodal point N in the upper left part of the Figure). Finally, the force components in the cutting direction (x) and orthogonal to the cutting direction (y) along the path of nodal points $x_0 \rightarrow x_n$ are presented in the lower left part of the Figure.

4.7 Powers, Torques and Forces in Drilling

The necessary power input in drilling depends on the shear or deformations and friction in the process. As described in Sect. 1.5 in drilling from the solid (with a double edged twist drill), two major cutting edges and two chisel edges each remove one chip, but with differences in the workpiece material deformation. In front of the major cutting edges, the chips are similar to those produced in turning

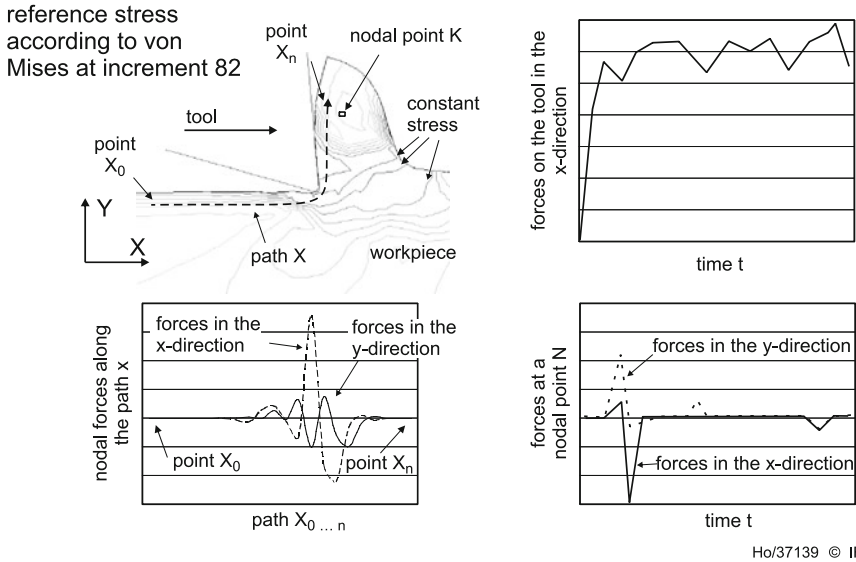


Fig. 4.19 Forces in the FE simulation

processes. However, they are produced at varying cutting speeds and with varying rake angles along the cutting edge. The chisel edges have highly negative rake angles (Figs. 1.14 and 1.15). Towards the center of the drill, the cutting speed decreases down to zero and the removed material in the form of a chip must be displaced in the transverse direction (in addition to its movement orthogonal to the cutting edge) in order to flow off the web of the drill into the flute. The corresponding shear and squeezing processes are more similar to extrusion [SHA84] than to the free chip formation in turning. The chip formation and displacement take place under high hydrostatic pressure in front of the cutting edges.

As in the turning process, friction occurs at the rake and flank faces. Additionally, the margins of the minor flank faces rub against the bore wall, while the chips formed by the major cutting edges and the chisel edges also rub against the flutes as well as the bore wall. As a consequence, the forces and moments in drilling processes are not constant along the drilling depth, but they increase. This increase is roughly proportional to the drilled depth while the drill point enters the workpiece and then rises more slowly in accordance with the increasing friction.

The contributions of the major cutting edges and the chisel edges to power, forces and torques in the process because of shear and friction can by approximation be determined using the principle of decomposition. For this purpose, the drilling process is divided into several parts (Fig. 4.20). In the “free drilling” process (B), a tubular workpiece with an outer diameter below the drilling diameter and an inner diameter above the radius of the drill web is used. Only the major cutting edges are engaged. The chips can flow off freely. The necessary

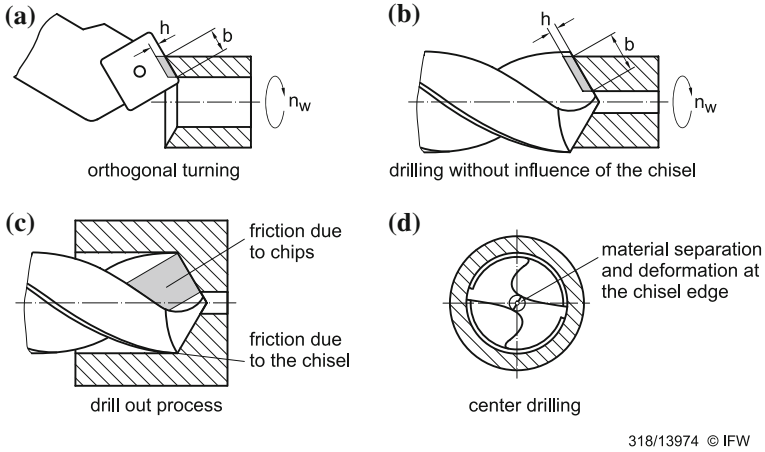


Fig. 4.20 Principle of decomposition

cutting power, the torques and the forces in the cutting and feed direction are in good approximation equal to those in turning (A).

The corresponding cutting power P_{ch} can be determined using the basic Eq. 4.8:

$$P_{ch} = k_{c1.1} \cdot \left(\frac{h}{h_0}\right)^{-m_c} \cdot Q_w \cdot \Psi_0 \quad (4.62)$$

In the drill out process (C), the chips cannot flow off freely. Additional friction forces occur. By comparing the process to drilling from the solid (D), we can determine the influence of the chisel edges. It leads to an additional cutting power component according to the effect of the chisel edge P_{cq} , thus

$$P_c = P_{cq} + P_{ch} \quad (4.63)$$

However, this decomposition would only be valid if the different parts of the process were independent from each other, which is strictly speaking, not the case, e.g., the chips produced by the chisel edges contribute to the chip friction.

The different process power components can be determined by torques measured in experiments according to Fig. 4.20. M_{ch} is the torque for the engagement of the major cutting edges, M_{cq} is that for the chisel edges, and the ratio between the two is $t_c = M_{ch}/M_{cq}$. Drilling of C45 steel leads to a measured torque ratio of about $t_c = 11$. This shows that the contribution of the chisel edge to the cutting torque and to the cutting power is low. With

$$M_{cq} = \frac{1}{t_c} \cdot M_{ch} \quad (4.64)$$

the total power is

$$P_c = \left(1 + \frac{1}{t_c}\right) \cdot P_{ch}$$

and

$$P_{ch} = \left(1 + \frac{1}{t_c}\right) \cdot k_{c1.1} \cdot \left(\frac{h}{h_0}\right)^{-m_c} \cdot Q_w \cdot \Psi_0 \tag{4.65}$$

with $h = \frac{1}{2} f \sin \sigma/2$ (f = drill feed)

Figure 4.21 shows the drill point and the applied forces, which are assumed to be discrete. The forces are transmitted as surface forces via the contact surfaces in the form of normal and shear stresses. For the following calculations these stresses are summarized as linearly distributed loads, which are composed of the cut load p_c and the feed load p_f with the chisel edges and major cutting edges folded into one plane. The influence of the radius on the specific cutting force is low, therefore, ω we can assume that the distributed load is constant within sections of the radii $0 < r \leq r_q$ and $r_q < r \leq r_a$. Accordingly, the drilling torque is

$$M_c = 2 \cdot \int_0^{r_q} p_{cq} \cdot r dr + 2 \cdot \int_{r_q}^{r_a} p_{ch} \cdot r dr \tag{4.66}$$

with the load ratio $s_c = p_{cq}/p_{ch}$ and the radius ratio $q = r_q/r_a$. For type N twist drills with diameters of 5–20 mm, the common radius ratio is $q = 0.19$.

$$M_c = p_{ch} \cdot r_a^2 \cdot (1 - q^2 + s_c \cdot q^2) \tag{4.67}$$

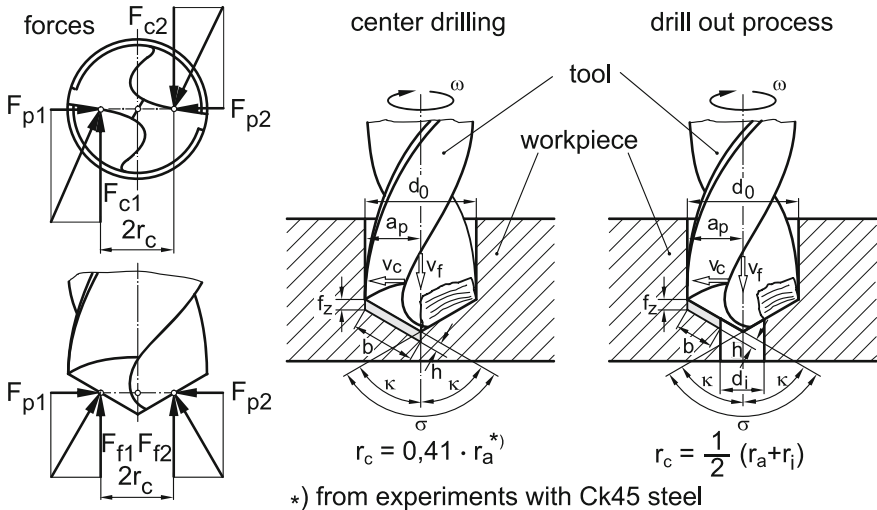
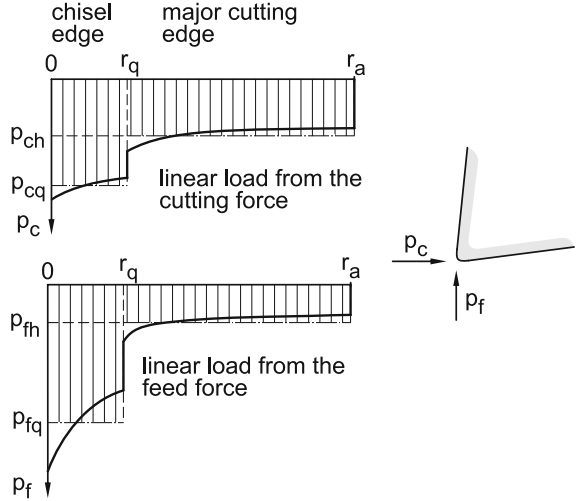


Fig. 4.21 Chipping geometry and resultant forces in drilling

Fig. 4.22 Load on the major cutting edge and the chisel edge



0/14417 © IFW

The ratio of the single torque components is

$$t_c = \frac{M_{ch}}{M_{cq}} = \frac{p_{ch} \cdot (1 - q^2)}{p_{cq} \cdot q^2} \tag{4.68}$$

This ratio can be used to determine the load ratio:

$$s_c = \frac{(1 - q^2)}{q^2} \cdot \frac{1}{t_c} \tag{4.69}$$

The corresponding value for C45 steel is $s_c = 2.4$. For the cutting force per cutting edge, we obtain

$$F_c = \int_0^{r_q} p_{cq} \, dr + \int_{r_q}^{r_a} p_{ch} \, dr \tag{4.70}$$

And with s_c and q :

$$F_c = p_{ch} \cdot r_a (1 - q + s_c \cdot q) \tag{4.71}$$

M_c and F_c can be used to calculate the effective radius r_c in drilling from the solid at which the discrete cutting force is applied:

$$r_c = \frac{M_c}{2 \cdot F_c} = \frac{1 + q^2 \cdot (s_c - 1)}{2 \cdot [1 + q(s_c - 1)]} \tag{4.72}$$

Thus, in drilling from the solid with C45 steel, $r_c = 0.41 r_a$ and

$$\frac{M_c}{2F_c} = 0,41 r_a \tag{4.73}$$

Using Eqs. 4.65 and 4.67 we can finally determine the linear load on the major cutting edge and by means of s_c , the linear load on the chisel edge, with ω as the angular speed of the drill:

$$p_{ch} = \frac{P_c}{\omega \times r_a^2 \times [1 + q^2(s_c - 1)]} \tag{4.74}$$

The feed force F_f per cutting edge is

$$F_f = \int_0^{r_q} p_{fq} \, dr + \int_{r_q}^{r_a} p_{fh} \, dr \tag{4.75}$$

With the force ratio $s_f = p_{fq}/p_{fh}$, we have

$$F_f = (s_f \cdot q + 1 - q)p_{fh} \cdot r_a \tag{4.76}$$

The force ratio is $s_f = 4$, thus

$$\frac{F_h}{p_{fh} \cdot r_a} = 0.76 + 0.81 \tag{4.77}$$

The first value in Eq. 4.77 represents the feed force at the chisel edge. The second value represents the feed force at the major cutting edge. This shows that the influence of the chisel edge is of the same order of magnitude as that of the major cutting edge. Please note that due to wear of the chisel edge and, to a smaller extent of the major cutting edge, the feed force in drilling from the solid can be increased by a factor of up to 2. Shortening the chisel edge by means of different methods (see Fig. 1.16) can reduce the feed force significantly, as evident from the reduction in the cutting edge ratio q in Eq. 4.76.

The specific feed force at the major cutting edge can be determined using the Kienzle equation. We obtain

$$p_{ch} = k_{c1.1} \frac{h^{(1-m_c)}}{\sin \sigma/2 \cdot [1 - q(1 - s_c)]}; \quad h = f_z \sin \sigma/2 \tag{4.78}$$

$$p_{fh} = k_{f1.1} \cdot \frac{h^{(1-m_f)}}{\sin \sigma/2 \cdot [1 + q(1 - s_f)]} \tag{4.79}$$

The presented derivations all refer to drilling from the solid. In contrast, for drill out processes of an initial bore with $r_i > r_q$, the influence of the chisel edge in Eq. 4.62 has to be omitted.

The moments and forces can be calculated accordingly:

$$M_{ch} = \frac{1}{\omega} \cdot P_{ch}$$

The effective radius r_c is

$$r_c = \frac{M_c}{2 \cdot F_c} = \frac{1}{2}(r_a + r_i) \quad (4.80)$$

and

$$F_c = \frac{M_c}{2 \cdot r_c} \quad (4.81)$$

The feed force in drill out processes according to Eq. 4.33 is

$$F_f = k_{f1.1} \cdot \frac{r_a - r_i}{\sin \sigma/2} \cdot h^{(1-m_f)} \quad (4.82)$$

In all derivations presented above, the influence of the chip and margin friction (case C in Fig. 4.20) has been neglected. In fact, the drilling torque increases with the drilling depth by about 10 % per depth of $2 r_a$. To limit the friction at the margin and to prevent it from being jammed, twist drills are slightly conical towards the shank (by 0.2–0.8 % of the drill diameter) to reduce the heating of the tool during the drilling process.

4.8 Power and Forces in Milling Processes

Equations 4.3 and 4.8 above for the calculation of the cutting power are generally also valid for milling processes.

$$P_c = F_c \cdot v_c \quad (4.83)$$

$$P_c = k_{c1.1} \cdot \left(\frac{h}{h_0}\right)^{-m_c} \cdot Q_w \cdot \Psi_0 \quad (4.84)$$

Equation 4.84 includes the undeformed chip thickness h that has to be determined for a milling tool with multiple cutting edges as indicated in Fig. 1.18. Evidently, in all processes with a varying feed motion angle φ (i.e., milling plus related processes and grinding), the undeformed chip thickness is not constant. Correspondingly, the instantaneous power and the instantaneous resultant force are not constant either.

Thus, to determine the average drive power as the minimum value that has to be supplied at the milling spindle, we have to average the power over the contact arc. To simplify matters, we assume that the factor k_{c0} (Eq. 4.8) sufficiently accounts for the influence of the undeformed chip thickness h on the specific energy k_c , so that this influence is negligible in the correction function Ψ_0 . We obtain:

$$P_{cm} = k_{c1.1} \cdot f_z \cdot \sin \kappa \cdot Q_w \cdot \psi_0 \cdot \frac{1}{\varphi_c} \int_{\varphi_E}^{\varphi_A} \sin^{-m_c} d\varphi \quad (4.85)$$

Equation 4.85 includes an integral which cannot be solved analytically. Therefore, the average power is most commonly determined by means of the average chip thickness h_m according to Eq. 1.17, which is assumed to be constant over the penetration angle φ_c .

$$h_m = \frac{1}{\varphi_c} \int_{\varphi_E}^{\varphi_A} h_{(\varphi)} d\varphi = \frac{1}{\varphi_c} \cdot f_z \sin \kappa \cdot (\cos \varphi_E - \cos \varphi_A) \quad (1.17)$$

Thus,

$$P_{cm}^* = \frac{1}{\varphi_c} \cdot k_{c1.1} \cdot Q_w \cdot \left(\frac{h_m}{h_0}\right)^{-m_c} \quad (4.86)$$

However, this is only an approximation because the average was not taken over the specific energy, but over the chip thickness. The error resulting from this approximation can be determined numerically, e.g., using MATLAB. The errors for an exponent of $m_c = 0.25$ are presented in Fig. 4.23.

$$\varepsilon = \frac{P_{cm}^* - P_{cm}}{P_{cm}} \quad (4.87)$$

It can be observed that, admittedly, the power determined by the approximative method is too low ($\varepsilon > 0$), i.e., that the value calculated over the average chip thickness is below the integral for all combinations of entrance (φ_E) and (φ_A) exit angles, but that this error is by all means very insignificant.

To determine the necessary drive power for the machine tool, we have to include the degree of efficiency for the drive section and an addition of 15 % to account for the deviations of the instantaneous power from the calculated average power.

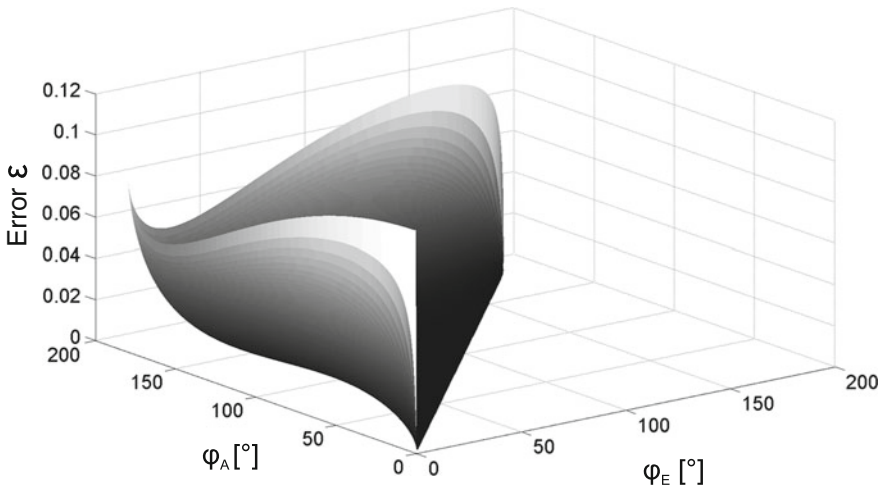


Fig. 4.23 Error due to the averaging of the integral

The average torque that has to be provided at the milling spindle results from the average cutting power and the angular speed ω of the milling spindle as

$$M_c = \frac{1}{\omega} P_{cm} \tag{4.88}$$

For the design of machine tool components, tools and clamping devices, the focus is not on the average of the torque and the resultant force, but on their maximum values. Therefore, we do not use the average chip thickness, but its maximum value. For

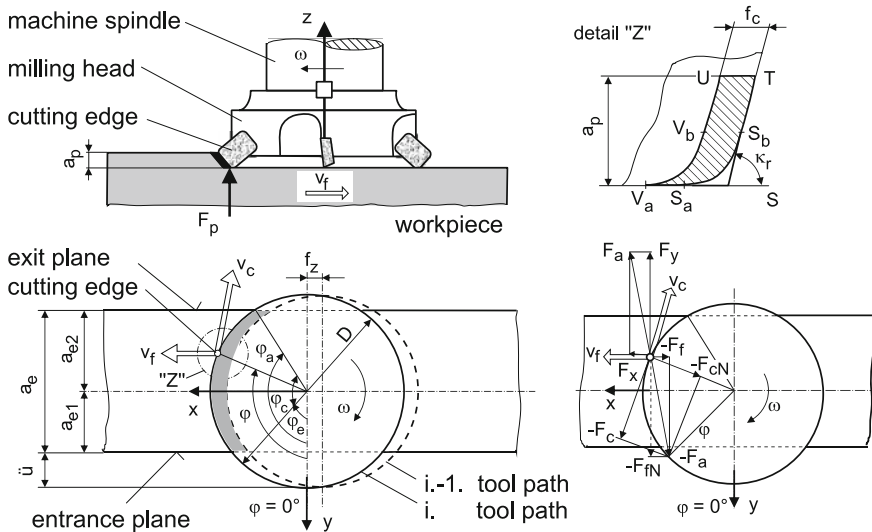
$$\begin{aligned} \varphi_E \text{ and } \varphi_A < 90^\circ : \quad h_{\max} &= f_z \cdot \sin \kappa \cdot \sin \varphi_A \\ \varphi_E \text{ and } \varphi_A > 90^\circ : \quad h_{\max} &= f_z \sin \kappa \sin \varphi_E \\ \varphi_E < 90^\circ \text{ and } \varphi_A > 90^\circ : \quad h_{\max} &= f_z \sin \kappa \end{aligned}$$

Accordingly, the components of the resultant force (Fig. 4.24)—the cutting force F_c , the normal cutting force F_{cN} and the passive force F_p —are acc. (Table 4.2).

$$F_i = a_e \cdot f_z \cdot k_{i1.1} \left(\frac{h_{\max}}{h_0} \right)^{-m_i} \quad \text{with } i = c, cN, p \tag{4.89}$$

However, to determine the total sum of forces acting on the spindle, we have to include the action of force of all engaged cutting edges.

Because of the rotating tool, measuring the forces applied to the milling cutter teeth is more difficult than the determination of forces in turning. Frequently, the resultant force components (F_f, F_p, F_{fN}) between the machine table and the tool are



36/11270 © IFW

Fig. 4.24 Engagement parameters and force diagrams in face plain milling

Table 4.2 Specific resultant forces in milling processes Dubbel [DUB94]

parameter workpiece material	Cutting speed v_c m/min	Cutting edge geometry	Specific resultant forces $k_{i1.1}$ (MPa)						Cutting material
			$k_{c1.1}$	$1 - m_c$	$k_{cN1.1}$	$1 - m_{cN}$	$k_{p1.1}$	$1 - m_p$	
St 52-3	120	Negative	1831	0.71	809	0.46	705	0.39	P25
		Positive	1469	0.75	447	0.43	174	0.44	P25
Ck 45	190	Negative	1506	0.55	708	0.38	653	0.38	P25
X22 Cr MoV121	120	Positive	1533	0.71	497	0.30	164	0.23	P40
Cutting edge geometry			a	r	a		s		chamfer (mm)
Negative	-4°		-7°	6°	23°	-6°	75°	90°	1.4/0.8/1.4
Positive	0°		8°	9°	29°	8°	75°	90°	0.8/1.4

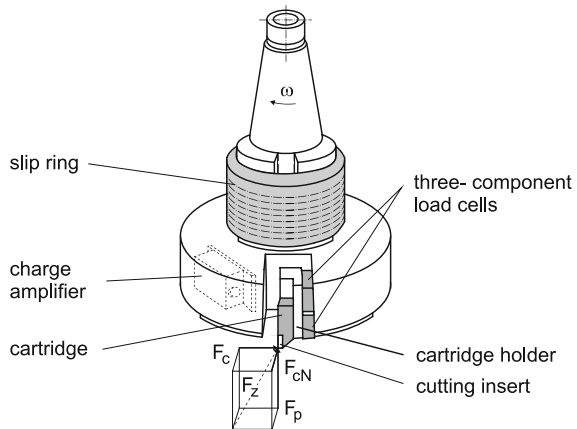
measured in a stationary coordinate system using a piezoelectric three-component measurement platform (see Fig. 4.9) [LAP02]. The coordinates then have to be converted into rotating coordinates to determine the resultant forces F_c and F_{cN} . The transformation matrix for the conversion is

$$\begin{bmatrix} F_c \\ F_{cN} \\ F_p \end{bmatrix} = \begin{bmatrix} \sin \varphi & -\cos \varphi & 0 \\ \cos \varphi & \sin \varphi & 0 \\ 0 & 0 & 1 \end{bmatrix} \cdot \begin{bmatrix} F_x \\ F_y \\ F_z \end{bmatrix} \tag{4.90}$$

However, the subtraction of components with high values can lead to an unacceptable raising of measurement errors.

Therefore, to measure the resultant forces in milling, the single-tooth milling cutter in Fig. 4.25 has been developed [BUS91]. This setup also measures the forces piezoelectrically by means of three three-component load cells, which are

Fig. 4.25 Determination of the resultant force components using a single-tooth milling cutter



positioned very closely to the zone of the force action. The measurement unit can be used for the direct determination of the resultant force components F_c , F_{cN} and F_p . The cutting inserts are fixed by a cartridge system in order to vary the cutting edge geometries and tool angles. The milling tool diameter of 200 mm is fixed.

4.9 Questions

1. Explain the different methods for the modeling of the cutting power respectively the cutting force.
2. To which extent do the separate resultant force components contribute to the power converted in the cutting zone?
3. Why does the Kienzle cutting force model not include the tool cutting edge angle?
4. What is the physical definition of the parameter k_c ? Does the ratio force/surface relation reveal stresses?
5. The Kienzle cutting force model is apparently dimensionally incorrect. What is the reason for this?
6. Why is the specific cutting force $k_{c1.1}$ used as a base value in Eq. 4.8?
7. Which parameter has a higher influence on the cutting force F_c —the undeformed chip width b or the undeformed chip thickness h ?
8. How does F_c change when the undeformed chip thickness h decreases, but the undeformed chip cross-section remains constant?
9. k_c is a stress parameter. What is the corresponding specific energy?
10. Specify the Kienzle relationship for optional reference values.
11. How does the deformability of the workpiece material affect the influence of the rake angle on the specific energy?
12. Name common methods of measuring the cutting force.
13. Which method would you choose for measuring resultant force components with a relatively high frequency?
14. Explain the method of resultant force measurement that is widely independent from the line of action of the forces.
15. Which extremal principle provides the basis for the plastomechanical determination of the shear angle relationship according to Ernst and Merchant?
16. Explain the simplifications or idealized assumptions that are part of the theory by Ernst and Merchant.
17. Hucks's plastomechanical theory is based on a volume element. Which stresses does it include and what are the interdependencies between these stresses?
18. What (qualitative) influence does the difference between the friction angle and the rake angle have on the shear angle according to the shear angle relationships defined by Ernst/Merchant and Hucks?
19. On that basis, what conclusions can be drawn if the shear angle increases?

20. Which methods are used to measure the shear stress?
21. What is the isothermal flow stress and what is the adiabatic flow stress?
22. Explain Atlán's method of reverse simulation for the determination of the flow curve.
23. Explain the decomposition principle for the determination of the torque and the feed force in drilling processes.
24. In drilling from the solid, the torque is a result of the cutting force F_c and the radius r_c that is assumed to be the point of action of the force F_c . Why does r_c depend on the workpiece material?
25. How can the milling force components that are in a fixed position within the room and towards the cutting part be converted into each other using equations?
26. Use the shear angle relationship by Ernst/Merchant and the flow criterion according to Tresca to calculate the tangential force $F_{T\phi}$ in the shear plane and the corresponding cutting force F_c for an orthogonal cut with a Ck45N workpiece. given: $k_f = 774 \text{ MPa}$, $\gamma = -6^\circ$, $h = 0.2 \text{ mm}$, $b = 2 \text{ mm}$, $\mu = 0.2$

References

- [ALS01] Altan, T.; Shatla, M.; Kerk, C.: Process modeling in machining—part I—determination of flow stress data. *J. Mach. Tools Manufacture* **41**, 1511 (2001)
- [BEN03] Ben Amor, R.: Thermomechanische Wirkmechanismen und Spanbildung bei der Hochgeschwindigkeits-zerspantung [Thermomechanical effect mechanisms and chip formation in high speed cutting]. Dr.-Ing. Diss. University of Hannover (2003)
- [BUS91] Bussmann, W.: Formfehleranalyse beim Planfräsen gehärteter Bauteile [Form errors at surface milling of hardened parts]. Dr.-Ing. Diss. University of Hannover (1991)
- [DEN92] Denkena, B.: Verschleißverhalten von Schneidkeramik bei instationärer Belastung [Wear behavior of cutting ceramics under transient loads]. Dr.-Ing. Diss. University of Hannover (1992)
- [DIN6584] Deutsches Institut für Normung/German Institute for Standardization (ed.): *DIN 6584: Begriffe der Zerspantechnik; Kräfte Energie, Arbeit, Leistungen/Terms of the cutting technique; forces, energy, work, power.* (Beuth, Berlin 1982)
- [DOE86] Doege, E., Meyer-Nolkemper, H.: *Fließkurvenatlas metallischer Werkstoffe* [Flow charts of metallic materials]. Hanser, München, Wien (1986)
- [DUB94] Dubbel.: *Handbook of Mechanical Engineering*, Chapter K. Springer, London (1994)
- [ELM04] El-Magd, E., Treppmann, C.: Stoffgesetze für hohe Dehngeschwindigkeiten [Material laws for high strain rates]. In: Tönshoff, H.K.; Hollmann, F. (eds.): *Spanen metallischer Werkstoffe mit hohen Geschwindigkeiten* Wiley-VCH, Weinheim (2004)
- [ERN41] Ernst, H.J., Merchant M.E.: Chip formation, friction and finish. *Trans. ASME* **29**, p. 299 (1941)
- [HUC54] Hucks, H.: *Zerspanungskräfte und Werkstoffmechanik. Fortschrittliche Fertigung*

- und moderne Werkzeugmaschinen [Cutting forces and material mechanics, Advanced manufacturing and modern machine tools]. 7. Aachener Werkzeugmaschinen Kolloquium/7th Aachen Machine Tool Colloquium (Essen), pp. 73–80 (1954)
- [ISO3002-4] International Standard Organisation (ed.): ISO 3002-4: basic quantities in cutting and grinding—Part 4. Forces, Energy, Power (1984)
- [JOC85] Johnson, G.R., Cook, W.H.: Fracture characteristics of three metals subjected to various strains, strain rates, temperatures and pressures. *Eng. Fract. Mech.* 21(1), pp. 31–45 (1985)
- [JOC83] Johnson, G.R., Cook, W.H.: A constitutive model and data for metals subjected to large strains, high strain rates and high temperatures. 7th international symposium on ballistics, The Hague (1983)
- [KAT57] Kattwinkel, W.: Untersuchungen an Schneiden spanender Werkzeuge mit Hilfe der Spannungsoptik [Investigations on cutting edges of tools by photoelasticity]. *Industrie-Anzeiger* 36, pp 29–36 (1957)
- [KIE54] Kienzle, O.: Einfluss der Wärmebehandlung von Stählen auf die Hauptschnittkraft beim Drehen [Influence of heat treatment of steels on the cutting force in turning]. *Stahl und Eisen* 74, pp. 530–551 (1954)
- [KIS09] Kistler Instrumente A.G, Winterthur/Switzerland (ed.): Zerspankraftmessung [Cutting force measurement]. Company leaflet (2009)
- [LAP02] Lapp, Chr.: Indirekte Erfassung und Regelung von Bearbeitungskräften an direkt getriebenen Vorschubeinheiten [Indirect identification and control at direct driven feed units]. Dr.-Ing. Diss. University of Hannover (2002)
- [OXL89] Oxley, P.L.B.: *Mechanics of Machining: an Analytical Approach to Assessing Machinability*. Halsted Press/Wiley, New York (1989)
- [SPA67] Spaans, C.: An exact method to determine the forces on the clearance plane. *CIRP Ann.* 15, 463–469 (1967)
- [UST60] Usui, E., Takeyama, H.: A Photoelastic Analysis of Machining Stress. *Trans. ASME J. Eng. Ind.* 82, 303–308 (1960)
- [ZIE95] Ziebel, F.: Mechanische und thermische Belastung von Zerspanwerkzeugen [Mechanical and thermal loads on cutting tools]. Dr.-Ing. Diss. University of Hannover (1995)
- [ZOD67] Zorev, N.N., Del. G.D. et al.: Spannungszustand in der Schnittzone [Stress state in the chip formation zone]. *Ann. CIRP* 14, 337–346 (1967)

Chapter 5

Energy Conversion and Temperature

5.1 Conversion Effects

Mechanical energy is introduced to the cutting process.

$$P_c = k_c \cdot Q_w \tag{5.1}$$

The power from the feed motion is negligible and not considered here (see Chap. 4). The mentioned cutting power is converted to thermal or potential energy by the following physical effects:

- plastic deformation, shearing,
- friction,
- material separation,
- change of material flow,
- residual stresses.

Below, these power fractions are referred to the removal rate or equivalently, the energy fractions to the removed material volume. In an energy balance the specific energy k_c equals the sum of the energy fractions of the plastic deformation k_ϕ , of the friction k_γ , of the material separation k_T , of the change of material flow k_M and of the spring energy or the energy by residual stresses k_{el} .

$$k_c = k_\phi + k_\gamma + k_T + k_M + k_{el} \tag{5.2}$$

The energy components are estimated qualitatively so that their main influences are apparent. For this purpose the shear plane model is used, which can be described analytically. This model postulates that the total plastic deformation takes place only in the shear plane. With the preconditions described in Sect. 4.4 it implies that a constant shear stress τ_ϕ acts in the shear area A_ϕ . The shear power referring to on the material removal rate is thus,

$$k_\phi = \frac{\tau_\phi \cdot A_\phi \cdot v_\phi}{Q_w} = \tau_\phi \cdot \frac{\cos \gamma}{\sin \phi \cos(\phi - \gamma)} \tag{5.3}$$

For the friction fraction only the energy conversion on the rake face is considered. Amontons' law is assumed with $\mu = \tan \rho$ (μ : friction coefficient, ρ : friction angle). The tangential force, which acts on the rake face according to Sect. 4.4.1 is:

$$F_{T\gamma} = \tau_\phi \cdot b \cdot h \cdot \frac{[\cos(\phi + \rho - \gamma) \cdot (\sin \phi)]}{\sin \rho} \quad (5.4)$$

and thus the specific friction energy is

$$k_\gamma = \tau_\phi \cdot \frac{[\cos(\phi + \rho - \gamma) \cdot (\sin \phi)]}{\sin \rho} \quad (5.5)$$

For the material separation, i.e. generating new surfaces, surface energy is applied. This energy follows from the surface tension T of the removed material against the surrounding medium. The energy is proportional to the area of the generated surface. The area related to the unit of time of these surfaces at the chip and at the workpiece is

$$\dot{A}_w = b \cdot v_c \quad (5.6)$$

and

$$\dot{A}_{ch} = b \cdot \frac{v_c}{\lambda_h} \quad (5.7)$$

It follows from there

$$k_T = \frac{\left(b \cdot \frac{v_c}{\lambda_h} + b \cdot v_c\right) \cdot T}{Q_w} = \left(1 + \frac{1}{\lambda_h}\right) \cdot \frac{T}{h} \quad (5.8)$$

Furthermore, there is an energy fraction from the change of the material flow. To determine this fraction the chip formation is seen as a pipe flow, which is deflected by the rake face. The impulse on the rake face is then

$$\vec{F}_M \cdot \Delta t = m \cdot \Delta \vec{v}_\phi \quad (5.9)$$

with the impulse force F_M in the direction of the shear speed v_ϕ and the time increment Δt , the mass m and the density ρ (attention: ρ is the density here and not the friction angle). Thus follows

$$\vec{F}_M = \rho \cdot Q_w \cdot \vec{v}_\phi \quad (5.10)$$

and

$$k_M = \frac{F_M \cdot v_\phi}{Q_w} \rho \cdot v_\phi^2 \quad (5.11)$$

or

$$k_M = \rho \cdot \frac{\cos^2 \gamma}{\cos^2(\phi - \gamma)} v_c^2 \quad (5.12)$$

As a final point, the energy fraction has to be estimated, which is stored as spring energy k_{el} —a consequence of residual stresses. This fraction is stored as elastic energy (potential energy) in the surface zone of the workpiece as well as in the chip.

An estimation of the stored maximal energy in the chip and in the workpiece can be achieved via the yield stress of the material. As a consequence it is simply assumed that

- the residual stresses cannot exceed the yield stress, because otherwise they are cut down by plastic flow
- for the load release, Hook’s law is applied and
- the estimation is done for the uniaxial state of stress.

Figure 5.1 shows the stress–strain curve for the uniaxial elastic–plastic state and the specific spring energy k_{el} .

The maximal energy stored in the chip and in the surface domain of the workpiece per volume unit is then

$$k_{el} = \frac{1}{2} \frac{k_f^2}{E} \tag{5.13}$$

The order of magnitude for the energy fractions shall be determined by a numerical example for common conditions: Normalized carbon steel is machined by carbide tools. With that the following parameters are given:

$E = 210,000 \text{ N/mm}^2$, $\rho = 7.8 \text{ g/cm}^3$, $k_f = 2 \tau_\phi = 660 \text{ N/mm}^2$, $\mu = 0.2$, $T = 40 \text{ mN/m}$

The cutting conditions should be: $Q_w = 250 \text{ cm}^3/\text{min}$ with $v_c = 250 \text{ m/min}$, $h = 0.3 \text{ mm}$ and $b = 3.3 \text{ mm}$

Fig. 5.1 Stress-strain curve

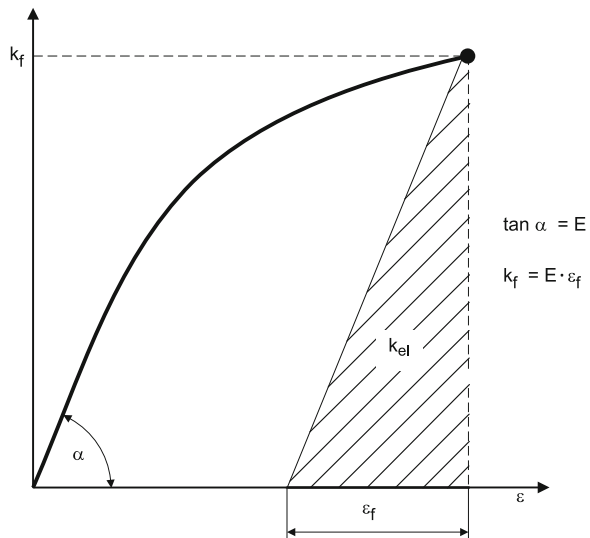
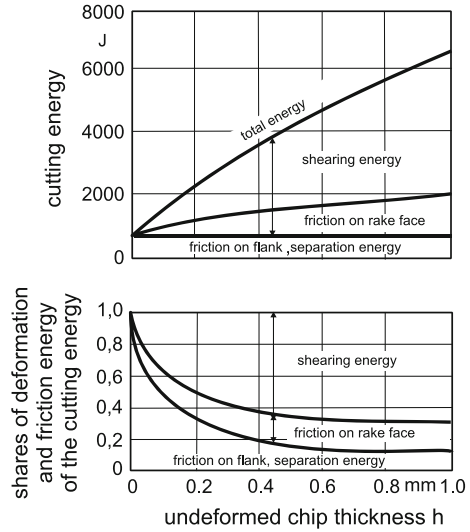


Fig. 5.2 Fractions of the cutting energy [VIE53]



The chip compression ratio was observed at $\lambda = 2.0$. The rake angle was $\gamma = 6^\circ$.

From Eq. 2.9 follows for $\lambda_h = \lambda$

$$\arctan \phi = \frac{\cos \gamma}{\lambda - \sin \gamma} \quad (2.9a)$$

Thus, the following energy fractions can be determined:

$$k_\phi = 760 \text{ N/mm}^2, \quad k_\gamma = 658 \text{ N/mm}^2, \quad k_T = 134 \times 10^{-3} \text{ N/mm}^2, \\ k_M = 0.155 \text{ N/mm}^2, \quad k_{el} = 1.4 \text{ N/mm}^2$$

This energy analysis leads to a numerical result that is approximately 40 % lower than that for the Kienzle formula (see Kienzle equation in Chap. 4), which is due to the different approaches. But it can be seen that the fractions k_T , k_M and k_{el} for common cutting conditions are by orders of magnitude smaller than the fractions k_ϕ and k_γ . However, k_T and k_M gain weight considerably in ultra-precision cutting with undeformed chip thicknesses of $h \approx 10 \text{ nm}$ or in high speed cutting with cutting speeds of $v_c \approx 10^4 \text{ m/min}$. Previous investigations by Vierge show results in similar fractions in the order of magnitude (Fig. 5.2).

5.2 Heat Flow

The cutting power, which is transformed by the dominant effects (k_ϕ and k_γ) is generally removed by heat. Smaller fractions are stored as elastic energy (potential energy by residual stresses) in the surface layers of the workpiece and in the chip.

The removed heat is distributed by the chip, by the workpiece and by the environment (convection). The heat flux in the environment is low, unless liquid coolant is applied. The distribution of the heat fluxes is strongly dependent on the cutting speed (Fig. 5.3).

This is due to the “solid body convection”, to the heat removed with the chip and to the limited heat conduction into the tool and the workpiece. The model in Fig. 5.4 is applied to estimate the fractions of the heat flux. The heat flux into the tool is small if the tool is permanently engaged, because of the high temperature level in the tool. The heat flux into the workpiece is dependent on its heat conductivity and on the relative speed between tool and workpiece, i.e. of the cutting speed.

The model in Fig. 5.4 is based on the assumption of a stationary process. The heat source $k_c Q_w$ is in the chip generating zone. Three fluxes flow from the source volume q_1 into the tool, q_2 into the workpiece and q_3 into the chip. A fourth flux into the coolant and the environment is neglected here. The partial fluxes q_1 and q_2 are based on heat conduction. They follow the general equation

$$q_i = \lambda \cdot \Delta x \cdot \left(\frac{1}{\delta}\right) \cdot \text{“1”} \cdot (\theta_0 - \theta_i) \tag{5.14}$$

where λ is the heat conductivity, $\Delta x \cdot \text{“1”}$ the area which the heat flux is lead on to (the extension perpendicular to the flux shall be “1”), with the width of the heated layer δ , the temperatures in the source volume θ_0 and in the adjoining body θ_1 . The heat flux with the chip is based on convection, it is

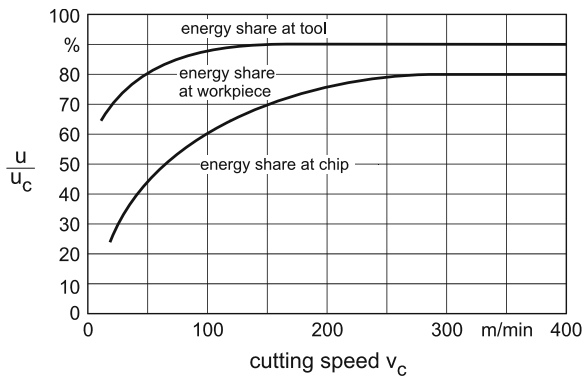
$$q_3 = c_p \cdot \rho \cdot Q_w \cdot \theta_0 \tag{5.15}$$

with c_p as heat capacity, ρ as density and θ_0 as the temperature of the source volume, from which the heat fluxes q_1 and q_2 flow in the adjoining bodies and whose contact surfaces have the temperatures θ_1 and θ_2 .

Thus are

$$q_1 = \lambda_1 \cdot \Delta x_1 \cdot \frac{1}{\delta_1} \cdot \text{“1”} \cdot (\theta_0 - \theta_1) \tag{5.14a}$$

Fig. 5.3 Energy distribution in the cutting region



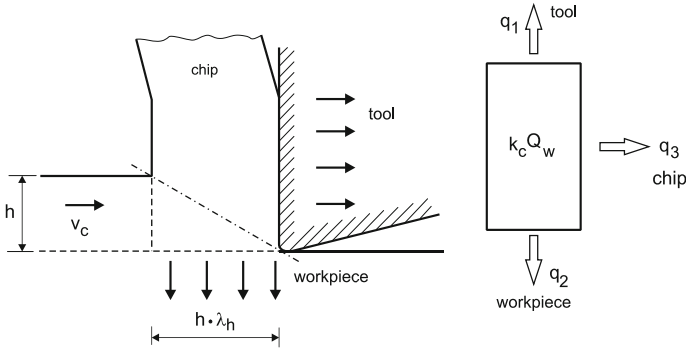


Fig. 5.4 Model of heat flux distribution

$$q_2 = \lambda_2 \cdot \Delta x_2 \cdot \frac{1}{\delta} \cdot \dots \cdot (\theta_0 - \theta_2) \tag{5.14b}$$

And finally following from the heat balance

$$k_c \cdot Q_w = q_1 + q_2 + q_3 \tag{5.16}$$

Some simplifications are carried out at this point. With modern cutting materials the cutting wedges heat up so strongly that there is practically no temperature gradient between the source volume and the cutting wedge, i.e. $\theta_1 = \theta_0$ and $q_1 = 0$. The undeformed cutting width is set for the heated layer, which is an assumption: $\Delta x_2 = \lambda_h \times h$.

So out of Eqs. 5.14 and 5.16 follows

$$\theta_0 = \frac{k_c}{c_p \cdot \rho + \lambda_2 \cdot \frac{\Delta x_2}{\delta \cdot Q_w}} \tag{5.17}$$

With practically common data for steel DIN C45N (AISI 1045)

$k_c = 2,500 \text{ N/mm}^2$, $v_c = 240 \text{ m/min}$, $\lambda_h = 1.5$, $c_p = 0.465 \times 10^3 \text{ J/(kg K)}$, $\rho = 7.8 \text{ g/cm}^3$ and $\lambda_2 = 50 \text{ J/(K m s)}$, $\delta = 0.1 \cdot h$, $h = 0.1 \text{ mm}$ results

$$\theta_0 = \frac{2,500 \times 10^6}{3.63 \times 10^6 + 1.25 \times 10^6} = 512 \text{ K} \tag{5.18}$$

that means 512 K higher than environmental temperature.

It can be seen from Eq. 5.18 that the fraction of the total cutting power $k_c \cdot Q_w = 1,000 \text{ J/s}$ —which flows into the chip by “solid body convection”—is bigger than the flux, which flows into the workpiece. For this example, it is

$$q_3 = c_p \cdot \rho \cdot Q_w \cdot \theta_0 = 744 \text{ J/s} \tag{5.19}$$

and accordingly the fraction, which flows into the workpiece $q_2 = 256 \text{ J/s}$. However, the assumption of the layer thickness in Eq. 5.14 is very critical. This value strongly influences the calculation. Therefore, the consideration can only

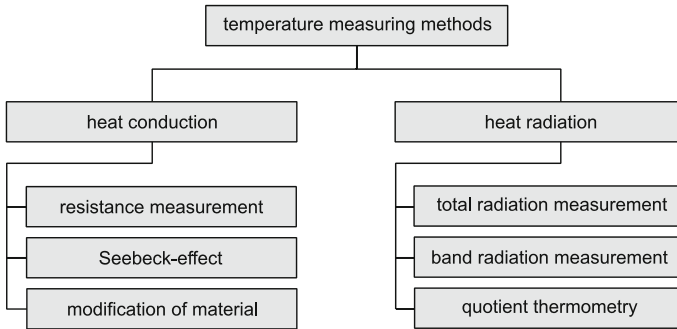


Fig. 5.5 Methods of temperature measurement

give the tendency of the relationship. But the energy partition correlates to Fig. 5.3 (in Fig. 5.3 the related energy is given by u), at least approximately.

5.3 Temperatures of Cutting Wedge and Workpiece

The temperatures in the cutting wedge are essential for the wear. Oxidation and diffusion, which partly cause the tool wear, are strongly accelerated at higher temperatures. The temperature distribution in the surface layers of the workpiece is decisive for surface integrity effects such as changes of hardness, residual stresses and alterations of the material structure.

5.3.1 Temperature Measurement

Therefore, various temperature measuring methods have been developed, which nevertheless all have process-specific disadvantages. Measuring is difficult due to small dimensions of the heated zone (only tenth of a mm^2), high temperatures (ca. $500\text{ }^\circ\text{C}$), steep temperature gradients ($d\vartheta/ds > 500\text{ K/mm}$), high mechanical load (more than $1,000\text{ MPa}$) and high speed of heating up ($d\vartheta/dt \geq 10^6\text{ K/s}$).

Figure 5.5 gives an overview of the currently applied measuring methods. Following the kind of heat transformation at the measuring device or sensor, it is possible to distinguish between heat conduction and heat radiation. The different methods have diverse properties, which make them suitable for different applications. Table 5.1 gives a comparison of the most important methods under different criteria.

The measurement of *electric resistance* is based on the effect that the electric conductivity of a conducting medium or of semiconductors changes with temperature and pressure. Metals (conducting media) change their conductivity almost

Table 5.1 Comparison of temperature measuring methods

	Resistance thermometer	Thermocouple	Dynamic thermo-couple	Thermal colors	One-color pyrometer	Two-color pyrometer
Temperature range	Molten metal	0–3.000 °C	Molten material	ϑ_{trans}	20–5.000 °C	0–5.000 °C
Spatial resolution	500 pm	>500 μm 10 μm	Contact averaging	100 Mm	5 μm	20 μm
Temporal resolution	2 ms	100 ms	–	Low	ms– μs	ms– μs
Manageability	Simple	Simple	Simple	Simple-medium	Difficult	Difficult
Major error influence	Material damage	Contacts	Contacts, dynamics of measurement	Influence of time	Emission coefficient	Gray body supposed
Cost	Low-medium	Low	Low	Low	Medium–high	Medium–high

linearly with the temperature coefficient α_θ and the pressure coefficient α_p and only if limited temperature or pressure domains are considered, even though the sensitivity to pressure is much less than to temperature.

$$\frac{\Delta R}{R} = \alpha_p \cdot \Delta p + \alpha_\theta \cdot \Delta \theta \quad (5.20)$$

Practically, α_p can be neglected for Platinum and Nickel. Thus, it can be said

$$\theta = \theta_{20} + (R/R_{20} - 1)/\alpha_{20} \quad (5.21)$$

with the measuring temperature θ , the room temperature θ_{20} , the measured resistance R , the resistance at room temperature R_{20} and the coefficient of resistance for room temperature α_{20} . For larger temperature ranges the coefficient has to be adapted. The linear dependency is not valid for semiconducting materials (thermistors).

Basically, all metals can be applied to measuring by resistance. Noble metals are used to avoid disturbing oxidations, but above all Platinum is applied. Resistance thermometers based on Platinum can be used up to 900°. Commercially they are available as wire from 0.9 to 4 mm. Their time constants are in the domain of 2–20 s for these dimensions and because of their size and their large time constants, such elements are only applied for nearly stationary cutting processes. The disadvantage of long time constants can almost be rectified, if thin foils or isolated layers are applied as resistance elements; obviously because the heating time and the time constant depend on the cross section of the heat conducting element.

To determine the temperature distribution in the contact zones between workpiece material and cutting material sensors in thin film technology were developed [TÖN94]. The thickness of the sensor is 0.2 μm , the width is 20 μm . To avoid short circuit with the flowing chip the current conducting layers are coated with a protective Al_2O_3 layer of 2 μm thickness. It is possible to measure the

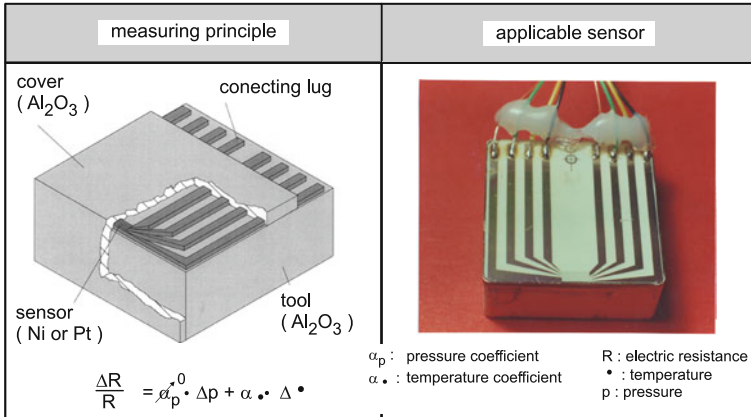


Fig. 5.6 Thin film sensor

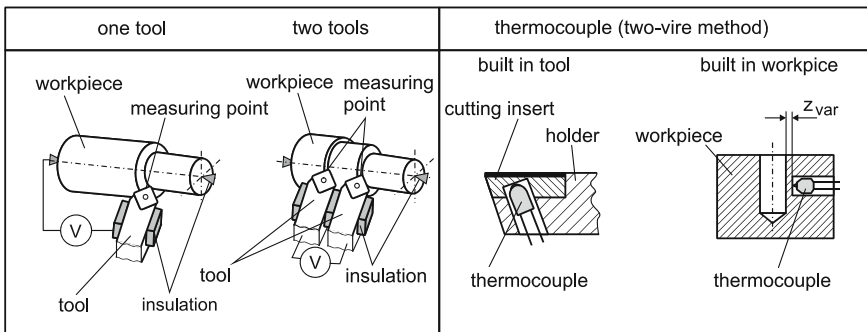


Fig. 5.7 Application of the thermocouple principle

temperature distribution over the rake face or the flank by arranging several resistance elements in a dense pattern during cutting. The measuring principle and a ready sensor with elements on the rake face are shown in Fig. 5.6.

Thermocouple elements work according to the Seebeck effect. The principle can be identified in Fig. 5.7. The bases of the thermo electricity are free movable electrons, which are able to drop off the surface of a metal, if their kinetic energy is at least equal to the separating energy. This energy depends on the material. Electrons pass over, if the surfaces of two materials touch each other closely. Thus, a contact voltage is generated whose magnitude is temperature dependent. A thermocouple has two of these touching points. If there is no temperature difference between these points, these contact voltages even out. If these touching points have different temperatures, a thermo current flows as a consequence of the thermo voltage. Its magnitude depends on the circuit resistance as well as on the involved materials, i.e. workpiece and tool material, and on the temperature difference. For limited measuring ranges the following thermo voltage is approximately

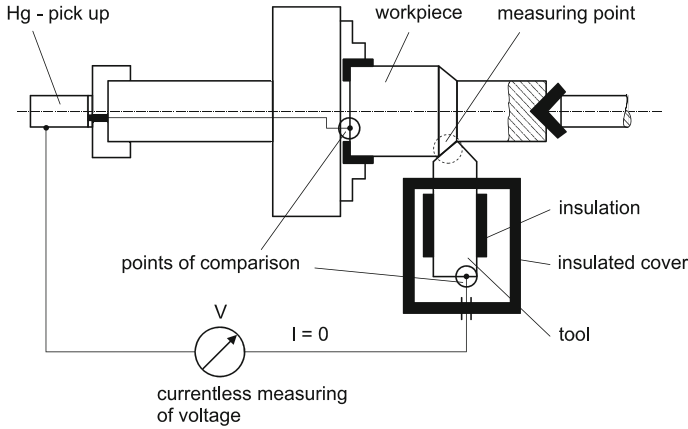


Fig. 5.8 Temperature measurement, single-tool method [OPI52]

$$U = k \cdot (\theta_1 - \theta_0) \quad (5.22)$$

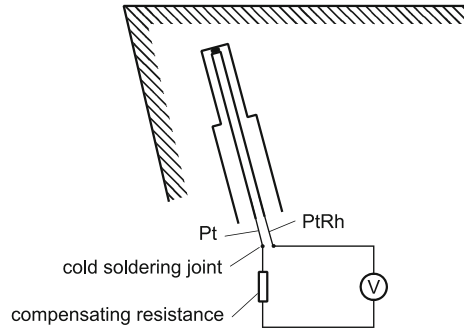
with k as Seebeck coefficient, which is dependent on the material matching and on the average working temperature. Typical material combinations are Pt and Pt/Rh with $k = 10 \mu\text{V/K}$ or NiCr and Ni with $40 \mu\text{V/K}$. Some applications of the Seebeck effect are shown in Fig. 5.7.

The single-tool method uses tool and workpiece directly as measuring elements. Thus, the two materials form the thermocouple. As the Seebeck coefficient of these metals is unknown, the sensitivity has to be determined by calibration, preferably in the temperature measuring range. Figure 5.8 shows a configuration in a turning machine.

The main difficulties with the single-tool method is the insulation of the potential carrying parts conducting the thermo current against the surrounding and the calibration of the thermocouple [OPI52]. Characteristically the measuring method used for and according to the single-tool principle, delivers only an average temperature reading over the contact area. It is not possible to determine the kind of averaging. Another problem is that the calibration has to be made for every material combination. So, if new work material is investigated or if another cutting material is applied, the system has to be newly calibrated respectively.

The calibration necessity of every material combination and the problems of conducting the thermo voltage from the rotating part, have led to the development of the two-tool method. This means cutting with two tools of different cutting materials and under equal conditions Between the two tools, which is the thermocouple, the thermo voltage is measured. Further variants of the thermo electric principle work with discrete thermocouples, which are built into the tool (Fig. 5.9) or the workpiece. It is also possible to place isolated wires in the workpiece. The wire then represents the thermocouple together with the chip or the workpiece. The defined positioning of the thermocouple makes it possible to determine the temperature distribution field in the tool or the workpiece.

Fig. 5.9 Thermocouple in the turning tool



The phenomenon that almost all materials change their structure with defined temperatures and by that, also their physical and chemical properties is the basis of further temperature measuring methods (*structure conversion*). The energy, which is necessary for these structural alterations, is taken from or given to the environment. Thus, temperatures have to affect certain time durations onto the materials to ensure reproducible values by the energy transport. Normally, short time temperature changes are not sufficiently captured and consequently, these measurements are limited to stationary temperature fields. Temperature sensitive colors, liquid crystals and thermo graphic chinks are available commercially. In the meantime, these transformable materials have been developed for a temperature range up to 2,000 °C [DAV07].

The energy radiated by a body is a measure of its temperature (*heat radiation*). According to Planck's law the radiated power per unit of area depends on the wavelength of the radiation λ and the temperature of the radiating surface. A "black body" radiates the energy per unit of area and per wavelength $E_{S\lambda}$, according to Wien's law (Fig. 5.10):

$$E_{S\lambda} = \sigma \cdot \theta^4 \quad (5.23)$$

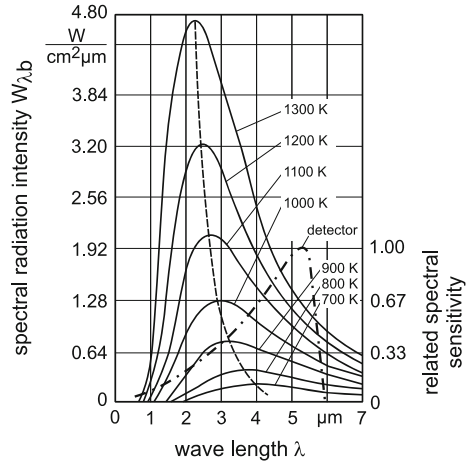
In Eq. 5.23 $\sigma = 5.67 \times 10^{-8} \text{ W/m}^2 \text{ K}^4$ is the radiation coefficient. Real bodies emit less power than a black body. That means the emission parameter ε has to be taken into account:

$$E = \varepsilon \cdot E_{S\lambda} \quad (5.24)$$

The difficulty is finding out the emission parameter, which has to be known for all bodies participating in the process.

Radiation thermometers are known as pyrometers. With a *total radiation thermometer*, the maximum radiation power over a large receiving cone is received in addition to the overall wavelengths. They can be applied to a wide range of temperatures varying between 200 °C and up to 1,800 °C. *Band radiation thermometers* receive radiation only over a defined range of wavelengths. They are often applied to temperature measurements for cutting processes, because they are

Fig. 5.10 Emitted power and temperature



easy to handle. *Quotient thermometers* receive radiations of two wavelengths and are thus able to eliminate the influence of the material dependent emission parameter with the help of setting the quotient of the received radiation energies and thus cancelling down the emission parameter. This implies that the emission parameter is independent of the wavelength. However, by using only two wavelengths the radiation energy is small and thus the sensitivity of the measurement is limited. This method is also used for temperature measurements of cutting processes.

The principle of typical radiation thermometers is shown in Fig. 5.11. Such temperature measurements have several advantages. The measurement is very fast—it takes 1–10 μs depending on the device. The possible measuring range is large. It lies between 300 and 3,500 °C. The measuring object is not influenced and temperatures of moving objects can also be determined. It is a disadvantage, however, that the emission parameter depends on the material, on its surface structure, on the received wavelength and on the temperature itself.

Nowadays, infrared detectors (photo-resistance (photoresistance with an upper cut-off wavelength)) are often used as radiation receivers. Figure 5.12 schematically shows a measuring device for infrared thermography.

It is possible to get moving pictures during cutting with the help of this method. Figure 5.13 is an infrared thermo-gram of the band chip generation during the orthogonal turning of AISI 1045 (DIN C45E). In 1933, Schwerd and Kramer from Hannover had already made the first measurements using this method to determine temperature fields when cutting [SCH33]. It is possible to overcome the problem of the temperature dependency of emission parameters with pointwise measurements, if the possible error is eliminated by calibration [DEN92].

Fig. 5.11 Principle of radiation thermometers [DAV07]

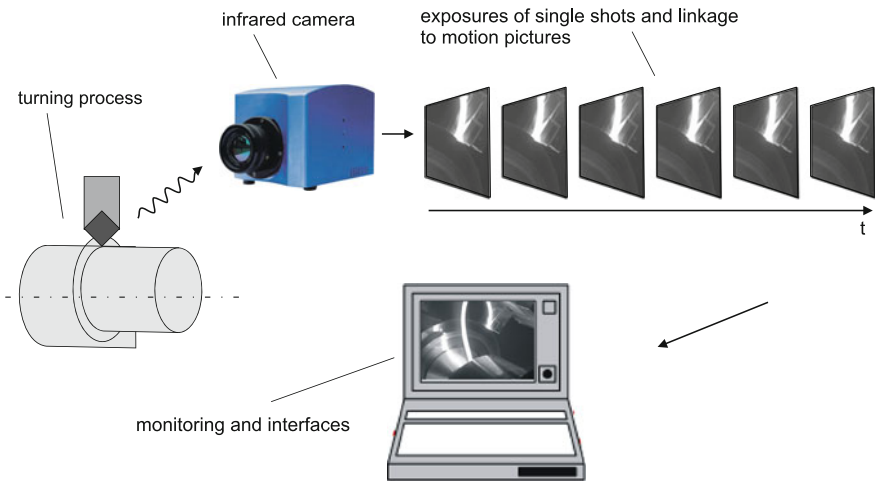
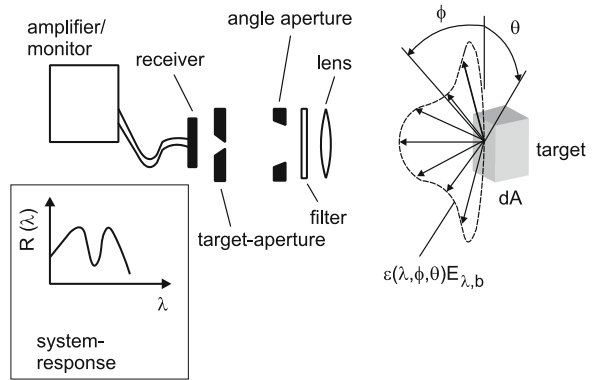


Fig. 5.12 Measuring device for infrared thermography for a cutting process

5.3.2 Temperature Fields

With the method shown in Fig. 5.12 temperatures on the rake face of a tool can be measured in interrupted cutting. It is possible to calculate the rake face temperature with sufficient accuracy from the cooling curves and by using a model of transient temperature distribution when the tool leaves the workpiece. Figure 5.14 shows temperature–time curves for turning processes with different ceramic cutting materials. Depending on the heat conductivity different exit temperatures are calculated.

The extension of the heated zone, as well as the temperature distribution in this domain and the temperature maximum are dependent on the properties of the cutting material, on the cutting conditions and due to different chip formation mechanisms, on the workpiece material. A distribution according to Fig. 5.15

Fig. 5.13 Infrared image cutting steel AISI 1045 (DIN C45E)

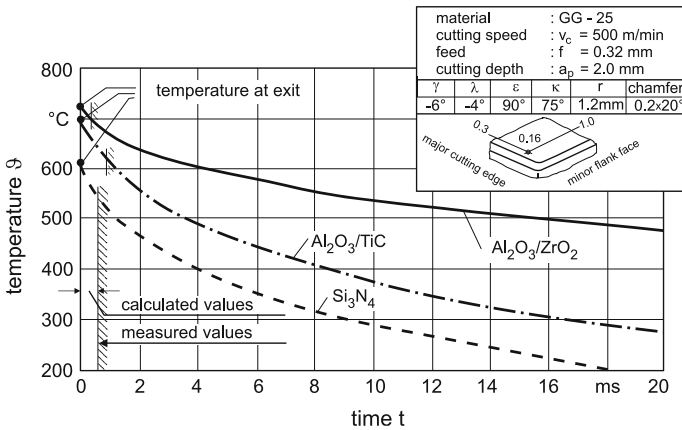
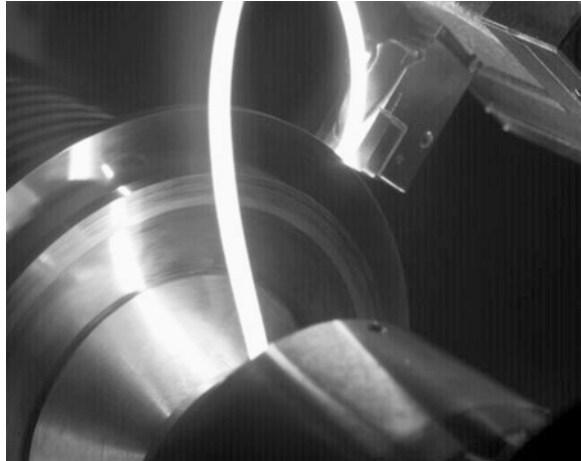


Fig. 5.14 Temperature—time curves for milling with different ceramic tools [DEN92]

results with an $\text{Al}_2\text{O}_3/\text{ZrO}_2$ -ceramic tool on grey cast iron. The temperature maximum is in the middle of the contact zone between tool and workpiece.

The influence of cutting speed and feed on the rake face temperature of different cutting ceramics can be seen in Fig. 5.15 for cast iron and in Fig. 5.16 for steel. The diagrams show that temperatures increase with the cutting speed and the feed. For the dispersion ceramic ($\text{Al}_2\text{O}_3/\text{ZrO}_2$) the temperature grows by an average of 100 K for 200 m/min up to 800 m/min speed difference, by 150 K for 0.1 mm up to 0.32 mm feed difference.

For the mixed ceramic and the Silicon–Nitride ceramic the temperatures are considerably lower as already shown in Fig. 5.13.

The comparison of grey cast iron with temperable steel shows a temperature increase of 50–100 K dependent on the process parameters, which can be seen in

Fig. 5.15 Temperature distribution on the rake face of a $\text{Al}_2\text{O}_3/\text{ZrO}_2$ -ceramic [DEN92]

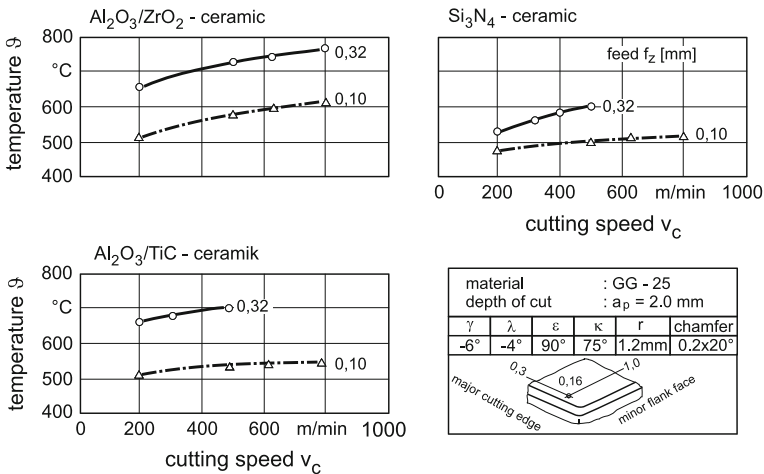
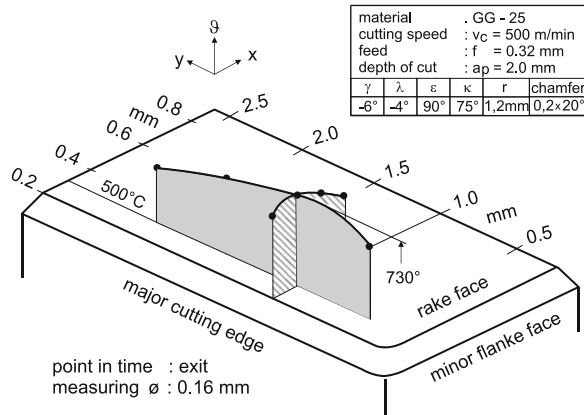


Fig. 5.16 Exit temperatures for milling of cast iron [DEN92]

Figs. 5.16 and 5.17. The temperature raise for Si_3N_4 -ceramic is remarkable, which is an explanation why this kind of ceramic is not suitable for steel. Very high wear rates follow the high thermal loading.

The temperature distribution on the minor flank face of the tool could be taken by an IR-camera [BAR88]. The minor flank face is always visible, so there is sufficient time to take a total image (Fig. 5.18). The influence of cutting speed of feed and of workpiece material on the temperature field at the minor flank face can be taken from Fig. 5.19. When comparing Figs. 5.17 and 5.19, it has to be observed that feeds are different.

Figure 5.20 shows the temperature distribution in a tungsten carbide tool. The temperature field on the rake face as well as in planes perpendicular and parallel to

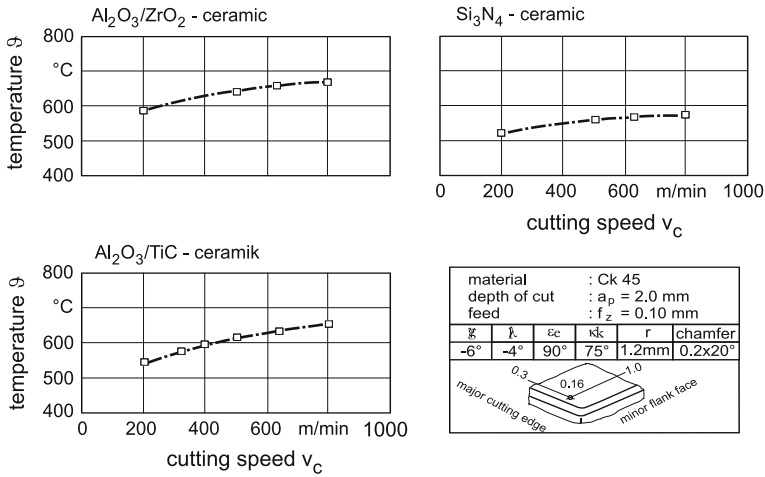


Fig. 5.17 Exit temperatures for milling of steel [DEN92]

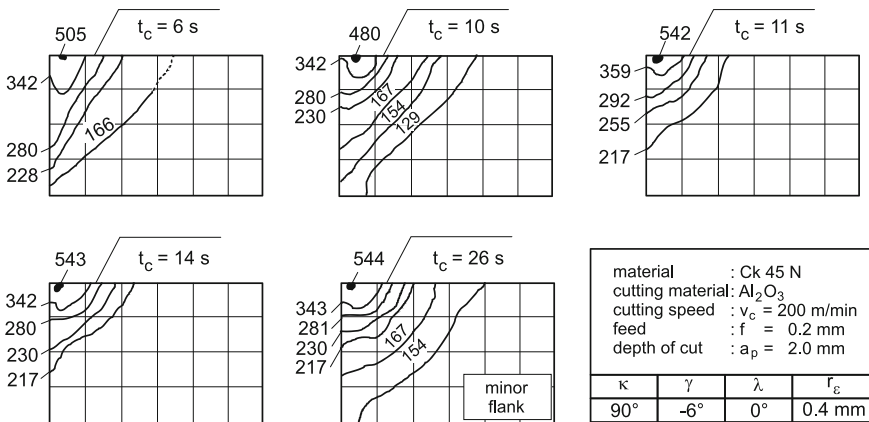


Fig. 5.18 Distribution of isotherms on the minor flank face when cutting steel [BAR88]

the major cutting edge, was determined by introducing thermocouples in the holes of the tool [KUE56].

The highest temperatures are generated on the rake face of a cutting wedge, as can be seen in Fig. 5.20. This is caused by friction between rake face and chip. Since these temperatures are of great importance for the wear behavior of the tool, an analytical estimation is introduced, which shall show the most important influencing variables [BAE94; BEN03].

The cutting wedge is considered as a unidirectional infinite body. According to Baehr, the temperature of the rake face θ_γ is

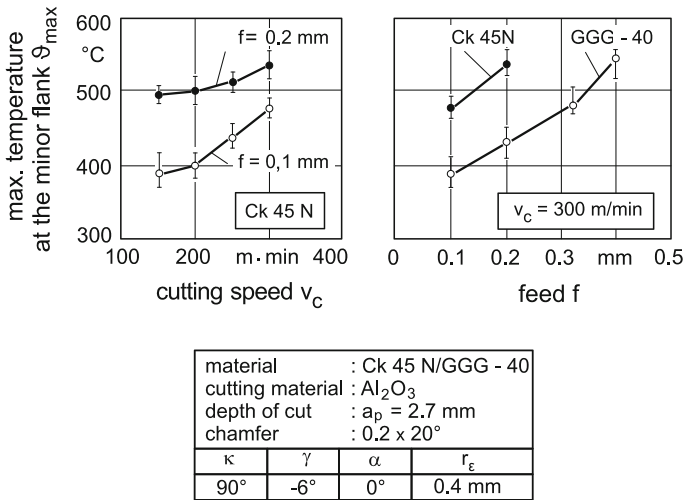


Fig. 5.19 Maximum temperature on the minor flank face [BAR88]

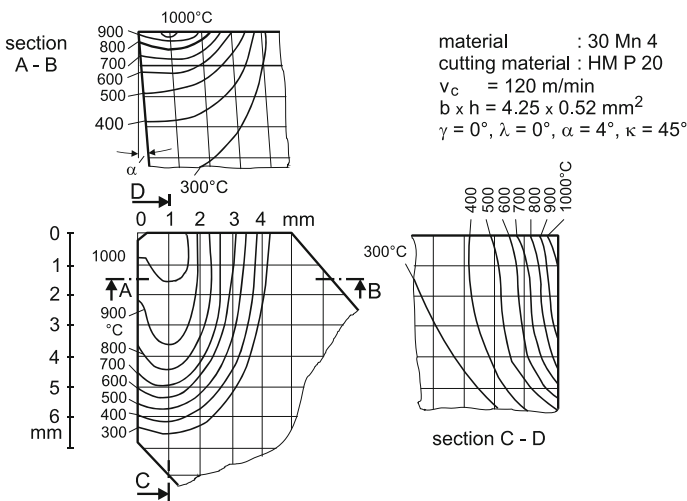


Fig. 5.20 Temperature field in a carbide turning tool [KÜS56]

$$\theta_\gamma = \theta_0 + \frac{\dot{q}}{b} \cdot \frac{2}{\sqrt{\pi}} \sqrt{t} \tag{5.25}$$

with the heat flux density \dot{q} , the heat penetration coefficient b and the contact time t . The heat flux density follows from the contact length CL and the chip width “1”, the chip velocity v_{ch} and the tangential force on the rake face $F_{T\gamma}$.

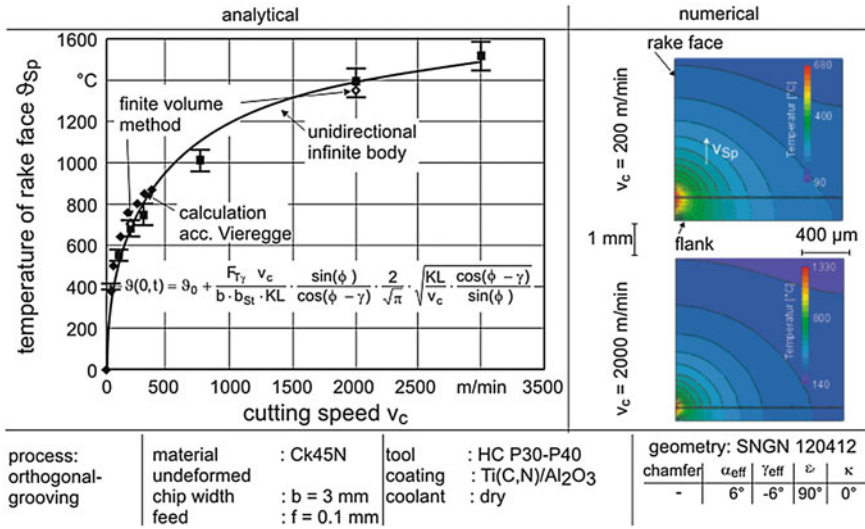


Fig. 5.21 Rake face temperature and cutting speed (acc. Ben Amor)

$$\dot{q} = \frac{F_{T\gamma} \cdot v_{ch}}{1 \cdot CL} \tag{5.26}$$

Applying the derivation of Sect. 5.1, the maximal rake face temperature ϑ_γ finally results to

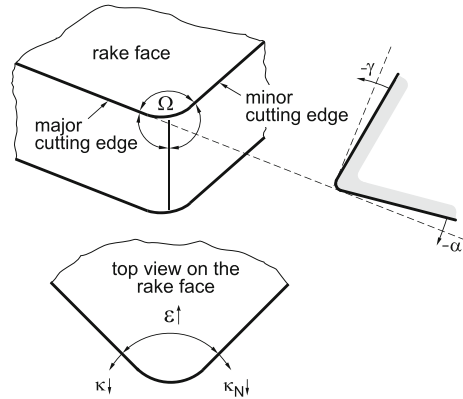
$$\theta_\gamma = \theta_0 + \frac{F_{T\gamma} \cdot v_c}{b \cdot 1 \cdot CL} \cdot \frac{\sin \phi}{\cos(\phi - \gamma)} \cdot \frac{2}{\sqrt{\pi}} \cdot \sqrt{\frac{CL}{v_c} \cdot \frac{\cos(\phi - \lambda)}{\sin \phi}} \tag{5.27}$$

The dependency of the rake face temperature on the cutting speed according to Eq. 5.27 is shown in Fig. 5.21 [BEN03].

5.4 Optimization of the Cutting Wedge

The wedges of cutting tools have to be matched with the specific application. This is particularly true for the angles of the wedge. The consideration of the solid angle Ω , which is formed by the rake face, the major and the minor flank face, gives an indication for the optimization of the cutting wedge (Fig. 5.22). For thermal and mechanical reasons, this solid angle is to be maximized so as to obtain a robust and stable cutting edge, which in addition, rapidly dissipates the heat from the cutting wedge via the wide solid angle and thus decreases the temperature level of the tool. A large solid angle Ω is reached by decreasing the rake angle γ , the flank (clearance) angle α and the cutting edge angle κ and by increasing the tool included angle ε , respectively. But there are limits by counter-directional influences:

Fig. 5.22 Optimizing the cutting wedge



- rake angle γ : decreasing γ increases the forces and the necessary power.
- flank (clearance) angle α : α should not fall below a minimum value of $\alpha_{\min} = 5^\circ\text{--}6^\circ$, otherwise the friction forces at the flank increase considerably and leads to higher power, which means higher temperatures in the tool due to the same reason.
- cutting edge angle κ : κ is usually chosen no lower than 45° —apart from increasing passive forces—the power determining cutting force gets higher for the same cutting cross section, because the undeformed chip thickness decreases.
- tool included angle ε : ε should be as large as possible with the application conditioned cutting edge position. The minor cutting edge angle κ_N may not fall below a minimum value, because of cutting stability to prevent chatter.

These limit considerations show, that a cutting wedge can be optimized according to its application (roughing or finishing, continuous or interrupted cut, predominantly thermal or mechanical load). Thus representing a compromise between favorable heat flux and large mechanical load capacity, a great variety of producible workpiece is shaped with the help of a small tool included angle ε and low friction load by enough flank (clearance) angle α and minor flank angle α_N .

5.5 Questions

1. What energy conversions take place in the working space?
2. What zones of energy conversion have to be distinguished?
3. How can the energy fractions in these zones be determined if a 3-component dynamometer is applied?
4. How can the energy fraction by “frozen” elastic deformation (residual stresses) be estimated?
5. How does the heat flux out of the cutting zone occur?
6. Outline a scheme of the model of heat dissipation.

7. Mention some possibilities of temperature measurement and discuss them.
8. What is the Seebeck effect?
9. Explain the 2-tool method. What advantage does it offer compared to the 1-tool method?
10. Indicate an upper boundary for the chip temperature.
11. What does “solid body convection” mean?
12. Compare the surface temperature of a workpiece machined with high and low cutting speed. In which case is more energy per volume unit transformed? How can the temperature differences be explained?
13. Outline a scheme of the isothermal curves in the cutting wedge viewing on the orthogonal plane (orthogonal to cutting plane and to cutting edge) and in a plane parallel to the cutting edge plane in a distance of two times the undeformed chip thickness from the cutting edge.
14. Which are the main influences on the temperature in the cutting wedge?
15. What surfaces is the solid angle, which encloses the cutting wedge, determined by?
16. Which counter-directed influences determine the optimum cutting edge shape?
17. High speed cutting (HSC) is continuously gaining importance (see also [Chap. 9](#)). Aluminum alloys are machined with speeds till $v_c = 10,000$ m/min compared to $v_c = 3,000$ m/min for conventional machining.
 - a. What factor does the specific energy fraction for the change of flow direction of material increase by at this change of speed?
 - b. What influence do the determining values have?
 - c. Determine the ratio of the energy fractions for the change of direction of material flow and for material deformation in both speed domains

conv.:	$v_c = 3,000$ m/min	$\lambda_{h, \text{ conv.}} = 1.6$
	$v_f = 6,000$ mm/min	$k_{f, \text{ conv.}} = 155$ MPa
HSC:	$v_c = 10,000$ m/min	$\lambda_{h, \text{ HSC}} = 3.5$
	$v_f = 6,000$ mm/min	$k_{f, \text{ HSC}} = 147$ MPa
orthogonal cutting,	$\gamma = 12^\circ$,	$\rho = 2.8$ kg/dm ³

References

- [BAR88] Bartsch, S.: Verschleiß von Aluminiumoxidkeramik-Schneidstoffen unter stationärer Belastung [Wear of aluminum oxide cutting materials under stationary load]. Dr.-Ing. Diss. Univ. Hannover 1988
- [BAE94] Baehr, H.D.: Wärme und Stoffübertragung [Heat and material transfer]. Springer 1994
- [BEN03] Ben Amor, R.: Thermomechanische Wirkmechanismen und Spanbildung bei der Hochgeschwindigkeitszerspannung [Thermomechanical effect mechanisms and chip formation at high speed cutting]. Dr.-Ing. Diss. Univ. Hannover 2003

- [DAV07] Davies, M.A., et al.: On the measurement of temperatures in material processing. *Ann. CIRP* **56**(2), 581–604 (2007)
- [DEN92] Denkena, B.: Verschleißverhalten von Schneidkeramik bei instationärer Belastung [Wear behavior of cutting ceramics at transient loads]. Dr.-Ing. Diss. Univ. Hannover 1992
- [KÜS56] Küsters, K. J.: Temperaturen im Schneidkeil spanender Werkzeuge [Temperatures in the cutting wedge of tools]. Dr.-Ing. Diss. RWTH Aachen 1956
- [OPI52] Opitz, H.: Meßgeräte zur Ermittlung der Schnittkraft und Schnitttemperatur bei Zerspanungsvorgängen [Measuring devices to determine forces and temperatures in cutting processes]. *Werkstatt und Betrieb*, 85 (1952) 2, pp. 43–47
- [SCH33] Schwerd, F.: Über die Bestimmung des Temperaturfeldes beim Spanablauf [On the determination of the temperature field at chip flow]. *Zeitschrift des VDI*, 77 (1933) 9, pp. 211–216
- [TÖN94] Tönshoff, H.K.; Wobker, H.-G.; Ziebel, F.: Distribution of temperature and stress in the contact zone of a cutting tool. *Ann. Ger. Acad. Soc. Prod. Eng.* **2** (1994)
- [VIE53] Vieregge, K.: Die Energieverteilung und die Temperatur bei der Zerspanung. *Werkstatt und Betrieb* [The energy distribution and the temperature in cutting], 86 (1953) 11, pp. 691–703

Chapter 6

Modeling and Simulation

The use of simulations in the field of machining is generally based on the combination of numerical methods or on the algorithmic geometry with the manufacturing processes, which are dealt with in this book. Therefore, not only the input data of the simulation, but also and especially the underlying models are crucial for the value and the expressiveness of the simulation.

On the other hand, the computer aided methods offer the possibility to calculate data in many variations and in speeds and resolutions, which would be unthinkable without them. The resulting consequences are opportunities for new models, which avoid previously necessary simplifications and therefore have a considerably increased significance. It should not be forgotten however, that despite the striking and illustrative moving pictures simulations always imitate reality—based on the view of reality filtered by the models. Before a conclusion on the basis of simulation results, it is therefore necessary to examine the applicability of the used models to each situation and to verify it, if necessary, by means of real experiments. So, the target of a simulation must always be to apply and to understand a model by the systematic running through numerous variants.

When executing a simulation, one has to distinguish between the time represented by the simulation—the **simulation time**—and the time actually required for the necessary calculations—the **real time**. These times are identical only in the rarest cases. If one examines, for example, how much material in one rotation of a milling cutter with a speed of 6.000 min^{-1} is removed, the simulation time for this is a one-hundredth second, regardless of what real time has passed in the meantime.

Two essential approaches are followed in the field of simulation of machining processes, which differ in their objectives and their degrees of detailing. Geometric simulation of material removal or **kinematic simulation** determines the shape of the removed area on the workpiece in discrete time steps and from this, the particular shape of the workpiece. Modern systems of computer aided process planning (*Computer Aided Manufacturing, CAM*) often contain simple variants of such simulations to visualize and to check the planned machining processes. In addition, specialized, commercial systems are offered to provide virtual images of

machine tools including kinematics, control and simulation of material removal. The objective of these systems is also the visualization and verification of process planning to date. In more recent times however, the determined geometric information is more frequently used to calculate technological quantities, such as process forces or temperatures.

The kinematic simulation distinguishes itself through the ability to map complex tool and workpiece shapes and is also able to model complicated movements of the components involved.

In contrast, the numerical simulation of machining processes is based on the **Finite Element Method (FEM)** or the **Molecular Dynamics (MD)**. These approaches consider the operations in a much more detailed way, but cover a much smaller time interval and a smaller geometric range because of this. At this, the calculation for a single cutting pass may take up to several days. It is obvious that the choice of an appropriate simulation approach depends on the objective of the desired research. Thus, for any kind of application one must proceed according to the principle: as detailed as necessary but with as little effort as possible.

6.1 Kinematic Simulation

Geometric models of workpiece and tool as well as the description of the performed movement are prerequisite to pattern the removal of material on the workpiece by a computer. Appropriate formats to describe the form of the involved components can be found in the area of **Computer Aided Design (CAD)**. In fact, these formats are already used in the planning of the machining processes by means of CAM and are suitable as input data for the simulation. It is an obvious method to pattern the shape of a machined work piece in a simulation, to modify the existing CAD model of the workpiece in the initial state by the continuous application of geometric cutting operations with the tool and to adjust it to the progress of the machining process. Basically, this can be done through the same mechanisms used in the CAD. But in most cases it makes sense to use a customized model on the objective. Here, the simulation time is divided into intervals that are considered only approximately, but are short enough to look at the respective change precisely enough. Since only the state at the beginning and the end of the time interval is considered for the calculation, we talk about time steps or **time discretization**.

Two essential criteria for the suitability of a model for a specific application are the expected calculation time and the memory consumption. Subsequently, it is not the absolute magnitude for a concrete simulation which is important, but the performance of the model with a growing degree of detailing. Depending on the model, the necessary storage requirement may grow by eight times by decreasing the maximal error to half (doubling in each space direction) or not increase at all. The same applies to the required computation time.

Direct interactive input or the existing NC code for programming the machine can be used for the description of movements, depending on the complexity. Within the simulation this format is transformed into the resulting movement of the tool relative to the workpiece. Both the model of the workpiece as of the tool consist of points, edges, faces and bodies, each described related to a local coordinate system. For cutters, the zero point is usually set to the top, with orientation of the Z axis along the rotation axis and is called tool coordinate system. The local coordinate system of the workpiece is called workpiece coordinate system. To describe the position of a component it is sufficient to set the position and orientation of the local coordinate system (Fig. 6.1). This is done by a spatial transformation matrix that describes the image of each point or vector in the target coordinate system. To represent a movement, such a matrix is set for each time t .

In case the NC program for the machine tool is used as input data, a mathematical model of the machine kinematics and a replica of the machine control must be used to calculate the actual motion to calculate the transformation matrix. The task of the machine control is to implement the described movements in the real machine. To work around the thus occurring physical restrictions, it is necessary to make modifications to the trajectories. A sudden change of direction is replaced, for example, with fillets, because the acceleration of the physical machine axes is limited. In addition, a machine deviates from the ideal path because of compliances and vibrations. The investigation of these deviations is often the target of the performed simulations. The more influences have to be patterned, the higher the necessary effort. Moreover, the objective of kinematic simulation is often focused

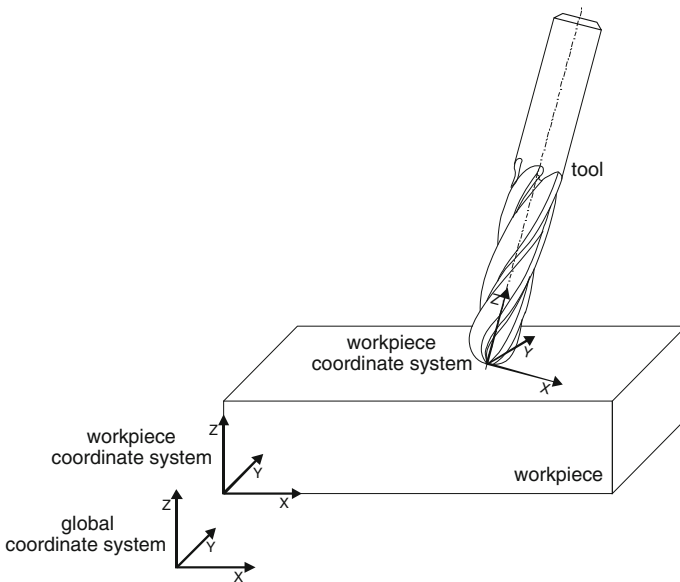


Fig. 6.1 Image of movements by transformation of the local tool coordinate system

on the use of the results in other simulations that mimic the behavior of the machine [WEI08, DEN06]. At this point, however, only the functionality of the calculations of the workpiece shape at every moment is to be described. Therefore, a given description of the motion function is assumed below.

To describe the spatial shape of tool and workpiece a suitable computer internal format is necessary, a so-called volume model. Regardless of the numerous data formats known from CAD, the methods of representation can be divided into three classes. *Volumetric models* apply small, easy-to-describe, contiguous, but not intersecting cells to combine these to a comprehensive model. In *connection models*, spatial objects such as spheres, cuboids, cylinders etc., which can be described by formulas, are combined by Boolean operations, i.e. by aggregation, penetration, or difference of the respective enclosed subset of the Cartesian space. In the *boundary representation model (B-Rep)*, the objects are described by the enclosing and adjacent surfaces [STR06]. These can be complex parameterized surfaces as well as a large number of triangles. For the simulation of material removal, different partly specialized variants of these classes are considered, which shall be described below.

6.1.1 Representation of the Workpiece

Before commenting on the representation of the requirements of the workpiece, a look should be taken at the requirements from the user's perspective. The requirements depend—as already mentioned—on the objectives of the planned investigations. Therefore, the following questions, according to which the models need to be evaluated, must be asked before selecting a model.

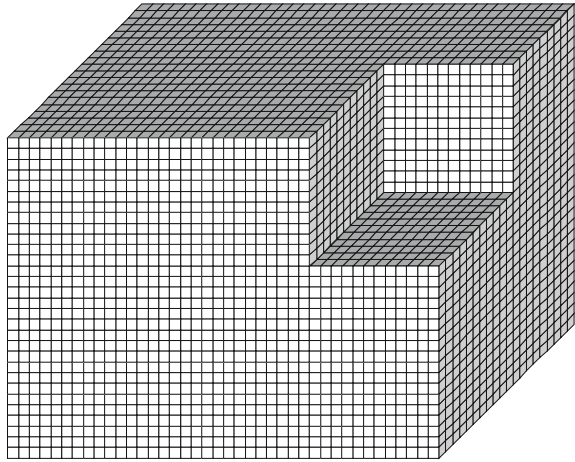
1. *What accuracy is the shape of the workpiece to be determined with?* The answer to this question influences not only the choice of the model as such—but using an approximated shape—the number of elements or the resolution of elements as well. Depending on the application, it can be sufficient to meet only a statement of the moment of contact between workpiece and tool or—on the other hand—to calculate the exact surface with high resolution. Higher accuracy typically results in a higher demand for disk space and adversely affects the speed of the simulation.
2. *Is the entire workpiece or only a detail considered?* Sometimes not the machining of the whole workpiece is of interest. Furthermore, possibly only one side of the workpiece has to be analyzed with high accuracy.
3. *What time resolution and what time interval will be investigated?* As already with the delineation of the kinematic simulation against FEM and MD, this question plays a role here as well. In general, a higher time resolution results in a longer calculation time. The memory requirement for the model does not increase, but more output data is generated.

4. *What real time has the simulation been performed in?* It is to be checked whether there are time restrictions for the duration of the calculations. This is especially the case for simulations, which run parallel to the real process to get additional information or to interfere by feedback control. In simulations for checking purposes of NC programs, it is naturally desirable to wait for the result only as shortly as possible.
5. *What kind of motion of the tool is expected and what does that mean for the generated shape?* A 3-axis milling process is limited in most cases from the outset on the surface of one side of a box. Choosing a suitable model can improve the value of the simulation or reduces the consumption of resources. The same applies to many processes that are composed of translational and rotatory movements. In particular, this can mean that the workpiece is rotationally symmetrical, at least in ideal shape, for example, in a turning or circular grinding process.
6. *How shall the resulting geometric data be further processed?* Depending on the aim of a geometrical simulation and specific processes different information shall be identified. This can be, for example, forces, temperatures, etc. The input data for the used technological calculations must be generated as simply as possible and with little losses from the simulation results. Under certain circumstances, they should be input data for other simulations. Conversely, the results of other simulations are the input data for the applied material removal model. For some applications, even a continuous exchange between different simulation systems is carried out to illustrate dynamic effects. The data exchange then heavily influences the choice of workpiece model.

6.1.1.1 Voxel Models

A *voxel model* is the simplest form of a volumetric representation of spatial objects. It is similar to bitmap formats for graphics. A discrete image of the workpiece is generated by three dimensional elements of small cuboids (building blocks) (Fig. 6.2). The blocks are called *Voxel*, an artificial word for volume element (in some references also volumetric pixel). Since a voxel has only two states, that is to say “material existing” and “no material existing”, it requires only one bit of memory. The location of a voxel is defined by the position in a three-dimensional matrix. At best, the accuracy of a voxel is given by the smallest mesh spacing and at worst by the length of the space diagonal of the voxel. As three-dimensional data fields are used, the memory requirement increases to third power, i.e. in doubling the resolution of any main direction the eightfold amount of memory is required. Thus, for a cube of 200 mm edge length and a mesh spacing of 0.1 mm a storage allocation of 1 Gigabyte is needed ($2,000^3$ Bit). The huge storage consumption of the voxel model can be weakened by a flexible variation of the resolution in different domains of the workpiece—for example by a so called octree structure—though this significantly increases the complexity of the calculations.

Fig. 6.2 Schematic view of a voxel model



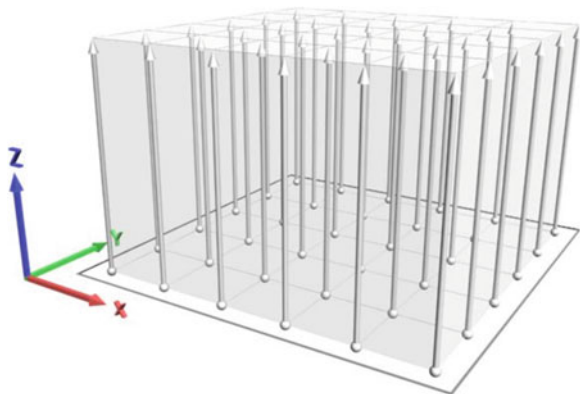
Overall, it is worth noting that voxel models are quickly applicable due to their simplicity and reach a very high computational speed at low resolutions. However, with an increasing number of voxels this procedure quickly reaches its limits.

6.1.1.2 Dixel Models

A very similar approach to the voxel model, the so called *dixel model*, represents the particular height of the top and the bottom of the workpiece on a two-dimensional matrix of equidistant, discrete X and Y positions. The resulting small rods at the matrix position are called dixel (depth element) [WEI02]. This is graphically similar to rectangular-arranged parallel pins on a board that are cut by the process (Fig. 6.3).

There is no material, so apparently not a pin for the case that the height values for both sides are identical.

Fig. 6.3 Dixel model of a block



The limitation of one dixel per position results in a constraint of the representability of any spatial object. In the direction of the dexels, no gap in the material is allowed. This can be avoided by an extension with a locally variable number of dexels, however it leads to higher memory consumption and a more complex data structure.

Compared with voxel models dixel models have the advantage that the memory requirements grow only by the second power. In addition, the accuracy in the dixel direction is much higher, because the height values can be represented with floating point accuracy instead of integer values. Any point on a surface approximately perpendicular to the direction of the pins can be very accurately determined by interpolation between the height values of adjacent grid points. But if the considered direction is on the level of the grid matrix, no higher accuracy is reached than by the voxel model. For a generally applicable material removal model it is not satisfying, if the computational accuracy relies strongly on the considered direction. This difficulty can be avoided by building up a specific dixel field for each main axis of the Cartesian workpiece coordinate system. However, this approach has the disadvantage that for further processing, for example, for visualization, three redundant data sets must be combined to a total model, a procedure which is quite elaborate.

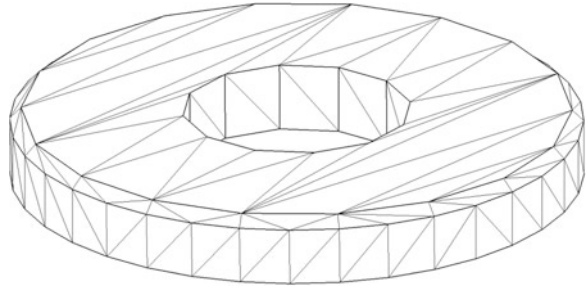
The storage requirement of the example already used with the voxel model of a cube with 2,000 elements per direction is—implying single floating point accuracy (32 bits) in the three spatial directions—at $2,000^2$ elements à 192 bits, which results in 96 Mb. Even with a more complex representation of the dixel and for this magnitude of workpiece and this resolution, a considerable lower memory requirement is to be expected than with the voxel model.

6.1.1.3 Polyhedron Model

Polyhedron models belong to the group of boundary surface models, i.e. a body is completely described by its surface. In the case of the polyhedral model, this surface consists only of flat polygons (facets), covering the surface to be represented with a maximal deviation, which has to be specified in advance (Fig. 6.4). To insure a consistent function the surface has to be closed, i.e. must not have openings or gaps.

Explained descriptively, this means that the described area is “waterproof”. To achieve this, the data structure for the model is often built as a hierarchical tree of bodies, surfaces, edges and nodal points. A surface is described within this tree by references to the boundary edges. These consist of references to start and end nodes. With multiple references to common elements, the risk of gaps is reduced and the testability of consistency of the model is eased. Two adjacent surfaces, for example, reference the same edge. To simplify graphic representations and the computer operations with the described bodies a normal vector is assigned to any surface, which points out of the body.

Fig. 6.4 Polyhedron model using triangles



Cut operations between bodies can be reduced in the polyhedral model to a number of cut operations between the facets of both bodies in contact. Separated by the traverses of the two surfaces of the bodies, four or more shell fragments are generated, which are joined according to the operation to the resulting body. In practical use, one often does without polyhedrons with more than three corners or sides respectively. This reduces the number of different configurations to be distinguished while intersecting. Elements with more corners can easily be decomposed into triangles.

The computational accuracy of the polyhedron model depends on the accuracy of the approximation. To carry out cutting operations it is somewhat difficult to identify two identical points as such, since identical coordinates do not exist—only two very close values because of calculation errors. This is avoided by introducing a threshold value, which defines two points below a minimal distance as being identical. However, for unfavorable configurations inconsistent data may occur, which have to be avoided either by case discrimination or corrected after subsequent review.

The computational time required for a cutting operation depends on the number of faces of the participating bodies. A doubling of the number of surfaces quadruples the number of necessary comparisons. The memory requirement is not directly predictable as is the case with the volumetric models. The example of the cube with an edge length of 200 mm can easily be represented as a polyhedron model—a cube is actually already described by the six sides with polyhedrons, namely squares. Only diagonals in the sides must be inserted for a representation with triangular surfaces. The resulting representation of the cube is in every respect mathematically correct and without errors and always requires the same memory space, regardless of the size of the cube. The more complex the shape of a workpiece, the larger the number of flats necessary. With this, a disadvantage of the polyhedron model becomes evident. By using each intersection operation with the tool normally more polyhedrons are added than removed. So the memory requirement grows with the progression of the simulation. The benefit of this approach is that locally very different accuracies can be created according to the needs in different areas of the workpiece.

6.1.1.4 CSG Models (Constraint Solid Geometry)

CSG models [WEI08] are formed by applying set operations on a basic set of simply describable spatial elements, the so called primitives, and are thus part of the link models. In contrast to the previously described models, the intersection operation is not carried out at the time of definition but the used bodies and operations are stored (Fig. 6.5). The data storage is carried out as a binary tree, whose leaves are formed by the individual primitives and its nodes by the respective set operation. In this structure, a cutting operation is very easy to add, as occurs in machining processes. In addition, the resulting shape of the workpiece is described exactly and analytically, depending on the accuracy of representation of the basic elements. During further processing, for example, for the graphical visualization or for the calculation of process variables, the tree of operations must however be analyzed again each time and converted into another model, because CSG models are only suitable for direct usage to a very limited extent. The cube, which has already been used as an example several times, creates a tree with a single node in the CSG model.

The tree grows with the number of operations. By that, the memory requirement and the calculation time grow for further evaluation. The storage of the cutting operation itself, however, can take place very quickly.

Fig. 6.5 CSG model of a ball end milling process (*upper*), resulting workpiece shape (*lower*)

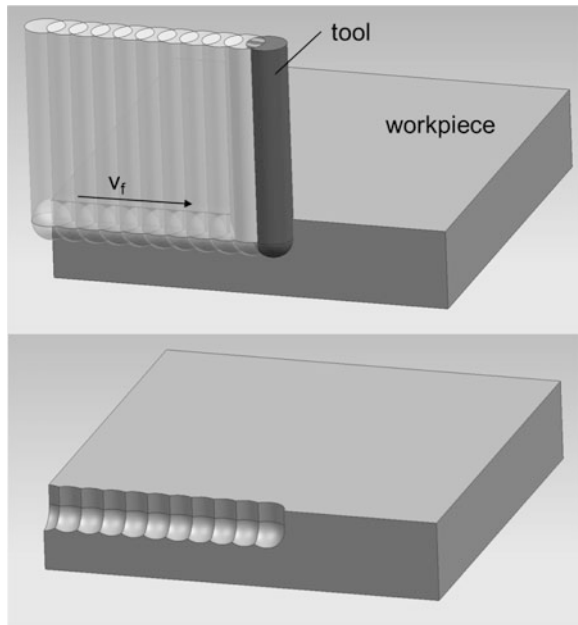
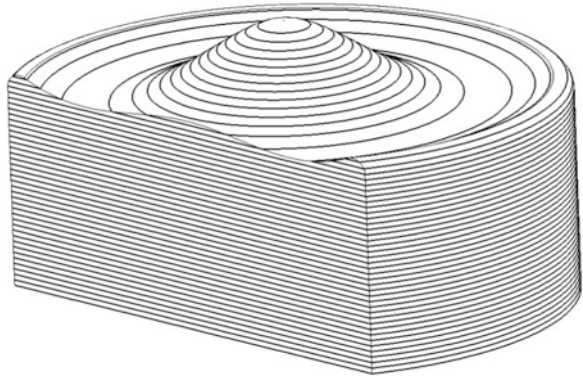


Fig. 6.6 Level curve model

6.1.1.5 Level Curve Model

Another model based on boundary representation is the *level curve model* (Fig. 6.6) [DEN07]. Similar to the depiction of landscape surveys in maps the workpiece is usually sliced with parallel planes, commonly parallel to one of the coordinate planes, and the intersection line is stored as a two-dimensional model. The intersectional line can be created either as polygon with appropriate constraint for the maximum deviation or as analytic description by parametric curves. In the case of polygonal lines one obtains a special case of a polygon model, because the nodal points of adjacent planes easily add to triangles. To intersect the represented workpiece with a tool it is sufficient to determine the section of the tool in the respective plane and to intersect the resulting section line with the respective level curve. This operation can be carried out much more easily than with the general polyhedron model since it is a two-dimensional intersection operation.

Another advantage of the level curve model is the lower effort for the reusing of the results. The volume removed during one time step is split into elements by the planes, which are limited by parallel planes in one direction, which simplifies further calculations.

6.1.2 Tool Model

Each of the described models for the workpiece is designed to be modified by a suitable model of the tool by geometric intersection operations. The model applied for the tool is not necessarily built up in the same way as the workpiece. In fact, it is of benefit to use a specific tool model, depending on the situation which is adapted on machining the workpiece model.

At this, it has to be especially observed that using a workpiece model with analytically described shape the advantage of high accuracy is nullified by

discretized tool models. As a whole, it is necessary to adapt the accuracy of the tool model on the accuracy of the workpiece representation. The same applies to the choice of the temporal resolution.

Still it is often useful to make simplifications for the tool model depending on the objective of the simulation. For most applications with rotating tools it is sufficient to look at the tool body resulting from the rotation as the movement of individual cutting edges is not considered in the time steps of the simulation. Therefore, CAD models of the real tool with a detailed representation of the discrete cutting edges are not applied. Instead, the tools are often specified via the contour curve of the rotational body. A representation with seven parameters is shown in ISO3592, which most of the milling tools can be specified by [ISO3592].

Despite the reduction of the tools on their rotational body, the rotational direction and speed or the concrete shape of the cutting edges can incidentally be reconsidered for the evaluation of the results.

Regardless of the used format or the level of detail of the tool model, for the intersection of the workpiece model not the tool model at a specific moment has to be considered but the space passed through by the tool—the trace—even at very high temporal resolving discretization. Therefore, a so-called swept volume has to be created from the tool model and the data of the applied movement by a further operation. This is especially not trivial for tool motions, which are combined by translational and rotational motions. However, for many models algorithms already exist, which can produce trace volumes.

Another important consideration when choosing a suitable tool model is the convexity. In the calculation of intersections between tool and workpiece, most of the procedures consider only the visible area of the tool surface from different views and make the intersection by this tool model. If there are undercuts in the considered view, i.e. the ray in line of the view would penetrate the material more than once, the hidden domain would not be recognized. This case can occur, for example, when grinding with a profiled grinding wheel (Fig. 6.7), with cup wheels or for the detailed examination of milling processes including specific cutting edges. Not only because of this, it is important to be familiar with the functionality of the models and the respective algorithms for the design of a kinematic simulation.

6.1.3 Determination of Process Values

So far it has been described how the shape of the removed material can be determined for a predefined time interval on the basis of purely geometric considerations. The input data of the analytical methods, as described in previous chapters contain no detailed information of the shape of the removed material, but have to make generalizations. In contrast, the simulation offers the possibility to determine a representation of the actual shape of the material removed per time step. On the one hand, this requires the obtained data to be processed for further

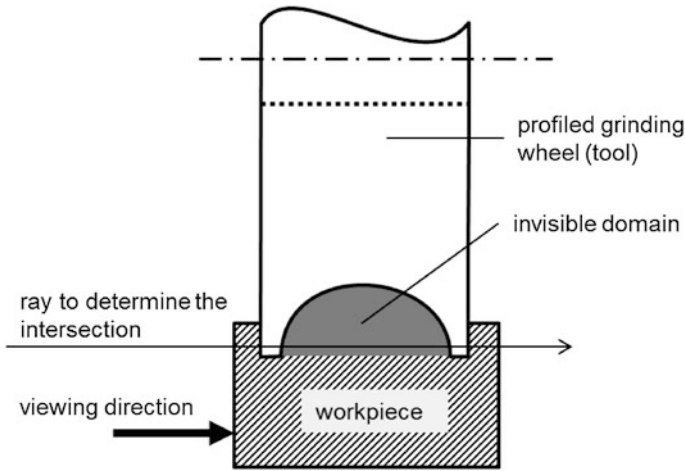


Fig. 6.7 Considering concave domains in the tool model

use and on the other hand, this offers the possibility to get a much more detailed picture of the ongoing process by integrating knowledge of other process parameters.

Some of the most important geometric input data in cutting are the cross section of the undeformed chip, the contact area between tool and workpiece and the removed volume per time unit. Especially for variable engagement conditions, the considered domain can be divided into smaller parts so as to be able to determine these values with higher precision. The different procedures for the calculation of other parameters, such as process forces, can then be applied separately, each with adapted parameters in the partial domains. As a consequence the parameters varying locally in practice such as the cutting speed, can be taken into better account.

As an example of an application to determine the shape of the undeformed chip cross section, a coupling of the calculated forces to a simulation of dynamic vibration behavior of the used machine tool shall be discussed. The objective is to simulate the stability behavior for the groove milling and to determine the influence on the workpiece surface by this effect. Due to the process force action the tool is deflected and pushed aside, which again influences the engagement of the tool and leads to varying forces. In connection with the vibration behavior of the machine dynamic effects are caused, which appear as irregularities on the surface of the workpiece.

To determine the forces under the varying engagement conditions purely analytic considerations are not sufficient. Also, a simplification of the material removal process by a mere intersection of the rotational body of the tool with the workpiece does not deliver a sufficient temporal resolution of the force course. In fact, it is necessary to include the position of the specific cutting edges of the cutter into the simulation and to compute the force course for the rotating tool. Figure 6.8

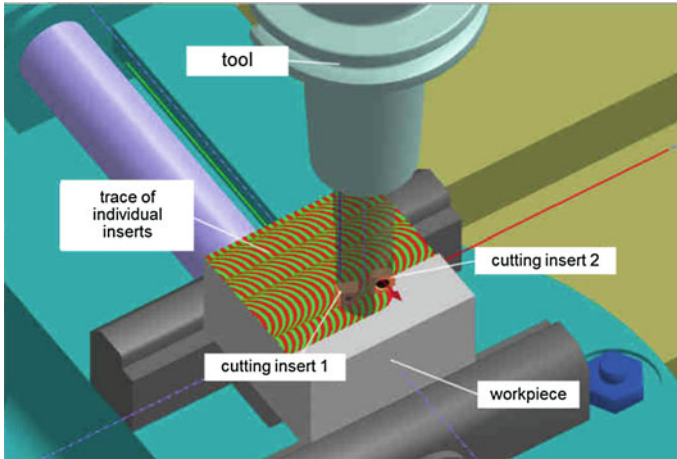


Fig. 6.8 Simulation of the material removal of single inserts in the rotating tool system

shows the material removal of two cutting edges of a torus milling cutter. The domains machined by both edges are colored differently to illustrate the areas processed by the two cutting edges.

To calculate the cutting forces for the process conditions of each time step, the geometric shape of the machined range is first determined from the used part model. It corresponds to the intersection of the trace body of the tool from the start to the end position of the current time step with the shape of the workpiece before the start time. It should be noted that each time interval contains an interval in the rotational movement of the milling cutter too. The time steps have to be taken small enough to be able to neglect the chord error resulting from building the trace body. In the application, a maximum increment of 10° of the tool rotation has proved to be suitable.

In the next step, the cross section of the undeformed chip is determined from the resulting volume element. The hereby relevant information for each particular point is the position in the reference system stretched from the milling cutter axis and the radius. Therefore, a projection of the body is taken in the space of the cylinder coordinates of these axes on the plane spanned by the radius and the tool axis.

The so resulting surface is decomposed into partial areas and for these the respective part of the force components are calculated (see [Chap. 4](#)).¹ The sum of the fractions results in the force component to be determined (Fig. 6.9).

Another application example, where less the cross section but rather the contact area between tool and workpiece plays a decisive role, is the adjustment of

¹ In the presented example a semi empirical force model introduced by Altintas was used to determine the forces. See also [ALT00].

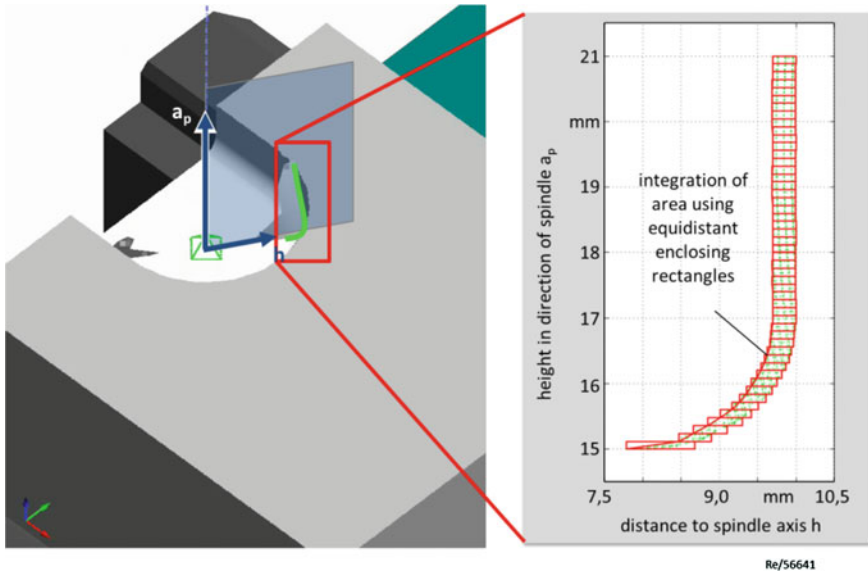
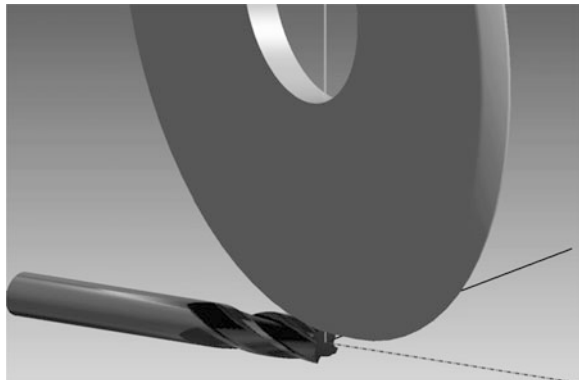


Fig. 6.9 Computation of the cutting forces by the cross section of the undeformed chip from the simulation

grinding processes for the manufacturing of milling cutters and drills of tungsten carbide [DEN08]. The flute in the workpiece—in this case the milling cutter or the drill—are produced by a profiled grinding wheel, which moves on several helix trajectories around the cylindrical workpiece (Fig. 6.10). Due to the hard material and the aimed high metal removal rate high process forces arise. This results in deviations of the set shape—as in the first example—in this case, however, by deflection of the workpiece. If the kind and size of this deflection is known, the error can be compensated by adapting the depth of the wheel.

The analytical view on geometric input values (see Sect. 12.7) ascribes grinding processes to surface grinding by transforming the individual values to

Fig. 6.10 Simulation of material removal in tool grinding



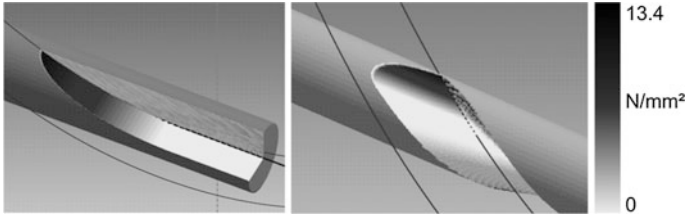


Fig. 6.11 Distribution of normal stresses on the contact area for straight (*left*) and helical flutes (*right*) determined by simulation

equivalent ones. For example, the equivalent radius r_{eq} or the equivalent chip thickness h_{eq} .

For this purpose, a generalization is made by replacing the actually locally varying values with average quantities. Since the axis of the grinding wheel is skewed against the feed direction, not only the cutting speed but also the contact length and the chip thickness vary over the contact area. Thus follows a non-uniform force distribution, which influences the deflection of the workpiece over time and position. An investigation by geometric simulation delivers the necessary data for a detailed consideration. For the evaluation the (not plane) contact area determined in the simulation is broken down into smaller fractions.

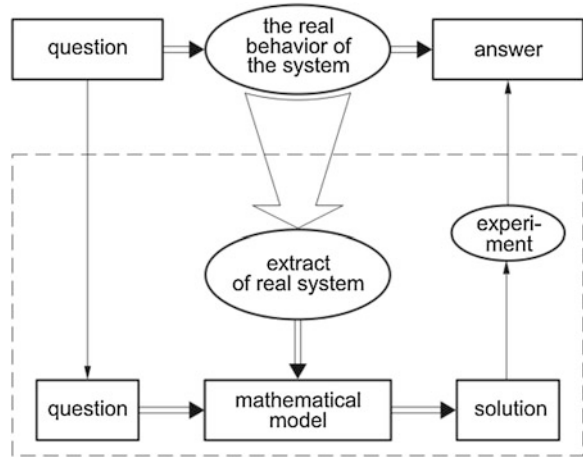
The removed volume in the specifically viewed time interval is assigned to each partial area by the calculated shape of the removed domain as determined in the first example. From this, the equivalent chip thickness h_{eq} and the equivalent chip width b_{eq} and the equivalent cross section $A_{eq} = b_{eq} \cdot h_{eq}$ can be determined respectively. These quantities are used for each partial area as input value for the calculation of the forces so as to obtain the normal stresses on the contact areas (Fig. 6.11).

With this distribution as input for a simulation of the deflection of the workpiece much more precise information about the deflection can be derived. If the computation of the forces is coupled to a suitable model, dynamic effects can be patterned—similar to the first example [DEI10].

6.2 Numerical Simulation by FEM

With the upcoming of powerful computers simulations based on numerical calculations have become possible. All of them are also based on models, which represent the real behavior of the system to be analyzed only in abstractions (Fig. 6.12). However, one is more independent in the choice of the included effects—subject to the effort—than using the closed analytical methods. But it should be realized: these numerical simulations also have to be verified in experiments. The occasionally used term “numerical experiment” is therefore mistaken.

Fig. 6.12 General formulation of engineering tasks



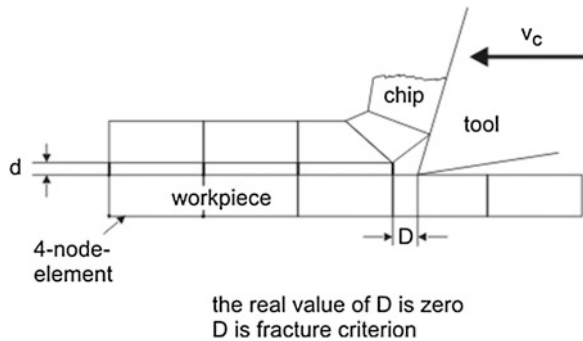
Among the numerical methods the Method of Finite Elements has been introduced in many fields of mechanics, thermodynamics and especially in continuum mechanics, as well as in the mechanics of large plastic deformations and for some years, also in cutting theory [STR90, MEI88].

FEM simulations are based on two fundamental principles, on the Lagrange- and the Euler-formulation. The Lagrange-formulation can be further distinguished into the implicit and the explicit mode. Simulations of cutting processes are run chiefly two dimensionally because of the high computing time. This approach corresponds to the orthogonal cutting.

A difficulty in the simulation of the cutting process after Lagrange is to pattern the extreme strain at the cutting edge. Two ways have been developed:

In the implicit Lagrange’s formulation (ILF), a parting line d is introduced (Fig. 6.13). A separation of the FE net is allowed only on this parting line. Chip and workpiece are represented by their own nets, which are connected until the actual separation by linking elements. The separation path is set as a parallel line to the workpiece surface on the height of the tool tip. Each linking element consists of two nodal points, which have the same coordinates, since the original length d is equal

Fig. 6.13 Presentation of the linking elements with a parting line in the ILF [ZHA94]



to zero. They have two states, the connection or the separation. These states are each subject to the distance D between the tool tip and the next element of the separation line. If D reaches a predefined value or less than that, the element is dissolved and chip and workpiece are separated. With the progression of the tool with cutting speed v_c the chip continues to be formed. The procedure of chip generation is considered purely geometrically. The influence of the cutting speed is hereby neglected. Initially, purely geometric sizes were adopted also in determining the timing of the network separation. Only later, material specific parameters (for instance maximal strain) were used as a separation criterion [LIN93].

In the explicit Lagrange's formulation (ELF), the equations of motion are integrated directly and explicitly. No global stiffness matrix is used in contrast to the implicit methods, where the FEM solution via the stiffness matrix is achieved. The stresses are directly calculated in the integration from the element stresses after each single time step. The advantage of this formulation is that no separation line has to be defined. To find the location of material separation in the model the maximal stresses are compared with a maximum value in a dedicated routine at every nodal point of the FE net—when this value is exceeded a separation by doubling the nodal points is carried out. Here, it becomes obvious that the strain energy density is a realistic criterion for the nodal point separation [MEI88].

The third possibility of simulation is a consideration according to the Euler-formulation, in which the structure to be investigated is viewed as a controlled volume. In this approach, the nodal points are stationary and not fixed to the physical material of the investigated structure. This has the advantage that the net can be intensely refined at the tool tip, where the highest stress and strain gradients occur as is necessary for a sufficient accuracy. It is important that there is no separation criterion in the Euler formulation in this method, since the stresses and velocities in the workpiece are calculated as a function of the spatial position and not as a function of the individual material particle. Given that the chip geometry in the Euler's representation is not known from the beginning and the material properties are partly dependent on the strain rate and on the changing temperature, the equations for the cutting model have to be solved iteratively [STR90] (Fig. 6.14).

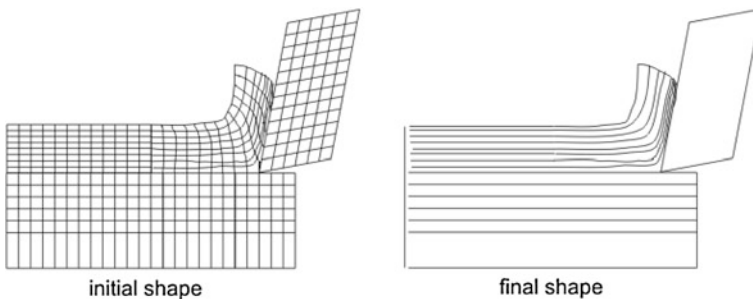


Fig. 6.14 Start and end contour of the Euler model, iteratively determined

A comparison of the different formulations shows:

Properties of the Euler formulation:

- visco-plastic flow process,
- no separation criterion necessary,
- forces and temperatures at the contact of tool-workpiece are realistically represented,
- a locally fixed net is applied, whose boundaries have to be known in advance,
- only stationary processes can be represented, i.e. no lamination or shear localizations,
- there are no extreme distortions in the cutting edge domain so that a constant computation mesh can be used.

Properties of the Lagrange formulation:

- elastic–plastic starting procedure,
- separation criterion necessary,
- at the cutting edge, extreme distortions of the net occur, which make remeshing necessary,
- chip geometry during or immediately after the chip generation results from the simulation and does not need to be provided in advance,
- transient processes can be patterned, i.e. the simulation is not limited to pure chip flow processes. This is especially interesting for shear localizations at chip compression or for the representation of segmented processes and variable cross section of undeformed chips,
- Lagrange simulations are considerably more complex than Euler computations because of the necessary remeshing and the link to material spots. However, they offer the chance to recognize material inhomogeneities in the first place, which is interesting especially in micro domains.

Most of the FE models described in literature are based on the Lagrange-formulation. Combinations of Lagrange and Euler formulations have been developed, which want to combine the advantages of both kinds of calculation [STR90].

During the FE analysis, considerable deformations of the net structure occur. Geometrically heavily distorted elements have a low quality of results and can lead to an interruption of the calculation, if the Jacobi determinant of the displacement vector becomes negative [MAR98]. Especially in the contact domain, where generally large deformations take place, state variables may adopt unrealistic values because of the element distortions. Thus, wrongly larger state variables are obtained by these analyses with a distorted net than by using repeated remeshing. Therefore, for a realistic process simulation a robust automatic remeshing procedure is essential, which generates a new net according to predefined criteria without intervention of the user.

There are several FEM programs applicable to chip building simulations. From among these, the following programs are often applied: SFTC/Deform, MSC/ Superform, Thirdwave AdvantEdge and ABAQUS. SFTC/Deform and MSC/

Superform are FEM programs to solve metal forming problems. ABAQUS is a FEM program to handle structure–mechanical, thermodynamic or acoustic problems. The above mentioned programs have to be adapted to cutting simulations. Third wave AdvantEdge was specifically configured for cutting simulations. The mentioned programs are based on the Lagrange’s approach. They differ in software architecture, in programming and the use of different algorithms for the remeshing of strongly distorted material domains.

A characteristic problem of the simulation of chip building, which does not exist for metal forming problems, is the material separation. It is different in Lagrange’s approaches:

- either the separation takes place alongside the element edges also providing the direction of separation by precisely these edges,
- or elements are removed from the net.

The example demonstrates the application of the FEM for chip formation processes, i.e. the deformations or the chip formation kinematic. Figure 6.15 shows the snapshot of a chip root simulated by FEM. A special advantage of the FEM is that by this method it is also possible to compute stress distributions and with that contact stresses, force and power requirements, heat fluxes, temperature distributions and in appropriate modeling, also alterations of surface layers, i.e. surface integrity effects.

6.3 Molecular Dynamic Modeling

The previously mentioned considerations were made phenomenologically on isotropic and homogeneous material. In the meantime, it has become possible to handle deformation and also wear problems on molecular or atomic basis (molecular dynamics (MD), minimum potential simulation (MPT)) [IKA92]. The

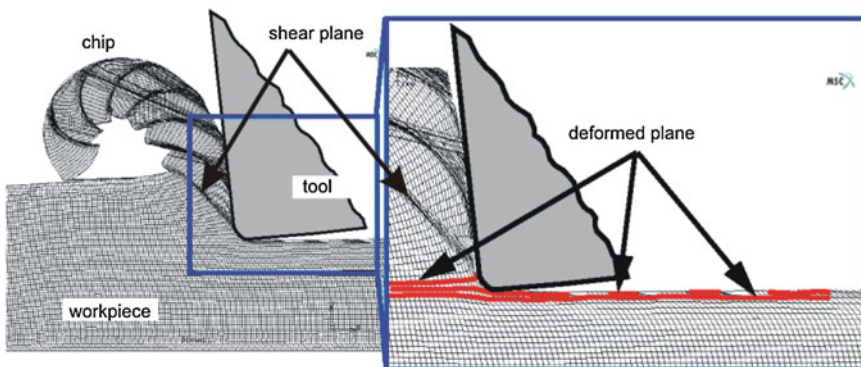
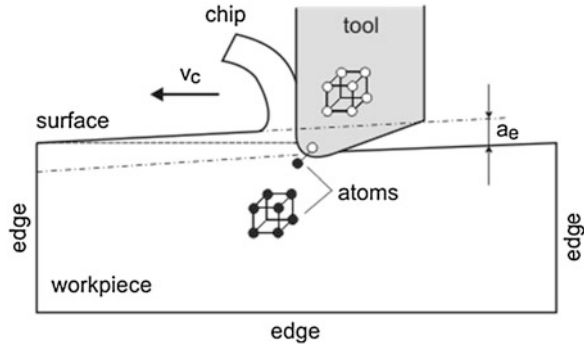


Fig. 6.15 Simulation of segmented chip formation

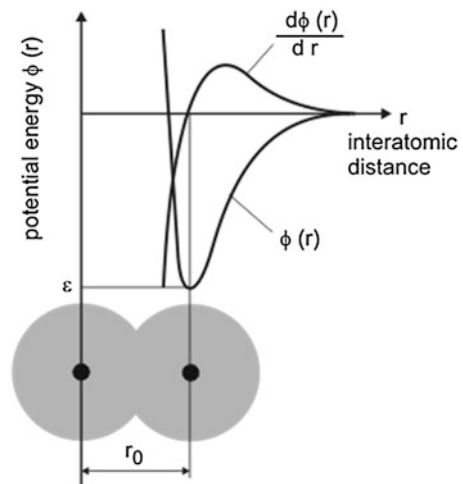
Fig. 6.16 Concept of cutting modeling by MD (acc. Rentsch)



interactions of atoms or molecules are modeled. Thus, mechanical and thermal states of an atomic lattice can be patterned.

Figure 6.16 shows the general concept of chip modeling by the MD method [REN95]. Obviously, orthogonal cutting is assumed, which is indispensable for two-dimensional analyses. The material properties, the interactions between the components, the contact and interface conditions between cutting wedge, tool and chip, as well as the environmental properties have to be defined in the model. Furthermore, the boundary conditions inside the model (surface to the base material) and the system boundaries to the not-modeled surrounding are of interest. The core of the MD method is the particle-to-particle interaction. This interaction is described by the potential energy between the particles. Figure 6.17 shows the potential energy as a function of the atomic spacing and derivation for the distance. Rentsch points out that the pair function cannot represent technical metals properly. For this, models based on multi-body interactions are needed, which cannot be addressed in detail here [REN09].

Fig. 6.17 Potential energy as function of atomic distance [REN09]



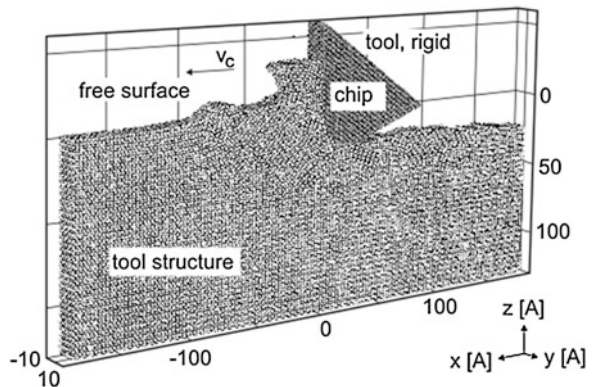
Cutting needs a relative motion between tool and workpiece, specified by the cutting speed v_c , which has to be introduced into the model. Furthermore, forces and moments introduced by the contact areas between tool and workpiece have to be supported by appropriate responses to avoid non-realistic movements of the system. Normally, the deformation process in front of the cutting edge is of interest. To limit the complexity the tool is mostly taken as rigid. In principle however, appropriate partial models can also be introduced to enable the simulation of wear caused by friction and thermal effects. Since energy is transformed into heat in the process, the temperature of the material increases. To maintain realistic conditions in the chip forming zone temperature controlling atoms are placed at the boundaries of the modeled body.

From the above it becomes obvious that these simulation calculations are very time consuming. Therefore, only limited sizes of volume or area can be modeled and simulated respectively. On the other hand, the volume must be large enough to keep artifacts negligible from the sides of the boundaries and as a consequence of elastic effects (Fig. 6.18).

However, with greater computing power this type of modeling can include the potential to pattern realistic scenarios of cutting. It is also interesting that approaches are pursued to combine MD models with FE models [HEI09]. Thereby, a part based on atomic view, considering local elastic and plastic deformations is complemented. A surrounding FE part takes care of elastic processes as it is indeed the case in the reality of cutting with a fading effect in the further surrounding of the effective point.

In any case, it was possible to show [REN09] that already today, the MD method is able to give interesting details on the deformation process in front of the cutting edge, on the thermal processes in the cutting zone and on the stress distribution in the workpiece material in micro machining in the nanometer regime of a crystalline material.

Fig. 6.18 MD simulation of orthogonal cutting according to Rentsch [REN95]



6.4 Questions

1. Explain the difference between simulation time and real time.
2. What considerations should precede the choice of models for the kinematic simulation?
3. How do the models for the representation of the workpiece differ for the simulation of the material removal?
4. Why is the adaptation of the tool model on the simulation target and the applied workpiece model important?
5. Explain the fundamental principles of the FEM.
6. What is implicit and what is explicit formulation?
7. Which principally different effects have to be considered in the FE simulation of cutting according to Lagrange compared to conventional forming processes as deep drawing or extrusion?
8. Why is a separation criterion not needed when using the Euler formulation?
9. Name typical problems of cutting which can be handled by FEM. Arrange these according to their complexity or the degree of difficulty.
10. Compare FEM and MD.
11. How is the interaction between atoms described in the MD method?

References

- [ALT00] Altintas, Y.: *Manufacturing Automation: Metal Cutting Mechanics, Machine Tool Vibrations and CNC Design*. Cambridge University Press, Cambridge (2000)
- [DEI10] Deichmüller, M., Denkena, B., Payrebrune, K.M.; Kröger, M., Wiedemann, S., Schroeder, A., Carstensen, C.: Determination of static and dynamic deflections in tool grinding using a dixel-based material removal simulation
- [DEN06] Denkena, B., Tracht, K., Rehling, S.: Technological NC-simulation—bringing NC-simulation to the next level. In: *Proceedings of the 5th CIRP International Seminar on Intelligent Computation in Manufacturing Engineering*, 25–28 July 2006, pp. 257–260 Ischia, Italien
- [DEN07] Denkena, B., Schmidt, C.: A flexible force model for predicting cutting forces in end milling. *Prod. Eng.* 1, S343–350 (2007)
- [DEN08] Denkena, B., Deichmüller, M., Kröger, M., Popp, K.M., Carstensen C., Schroeder, A., Wiedemann, S.: Geometrical analysis of the complex contact area for modeling the local distribution of process forces in tool grinding. In: *Proceedings of the 1st International Conference on Process Machine Interactions*, Hannover, S. 289–298 (2008)
- [HEI09] Heinzel, C.: *Scheifprozesse verstehen [To Understand Grinding Processes]*. Habil. Schrift Univ., Bremen (2009).
- [IKA92] Ikawa, N., Shimada, S., Ohmori, G., Tanaka, H.: Moleculardyna-mics analysis as compared with results of micromachining. *Ann. CIRP* 41(1), S. 117–120 (1992)
- [ISO3592] ISO 3592:2000: *Industrial automation systems—Numerical control of machines—NC processor output—File structure and language format*. International Organization for Standadization (2000)

- [LIN93] Lin, Z.C., Pan, W.C.: A thermo-plastic large deformation model of orthogonal cutting with tool flank wear—part 1: computational procedures. *Int. J. Mech. Sci.*, Bd. 35, Heft 10, S. 829–840 (1993)
- [MAR98] N.N.: MARC Volume A: Theory and User Information, Version 7.3, Part Number RF-3001-07.3. Revision Date: August 1998, MARC Analysis Research Corporation
- [MEI88] Meir, G., Hashemi, J., Chou, P.C.: Finite-Element Simulation of Segmented Chipping in High-Speed Machining, p. MR88-120. Society of Manufacturing Engineers, Dearborn, Mi, USA (1988)
- [REN95] Rentsch, R.: Molecular dynamics simulation for nanometer chip removal processes. PhD-Dissertation, Keio University (1995)
- [REN09] Rentsch, R.: Molecular dynamics of nanoscale cutting. In: Davim, J.P., Jackson, M.J. (eds.) *Nano and Micromachining*. ISTE-Wiley Publ, NY (2009). ISBN 978-1-84821-103-2
- [STR90] Strenkowski, J.S., Moon, K.J.: Finite element prediction of chip geometry and tool/workpiece temperature distribution in orthogonal metal cutting. *J. Eng. Indus.*, Bd. 112, Heft 4, S. 313–318 (1990)
- [STR06] Stroud I.: *Boundary representation modelling techniques*. Springer Verlag, London (2006)
- [WEI02] Weinert, K., Stautner, M.: An efficient discrete simulation for five-axis milling of sculptured surfaces. *Prod. Eng.* IX/1 (2002), S. 47–51
- [WEI08] Weinert, K., Kersting, P., Surmann, T., Biermann, D.: Modeling regenerative workpiece vibrations in five-axis milling. *Prod. Eng.* 2(3):S. 255–260
- [ZHA94] Zhang, B., Bagachi, A.: Finite element simulation of chip formation and comparison with machining experiment. *J. Eng. Indus.* 116:S. 289–297 (1994)

Chapter 7

Wear

7.1 Wear Forms

Cutting tools wear during operation. Typical wear forms develop at the cutting wedge. These wear phenomena depend on the materials of tool and workpiece and on the cutting conditions. The mechanisms of wear (also called wear causes) have to be distinguished from the wear forms. Thus, the following chain of effects results:

loading → wear mechanisms → wear forms.

The most important wear forms are shown in Fig. 7.1 together with the parameters which describe them quantitatively.

Flank wear develops at the major and minor flank of the tool. The just generated cut surfaces of the workpiece slide at these wear faces. Significant marks are formed. Their extension in cutting direction is called width of flank wear land VB . Since different flank wear marks may form alongside the cutting edge, one distinguishes wear at the corner rounding VB_C (maximum value at the corner rounding, C for corner), VB_B (average value) at the straight part of the cutting edge and VB_{max} as maximum heights and VB_N (N for notch) with the formation of a notch (notch wear) at the end of the active cutting edge in the area of interaction with the uncut surface.

The flank wear is normally monotonic. The volume removed from the cutting wedge V_T referred to the cutting edge length, depends on the clearance angle of the tool α (assuming constant wear development alongside the cutting edge) as follows:

$$V_T = \frac{1}{2} VB^2 \tan \alpha \quad (7.1)$$

A small clearance angle α causes a stable cutting wedge. However, a small clearance angle enlarges the friction area and so intensifies the friction effect between the tool and the workpiece. Generally, a clearance angle is indispensable, because otherwise the tool would only push and not be able to cut. From the hodographs in Fig. 7.2 follows

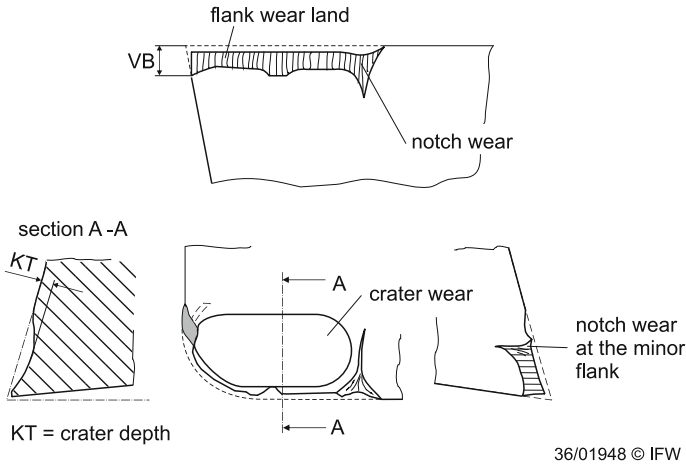


Fig. 7.1 Wear forms in turning (acc. ISO 3685)

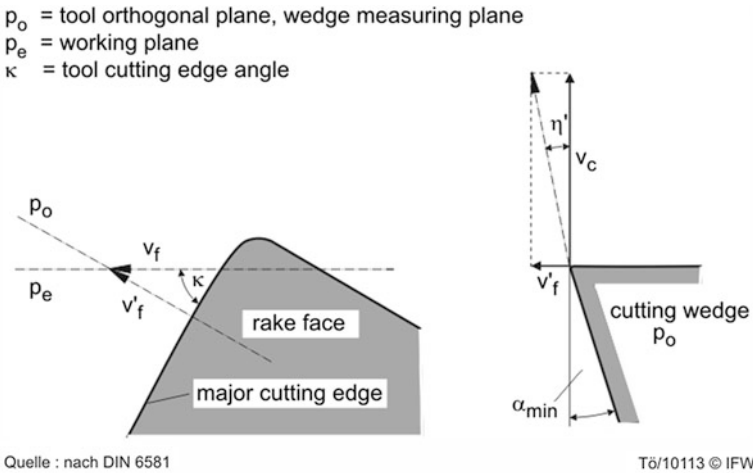


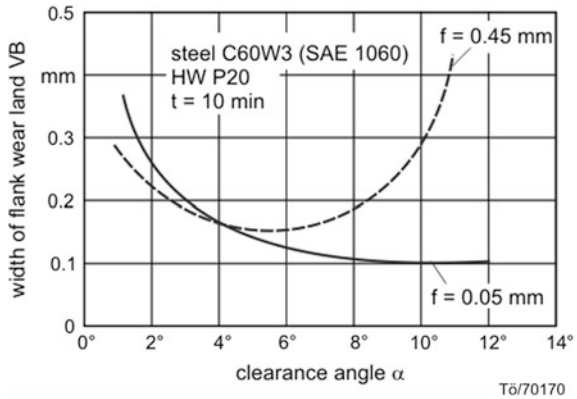
Fig. 7.2 Kinematic clearance angle minimum

$$\tan \alpha_{min} = \frac{v_f}{v_c} \sin \kappa \tag{7.2}$$

For kinematic reasons the clearance angle α has to be greater than the effective cutting speed angle η' . However, this consideration does not yet regard any elastic deformations of the effective pair (i.e., tool and workpiece). Therefore, the clearance angles are in practice by 4° greater than calculated, according to the above relation.

Figure 7.3 shows that the flank wear increases at very small clearance angles due to the increasing friction, but this occurs also for higher loading and a large clearance angle because the cutting wedge is then weakened.

Fig. 7.3 Influence of the clearance angle on the flank wear

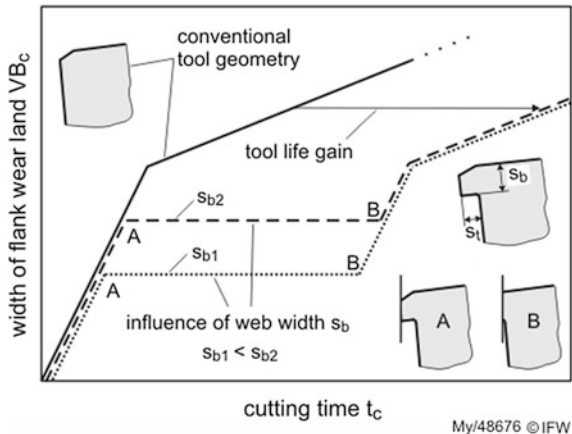


It is interesting that you can reach a significant reduction of wear in the initial phase by only a small reset of the flank according to Fig. 7.4 [DEN08]. In addition, the contact length between flank and workpiece is kept nearly constant over a certain cutting time. This is important, for example, for hard machining as this influences the passive force and the residual stress state in the surface layer of the workpiece (for this, see also Chaps. 10 and 11).

The *crater wear* forms as a crater of removal of tool material on the rake face (Figs. 7.1 and 7.5). It is described by the crater depth KT or the crater ratio $K = KT/KM$ as a quotient of crater depth and crater center distance KM . The crater ratio is a measure of the weakening of the crater lip which could result in the risk of it breaking out.

Further wear phenomena such as plastic deformation of the cutting wedge, formation of cracks, slate-like wear and fracture are discussed with the wear mechanisms.

Fig. 7.4 Flank reset and wear (principle)



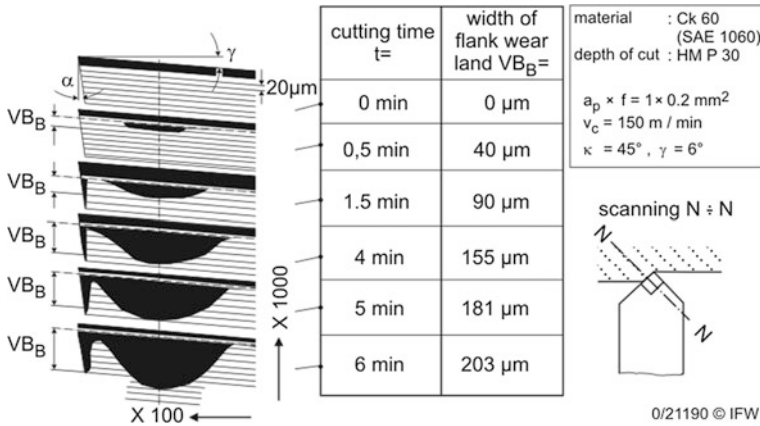


Fig. 7.5 Influence of cutting time on the wear of a turning tool

7.2 Loading

The active parts of cutting tools- the cutting wedges- are mechanically, thermally and chemically loaded (Fig. 7.6). This loading may be temporally constant (turning in continuous cut or drilling). The loading for milling or turning in interrupted cut is transient, i.e., temporally changing.

The *mechanical loading* of the cutting wedge follows from the introduction of forces via the contact areas on the rake face and the major and minor flank faces. The so caused stresses may be computed, for instance, by the method of finite elements (FEM). Prerequisite is that the distribution of surface forces on the contact areas is known. From measurements and analytical calculations generally

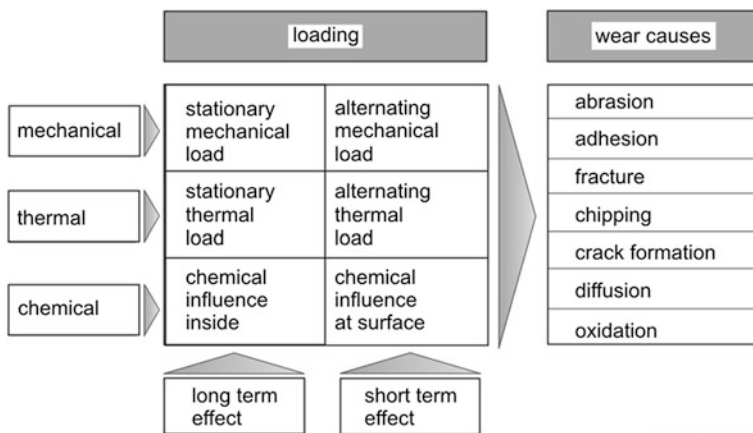


Fig. 7.6 Loading and wear mechanisms of cutting materials

only the global force components can be specified, whose vectorial sum is the resultant force and the surface forces (distribution of contact stresses) are difficult to determine (Sect. 4.5).

The procedure of calculation and the necessary assumptions shall be explained by the example of a milling process [DEN92]. From the resultant force or its components taken in a measuring coordinate system, the force components referred to the cutting wedge, i.e., the force components acting normally and tangentially on the contact areas have to be calculated. This is carried out by the values and angles shown in Fig. 7.7 by a coordinate transformation.

$$(F_x, F_y, F_z)^T = \underline{T}_{FS} \cdot (F_c, F_{cN}, F_p)^T \tag{7.3}$$

where \underline{T}_{FS} is the transformation matrix, which contains the trigonometric functions of the tool angles κ , γ_a and γ_r . The forces for milling of steel AISI 1045 (DIN Ck45N) with a ceramic cutting tool change with the engagement angle φ as illustrated in Fig. 7.8. From the thus determined components the fractions acting on the rake and flank faces have to be derived (Sect. 4.7). For this purpose the investigations of Spaans [SPA67] can be applied, who determined the following partial components for the flank (F_α) and the rake face (F_γ):

$$F_{\alpha y} = 0.1 F_y \quad F_{\alpha x} = 0.4 F_x \tag{7.4}$$

$$F_{\gamma y} = 0.9 \cdot F_y \quad F_{\gamma x} = 0.6 \cdot F_x$$

The force shares transmitted over the minor cutting edges are negligible in roughing-finishing conditions.

Now, the distribution of discrete normal and tangential forces on the contact surfaces has to be determined according to Chap. 4. The width of the contact

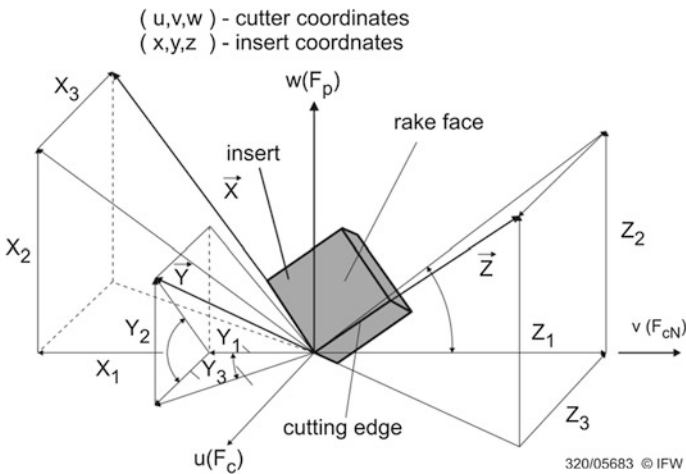


Fig. 7.7 Transformation of coordinates: milling head to indexable insert

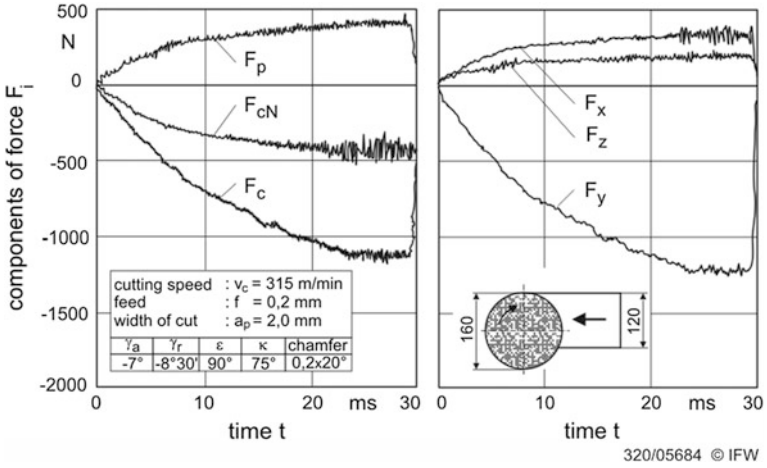


Fig. 7.8 Force components in coordinates of milling head and cutting insert

surface corresponds to the width of cut b ; the contact length in direction of the chip flow is about 2.5 times the undeformed chip thickness h . However, the contact length can double towards the end of the tool life [DEN92]. Therefore, an experimental determination by means of the contact imprint at the cutting wedge is recommended. Hence, the surface stresses are derived which have to be known as boundary conditions for a FEM calculation.

Figure 7.9 shows the main stresses on the basis of selected points of the insert based on the load given in Fig. 7.8. The calculated stresses are not critical for the investigated cutting material, but once the force increases, for example due to wear, the stresses could reach critical values.

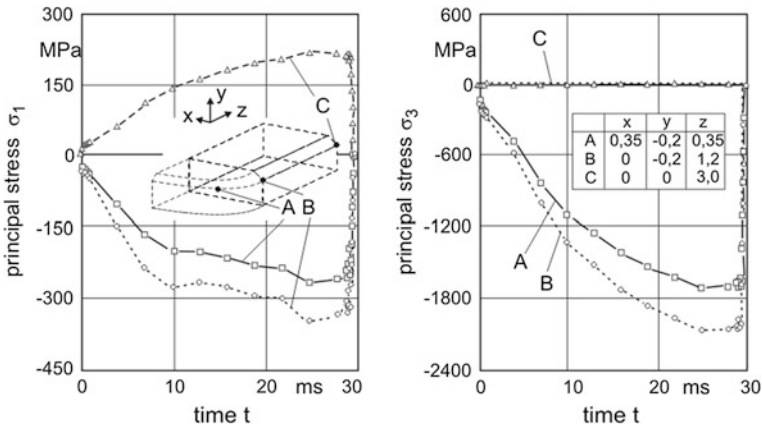


Fig. 7.9 Principal stresses during the engagement phase

The *thermal loading* of a cutting wedge can also be determined by FEM if the heat flux, which enters the cutting wedge and its distribution are known. The power transformed at the cutting edge leads to heat fluxes via the chip, the workpiece, the tool and the environment. The cutting wedge is permanently in the heat flux—different from the other three elements. Consequently, the temperature rises considerably and steep temperature gradients are generated dependent on the thermo-physical properties of the tool material. To determine them the following assumptions and steps are necessary:

- The supplied mechanical power is almost totally transformed into heat.
- The fraction of heat dissipated via the tool is only 5–20 %. Knowledge about this is consequently critical for the determination of thermal stresses.
- From the heat flux, which goes through the contact surface of the cutting wedge, temperature distributions can be determined, for instance by the finite elements method. Prerequisite for this is the knowledge of the thermo-physical data and of the heat dissipation via the tool surface into the environment and into the tool holder. The measurement of the temperature distribution was dealt with in [Chap. 5](#). Due to the difficult data situation, one generally cannot do without measurements.
- The thermal stresses in turn can be calculated by FEM from the temperature distribution knowing the thermal expansion coefficient and the elastic constants.

Thermal stresses have to be superimposed to the stresses resulting from mechanical loads. As far as there is no plastic flow or cracks nor nonlinear effects, mechanical and thermal stresses can be added. Figure 7.10 shows temperature and stress distributions by thermal load of a ceramic insert.

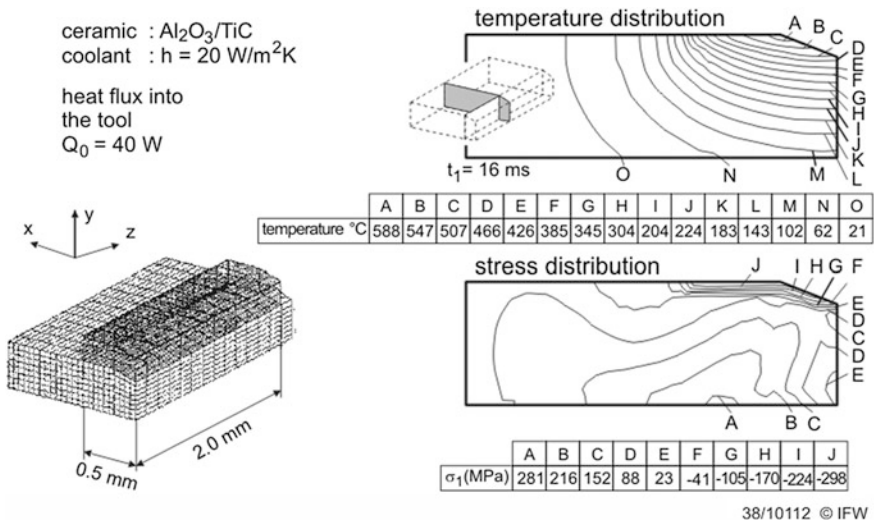


Fig. 7.10 Temperature and stress distribution perpendicular to the major cutting edge [[DEN92](#)]

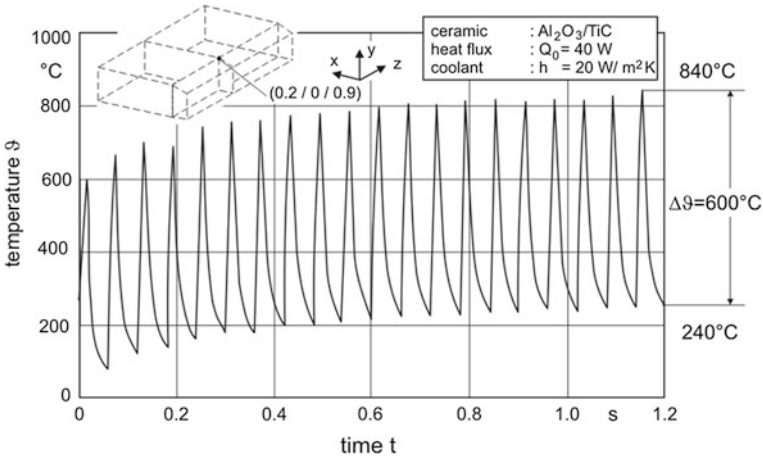


Fig. 7.11 Time temperature characteristic at the chamfer edge [DEN92]

The transient case is of particular interest for thermal stresses, because it can lead to stress inversions due to the temperature alternation. In Fig. 7.11, the contact temperature by milling is shown for a point on the rake face. After a short time, alternating heating and cooling phases lead to an increase of the average temperature until a steady state has been reached. For the considered point on the rake face the stress curves of a heating and cooling period follow (Fig. 7.12).

The main stress σ_3 is proportional to the tool temperature. During the heating phase its value increases depressively to the stress maximum at the end of this phase, then the value decreases exponentially according to the temperature characteristic.

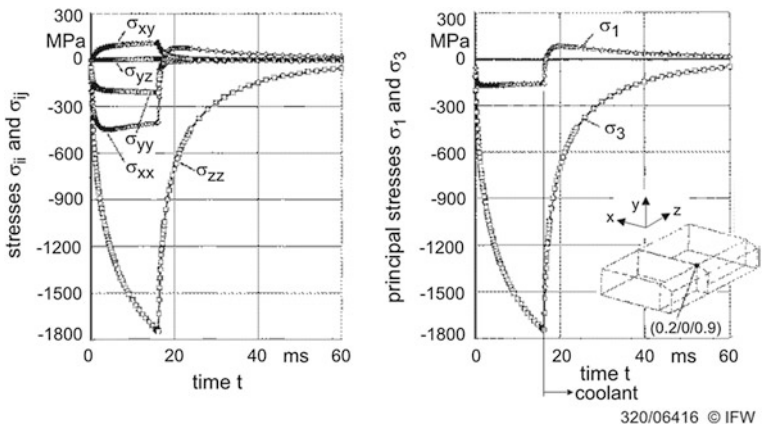


Fig. 7.12 Stresses in the surface [DEN92]

The other main stress σ_1 is significantly different. During the total heating phase the stress value remains nearly constant. With the beginning of the cooling phase, the stress value changes from compression to tension, where the stress maximum $\sigma_1 = 90$ MPa lies about 4 ms behind the beginning of the cooling. The correlation of the normal and main stresses shows that σ_3 basically corresponds to σ_{zz} , whereas σ_1 corresponds to σ_{xx} [DEN92].

For the development and selection of cutting tool materials the influence of the thermal constants such as the heat capacity c_p , the heat conductivity λ and the temperature diffusivity α or the density ρ respectively are of interest. With the example of one-dimensional heat conduction, when a rod with the cross section A is thermally loaded at its front face by the heat flux Q_0 , the temperature inside the rod can be estimated as follows:

$$\Delta\vartheta_{0,t+1} = \frac{1}{\rho \cdot c_p} \cdot \frac{\Delta t}{\Delta z} \cdot \left[\frac{Q_0}{A} + \frac{\lambda}{\Delta z} (\vartheta_{k,t} - \vartheta_{0,t}) \right] \quad \text{with} \quad \alpha = \frac{\lambda}{\rho \cdot c_p} \quad (7.5)$$

with the surface temperature $\vartheta_{0,1}$ and the temperature inside the rod $\vartheta_{k,1}$. Figure 7.13 shows the surface temperature over the temperature diffusivity α , where in one case λ is varied ($\rho \cdot c_p = \text{const.}$) and in the other case $\rho \cdot c_p$ is variable ($\lambda = \text{const.}$).

The heat transport is accelerated by increasing the heat conductivity λ ; the surface stresses are reduced. The heat capacity $\rho \cdot c_p$ is a measure of the implementation of heat in temperature. An increase of the heat capacity therefore also causes temperature reduction [DEN92].

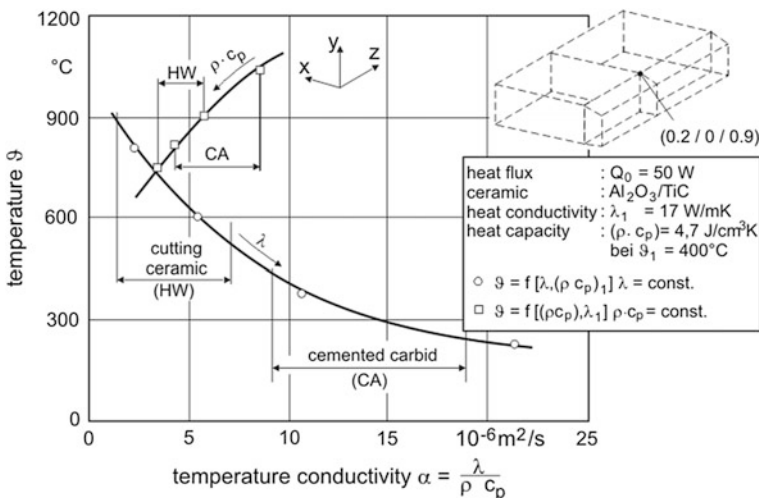


Fig. 7.13 Surface temperature of the cutting face over thermal properties of the cutting material [DEN92]

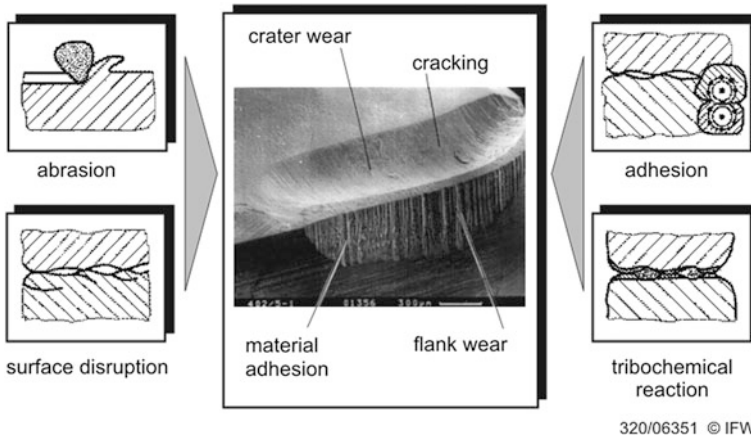


Fig. 7.14 Wear mechanisms and wear forms [DEN92]

7.3 Wear Mechanisms

Depending on the load and its temporal characteristic, different wear causes with different wear mechanisms appear (Fig. 7.14).

Abrasion occurs due to sliding between the active partners through hard constituents of the work material (Fig. 7.15) [VIE70]. It is a purely mechanical process, comparable to micro cutting (micro filing): This process is supported by high surface temperatures of the cutting wedge on the rake and flank face and the linked softening of the cutting material. Under the effect of normal and shear forces,

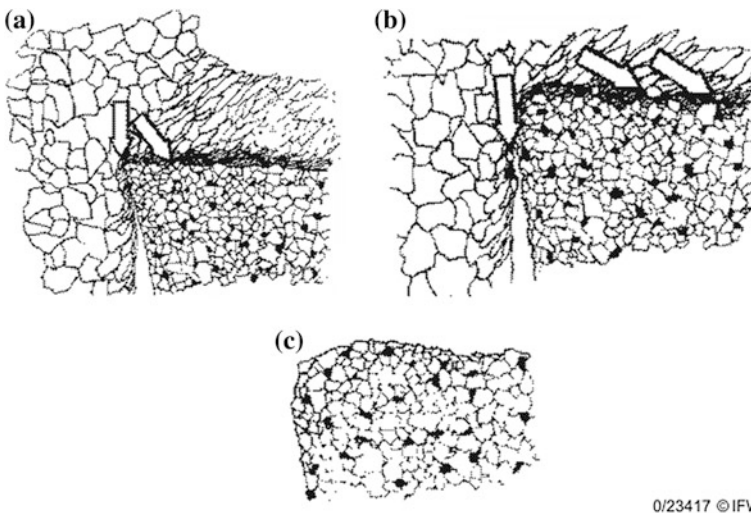


Fig. 7.15 Schematic views of the tool wear by abrasion [VIE70]

softer parts of cutting material are taken away. A fine finished surface of cutting the wedge can become rougher with the operating time. Its micro geometry affects the wear progress only initially, later there is no influence.

Adhesive wear occurs, if particles of the cutting material are transported to the chip or to the cut face of the workpiece by adhesion, i.e., by atomic boundary forces at micro contact spots. Adhesion in cutting is supported by the fact that the faces of the cutting wedge are kept free from passivized layers by a permanent passing-by of material, which itself is of high purity because it is *in statu nascendi*. Basically, two mechanisms of adhesive wear can be distinguished:

- It comes to cold welding (pressure welding) on the cutting wedge. The thus formed deposits are later disrupted—after further growth—out of the cutting material, which means material loss or wear.
- Particles of cutting material weld directly with the cut face and the bottom of the chip and are thereby separated.

Both of these effects decrease with higher sliding speed, i.e., with the cutting speed.

Tribo-chemical wear in cutting results by *diffusion*. With growing temperature of the material the movability of its atoms and molecules increases. Thermally activated migration of constituents of the cutting material into the work material or migration in the opposite direction can occur. Chemical reactions of the immigrated particles with the cutting material or the separation of constituents can cause the development of soft layers, which are removed. During the cutting of carbon steel by tungsten carbide tools, consisting of WC and Co, the following reactions take place:

- Fe diffuses into the binder phase Co. It comes to the formation of Fe-Co-mixed crystals.
- Co migrates off the tungsten carbide towards the Fe and forms mixed crystals.
- C migrates from the steel via the cobalt phase into the cutting material and leads to the decomposition of the WC by forming softer iron-tungsten-mixed carbides.

A further cause of tribo-chemical wear is *oxidation*. It can occur at the edges of the contact zones, if the surface temperature and the tendency of oxidation are high enough. As illustrated in Fig. 7.16, the oxidation wear is negligible for stellites due to a low tendency to oxidation and for not alloyed tool steels and high speed tool steel because of softening even at low temperatures.

Schematically, the importance of the different types of wear mechanisms on the total wear in steel cutting depending on the cutting speed and thus on the cutting temperature is shown in Fig. 7.17.

The partition of the different types of wear mechanisms cannot be generally indicated. Depending on the matching of work material—tool material and depending on the cutting edge temperature and cutting speed, the one or the other type can be dominant.

Cracks occur especially under transient cutting edge loading. Parallel cracks (lateral cracks) and cracks perpendicular (normal cracks) to the cutting edge can be

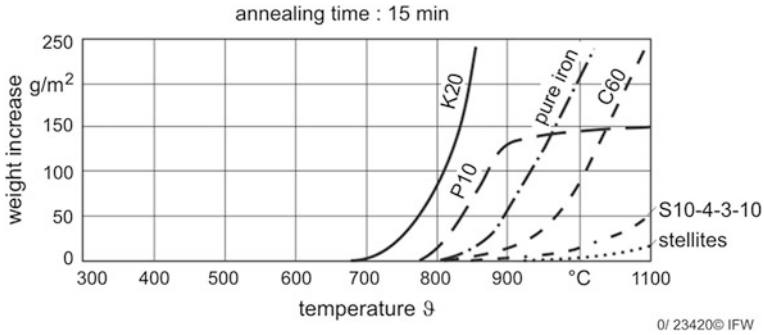
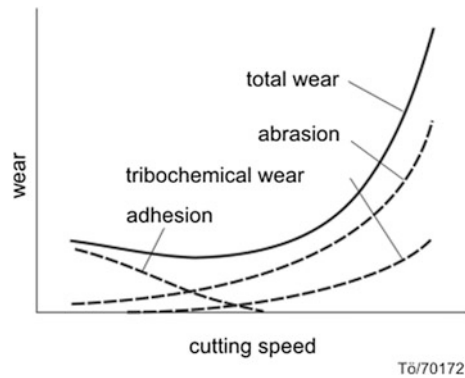


Fig. 7.16 Increase of weight by heating of different cutting materials

Fig. 7.17 Influence of speed on wear mechanisms



distinguished (Fig. 7.18). Normal cracks often occur with regular distances. They are called comb cracks and are of thermal origin [BAR88].

For these cracks, elastic or—depending on the deformability—elastic–plastic mechanisms can be dominant. Perpendicular to the rake face, a sloping temperature characteristic occurs (Fig. 7.19). By cooling from the outside the temperature near the cooled surface decreases, finally resulting in tension thermal residual stresses. If plastic compression ($\epsilon < 0$) takes place during cutting, tensile stresses in the surface follow after cooling. Both effects can lead to cracks. The regularity of the comb cracks follows from the fact that the critical tensile stresses of volume changes are dependent on distance.

7.4 Tool Life

Tool life is the time T , during which a tool cuts from the first cut up to the achievement of a previously set wear limit under given conditions.

Fig. 7.18 Wear at the cutting edge

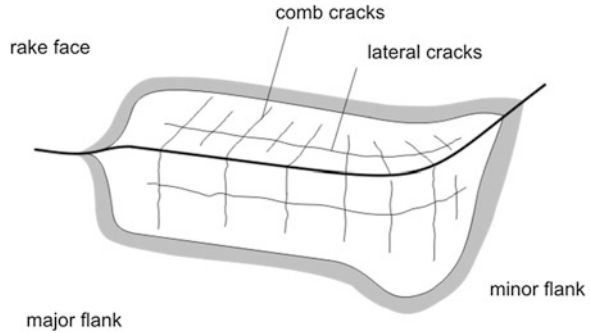
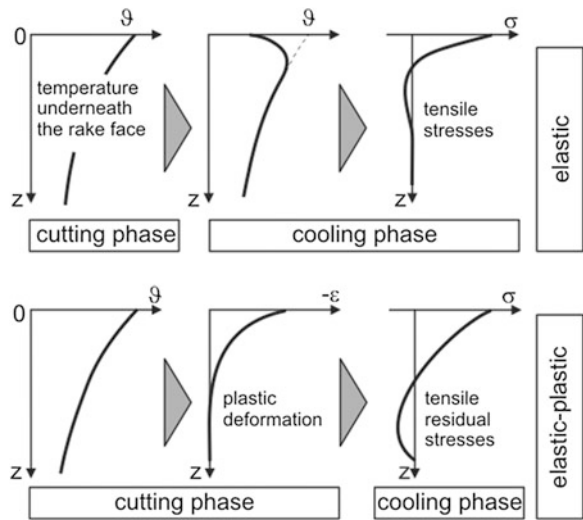


Fig. 7.19 Thermally induced generation of cracks



320/06773 © IFW

The tool life of a tool depends on the tool material-work material matching, on the machining conditions, under which the tool is applied and on the cutting wedge geometry. Different tool life criteria are applied to assess the temporal alteration of the tool and to determine the end of the tool life.

The appropriate effort to determine the tool life criterion is dependent on the type of operation and on the batch size to be machined. Generally the following applies:

- large batch production \Rightarrow test for the given conditions
- piece or small batch production \Rightarrow empirical values.

Maximum values for the size of flank wear land are given in Table 7.1. For the crater wear the following critical values are generally assumed:

crater depth: $KT_{tol} = 1.0-1.5$ mm

crater ratio: $K_{tol} = 0.4$

Table 7.1 Allowable widths of flank wear land

VB_{tol}	High speed steel/carbide (mm)	Ceramic (mm)
Roughing	0.8–1.0	0.3
Finishing	0.2–0.4	0.3

However, the tolerable crater depth according to ISO3685 depends on the set feed.

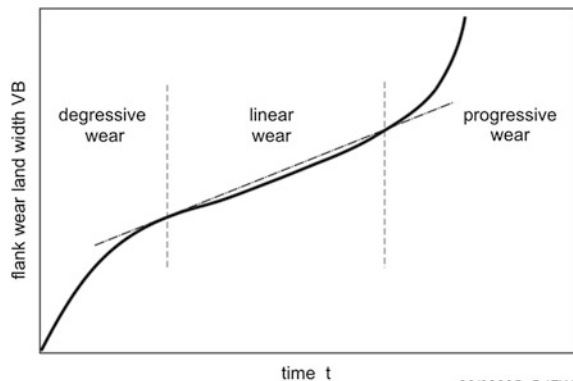
Tool life times refer to a certain criterion, for instance $T_{VB0.4}$ means a tool life time up to a flank wear land of $VB = 0.4$ mm. The typical temporal development of the flank wear is shown in Fig. 7.20.

On the one hand, the wear depends on fixed or optimized parameters which are generally no longer influenced during the operation:

- cutting material,
- work material,
- tool geometry,
- cutting fluid, dynamic behavior of tool, workpiece and machine,
- and, on the other hand, on parameters to be set:
- cutting speed v_c ,
- feed f ,
- cutting depth a_p .

The cutting speed has the strongest influence on continuously progressing wear such as flank and crater wear. Similar but differently steep wear curves over cutting time are plotted in Fig. 7.21. At the tool life criterion, the tool life times assigned to each cutting speed can be metered [TAY07].

F.W. Taylor (USA, 1856–1915) detected an exponential correlation between cutting speed and tool life for a given criterion as flank wear VB_{tol} or crater wear KT_{tol}

Fig. 7.20 Timewise development of the flank wear

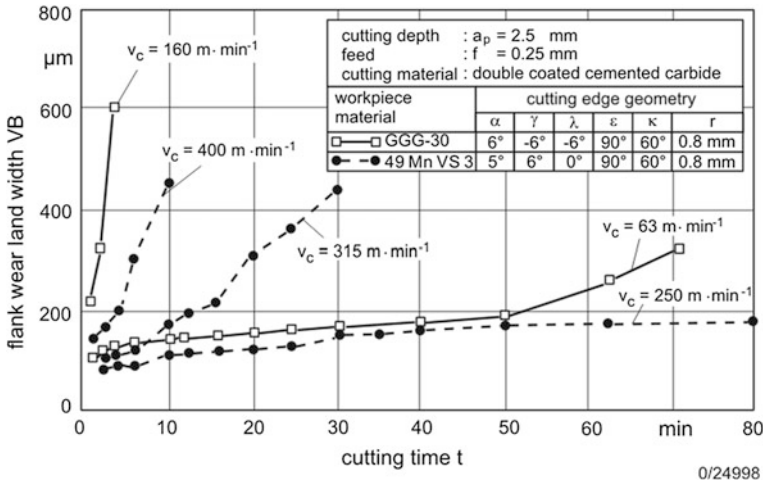


Fig. 7.21 Comparison of flank wear lands for the machining of steel and cast iron

$$v_c = C \times \left(\frac{T}{T_0}\right)^{1/k} \tag{7.6}$$

with $T_0 = 1$ min and the Taylor coefficient C (related cutting speed for 1 min of tool life). The relationship is generally written as a numerical value equation:

$$v_c = T^{1/k} \tag{7.7}$$

This equation can be plotted as a straight line in double logarithmic coordinates. These lines are called “Taylor lines” (Fig. 7.22). The constants k and C may be taken from tables (Table 7.2)

The slope of the straight line indicates the sensitivity of a tool material-work material combination against cutting speed increase. The width of the scattering band allows to conclude on the reliability of the tool life or respectively the probability of the tool life criterion happening (see Sect. 7.5). Thereby, the flank face or the crater wear may be critical depending on the tool material-work material combination and on the machining conditions. If both wear forms occur, the wear of flank face generally determines the tool life in the lower speed domain, whereas the crater wear determines in the higher speed range. The Taylor line for the wear of the flank face is shallower than for the crater wear.

Figure 7.23 indicates the influence of the work material on the position of the Taylor line. Higher strength reduces the tool life as the comparison of globular cast iron EN-GJS-700-2 and EN-GJS-600-3 shows. On the other hand, the composition and the structure have a decisive impact, which can be taken from the Taylor lines of globular cast iron EN-GJS-700-2 and micro alloyed steel 49MnVS3 of equal strength.

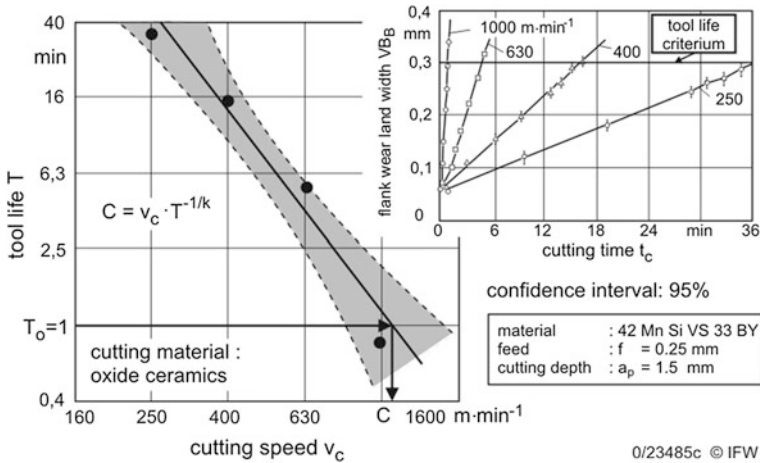


Fig. 7.22 Determination of Taylor lines

Table 7.2 Coefficients to determine the Taylor lines

Taylor function $v_c = C \cdot T^{1/k}$	Uncoated carbide		Coated carbide		Oxide ceramic (steel) nitride ceramic (cast iron)	
	C (m/min)	k	C (m/min)	k	C (m/min)	k
St52-2	299	-3.85	385	-4.55	1,210	-2.27
St70-2	226	-4.55	306	-5.26	1,040	-2.27
Ck45 N	299	-3.85	385	-4.55	1,210	-2.27
16MnCrS5BG	478	-3.13	588	-3.57	1,780	-2.13
20MnCr5BG	478	-3.13	588	-3.57	1,780	-2.13
42CrMoS4 V	177	-5.26	234	-6.25	830	-2.44
X155CrVMoV51G	110	-7.69	163	-8.33	570	-2.63
X40CrMoV51G	177	-5.26	234	-6.25	830	-2.44
GG-30	97	-6.25	184	-6.25	2,120	-2.50
GG-40	53	-10.0	102	-10.0	1,275	-2.78

Tool life and cutting speed may be optimized according to economic aspects. Optimizing criteria may be:

- minimum machining time,
- minimum costs per piece or,
- minimum period costs.

The optimum of machining time, of machining costs or of period costs follows from opposed time or cost fractions related to the tool (increasing with v_c) on the one hand and the machine occupancy (decreasing with v_c) on the other hand (Fig. 7.24). For the piece cost optimization the following applies:

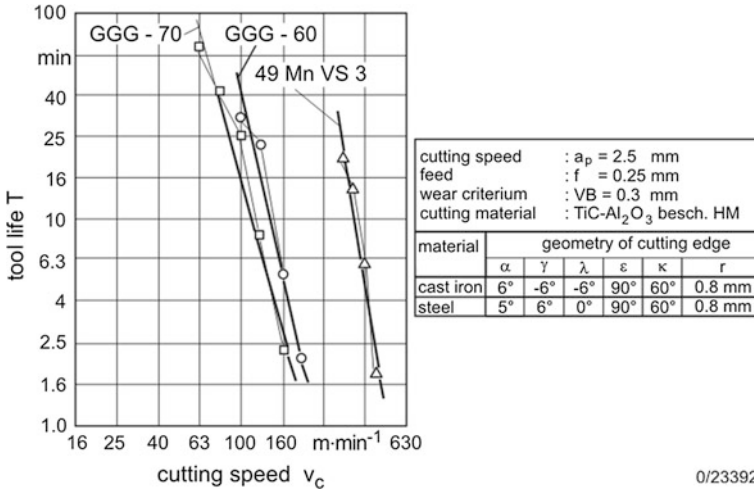
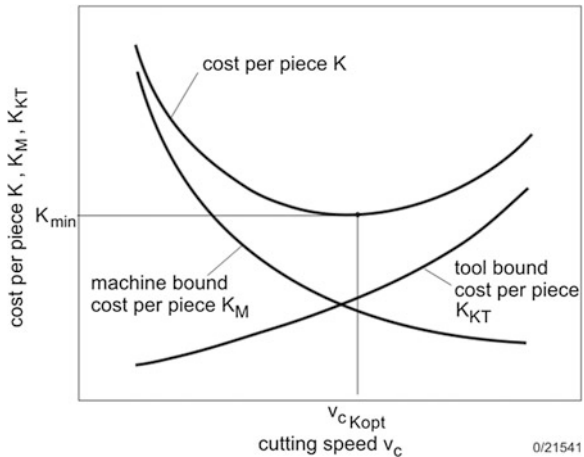


Fig. 7.23 Comparison of tool life for machining steel and cast iron

Fig. 7.24 Machining costs as function of the cutting speed



$$v_{c,Kopt} = C \cdot [(-k - 1) \cdot (t_{tl} + K_{KT}/K_M)]^{1/k} \tag{7.8}$$

The cutting speed for minimum period costs $v_{c,Pop}$ lies between $v_{c,Copt}$ and $v_{c,top}$. The minimum period costs result from an optimization of piece time and piece costs. The following relationships between the different criteria of optimized cutting speeds exist (Table 7.3).

In a *weak economic situation*, it is reasonable to reduce the cutting speed in order to minimize the tool costs since the machine is not fully exploited anyway.

Table 7.3 Optimizing criteria for the cutting speed

$V_{c,Kopt}$	$V_{c,Popt}$	$V_{c,topt}$
Minimum piece costs	Maximum profit	Boom conditions
Normal occupation	Low transparency of market	to allow to keep markets
Long term	Short term	

So other cost fractions such as the energy costs also decrease. Yet it has to be observed that this may lead to a possible increase in staff costs.

A cost optimum is reached by minimizing the tool change time and the tool costs per tool life. This strategy is generally followed in *balanced markets*. The illustrated relationship cannot simply be generalized, especially if a cost comparison with geometrically complex tools is concerned. In Fig. 7.25, the direct cost comparison between two different turning tools is shown. The cutting insert technology enabled a decrease of costs.

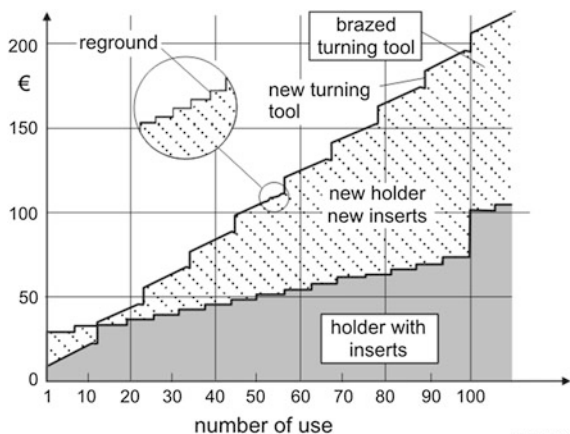
Beside the cutting speed, the set feed also influences the tool life although in a far less sensitive way. The feed, however, may not be freely chosen for many applications, for example, if the surface roughness is required.

7.5 Tool Life Scatter and Process Reliability

In operational practice, it must be noted that the wear development and thus the tool life underlies heavy scattering, even if work materials of the same standard designation are machined with the same tools under identical cutting conditions [VOS76]. The causes are fluctuations of the input parameters (Fig. 7.26).

The set values as input parameters are generally kept constant in narrow limits, if the same machine is applied. Important disturbing quantities are geometric

Fig. 7.25 Cost comparison of two turning tools



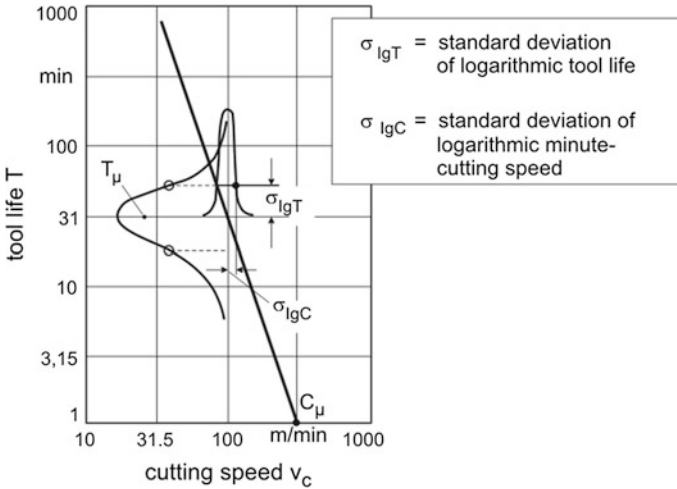


Fig. 7.26 Scattering of tool life and cutting speed [VOS76]

deviations of the unfinished parts [PAT87] and chemical and physical property scattering of the work and tool materials.

The tool life is thus a random variable. Experiments showed that this variable follows the logarithmic Gaussian distribution. So the density of the logarithmic tool life can be specified as

$$f(\lg T) = \frac{1}{\sigma_{\lg T} \sqrt{2\pi}} \cdot e^{-\frac{(\lg T - \lg T_\mu)^2}{2\sigma_{\lg T}^2}} \tag{7.9}$$

with T_μ as the average value and $\sigma_{\lg T}$ as the logarithmic standard deviation of the tool life. The failure probability of the tool $P(A)$ is of interest.

$$P(A) = P(T < T_\mu) = F(\lg T) = \int_0^{\lg T} f(\lg T) d(\lg T) \tag{7.10}$$

By a fast converging series expansion one can write with $|u| < 1$

$$P(A) = \frac{1}{2} - \frac{1}{\sqrt{2\pi}} \left[|u| - \frac{|u|^3}{6} \right] \tag{7.11}$$

with

$$u = \frac{\lg T - \lg T_\mu}{\sigma_{\lg T}} \tag{7.12}$$

The tool life reliability is then

$$R(T) = 1 - P(A) \tag{7.13}$$

The logarithmic Gaussian distribution is suitable for integration into the Taylor relationship. It is simply

$$\sigma_{lg C} = -\frac{1}{k} \sigma_{lg T} \tag{7.14}$$

This relationship is shown in Fig. 7.26. The consequence is that for the complete representation of the Taylor relationship a value triple should be taken into account, considering the random character of the tool life.

$$C_\mu, k \text{ and } \sigma_{lg C} \tag{7.15}$$

The tool life line, whose position is described by C_μ , means a reliability of 50 %, measured at the tool life criterion. The further a parallel line is moved to the left (to lower cutting speeds), the greater the reliability. In Fig. 7.27, the line of the distribution function is displayed in a probability net and the tool life lines in the T- v_c -diagram. For $C_\mu = 300$ m/min the failure probability is 50 %, for $C = 230$ or 180 m/min respectively, however, only 5 % or 0.1 %.

7.6 Influence of Work Material on Wear

The machinability of a work material shall be assessed to the criteria tool wear, forces, chip formation and surface quality. It depends on the material composition,

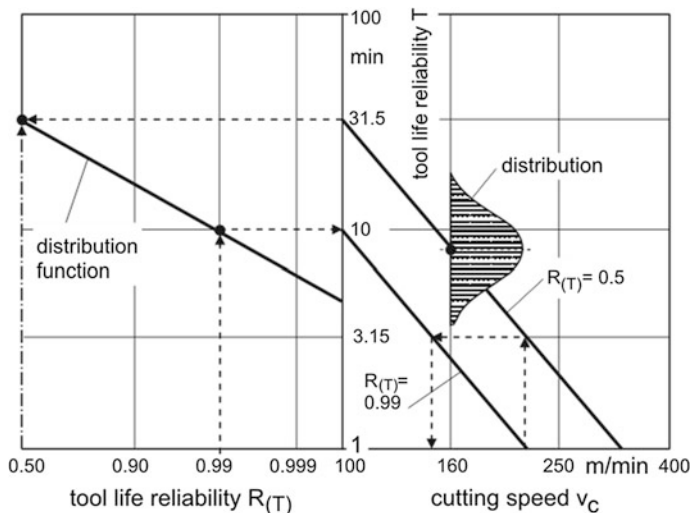


Fig. 7.27 Tool life reliability and Taylor line [VOS76]

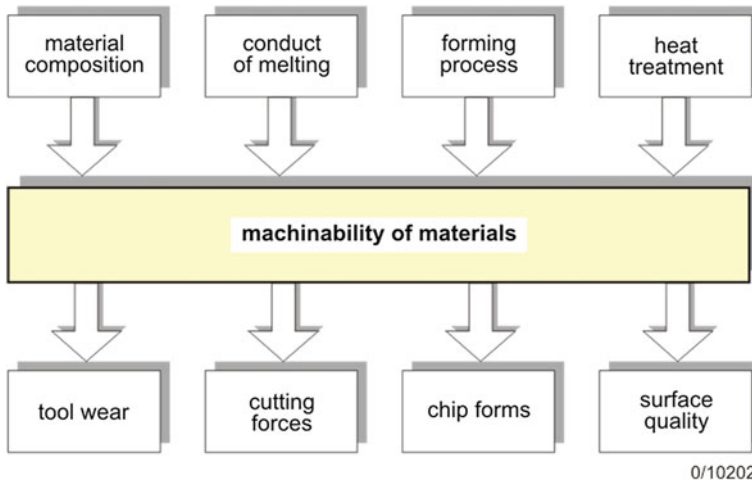


Fig. 7.28 Influence factors and assessment criteria of machinability

the melting procedure, the forming processes and the heat treatment (Fig. 7.28) [VIE70, WIN83]. The influences on the wear are illustrated by examples of hypereutectoid and low alloyed carbon steel.

7.6.1 Work Material Composition

The most important companion of steel is *carbon*. Carbon exists mainly in a bonded form in iron carbide, cementite (Fe_3C). Cementite with a C content of 6.67 % is rhombic crystalline and has a high hardness of $\text{HV} \approx 1,000$. The other basic component is the α -mixed crystal, ferrite, with a C content of less than 0.02 %. Ferrite is body-centered and only has a low hardness around $\text{HV} \approx 90$. The eutectoid perlite (0.86 % C) consists of a fine mixture of ferrite and cementite. Hypo-eutectoid steels consist of a mixture of ferrite and cementite, hypereutectoid ones of secondary cementite and perlite.

The percentage of hard components provides an indication to the wear tendency of steels. The force components increase with the C content. Though some steels with a low C content ($<0.02\%$), such as softly annealed case hardening steels, have a tendency to sticking and to adhesion, which again worsens the machinability.

Oxygen gets into the steel during manufacturing. It is found only as oxide inclusions, such as manganese oxide, silicon oxide (silicates) and aluminum oxide. All oxides have wearing effects, particularly alumina [WIN83].

Silicon easily combines with oxygen and yields hard silicate inclusions. It leads to an increase of the strength of ferrite and increases the tool wear.

Sulfur has a low solubility in steel, forming stable sulfides. Its binding ability to metals increases in the order of nickel (Ni), cobalt (Co), molybdenum (Mo), iron (Fe), chromium (Cr), manganese (Mn), zirconium (Zr), and titanium (Ti). Which sulfides arise therefore depends on the alloying constituents of the steel. Iron sulfide is undesirable, because it has a low melting point and is deposited at the grain boundaries. Red or hot shortness may occur during hot forming. Manganese, which has a greater affinity to sulfur than iron, can lead to the development of manganese sulfides (MnS), which have a higher melting point than iron sulfides and thus red or hot shortness can be avoided. Manganese sulfides act in a wear reducing manner.

Manganese binds sulfur and so also helps steel to achieve better mechanical properties. For a manganese/sulfur ratio greater than $Mn/S = 1.7$ the entire sulfur is set to manganese sulfur with the melting point at 1,600 °C or to other manganese-containing sulfides. In flow chip formation, manganese sulfides can moreover apply a covering and lubrication effect on the cutting wedge (see melting procedure, Sect. 7.6.2).

A *phosphorus* content of up to 0.1 % benefits the machinability with the fact that the steel becomes brittle and thus more advantageous chip forms occur. However, the increase in hardness can reduce the tool life. Figure 7.29 shows an overview of the effects of the steel composition on the tool wear or the tool life respectively.

alloy elem.	effect	cause, condition	alloy elem. (hardness)	effect	cause, condition
C	T ↓	if R_m is set by C	Cr	T ↓	if carbides are existing
Si	T ↓	strength of ferrite ↑, silicates	Mo	T ↓	
Ni	T ↓	toughness increases	W	T ↓	
Mn	T ↑	for $MnS > 1.7$ formation of MnS, parallel shift of tool life line	Pb	T ↑	
S	T ↑		Bi	T ↑	
Ca	T ↑	formation of globular non-metallic inclusions, formation of protective layers	V	T ↓	strength increases by fine carbide and carbonitride precipitations
Te	T ↑	formation of globular non-metallic inclusions	Ti	T ↓	
P	T ↑	A ↓ decreases	HB	T ↓	rake face temperature increases

assumed is in each case an increase of the alloy content of the hardness respectively
T = tool life

319/05420

Fig. 7.29 Influence of alloy constituents and hardness on tool life

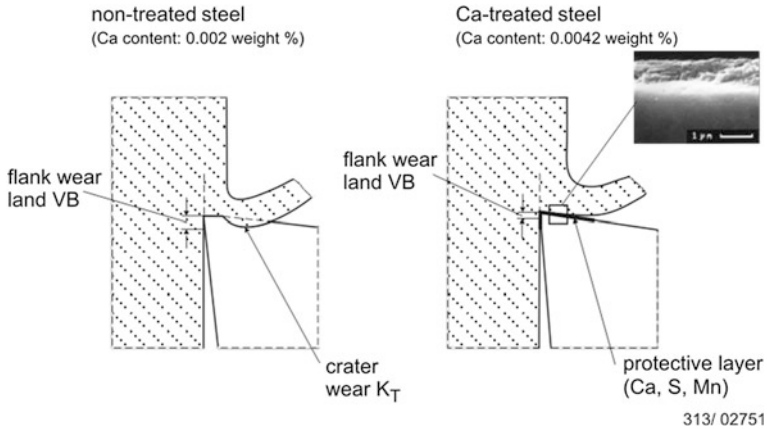


Fig. 7.30 Wear reduction by separating layers

7.6.2 Melting Procedure

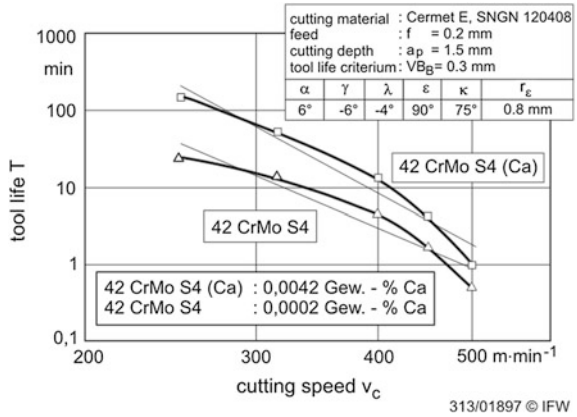
By adding deoxidizing agents such as aluminum, silicon or manganese which have a high affinity to oxygen, a strong gas development is suppressed during the solidification of the melt. The released oxygen gets bound. Alumina and silicon oxides are hard inclusions and not formable. Tool wear is especially increased, if the oxide inclusions exist in large quantities or in line form in the steel. The choice of suitable deoxidizing agents can favorably influence the wear. Steels deoxygenated with calcium-silicon or ferro-silicon generates wear-inhibiting oxide and sulfide protective coatings on tungsten carbide and ceramic cutting edges. In Fig. 7.30, the mechanism of the wear-reducing effect of the coatings is shown.

The coating consisting of (Mn,Ca)S (thickness ca. 1 μm) has a separating and lubricating effect, which especially diminishes crater wear clearly. The reduction of the friction generated at the cutting edge results in a lower thermal load of the tool. The coating can also act as a diffusion barrier between tool and work material. Figure 7.31 shows the tool life depending on the cutting speed for a calcium-treated and an untreated steel.

The gains in tool life due to the treatment are considerable. EDX analyses show that in the crater zone of Ca treated steel deposits with Ca concentration exist and especially in the zone of notch wear accumulations of sulfur and manganese occur (Figs. 7.32 and 7.33) [TÖN89]. A comparison of the EDX analyses of iron and silicon shows that in the domain covered by calcium almost no iron exists. Therefore, the direct contact between iron and the tool insert is inhibited.

A high concentration of iron exists in the flank wear zone, in the crater ramp and in the notch wear zone when machining untreated steel. The existence of a cover of (Ca,Mn)S cannot be proved so that a direct contact of steel and incorporated carbides (and also aluminum oxides) occurs here, which results in a higher wear at the flank and at the crater zone.

Fig. 7.31 T - v_c -dependency, Ca-treated and untreated steel



7.6.3 Heat Treatment

By means of the heat treatment the texture of steels can be influenced to a large extent. The following components influence the wear unfavorably in rising order:

- ferrite
- perlite with mould-in cementite
- course perlite
- fine perlite

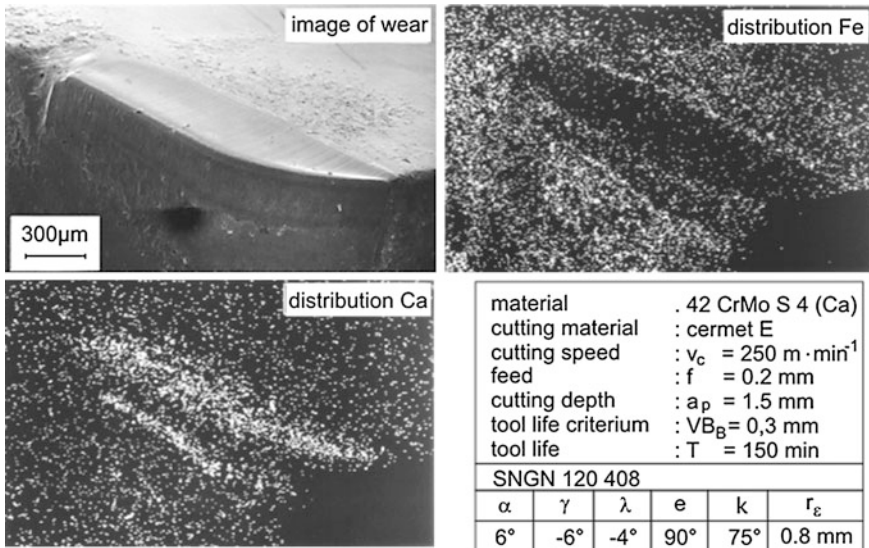


Fig. 7.32 Distribution of elements after machining Ca-treated steel

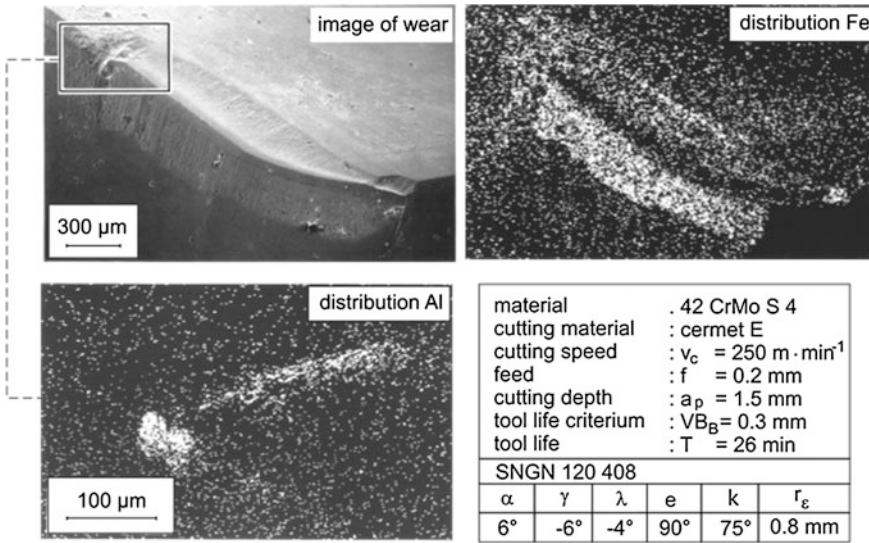


Fig. 7.33 Distribution of elements after the machining of non-treated steel

- bainite
- martensite
- cementite.

In addition, a considerable decrease of wear can result at equal strength from the coarseness of work material grains such as a BY-treatment (controlled cooling from forging heat), i.e., precipitation hardening ferritic-pearlitic steel (Fig. 7.33). The coarse structure of the texture is seen as the cause [WIN83].

7.7 Rounding of the Cutting Edge

In addition to the macro geometry of a cutting tool (rake angle, clearance angle, etc.), it is the micro geometry of the cutting edge, which determines the performance and the wear characteristic. The cutting edge shape, for instance, is of special importance for hard turning operations when high demands exist at the workpiece surface. Above all, cutting a workpiece surface of high quality requires a well-defined cutting edge. The cutting edges endure high force and temperature loads. Hyper sharp cutting edges cannot meet these requirements and have only a short life time. Despite the low strength of the cutting edge, small break-outs of hard carbide particles out of the bonding are causal due to the grinding process [DEN02] (Fig. 7.34, left upper part). The targeted rounding or chamfering of the cutting edge allows a uniform quality of the machined part and an increase of performance and tool life.

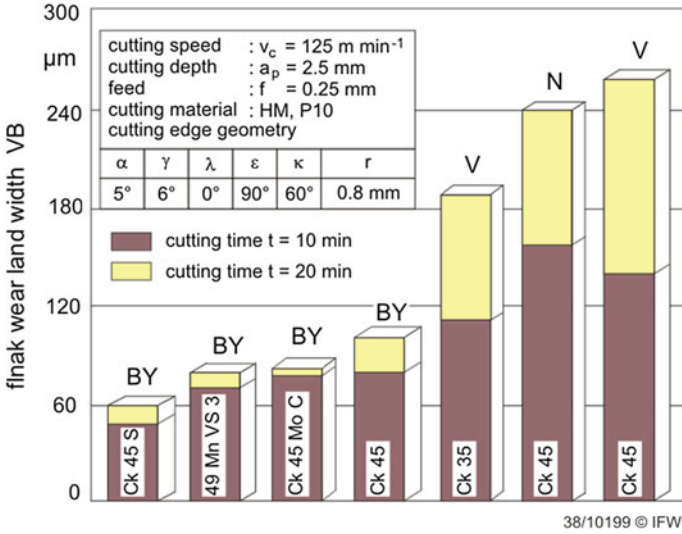


Fig. 7.34 Influence of work material modification and heat treatment on wear [WIN83]

For the rounding or chamfering of the cutting edge, it is subjected to an additional processing step after grinding. Different methods are applied for this preparation. Among these are brushing, abrasive blasting or polishing as well as several grinding processes [FRI02].

A rounding of the cutting edge is not necessarily circular. As a matter of fact it can be expected that due to the oriented indentation of the cutting wedge into the work material, deviation from circular shape brings benefits. However, a broader definition of the edge geometry is needed. To come to a more detailed characterization of the cutting edge, four parameters are introduced: Δr , φ , S_x , S_y . The procedure of measurement is shown in Fig. 7.35. The parameter Δr describes the size of the rounding, the angle φ (not to be confused with the feed motion angle) describes the displacement of the cutting edge either to the rake or to the flank face and the parameters S_x and S_y describe the sharp or blunt course to the rake or the flank face. These parameters can be measured automatically with little effort by means of a mechanical stylus and a measuring program or optically. The so measured values allow a defined characterization of the cutting edge geometry and a systematic identification of the influencing values for an optimized cutting process.

Commonly-practiced edge roundings for the machining of steel are in the domain of $\Delta r = 10\text{--}30 \mu\text{m}$. The machining of titanium requires a sharp edge as far as possible, i.e., $\Delta r \approx 0$. Tests of orthogonal grooving, where different edge shapes have been processed in a targeted way, show that the uniform rounding with $\varphi = 0$ results in the maximal machining forces in all cases (Fig. 7.36). It also shows that cutting edges with unequal forms—whether in a positive or negative direction (+ or $-\varphi$)—result in lower machining forces.

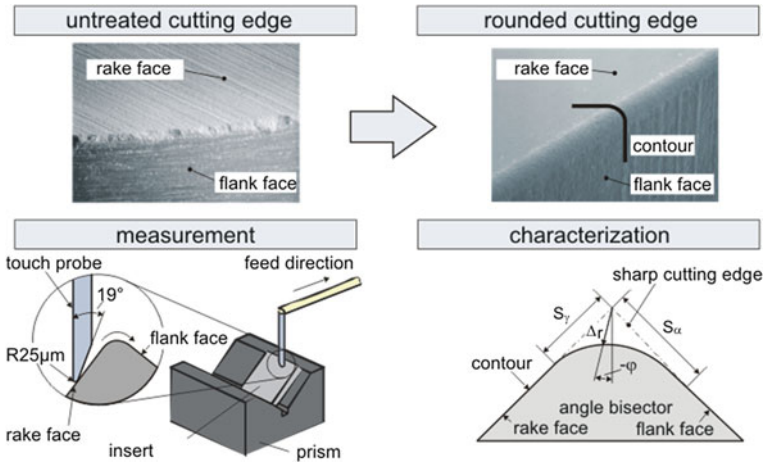


Fig. 7.35 Break-outs at the cutting edge

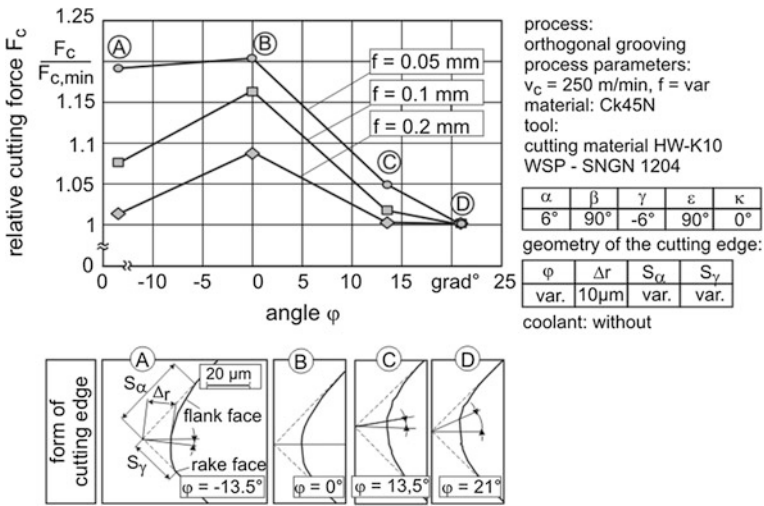


Fig. 7.36 Characterization of the cutting edge by new parameters—influence on the cutting force

With smaller feeds the force alterations by changes of the angle φ are greater than with larger feeds. It can be recognized from this, that the influence of the micro-geometry of the cutting edge is greater in finishing – which was to be expected. The machining forces can be reduced by unequally rounded cutting edges. Thus an increased quality of the surface and reduced wear can be achieved.

7.8 Questions

1. Characterize the interaction between wear, temperature and forces in cutting.
2. What types of wear forms do you know?
3. Explain the influence of the clearance angle on the flank wear.
4. What lower bound of the clearance angle can be derived from the movement components of cutting?
5. How does wear influence the chip formation and the process result?
6. What kind of wear mechanisms (wear causes) do you know?
7. Why does the adhesive wear decrease with higher speeds?
8. How can the shape of the crater wear be explained?
9. Why has cast iron with lamellar graphite to be machined by tungsten carbide with lower speeds than carbon steel?
10. What chemical effects influencing the wear do you know?
11. What principles can be applied to measure the wear?
12. How is tool life defined? How is tool life determined?
13. What circumstances can limit the tool life?
14. What conditions or parameters respectively does the wear depend on?
15. Outline the typical course of the flank wear land over cutting time.
16. What dependency exists between speed and tool life and how can it be described?
17. What influence do feed and tool life criterion have on the Taylor relationship? Outline the changes.
18. Give a qualitative outline of the dependence of tool cost, machine cost and piece cost on the cutting speed.
19. What is the minimum of piece costs?
20. What is the minimum of period costs?
21. According to what criteria can the tool life be optimized?
22. What parameters determine the time-optimal cutting speed?

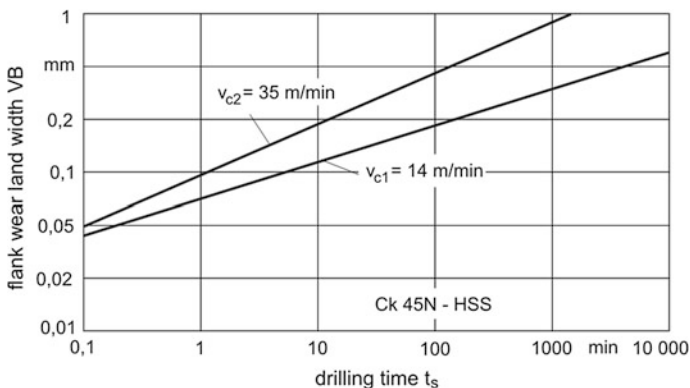


Fig. 7.37 Flank wear land dependent on drilling time

23. Where are the values of optimized cutting speed following the criteria piece cost, period cost or piece time?
24. The time-optimal cutting speed has to be determined for a drilling operation by a twist drill. The wear characteristic follows from the diagram in Fig. 7.37. The flank wear land of $VB = 0.2$ mm should be taken as the wear criterion. Furthermore, the tool changing time of $t_{tc} = 6$ min is known.

References

- [BAR88] Bartsch, S.: Verschleißverhalten von Aluminiumoxid-Schneidstoffen unter stationärer Belastung [Wear behavior of aluminum cutting ceramics under stationary load]. Fortschritt-Berichte VDI Reihe 2, Nr. 161
- [DEN92] Denkena, B.: Verschleißverhalten von Schneidkeramik bei instationärer Belastung [Wear behavior of cutting ceramics under transient loads]. Dr.-Ing. Diss. Univ. Hannover (1992)
- [DEN02] Denkena, B., Friemuth, T., Fedorenko, S., Groppe, M.: Neue Parameter zur Charakterisierung der Schneidengeometrien an Zerspanwerkzeugen [New parameters to characterize the cutting geometry at tools]. Werkzeuge-Sonderausgabe der Zeitschrift Fertigung, 24–26 (2002)
- [DEN08] Denkena, B., Boehnke, D., Meyer, R.: Reduction of wear induced surface zone effects during hard turning by means of new tool geometries. Prod. Eng. Res. Dev. **2**, 123–132 (2008)
- [FRI02] Friemuth, T.: Herstellung Spanender Werkzeuge [Manufacturing of Cutting Tools]. Universität Hannover, Habilitationsschrift (2002)
- [PAT87] Patzke, M.: Einfluss der Randzone auf die Zerspanbarkeit von Schmiedeteilen [Influence of the surface zone of forged components on the machinability]. Dr.-Ing. Diss. Univ. Hannover (1987)
- [SPA67] Spaans, G.: An exact method to determine the forces on the clearance plane. CIRP Annals **15**, 463–469 (1967)
- [TAY07] Taylor, F.W.: On the art of cutting metals. Trans. Am. Soc. Mech. Eng. **28**, 31–279 (1907)
- [TÖN89] Tönshoff, H.K., Kaestner, W., Schnadt, R.: Metallurgische Auswirkungen der Calciumbehandlung von Stahlschmelzen auf die Bearbeitbarkeit [Metallurgical effects of the calcium treatment on the machinability]. Stahl und Eisen **109**(13), 651–660 (1989)
- [VIE70] Vieregge, F.: Zerspanung der Eisenwerkstoffe [Cutting of ferrous materials]. 2. Stahl Eisen M.B.H. Verlag, Auflage, Düsseldorf (1970)
- [VOS76] Voss, W.: Optimierung Spanender Fertigung [Optimization of Cutting Production]. Technischer Verlag Resch, München (1976)
- [WIN83] Winkler, H.: Zerspanbarkeit von niedriglegierten Kohlenstoffstählen nach gesteuerter Abkühlung [Machinability of low alloyed carbon steels after controlled cooling]. Dr.-Ing. Diss. Univ. Hannover (1983)

Chapter 8

Cutting Materials

Cutting materials determine the economic viability of a cutting process to a great extent. The development of the cutting technology is therefore directly linked to the development of the cutting materials. Figure 8.1 shows the hour cutting speed. That is the cutting speed applicable for one hour of tool life, which has become possible due to new developments since the last turn of the century. Per decade, the possible cutting speed is approximately doubled.

In addition to the still often applied high speed steels the following hard cutting materials can be named, classified according to [DIN ISO 513](#):

- tungsten carbide
- cutting ceramics
- diamond
- boron nitride.

8.1 Requirements on Cutting Materials

Cutting materials have to be wear resistant (hard) and sufficiently tough to ensure a long tool life and high process reliability. Both requirements cannot be fulfilled simultaneously for the reason that hard materials are generally not tough and vice versa (Fig. 8.2). The loads and the wear mechanisms (see [Chap. 7](#)) require the following properties [[VIE70](#), [TÖN90](#)]: Hardness, hot hardness, toughness and chemical stability (Table 8.1).

Hardness: Hardness is a measure of the wear resistance of the cutting material. It counteracts abrasive and adhesive wear. Cutting materials can take their hardness from the base material, from hard particles incorporated in a binding matrix or exclusively by hard crystallites, which are directly connected by grain boundaries. The hard material content is accordingly different (Fig. 8.3).

Hot hardness: Even under high temperatures of the cutting wedge, the hardness has to be maintained to counteract abrasive wear and plastic deformations (Fig. 8.4).

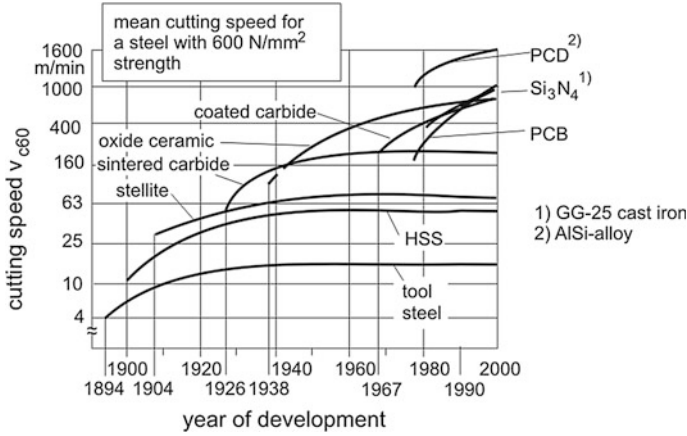


Fig. 8.1 Development of cutting materials

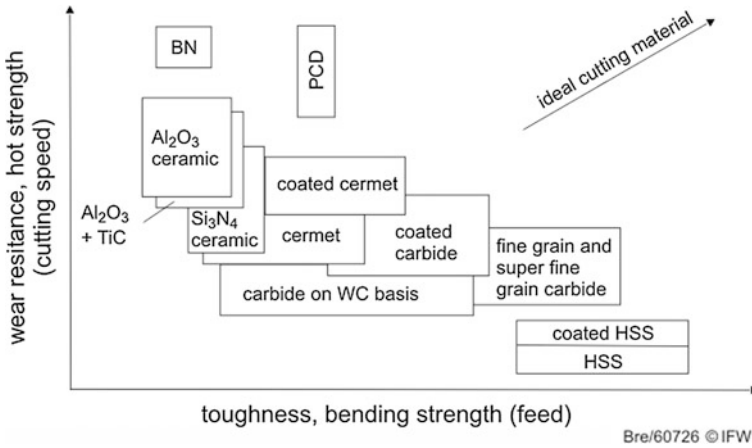


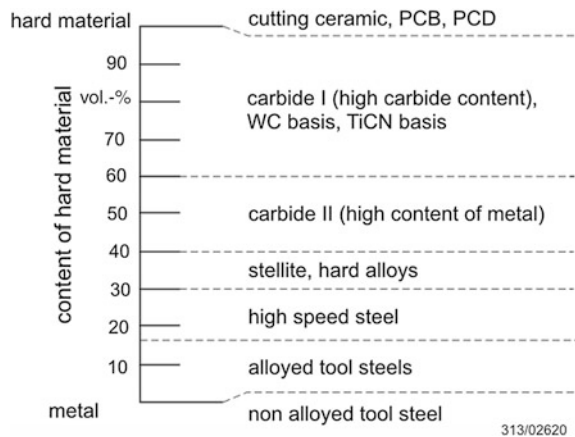
Fig. 8.2 Cutting materials and their wear resistance and toughness [KLO08]

Toughness: The ability of materials to withstand the propagation of cracks is called toughness. The fracture mechanics deliver a measure for the toughness by the stress intensity factor, the K_{Ic} -value (also called the fracture toughness). The K_{Ic} -value is determined with a technological test procedure with prescribed sample geometry after a numerical value equation. According to Fig. 8.5, a sample with defined initial fracture incipient crack (for instance a fatigue crack introduced by a tension pulsating stress) is loaded in a tension or 3-point bending test so far that the crack is unstable, i.e. abruptly propagating. The applied fracture stress is σ_b ; a is the length of the crack; Y is a calibrating factor, that takes the sample geometry into account.

Table 8.1 Properties of cutting materials

	Hardened steel	HSS	Carbide	Cutting ceramic	PCB	PCD
Density [g/cm ³]	7.8	8.0–8.8	6.0–15.0	3.8–7.0	3.4	3.5
Hardness HV 30	700–900	750–100	1,300–1,700	1,400–2,400	4,500	7,000
Young's modulus [GPa]	220	260–300	430–630	300–400	680	890
Melting point [°C]	1,200–1,400	1,300–1,400	~ 1,300	1,700–2,050	2,700	3,700
Temperature stability [°C]	200–300	600–800	800–1,200	1,300–1,800	1,500	600
Temperature expansion coeff. at room temperature [10 ⁻⁶ /K]	13–15	9–12	5–7.5	7.4–9	3.6	0.8
Compression strength [N/mm ²]	2,000–3,000	2,500–3,500	4,000–5,900	2,500–4,500	4,000	3,000
Bending strength [N/mm ²]	1,800–2,500	200–3,800	800–2,200	300–700	600	300

Fig. 8.3 Hard constituent in cutting materials



The stress intensity factor K_{Ic} of cutting materials lies between 13 and 30 MPa m^{1/2} for high speed steels, 8 and 18 MPa m^{1/2} for tungsten carbide and 2 and 7 MPa m^{1/2} for cutting ceramics.

For ceramics, which show brittle behavior, the bending fracture strength also gives an indication on the toughness. Its numerical value given in MPa is 100–200 times as much as the K_{Ic} -value. The toughness affects the fracture tendency of the cutting material and the wear resistance in transient mechanical and thermal loading. For instance, the latter loading is called thermo shock. The resistance against temperature change is called temperature change resistance or thermo-shock resistance.

Chemical stability: To counteract tribo-mechanical wear cutting materials should be inert against work materials and environmental agents such as air and cutting fluids. Chemical stability is a prerequisite for the use of a cutting material under high temperatures. A measure for the chemical stability is the bond

Fig. 8.4 Hot hardness of cutting materials

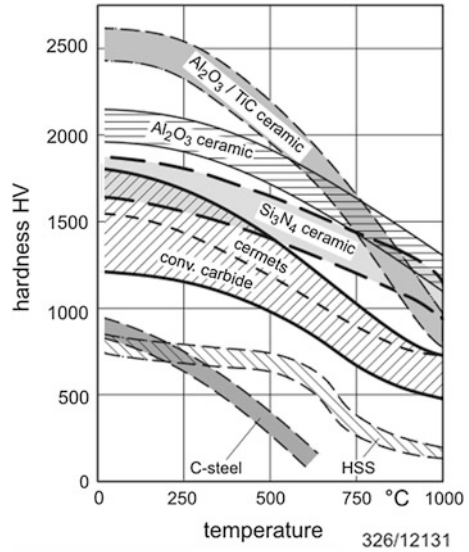
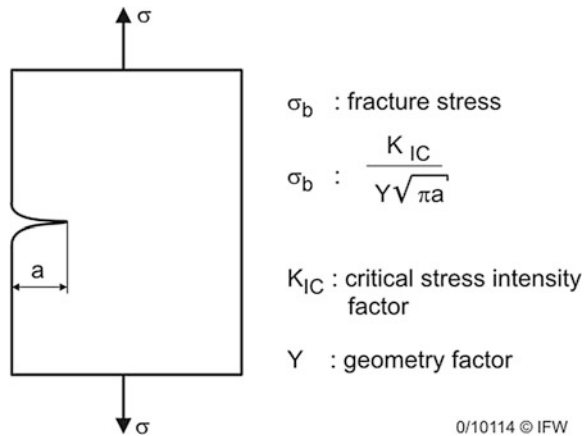


Fig. 8.5 Definition of fracture toughness



enthalpy. A large negative bond enthalpy of an alloy corresponds to high chemical stability, which means a large amount of heat energy has to be introduced to cause a chemical reaction.

There is no ideal cutting material, which fulfills all demands named above. For all cutting materials the fundamental dualism applies to be either hard and wear resistant or tough and resistant against transient loads.

8.2 Tool Steels

One distinguishes between unalloyed and alloyed tool steels. Unalloyed tool steels (Carbon steels) contain 0.6–1.3 % carbon. They get their hardness and wear resistance by hardening, which generates a martensitic structure. Alloyed tool steels for higher loads additionally contain up to 5 % shares of Cr, W, Mo and V. Compared to unalloyed tool steels they have an elevated wear resistance (additive of carbides generating elements) and a greater hardness (carbon passed into solution). Due to the limited hot hardness of tool steels (Fig. 8.4) only lower cutting speeds can be applied so that tool steels are hardly used on machine tools for the machining of metals. They are primarily applied for cutting manually-driven tools, for hand tools such as files and hand-reamers and for woodworking tools.

8.3 High Speed Steels

High speed steels (HSS) are ledeburitic, highly alloyed tool steels with alloy contents of up to 35 %. They are used as tools for drilling, milling, reaming, sawing and turning. In contrast to the tool steels mentioned above they have a higher annealing temperature and a hot hardness of up to 600 °C (Fig. 8.4).

The alloy elements bound as carbides do not determine the higher annealing stability, but therefore the alloy elements in the matrix do. The hardness and the high wear resistance also arise from the martensitic matrix as well as from the incorporated W, W-Mo, Cr, and V carbides.

The properties of high speed steel are primarily governed by the alloy elements W and Mo. The tungsten and molybdenum contents are therefore used to classify the high speed steels according to [DIN EN 10027-1] into four groups (Table 8.2).

Table 8.2 Alloy groups of high speed steels

Class	Name acc. [DIN EN 10027-1]	Fractions in %					Applications
		C	W	Mo	V	Co	
6 % W, 5 % Mo	HS6-5-2	0.85	6.5	5.0	2.0	-	- Drills - Taps
	HS6-5-3	0.85	6.5	5.0	2.8	-	- Milling cutters
	HS6-5-2-5	0.85	6.5	5.0	2.0	4.75	- Reamers
	HS10-4-3-10	1.25	10	4.0	3.25	10.0	- Tuning tools
2 % W, 10 % Mo	HS2-10-1-8	1.1	2.1	10	1.2	7.9	- End milling cutters
12 % W	HS12-1-4-5	1.45	12	0.8	3.75	4.75	- Turning tools - Turning tools
18 % W	HS18-1-2-5	0.80	18	0.8	1.5	4.75	- Planning tools - Milling cutters

They are marked by HS for high speed steel and the percentage contents of the alloying elements W-Mo-V-Co. The universal type HS6-5-2 covers more than 50 % of the totally manufactured high speed steel. The varieties mentioned in the 6 % W and 5 % Mo-classes cover approximately 90 % of the manufactured quantity [HAB88].

The alloying elements affect specific properties of the high speed steels:

- C Carbon is essential for the hardness and necessary for the formation of carbides.
- W Tungsten is a carbide former and increases the tempering resistance and the wear resistance.
- Mo Molybdenum increases the ability of through-hardening and the toughness; it can replace tungsten. Due to the half density lower mass contents are required compared to tungsten.
- V Vanadium, similar to tungsten, is a carbide former and increases the wear resistance.
- Co Cobalt is able to raise the hardening temperature. Thereby, more alloy contents of carbide formers can be solved, i.e. the hot hardness and the tempering resistance increase.

High speed steels are produced by melting processes. The hardening temperature (1,180–1,280 °C depending on alloy elements) and the immersion time during the tempering procedure are chosen so that the largest possible fraction of carbides is solved but no coarseness of grains is generated. The remaining part of austenite can be reduced by repeated annealing (540–580 °C). The precipitation of carbides works against the decrease of hardness by collapsing martensite connected with the annealing. The decrease of hardness, however, is connected with an increase of toughness.

In the melting process, the high speed steels tend to segregation during the solidification phase, which is detrimental on the wear resistance. To avoid these disadvantages, electro slag remelting processes (ESU) and powder metallurgy manufacturing (PM) are applied. Either method leads to a more uniform structure and finer grains. PM steels have better edge strength and cutting edge durability. They are used for threading and reaming tools. With higher carbide fractions they are better grindable than molten high speed steel. The higher manufacturing costs are detrimental.

Longer tool life and higher cutting speeds can be reached with high speed steel by coating with titanium nitride (TiN). The layers have a thickness of 2–7 µm. Friction between tool and work material and thus the adhesive wear can be reduced by TiN. The lower friction leads to a reduction of the necessary cutting power and the cutting forces by 10–20 %.

The rake face is heated by friction especially at higher cutting speeds. The greater part of the power transformation takes place in the chip formation zone (see Chap. 5), the shearing energy contributes but little to the temperature at the tool surface. Therefore, a reduction of the total power as a result of lower rake face friction has the following effect:

$$k_c = k_\Phi + k_\gamma \quad \text{without coating} \quad (8.1)$$

$$a \cdot k_c = k_\Phi + b \cdot k_\gamma \quad \text{with coating} \quad a, b < 1 \quad (8.2)$$

$$b = 1 + \frac{k_c}{k_\gamma} \cdot (a - 1) \quad (8.3)$$

The total specific energy k_c divides itself into the friction share on the rake face k_γ and the shearing share (plus the friction at the flank face) k_Φ . With a coating, the total energy decreases to $a \cdot k_c$ as a result of the lowered friction at the rake face to $b \cdot k_\gamma$. With the values from [Chap. 5](#) for the shearing and the friction energy and $a = 0.8$ (i.e. reduction of the cutting power to 80 %) follows $b = 0.2$ of the original value without coating. The temperatures in a high speed tool can be lowered significantly by a TiN coating, which results in a considerable gain in the possible cutting speed or the tool life respectively. In addition, the abrasive wear is reduced by the higher hardness of the TiN layer in the range of HV05 = 2,400 compared to the substrate with the hardness of HV05 = 900 at room temperature.

Due to the lower process temperatures during the vapor deposition of layers high speed steels are coated by physical vapor deposition (PVD). Typical coating temperatures in this process are lower than 500 °C. Thereby, hardly any annealing effects occur. For chemical vapor deposition (CVD) the process temperatures are 900–1,000 °C, which is far above the annealing temperature of high speed steel. CVD-coated tools therefore have to be post-hardened. Because of the connected risk of warpage this is achieved only for simple shapes such as cutting inserts. [Section 8.5](#) gives further explanations concerning the various vapor deposition methods.

Coated tools have a significantly longer tool life. Even reground tools still show a clear effect. The causes are the supporting and protecting effects by TiN-carryovers. Beside others, twist drills, milling cutters, hobs, taps, broaches and reaming tools are coated. They can then be used for partly decisively higher cutting and feed speeds. [Figure 8.6](#) shows the recommended cutting and feed speeds of differently coated twist drills of high speed steel and of solid tungsten carbide for a drill diameter of 6 mm.

8.4 Stellites

Stellites are cast hard alloys (not to be confused with hard metals, which are sintered). They are naturally hard so they need not be hardened. They were developed for the first time by E. Haynes in 1915. Stellites have the following composition: 42–53 % Co, 24–33 % Cr, 11–22 % W and 1.8–3 % C. Cr and W form carbides. Stellites have a hardness of HV0.5 = 700–750 at room temperature. At low cutting speeds they are inferior to high speed steel, at higher cutting speeds they are inferior to tungsten carbide materials ([Fig. 8.4](#)). The possibilities

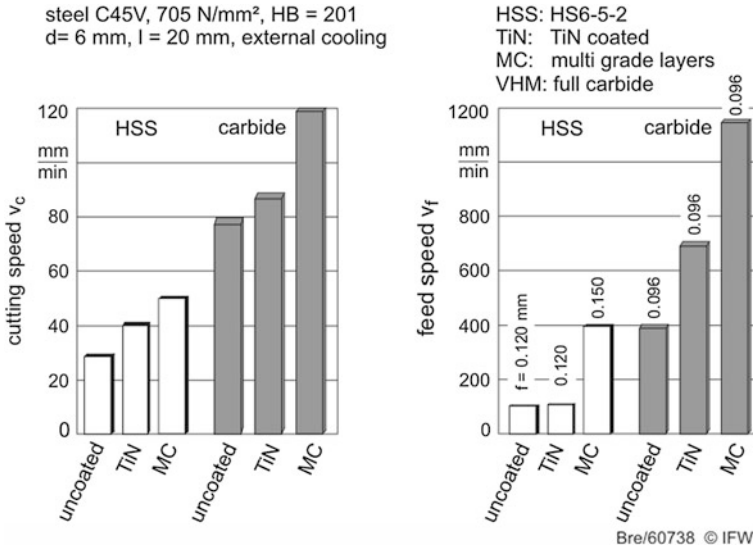


Fig. 8.6 Recommended cutting speeds and feed speeds of various coated twist drills (acc. to Guehring)

of shaping by casting can be beneficial for large profile tools. The high oxidation resistance of stellites can be of interest for materials, which tend strongly to oxidation wear.

8.5 Cemented Carbides

Cemented carbides are two- or multi-phase powder metallurgically produced alloys of a binding metal (β -phase) which determines the toughness -, and metal carbides or -carbonitrides as the hardness carrier [KIE53]. As hard materials, tungsten carbide (WC, called α -phase), titanium-, tantalum- or niobium-carbide (TiC, TaC, NbC, called γ -phase) or titanium carbonitride or other titanium mixed carbides are used. The first basic patent on a WC–Co cemented carbide was granted to K. Schroeter of the Osram-Studiengesellschaft in 1923. The beneficial combination of properties is due to the fact that tungsten carbide is very well wetted by cobalt (β -phase) and that cobalt is able to solubilize larger shares of tungsten carbide. The good wettability is such that tungsten carbide never breaks interfacially alongside the bonding metal-carbide boundaries. The solvent power causes high internal binding forces and a good edge strength of the carbide.

By variation of the α - and β -phase shares the cutting material can be tailored to a certain extent. Tough carbides contain up to 15 % Co, wear resisting in contrast only up to 5 % Co (Table 8.3). The diffusion tendency of WC carbide can be reduced by titanium carbide, which leads to better hot wear resistance of cemented

Table 8.3 Composition and properties of various cemented carbides

	WC	γ -phase	Co	HV30	Bending strength [MPa]	Application
P01	32	60	8	1,670	750	Fine turning
P10	55	36	9	1,600	1,300	Finishing (turning and milling)
P25	70	20	10	1,450	1,750	Milling
P40	74	12	14	1,350	1,900	Interrupted cut, turning and planning
K05	92	2	6	1,750	1,350	Finishing
K30	93	–	7	1,400	2,000	Milling, rough turning
M10	84	10	6	1,700	1,350	Turning

carbides in spite of the higher hot hardness of WC (HV05 = 1,800 at room temperature, HV05 = 800 at 1,000 °C) compared to TiC (HV05 = 3,000 at room temperature, HV05 = 400 at 1,000 °C). However, the binding capacity and hence the toughness and edge strength is reduced. Additions of TaC and NbC counteract this tendency by grain fining and thereby increase the toughness.

The most important new developments to increase the hardness of WC–Co carbides are the fine grain and the ultra-fine grain cemented carbides with a WC grain size of 0.5–0.8 μm and 0.2–0.5 μm respectively with a cobalt content of 6–16 % by mass. These fine powders have a nearly round grain shape in contrast to standard materials, which not only has a positive influence on the homogeneity of the microstructure generated by sintering but also on the reachable density.

A recent development in the field of carbides is a functional gradient set into the surface zones of cutting tools (FGH, functionally graded hard metal). Such a functional gradient is a precise, finely varying distribution of phases and/or composition of elements, which provides a resistant surface zone, able to withstand the interactions between workpiece and tool under high temperatures. So, for example, the Co content is increased in the surface area to selectively enhance the toughness and to reduce cutting edge breakages [BOE02].

According to [DIN ISO 513], the cemented carbides are classified into three groups. The so-called cutting application groups, P, K and M. The WC- (TiC, TaC-, NbC-) Co alloys in the P group (P for plastic) are used to machine long chips forming ferrous materials as steel. The TiC-/TaC- alloys, largely free of WC–Co, of the K group are applied for the machining of non-ferrous metals, ferrous cast iron materials, AlSi alloys, plastics and wood. The transition between the P and K groups form the cemented carbides of the M group, which are used for alloyed austenitic and ferritic steels respectively and for alloyed cast iron. Toughness and wear resistance are marked by appending digits within each application group. With increasing numbers the toughness increases and the wear resistance is reduced. Table 8.3 lists typical compositions and properties of cemented carbides.

The characteristic and at the same time limiting dualism for cutting materials, to have a high hardness and wear resistance on one hand and a high bending strength and toughness on the other, can be overcome largely by coatings of the substrate. This principle of functional separation combines wear resisting layers with tough

base material. Due to great temperature differences which occur in cutting tools, the control of temperature cracks as a result of different thermal expansion coefficients is a prerequisite for durable and crack free coatings.

Titanium carbide (TiC), titanium nitride (TiN), titanium carbonitride (TiCN) and titanium aluminium nitride (TiAlN) still have a large proportion of the coating materials. Selected properties of some of these materials compared to tungsten carbide are shown in Table 8.4. The properties of these hard materials are mainly determined by the kind of chemical bond. Good layer adhesion, for example, is best achieved by metallic bonding since it has the greatest adhesion forces. High hardness for optimal wear resistance is best achieved by covalent bonding. The also required chemical stability is predominantly due to ionic bonding. TiN holds shares of all three types of bonding. Therefore, it was successfully used as the first layer [BOB08].

New PVD layers consist of systems of TiN/TiAlN or hard-soft combinations such as TiAlN + WC/C in several folds or multiple fold layers. Nano-structured layers of TiSiN, TiAlN, TiAlSiN or TiAlBN have already been in use for several years. CrAlN, CrAlSiN or Al₂O₃ are components of multilayers coatings, which are successfully used for the machining of hard materials [BOB08].

Additionally in the CVD coating of multiple layers, coatings with oxide ceramic shares affect beneficially. Combinations of TiC, TiN, TiCN, and Al₂O₃ were advantageous. For the turning of steel and cast iron materials a layer package of TiN, TiCN, Al₂O₃ and ZrCN proved value. Improvements of performance of CVD coatings can be achieved by quaternary coating materials like (T,Zr)(C,N) or (Ti,Hf)(C,N) [DRE01].

Titanium carbonitride coatings can be built up on TiC with a monotonous transition of the shares up to pure TiN. TiN is chemically inert and therefore counteracts the wear by diffusion and oxidation. In addition, it has a low adhesion tendency and reduces the respected wear. Aluminum oxide is also inert. It serves as a protection against oxidation.

(Ti,Al)N benefits at high process temperatures and forms a thin, passive layer on the tool surface, which prevents fast growing wear by diffusion and oxidation. High ionization pulse processes allow the production of non-conducting nitride layers with a high content oxide forming components such as (Al,Ti)N super nitride layers with more than 65 mol % of aluminum nitride. This further development of tool coatings aims at an improved wear behavior. Figure 8.7 shows the basic structure of different layer concepts in principle.

The single or multi-layer coatings are 2–10 µm thick in total. They are generated by vapor deposition. Chemical vapor deposition (CVD) works with process temperatures of 900–1,000 °C. Figure 8.8 shows the process of the deposition of TiC layers according to the following reaction formula



Methane (CH₄) and titanium chloride (TiCl₄) are gaseously sent to a heated reactor, where metallic substrate plates of the highest pureness possible are

Table 8.4 Properties of coating materials

	WC	TiC	TiN	TiCN	(Ti,Al)N	Al ₂ O ₃
hardn. HV0.05 at RT	1800	3000	2400	3000	2800	2200
at 1000°C	800	400	450	790	1250	1100
thermal expansion coefficient 10 ⁻⁶ K ⁻¹	7.3	7.8	9.4	7-8	7.6	8.3
thermal conductivity W/mK	90	30	39	50-100	50-100	25
Young's modulus GPa	690	450	256	372	390	410
enthalpy of formation kJ/mol bei 1450°C	-54	-165	-335	-268	-210	-1670
flank face wear		+	0	+	+	0
crater wear		0	0	0	0	+
toughness		+	+	+	0	0
bonding capacity		+	+	+	+	0
friction coefficient		+	+	0	0	0
separation function		0	+	0	+	+

+ = ideally suited; 0 = adequate

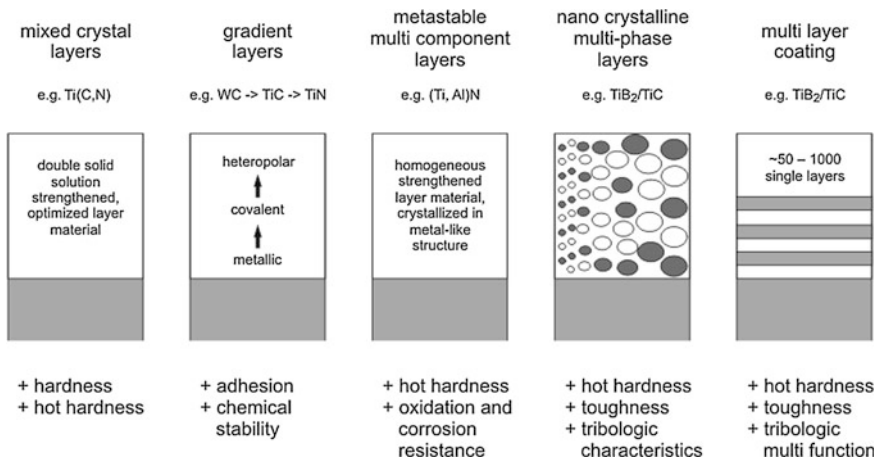


Fig. 8.7 Structure of different concepts of cover coating

located. At the heated surface of the substrate, the gases decompose into the respected solid material (TiC) and into volatile by-products (HCl). The layers grow up granularly (TiC, Al₂O₃) or fibrously (TiN). First, the growth of TiC occurs with a high coating rate. With a growing coating thickness the coating rate slows down, while the grain size of the layer increases. With CVD tensile stresses occur in the layers because of the different thermal expansion coefficients and because of the cooling down after coating. These stresses can exceed tensile strength and thus generate cracks.

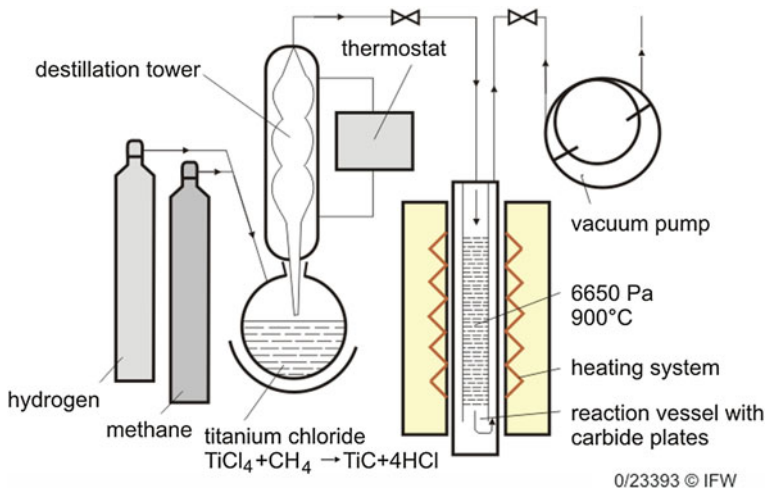


Fig. 8.8 Deposition of TiC coated carbide inserts by the CVD process

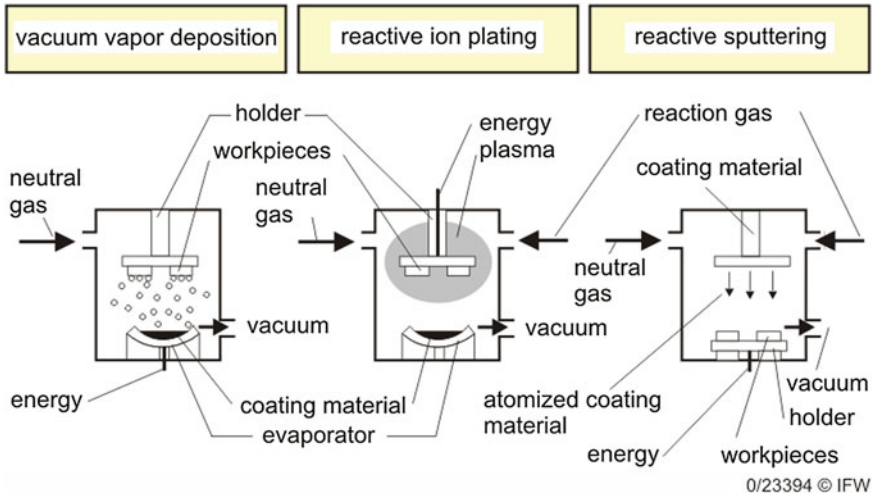


Fig. 8.9 PVD processes for coating

Physical vapor deposition (PVD) works at lower temperatures of about 500 °C. Ion plating or cathode sputtering is applied (see Fig. 8.9). The layers develop by the acceleration of loaded particles and by the bombardment of the substrate. Geometric limitations result, which can be partly neutralized by rotating the samples, because the faces to be coated have to be accessible. Residual stresses also develop in the coatings. However, they are hardly caused by the differences in thermal expansion, but rather by the ion bombardment. Compressive stresses are generated, which possibly benefits transient thermal loading, since the compressive residual stresses compensate the thermal stresses in the layers.

The plasma-CVD process avoids the limitations of the CVD and the PVD procedure (Fig. 8.10). The procedure no longer uses only thermal energy to activate the chemical reactions, but the process is activated by a plasma in the reactor. On the one hand, the plasma has a catalytic effect. On the other hand, its task is energy coupling. Thus, the reactions can occur at lower temperatures or only become due to them.

The PACVD can generate nitride, carbide or also carbonitride layers depending on the gas feeding. The coating according to the PACVD process implements substrate temperatures below 500 °C.

In contrast to the CVD coating diffusion actions, phase transforming and replacement reactions as well as the connected embrittlement effects between substrate and layer are therefore excluded. In contrast to layers generated by PVD, which are also superimposed under lower temperatures, the PACVD layers show high adhesion strengths and lower residual stresses as well as a smaller influence on the bending strength of the substrate. Furthermore, the adjusting and charging necessary with the PVD process to obtain a uniform layer thickness is omitted.

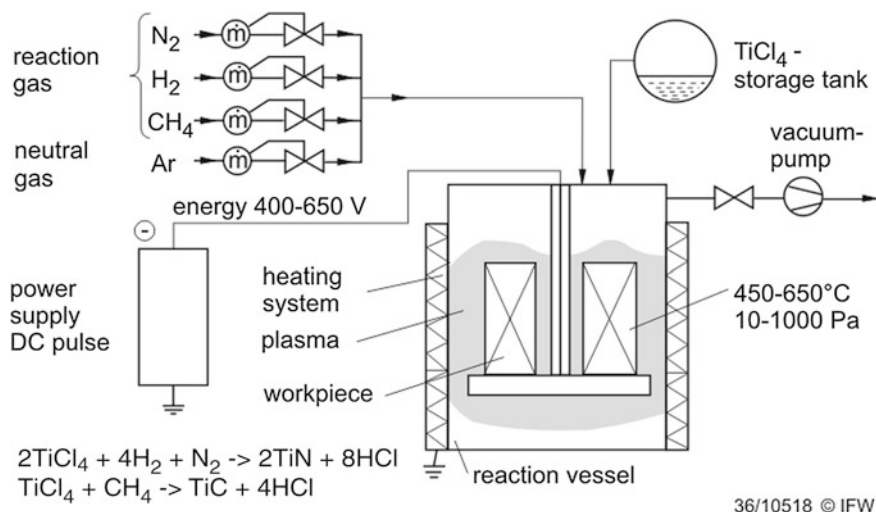


Fig. 8.10 Manufacturing of TiN-coated inserts by the PACVD process

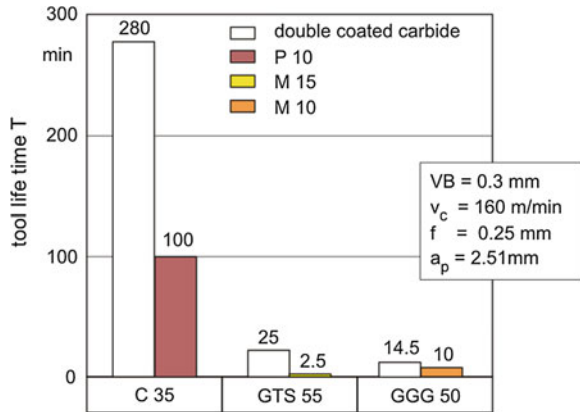
Very hard layers of diamond can be applied on cutting inserts and on shank tools by means of the CVD process. As substrate materials fine grained tungsten carbides or silicon based ceramics are suitable. The cobalt content is responsible for the strength of the CVD-diamond coated carbide tools [UHL04].

First successful trials with CBN coatings have also been documented [WIE07, UHL04]. Improvements to PVD coating techniques and plasma-assisted CVD resulted in CBN layers with more than 1 μm thickness deposited on carbide inserts. These layers are more than twice as hard as TiN layers and show more than a tenfold resistance to abrasive wear, where the coefficient of friction against steel is only half the size. Application attempts when turning steel, partially hardened and cast materials show the potential of the CBN layers but also the great amount of research to be done [UHL04].

Thin amorphous carbon layers were successfully synthesized 40 years ago, reminding of diamond as far as transparency, refraction index, insulation, hardness and chemical resistance is concerned. They are therefore called diamond-like carbon (DLC) [AIS71]. This material allows a wide variety of properties by means of the insertion of hydrogen, metallic or nonmetallic elements, which allows a significant determination of its properties. DLC coated tools are used to cut Al- and AlSi-alloys [SAN07, FUK04]. The tendency to build up edges is suppressed and the surface roughness of the workpiece is reduced.

Nowadays, 80 % of the carbide tools are PVD or CVD-coated [BOB08]. But they did not prove worthy for the machining of non-ferrous metals, highly nickel containing steels or nickel based alloys and austenitic and ferritic stainless steels. It also has to be noted that coated carbides have larger cutting edge radii by principle (equidistant, process necessary rounding). For very small undeformed chip thicknesses this leads to highly negative rake angles with the result that coated

Fig. 8.11 Comparison of tool life between cutting materials for cast iron and steel



tools are not usable for fine finishing operations. For the rest coated carbides are clearly superior to non-coated inserts as far as the wear behavior is concerned (Fig. 8.11). Besides, an economic reduction of grades is achievable due to the coating because a close adaptation to the machining conditions or to the machined material is no longer necessary.

Coated carbides wear slowly and show a characteristic wear development (Fig. 8.12). Even if the layer is penetrated, there is still a protective effect as can be seen in the moderate wear progress. It is explained by retain effects and a continuous plating by adhesion. After further use the typical steep wear occurs.

To assess the wear status of tools the crater depth KT can be applied beside the width of flank wear land. Figure 8.13 indicates the wear behavior of a TiC-Al₂O₃ carbide.

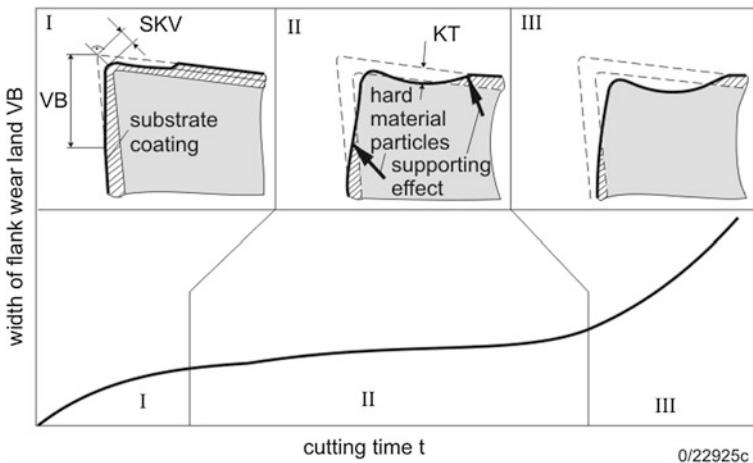


Fig. 8.12 Wear procedures in the case of coated carbides

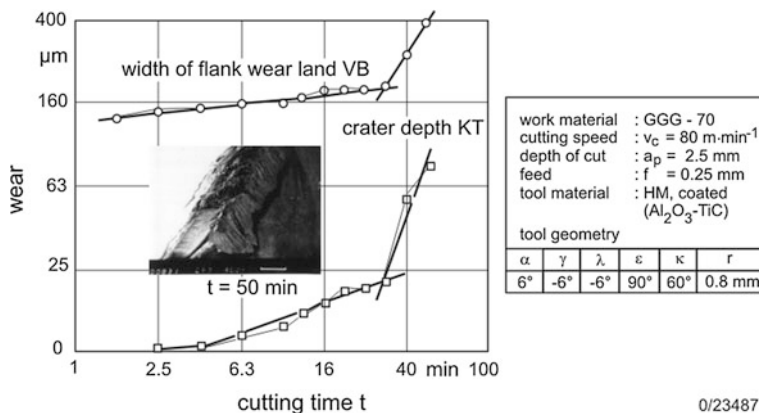


Fig. 8.13 Wear characteristic parameters of double-coated carbide when turning cast iron with globular graphite

A change of the properties of carbides, particularly of hardness, toughness and wear resistance is possible due to the change in the grain size and the shape of the carbides. This led to the development of ultra-fine grain hard metals. By using fine grain carbides (grain size $< 1 \mu\text{m}$) hardness, fracture toughness, compressive strength, wear resistance and edge strength are increased. Due to the small grain size and the material properties, particularly sharp and highly loadable cutting edges can be achieved with ultra-fine grain carbides. Accordingly, ultra-fine grain carbides are applied in finishing and fine finishing operations as well as for drills. Advantages exist for drill operations particularly when cutting with low cutting speeds ($v_c < 60 \text{ m/min}$). Here, the high toughness of the cutting material comes into play. So, clear tool life improvements have been achieved compared to conventional hard metals (Fig. 8.14).

8.6 Cermets

Hard metals without free tungsten carbide are called Cermets (from the word stem “ceramics” and “metals”) [ETT88]. They are multi-component hard metals based on titanium carbonitrides with tantalum, niobium and vanadium in the hard phase. The binder contains nickel and cobalt. Mixed crystal hardening can increase the wear resistance from the binder side, also by means of molybdenum, titanium, and aluminum. In contrast to tungsten carbides the cermets have a significantly higher chemical stability at high temperatures, i.e. less diffusion and oxidation wear. In addition, cermets offer a far higher edge stability. The sustainable cutting speeds are higher than those of coated tungsten carbides (Fig. 8.15).

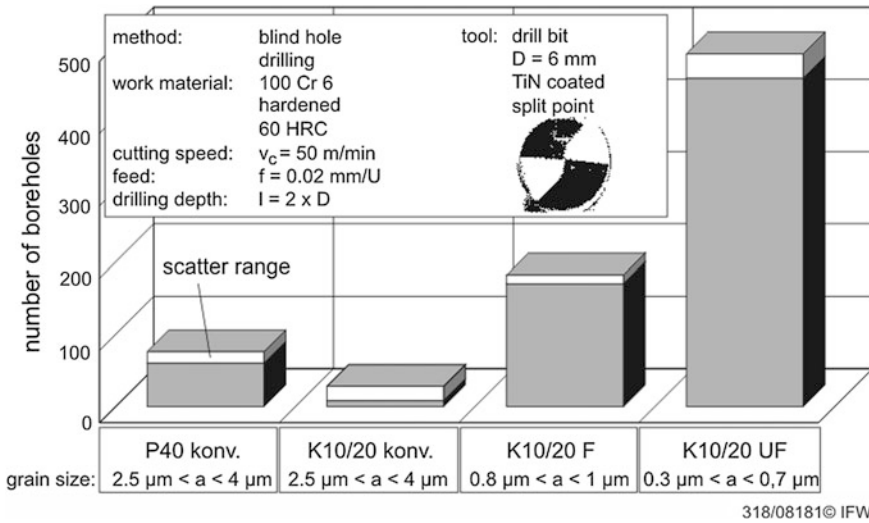


Fig. 8.14 Influence of carbide grade on the toll life behavior

The fracture toughness of cermets is lower (Table 8.4) than that of tough WC hard metal. Large differences exist in the thermal expansion coefficient and in the heat conductivity, which affects the application behavior in transient loading (see Chap. 7).

Cermets can be used for finish turning, thread turning and milling of steel and cast iron. The tendency of the batch production to use formed and molded parts with little allowance (near net shape technology) complies with the use of cermets.

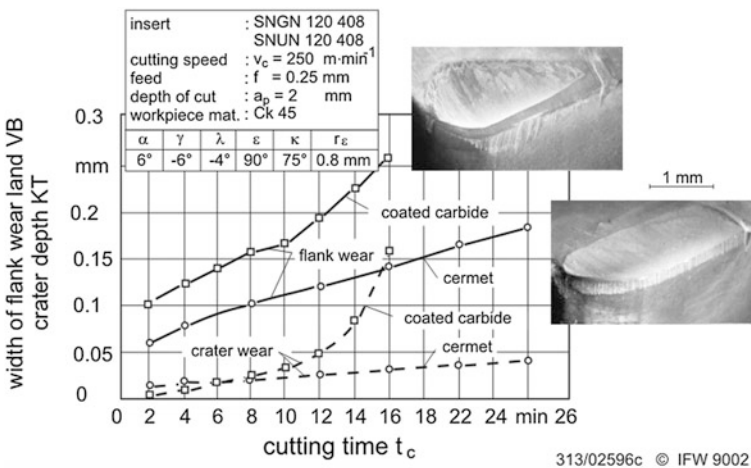
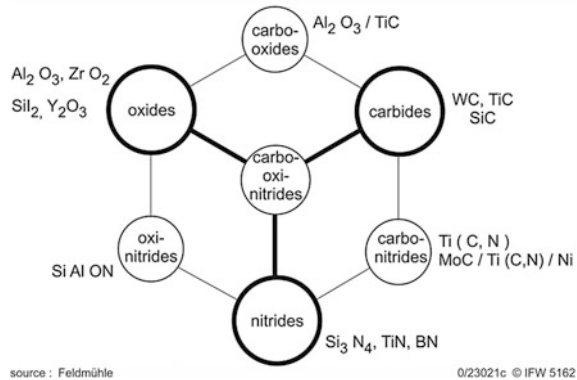


Fig. 8.15 Wear development of cermets and coated tungsten carbides over cutting speed

8.7 Ceramics

Cutting tools of ceramic materials are manufactured by sintering metal oxides, nitrides and carbides [FRI88, MOM93]. The ceramic base materials are divided into oxide and non-oxide ceramics. Aluminum and zirconium oxide belong to the most important oxide-ceramic cutting materials, silicon nitride, titanium carbide and nitride to the non-oxide ceramics (Fig. 8.16). Compounds and mixed crystals (for instance SiAlON) are used to combine the advantageous properties of various base materials.

Fig. 8.16 Base materials for ceramics

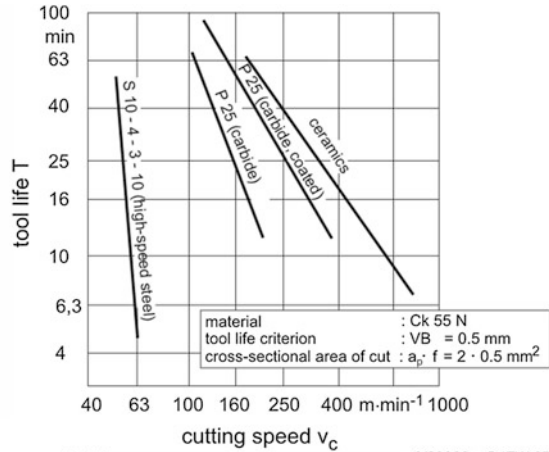


The most important properties of ceramics are their great hardness and their wear resistance. With increasing temperature the hardness of ceramics decreases more slowly than that of cemented carbide, whose hard particles are embedded into a metallic binder phase. Thus, ceramic cutting materials have a very good wear resistance even at high cutting speeds (Fig. 8.17). Their chemical inactivity reduces material adhesions and crater wear.

The toughness of ceramic cutting materials is limited. Ceramics break in a brittle way at mechanical overload, practically without any preceding plastic deformation. Compared to metals the expansion of a crack in ceramic materials requires only little energy. Therefore, ceramics are very sensitive towards external kerfs and internal material defects, where stress superelevations take place. The strength of a ceramic part is determined by the size of its biggest defect. Since the sizes of texture and surface defects are subject to statistic distributions, the fracture strength of ceramics varies in wide limits. It can be described by the Weibull distribution (Fig. 8.18). These relationships can affect the process reliability of applying ceramic cutting materials.

It was Osenberg who applied ceramic material for the first time as cutting tool in 1938. But he was unsuccessful, because he used pure aluminum oxide (alumina) which is a very brittle material [OSE38]. Enhanced oxide ceramic cutting

Fig. 8.17 Influence of cutting speed on tool life



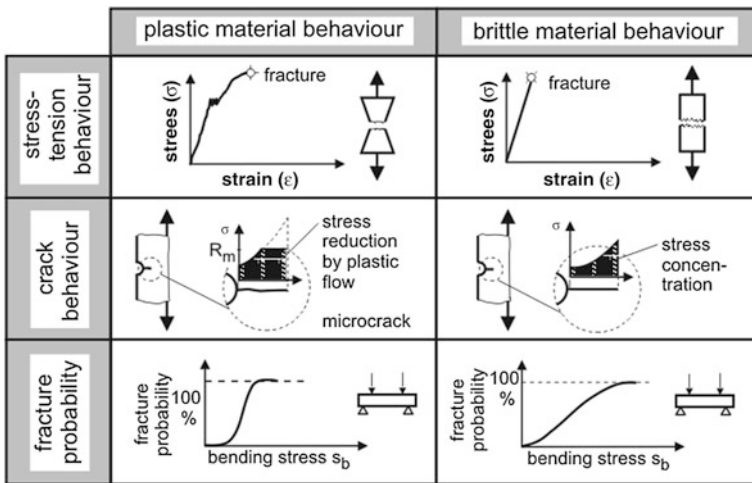
source : INFOS

0/23022c © IFW 0741

materials have been available since the 1960s. They contain 5–15 % zirconium oxide or up to 40 % titanium carbide and nitride (“black” mixed ceramic) besides the 60–95 % of the hardness carrier alumina.

The addition of finely distributed zirconium oxide (ZrO_2) enhances the fracture toughness. This dispersion strengthening is based on three mechanisms: the stress inducing, the crack deflection and the crack furcation (Fig. 8.19).

Under mechanical load in the neighborhood of a crack from its metastable tetragonal high-temperature phase, the ZrO_2 converts into the monocline low-temperature phase. Since monocline ZrO_2 has a 4 % lower density than tetragonal ZrO_2 the particles tend to increase their volume. At this, they generate stress fields



0/23395c © IFW 5161

Fig. 8.18 Fracture behavior of metals and ceramics

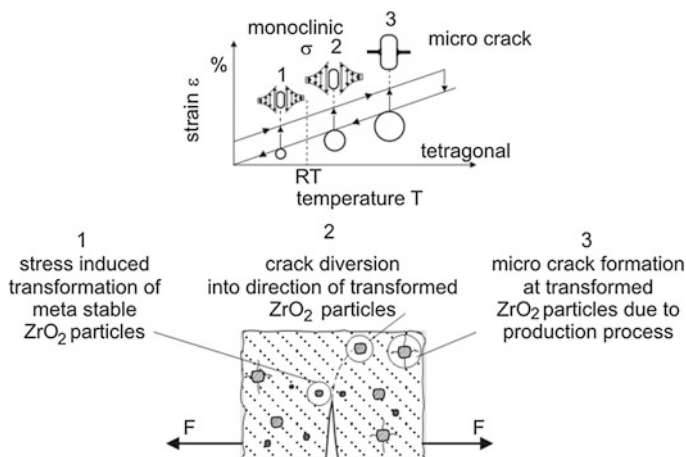


Fig. 8.19 Strengthening mechanisms of dispersion ceramics

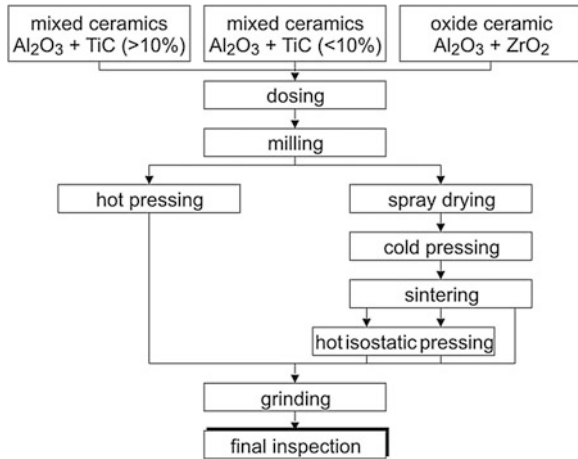
in the Al_2O_3 matrix. Cracks are deflected onto ZrO_2 particles and stop there (*crack deflection*). However, local stress fields are already generated in Al_2O_3 - ZrO_2 ceramic during the cooling of the sintering temperature. They are the result of the different thermal expansion coefficients of the two materials (*thermal misfit stresses*). These stresses can be adjusted by the grain size of the zirconium oxide in such a way so that they generate a great number of micro cracks (0.01 – $0.1 \mu\text{m}$) around the ZrO_2 particles. Because of their small size these cracks do not reduce the strength of the cutting ceramic. If an external crack encounters such a micro-crack network, its surface is greatly enlarged and the necessary energy to spread further increases correspondingly (*crack furcation*).

Dispersion-reinforced aluminum oxide ceramic is applied for the rough and finish turning of steel and cast iron up to a hardness of 48 HRC or 400 HV respectively. To cut aluminum alloys aluminum oxide ceramics are not suitable due to the chemical attack.

Titanium carbide and titanium nitride increase the hardness and abrasive wear resistance of the pure alumina. Their predominant covalent bondings give these materials a particularly high hot hardness compared to the predominant ionically-bonded alumina. This means that hardened steels up to 64 HRC can also be machined. The main application area of Al_2O_3 -TiC/TiN ceramic is finishing at high cutting speeds. The significantly elevated heat conductivity allows the use at rapidly varying thermal loads of interrupted cutting.

Silicon nitride (Si_3N_4) was introduced to machine cast iron and highly heat resistant materials at the beginning of the 1980s. The hardness of these non-oxide ceramics depends little on temperature. Due to beneficial thermal properties and a higher toughness, the silicon nitride ceramic is much less sensitive to thermal shock than pure oxide ceramic so that it can also be used in interrupted cutting. However, silicon nitride reacts at temperatures above $1,200^\circ\text{C}$ with iron forming

Fig. 8.20 Sintering of oxide ceramics



ferro-silicides. Therefore, it is not applicable for cutting steel, if such high temperatures are reached.

All cutting ceramics are produced by the sintering of fine powders. Thereby, the operational steps for cutting materials on the base of alumina and silicon nitride differ substantially. Figure 8.20 indicates the possible process steps for oxide ceramics. As precursors and in the form of powders, the intended basic materials and small shares of sintering additives are used, then weighed together in the required portions and finally subjected to a crushing and grinding procedure in a ball mill. This destroys the agglomerates of fine powder particles, which otherwise would lead to sintering defects. The grain size is set by the powder production (precipitation, gas phase reaction) and is generally not reduced any further here. The processed powder mixture can now be processed to solid ceramic bodies in different ways. The older procedure includes a compacting of the powder at room temperature and pressure of several hundred bar in a press form and then a non-pressure sintering of the semi-solid green body between 1,500 and 1,800 °C. These two process steps are combined in one single operation by means of the hot sintering mode. In both cases, the cutting insert is individually pressed and not cut from a larger sintered body. For particularly higher demands concerning pore free products and strength, the completed tools can be repressed isostatically at a high gas pressure and high temperatures. Prerequisite for this is an already closed porosity, at least at the surface. The sintered tools must finally be set to the required form and dimension by diamond grinding and polishing. The required high surface quality is also produced in this process step.

Figure 8.21 explains the cutting ceramic on the base of silicon nitride. Raw materials can be silicon nitride as well as silicon powders. The latter reacts only when sintering at the nitrogen atmosphere of the furnace to α - and β -silicon nitride (reaction bonded Si_3N_4). All silicon nitride ceramics must be sintered under high nitrogen pressure, because Si_3N_4 dissolves into its elementary constituents at

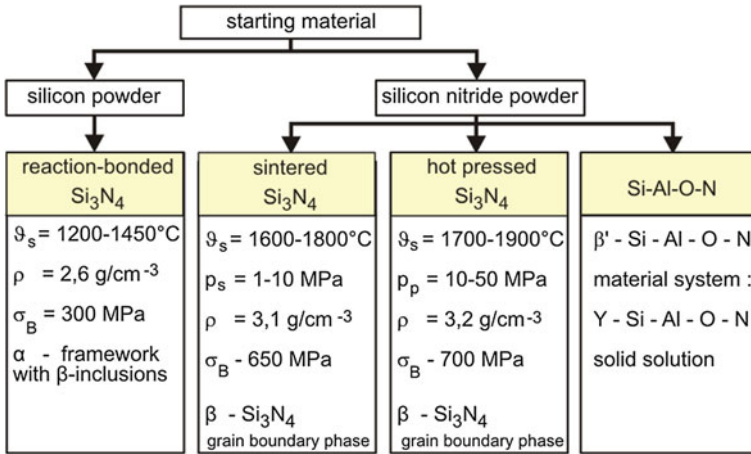


Fig. 8.21 Silicon nitride ceramic

normal pressure and high temperatures. Furthermore, sintering aids (yttrium-manganese- silicon-oxides) have to be added to build a silicate glass phase, which binds the needle-shaped silicon nitride crystals to a dense, pore-free structure. Because glasses have no fixed melting point but soften at elevated temperatures, the high temperature strength of silicon nitride cutting materials is reduced by the glass phase. The result is creeping, i.e. slow plastic deformation follows under mechanical load. The Si_3N_4 - crystals slip against each other alongside the grain boundaries. To increase the maximum applicable temperature of usage, the glass can be totally or partly crystallized out by subsequent tempering (aged at elevated temperature). Thus, between the Si_3N_4 -needles a matrix of garnet crystals is built with a high melting point temperature, which is far more creep-resistant.

Cutting inserts of hot pressed silicon nitride are sintered in the form of large plates and subsequently separated by laser. In contrast to oxide ceramic, laser cutting is unproblematic in this case as silicon nitride has no melting phase but sublimates at $1,900^\circ\text{C}$. To achieve form, dimension and surface-quality the silicon nitride inserts are also finished by diamond grinding. Due to the high hardness and the relatively high toughness, the grinding of ceramics is very expensive and causes a high partition of the total manufacturing cost of cutting tools.

The new developments of ceramic cutting materials aim towards an increase in process reliability. Therefore, the ceramics are strengthened by ceramic fibers, high strength fiber-shaped single crystals (whiskers) and platelets. They increase the bending strength and particularly the fracture toughness by means of crack deflection, crack bridging and thus stress reduction at the crack front. However, these measures complicate the grinding processes and increase the cost of the ceramic tools. In the case of whiskers there are health hazards in handling the powder, which is why the production was abandoned in Germany for the time being.

8.8 Diamond

Diamond and cubic crystalline boron nitride belong to the super hard cutting materials. Diamond is the hardest known substance. It consists of pure carbon. Elemental carbon co-exists in the stable modification, i.e. graphite and in the unstable high pressure modification, i.e. diamond. Diamond solidifies cubic crystalline, where each carbon atom is surrounded by four neighboring carbon atoms in the lattice. The C-atoms are tetrahedrally linked by covalent bonds. The high hardness of the diamond follows from the high binding energy of the atoms.

Diamonds are found and mined in nature. Since the 1950s [BUN55], diamonds are also being produced synthetically. Both modifications may exist as mono-crystalline or poly-crystalline diamonds.

8.8.1 Mono-Crystalline Diamond

Diamonds found in nature are mostly applied as single crystals, namely where cutting edges of highest sharpness and lowest chipping are required. Typical application domains are the ultra-precision cutting and the shine cutting of non-ferrous metals such as aluminum, copper and their alloys. Using the crystallographic orientation of the diamond, the crystal can be shaped by means of grinding and polishing to the minimum cutting edge radius $r_\beta \sim 1 \mu\text{m}$. The cutting edges are ground in a faceted way, i.e. with several major cutting edge angles and small minor cutting edges of $1^\circ\text{--}3^\circ$, or as arc edge (large radius r_e). The mono crystals are soldered or clamped in a holding element. Mono-crystalline diamond has strong direction-dependent physical properties (anisotropic material behavior), for instance hardness, strength, Young's modulus and heat conductivity. This anisotropy is used to modify diamond by cleaving, grinding and polishing. For its application as a tool it is orientated as far as possible into its hard, wear resistant directions. Basically, large mono-crystalline diamonds can also be produced synthetically. So far, however, due to the high cost of equipment and of tools for the production of large crystals for the application in geometric defined processes (for cutting in contrast to abrasive processes), natural diamonds as large mono-crystals are more economic.

8.8.2 Polycrystalline Diamond

The first diamond synthesis is said to have been successful in 1953 at ASEA, Sweden. In 1955, the synthesis was published in Nature by Bundy and others (General Electric, USA) [BUN55]. The first patents for industrial application were granted in 1960 [HAL60]. At that time, the production of smaller diamonds

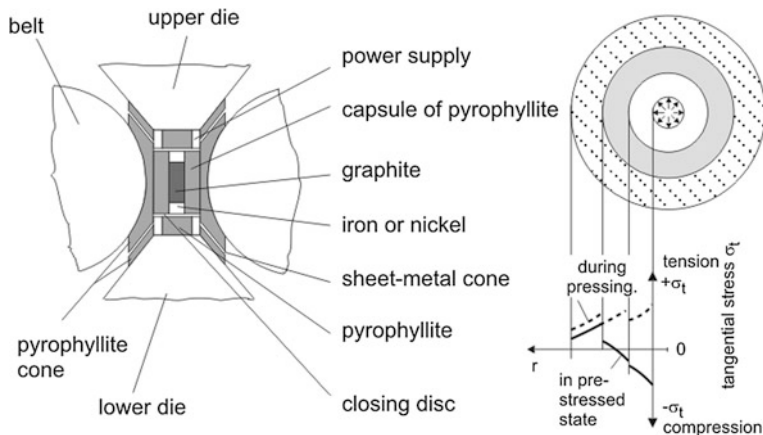


Fig. 8.22 Belt press for the production of synthetic diamonds [HAL60]

directly from graphite at high temperatures of 3,000 °C and high pressures of 10 GPa was initially successful. Adding solvents and catalysts (for instance cobalt, nickel, silicon, boron, beryllium and iron) can reduce the conditions of synthesis to 6 GPa and 1,500 °C. Cobalt, for example, has dissolving properties for carbon depending on pressure and temperature. Under conditions of synthesis in the metastable diamond-range cobalt is liquid. With increasing pressure and temperature the liquid solubility for carbon decreases, diamond is segregated. Repeated cyclic traversing of the synthesis range can enhance the conversion. This kind of synthesis generates single crystals, whose growth rate can be changed by systematical pressure and temperature control as well as by the quantity of seed crystals (density of nucleuses). The size of the crystallites can thus be influenced in a well-targeted way. To generate the necessary pressures for the diamond synthesis presses as shown in Fig. 8.22 are used.

Diamond synthesis generates grains in the range of 2–400 μm , which can be combined to a poly-crystalline matrix (PCD) after sorting in a further process by means of high-pressure-liquid-phase sintering. In this second process, the catalytic effect of the metallic companion is used again (Fig. 8.23). An adhesion enhancement can be achieved by means of a cobalt rich intermediate layer. If metallic phases are used as sintering aids, their liquidus line will lie below the sintering temperature even in the high pressure domain.

The properties of the poly-crystalline diamond layers can be controlled by the size of the applied grit and by the kind and quantity of the metallic phases. Grain sizes of 2–60 μm can be achieved in the final state, whereupon the grain size decreases during the sintering process. The Co-content after sintering decreases with the growing grain size of the base material [SIE91]. Consequently, it can be assumed that larger grits have higher shares of covalent bonds. That is the reason why PCD with coarser structures has the highest wear resistance but also the lower edge quality (possible sharpness).

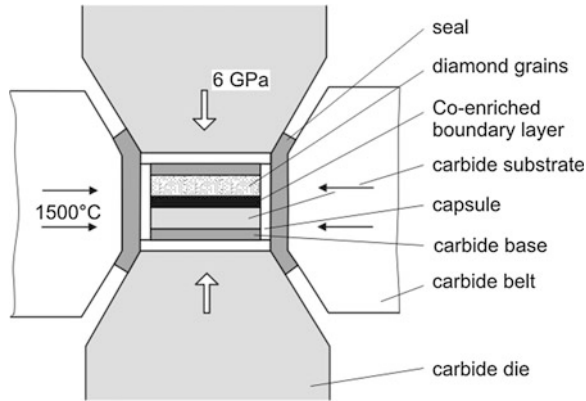


Fig. 8.23 High-pressure-liquid-phase sintering of PCD on substrate

Polycrystalline diamonds are largely isotropic because of the non-directed allocation they are composed of. They are, however, less hard than mono-crystals. They are much tougher than mono-crystals because of their isotropy, their grain boundaries and metallic inclusions.

Their application domain is the roughing-finishing machining of non-ferrous metals at set conditions, which no chemical wear and cutting wedge temperatures above 700 °C occur at. The tolerable temperature is not limited by the temperature of graphitizing at 900 °C but already at 650–800 °C. The reason is the enrichment of cobalt occurring in this temperature range resulting from the volume expansion of cobalt compared to diamond. However, this effect depends on the disposition time [SIE91]. Metallic materials such as aluminum, copper and their alloys, non-metals such as plastics, wood and graphite can be beneficially machined by PCD. PCD is particularly applied for highly abrasive material such as hypereutectic aluminum–silicon alloys (pistons, cylinder blocks), glass fiber reinforced plastics and wood-

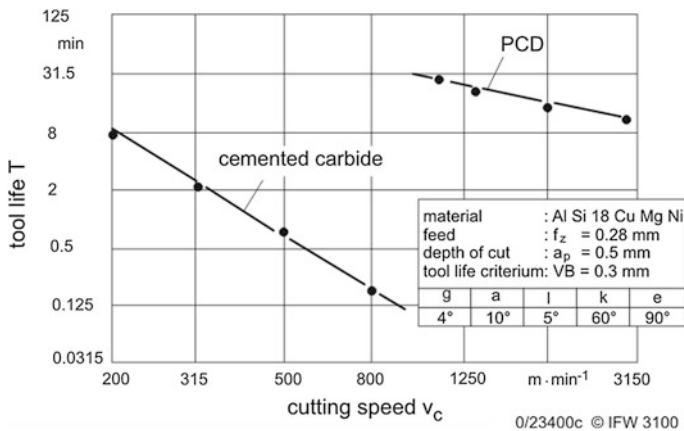


Fig. 8.24 Tool life for the milling of aluminum

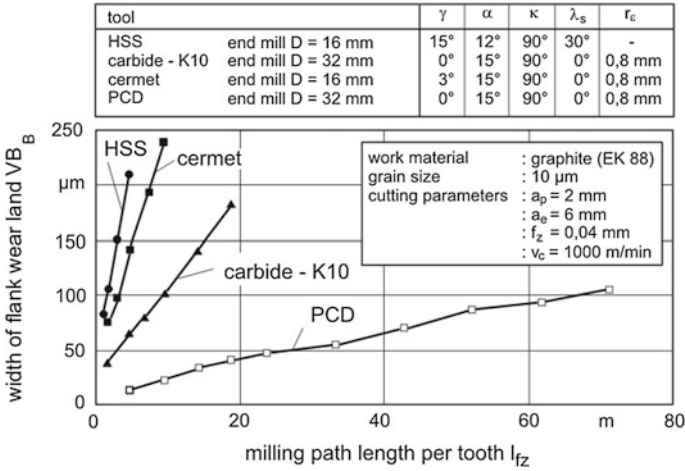


Fig. 8.25 Flank wear land for various cutting materials

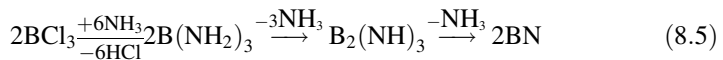
plastic-filling compound material seeing as very long tool lives can be reached in contrast to high speed steel, cemented carbides or ceramics (Figs. 8.24 and 8.25).

For soft materials declining to adhesion such as forgeable aluminum alloy, it may be of interest that adhesion and pseudo-chip building can be prevented or delayed by PCD because of its good cutting edge resistance (geometrical effect, delay of cutting edge rounding) and because of its low friction co-efficient (tribo-effect).

8.9 Boron Nitride

Cubic crystalline boron nitride (CBN) is the hardest cutting material beside diamond (Table 8.1). Unlike diamond, CBN is chemically resistant towards iron and other carbide building materials. It is stable up to temperatures of 1,400 °C. In the normal atmosphere, a protective layer of boron oxide (B_2O_3) prevents oxidation up to 1,300 °C. Therefore, CBN tools can be used to cut hardened steels, hard cast iron, nickel base alloys and to machine sputtered or welded hard layers.

Boron nitride naturally exists only in the hexagonal crystalline form, having a similar consistency as graphite. Boron and nitrogen are the elements directly next to carbon in the periodic system. Boron nitride can be transformed into the cubic crystalline modification as diamond through high-pressure- high-temperature synthesis. This kind of structure has a covalent binding. There is also a further lattice type of high hardness (but not as hard as the cubic type), the wurzite-modification. Hexagonal boron nitride is obtained by pyrolysis from boron-halogen compounds.



Boron nitride can be produced in various ways, differing in the number of process steps and in the use of additives. With the one-step process polycrystalline CBN is directly produced from the hexagonal modification and with the two-step process the CBN is first synthesized and in a subsequent sintering process the grit is treated to poly-crystalline material [KRE07].

For the pyrolysis metallic catalysts are mostly applied, where lithium is most frequently used, which leads to brown to black CBN. The further processing of the CBN grit produced in the pyrolysis to abrasive tools occurs in the same way as with the synthesized diamond.

Cubic boron nitride was first produced in 1957 [WEN57]. The synthesis requires the same arrangement as the synthesis of diamond. Pressures of 5–9 GPa and temperatures of 1,500–2,000 °C have to be applied [WEN61]. Alkali metals serve as catalysts, which allow the reduction of the synthesis temperature to the specified range.

Similar to diamond the CBN grit can be processed to thick poly-crystalline layers (layer thickness 0.5 mm) on cemented carbide or to solid CBN bodies by means of high-pressure-high temperature synthesis (Fig. 8.22). This poly-crystalline boron nitride (PCB) is available in two types of cutting material. One type being PCB with a high content of hard substance and strong penetration of the grains and the second type, with small content of hard substance and without grain penetration. The binder phase contains titanium carbide or titanium nitride. PCB with a lower hard substance content has a much lower heat conductivity ($\lambda = 40$ W/mK compared with 100–200 W/mK for the material with larger hard substance content).

PCB wears significantly less than cemented carbide (Fig. 8.26). Thus, higher cutting speeds can be reached for equal tool life by orders of magnitude [HER91]. When machining high strength materials with slender tools or workpieces of high compliance, it is of interest that lower cutting forces occur due to geometric (sharp cutting edges) and tribological (less friction) reasons (Fig. 8.27).

PCB is of great importance for the hard machining of steel, particularly under instable machining conditions or for interrupted cuts. For appropriate machining operations grinding can be replaced by turning, milling or drilling with PCB (see Chap. 10). Appropriate machining operations mean:

- small faces to be machined to keep form errors within limits
- limited demands on the dimensional and form accuracy
- compact, stiff workpieces, which are not inadmissibly deflectable by passive forces

If these conditions are met, considerable rationalization effects are achievable by means of higher material removal rates and shorter operation sequences.

8.10 Questions

1. Mention the types of loading on cutting tools.
2. What properties should cutting materials have?

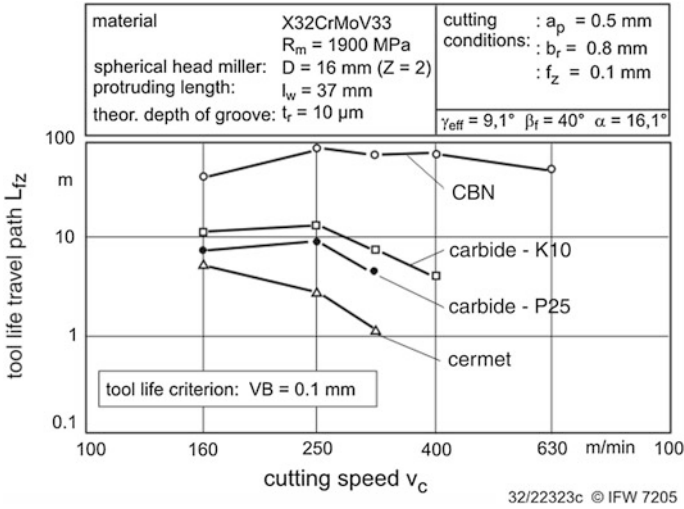


Fig. 8.26 Tool life travel of various cutting materials depending on cutting speed

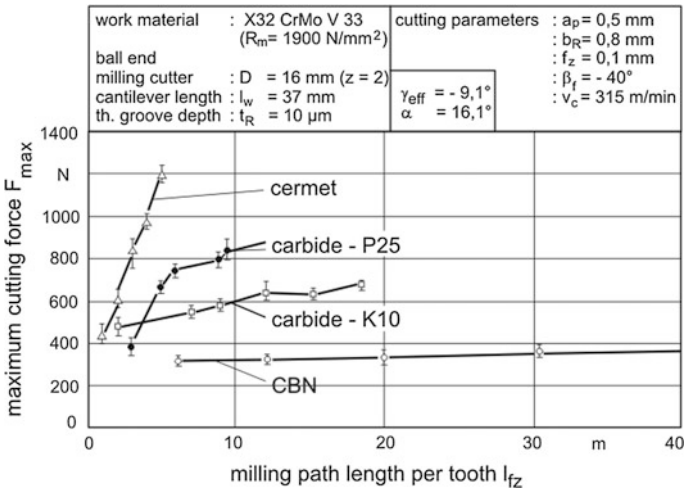


Fig. 8.27 Resultant force of various cutting materials

3. What cutting processes have special requirements concerning the mechanical and thermal fatigue strength?
4. What effect does the inclusion of hard substances into the cutting material matrix have?
5. Which classes of hard substances do you know? (4 classes)
6. Give one example for each class of hard substances.
7. Name at least 5 different cutting materials and order them by their wear resistance.
8. What is the carbon content of unalloyed tool steels?

9. Which main alloy elements form carbides?
10. What is the meaning of HS 10-4-3-10?
11. What does the marking HSS mean and what kind of tools is this cutting material preferably used for?
12. How are tungsten carbides produced and which main phases are they composed of?
13. Why are tools coated and what problems occur during coating? What ranges does the deposited layer thickness lie in?
14. Explain the differences between PVD, CVD and PACVD processes.
15. What benefit does one expect from TiC coated cemented carbides?
16. What are cermets?
17. How do cermets and WC containing carbides differ? What are the respective application domains?
18. What are the advantages and disadvantages of cutting inserts out of ceramics?
19. What is the essential difference between cemented carbides and ceramics regarding the composition? What sorts of ceramic are known to you?
20. What do you understand by the transformation strengthening of ceramics?
21. What is PCB and what properties does this material have?
22. What types of PCB exist and how do they differ?
23. Describe the process for the production of PCD.
24. What is the strengthening effect of a Belt-press?

References

- [AIS71] Aisenberg, S., Chabot, R.: Ion beam deposition of thin films of diamondlike carbon. *J. Appl. Phys.* **42**(7) 2953–2958 (1971)
- [BOB08] Bobzin, K., Bagcivan, N., Immich, P., Pinero, C., Goebbels, N., Krämer, A.: PVD – Eine Erfolgsgeschichte mit Zukunft [PVD – A success story with future]. *Materialwissenschaft und Werkstofftechnik* **39**(1) 5–11 (2008)
- [BOE02] Böhlke, W.: Hartmetall – ein moderner Hochleistungswerkstoff [Cemented carbide – A modern high performance material]. *Materialwissenschaft und Werkstofftechnik* **33** 575–580 (2002)
- [BUN55] Bundy, F.P., Hall, H.T., Strong, H.M., Wentorf, R.F.: Man-made diamonds. *Nature* **176** 51–55 (1955)
- [DIN EN 10027-1] Bezeichnungssysteme für Stähle – Teil 1: Kurznamen [Designation systems for steels – Part 1: Steel names]. Beuth, Berlin (2005)
- [DIN ISO 513] Klassifizierung und Anwendung von harten Schneidstoffen für die Metallzerspanung mit geometrisch bestimmten Schneiden – Bezeichnung der Hauptgruppen und Anwendungsgruppen [Classification and application of hard cutting materials for metal removal with defined cutting edges – Designation of the main groups and groups of application]. Beuth, Berlin (2005)
- [DRE01] Dreyer, K., Kassel, D., Schaaf, G.: Feinst- und Ultrafeinkornhartmetalle:

- Tendenzen und Anwendungen [Fine and ultrafine carbides: Tendencies and applications]. *Materialwissenschaft und Werkstofftechnik* **32** 238–248 (2001)
- [ETT88] Ettmayer, P., Kolaska, H.: Cermets. Schmid, Freiburg 163–193 (1988)
- [FRI88] Fripan, M., Dworak, U.: Keramische Hochleistungsstoffe [Ceramic high performance materials]. Schmid, Freiburg 194–214 (1988)
- [FUK04] Fukui, H., Okida, J., Omori, N., Moriguchi, H., Tsuda, K.: Cutting performance of DLC coated tools in dry machining aluminum alloys. *Surface & Coatings Technology* **187** 70–76 (2004)
- [HAB88] Haberling E.: Schmelzmetallurgisch hergestellte Schnellarbeitsstähle [High speed steels produced by melting]. Schmid, Freiburg 47–73 (1988)
- [HAL60] Hall, H. T.: Ultra-high-pressure, high temperature apparatus: “Belt”. *Review of Scientific Instruments* **31**(2) 125–131 (1960)
- [HER91] Hernandez-Camacho, J.: Frästechnologie für Funktionsflächen im Formbau [Milling technology for functional faces in mould manufacturing]. PhD Thesis Universität Hannover (1991)
- [KIE53] Kiefer, R., Schwarzkopf, P.: Hartstoffe und Hartmetalle [Hard materials and hard metals]. Springer, Wien (1953)
- [KLO08] Klocke, F., König, W.: *Fertigungsverfahren Bd. 1: Drehen, Fräsen, Bohren [Manufacturing methods vol. 1: Turning, milling, drilling]*. 8th ed. Springer, Berlin, Heidelberg, New York (2008)
- [KRE07] Kress, J.: Auswahl und Einsatz von polykristallinem kubischen Bornitrid beim Drehen, Fräsen und Reiben [Selection and application of polycrystalline boron nitride in turning, milling and reaming]. PhD Thesis, Universität Dortmund (2007)
- [MOM93] Momper, F.: Systematische Einführung von Schneidkeramik in die Produktion [Systematic introduction of cutting ceramics into production]. Expert Verlag, Reihe Kontakt und Studium, Band **370** 100–122 (1993)
- [OSE38] Osenberg, W.: Die Bearbeitbarkeit von Kunststoffen mit keramischen Werkzeugen [The machinability of plastic with ceramic tools] . *Maschinenbau*, **17**(5/6) 127–130 (1938)
- [SAN07] dos Santos, G. R., da Costa, D. D., Amorim, F. L., Torres, R. D.: Characterization of DLC thin film and evaluation of machining forces using coated inserts in turning of Al-Si alloys. *Surface & Coatings Technology* **202** 1029–1033 (2007)
- [SIE91] Siebert, J. Ch.: Polykristalliner Diamant als Schneidstoff [Polycrystalline diamond as cutting material]. PhD Thesis, TU Berlin (1991)
- [TÖN90] Tönshoff, H. K.: *Schneidstoffe [Cutting materials]*. Dubbel, Chap. 4.2.6, 17th ed. p. 50 (1990)
- [UHL04] Uhlmann, E., Braeuer, G., Wiemann, E., Keuneke, M.: CBN coatings on cutting tools. *WGP-Annals XI/1* (2004) pp. 45-48
- [VIE70] Vieregge, G.: Zerspanung der Eisenwerkstoffe [Machining of ferrous material]. *Stahleisen*, Düsseldorf (1970)
- [WEN57] Wentorf, R. H.: Cubic form of boron nitride. *Journal of Chemical Physics* **26** 956 (1957)
- [WEN61] Wentorf, R. H.: Synthesis of the cubic form of boron nitride. *Journal of Chemical Physics* **34**(3) 809–812 (1961)
- [WIE07] Wiemann, E.; Koenig, J.; Keuneke, M.; Richter, V.: Superhard coatings for cutting tools. *Industrial diamond review* 1/07 19–22 (2007)

Chapter 9

High Speed Cutting

9.1 Definition

Cutting at high speeds has gained great importance in recent years after the technical prerequisites were met by cutting materials, main spindles of machines, feed drives and control. The term “high speed cutting” or “HSC” is used in this context without having a clear definition on physical principle basis. “High speed” or “high power” are indefinite, upwardly open concepts. There have been several approaches to give a definition, going back to the 1930s (Fig. 9.1).

Salomon [SAL31] thought to have discovered a fundamental change in chip formation mechanisms at very high speeds. He pointed out in his patent that the load and the wear of tools are greatly reduced in this speed range. This assumption could not be proved. Already in 1932, motion pictures made by Schwerd/Hannover [SCH36] showed that the chip formation mechanisms at high speed are not fundamentally different compared to standard speeds. Icks [ICK81] showed that high speed cutting is dependent on the kind of machining process. Schulz [SCH94] defined high speed domains connecting them to the material properties to be machined. Ben Amor [TÖH05, BEN03] succeeded for the first time, to develop a physically based definition due to experimental force and power measurements.

It was observed that a characteristic force curve is given for almost all materials depending on the cutting speed (Fig. 9.2).

Thereafter, cutting and feed force drift asymptotically against a constant value, which in the case of the cutting force is marked with $F_{c\infty}$. Ben Amor was able to show that the variable part of the cutting force can be well described by an exponential decaying function.

$$F_c(v_c) = F_{c\infty} + F_{c\text{var}} e^{\left(\frac{-2v_c}{v_{\text{HSC}}}\right)} \quad (9.1)$$

Thereby, a limit speed v_{HSC} was introduced. v_{HSC} is apparent according to Eq. 9.1. v_{HSC} is seemingly the speed, which the variable part of the cutting force was dropped at by 86.5 % (exponent-2). A plausible explanation is achieved through the power fractions (Fig. 9.3).

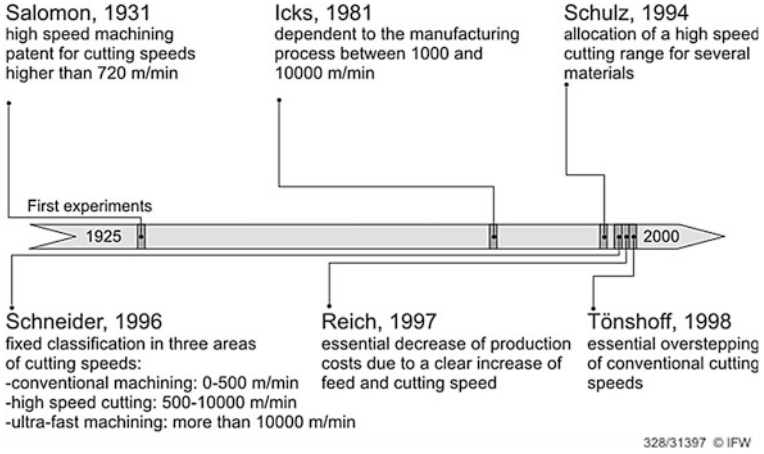


Fig. 9.1 Definitions of high speed cutting

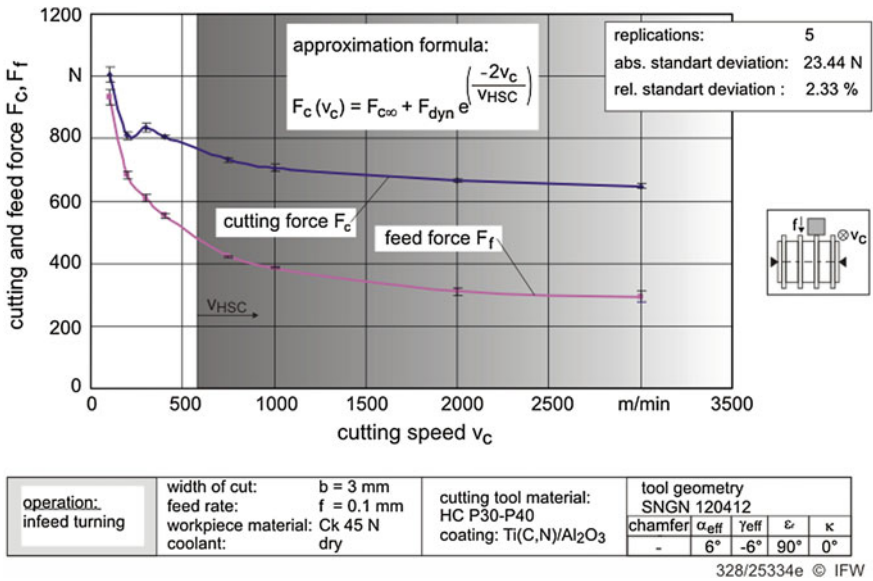


Fig. 9.2 Characteristic of cutting force depending on the cutting speed

According to Fig. 9.3 there is a cutting speed, which the function of the variable power P_{cvar} has an inflection point at and thus the deviation of P_{cvar} over v_c adopts a minimum. This cutting speed is referred to as limit speed. According to Ben Amor's definition it marks the beginning of high speed cutting. This limit speed can be correlated with the tensile strength of many practically important metals (Fig. 9.4). The function of approximation

example for C45E W1

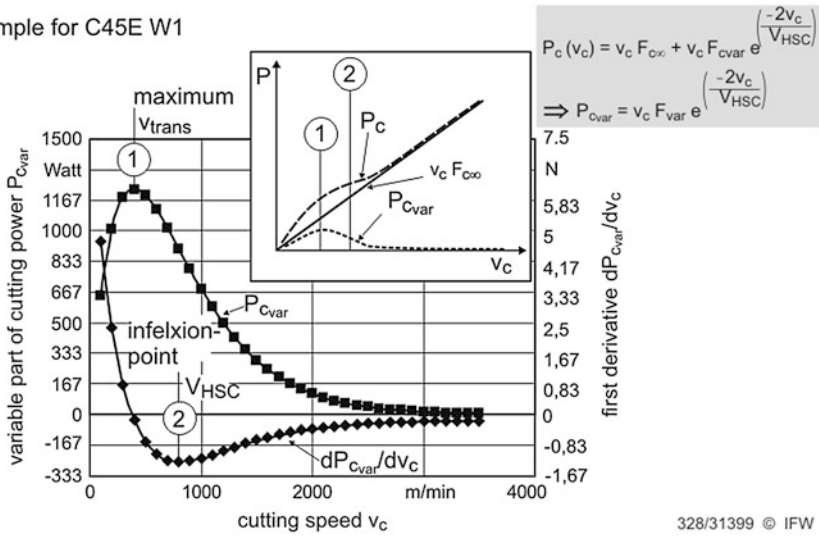


Fig. 9.3 Influence of cutting speed on the power superlevation

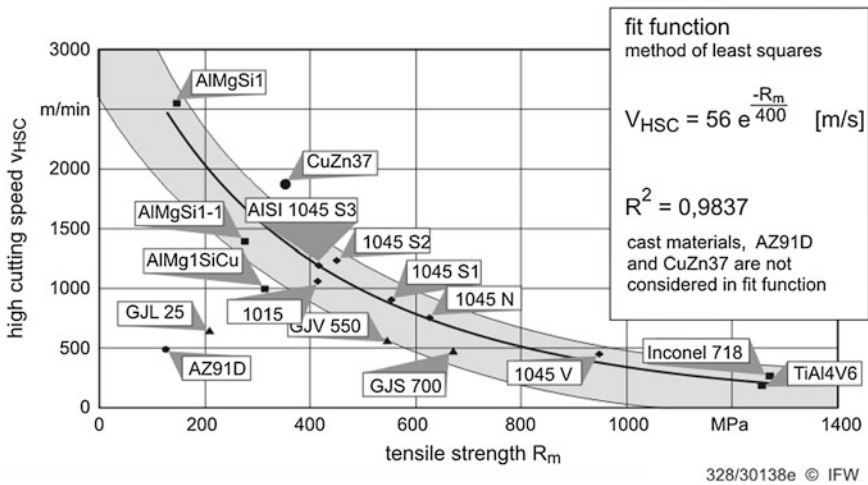


Fig. 9.4 Limit speed and tensile strength

$$v_{HSC} = 3.360 \times e^{\frac{-R_m}{400}} \tag{9.2}$$

with v_{HSC} [m/min] and R_m [MPa] describes the dependency on the strength with a high degree of certainty ($R = 0.984$). Only some of the investigated metals like cast iron, brass CuZn37 and manganese AZ91D make an exception.

9.2 Chip Formation

When machining at high speeds, a significant change in the chip formation occurs. Visible or measurable phenomena are:

- the decline of the cutting force and the other force components for all the other previously investigated ductile metals,
- an increase of the shear angle and thus a reduction of the chip compression,
- a clear segmentation of the chip and a concentration of plastic deformations in shear localizations, although this phenomenon strongly depends on the material,
- an unstable formation of highly concentrated shear bands, depending on the material and the texture.

The distinct decrease of the cutting force is observed consistently as long as no brittle discontinuous chips are formed and ripped out of the material. Baeker has named possible causes, as they are also divergently proposed in literature [BÄK03]. He can explain conclusively by simulation that it is neither the segmentation nor the alteration of the friction coefficient, which can interpret these experimental observations but that an adiabatic decline of the deformation strength dependent on the strain rate can fully explain the experimental observations [ELM05]. This is followed by an increase of the shear angle as can be seen for carbon steel in Fig. 9.5.

Independently of that, a characteristic chip segmentation occurs for metals of sufficient strength. For titanium alloys this happens at all, even very low, cutting speeds. Ductile steels of elevated strength show chip segmentation only with higher speeds, for particularly soft steels segmentation does not occur at all. Shear

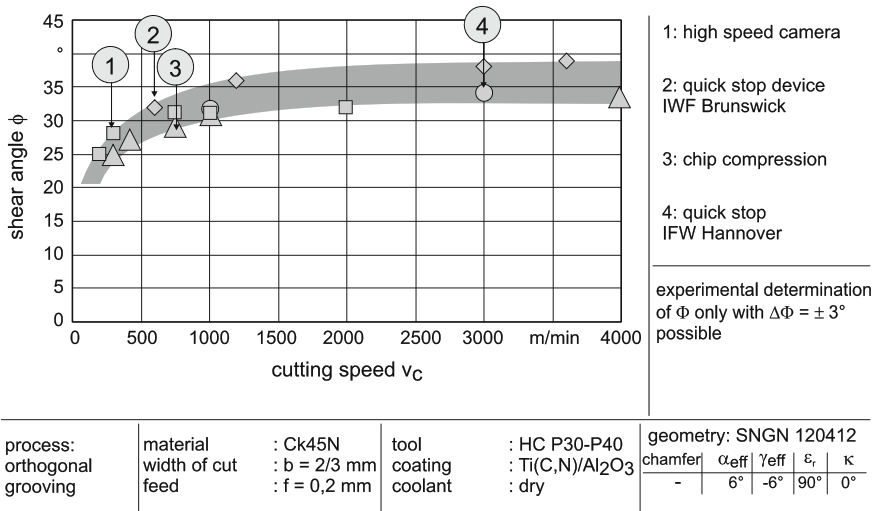


Fig. 9.5 Influence of cutting speed on the shear angle

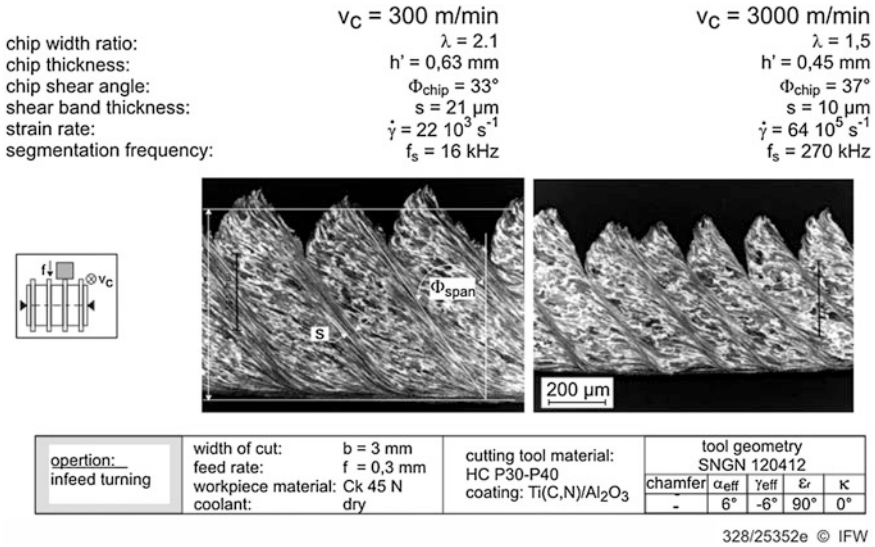


Fig. 9.6 Chip formation at high feeds

bands can be observed in metallographic sections (Fig. 9.6) and with micro hardness measurements (Fig. 9.7)

Figure 9.8 represents a model distinguishing compressive and shearing phases during the chip formation. These phases alternate nearly periodically. Such periodicities can also be seen on the workpiece surface, which also means periodic force courses between workpiece and tool.

9.3 Application

According to previous experimental results, high speed cutting is not fundamentally different from cutting in conventional speed domains. Nevertheless, some effects can be used which are of interest for practical application.

With higher cutting speeds the *material removal rate* initially increases for all cutting processes, if the chip cross section remains constant. This can especially be used when machining with rotating tools. For processes and machines, where the workpiece is rotated, limits mostly occur due to the clamping technology because the centrifugal forces, pushing the clamping jaws outward, counteract the clamping forces and reduce them with the 2nd order of the rotational speed (rpm). In addition, for heavy workpieces and clamping devices the accelerating and breaking times can become so long—and they grow also with the 2nd order of the rpm—that thereby the idle times question the economic success. High speed cutting for rotating workpieces is thus limited by

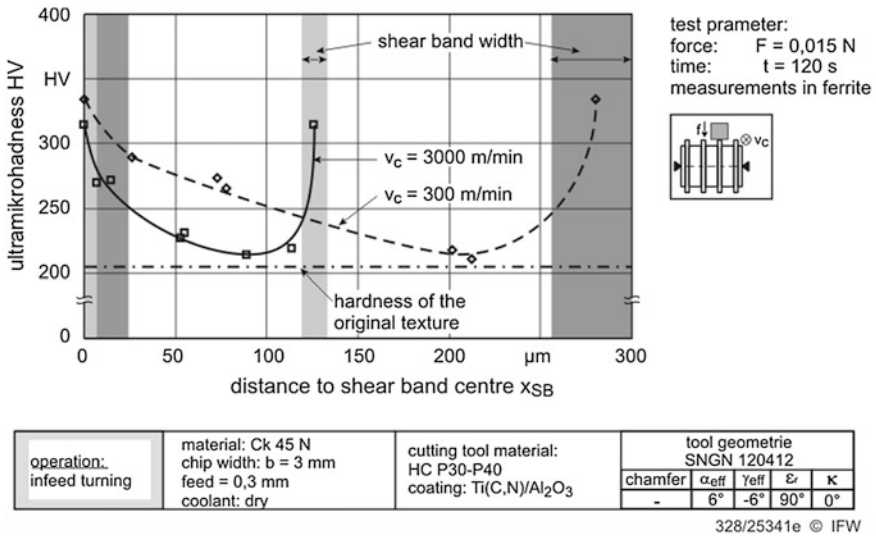


Fig. 9.7 Micro hardness in the segment domain [TÖD05]

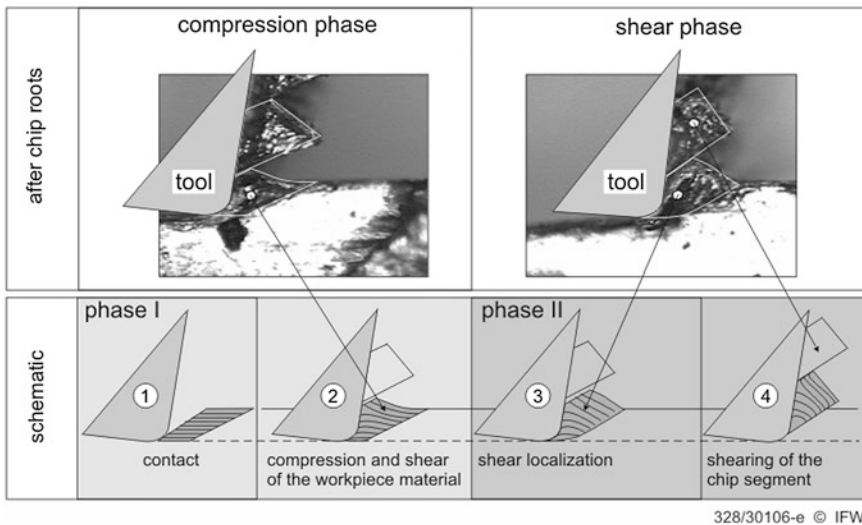


Fig. 9.8 Material deformation during segmentation

- the influence of the workpiece clamping with the 2nd order of the rpm,
- the necessary strengthening of the safety devices against release of rotating elements,
- the increase of idle times for accelerating and breaking phases.

When cutting with rotating tools, these disadvantages have less effect or none at all. As a rule, the rotating masses or the moments of inertia are considerably lower

so that acceleration and breaking procedures have less effect on the increase in idle time, although the effect must not be neglected as the material removal rate grows with the first order and the acceleration/breaking durations with the second order of the rpm or the speed respectively. Special precautionary measures also have to be observed for the clamping of tools under high speed conditions as clamping by hollow shaft cones.

The advantage of cutting with high speeds is that cutting and feed forces are considerably reduced. Filigree parts with small wall thickness can thus be machined with less elastic deformations caused by the force components (for example in aircraft manufacturing). However, the effect of minimizing the chip cross section is stronger for finishing operations, where this effect alone is interesting; since it is (see [Chap. 4](#))

$$F_{c,f,p} = k_{c,f,p} \cdot A \tag{9.3}$$

- $k_{c,f,p}$ specific energy for cutting, feed and passive direction
- A chip cross section
- $k_{c,f,p}$ decreases with $e^{-v_c/v_{HSc}}$ whereas A is proportional in [Eq. 9.3](#)

The power converted in the chip forming zone increases with the cutting speed—although sub proportionally due to the decreasing cutting force. The powers converted at the contact areas (index α for the flank face, and index γ for the rake face) result with the tangential forces $F_{T\gamma}$ and $F_{T\alpha}$ to

$$P_\gamma = \frac{1}{\lambda} F_{T\gamma} \cdot v_c \quad \text{and} \quad P_\alpha = F_{T\alpha} \cdot v_c \tag{9.4}$$

Accordingly, the temperatures rise in the contact zones and thus in the cutting wedge. It should be noted that the *energy per time unit* (i.e., the power) is relevant in the heat balance with respect to the tool, since the cutting wedge is engaged permanently or for longer durations. The heat balance, however, is different considering the work material, e.g., the surface integrity of the newly generated surface or the average temperature in the chip. In this case the *energy per removed volume* is relevant.

A strong increase of the thermally induced wear occurs due to the temperatures in the contact zones and in the cutting wedge, increasing with the cutting speed. Thus, the cutting speed is economically limited when machining steel and other materials of higher strength. Only with materials of relatively lower melting temperatures, such as aluminum- and magnesium-alloys, is the thermal loading uncritical. Cutting speeds of more than 3,000 m/min are achievable.

However, such high temperatures cannot be often reached in interrupted cutting, because of the cooling effect when the cutting edge is not engaged, for instance in milling, which would then result in non-economical tool life. Therefore, high speed milling is also used with good results when machining casings made of steel or cast iron or in die and mold manufacturing. For finishing

operations it can be useful not to utilize the totally possible speed increase to enhance the metal removal rate, but to use a part of the gain to optimize and reduce the undeformed chip thickness. This allows high surface qualities particularly useful in die and mold manufacturing or in circular milling when machining bore holes of a bigger diameter. In die and mold manufacturing it can thus be achieved that the share of the manual bench work for finishing and fine finishing of milled surfaces is considerably reduced and at the same time the dimensional and form accuracy is significantly enhanced. Circular milling of holes in the domain of IT 7 and IT 6 is advantageous because dimensionally independent tools can be used. If a hole is drilled by conventional techniques, a dimensionally dependent tool has to be used. In contrast, circular milling can cover a larger diameter range with the same tool. This eliminates downtime tool cost for tool change and reclamping.

9.4 High Power Cutting

Beside the speed, the torque or the power may also be limitations of a cutting process. Consequently, the concept of high power cutting was developed [AND02]. High power cutting is based on four process boundaries,

- the maximum machine power,
- the maximum torque and the maximum feed force,
- the maximum tool load and
- the maximum feed speed, which can be achieved due to the drives and control system.

The dependencies are shown in Fig. 9.9 using an example of the power limitation and of machining of an aluminum alloy as used in aircraft manufacturing. Power losses increase with growing cutting speed and thus growing rpm of the spindle. So there is less power available at the working spindle at high speeds. However, this is counteracted by the fact that the specific energy decreases (see above).

Finally, it is to be noted that for a given power limit the specific energy increases by reducing the undeformed chip thickness. These factors mean that there is an optimum in the per kW achievable material removal rate as has been shown theoretically and experimentally [AND02]. This optimum, however, depends on the boundary conditions of the machine, the tool and the material.

9.5 High Power Drilling

The material removal rate cannot be arbitrarily raised by increasing the cutting speed for drilling either. The limited accelerating ability of the spindle and feed drives are decisive for this, apart from the technological reasons [AND02].

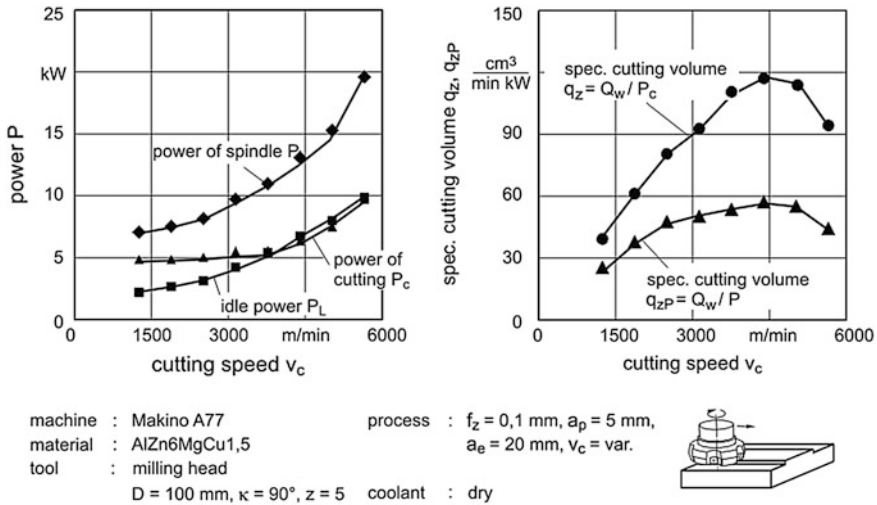


Fig. 9.9 Power requirement dependent on the cutting speed

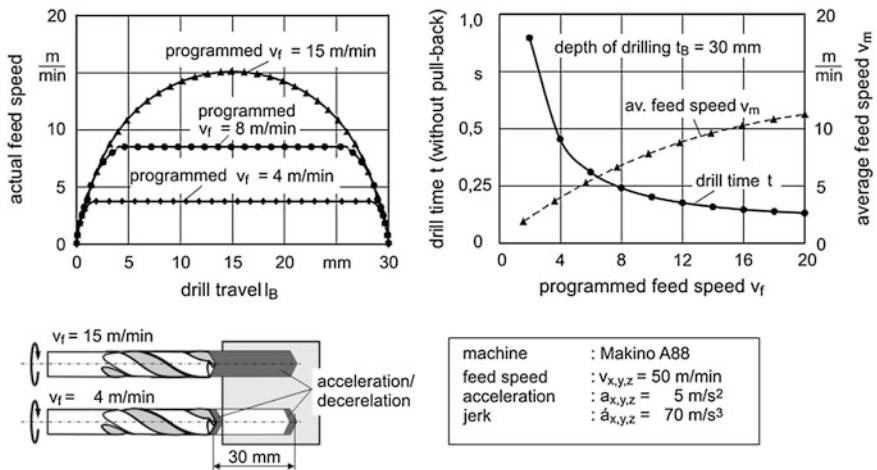


Fig. 9.10 Speed courses at drilling

Figure 9.10 shows the feed speeds (left part of the figure) achievable by the limits for the acceleration and the jerk of a high speed milling machine. The achieved average speeds and the drill times were measured for a given drill travel (right part of the figure). It therefore also follows here that the rpm can be optimized according to the given conditions (Fig. 9.11). Thereby, the spindle run-up time can have a substantial part of the total drill time. Consequently, the number of holes has to be regarded, which is obtainable without a spindle stop.

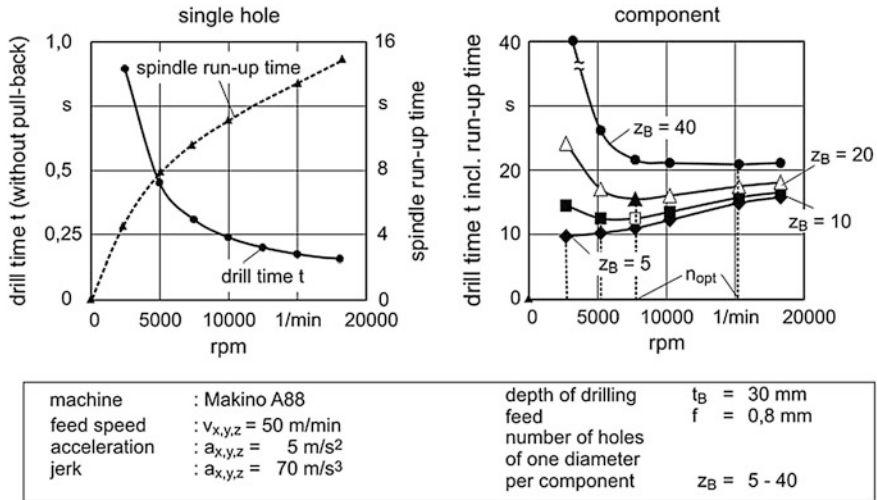


Fig. 9.11 Determination of the optimal rpm at drilling

9.6 Questions

1. What developments of machine tools and cutting materials enabled high speed cutting (HSC)?
2. Explain the definition of high speed cutting according to Ben Amor. Can you find a physical/metallurgical justification within it?
3. How does the chip formation change at high cutting speeds?
4. What are shearing locations, shear bands?
5. Discuss the thermal conditions in the chip forming zone dependent on the cutting speed.
6. Why is high speed cutting in turning less interesting?
7. Discuss the concept of high power cutting using process boundaries.
8. What economic limits do you see in high speed drilling/boring?
9. What advantages does circular milling offer?
10. Give typical cutting speeds in the HSC domain for AlMgSi1, CK45 N, Inconel and TiAl4V6.
11. Try to give a tribological and/or physical explanation for the strong differences of cutting speeds.

References

- [AND02] Andrae, P.: Hochleistungszerspanung von Aluminiumlegierungen [High power cutting of aluminum alloys]. Dr.– Ing. Diss. Universität Hannover (2002)
- [BÄK03] Bäker, M.: An investigation of the chip segmentation process using finite elements; to appear in: Technische Mechanik 23, (2003)
- [BEN03] BenAmor, R.: Thermomechanische Wirkmechanismen und Spanbildung bei der Hochgeschwindigkeitszerspanung [Thermo-mechanical effect mechanisms and chip formation in high speed cutting]. Dr.–Ing. Diss. Universität Hannover 2003
- [ELM05] El Magd, E., Treppmann, C. et al.: Experimentelle und numerische Untersuchungen zum thermo-mechanischen Stoffverhalten [Investigations on the thermo-mechanical material behavior]. pp. 183–206, Wiley, Verlag, (2005)
- [ICK81] Icks, G.: Maschinenseitige Grenzen des Hochgeschwindigkeitsdrehens [Machine dependent limits of high speed turning], Dr.-Ing. Diss., University Stuttgart (1981)
- [SAL31] Salomon, C.: Deutsches Patent [German patent] Nr. 523594, April (1931)
- [SCH36] Schwerd, F.: Filmaufnahmen des ablaufenden Spans bei üblichen und sehr hohen Schnittgeschwindigkeiten [Motion pictures of the chip flow at comon and very high cutting speeds]. Z. VDI (1936)
- [SCH94] Schulz, H.: Hochgeschwindigkeits-Bearbeitung - Technologie mit Zukunft [High speed cutting – a technology with future]. Werkstatt und Betrieb **127**(7–8), 539–541 (1994)
- [TÖD05] Tönshoff, H.K., Denkena, B., et al.: Spanbildung und Temperaturen beim Spanen mit hohen Geschwindigkeiten [Chip formation and temperatures in cutting with high speeds], pp. 1–40, Wiley, Verlag (2005)
- [TÖH05] Tönshoff, H.K., Hollmann, F., Hrsg.: Hochgeschwindigkeitsspanen [High speed cutting], Wiley-VCH, Verlag (2005)

Chapter 10

Hard Machining, Process Design

The cutting of hardened ferrous materials and hard coatings with hardnesses above 47 HRC is referred to as hard machining (more precisely: cutting with geometrically defined cutting edge). These hard materials have been machined—apart from repair cases—exclusively by grinding and brought into their final shape until this technology came up [TÖN81, TÖN86]. The development of cutting materials of high hardness and heat resistance made hard turning, hard milling and hard drilling, which are mentioned here and also hard broaching, hard shaving and hard reaming both possible and economical. Table 10.1 gives an overview of the conditions, under which these processes can be performed.

In many areas of mechanical engineering, automotive and machine manufacturing, components are exposed to higher force and power density. Therefore, they have to be firmer, harder and more wear resistant. Where materials, particularly steels with merely moderate strength were previously sufficient, increasingly highly-tempered or hardened materials are now used. For a number of components the spectrum of the rough and finish machining processes can be extended by methods of hard machining besides grinding [KLB05]. In addition to the strength and hardness the quality requirements for highly-stressed components have grown significantly at the same time (Fig. 10.1). These requirements must also be met by hard machining with geometrically defined cutting edges, i.e. by cutting [KAN04].

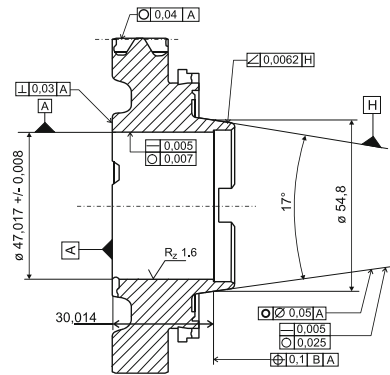
10.1 Hard Turning

In turning the cutting edge is usually continuously engaged. The energy density implemented in the chip formation zone is high, which leads to a high thermal load on the cutting wedge [Sch99]. Therefore, cutting speeds must be limited with respect to the tool wear (Table 10.1). Cutting ceramics (mixed ceramics of Al_2O_3 and TiC) are applied at 150 m/min and poly-crystalline boron nitride (PCBN) up to 220 m/min, at lower levels of hardness higher speeds can also be used [HER91]. Usual cutting depths are in the range $a_p = 0.05\text{--}0.3$ mm. Feeds significantly determine the

Table 10.1 Boundary conditions for hard cutting

Process	Cutting material	Cutting parameters	Roughness, accuracy
Hard turning	PCB, mixed ceramic, ultrafine carbides	$v_c = 100\text{--}220$ m/min $f = 0.05\text{--}0.2$ mm	$R_z = 1\text{--}3$ μm IT6–IT7
Hard drilling	Carbide, TiN coated	$v_c = 40\text{--}60$ m/min $f = 0.02\text{--}0.04$ mm	$R_z = 2\text{--}4$ μm IT7–IT9
Hard milling	PCB, ultrafine carbides	$v_c = 200\text{--}350$ m/min $f_z = 0.1\text{--}0.2$ mm	$R_z = 2\text{--}5$ μm IT7–IT10

Fig. 10.1 Typical quality requirements for hard machined components [KAN04]



surface quality. Depending on the requirements of the surface roughness, feeds of $f = 0.05\text{--}0.2$ mm are set. The tool life depends significantly on the hardness of the material, as shown in a tendency illustration referring to hardened steel materials in Fig. 10.2. The maximum achievable speeds are also visible. In addition to hardened steels basically hard cast iron, nickel-based alloys and sintered and hardened steels can be machined by PCB [KLB05]. Figure 10.3 shows the dependency of tool life and cutting speed in a Taylor diagram for the use of poly-crystalline boron nitride. From the atypical curves, if compared with the straight lines in soft material cutting, it can be found that a limited window of cutting speed must be maintained.

In Fig. 10.3, in addition to the cutting speed the hardness of the material was varied [KOC96]. Here you can see a strong influence of the hardness, with the hardness of the martensitic 100Cr6 and the hardness of martensite and carbides in high speed steel which tend to similar effects. For practical purposes it is applicable that a slight lowering of the hardness brings a significant gain in tool life.

In hard turning one usually works with relatively low feed rates and large corner radii r_e of the cutting edge. This allows the keeping of the cutting edge load within limits. Figure 10.4 shows the engagement conditions in hard turning, where f , a_p , r_e and r_β are shown to scale. It can be seen in the top view on the rake face that the actual cutting edge angle along the engagement arc changes heavily and that the nominal cutting edge angle does not come into effect. To estimate the load

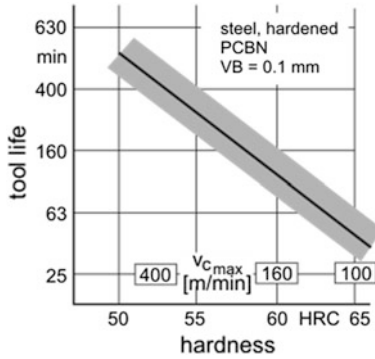


Fig. 10.2 Influence of hardness on tool life

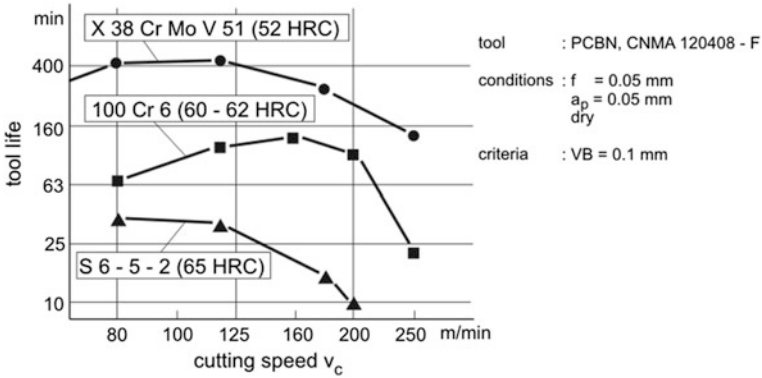


Fig. 10.3 Wear behavior of PCB

conditions of the cutting edge an effective angle κ_{eff} is defined, which corresponds to half the contact angle ψ . It is

$$\kappa_{eff} = \frac{1}{2} \arccos \left(\frac{r_\epsilon - a_p}{r_\epsilon} \right) \tag{10.1}$$

In the orthogonal plane perpendicular to the cutting edge, geometric conditions also differ from conventional machining because of the small undeformed chip thickness, which also varies heavily from $h = 0$ to the maximum value $h_{max} = f \cdot \sin 2 \kappa_{eff}$. The length of contact arc l_c , which is part of the cutting edge in engagement, follows from

$$l_c = 2 \kappa_{eff} r_\epsilon \tag{10.2}$$

The right part of Fig. 10.4 shows that the actual rake angle γ_{eff} , which is taken from the reference plane (approximately normal to the cutting speed vector) to the varying undeformed chip thickness h , is usually negative due to the cutting edge radius r_β . It applies to the sharp edge for $h < r_\beta$

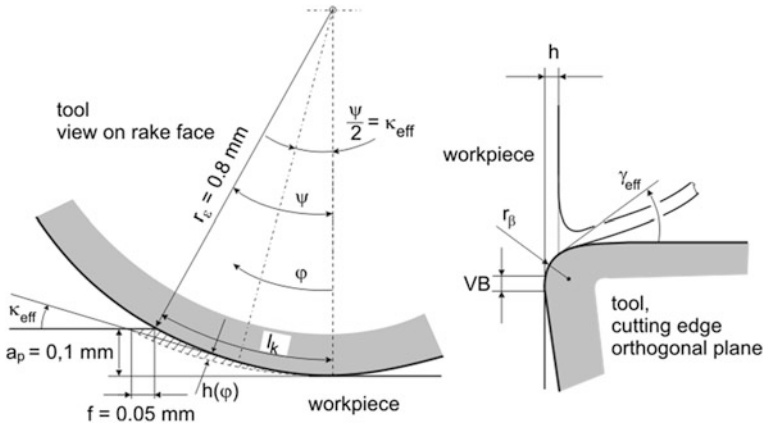


Fig. 10.4 Engagement conditions in hard turning

$$\gamma_{\text{eff}(\varphi)} = \arcsin \frac{r_\beta - h(\varphi)}{r_\beta} \tag{10.3}$$

For $h \geq r_\beta$ the rake angle given by the rake face applies, although an additional chamfer is mostly intended to strengthen the cutting wedge. With a negative rake angle of $\gamma = -6^\circ$ (negative cutting insert), for example, and a chamfer of $\gamma_n = 20^\circ$, a resultant rake angle $\gamma = -26^\circ$ follows.

As a final machining process, hard turning is aimed at the substitution of grinding operations. In Fig. 10.5, a best practice is shown, where hard turning is significantly more favorable [BRA95]. A friction disc of bearing steel 100Cr6 is precision-turned on three surfaces, an outer cylinder, a flat surface and a short inner cylinder. The economic and environmental benefits are indicated in the figure.

For $h \geq r_\beta$ the rake angle given by the rake face applies, although an additional chamfer is mostly intended strengthen the cutting wedge. With a negative rake angle of $\gamma = -6^\circ$ (negative cutting insert), for example, and a chamfer of $\gamma_n = 20^\circ$, a resultant rake angle $\gamma = -26^\circ$ follows thus.

As a final machining process hard turning is aimed at the substitution of grinding operations. In Fig. 10.5, a best practice is shown, where hard turning is significantly more favorable [BRA95]. A friction disc of bearing steel 100Cr6 is precision-turned on three surfaces, an outer cylinder, a flat surface and a short inner cylinder. The economic and environmental benefits are indicated in the figure.

However, a comparison between grinding and hard turning depends strongly on the machining task and certainly not without ambiguity. In addition, different criteria can be applied to the process such as manufacturing costs per part, flexibility, component quality or ecological compatibility. A comparison of the material removal rates Q_w (removed volume per time) and the surface rate A_w (the machined surface per time) is shown in Fig. 10.6. It is apparent that especially for the surface rate significantly larger values are in favor of grinding. The advantage exists only where large surfaces have to be machined. It is also important that

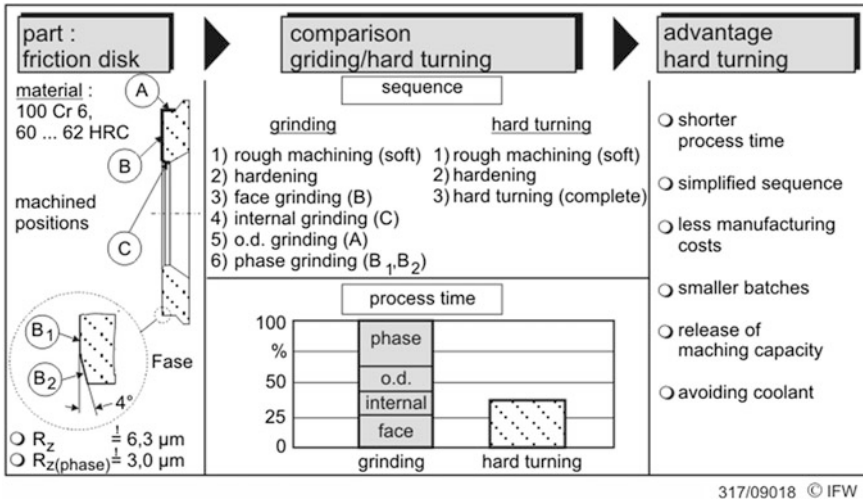


Fig. 10.5 Economic manufacturing by hard turning

when turning and generally when hard cutting a minimum undeformed chip thickness exists, which must not be under-run, otherwise no cutting takes place. This means that not any optionally small depth of cut can be used. In contrast, in grinding the process can be set so far by spark-out till the normal force disappears. Consequently, hard cutting processes are hardly applicable, if long, slender and pliable workpieces must be machined because then the higher surface rates of grinding can be generally used (Fig. 10.6).

An advantage of hard turning, which is advantageous in many cases, is the form flexibility of the process. The workpiece is machined via the control system, whereas when using grinding it is mostly machined by plunge grinding or at least by copying the profile of the grinding wheel onto the workpiece. In turning, workpieces can be machined by one or several tools, which are easily changeable. This often leads to a considerable shortening of the process chain in the sense of a complete machining, to less complexity costs and to lower investment.

Material and energy flows are compared from an ecological point of view. An example for manufacturing a center gear for a friction transmission shows the material flows for grinding and hard turning from the production of 5,000 parts (Fig. 10.7). On the basis of the allowance of the parts a mass of 50 kg of chips is generated per year. The grinding fluid used in the required 4 grinding machines adds up to 8 t per year, if a bi-annual change is used. In addition 20 cm³ of abraded wheel material (depending on the wheel material) accumulate, caused by the grinding process, is accumulated by dressing and by additional filter materials. It is especially critical when the material flows mix, so that generally the entire material flow has to be disposed of. There are technologies to dry generated chips to a residual level of 3 % so that they are recaptured, but this requires an additional energy effort [WOB96].

	grinding	cutting
principle		
material removal rate	$Q_w = a_p \cdot Q_w'$	$Q_w = a_p \cdot f \cdot v_c$
spec. material removal rate	$Q_w' = d_w \cdot \pi \cdot v_{fr}$	$Q_w' = \frac{a_p \cdot f \cdot v_c}{l_c}$
surface rate	$\dot{A}_w = a_p \cdot v_{fr,w}$	$\dot{A}_w = f \cdot v_c$
characteristic parameter	$a_p = 5 - 20 \text{ mm}$ $v_{fr,w} = 1 \text{ m/s}$	$a_p = 0,05 - 0,3 \text{ mm}$ $f = 0,05 - 0,2 \text{ mm}$ $v_c = 150 \text{ m/min}$
typical values	$Q_w' = 2 - 12 \text{ mm}^3/\text{mms}$ $Q_w = 10 - 240 \text{ mm}^3/\text{s}$ $\dot{A}_w = 5000 - 20000 \text{ mm}^2/\text{s}$	$Q_w' = 22 - 242 \text{ mm}^3/\text{mms}$ $Q_w = 6 - 150 \text{ mm}^3/\text{s}$ $\dot{A}_w = 125 - 500 \text{ mm}^2/\text{s}$

31/3/20523 © IFW

Fig. 10.6 Comparison of hard turning and grinding

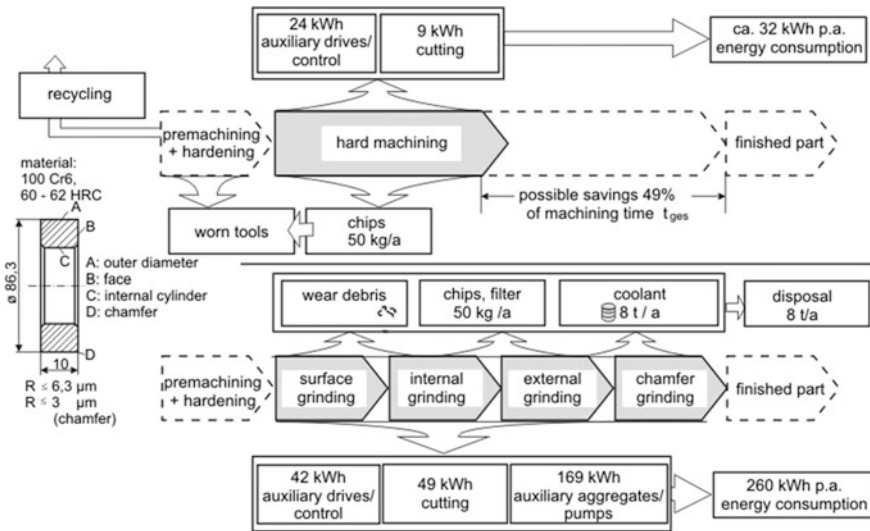


Fig. 10.7 Comparison of energy- and material flow for hard turning and grinding (acc. H.-G. Wobker)

In contrast, for hard turning a more favorable picture emerges since machining can be performed in a dry way, the chips can be recaptured without further treatment in the material cycle. The small additions of tool material abrasion are irrelevant for the recycling process. The used and worn tools can be disposed of

according to their substrate (ceramics) or it is possible to rework them (PCB). Thus, the balance of the material flow is more advantageous for hard machining, resulting from the lower pending disposal quantities and the higher purity.

A comparison of hard turning and grinding was made for the production of roller bearing rings in terms of energy demand. Compared with the conventional production sequence, 34 % of primary energy and 15 % material can be saved on the hard turning of the hardened bearing rings, which are directly hardened out of the forming heat by an optimized working process sequence. In addition to the clearly reduced energy consumption, more significantly reduced processing times and easily recyclable metal waste are the benefits [WIN96].

To reach the common tolerances in the range of IT 6 and improved special demands on turning machines are often provided. This applies to the dimensional and form accuracy, the achievable surface quality and the minimum undeformed chip thickness, dependent on the stiffness of the machine. In addition to conventional turning machines with special construction as far as static and dynamic stiffness and resolution of the position measuring systems are concerned, precision turning machines (also called high precision machines) are used. These machines have a machine bed of granite to improve the dynamic and thermal behavior. The headstock can also be made of granite. To reduce thermal displacements the electrical, pneumatical and hydraulical supply units are arranged separately from the basic structure of the machine, which consists of frame, bed and slides with drives, bearings and guideways.

Figure 10.8 shows to what extent the surface quality can be improved when using precision turning machines in comparison to conventional turning machines. In particular, surfaces in finish grinding and honing quality ($R_z < 1 \mu\text{m}$) can only be reliably achieved with precision turning machines using feeds of $f < 0.1 \mu\text{m}$. This result is due to the hydrostatical spindle bearing and thus a high run-out accuracy of $0.1 \mu\text{m}$, whereas in the conventional machine the achievable roughness is limited because of the spindle concentricity in the range of about $1 \mu\text{m}$. However, applying higher feeds causes the quality ranges for both types of machine to overlap, because the influence of the theoretical roughness, dependent of the feed and the cutting edge radius, predominates.

10.2 Hard Drilling

Holes also have to be regularly brought into turned parts. Regardless of whether hard workpieces are manufactured by grinding or turning/milling, such parts must be machined by hard drilling. For case-hardened workpieces, i. e. parts with a 0.5–1.5 mm thick layer and tough base material, the additional difficulty often arises that one has to drill in the hard as well as the soft texture.

Figure 10.9 shows that a limited process window should be met when drilling. Solid carbide drills are generally applied. Thus, fine grain carbides have been especially proven. Drilling tools with cutting inserts are only used for large

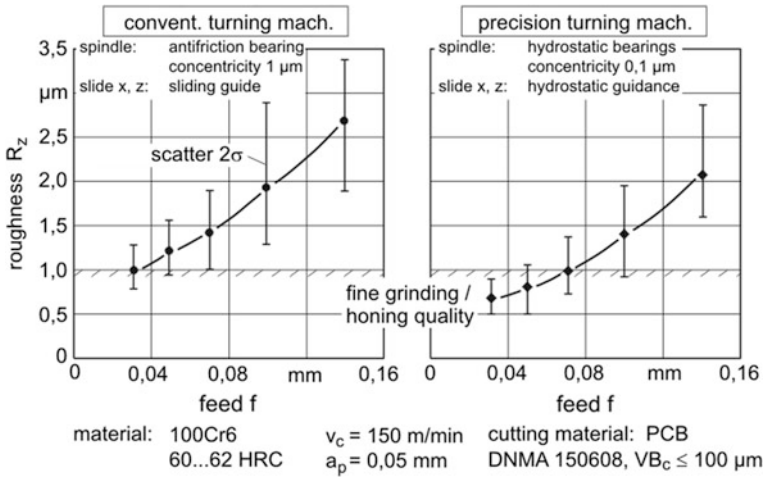


Fig. 10.8 Comparison of the surface quality using conventional and precision turning machines

diameters. For this purpose, tools coated with titanium nitride have been introduced. They offer the advantage of minimizing the friction between the drill and the bore wall and between the chip and the flute in addition to wear reduction. Under finishing conditions, dimensional accuracies in the range of IT 7–IT 9 and surface qualities of $R_z = 2\text{--}4$ µm, in special cases also $R_z = 1$ µm, can be reached by hard drilling with solid carbide drills. The manufacturing sequence can be significantly reduced precisely for case-hardened parts. It is exceptionally interesting that the split heat treatment (carburizing and hardening) or the necessary covering while carbonizing may be omitted (Fig. 10.10).

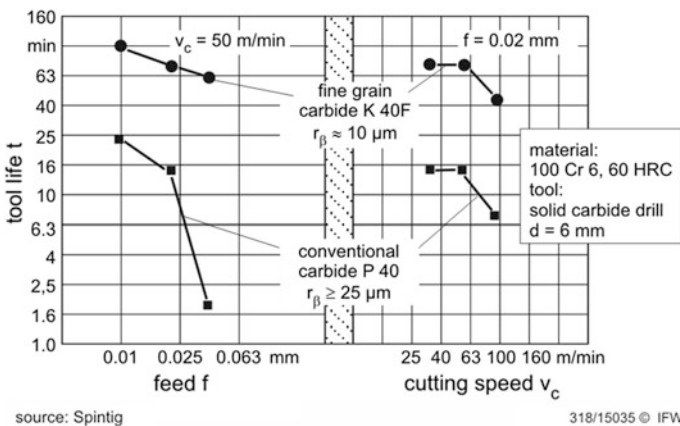
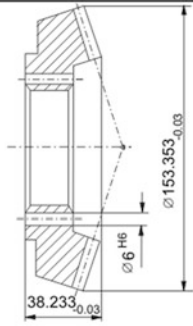


Fig. 10.9 Tool life for hard drilling dependent on the cutting parameters

up to now	part	in future
<ol style="list-style-type: none"> 1. stress free annealing 2. turning both sides 3. drilling holes 4. intermediate 5. inspection 6. set cylinder pins in holes 7. gear cutting 8. remove pins 9. reaming of fit holes or tapping 	 <p>material : 15 CrNi 6 number of teeth : $z_n = 36$ real module : $m = 2.5$</p>	<ol style="list-style-type: none"> 1. stress free annealing 2. turning both sides 3. gear cutting 4. case hardening 5. drilling and reaming or tapping

318/04897c

Fig. 10.10 Reduction of the production steps using hard drilling

The heat dissipation is particularly unfavorable when hard drilling. On the one hand, high power density because of the hardness and strength is generated and on the other hand, the heat dissipation from the drill point is disabled. Therefore, the tool heats up heavily during the drilling operation, expands and can be heated up additionally by the wall friction and consequently it clamps. Therefore, it has been proven to form the drilling tool with a shallow conical taper onto the shaft [SPI95].

10.3 Hard Milling

Hard milling is applied in mechanical engineering and tool making. The finishing of sliding guide way surfaces for machine tools requires elaborate guide way grinding machines, representing significant investments, because of their large working area. Therefore, it is interesting to substitute grinding by milling. An alternative is the development of hardened strips on a machine bed of soft cast iron or steel. However, such strips must be finished in the hardened state too.

Figure 10.11 shows wear over the feed travel of a milling tool of PCB. A carbon steel Cf53 was machined, which is appropriate for guideways because of its low tendency to distort. It is striking, that compared to turning and drilling significantly higher cutting speeds and feed rates (here feed per tooth f_z) were used. This can be explained by the fact that a milling cutting edge is engaged only timewise, which does result in the thermal and mechanical loading occurring shockwise, but the temperature level in the cutting wedge is significantly lower. For the choice of feed the required surface quality is determining in addition to the form of the cutting edge. Surface roughnesses of $R_z = 2\text{--}5 \mu\text{m}$ are quite

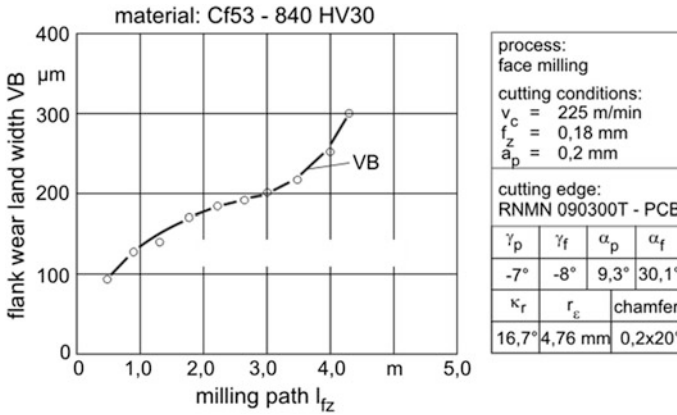


Fig. 10.11 Flank wear in hard milling

accessible. For the dimensional and form accuracy needs one has to consider that by heating the component, by inserting or/and releasing residual stresses and due to the temperature variation of the machine systematic errors can occur, which partly compensate each other, however (Fig. 10.12) [BUS91].

In the die and mold industry, hollow tools are manufactured for molding and forming. Such cavities are partially hardened to reduce wear. After hardening, they have to be brought into their final shape, where partially substantial material volumes of the workpiece have to be removed by cutting due to unavoidable hardening distortion. Here lies another application field for hard milling [HER91, FAL98]. Figure 10.13 shows the use of different cutting materials on a hot working steel as used for die forging and die casting tools.

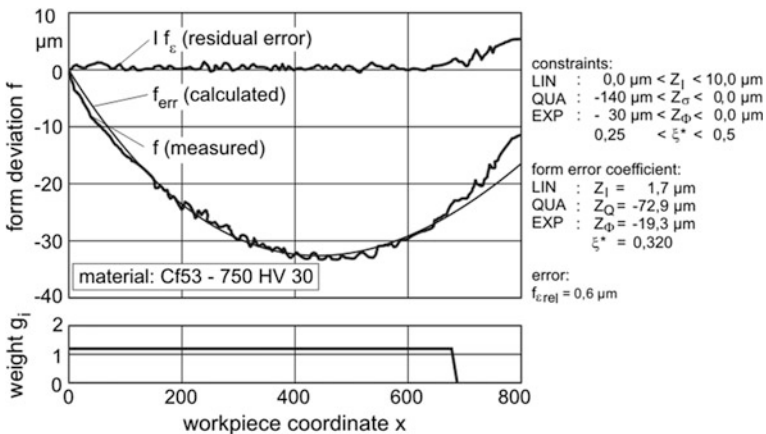


Fig. 10.12 Compensation of form errors

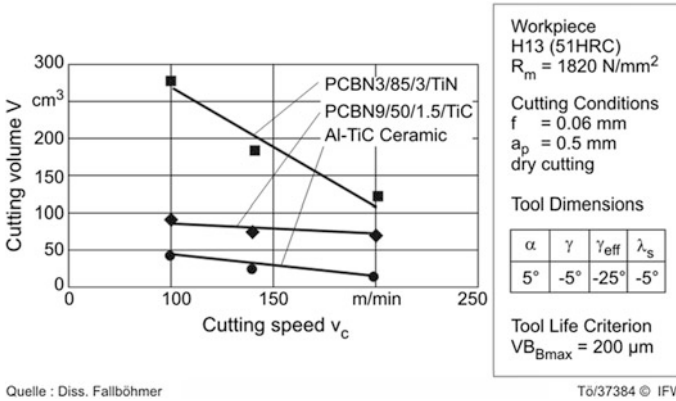


Fig. 10.13 Tool life for different cutting tools in the hard turning of AISI H13

10.4 Materials

Tribologically-loaded components can experience damaging, due to contact deformation (plastic deformation of surface near layers) by friction and wear. Where high energy densities or mass or volume reductions produce higher area-dependent loads, sufficient strength and hardness are required to avoid damage. Coating with wear-resistant protective layers or—for ferrous materials—hardening are common measures to improve their tribological behavior. As far as thick layers (casings) of hard metals such as stellites are applied the surfaces have to be machined. This also applies to functional surfaces of hardened components, because the necessary dimensional and form accuracy and the surface quality are lost due to the heat treatment. The more the risk of distortion by a coating or a heat treatment, the larger the allowance has to be provided on the surfaces to be machined for them to become completely “clean”.

Steels and other ferrous materials can be brought to higher hardness by transformation in the martensitic region and by insertion of carbides. Dahl distinguishes between the ability of intrinsic hardening and hardness penetration [DAH93]. The external hardening determines the highest achievable hardness given by the carbon content. The hardness penetration features the depth of hardening. It is mainly determined by the alloying elements. The following heat treatment techniques are applied to increase the hardness: case hardening, tempering, nitriding and surface-near zone hardening. Depending on the application scope the standards differentiate the following material groups: tool steels, bearing steels, carbon steels and case-hardening steels. The tool steels include high speed steels, hot work and cold work steels [TÖA00]. Figure 10.14 gives an overview of the material groups according to their hardening abilities. The hardness ranges usually mentioned in practice are specified for the material groups. At this, the underlying hardening mechanism, namely by martensite formation or by the formation and insertion of

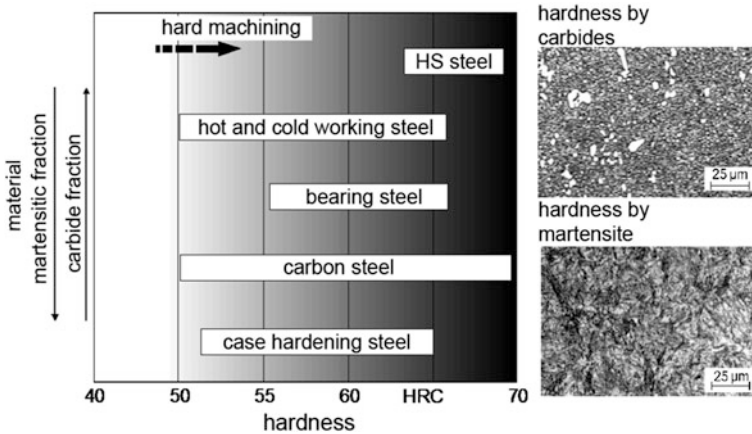


Fig. 10.14 Hardening ability of steels

hard carbides, resulting from the compound of carbon with alloying elements in steel are to be distinguished.

10.5 Chip Formation, Forces and Temperature

As pointed out in [Chap. 2](#), high plastic deformations occur during cutting. In hard cutting, the question rises as to whether the hard materials or the hardened metals can endure such high deformations or whether there is a risk of cracks occurring in the newly-generated surface due to insufficient deformability. The theory of hydrostatic pressure gives an explanation for a crack-free chip formation process [TOEN93]. Large compressive stresses with a high proportion of hydrostatic pressure occur in the chip forming zone due to the low undeformed chip thickness and at the same time strong negative rake angle. The critical flow shear stress is reached without material cracks by means of the tri-axial pressure state. With these considerations the findings of von Kármán, namely that under the influence of high compressive stresses even brittle materials such as marble are plastically deformable, are transferred onto the occurrence involved in fine turning. In a simplified way, the mechanism can be represented at the Mohr's circle for the bi-dimensional case. Using the extended stress hypothesis after Mohr, different limiting stress states arise, whose exceedance leads either to brittle fracture, gliding fracture or plastic deformations (Fig. 10.15).

While the occurrence of brittle fracture is determined by the tensile strength (circle No. 1), the material breaks down by reaching the shear strength limit by gliding fracture (circle No. 2). The shear stress necessary for this is lower if there is tension at the same time. If, however, the compressive stress exceeds a material-

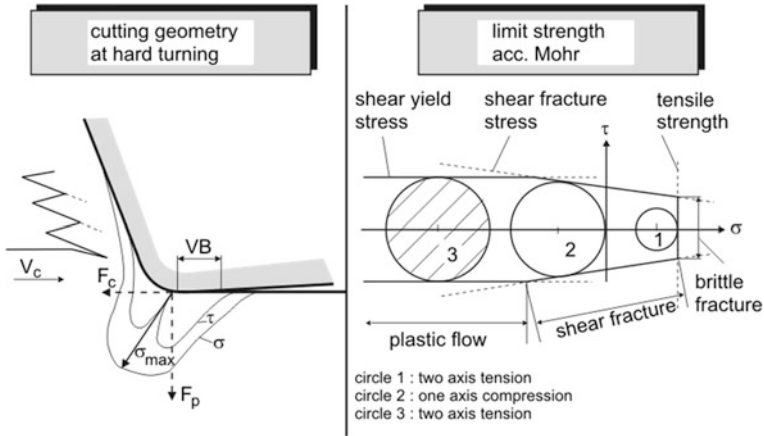


Fig. 10.15 Boundary conditions for plastic flow in hard machining

dependent threshold, a further increase of stress is prevented not by breakage but by plastic flow.

As a result of the small undeformed chip thickness, the chip formation takes place entirely in the region of the rake face chamfer or the cutting edge radius respectively. This leads to the already described severe negative rake angles. Therefore, the passive force F_p becomes the dominant force component in hard turning. Furthermore, using tools with a large corner radius leads to a large contact length, which also contributes to high passive forces. It also turns out that the resulting force components very much depend on the tool wear, which almost linearly rises with the cutting time (Fig. 10.16). This leads to extremely high pressings in the contact area between workpiece and flank face of the tool resulting in a high mechanical and thermal load of the workpiece surface-near zones of the workpiece.

The hardness of the material has great impact on the force components or the specific forces (Fig. 10.17). Here, the passive force is also particularly concerned as hard milling tests show [BUS91].

A comparison of the force effects when machining soft and hard steels shows that the global loads in hard machining are not particularly large because the undeformed chip sections are comparably small. The conditions when looking at the force related to the contact length F_z/l_c or the force related to the contact area F_z/A_C show a different situation as illustrated in Table 10.2.

With some assumptions one can make conclusions concerning the distribution of the forces on the cutting wedge from the heavy dependence of the forces of the wear. It is assumed that the energy transformation and the force effect are composed of two mechanisms, the forming or shearing process in the primary shear zone and the friction and plastic deformations near the rake face and the flank face of the major and minor cutting edge, which result from the friction. These assumptions reflect the real situation as a good approximation.

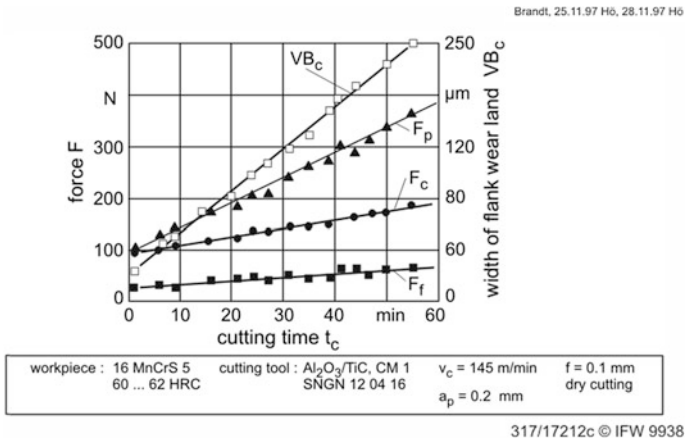


Fig. 10.16 Interdependence between cutting time, tool wear and force components

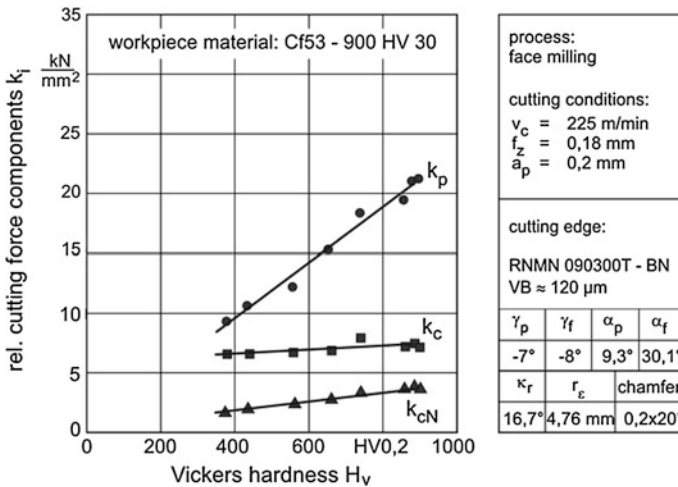


Fig. 10.17 Influence of hardness on the specific force components

Table 10.2 Force effect when turning soft and hard steels

Material	F_z [N]	F_z/l_c [N/mm]	F_z/A_c [N/mm ²]
Steel C45 N			
• finishing	600	300	500
• roughing	3.000	1.000	1.650
16MnCr5, 60 HRC			
• hard turning	490	620	4.450
$VB_c = 200 \mu\text{m}$			

It is also assumed that only the wear at the flank face has to be considered and that this does not affect the deformation situation in the primary shear zone and on the rake face. It is therefore assumed that the effect of flank wear alone affects the force shares in front of the flank face. This assumption is less secured, because the stress and strain states in the primary shear zone may also change due to strong friction effects on the flank face. However, a sufficient approximation seems to be given. Finally, it is assumed that the friction on the flank faces can be described by Amonton's law and that the coefficient of friction does not change with the progressive wear. The balance of the energy input to the energy transformed can then be described as follows:

$$P_c = P_\phi + P_\gamma + P_\alpha = P_{\phi\gamma} + P_\alpha \quad (10.4)$$

In Eq. 10.4, the power fractions P_ϕ and P_γ are composed to $P_{\phi\gamma}$. Here, P_ϕ and P_γ are independent of the wear according to the assumption. At this, the thrust force F_d

$$F_d = \sqrt{F_p^2 + F_f^2} \quad (10.5)$$

acts on the flank face.

In the unworn state, i.e., sharp condition, so when $t_c \approx 0$, F_{d0} is effective. With progressive wear, F_{d0} grows with the rate f_d as shown by the tests (Fig. 10.16).

$$F_d = F_{d0} + f_d \cdot t_c \quad (10.6)$$

The parameters F_{d0} and f_d are determined from experiments using linear regression.

With the approach for the power follows

$$P_c = P_{c0} + p_c \cdot t_c \quad (10.7)$$

P_{c0} contains $P_{\phi\gamma}$ and the time-independent part of P_α . The parameters are determined from experimental results. With the friction law follows

$$p_c = \mu \cdot f_d \cdot v_c \quad (10.8)$$

or

$$\mu = \frac{P_c}{f_d \cdot v_c} \quad (10.9)$$

From test results for conditions common in practice according to the method Wobker [WOB96] described a coefficient of friction of

$$\mu = 0.26.$$

Herewith, the power transformed at the flank can be determined.

The cutting force F_c can also be taken as composed of a part following from forming or shearing $F_{\phi\gamma}$ and another part following from friction at the flank face

$$F_c = \mu \cdot F_d + F_{\phi\gamma}$$

Below, it is further assumed that the same conditions of friction exist on the rake face and the flank face, i.e., the same coefficient of friction. The thrust force and the cutting force can then be written from the normal and tangential parts, the latter via the friction coefficient from the normal force

$$F_d = F_{N\alpha} + \mu F_{N\gamma} \quad (10.10)$$

$$F_c = F_{N\gamma} + \mu F_{N\alpha} \quad (10.11)$$

A transformation results in

$$\mu F_d = \mu^2 F_{N\gamma} + \mu F_{N\alpha}$$

$$F_c = F_{N\gamma} + \mu F_{N\alpha}$$

$$F_c - \mu F_d = F_{N\gamma} (1 - \mu^2)$$

From this, the force effects on the rake and flank face can be given after transformation as

$$F_{N\gamma} = \frac{1}{1 - \mu^2} (F_c - \mu F_d) \quad (10.12)$$

$$F_{N\alpha} = \frac{1}{1 - \mu^2} (F_d - \mu F_c) \quad (10.13)$$

As explained above, the power introduced into the process is by far mostly converted into heat. With thermographic measurements the temperatures at the workpiece surface during turning can be recorded. It turns out that the contact determining parameters, corner radius and chamfer of the rake face, have greater influence on the workpiece temperature than the power affecting parameters, cutting speed and feed. The course of the workpiece temperature shows a good correlation with the course of the frictional power related to the length of cutting edge at the flank P'_α . This part of the power is

$$P'_\alpha = \frac{P_\alpha}{l_c} = \frac{\mu \cdot v_c \cdot \sqrt{F_p^2 + F_f^2}}{l_c} \quad (10.14)$$

For the sliding friction coefficient values of $\mu = 0.25\text{--}0.28$ can be taken [WOB96].

The friction power related to the contact length was derived as an indicator for the turning of hardened steels in order to quantify the mechanical and thermal effects. They are particularly influenced by the shape of the cutting edge and the wear state of the tool. Figure 10.18 represents the maximum surface temperatures in hard turning [SCH99].

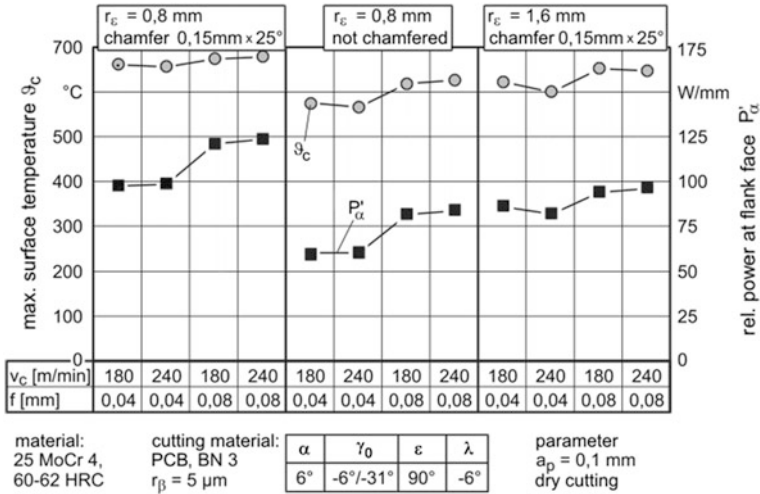


Fig. 10.18 Related power at the flank face and workpiece temperature

10.6 Cutting Materials and Tool Wear

While hard cutting, a tool is subjected to high loading causing abrasive and adhesive wear. Here, the workpiece structure is very important. For instance, deposited hard carbides, as they typically exist in cold working steels lead, to increased abrasive wear. The cutting materials have to have a high hot hardness due to this kind of loading. High speed steels and conventional tungsten carbides are therefore not suitable for hard cutting. However, applicable are fine and super fine tungsten carbides as well as mixed ceramic and polycrystalline boron nitride (PCB) [TÖN93].

Hard turning is largely covered with mixed ceramics $\text{Al}_2\text{O}_3/\text{TiC}$ and with PCB. Both materials can be used in continuous cutting. If, however, interrupted cuts make higher demands on the fracture toughness of the cutting material, PCB has to be used. For hard drilling, especially titanium nitride-coated ultra-fine tungsten carbides are significant, as for this application PCB or ceramic tools are not available or are too expensive [TÖN93]. Hard milling can be carried out with fine tungsten carbides or PCB.

Flank wear and crater wear are the dominant forms of wear using PCB or ceramic cutting materials in hard turning. Figure 10.19 shows scanning electron microscopic images of worn tools of PCB, which had different starting cutting edge radii. The formation of the distinctive cratering is primarily determined by abrasion. The tool life-decisive criterion is the wear at the major flank face VB_C or at the minor flank face VB_N respectively.

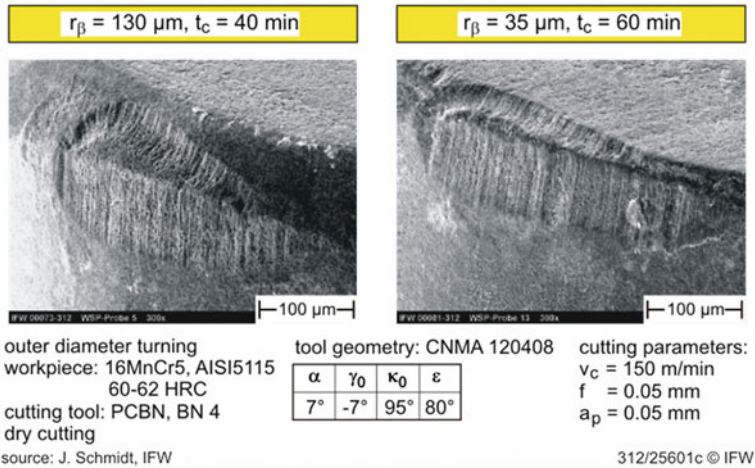


Fig. 10.19 Typical wear forms in hard turning

10.7 Questions

1. What (restricted) importance did hard cutting get due to the developments of cutting materials?
2. What materials in what state are hard machined in this sense?
3. What cutting materials are used for hard cutting?
4. How does the hardness of the workpiece material tend to affect the tool life?
5. What indication do you take from the course of the tool life—cutting speed function in Taylor's diagram?
6. What values do the effective cutting edge angle and the effective rake angle typically take in hard cutting?
7. Note typical values which indicate the productivity of grinding compared to hard turning. Can you derive preference geometries from this for workpieces?
8. Often, the material removal rate or the surface rate are less decisive for the substitution of grinding by hard turning, but rather?
9. What characteristics are important for hard turning machines?
10. Hard drilling often follows inevitably from hard turning, why?
11. Why are hard turning and hard drilling particularly interesting for case-hardened steel?
12. Why are solid carbide drills shaped with a shallow taper?
13. How do you explain, that for hard milling significantly higher cutting speeds are chosen than for hard turning?
14. What is a wide finishing cutting edge (wiper cutting edge)? Why is it applied for the milling of guide ways?
15. What systematic causes do you see for distortions when milling guide way strips?

16. What application domains do you see for hard milling?
17. What cutting materials are used for hard milling?
18. What hardness enhancement mechanisms do you know?
19. Compare the formability of hardened steel with the deformations as they occur during cutting.
20. How can it be explained, that the surface of the workpiece after hard machining does not show any cracks, but is generated solely by plastic deformation?
21. How do the force components change with application time in hard machining?
22. Based on what assumptions can the power conversion at the flank face be split into a part by forming and another by friction?
23. Name the most important influencing factors on the friction power at the flank face.
24. What are the typical wear forms of tools for hard cutting?
25. Compare hard turning and plunge grinding of hardened parts. What are the advantages, what are the disadvantages?

References

- [BRA95] Brandt, D.: Randzonenbeeinflussung beim Hartdrehen [Surface zone influence in hard turning]. Dr.-Ing. Diss. Universität Hannover, (1996)
- [BUS91] Bussmann, W.: Formfehleranalyse beim Planfräsen gehärteter Bauteile [Form error analysis in face milling of hardened components]. Dr.-Ing. Diss. Universität Hannover, (1991)
- [DAH93] Dahl, W.: Eigenschaften und Anwendungen von Stählen [Properties and applications of steels]. Band 1 und 2. Aachen (1993)
- [FAL98] Fallböhrer, P.: Advanced cutting tools for the finishing of dies and molds. Dr.-Ing. Diss. Univ. Hannover (1998)
- [HER91] Hernandes-Camacho, J.: Frästechnologie für Funktionsflächen im Formenbau [Milling technology for functional surfaces in mold making]. Dr.-Ing. Diss. Universität Hannover, (1991)
- [KLB05] Klocke, F.; Brinksmeier, E., Weinert, K.: Capability profile of hard cutting and grinding processes. *Annals of the CIRP* **54**(2):557–580 (2005)
- [KOC96] Koch, K.-F.: Technologie des Hochpräzisions-Hartdrehens [Technology of high precision hard turning]. Dr.-Ing. Diss. RWTH Aachen (1996)
- [SCH99] Schmidt, J.: Mechanische und thermische Wirkungen beim Drehen gehärteter Stähle [Mechanical and thermal effects in turning of hardened steels]. Dr.-Ing. Diss. Universität Hannover, (1999)
- [SPI95] Spintig, W.: Werkstoffbeeinflussung und Prozessführung beim Hartbohren [Material influencing and process design in hard drilling]. Dr.-Ing. Diss. Universität Hannover, (1995)
- [TÖA00] Toenshoff, H.K.; Arendt, C.; Ben Amor, R.: Cutting of hardened steel. *Annals of the CIRP*, **49**(2):547–566 (2000)
- [TÖN81] Tönshoff, H.K.; Chryssolouris, G.: Einsatz kubischen Bornitrids (CBN) beim Drehen

- gehärteter Stähle [Application of boron nitride (CBN) in turning of hardened steels]. Werkstatt und Betrieb **114**(1):45–49 (1981)
- [TÖN86] Tönshoff, H.K.; Bußmann, W.; Stanske, C.: Hartbearbeitung durch Drehen und Fräsen [Hard machining by turning and milling]. tz für Metallbearbeitung **80**(12):35–40 (1981)
- [TÖN93] Tönshoff, H.K.; Spintig, W.: Prozesssicheres Bohren gehärteter Stähle [Process reliable drilling of hardened steels]. Werkstatt und Betrieb **7**:390–392 (1993)
- [WIN96] Winands, N.: Hartdrehen aus der Umformwärme gehärteter Wälzlageringringe [Hard turning of bearing rings hardened from the forming heat]. Dr.-Ing. Diss. RWTH Aachen, (1996)
- [WOB96] Wobker, H.-G.: Hartbearbeitung [Hard machining]. Habilitationsschrift Universität Hannover, (1996)
- [KAN04] Kanfir, H.: Industrial Performances in Gear Hard Turning at Renault. Presentation of Advanced Machining Processes, Power Train Department., Renault in [KLB05]

Chapter 11

Hard Machining, Component Quality

For the application of components under tribological, corrosive or dynamic operational loads, the properties of their surfaces and subsurface zones are of crucial relevance. These are the areas of the workpiece where property alterations will arise due to the impact of a manufacturing process. This affects the geometric as well as the physically-material condition. Surface topography and roughness are mainly consulted for the description of the geometric surface properties, whereas the physical properties are described based on the features residual stress, crystalline structure and hardness. Thus, the hard machining alters the component quality. We differentiate between alterations of

- macro geometry,
- micro geometry and the
- physical properties of the subsurface zones.

11.1 Macro Geometrical Deviations

When using conventional lathes, dimensional accuracies of ISO qualities IT6 to IT7 are achievable. The roundness deviations in cylindrically shaped components are below $2.5 \mu\text{m}$. The cylindricities achieve values below $2 \mu\text{m}$ [WEL98]. The average depths of surface roughness lie between $R_z = 2$ and $6 \mu\text{m}$.

Hard turning on especially designed precision lathes permits dimensional accuracies in the ISO quality ranges IT5-IT6. Circularities of $0.2 \mu\text{m}$ and cylindricities below $1.0 \mu\text{m}$ are achievable. The average depth of roughness R_z of the hard turned surfaces is approximately $0.5 \mu\text{m}$.

Impacts on the macro geometrical deviations meaning deviations of form, dimension and position (see Chap. 16), thus component alterations which are generally undesired, can be ascribed to all the partial systems involved in the

process. The following sources for alterations can be assigned to the partial systems workpiece, tool, machine and environment:

Workpiece

- deviations of dimension, form or position of the raw part,
- variations in material strength,
- activation and/or introduction of residual stresses,
- locally and temporally variable temperature fields.

Tool

- compliance of the tool/tool holder,
- tool wear,
- deviations of position during tool change.

Machine

- geometrical deviations,
- kinematic deviations (feed, control),
- compliance of the machine in force flux,
- thermally-caused deformations,
- load alterations during the machining.

Environment

- external heat sources (radiation),
- alterations of the environmental temperature (convection),
- alteration of the cutting fluid.

In part, there is interaction between the influences. For example, the increase in cutting force resulting from deviations in the material strength has an increased impact the higher the compliance of the machine. Tool wear alters the position of the cutting edge and can thus directly result in deviations of dimension and form. Yet, the wear also generally leads to increased cutting forces and thus to deviations of dimension and form via the compliance of the machine.

The forces active in the process as well as the connected heating of tool and workpiece influence the accuracy of form and dimension considerably. In this context, the tool wear which rises approximately linearly with the cutting time (see Fig. 10.16), shows a dominant influence. All three force components increase steadily, whereas the passive force shows significantly higher values than the cutting and feed force. Since the system workpiece-tool-machine only possesses a finite stiffness, which also differs along the feed travel according to the workpiece (correspondingly to a bar on 2 supports), the passive force results in relative displacements between cutting edge and workpiece, which have a direct effect on the accuracy of dimension and form. The left side of Fig. 11.1 illustrates the deviation in dimension δ_x in radial direction at differing system stiffnesses c_x and passive forces F_p . In addition, the displacement of the cutting edges which rises with increasing tool wear, also results in a dimension error.

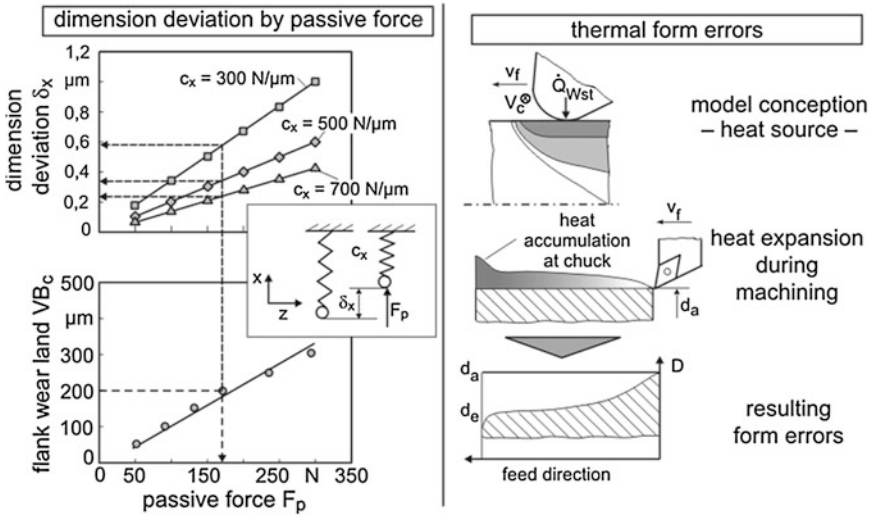


Fig. 11.1 Dimension and form errors in hard turning

While the resultant force components, especially the high passive force, mainly lead to dimension deviations, the heat flux into the workpiece brings about form errors. The temperature increases in the workpiece, which occur during the usual dry machining, are causes of this form error. In cylindrical workpieces, a form error arises along the axial length. This form error can be attributed to an inhomogeneous heating with elastic deformation of the workpiece. The radial expansion which increases together with the feed travel causes an increased material removal at an ideal tool motion so that a residual form error exists after cooling off (Fig. 11.1, right image section).

Concerning the set diameter, a heating on the outer surfaces (shafts) leads to a diameter reduction and on inner surfaces (holes) to a diameter expansion. At this, the measurement of the form deviation is mainly dependent on the wear and can rise from three to five times its original value at a flank wear land of $VB_c = 200 \mu\text{m}$.

Even if dry machining is often aspired due to ecological reasons, the use of cutting fluid can compensate the form errors generated by the heating of the workpiece. Air cooling is another means of considerable improvement compared to dry machining [BOR01]. Should there be tolerances of 0.01 mm during hard turning and the use of cutting fluid is unwished for, then it is recommendable to primarily process the close-tolerance functional surfaces so as to minimize the heat flow into the workpiece. A compensation by controlling the machine tool represents another option to avoid form errors. For this purpose, the form deviation resulting from the workpiece heating has to be allocated with the support points for the feed motions of the axes in the controlling of the machine tool.

The influence of the heating is especially critical in the case of components, which are machined asymmetrically, e. g. flat prismatic workpieces such as guide ways. The removal of residual stresses caused by hardening, the thermic expansion during the process, the generation of residual stresses resulting from the plastic deformations underneath the machined surface, the displacement of the cutting edge and the increase in passive force as a result of wear interact. Form measurement of the machined workpiece can serve as a form error analysis according to [BUS91] by using them to try to separate the individual causes. A similar procedure for the machining of thin, hardened rings is being developed in [SÖL10].¹

11.2 Micro Geometrical Properties

The surface roughness after hard turning is fundamentally influenced by the choice of the cutting angle radius, the cutting speed and the feed (see also Chap. 16). Figure 11.2 illustrates the influence of the manipulated variables feed and cutting speed at roughness of R_z (mean peak to valley height) at a given corner radius r_g . It is initially surprising that roughness increases with a lower speed, since the dynamic effects decrease, e. g. due to imbalance incitement. The explanation is that lower speeds increasingly lead to irregular segmented chip formation and thus higher roughness.

The development of the roughness R_z at a variation of the feed f , illustrated on the right side of Fig. 11.2, shows that for reasons of surface quality it is not sensible to set the feed smaller than $f = 0.05$ mm. In this area, the theoretical roughness R_{th} merely specifies the conditions in an insufficient way. This is to be attributed to an underrun of the minimum undeformed chip thickness before the contact bow along the cutting edge, which occurs especially in the case of small feeds. The underrun of the minimum undeformed chip thickness leads to pinches and deformations by compressions on the newly generated surface, which results in an increase of the roughness depth R_z .

In Fig. 11.3, weightings of the influences feed, cutting angle radius, machine and tool wear are registered based on experiment. Even if this illustration has no universal validity, we can gather tendencies from it [KLB05].

¹ The research work is part of the Special Research Centre (SFB) 570 “Distortion Engineering” of the University of Bremen, where problems of distortion are dealt with.

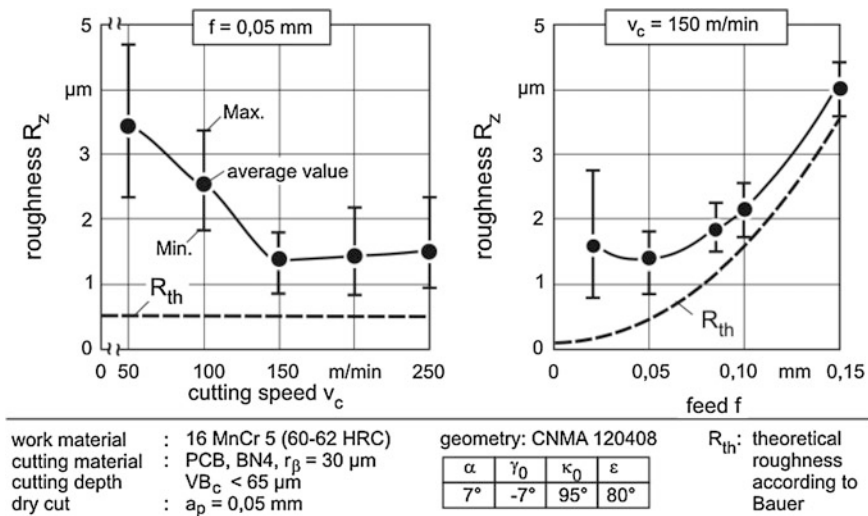
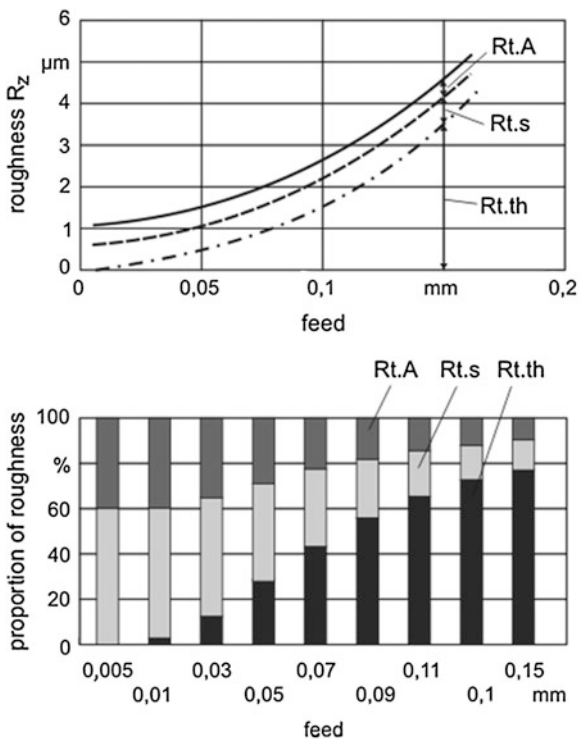


Fig. 11.2 Surface performance as a function of cutting speed and feed

Fig. 11.3 Influences on the roughness with hard turning (after Jochmann)



11.3 Physical Influence

Along with the geometrical shape of technical surfaces, the physical properties of the subsurface zones are relevant for the functional behaviour of the components. Metallographic and X-ray examinations on hard-turned workpieces prove that hard turning can procreate considerable influences of subsurface zones. These manifest in altered residual stress conditions, in the development of rehardened zones as well as in areas of tempered structure.

The reason for this behaviour are the high stresses and temperatures during cutting as well as the high stress and temperature gradients, due to the outer subsurface zone being exposed to considerable plastic deformations, structure alterations and other thermic influences.

The tool wear on the flank face decisively influences the properties of the subsurface zones. The thermo-mechanic loads of the subsurface zones rise with an increased tool wear. A cohesive rehardened layer, which appears white in the polished section and a tempered zone located below, which appears dark in the grinding pattern in Fig. 11.4, develop. The degree of structure influence is independent of the used cutting material at an equal geometrical construction of the tool. The rehardened layer, where hardness values of up to 1,000 HV (0.025) are measured, appears white because it is difficult to etch during the metallographic preparation. Therefore, it is often called the “white layer”. The basic structure shows hardnesses of approx. 800 HV (0.025). The tempered areas show lower hardnesses of approx. 600 HV (0.025).

As a consequence of the thermic influence, tensile residual stresses occur at the subsurface. These continue to rise with increasing tool wear. The occurring

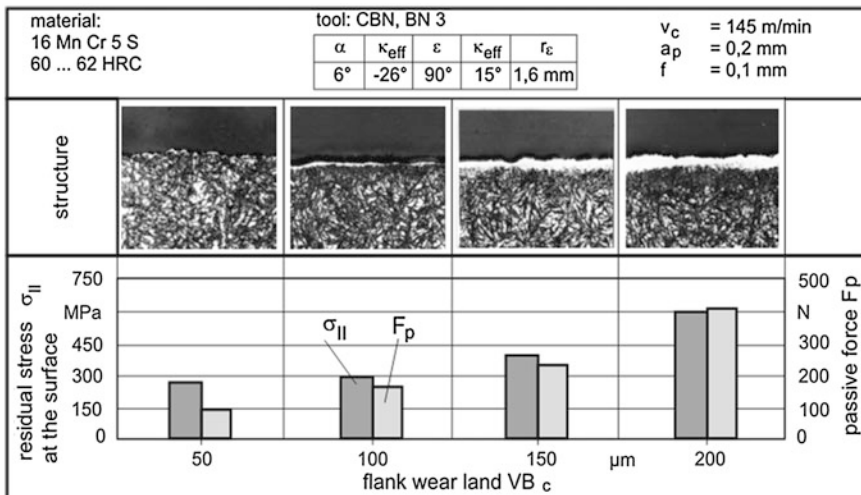


Fig. 11.4 Condition of subsurface zones depending on tool wear

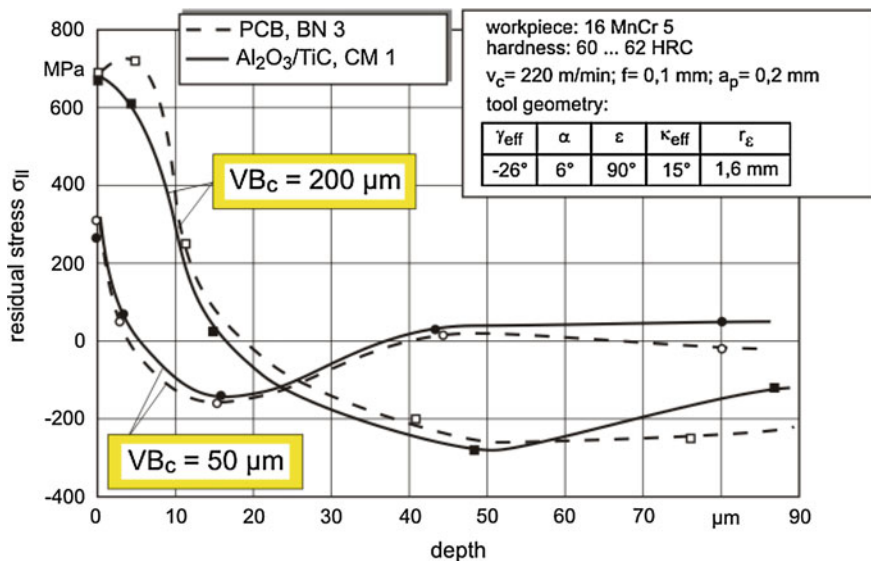


Fig. 11.5 Residual stress development below the workpiece surface

influences on the subsurface zones then correlate with an increase in the passive forces.

This effect of the process can be explained using the following model: The high passive forces and the accompanying frictional power lead to a strong heating of the surface layer. The material expands; high compressive stresses and plastic flow occur. The heat source, i. e. the flank face contact, abandons the regarded place at cutting speed. The material is cooled down rapidly by means of auto-chilling. The previously compressed surface layers are extended and residual tensile stresses with gradients develop. The stronger the friction, i. e. the flank wear land and thus the passive forces, the more pronounced the effect (Fig. 11.5). The stresses can additionally be aggravated or weakened by superposed transformation-dependent stresses, if phase transformations linked with volume alterations occur during the machining.

Figure 11.6 shows an estimate of the power flux into the surface of a component and thus the thermic load for a hard turning and a grinding process, based on measured forces and tool wear [TÖK97].

11.4 Rolling Fatigue Strength

Structure alterations, residual stress distributions and hardness alterations can affect the component behaviour depending on the operational load. A multitude of hardened surfaces underlie rolling fatigue loads in practical use. Whether hard-

	hard turning	grinding
set value	$v_c = 150 \text{ m/min}$ $l_c = 0,8 \text{ mm}, VB = 0,2 \text{ mm}$	$v_c = 35 \text{ m/s}, a_p = 2,5 \text{ mm}$ $l_g = 0,6 \text{ mm}$
forces	$F_c = 300 \text{ N}$	$F_t = 70 \text{ N}$
power	$P_c = F_c \cdot v_c = 750 \text{ W}$	$P_c = F_t \cdot v_c = 2.450 \text{ W}$
related power	$P_c'' = P_c / (a_p \cdot l_c)$ $= 4.688 \text{ W/mm}^2$	$P_c'' = P_c / (a_p \cdot l_g)$ $= 1.633 \text{ W/mm}^2$
power distribution	$R = 0,15$	$R = 0,35$
related heat flow	$q_w'' = R \cdot P_c'' = 703 \text{ W/mm}^2$	$q_w'' = R \cdot P_c'' = 572 \text{ W/mm}^2$
contact time	$t_c = VB/v_c = 0,08 \text{ ms}$	$t_c = l_g \cdot v_c = 28,8 \text{ ms}$
related path energy	$e_c = q_w'' \cdot t_c = 0,056 \text{ J/mm}^2$	$e_c = q_w'' \cdot t_c = 16,5 \text{ J/mm}^2$

Fig. 11.6 Estimate of the power distribution in hard turning and grinding [TÖK97]

turned surfaces are convenient or inconvenient for this case of application depends on the fatigue strength. The factors of influence are roughness, residual stress condition after hard turning and after rolling fatigue load, surface quality and structure pattern. The plastic deformation of the surface arising under usual conditions of mixed friction in the rolling contact leads to a reduction of the residual tensile stresses, which exists after hard turning on the workpiece surface. This was detected in experiments [BOR01, LIE98]. Thus, they have no negative influence on the rolling strength. The structural texture is basically maintained after the rolling load, even though a removal of the white layer is noticeable at very high load cycles. However, this is normal wear and not to be regarded as failure. For a defect development, the surface quality is of primary relevance. A lower roughness is especially necessary under slip compared with slip-free conditions to avoid the formation of pitting. The formation of pitting is a fatigue of the material in rolling contact, which is accompanied by a progressive defect development with shell-shaped flakings of the workpiece.

Life cycle analyses of hard turned inner rings of cylinder roller bearings show that at a similar arithmetic average roughness R_a , hard-turned bearings achieve a life cycle comparable with that of ground and honed bearings. The mathematically established life cycles of the rolling bearings are confirmed on the test stand, even if subsurface zone damages in form of white layers in the surface zone occur.

11.5 Fatigue Strength

Another decisive component characteristic, especially for hardened workpieces, is the fatigue strength. It reacts extremely sensitive to alterations in the subsurface zone, since fatigue tears generally start at the surface [SIG93].

Fatigue strength is of special relevance for components with strongly-pronounced constructive notches. Large cross-section transitions, grooves, undercuts and recesses which can be found as form elements for example in gear shafts, crank shafts or axle journals, represent constructive notches. A stress exaggeration in the notch groove, which can lead to a weakening of the component, is a result of the geometric notch effect. In addition, a micro geometric notch influence occurs due to the surface roughness.

In contrast with the fatigue load, in the case of torsion and bending loads the maximum stress appears directly at the surface, which is also where the hard turning has caused the critical alterations in the condition of the subsurface zone.

To examine the fatigue strength of components it is common to carry out stress-cycle experiments under a vibratory load. A number of trials sufficient for the application of statistic methods undergo a test cyclus up to breakage at different amplitudes of the bending load. As schematically illustrated above on the right in Fig. 11.7, the obtained number of stress reversals is applied logarithmically above the amplitude of the bending load. The result is a straight line with a negative gradient, which kinks to a horizontal at a certain stress value and a certain number of stress reversals. Below this horizontal line, the components are considered fatigue durable.

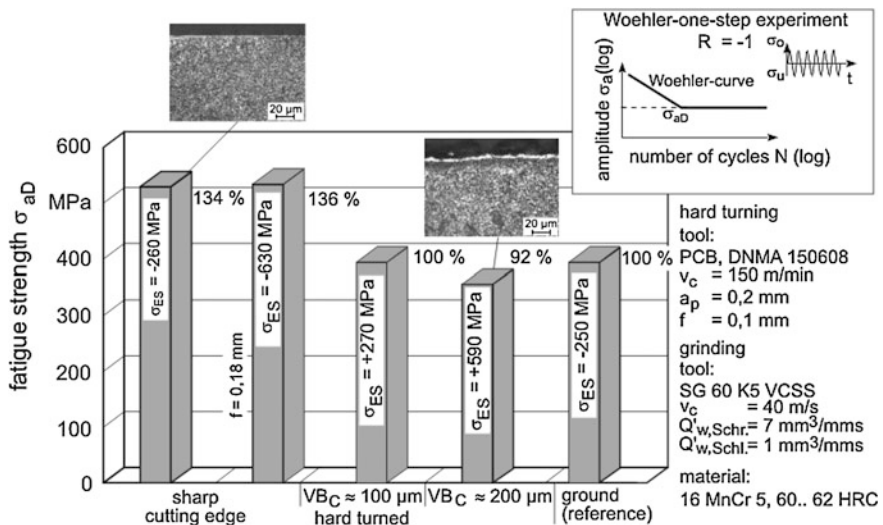


Fig. 11.7 Fatigue strength of hard-turned components under bending cycle load

When loading hard-turned components by bending cycles with loads considerably smaller than the fatigue limit of the material, the residual stress condition after hard turning will have a decisive influence on the fatigue strength. Figure 11.7 illustrates the fatigue strength of hard-turned components compared to a ground reference component. If medium–high residual tensile stresses at approx 150–350 MPa are detected after hard turning with worn tools ($VB_c = 100 \mu\text{m}$), the fatigue strength will decrease noticeably compared with components machined with a sharp-cutting edge. Hard-turned and ground (afflicted with residual compressive stresses) surfaces achieve almost the same fatigue strengths at a comparable surface roughness $R_z \approx 3 \mu\text{m}$. At very high residual tensile stresses after hard turning with even more worn tools ($VB_c = 200 \mu\text{m}$) a fatigue strength decrease of approx. 8 % can be detected compared with the ground reference. The highest fatigue strengths are achieved by the hard-turned samples, which were machined with a sharp cutting edge. An increase of the feed from $f = 0.1 \text{ mm}$ to $f = 0.18 \text{ mm}$ leads to a higher mechanical load in the surface zone of the workpiece. This causes higher residual compressive stresses of -630 MPa at the workpiece surface. However, compared with the lower feed $f = 0.1 \text{ mm}$ with residual compressive stresses of -260 MPa , there is no significant difference in the achievable fatigue strength [BOR01].

11.6 Sealability

The quality of the shaft surface is of decisive importance for the sealing function of a radial shaft sealing ring. The usage of radial shaft sealing rings, as a dynamic sealing element on a large number of power train components, requires certain roughness values for a safe sealing function. The corresponding standards stipulate average surface roughnesses from $R_z = 1\text{--}4 \mu\text{m}$ and maximum surface roughnesses of $R_{\text{max}} = 6.3 \mu\text{m}$ [DIN3761]. In addition to the requirement for the surface quality, there is a total absence of twist in the grinding structure of the counter surface. Therefore, the grinding structure has to lie in peripheral direction and must not possess any superposed periodic and regular undulation parts.

Twist occurs during grinding, due to the dressing process of the grinding wheel or due to parallelity deviations between the axes of the grinding wheel and the workpiece. The dressing and zero twist are to be assigned to the undulation according to their specification and superposed to the grinding structure. The course of a twist constantly rotates around the circumference. The continuity is given as long as the undulation part of the twist is at least as strongly pronounced as the surface roughness of the grinding structure. The bigger the twist angle and the bigger the cross-section of one or more drifts, the more the twist specification will influence the sealing function of the surface [KER92].

The counter faces for radial shaft sealing rings are manufactured conventionally by means of plunge grinding. According to the current state of knowledge, grinding in the plunge is the least problematic process. Due to the process, a twist

structure occurs during longitudinal turning which means also during longitudinal turning of hardened functional surfaces. The feed motion of the tool causes a helical twist structure, which practically shows a drift on the shaft surface. Therefore, for a long time longitudinal turning was considered inappropriate as a machining process for seal seats.

Meanwhile it has become clear that processes such as hard turning and hard turning with subsequent hard roller burnishing are generally appropriate for the machining of counter faces for seal seats [RAA99]. The hard-turned shafts are advantageously used in aggregates, which are predominantly operated in only one direction, e. g. engine, entrance of gear drive with restriction drive exit, axis entrance.

However, for an unproblematic use there is still a lack of experience concerning the influences of machining parameters. For instance, more recent tests have shown that the different inclinations of the helical twist structure caused by different feeds, have no influence on the delivery rates. The delivery rate of a seal system is a characteristic parameter for the description of the leakage proneness of the system radial shaft sealing ring-counter surface. Higher delivery rates point at possible leakages. The delivery rates for hard-turned seal seats actually rise with increasing tool wear, but still turning does not reach resp. surpass comparable delivery rates through grinding.

11.7 Post-Treatment Processes

One possibility to influence the workpiece subsurface zone appearing after the hard machining is the post-treatment process by means of cutting, forming or other processes that alter properties. The application of an additional process does not necessarily have to be assessed negatively under the aspect of profitability. For instance, in the meanwhile there is a multitude of industrial applications, that process combinations have established due to the more convenient component behaviour, such as grinding/honing of bearing races [SCH76], grinding/rolling of crank shafts or grinding/shot peening of gears. In the post-treatment process of hard-turned workpieces, especially the process hydro-static rolling or water peening have a larger spreading.

11.7.1 *Hard Roller Burnishing*

Using tools especially adapted to the requirements of high-tensile materials for roller burnishing, the machining of hardened steels with hardnesses of up to 62 HRC is possible. In this context, we talk about hard roller burnishing. Typical applications of roller burnishing are the post-processes of sliding components such as bearing studs, valve rods, shaft seal seats, guideways and brake cylinders. The

economic advantages of hard roller burnishing result from short essential operating times, comparable with turning, a low use of cutting liquid, long component durability and the possibility of machining in a clamping [ECO99]. The hard roller burnishing tool can be applied both in conventional and CNC-controlled turning machines at which the tool can be clamped into standard tool holders using a clamping strip.

The mode of operation of the hard roller burnishing tool is based on the hydrostatic principle. A ceramic hard roller sphere is pushed through a pressurizing medium against the workpiece surface. At this, roller pressures of up to 50 MPa are reached. The sphere swims on a pressurizing capping and is thus supported at a low friction. As shown in the left image area of Fig. 11.8, the kinematics of hard roller burnishing is characterised by a rotatory motion of the workpiece (roller speed v_w) and a feed motion of the tool along the longitudinal axis of the workpiece (roller feed f_{ro}) analogue to turning.

In hard roller burnishing, due to the low diameter of the ceramic sphere, comparatively low forces already cause high Hertz pressings, which lead to the surpassing of the yield strength and to a levelling of roughness peaks. At a roller pressure of 30 MPa, for instance, a maximum Hertz compression of approx. 7.500 N/mm^2 is reached. At this, a roller force of about $F_{ro} = 850 \text{ N}$ acts on the workpiece surface via the roller sphere.

Due to the plastic deformations in the subsurface zone, tensile stresses after hard turning with worn tools are conveyed into the compressive stress zone. Surface roughness variations resp. the increase in surface roughness resulting from tool wear can be reduced by hard roller burnishing.

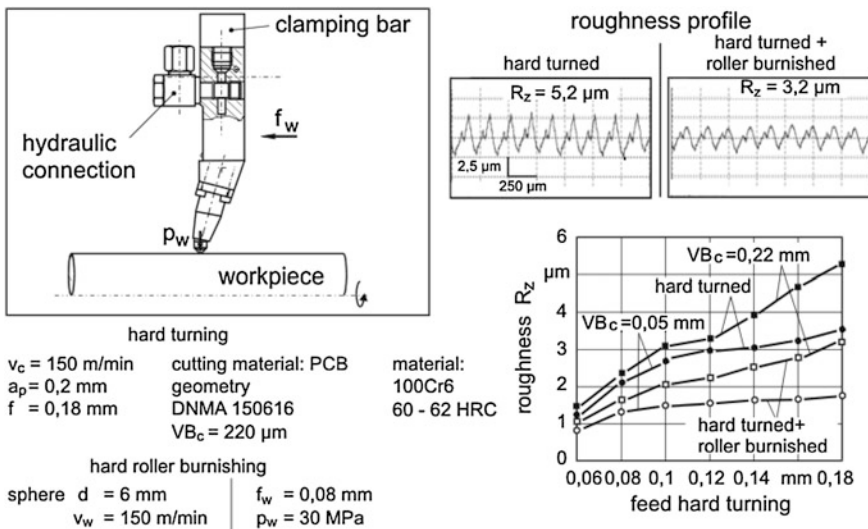


Fig. 11.8 Surface quality after hard turning and hard roller burnishing

The comparison of the roughness profile after hard turning and subsequent roller burnishing, illustrated in the top right image section of Fig. 11.8, shows a noticeable levelling of the roughness peaks. The characteristic profile of a turned surface remains intact.

The bottom right section of Fig. 11.8 illustrates the dependence of achievable surface quality after roller burnishing from the level of the original roughness after hard turning. For this purpose, different original roughnesses were adjusted depending on feed and tool wear.

If the original roughnesses are above an average surface roughness of $R_z = 2 \mu\text{m}$, it is possible to achieve an improvement of the surface quality of between 40 % to almost 50 %. At an original roughness of below $R_z = 2 \mu\text{m}$, a reduction of the roughness value of up to 30 % is still possible. This can be attributed to the fact, that an increasing profile depth also means an increased material volume which has to be plastically deformed. As demonstrated, surface qualities between $R_z = 1$ and $2 \mu\text{m}$ are achievable even in roller burnishing.

The mechanical load in roller burnishing does not only lead to an alteration of the surface quality, but also to a modification of the residual stress condition. The very high residual tensile stresses existing on the workpiece surface after hard turning can be almost abolished by roller burnishing at a rolling pressure of $p_{ro} = 20 \text{ MPa}$. At a rolling pressure of $p_{ro} = 30 \text{ MPa}$ it is possible to achieve a complete shift of the residual stress distribution at surface into the pressure area. With increasing workpiece depth, roller burnishing induces very high and pronounced compressive residual stresses, which reach maximum values of -900 MPa in tangential direction. The structure transformations in form of white layers resulting from the hard turning are not influenced by the hard roller burnishing.

11.7.2 Water Peening

High pressure water peening has been known as a separating process for a long time. However, water drops can also increase the strength of steel materials, if they hit the surface with a correspondingly high kinetic energy. Based on this knowledge, water peening has also developed into a process of surface treatment in the last years [KRO95]. A considerable advantage compared with shot peening is the applicability for a large spectrum of component geometries. The strength-increasing effect of water peening lies in the insertion of residual tensile stresses, as well as the increase of the hardness.

The cause for the development of residual tensile stresses close to the surface zone, due to water peening is the impact of liquid particles on the solid material surface with high local pressure peaks. A plastic deformation of the material zones close to the surface zone takes place, with parallel strain hardening. After the treatment with water peening, the workpiece surfaces show no traces of visible plastic deformation. In contrast to the processes rolling and shot peening, the surface topography and the roughness depth are not altered in this case [KRO95].

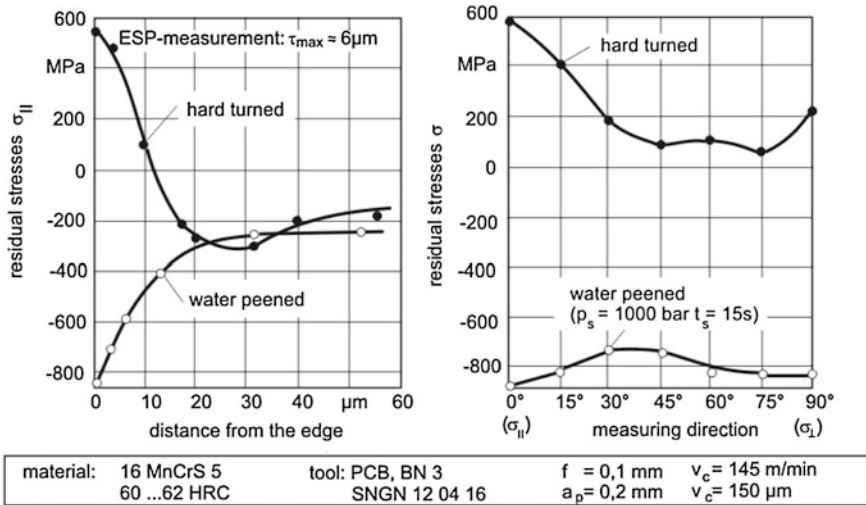


Fig. 11.9 Residual compressive stresses in hard turned workpieces by means of water peening

Preconditions for the use of water peening as a surface layer-hardening process are sufficiently high peening pressures and suitable nozzle geometries. When water peening case-hardened materials which are machined by hard turning with worn tools, the typical course of residual stresses underneath the surface with residual tensile stresses in surface-near areas is significantly shifted into the compressive stress area due to the water peening (Fig. 11.9). The effective dwell time with water peening represents $t_s = 15$ s for hardened materials at a peening pressure of $p_s = 100$ MPa. The effect of the peening treatment is at its highest directly at the surface and decreases continuously with a growing distance from the surface. At a depth of approx. 15–20 μm , the stress course is no longer influenced. Thus, the basically lower penetration depth compared with the use of shot peening does not represent a disadvantage when using high pressure water peening in the process chain hard turning/water peening, since the critical effects of hard turning do not generally reach greater depths.

For case-hardened, ground rotary bending samples, a significant increase in the bending cycle strength of approx. 30 % appears after high pressure water peening. For hard turned samples, machined with worn tools the fatigue strength drop, resulting from high pressure water peening, can be compensated again [BRA95].

To mention further advantages of the process: minimal costs for the supply and processing of the peening material, flexible applicability to a large variety of workpiece geometries and simple quality control by process parameters easily to be monitored.

11.8 Questions

1. How do form errors occur with hard turning or hard milling?
2. How is “theoretical roughness” defined in turning and what are the influencing factors?
3. In hard turning, what is the explanation for the stronger deviation of the actual roughness from the theoretical roughness at lower cutting speeds?
4. What are the typical subsurface zone alterations produced by hard machining?
5. What is the explanation for the development of residual tensile stresses at the surface and what is the consequence of higher tool wear?
6. Name properties of surface and surface near zones, which can influence the operating behaviours of components.
7. Which effects have been detected as a consequence of influences to surface and surface near zones?
8. Which post-processes do you know? What do they cause?

References

- [BOR01] Borbe, C.: Bauteilverhalten hartgedrehter Funktionsflächen [Component behavior hard turned functional surfaces]. Dr.-Ing. Diss. Universität Hannover (2001)
- [BRA95] Brandt, D.: Randzonenbeeinflussung beim Hartdrehen [Surface integrity in hard turning]. Dr.-Ing. Diss. Universität Hannover
- [BUS91] Bußmann, W.: Formfehleranalyse beim Planfräsen gehärteter Bauteile [Form error analysis in face milling of hardened components]. Dr.-Ing. Diss. Univ. Hannover (1991)
- [DIN3761-1] Radial-Wellendichtringe für Kraftfahrzeuge; Begriffe; Maßbuchstaben, zulässige Abweichungen, Radialkraft/Rotary shaft lip type seals for automobiles; terms, formula, symbols, tolerances. Hrsg. Beuth Verlag (1984)
- [ECO99] Hartglattwalzen-Status von Forschung und Anwendung. Anwendungsbeschreibung [Hard roller burnishing—status of research and application. Description of application] Nr. 5593, Fa. Ecoroll, Celle (1999)
- [KER92] Kersten, W.: Optische und antastende Prüfung der Gegenlauffläche von Radialwellendichtringen [Optical and touching testing of radial shaft sealing rings]. Dr.-Ing. Diss. Universität Hannover (1992)
- [KLB05] [KLB05] Klocke, F., Brinksmeier, E., Weinert, K.: Capability profile of hard cutting and grinding processes. *Annals of the CIRP* **54**(2), 557–580 (2005)
- [KRO95] Kroos, F.: Randschichtverfestigung durch Hochdruck-Wasserstrahlen [Surface layer hardening by high pressure water peening]. Dr.-Ing. Diss. Universität Hannover (1995)
- [LIE98] Liermann, J.: Hartdrehen wälzbelasteter Bauteile [Hard turning of rolling loaded components]. Dr.-Ing. Diss. RWTH Aachen (1998)
- [RAA99] Raab, H., Haas, W.: Tribologische Partner: Radialwellendichtring und Gegenlauffläche Antriebstechnik [Tribological partner: radial shaft sealing ring and counter surface], Band **38**(Heft 4), Seite 133–135 (1999)

- [SCH76] Schreiber, E.: Die Werkstoffbeeinflussung weicher und gehärteter Oberflächenschichten durch spanende Bearbeitung [The material influencing of soft and hardened surface layers by cutting]. VDI-Bericht Nr. **256**, S. 67–79 (1976)
- [SIG93] Sigwart, A.: Bauteilrandschicht und Schwingfestigkeit [Subsurface zone and fatigue strength]. Dr.-Ing. Diss. TU Clausthal (1993)
- [SÖL10] Sölter, J.: Ursachen und Wirkungsmechanismen der Entstehung von Verzug infolge spanender Bearbeitung [Causes and effect mechanisms of the generation of distortions as a result of cutting]. Dr.-Ing. Diss. Univ., Bremen (2010)
- [WEL98] Welk, R.W.: Erfahrungen und Grenzen bei der Hartfeinbearbeitung auf CNC-Drehmaschinen [Experiences and limits in hard fine machining on CNC turning machines], VDI-Seminar, Rationalisierungspotentiale in der spanenden Bearbeitung, **5**,-6. März (1998)
- [TÖK97] Tönshoff, H.K., Karpuschewski, B., Borbe, C.: Comparison of basic mechanisms in cutting and grinding of hardened steel. *Prod Eng* **IV/2**, 5–8 (1997)

Chapter 12

Broaching

12.1 Broaching Process

Broaching is a productive cutting process of serial production. Functional surfaces of high surface quality at a high dimension and form accuracy can be generated by a single tool stroke. The process is characterised by a high material removal rate.

A broaching tool, which carries out a straight cutting motion, is composed of several/many offsetwise positioned cutting edges (Fig. 12.1). Special variants (rotary broaching, gear shaving of involute surfaces) cut with rotary cutting motions. Broaching is the only cutting process, which works without feed motion given that the engagement from cutting edge to cutting edge is achieved by their grading or offset. Thus, the undeformed chip thickness is predefined by the tool.

One must differentiate between internal and external broaching. During internal broaching, a tool is pulled or pushed through a prefabricated hole [DIN8589-5].

Internal broaching is typically applied for the manufacturing of profiled holes such as quadrangular, polygonal and spline profiles, internal gearing and grooves (Fig. 12.2). Since the tools which are bound to the profile and due to the offset (undeformed chip thickness) mostly also to the material, are very elaborate because of their complex construction, internal broaching is only applied either in serial production or for the manufacturing of standardised profiles, if an elaborate tool can be amortised by means of a higher number of orders or different applications (example: standardised spline profiles). External broaching is used for the manufacturing of plan or profiled surfaces. Frequently, it is the more productive alternative to milling. Yet, a sufficient serial size should also be required in this case (Fig. 12.2).

During a tool stroke, roughing, finishing, fine finishing and sizing processes are generally carried out. The undeformed chip thicknesses can be adapted accordingly by varying the offset. The strongest forces occur during the roughing phase.

High dimension and form accuracies up to IT7 (normal IT8) can be achieved by broaching. It is also possible to generate high surface qualities of R_z up to 5 μm (normal $R_z = 6, 3\text{--}25 \mu\text{m}$, with special effort up to 1 μm). However, the position

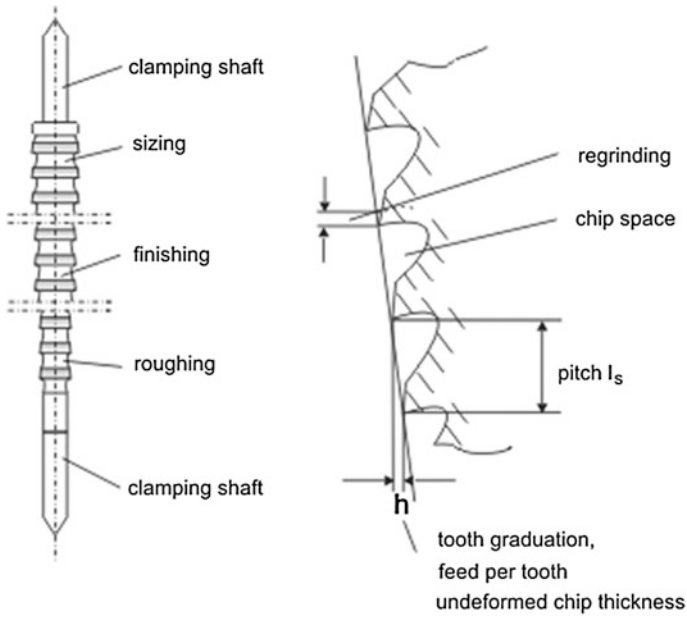


Fig. 12.1 Internal broaching tool with tooth graduation

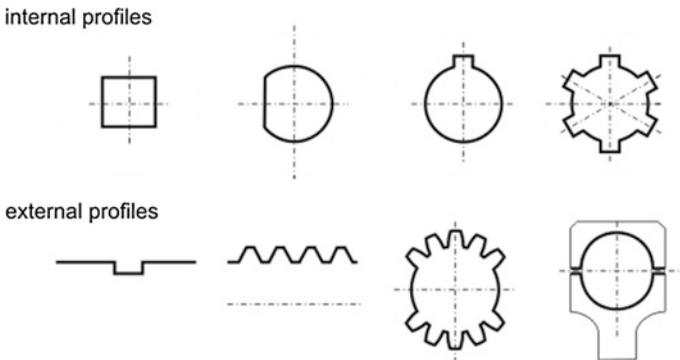


Fig. 12.2 Internally and externally broached profiles

accuracy during internal broaching may be critical, since the workpieces are mostly supported afloat and the slender tools possess only a low transverse stiffness.

Broaching tools are mostly manufactured from high speed steel. The cutting materials HS 6-5-2, HS 6-5-2-5 or HS 2-9-2 with hardnesses of 64 HRC to 66 HRC are common. Due to the percussion-type load of the cutting edges, the cutting material has to be tough enough. The broaching tools can be coated with titanium nitride (TiN) or titanium carbonitride (TiCN) so as to increase the tool life

travel path. Only coating processes with working temperatures below the annealing temperature can be applied because of the hardened high speed steel. These are PVD processes at 480–500 °C. Due to their high value, the broaching tools are reground repeatedly. This occurs at the rake face, at which the first coating is lost. Nevertheless, the coating has a supportive effect on the flank face and delays the wear. So as to limit the regrinding depth, it is advantageous to work only up to a flank wear land of 0.2 mm. In some cases broaching tools with cemented carbide elements are used for high volume production. The profitability for the choice of the cutting material is to be considered.

Materials with strengths in a wide area of 400–1,000 N/mm² can be broached. However, it has proved of value to hold steel workpieces at strengths of 500–900 N/mm², so as to avoid overstressing the cutting edges (high strength of material) or smearing and unfavourable long chips (low strength).

A linearly distributed, spatially inclined resulting force acts at every cutting edge. It can be summarised in one discrete force F_z and broken down into three components: the cutting force F_c in cutting direction; perpendicular to it and normal to the created surface, the normal cutting force F_{cN} and vertical to both components, the passive force F_p (Fig. 12.3).

Only if the cutting edges are inclined against the cutting direction ($\lambda \neq 0$), does the passive force F_p not disappear. The cutting force can be determined with the approach of Kienzle via the specific cutting force k_c —as stated before:

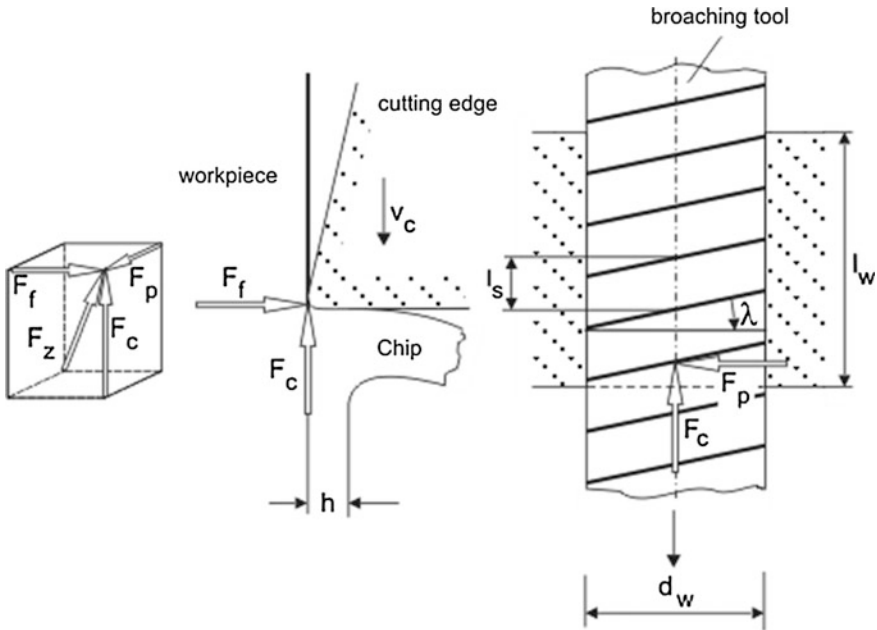


Fig. 12.3 Forces at the cutting edge

Table 12.1 Undeformed chip thicknesses, cutting space values and cutting speeds

Material	f_z (μm)		c	v_c (m/min)
	Roughing	Finishing		
Steel	10–150	3–30	5–15	6–25
Non ferrous metals	20–200	10–40	3–12	10–40
Synthetics	30–60	10–30	5–15	10–40

$$k_c = \frac{P_c}{Q_w} = k_{c1.1} (h/h_o)^{-m_c} \quad (12.1)$$

and so the cutting force is

$$F_c = k_c \sum_{j=1}^z b_j h_j g_j \quad (12.2)$$

In Eq. 12.2, the cutting width b_j is given by the length of the engaged cutting edge j . For example, if a circular hole is broached that is then the circumference. The undeformed chip thickness h_j results from the graduation and z is the number of cutting edges. The factor g_j considers whether the corresponding cutting edge is in the engagement or not and is accordingly either 1 or 0. The tool tooth pitch l_s determines the length of the broaching tool, which is limited by the maximum stroke of the broaching machine, via the offset. The minimum tooth pitch $l_{s,\min}$ results from the necessary cutting space to be provided between the single cutting edges, an addition for the regrinding at the cutting surfaces of the cutting edges and a rest thickness of the cutting wedge (see Fig. 12.1). A common experience formula is [SCH80]

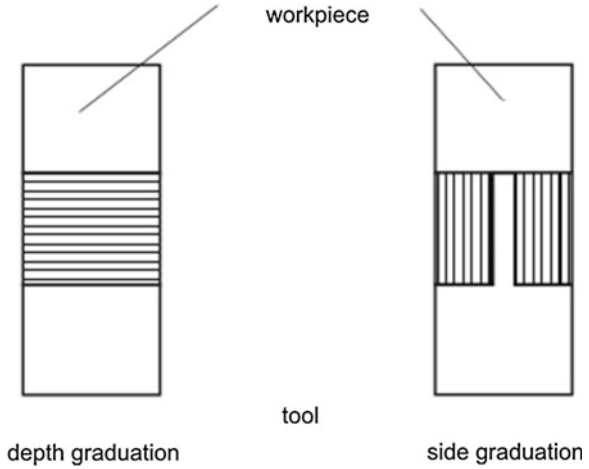
$$l_s = 2,5 \sqrt{h \cdot l_w \cdot c} \quad (12.3)$$

with the undeformed chip thickness h , the cutting path l_w and the chip space factor c (see Table 12.1). Depending on the material (Table 12.1), the chip space factor is determined.

The positioning of the cutting edges is generally adjusted to generate an offset in depth. That means that the cutting edges are placed parallel to the final contour. In lateral offset, the material is broached diagonally to the final contour (Fig. 12.4). Lateral offset is applied so as to avoid excessive wear on the casting or forging skin of a workpiece. The undeformed chip thicknesses are determined by the offset of the broaching tool. Table 12.1 provides some reference values, at which we must differentiate between roughing and finishing [LAN05].

The periodical cutting edge engagement leads to force fluctuations and thus to the vibrational excitation of the machine. Figure 12.5 illustrates the force–time course for a straight-grooved ($\lambda = 0$) and a diagonally-grooved ($\lambda \neq 0$) tool. For internal broaching, straight-grooved tools are generally used, because diagonal grooves are more difficult to manufacture. Whereas during external broaching, a finite inclination angle arranges for a smoother force increase, so that the dynamic

Fig. 12.4 Offset or graduation of broaching tools



load on the system machine-tool-workpiece is considerably lower. A Fourier analysis of the trapezoidal force course results in

$$F_{cTR} = \frac{4 \hat{F}_c}{\pi \alpha} \left[\frac{1}{1^2} \sin \alpha \sin \Omega + \frac{1}{3^2} \sin 3\alpha \sin 3\Omega t + \frac{1}{5^2} \sin 5\alpha \sin 5\Omega \dots \right] \quad (12.4)$$

with the time t and

$$\alpha = \frac{2\pi}{l_w} a ; \Omega = \frac{2\pi}{l_s} v_c ; a = d_w \tan \lambda$$

In the case $\lambda = 0$, the function is not explained according to Eq. 12.4, because the numerator and denominator disappear at the same time. With the rule by L'Hospital it is possible to name a limit value for the rectangular force course F_{cRE}

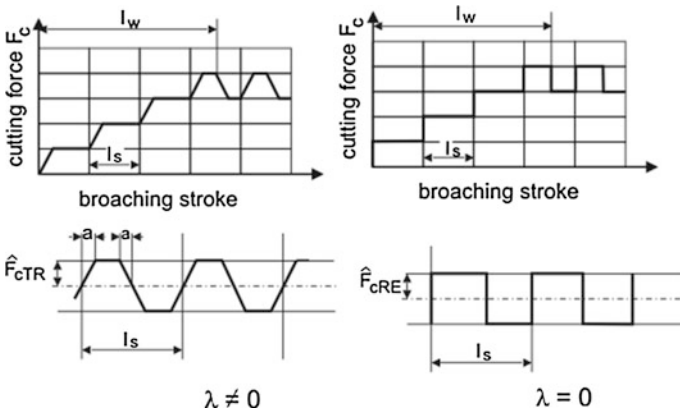


Fig. 12.5 Cutting force time course

$$F_{\text{cRE}} = \lim_{\lambda \rightarrow 0} F_{\text{cTR}} = \frac{4 \hat{F}_c}{\pi} \left[\sin \Omega t + \frac{1}{3} \sin 3\Omega t + \frac{1}{5} \sin 5\Omega t + \dots \right] \quad (12.5)$$

Equation 12.4 shows that the excitation with the basic frequency $f = \frac{1}{2\pi} \cdot \Omega = v_c/l_s$ is dominant. This is different with inclined steep engagement F_{cRE} (see chart 12.5). On the one hand, the amplitude relation (only calculated with the first element) is higher by the factor,

$$F_{\text{cRE}}/F_{\text{cTR}} = \alpha/\sin \alpha \quad (12.6)$$

On the other hand, all the following elements of the series are considerably higher with a steep gradient. This means that the acceleration is several times stronger at $\lambda = 0$ and higher natural frequencies are also stimulated to a considerably higher degree. In this case—that means especially for internal broaching—the dynamic behaviour of the machine and the broaching tool with its clamping are especially critical.

12.2 Machine Development

Most internal broaching machines work with pulled tools. So the unloaded part of the broaching tool is long and tends to considerable bending vibrations, especially in the initial or roughing phase. Some internal broaching machines therefore work with pushed tools. This constellation may have the advantage that the tool is well-guided after its clamping, but it also has the disadvantage that the tools are loaded at buckling, which can be critical.

A constellation of interest in this context is the pull–push-broaching machine. The tool is tightly clamped at both ends by means of a thrust rod, both clamping bridges are tightly connected with each other and jointly driven. The principle and a spring representation are shown in Figs. 12.6 and 12.7.

Dependent on the design of the broaching tool, this can be the most compliant element in the force flow. In a mechanical sense, the force-penetrated components of a broaching machine can be understood as a chain of springs connected in series from the point of action, where the tool and the workpiece are in contact, over the broaching tool, the broaching slide(s), the base frame of the machine up to the tool bridge. The total stiffness k_{ges} results from

$$\frac{1}{k_{\text{ges}}} \geq \sum_{i=1}^n \frac{1}{k_i} \quad (12.7)$$

That means that the total stiffness is always lower than the lowest stiffness of one of the components.

As visible in Fig. 12.6, the broaching tool is clamped between an upper and a lower bridge, after having been inserted into the workpiece. Both bridges are moved concurrently.

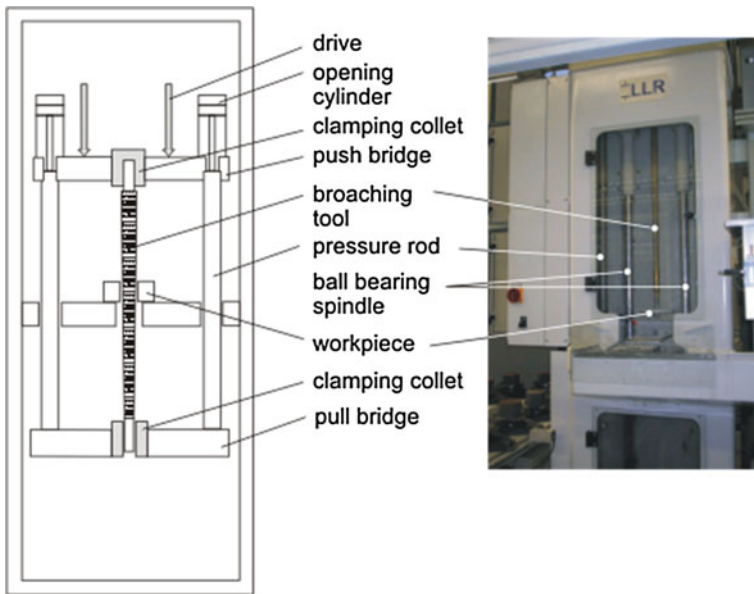


Fig. 12.6 Pull-push internal broaching machine (type LLR, Balve)

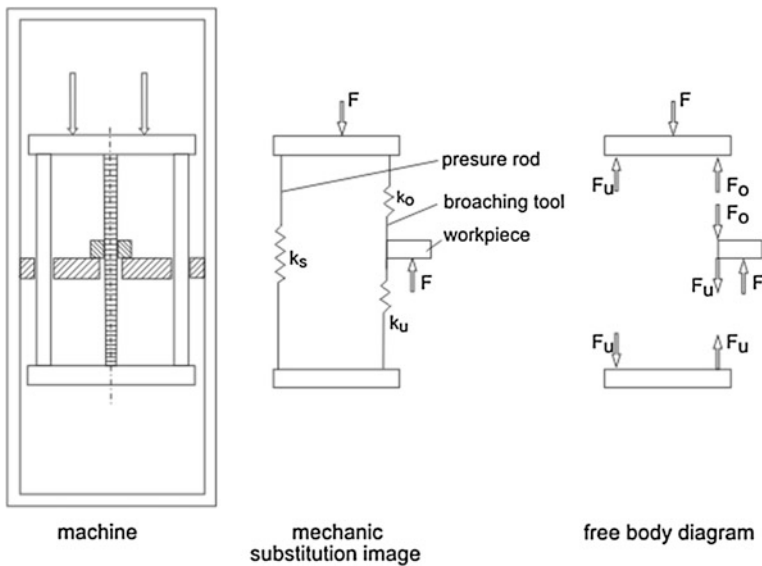


Fig. 12.7 Force balance

Broaching force F acts between the tool and the workpiece. This force is determined by the cutting process. On the one hand, the broaching force is supported by the workpiece bridge and, on the other hand, transmitted into the base frame of the machine by the mobile slides, i. e. the push-and pull-bridge. The system is symmetrically designed. Thus, no tilting or bending moments occur, which develop in an unsymmetrical constellation and then have to be supported by the guideways of the broaching slide against the base frame of the machine.

How the broaching force is introduced into the driven pushing bridge via the mobile part, i. e. what pull and push forces develop in the broaching tool, depends on the stiffnesses of the transfer elements. The spring representation illustrated in Fig. 12.7 is used to determine the force distribution. The compliance of the push and pull bridge (bending) and the ball bearing spindle as well as the connecting rods (pressure) is reproduced by the spring constant k_s . The springiness of the upper and lower part of the broaching tool is characterised by the spring constants k_o (upper part) and k_u (lower part).

Thus, only the forces F and $-F$ act on the spring system from the outside. On the inside of the system, F_u (lower part) and F_o (upper part) act in the broaching tool. The forces are transferred onto the pushing bridge (upper part) via the ball bearing spindles. Thus, the following applies:

$$F - F_o - F_u = 0 \quad (12.8)$$

Under the influence of these forces, their points of action are displaced by the small dislocation x_1 at the point of action of the broaching force and x_u at the pushing bridge (lower part).

Therefore, the following applies:

$$F - F_u = k_o \cdot x_1 \quad (12.9)$$

and

$$F_u = k_s \cdot x_u \quad (12.10)$$

Since F_u also acts in the thrust rod as well as in the lower part of the broaching tool, the following also applies:

$$F_u = k_u \cdot (x_1 - x_u) \quad (12.11)$$

The spring constants k_s , k_u and k_o can be calculated from the sizes and the elastic properties of the force penetrated components. So after a force balance, the following applies:

$$F_o = \frac{k_o \cdot (k_u + k_s)}{k_o k_u + k_o k_s + k_u k_s} \cdot F \quad F_u = \frac{k_u \cdot (k_u + k_s)}{k_o k_u + k_o k_s + k_u k_s} \cdot F \quad (12.12)$$

So as to simplify the calculation, it is to be assumed that k_s is much larger than k_o and k_u

$$k_s \gg k_o, k_u$$

The Eq. 12.12 will then become

$$F_o = \frac{k_o}{k_o + k_u} \cdot F \quad F_u = \frac{k_u}{k_o + k_u} \cdot F \quad (12.13)$$

In principle, this simplification is not necessary for the calculation.

For an elastic calculation, the broaching tool is understood as a cylindric bar. Furthermore, it is assumed that the stiffnesses of the push and pull bridge are irrelevant for a comparison, regardless of their type of drive. They are, however, loaded by bending and therefore definitely contribute to the total compliance.

The spring constants k_o and k_u are variable along the travel x with the E-module E , the cross-section A and the bar length l . Thus, the following applies:

$$k_u = \frac{E \cdot A}{x} \quad k_o = \frac{E \cdot A}{l - x} \quad (12.14)$$

With Eq. 12.7, the following results:

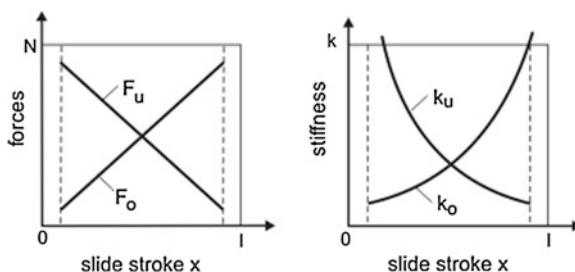
$$F_o = \frac{x}{l} \cdot F \quad F_u = \frac{l - x}{l} \cdot F \quad (12.15)$$

The force course is illustrated in Fig. 12.8.

So one can recognise that the pressure force in the broaching tool is low, if the free buckling length is big and vice versa. As a consequence, the danger of buckling is considerably reduced in spite of the proportionate pressurisation of the tool. Then again, the tool is actively guided at both ends. Practical experiments have shown that the tool life quantities at internal broaching on the machines, according to the push and pull principle can be increased considerably, compared with conventional machines [TÖN03].

Characteristics for broaching machines are the maximum broaching force and the maximum broaching length. Internal and external broaching machines with broaching forces of up to 1,200 kN and broaching strokes of up to 3,000 mm are on offer. The drives can be carried out electro-mechanically or with hydraulic. Broaching is a difficult cutting process with high technological requirements. For internal broaching, the pilot holes have to lie within tight tolerances, which have to be lower than the maximum undeformed chip thickness. Too small pilot holes make broaching impossible. If the pilot holes are too big, drifts and strong position

Fig. 12.8 Forces and stiffnesses



deviations are to be expected. This error can also lead to the jamming and tearing of the tool. In addition, the contact surface of the workpiece has to be at a right angle to the pilot hole. If special position or angle tolerances are predetermined, the internal broaching operations should be carried out first before the external machining. Even if that means clamping in the broached surfaces and considering these tolerances, which are not easily complied with. Hardened workpieces can also be broached. In that case, hard metal or cubic crystalline boronitride (PCB) is used as a cutting material. Machines and tools have to be apt for hard broaching. In view of the technological difficulties of the process broaching, all precautions have to be made so as to avoid tearing or badly damaging the complex tools.

12.3 Questions

1. Which motion does a broaching tool carry out?
2. What does the undeformed chip thickness result from?
3. Name typical applications of broaching.
4. What is lateral offset applied for?
5. What does the tooth pitch of a broaching tool result from?
6. Why is there a limit to the workpiece height for a given broaching machine?
7. Name orders of magnitude for undeformed chip thicknesses in broaching. What differentiation has to be carried out?
8. Outline the dynamic cutting force course in broaching for $\lambda = 0$ and $\lambda \neq 0$.
9. Why does one work mostly at $\lambda = 0$ in internal broaching?
10. How can the acceleration frequencies be determined from the time course of the cutting force?
11. What are the advantages and disadvantages of internal broaching machines with pushed tools?
12. Describe the force course of an internal broaching machine in a push–pull-constellation?

References

- [DIN 8589-5] DIN 8589-5: Fertigungsverfahren Spanen, Teil 5: Räumen, Einordnung, Unterteilung, Begriffe/Manufacturing processes chip removal—Part 5: Broaching; classification, subdivision, terms and definitions, Beuth (2003)
- [LAN05] Lang, H.: Trockenräumen mit hohen Schnittgeschwindigkeiten—Werkzeug und Prozesskenngrößen für die Weich- und Hartbearbeitung [Dry broaching with high cutting speeds—tool and process parameters for soft and hard machining]. Dr.-Ing. Diss. Universität Karlsruhe (2005)
- [SCH80] Schweitzer, K.: Räumen [Broaching]. In: Spur, G. Th. Stöferle (Hrsg.): Handbuch der Fertigungstechnik (Band 3/2), Hanser-Verlag (1980)
- [TÖN03] Tönshoff, H.K., Lübbers, E.: Produktivitätssprünge beim Räumen [Productivity leaps in broaching]. ZWF 7/8 (2003)

Chapter 13

Grinding

13.1 Cutting with Geometrically Undefined Cutting Edges

The process of the group “abrasive processes” or “Cutting with geometrically undefined cutting edges” is structured according to [DIN8589-0](#) (see [Sect. 1.2](#)), in the processes grinding with rotating tools, belt grinding, stroke grinding, honing, lapping, free abrasive cutting and abrasive blast cutting (Fig. 13.1). Processes with fixed and loose abrasive particles can be distinguished. These processes are mainly finishing processes. But nowadays, the development of high power grinding processes permits the economic realisation of high material removal rates, so that the areas of application of the processes with a geometrically undefined cutting edge is no longer limited to finishing.

The removal of material can be a path-linked manner (grinding, honing), force-linked (lapping) or energy-linked (blasting). The cutting edges of the abrasive particles are thereby moved tangentially (e.g., in grinding) or normally (e.g., in lapping) to the existing surface (Fig. 13.2). This effective motion determines the effective mechanism: During the *normal* penetration of the single cutting edges material is displaced and as a consequence of these wedge-type, plastic deformations is also tangentially shifted. Several or many such displacement processes [SIM88] in one place, e.g., during lapping, lead to the disruption and separation of material parts. The abrasive particles roll off on the workpiece driven by the lapping wheel and are thereby continuously pressed, normally into the workpiece surface.

When the single cutting edges penetrate *tangentially* e.g., during grinding, the process generally resembles cutting with a geometrically defined cutting edge. In principal, the same separating mechanisms occur during the processes of both groups (Fig. 13.3). In grinding, however, the cutting edges are formed by hard material abrasive particles at which one abrasive particle can have several active cutting edges. In general, the dimensions of the elements involved are considerably smaller than in cutting with geometrically defined cutting edges. Cutting with bond abrasive particles generally occurs with a strongly negative cutting angle. When cutting with rotating tools, the paths of the cutting edges correspond to epicycloids (by means of cutting and feed motions). The form of the cutting

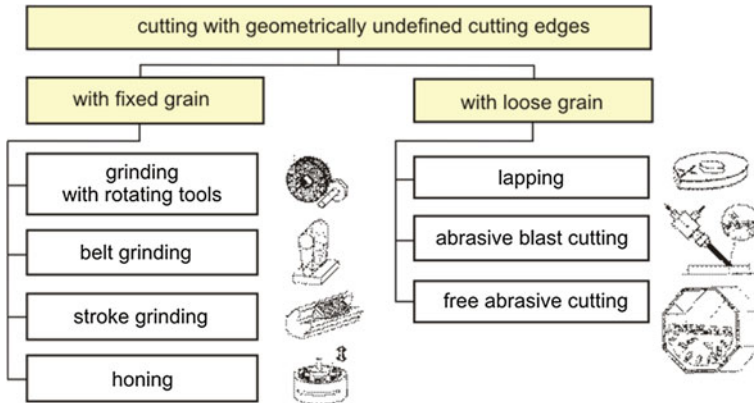


Fig. 13.1 Abrasive processes or cutting with geometrically undefined cutting edges (according to DIN 8589-0)

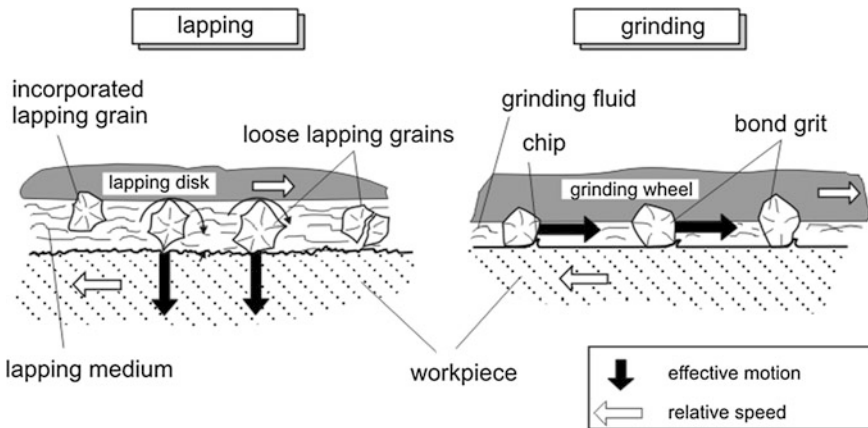


Fig. 13.2 Effective principles and mechanisms during lapping and grinding [SIM88]

wedges and thus the cutting angles, the cutting thickness at each single cutting edge and also the process variables active on the single abrasive particle, such as forces and temperatures, can only be described statistically, e.g., by means of averages, variances and distributions.

The cutting thicknesses during grinding are so small that elastic shares in the deformation are not to be disregarded. Figure 13.4 illustrates the different phases in chip formation. During the cutting edge penetration, after a purely elastic deformation (1), the plastic flow of the material occurs (2). The actual chip formation takes place after another penetration of the cutting edge into the material (3). Apart from the shearing of the chip (4), this area is characterised by elastic as well as plastic deformations. Compared with this, immediately before the abrasive particle leaves the material, there are only elastic deformations and

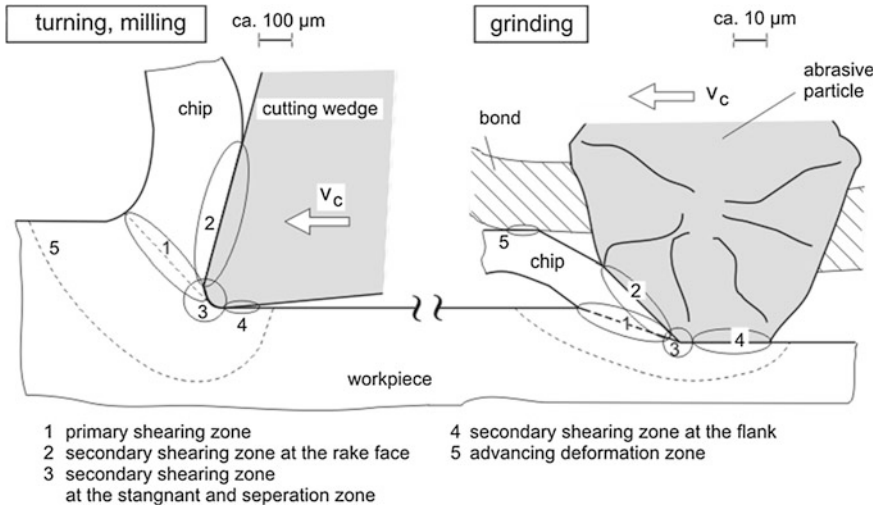


Fig. 13.3 Chip formation

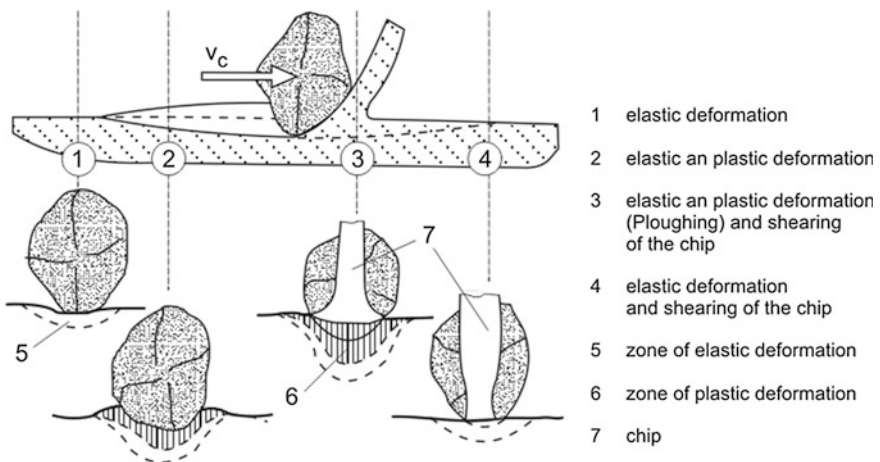


Fig. 13.4 Phases of chip formation during grinding

the shearing of the chip (4). Despite the similarity between grinding and the processes of cutting with geometrically defined cutting edges, several basic differences do exist: In grinding, lateral material flow occurs in front of the cutting edge, the deformation status is triaxial in contrast to a mainly biaxial flow in cutting with a geometrically defined cutting edge [HAH63].

13.2 Grinding Materials

The usual hard materials for grinding are aluminum oxide, silicon carbide, cubic crystalline boron nitride, and diamond. Nowadays, these hard materials for grinding purposes are exclusively produced synthetically, because that way favourable material properties can be reached within tight limits. The grinding materials differ considerably in their degree of hardness and thus in their wear resistance (Fig. 13.5). However, there are also large differences in the other physical characteristics (Table 13.1) [DOW72]. Here, the hardness of diamond has been converted into Knoop resp. Vickers hardness. A direct measurement of diamond hardness is not possible with this process, in fact the hardness is determined indirectly via Young's modulus (E module).

Apart from the hardness, the friability of grinding materials is of interest with regard to the wear behaviour. The friability is determined in a technological—not standardised—process by ball milling coarse grains (particle size 12 US mesh), under determined conditions (ball mass, milling time, etc.). The process goes back to the “friatester” developed by the company DeBeers [ANSB7418]. The friability index (breakage index) of the grinding material is determined by the proportion of the particles that fall through a mesh with particle size 16 US mesh. Since the process of meshing only uses one mesh width, it is hardly possible to make a statement about the distribution of sizes and thus about the fine friability of interest for the splintering.

In addition, the index numbers for different sizes of abrasive particles are not comparable because smaller sizes generally generate a smaller index number. Friability indices for aluminum oxide of different degrees of hardness were entered in Fig. 13.6 as an example.

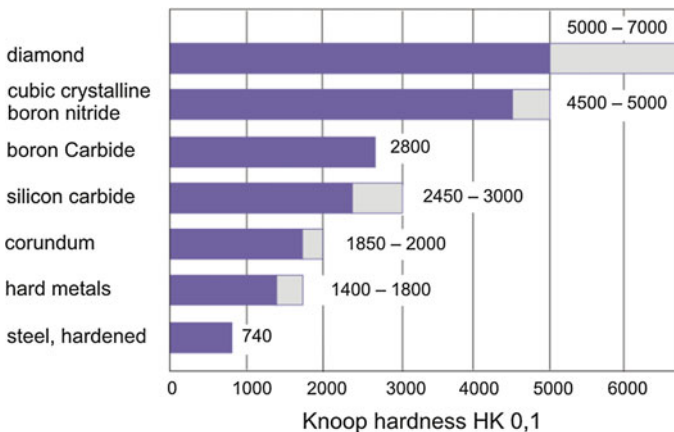


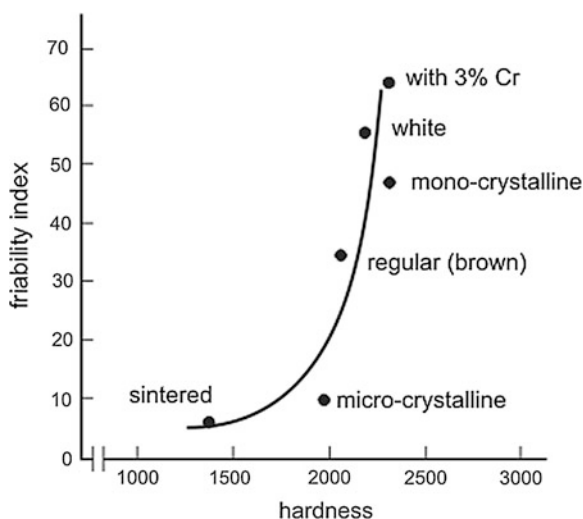
Fig. 13.5 Hardness of abrasives and other materials

Table 13.1 Physical properties of different grinding materials

	Al ₂ O ₃	SiC ¹	CBN	Diamond
Density (g/cm ³)	3.96	3.15	3.48	3.52
Hardness	HK01	2,450–3,000	4,500–5,000	5,000–7,000
	HV01	2,100	2,500	6,000
Young's modulus (GPA)	400	400	680	890
Poisson ratio(–)	0.2	0.17	0.17	0.2 ⁴
Friction co-efficient (–)	0.34	2.300	0.19	0.05–0.15 ⁴
Melting point (°C)	2,050		2,730	3,700
Temperature stability (°C)	1,750	1,500	1,200	900
Heat expansion co-efficient (10 ⁻⁶ /K)	7.4(<500 °c) 7.5–8.5 (>500 °c)	4.7	3.6	0.8 (RT) ⁴ 1.5–4.8 (>500 °C)
Heat conductivity (W/mK)	30 (RT) 14 (400 °C)	110 (RT) ² 55 (600 °C)	200 (400 °C) ³	600–2,000 (RT) ⁴
Related heat (J/gK)	1.08 (400 °C)	1.1 (500 °C)	1.57 (400 °C) ³	6.19 (RT) ⁴

Source 1 Saint Gobain Abrasives; 2 Salmang, Scholze; 3 De Vries; 4 Element Six

Fig. 13.6 Friability index and hardness, according to Malkin [MAG08]



13.2.1 Corundum

Corundum is a crystalline aluminum oxide (also called alumina) (Al₂O₃). The mechanical properties are determined by the purity degree to a large extent. We differentiate between regular or brown, white and modified aluminum oxide.

In the production of corundum, bauxite serves as a raw material for all qualities, a mixture of different aluminum oxide hydrates which is polluted with ferric hydroxides, silicates and titanium alloys [SAL82]. In the most frequently used Bayer process, ground bauxite with an Al₂O₃ content of 55–60 % is treated with caustic lye at approx. 250 °C under a pressure of 4 MPa. The aluminum oxide

hydrates dissolve as sodium aluminate, the pollutions are separated as so-called red mud. The sodium aluminate lye is stowed with finely dispersed aluminum hydroxide, which as a crystallisation seed, leads to the growth of $\text{Al}(\text{OH})_3$ crystals. The calcination of the aluminum hydroxide in fluidised-bed furnaces at 1,200–1,300 °C produces Al_2O_3 (alumina) [SAL82].

Melting the alumina in an electric furnace at temperatures of approx. 2,000 °C generates corundum (Al_2O_3). With this process, it is possible to obtain a high purity degree. The sizes of abrasive particles required for the grinding materials are produced by means of controlled crushing in crushers. Chemical post-treatment process by means of calcination and washing in lyes and acids lead to an improved surface structure of the abrasive particles and targets an increase in their adhesion within the bond.

A very fine original abrasive particle is obtained by means of the *sol-gel process*, which emanates from a liquid or easily soluble compounds. The sol-gel process allows the production of ceramic and glassy compounds at low temperature. The process is characterised by the changeover of a liquid or colloidal solution (smallest particles of the dimension 10^3 – 10^4 atoms, mixed with molecules of the solvent) into a solid gel.

For the production of Al_2O_3 with the sol-gel process, a solution of aluminium and an organic ester ($\text{Al}(\text{OC}_3\text{H}_7)_3$) is hydrolysed with H_2O and then condensed under dehydration, which generates a very fine gel well suitable for sintering.

A performance increase of corundum grinding materials can be obtained by altering the structure and shape of the abrasive particles (Fig. 13.7). During the grinding process, the number of sharp cutting edges per abrasive particles can be increased, thus improving the tool life and the power conversion compared with untreated melted corundum. On the other hand, an increase in wheel porosity at

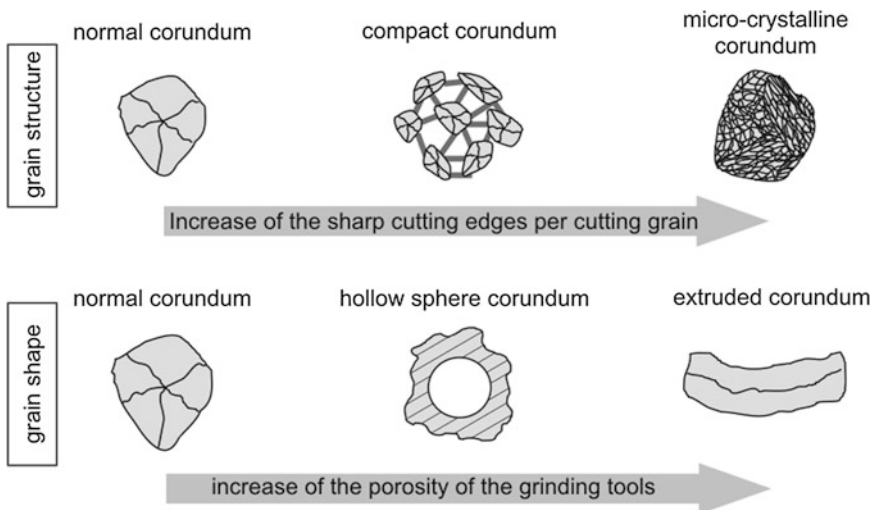


Fig. 13.7 Possibilities of power increase when using aluminum oxide

unaltered wheel strength allows an easier removal of the chips from the effective zone. In addition, the feed of cutting fluid to the contact zone is better at an increased wheel porosity.

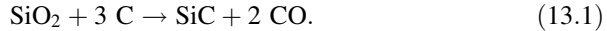
During the grinding process, suitably distributed abrasive particles may wear to such a degree that extensively sharp cutting edges are generated. This resharpening or self-sharpening process can be obtained by using compact abrasive particles or particles with a micro crystalline structure. The compact abrasive particles consist of a multitude of small grains, which have been clinkered into a large abrasive particle by means of a bond. The process-related wear on each small grain leads to a local increase in the specific grinding force on the worn abrasive particle. When the bonding forces are surpassed, the blunt abrasive particle detaches itself from the compound of the compact abrasive particle and exposes a new sharp abrasive particle located underneath. This type of resharpening process of abrasive particles is preferably used for abrasives on backing materials, e.g., belt grinding processes [ARG00].

Resharpening is also transferable to each single grain by producing micro crystalline Al_2O_3 according to the sol-gel process. At this, grain fracture and thus sharp cutting edges can occur during the grinding process. In contrast with the coarsely crystalline melting corundums, this mechanism leads to a considerably reduced wear with decreased grinding force and temperature at the same time. This results in longer wheel life, longer dressing intervals and allows an increase of the material removal rate [UHL87, BRU98, MÜL01]. At this, different micro crystalline corundums differ considerably in the height of the initial force required for resharpening [STA02].

In grinding processes with a high material removal rate, grinding wheels with high pore proportions are applied. The maximum porosity readily accounts for about 50 %. A further increase leads to a lower strength, which limits the maximum cutting speed and increases the wear rate. By inserting hollow ball corundum, a hollow corundum grain, into the grinding wheel structure, the porosity can mount to 60 % [MAH00]. Special machining processes can produce grains with large length/diameter relations (aspect ratio) of up to 8. In comparison, the normal corundum grain has an aspect ratio of 1. An advantage of elongated particles is the extension and improvement of the natural packing porosity of the particles. Grinding wheels with a porosity of up to 80 % can be produced without artificial pore builders.

13.2.2 Silicon Carbide

Silicon carbide is one of the important ceramic materials. It is also used as a grinding material. The technical production of SiC takes place according to the *Acheson process* from quartz sand (SiO_2) and petrol coke at a temperature of 2,000–2,300 °C after the stoichiometric reaction



At this, the reactions also occur via intermediate reactions following the presence of gasiform silicon and carbon compounds. The silicon carbide gained by means of the Acheson process occurs at a purity of 98–99 %. The pollutions (Fe, Mg, Ca) are accumulated at the grain edges or in the pores. The material is crushed, cleaned and separated by meshes according to the particle sizes. A multi-step washing process allows the cleaning of the SiC. An acid treatment loosens existing iron residues. Free silicon and silicon compounds are separated with soda lye and graphite with water.

The colour allows the differentiation of the two qualities of SiC, which are characterised by their chemical composition. Black SiC ($\approx 98\%$) compared to green SiC ($\approx 99.5\%$) shows greater pollutions of free carbonate and elements such as Fe, Al, Ca, Mg and free silicon. The pollutions show no influence on the hardness. However, the ductility of black SiC is higher than that of green SiC.

13.2.3 Cubic Crystalline Boron Nitride and Diamond

Grinding materials made of cubic crystalline boron nitride, also called Cubic Boron Nitrides (CBN) and diamond are extremely hard grinding materials, which are summarised under the term “superabrasives” in English language use. The structure and production process are illustrated in [Chap. 8 \[BUN55, HAL60\]](#). While the production of CBN is only synthetic, diamond can be differentiated into natural and synthetic. As grinding materials in grinding wheels, exclusively synthetic diamond is used nowadays. CBN has a cubic face centred crystal lattice of nitrogen and boron atoms similar to diamond, which also has a cubic face centred lattice with four additional carbon atoms [\[KEL80\]](#). Different crystal forms can occur due to the different sliding planes (Fig. [13.8](#)). For synthetic diamond, these range from the octahedron (111 plane) to the cube (100 plane). The diamond is anisotropic, e.g., the hardness is higher in the 111 plane than in the 100 plane [\[RAM78\]](#). Because of the slightly different crystal structure, CBN crystals can take up further shapes from the octahedron to the tetrahedron.

Due to their crystal structure, the grains contain cleavage planes, which they preferably split along. During the grinding, the abrasive particles blunt. Thus, they are loaded more strongly and split. This generates new cutting edges, which is called self-sharpening. According to the type and number of cleavage planes, one can differentiate mono, macro and micro crystalline structures.

Diamond is the hardest known material. In connection with its high wear strength, it is predestined for the use as a cutting material for the machining of hard materials such as glass, hard metal and ceramic. However, at temperatures above $650\text{ }^\circ\text{C}$ in the air, diamond transforms into the energetically more convenient modification of graphite with iron and nickel acting as catalysts and shifting the transformation point to lower temperatures [\[MAR01\]](#). Carbon also shows a high

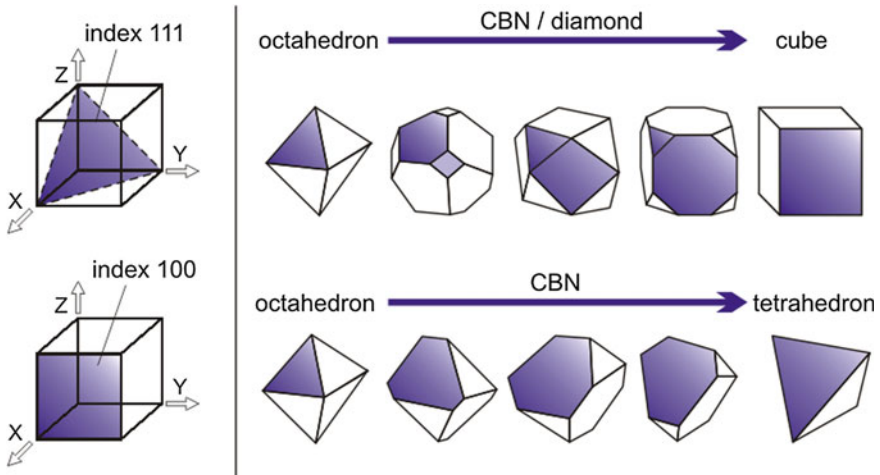


Fig. 13.8 Possible crystal forms of CBN and diamond (*Source* Element six)

affinity to iron so that chemical wear occurs at higher temperatures—thus at higher cutting speeds. Both effects, the graphitisation and the chemical wear lead to the fact that diamond is not used as a grinding material for the machining of steel materials. In contrast, CBN shows no reaction of this kind and is stable at an atmospheric pressure of up to a temperature of 1,400 °C and thus suitable for the machining of ferrous workpieces.

The friability test is a recognised method for the strength determination of diamonds. It is based on the measurement of the impact strength of a defined number of diamonds of a certain abrasive particle size. The number of diamonds that resist the “crushing effort” is a measure for the strength of the examined type of diamond (TI) (also see Sect. 13.2). To determine their thermal stability, diamonds are thermally loaded under protective gas at 1,100 °C for 20 min and then again submitted to the friability test (TTI). The difference between the strength before and after the thermal load is a measure for the thermal stability of the material. This thermal stability is relevant for the application of the tool, but also in the manufacturing of a grinding wheel by sintering [VOL00].

13.2.4 Grain Sizes of Grinding Materials

Abrasive particles are characterised by physical properties, such as hardness, elastic modulus, density, heat conductivity and heat capacity but also by geometrical properties, such as grain size and grain shape. The abrasive particle size in grinding materials from aluminum oxide and silicon carbide up to grit size 220, which corresponds to a medium abrasive particle diameter of about 58 µm, results

sieve grit sizes				
Europe (metrical)		sieve mesh width in μm	USA (mesh)	
(1)	(2)		(1)	(2)
1181	1182	1180 - 1000	16 / 18	16 / 20
1001		1000 - 850	18 / 20	
851	852	850 - 710	20 / 25	20 / 30
711		710 - 600	25 / 30	
601	602	600 - 500	30 / 35	30 / 40
501		500 - 425	35 / 40	
426	427	425 - 355	40 / 45	40 / 50
356		355 - 300	45 / 50	
301	-	300 - 250	50 / 60	-
251	252	250 - 212	60 / 70	60 / 80
213		212 - 180	70 / 80	
181	-	180 - 150	80 / 100	-
151	-	150 - 125	100 / 120	-
126	-	125 - 106	120 / 140	-
107	-	106 - 90	140 / 170	-
91	-	90 - 75	170 / 200	-
76	-	75 - 63	200 / 230	-
64	-	63 - 53	230 / 270	-
54	-	53 - 45	270 / 325	-
46	-	45 - 38	325 / 400	-

Fig. 13.9 Classification system for abrasive particle sizes of super hard grinding materials (according to FEPA¹)

from meshing. For this, standardised wire sieves are used [DIN ISO8486-1]. Due to the heterogeneous grain shapes, there is a statistic distribution of the abrasive particle diameter after meshing, so a classification of the permitted deviations was carried out. This classification is standardized by the FEPA.¹ A grain mixture, for example generated by crushing and milling, is routed to increasingly tighter aperture by means of sieves. In the case of aluminum oxide and silicon carbide, the grain size is defined by the number of meshes per inch of the meshing sieve at a determined wire diameter. A grit size of 60 is removed from the grain compound with a sieve of 60 meshes per inch, which corresponds to a mesh distance of 0.42 mm. Grain sizes finer than 220 are determined by optic sedimentation from a suspension. The sieve analysis entails that the abrasive particles occur in fractions with typical distributions, which also depend on the grain shape.

The super hard grinding materials diamond and CBN are marked according to the clear mesh width of the sieves, i.e., the index correlates directly with the grain diameter. Figure 13.9 contrasts the classification system used in Europe with the US system (mesh). To extend the field of tolerance, one can differentiate between a narrow (1) and a wide dispersion area (2). Both systems are only defined up to a medium grain diameter of $d_g = 46 \mu\text{m}$. Smaller grain sizes are defined by the producers of grinding materials themselves.

¹ FEPA: Federation Europeene des Fabricants de Produits Abrasifs—Federation of European Producers of Grinding Materials.

13.3 Bonding

The abrasive particles are bonded by bonding materials or bonds in the grinding tool. The most important bonds are vitrified bonds, synthetic resinoid and metal bonds.

Vitrified bonds consist of kaolin, clay, quartz, feldspat and flux material [KLO86, PAD93, COL81]. Magnesium oxide or borosilicate containing glasses are used as flux materials to reduce the calcination temperature. The charges fired together with the abrasive particles to grinding tools, at temperatures of 1,100–1,400 °C maximum for corundum and silicon carbide wheels, below 1,000 °C for boron nitride and below 700 °C for diamond. The choice of the charge materials allows the attainment of melting with different viscosity and surface tension. Thus, the structure resp. the porosity of the vitreous-bound grinding wheels can be adjusted.

Synthetic resinoid bonds mainly consist of thermosets, i.e., phenolic resin or compounds with phenolic resins with other resins. They are converted into grinding tools together with the abrasive particles by means of hot pressing. The pressing temperatures are between 150 and 170 °C.

Metal bonds are produced by pressing and sintering bronze, steel or hard metal powders or applied by the galvanic coating with nickel or nickel compounds. Bonds created on the basis of metal powder are sintered under pressure at temperatures of 700–900 °C. Metal bonds are applied for extremely hard grinding materials. They offer a good heat removal from the active grinding layer, have good form stability and show a high adhesion to the abrasive particles. They are often used for profile grinding. Electro-plated grinding wheels mostly feature only one grain layer and are generally not dressed (see Sect. 13.5). By crushing (pressing), dressable metal bonds have been developed by means of inserting brittle fillers.

Other bonding materials are employed for special purposes, e.g., mineral bonds (silicate, magnesite bonds), glue or rubber bonds. The *rubber bond* based on synthetic rubber is used for especially temperature-sensitive processing tasks (knife sharpening), for example.

An important characteristic of a grinding tool is its hardness, which is determined as the resistance opposed by the bond to the quarrying out of abrasive particles. Thus, the hardness of a grinding wheel is basically defined other than usual, since generally the hardness of indentation is determined. The hardness of the wheel or bond is of great relevance for the grinding process. It determines how long a worn abrasive particle is kept in the bonding formation. A soft bond releases abrasive particles at an early stage; the grinding wheel remains sharper compared with a wheel with a hard bond. The practical rule resulting from this: soft, less wearing materials are processed with hard wheels and hard materials with soft wheels. Harder wheels are also recommended for low chip thicknesses, i.e., in short contact lengths or low speed conditions.

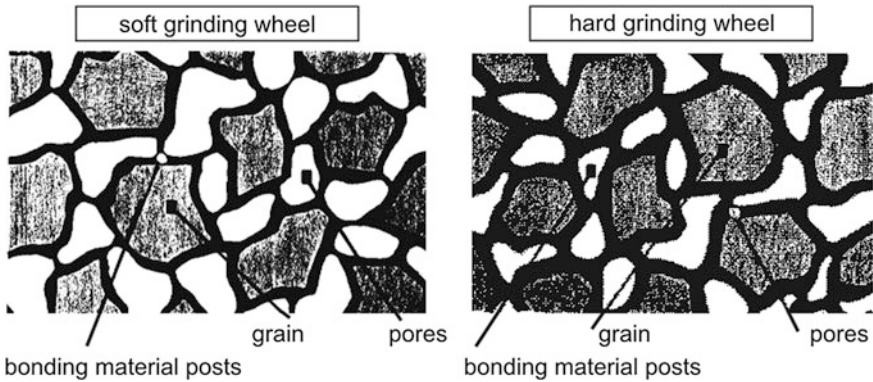


Fig. 13.10 Structure of a vitrified grinding wheel (Source “Saint Gobain Abrasives”)

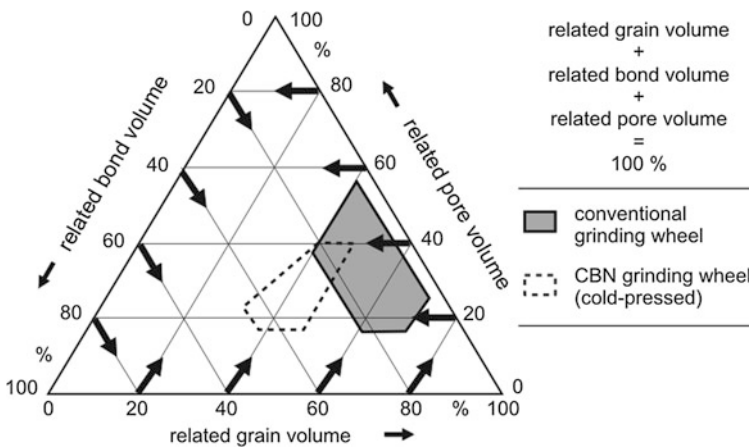


Fig. 13.11 Volume shares of vitrified grinding wheels

For vitrified-bond grinding wheels, the hardness is mainly determined by the abrasive particle size and the thickness of the bonding bridges (Fig. 13.10). Stronger bonding bars maintain the abrasive particles within the structure more strongly and thus provide a higher degree of hardness of the grinding wheel. Figure 13.11 illustrates the areas of common configurations for grinding wheels.

13.4 Grinding Wheels

The material classification of conventional grinding wheels takes place according to [DIN ISO 525] (Fig. 13.12). It contains eight codes including two free codes, i.e., they can be freely chosen by the producer.

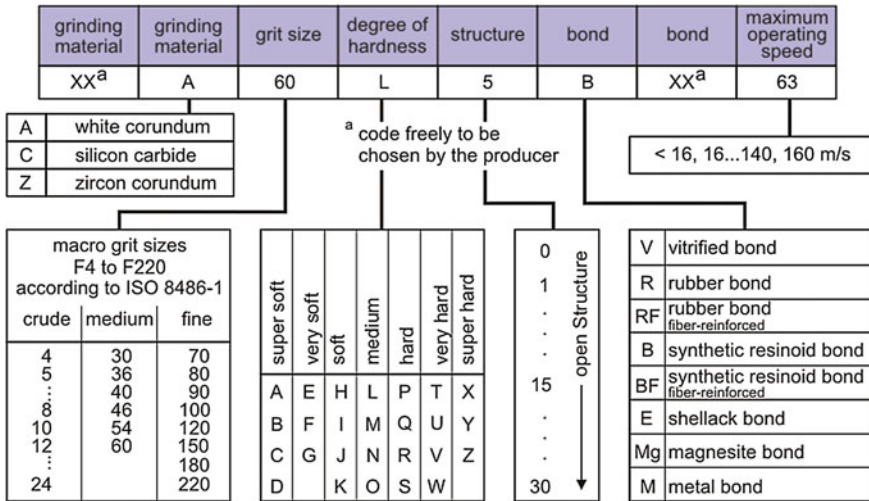


Fig. 13.12 Classification of corundum and silicon carbide grinding wheels (according to DIN ISO 525:2000)

The hardness of a grinding wheel is classified according to the Norton scale with code letters from A (extremely soft) to Z (super hard). The area from E and G (very soft) till P and S (hard) is actually used in practice.

The manual scratch test with a stylus and the comparison with known wheels is subjective and offers no absolute data. A variant of this manual test developed for research purposes is the scratch test according to Peklenik [PEK57], at which a scratching tool is pulled over the surface of the active grinding wheel surface under defined normal load and abrasive particles or parts of them break off in this test. The emerging tangential forces are a measure for the hardness of the wheel. This test comes as close as possible to the definition of hardness, however it is not suitable as a shop testing process.

The hardness test of grinding wheels by means of the shot blasting process according to C. Zeiss and M. Mackensen (tester of Mengrinhhausen company, Iserlohn) is defined in guideline 102 of the German Grinding Wheel Committee. In this process, a defined volume of a certain sand grit is blown onto the surface of the grinding wheel with pressurised air at a determined static pressure and defined blast cross-section. Figure 13.13 illustrates the structure of a blast tester. The depth of the developing calotte, the so-called blowing depth, is consulted as a measure for the hardness of the grinding wheel. A disadvantage of this process is that it does not work without damage and that the kind of load on the abrasive particles and the bonding is not identical with the hardness definition.

Concerning the load, it is similar to the crushing process (Fig. 13.14). At this, a steel wheel with defined pressure is pressed against the grinding wheel to be tested. Grinding wheel and roller roll against each other. The rolling depth reached after a certain number of rotations is correlated with the wheel hardness. From the

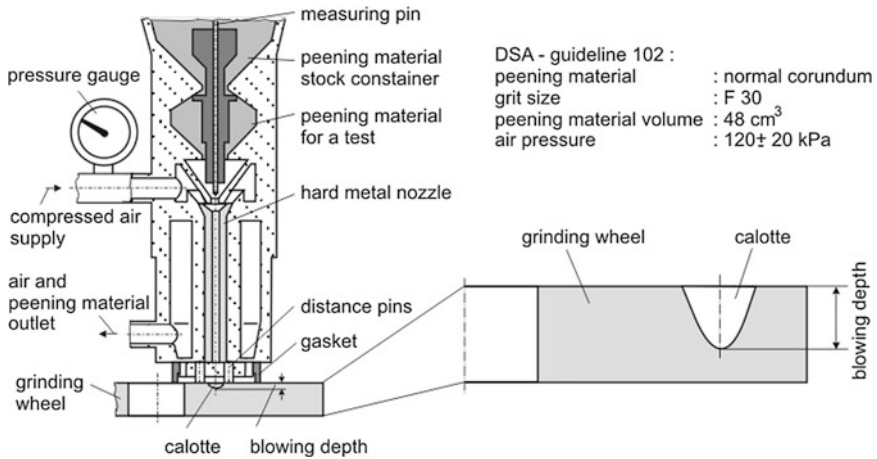


Fig. 13.13 Hardness test of grinding wheels by determination of the blowing depth

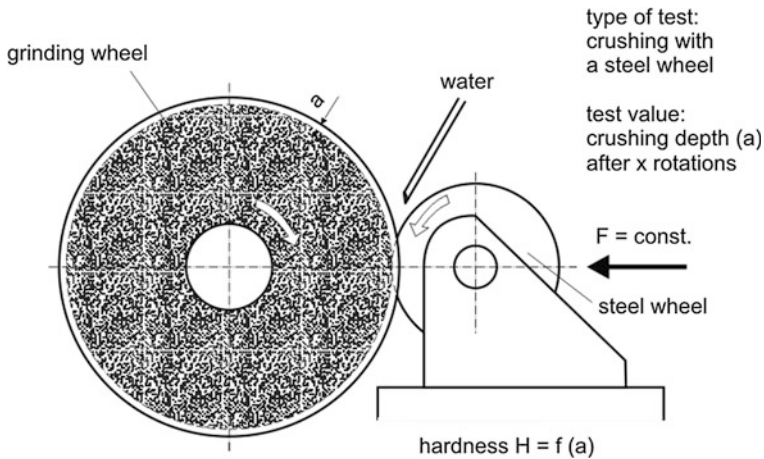


Fig. 13.14 Grinding wheel hardness test according to the rolling process (Source Opitz)

perspective of the load on abrasive particles and bonding, the hardness test B according to Rockwell (ball groove test), which mainly tests very fine-grained grinding tools (honing and oil stone tools), is comparable with the rolling process.

A test process, which provides a physical value, is the eigenfrequency measurement (grindo-sonic process) according to R. Snoeys [PET68]. At this, the first eigenfrequency of the grinding wheel is determined by striking in the attenuation test (Fig. 13.15). The eigenfrequency is proportional to the root of the apparent E module of the grinding wheel. With the diameter of the wheel d_a and the hole d_i , the wheel thickness b_s , the average (apparent) density ρ_s and the Poisson's ratio ν ,

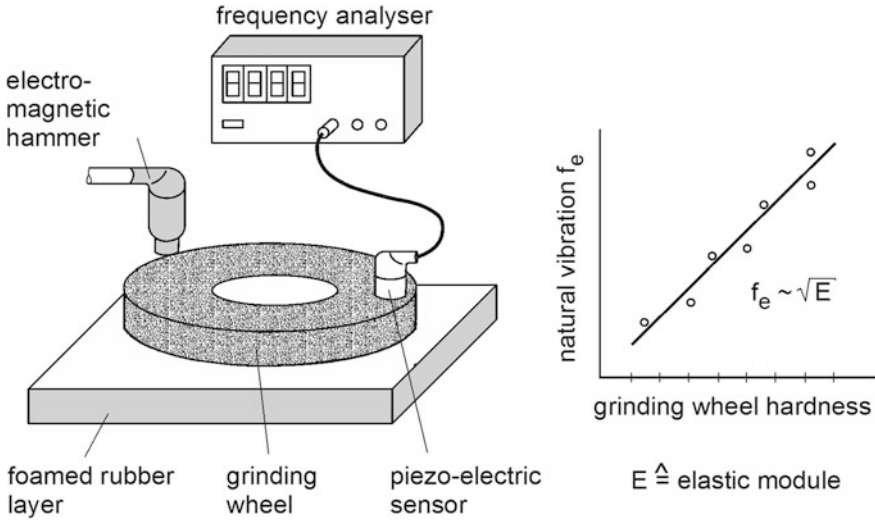


Fig. 13.15 Grinding wheel hardness and E module

the following is valid for the eigenfrequency f_e of the natural oscillation with three node diameters under the condition $d_i/d_a < 0.25$ [PET68]:

$$f_e = \frac{b_s}{d_a^2} \cdot \left(\frac{1 - (d_a/d_i)^2}{1.07(1 - \nu^2) \cdot \rho_s} E \right)^{1/2} \tag{13.2}$$

The specimen, which consists of several components, can be described only as an apparent E module. The thicker the bonding bars, the bigger the E module. This provides a correlation between the E module determined that way and the hardness of the wheel.

The testing process of conventional grinding wheels is transferable to super hard grinding wheels only to a limited extent. There are first method approaches to do determine the fracture behaviour (bonding, abrasive particle) resp. the compliance of super hard vitrified-bound grinding wheels. They apply test loads to single abrasive particles [KLO02] or groups of abrasive particles with a defined tester [DEN03].

13.5 Burst Safety of Grinding Wheels

Grinding wheels run at high circumferential speeds. As a consequence, they are submitted to high radial accelerations, which in turn cause high stress through the centrifugal effect. These stresses can lead to the destruction of the grinding wheels, which is to be avoided. So the loads as a result of the centrifugal forces and their parameters of influence have to be determined.

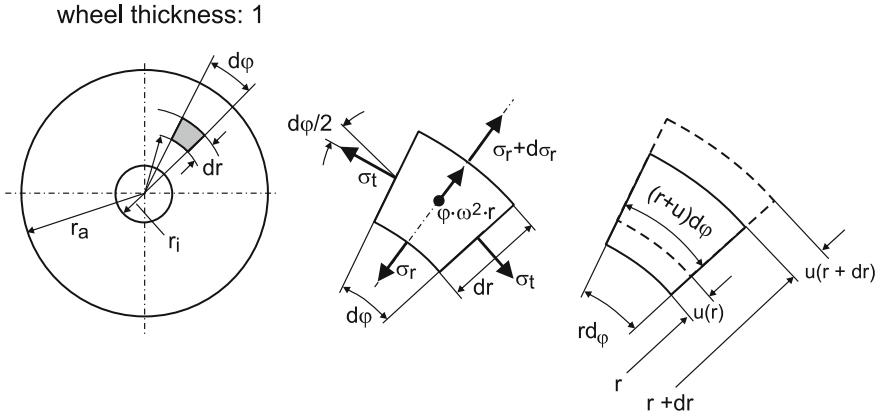


Fig. 13.16 Stresses and strains on the volume element

Figure 13.16 shows stresses and strains on the volume element of a wheel. Due to the low extension vertically to the drawing plane, biaxial stress condition can be presumed. From the balance of the forces in radial direction, it can be written

$$\left(\sigma_r + \frac{\partial \sigma_r}{\partial r} dr \right) \cdot (r + dr)d\phi \cdot 1 - \sigma_r \cdot r \cdot d\phi \cdot 1 - 2 \cdot \sigma_t \cdot dr \cdot 1 \cdot \sin \frac{d\phi}{2} + \rho \cdot r^2 \cdot \omega^2 \cdot dr \cdot d\phi = 0 \quad (13.3)$$

In addition, the following is valid for small sections

$$\sin \frac{d\phi}{2} = \frac{d\phi}{2}$$

So in summary, it can be written

$$\frac{\partial(\sigma_r \cdot r)}{\partial r} \cdot dr \cdot d\phi - \sigma_t \cdot dr \cdot d\phi + \rho \cdot r^2 \cdot \omega^2 \cdot dr \cdot d\phi = 0 \quad (13.4)$$

A link between σ_r and σ_t is obtained using the material law for elastic behaviour, the Hook's law. As shown in Fig. 13.16, the strains result from the displacements u in radial direction.

$$\epsilon_r = \lim_{\Delta r \rightarrow 0} \frac{u_{r+\Delta r} - u_r}{\Delta r} = \frac{\partial u}{\partial r} \quad (13.5)$$

and

$$\epsilon_t = \frac{2\pi(r + u) - 2\pi r}{2\pi r} = \frac{u}{r} \quad (13.6)$$

The Hook's law for the plane stress conditions adds up to:

$$\begin{aligned} \varepsilon_r &= \frac{1}{E} [\sigma_r - \nu \cdot \sigma_t] \text{ and} \\ \varepsilon_t &= \frac{1}{E} [\sigma_t - \nu \cdot \sigma_r] \end{aligned} \tag{13.7}$$

which finally results in the differential equation, solvable by means of two-fold integration:

$$\frac{d}{dr} \left[\frac{1}{r} \cdot \frac{d}{dr} (u \cdot r) \right] = - \frac{\rho \cdot (1 - \nu^2)}{E} \cdot r \cdot \omega^2 \tag{13.8}$$

The following solutions result with the boundary conditions for the force-free edges and the (for a dimension-free illustration) radiuses $Q = r/r_a$ and $Q_i = r_i/r_a$ related to the external radius r_a

$$\frac{\sigma_r}{\rho \cdot r_a^2 \omega^2} = \frac{3 + \nu}{8} \left(1 + Q_i^2 - \frac{Q_i^2}{Q^2} - Q^2 \right) \tag{13.9}$$

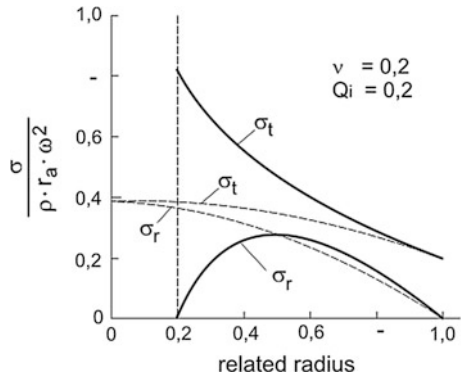
$$\frac{\sigma_t}{\rho \cdot r_a^2 \omega^2} = \frac{3 + \nu}{8} \left(1 + Q_i^2 + \frac{Q_i^2}{Q^2} - \frac{1 + 3\nu}{3 + \nu} Q^2 \right) \tag{13.10}$$

Figure 13.17 shows that the maximum load of a grinding wheel occurs as a consequence of centrifugal forces at the internal edge. In fact, wheels, which are operated above their burst speed, are dispersed into segments with radial breaking faces.

For a full wheel, which would then be held to a holding adapter [GRE58] for example, a totally different stress course results theoretically (holelessness). In Eqs. 13.9 and 13.10, the following limit has to be generated according to the law by de L'Hospital:

$$\lim_{Q \rightarrow 0} \frac{Q_i^2}{Q^2} = 0 \tag{13.11}$$

Fig. 13.17 Radial and tangential stresses through centrifugal forces



Thus, the stresses in the centre of the wheel become $Q = Q_i = 0$

$$\frac{\sigma_r}{\rho \cdot r_a^2 \omega^2} = \frac{\sigma_t}{\rho \cdot r_a^2 \omega^2} * = * \frac{+ v}{\circ} \quad (13.12)$$

In Fig. 13.17, the stress course of a full wheel has been entered in a dotted way. It is recognisable that the tangential and radial stresses in the middle change discontinuously compared with the holed wheel. They are equal, the tangential stress reduces to half of the value of the holed wheel. However, it remains questionable whether “holelessness” can actually be assumed in a porous wheel such as in a vitrified bound one.

The bursting is critical, especially in the case of vitrified bound wheels. In contrast to this, the trend is to increase the grinding speed. The following measures are suitable to increase the burst rpm of the grinding wheel:

- Fitting of reinforcements in the highly-loaded zones (stronger bonds, fiber reinforcement).
- Insertion of a steel ring into the wheel hole and creation of a pull-loadable connection, e.g., by gluing.
- Dissolving the wheel into segments, who do not transfer tangential stresses; however, this requires a safe radial clamp of the segments.
- Double-cone-shaped construction of the wheel so that the stress is reduced against the internal edge.

Due to the high energy content of the grinding wheels or their fragments at high grinding speeds (the speed effects in the 2nd order), special safety requirements are to be observed. In grinding machines (stationary machines), only grinding wheels authorised according to DIN ISO 13236 and according to DIN ISO 12413 for conventional grinding wheels are allowed for operation. The inscription and coloured mark indicate the permissible maximum working speeds. This maximum speed v_s is considerably lower than the bursting speed v_{br} determined in the experiment depending on the safety factor S_{br} . Due to the square connection with the turning energy, the following relation applies:

$$S_{br} = \left(\frac{v_{br}}{v_s} \right)^2 \quad (13.13)$$

For machine-operated grinding with a closed working area (safe covering of the workspace) $S_{br} = 1.75$, without covering $S_{br} = 3$ has to be complied with. When a wheel is first introduced into a clamp (mostly clamping flanges), the following tests have to be carried out by the specialised staff:

- Visual test for tears, bursts or other damages.
- Ring test (only sensible for vitrified-bound wheels) for clear sound (ok) or rattling resp. dull sound (not ok).
- Clamping in special flanges.

- Test run in the machine with the maximum drive of the grinding spindle, maximum speed of the wheel, duration 1 min.

For the operation it is to be observed that porose grinding wheels are not allowed to be flooded by cutting liquid when stopped due to the risk of imbalance.

13.6 Grinding Processes

The grinding process can be described by input, process and output variables from a system-technical point of view (see also Sect. 1.3). The input variables are divided into system and manipulated or set variables (Fig. 13.18). The system variables are described by the workpiece (physical, chemical properties, original and machined part form and dimensions), the grinding wheel specification, the machine (type, static and dynamic properties), the dressing tool and the cooling lubricant system. The manipulated or set variables are cutting speed, depth of cut, feed and dressing result as well as the set pressure and the flow rate of the cooling lubricant. In contrast with the system variables, the manipulated variables can be adjusted to the process quickly. The evaluation of the grinding process occurs via process variables by means of the cutting forces, power, energies, temperatures, vibrations as well as the grinding time. Workpiece-specific variables such as form and dimension accuracy, surface quality as well as surface zone properties, which have considerable influence on the functional performance of the component, are used to describe the output variables. Further output variables are wear, micro-

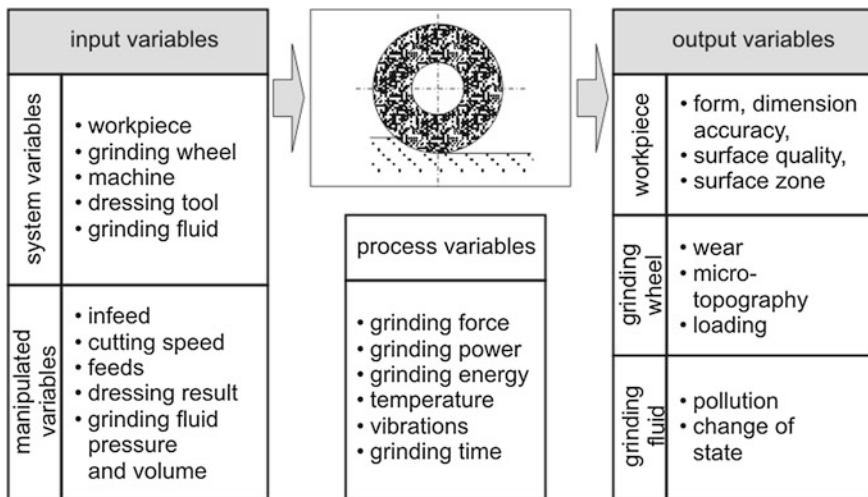


Fig. 13.18 Characteristics of the grinding process

topography and the loading-up of the grinding wheel as well as the pollution and alterations of the grinding fluid.

13.6.1 Input Variables

The productivity of the grinding process is described by the material removal rate Q_w (material flow rate, which is separated from the workpiece) [SAL91]. Figure 13.19 shows the variables required for the peripheral and side surface grinding to calculate the material removal rate. It follows at

$$Q_w = a_e \cdot a_p \cdot v_{ft} \quad (13.14)$$

from the working depth of cut a_e and the width of cut a_p , which add up to the engagement cross-section $A_w = a_e \cdot a_p$ and from the tangential feed speed v_{ft} , which stands normally to the cross-section. The depth of cut a_e is measured in the working plane (spanned between feed and cutting speed vector), the width of cut a_p is measured normally to the working plane. Figure 13.20 contains information on the material removal rates for other grinding processes than the peripheral and side surface grinding. Generally, the following applies to other surface grinding processes,

$$Q_w = A_w \cdot v_f, \quad (13.15)$$

where A_w ² is the engagement cross-section normal to the main feed speed v_f .

The geometrical and kinematic engagement conditions are of relevance to the chip formation in the effective zone. The geometric contact length l_g is entered in Fig. 13.19. Together with the width of cut, the geometric contact surface $A_k = a_p \cdot l_g$ results from this. The geometric contact length can be determined from the grinding wheel radius r_s and the depth of cut a_e at

$$l_g = r_s \cdot \arccos\left(\frac{r_s - a_e}{r_s}\right) \quad (13.16)$$

or for $r_s \gg a_e$

$$l_g = \sqrt{2 \cdot r_s \cdot a_e} \quad (13.17)$$

For a determination of the contact length and the contact surface independently from the tool and workpiece measurements and, in addition, independently from the process, the equivalent (equivalent to surface grinding) radius r_{eq} resp. diameter d_{eq} is defined. The following applies

² Here A_w determines the engagement cross-section and is not to be confused with the removal surface rate.

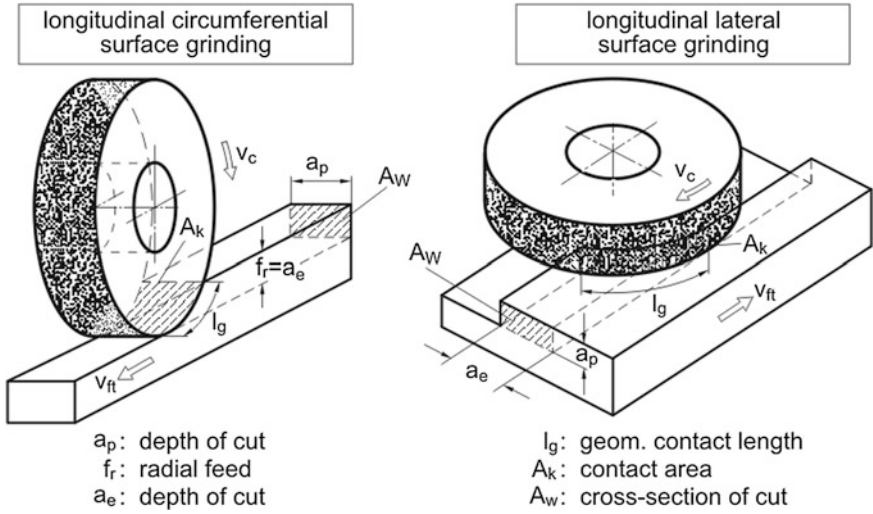


Fig. 13.19 Characteristics of the grinding process

		peripheral-		side-	
		longitudinal-	cross-	longitudinal-	cross-
surface-	surface-				
	round-	external- 	cross- 	longitudinal external profile 	cross-
	internal- 	cross- 	longitudinal external generating 		

Fig. 13.20 Important grinding processes (according to DIN 8589)

$$r_{eq} = \frac{r_w \cdot r_s}{r_w \pm r_s}, \tag{13.18}$$

at which the addition in the denominator stands for external cylindrical grinding and the subtraction for internal cylindrical grinding. Figure 13.21 represents the concept figure for the identification of r_{eq} and shows a comparison for external and internal cylindrical grinding at different radius conditions.

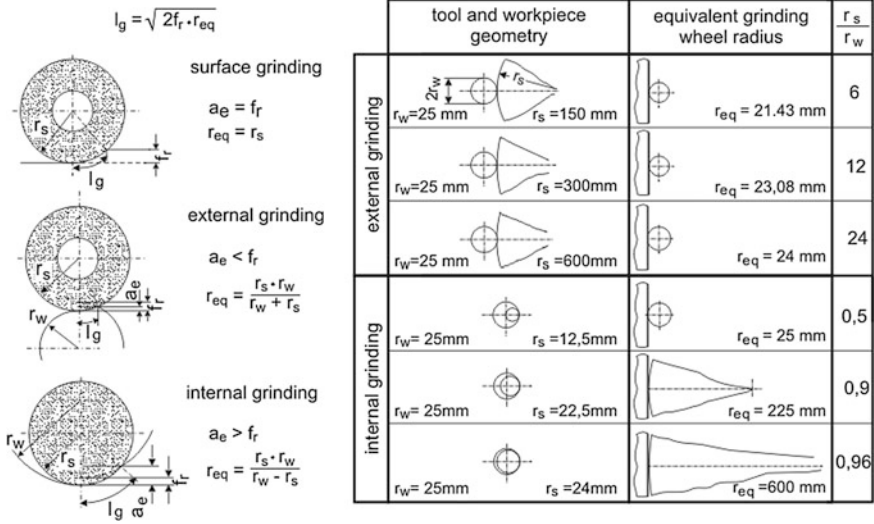


Fig. 13.21 Description of the equivalent radius

The geometric contact length is a calculation variable, which contains several simplifications as an approximation. It does not consider

- the entire kinematic of the effective partners, i.e., the cycloidal cutting path of the tool against the workpiece,
- the elastic deformation of the bodies involved as a consequence of the grinding forces,
- the fact that the surfaces of the grinding wheel and the workpiece, which are in contact, are not geometrically smooth but actually very rough and
- that the real contact surface only represents a fraction (in an order of 1 %) compared with the total surface of the workpiece engaged due to the contact of only single grains or cutting edges of the grinding wheels.

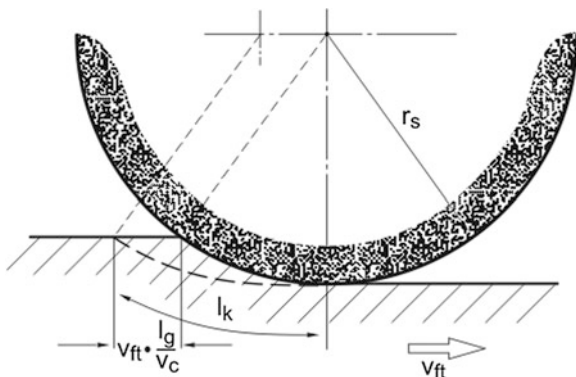
The kinematic contact length l_k considers the feed and cutting speed and assumes smooth effective partners. At a good approximation, it is

$$l_k = l_g \left(1 \pm \frac{1}{q} \right), \quad (+ : \text{down grinding}, - : \text{up grinding}) \quad (13.19)$$

at which the speed relation is $q = v_s/v_f$ (Fig. 13.22). At this, the addition stands for the up grinding, the subtraction for the down grinding. So in common grinding processes with $q = 60$, l_k and l_g differ from each other by 1.6 %. In creep feed grinding ($v_{ft} \ll v_c$), the difference is considerably lower. Noteworthy differences can only occur in speed stroke grinding, i.e., very high feed speed.

So far, it has not been considered that the actual contact between grinding wheel and workpiece only takes place via the active abrasive particles. So the real

Fig. 13.22 Kinematic contact length



contact surface is far smaller than calculated so far. A rough estimation of the relation between the real and the so-far mathematically determined contact area A_e/A_c is possible by considering the yield strength of the material [ROW93]. If the average pressing under the abrasive particles tolerable until material flow is p_{max} , the following applies:

$$F_n = A_e \cdot p_{max}, \tag{13.20}$$

and thus

$$\frac{A_e}{A_c} = \frac{F'_n}{p_{max} \cdot l_c} \tag{13.21}$$

Tests show an order of $A_e/A_c < 0.01$.

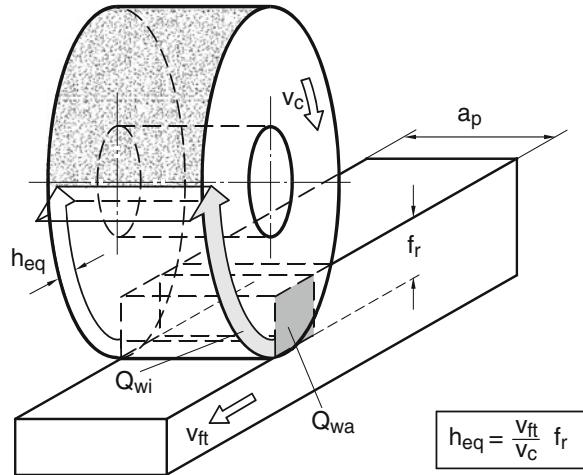
Since the grinding width or the depth of cut is generally large compared with the occurrence at the single grain, it is assumable with sufficient approximation that the same chip formation conditions apply along the width of cut. Thus, the set and process variables are sensibly related to the width of cut, such as e.g., the related material removal rate

$$Q'_w = \frac{Q_w}{a_p} \tag{13.22}$$

Forces, energies or powers, such as wear volumes are purposefully divided by the width of cut so as to make them technologically comparable.

The material removal rate is established by externally determined variables. So Q_w is also called the external material removal rate Q_{wa} . This external material removal rate has to be identical with the volume, which is cut per time unit by the cutting motion—marked by the cutting speed v_c —and the engagement of the single cutting edges. The volume rate produced by the cutting motion is indicated as the internal material removal rate Q_{wi} . If, according to Kurrein [KUR27], one assumes that a “material band” of the thickness h_{eq} is separated from the workpiece with the cutting speed, the following results (Fig. 13.23).

Fig. 13.23 Equivalent chip thickness h_{eq}



$$Q_{wi} = h_{eq} \cdot a_p \cdot v_c. \quad (13.23)$$

From the mentioned identity

$$Q_{wa} = Q_{wi} \quad (13.24)$$

the equivalent chip thickness results at

$$h_{eq} = f_r \cdot \frac{v_{ft}}{v_c} \quad (13.25)$$

or with the speed relation $q = v_c/v_{ft}$

$$h_{eq} = \frac{f_r}{q} \quad (13.26)$$

h_{eq} is a mathematical variable, which does not indicate the actual cutting thickness but a far smaller one, since a continuous band is not cut from the workpiece, only single grains or cutting edges are effective.

According to M. C. Shaw [REI56], the average chip thickness at the grain resp. the cutting edge h_c can be determined from the number of grains resp. cutting edges N_A per unit area of the active grinding surface. If N_A is detected by counting the grains in the top view of the grinding wheel, the following assumptions are made:

- every grain participates in the cutting,
- every grain lies at the same height in the external diameter,
- every grain separates the overlapping volume that it penetrates on the workpiece. Elastic deformations and plastic displacement (ploughing) or chipping of material does not occur,
- every grain has a free contact length without any cutting overlapping with grains moving before or after (no path overlappings) occurring.

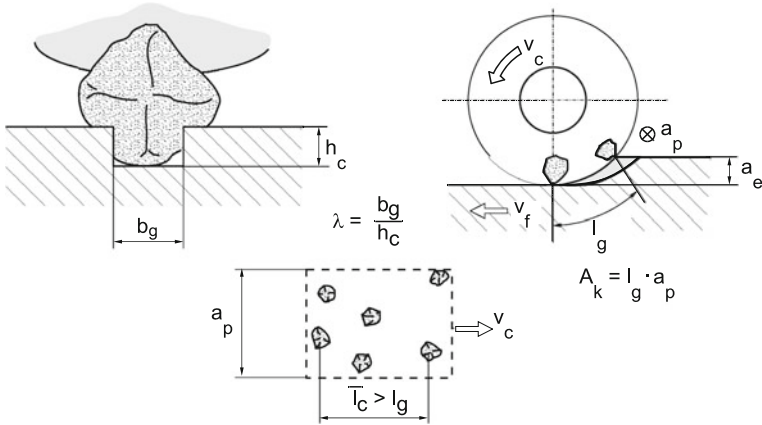


Fig. 13.24 Grain form and grain density

According to Fig. 13.24, the effective average cross-section of a grain is

$$A_g = b_g \cdot h_c \tag{13.27}$$

and with the form factor

$$\lambda = \frac{b_g}{h_c} \tag{13.28}$$

the total of the cross-section area A_c cut with the cutting speed is

$$A_c = \sum A_g = A_g \cdot N_A \cdot A_k = \lambda \cdot h_c^2 \cdot N_A \cdot a_p \cdot (2 \cdot f_r \cdot r_{eq})^{1/2} \tag{13.29}$$

at which A_k is the contact area with $A_k = l_g \cdot a_p$. Consequentially, equalizing the internal and external material removal rate results in $Q_{wi} = Q_{wa}$:

$$A_c \cdot v_c = f_r \cdot a_p \cdot v_{ft} \tag{13.30}$$

the average chip thickness

$$h_c = \left(\frac{v_{ft}}{v_c} \cdot \frac{1}{N_A \cdot \lambda} \cdot \frac{f_r}{l_g} \right)^{1/2} \text{ with } l_g = \sqrt{2 \cdot f_r \cdot r_{eq}} \tag{13.31}$$

Obviously, the assumption that all grains participate equally in the grinding process, i.e., with the same cross-section A_g , is actually not fulfilled; since the abrasive particles are generally arranged without rules within the bonding (except in a galvanic bonding). A further-going theory therefore considers the distribution of the grains perpendicular to the active grinding plane. Büttner and Triemel determined the grain distribution from the concentration of the grinding material in the volume of the grinding wheel [BÜT68, TRI76].

For the wheel volume V_s , the following applies

$$V_s = V_g + V_b + V_p \tag{13.32}$$

with the grinding material volume V_g , the bonding volume V_b and the pore space V_p . The composition is to be detected by an Archimedean weighting or from the manufacturer specification.

The number of grains per volume unit N_V can be defined as follows with the aid of the average volume of a grain V_{ge} or from the grain concentration C and the density of the grinding material ρ_g

$$N_V = \frac{V_g}{V_{ge} \cdot V_s} = \frac{C}{\rho_g \cdot V_{ge}} \tag{13.33}$$

The following applies for the volume of a grain with the shape factor q_e , which turns into $q_e = 1$ for the ball shape:

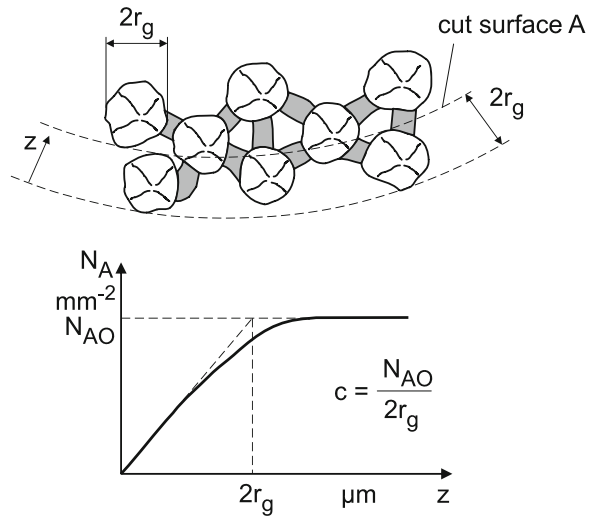
$$V_{ge} = q_e \frac{1}{6} \pi d_g^3 \tag{13.34}$$

According to Fig. 13.25, an imaginary area of size “1” in distance $z \geq d_g$ off the grinding wheel periphery is penetrated by a grain number N_{A0} . The following applies

$$d_g \cdot N_V \cdot \text{“1”} = N_{A0} \cdot \text{“1”} \tag{13.35}$$

$$N_{A0} = d_g \cdot N_V \tag{13.36}$$

Fig. 13.25 Grain distribution and grain density



At this it is pre-assumed that the volume-related grain density N_v is constant, independently from z . This does not apply to $z < d_g$. In fact, the area-related grain number N_A increases linearly with z in this domain. In addition, the limit value N_{A0} is already reached at a low penetration depth z into the grinding layer due to influences of the free edge. Figure 13.25 illustrates the gradient of the grain number per area unit above z

$$c = \frac{dN_A}{dz} = \frac{N_{A0}}{2r_g} \tag{13.37}$$

$$c_0 = N_v \tag{13.38}$$

It was possible to determine the grain density by measurement with a thermo-electric method [KAI75]. According to this, we can actually assume a constant grain density c_0 in the active cutting edge space (Fig. 13.26), which reaches down to a cutting edge space depth of $z \approx 0.3 d_g$. The cutting edge space depth decreases with an increasing cutting edge density, i.e., higher grain concentration, finer grains and higher grain holding capacity of the bonding.

The determination of the grain density resp. grain number per area unit from the grinding material concentration presumes that every grain has only one cutting edge. Depending on the dressing process and the type of bonding and the grinding material, a grain can develop several cutting edges [WER71, LOR75]. But even in that case, it is possible to assume with sufficient approximation that the cutting edge density is constant, i.e., the number of cutting edges per area unit increases linearly with the penetration depth into the cutting edge space. The chip thickness h_c can then be determined with the grain resp. cutting edge distribution.

With this knowledge of the cutting edge resp. grain distribution over the penetration depth into the active grinding space, an extended chip thickness model can

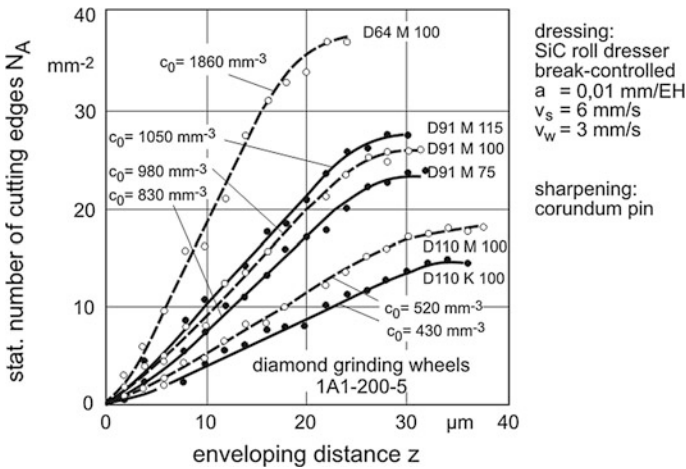
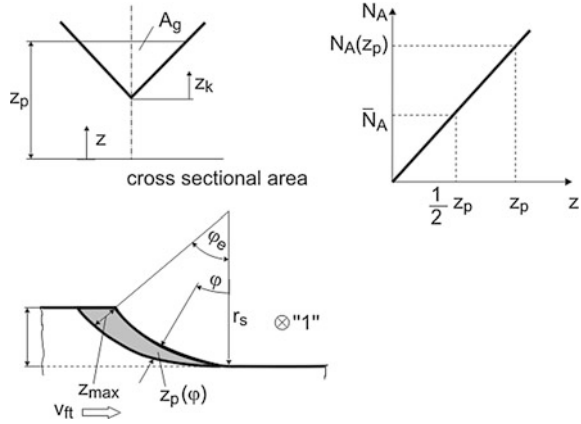


Fig. 13.26 Sum frequency of cutting edges in diamond grinding layers

Fig. 13.27 Grain shape, grain distribution and kinematics for the chip thickness model



be developed, based on the considerations of Büttner [BÜT68], Triemel [TRI76], Kassens [KAS69] and Lortz [LOR75].

The internal material removal rate results from the number of grains currently engaged N and the average cutting cross-section per grain A_g

$$Q_{wi} = N \cdot A_g \cdot v_c \tag{13.39}$$

An average grain shape with an obtuse angled cross-section (triangle) is assumed for the average grain cross-section (Fig. 13.27),

$$A_g = c_1 \cdot z_K^2 \tag{13.40}$$

with c_1 describing this grain shape. In principle, a different function, e.g., an exponential function as in [WER71] could be determined for A_g . However, since the determination of the average grain shape is only possible with limited accuracy in any case, this bears no advantage. The number of engaged grains results from the grain distribution with

$$N_A = c_0 \cdot z_p \tag{13.41}$$

where z_p is the penetration depth of a grain into the material (Fig. 13.27). Due to the constant grain density above z , the average number of grains per area at any position φ of the engagement bend is

$$\bar{N}_A = \frac{1}{z_p} \cdot \int_0^{z_p} c_0 \cdot z \cdot dz = \frac{1}{2} c_0 \cdot z_p \tag{13.42}$$

dN grains are active above a bend increment of the length $r_s \cdot d\varphi$ and the width "1".

$$dN = \bar{N}_A \cdot \text{"1"} \cdot r_s d\varphi \tag{13.43}$$

Due to the constant grain density, the average grain cross-section at a point φ is

$$A_{g(\varphi)} = \frac{1}{z_p} \cdot \int_0^{z_p} c_1 \cdot (z_p - z) dz = \frac{1}{3} c_1 \cdot z_p^2 \quad (13.44)$$

Thus, over the entire engagement bend, the sum of the grain cross-sections is

$$\sum A_g = \int_0^{\varphi_e} A_{g(\varphi)} dN = \frac{1}{6} c_0 \cdot c_1 \cdot \text{''1''} \cdot r_s \cdot \int_0^{\varphi_e} z_p^3 d\varphi \quad (13.45)$$

For the kinematics of the peripheral grinding, the following applies

$$\frac{\varphi}{\varphi_e} = \frac{z_p}{z_{\max}} \quad (13.46)$$

and with

$$\varphi_e \approx 2 \cdot \left(\frac{f_r}{2r_s} \right)^{1/2} \quad (13.47)$$

the sum of the grain cross-sections over the entire engagement bend is then $r_s \cdot \varphi_e$

$$\sum A_g = \frac{1}{12} \cdot c_0 \cdot c_1 \cdot \text{''1''} \cdot r_s \cdot z_{\max}^3 \left(\frac{f_r}{d_s} \right)^{1/2} \quad (13.48)$$

From $Q_{wi} = Q_{wa}$ results

$$f_r \cdot \text{''1''} \cdot v_{ft} = \sum A_g \cdot v_c \quad (13.49)$$

and thus finally the maximum grain penetration depth (cutting depth)

$$z_{\max} = \left(24 \cdot \frac{v_{ft}}{v_c} \cdot \frac{1}{c_0 \cdot c_1} \right)^{1/3} \cdot \left(\frac{f_r}{d_s} \right)^{1/6} = \left(24 \cdot \frac{1}{c_0 \cdot c_1} \cdot \frac{Q'_w}{v_c \cdot l_g} \right)^{1/3} \quad (13.50)$$

A simplified illustration of the correlations between the grain penetration depth and the manipulated variables of the grinding process illustrate the possibilities of influence on the cutting depth in the grinding process

$$z_{\max} \approx \frac{1}{d_g} \left(\frac{Q'_w}{c_1 \cdot v_c \cdot l_g} \right)^{1/3} \quad (13.51)$$

Further models on grinding forces, roughnesses and grinding energies can be established on the basis of this chip thickness model [WOB91, TÖN92, PAU94, FRI02].

13.6.2 Process Variables

The mechanical energy applied during the grinding process is almost totally transformed into thermal energy. This amount of heat can evoke geometrical deviations on the workpiece, alter its surface zone and accelerate the tool wear. Thus, the contact zone temperature represents an important process variable. It is, however, difficult to measure due to the rapid temperature changes and the resulting steep temperature gradients. In addition, the contact zone is not readily accessible and mostly surrounded by cutting liquid. In principle, the temperature measuring process can be differentiated into heat conduction and heat radiation. The most common methods are illustrated in Fig. 13.28 [KAR01].

Due to the necessity to measure as closely as possible to the contact point, the workpiece or the grinding wheel has to be prepared for all methods, which use heat conduction, and for the pyrometer measuring process. Therefore, the listed measuring methods are only applied in research. A direct temperature measuring method applicable in practise for process supervision does not exist until now. It is possible, however, to indirectly draw conclusions concerning the surface zone influence in the workpiece as described in Chap. 15. The temperatures mentioned in Fig. 13.29 are recorded during external plunge grinding with a minimum quantity lubrication (MQL) and without any kind of cutting lubrication with a thermographic system at a distance of 30 mm from the contact zone. The tests include different combinations of cutting and feed speed and material removal rates during the grinding process of ball bearing steel 100Cr6 with micro-crystalline Al_2O_3 and CBN grinding wheels.

In Fig. 13.29, the X-ray-measured workpiece residual stresses are set at the measured temperatures ϑ_M . The result is a uniform transfer function for different

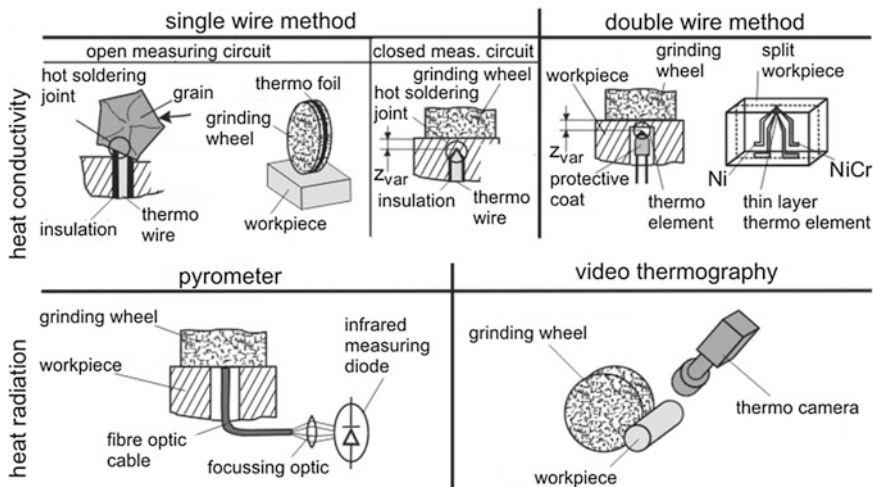


Fig. 13.28 Temperature measuring methods for geometrically-undetermined cutting (according to Karpuschewski)

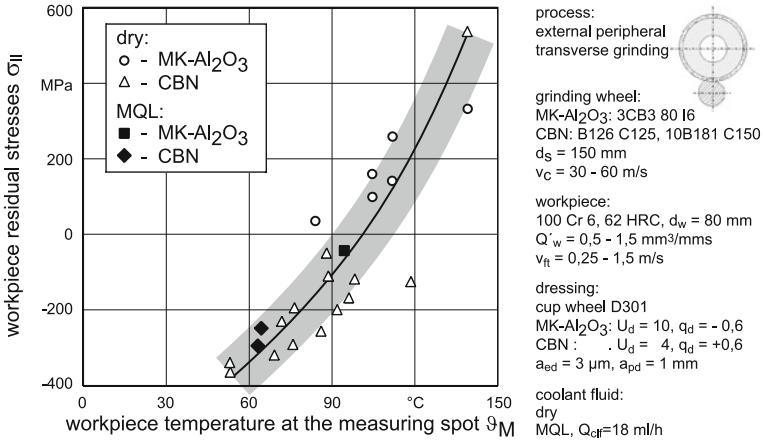


Fig. 13.29 Workpiece residual stresses depending on the workpiece temperature

tools and engagement conditions. Workpiece residual stresses between -400 and 500 MPa can be assigned to the temperatures. An increase of the temperatures and thus of the residual stresses can be detected at an increase of the material removal rate with any kind of grinding material. An increase of the measured temperatures is detectable at an increasing cutting speed and using the micro-crystalline Al_2O_3 grinding wheel. In CBN grinding, the variation of the cutting speed does not influence the temperature. A decrease of the workpiece temperature can be reached by increasing the workpiece speed (tangential feed speed). The differences between the two grain types can be explained with the different properties. CBN grains have a high wear resistance and heat conduction. Accordingly, the heat amount, which arrives inside the workpiece is lower, which results in lower workpiece temperatures [BRU98].

The mechanical power P_c is fed into the grinding process.

$$P_c = F_t \cdot (v_c \pm v_{ft}) \quad (+ : \text{up grinding} - : \text{down grinding}) \quad (13.52)$$

Since $v_c \gg v_{ft}$ generally applies, the following can be concluded:

$$P_c = F_t \cdot v_c \quad (13.53)$$

Apart from a negligible rest of $(1 - k_1) < 0.03$, which is transformed into dislocation energies and lattice distortion, i.e., residual stresses, this power is transformed into heat. The heat flow is $L = k_1 P_c$. This heat flow drains off via the tool L_s , the workpiece L_w , the chips L_{ch} , the cutting fluid L_f and the environment L_r . The main proportion is absorbed by tool and workpiece [CHO86].

$$L_s + L_w = k_2 \cdot L, \quad (13.54)$$

$$k_2 \approx 0.8 \div 0.9 \quad (13.55)$$

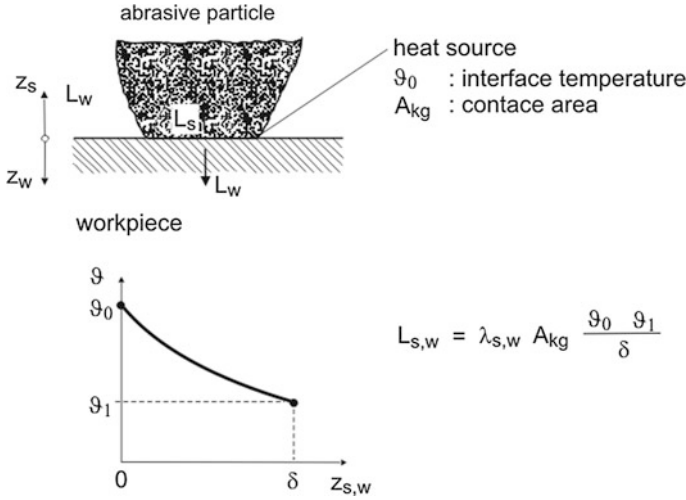


Fig. 13.30 Energy balance on the abrasive particle

A simplified consideration of both parts is useful to explain the different thermal surface zone influences in the case of conventional grinding materials and boron nitride (Fig. 13.30). At this, a unidimensional, stationary heat conduction is pre-supposed and that the same temperature ϑ_1 prevails in the media involved at a distance $\delta_s = \delta_w = \delta$ from the contact plane. Then the following applies:

$$L_{s,w} = \lambda_{s,w} \cdot A_{kg} \frac{\vartheta_0 - \vartheta_1}{\delta} \tag{13.56}$$

with the heat conduction co-efficients $\lambda_{s,w}$. The following results from $k_2 \cdot L = L_s + L_w$:

$$L_s = \frac{k_2 L}{1 + \lambda_w / \lambda_s} \tag{13.57}$$

$$L_w = \frac{k_2 L}{1 + \lambda_s / \lambda_w} \tag{13.58}$$

For grinding materials with different heat conductions, such as corundum with λ_{sk} and boron nitride with λ_{sb} , the following results for the heat flows L_{wk} , L_{wb}

$$\frac{L_{wk}}{L_{wb}} = \frac{\lambda_w + \lambda_{sb}}{\lambda_w + \lambda_{sk}} \tag{13.59}$$

For the media steel ($\lambda_w = 50$ W/mK), corundum ($\lambda_{sk} = 29$ W/mK) and boron nitride ($\lambda_{sb} = 1,300$ W/mK) follows

$$\frac{L_{wk}}{L_{wb}} = 17 \tag{13.60}$$

This means that when grinding with corundum, the 17-times heat amount flows into the workpiece compared with boron nitride. The grinding wheel based on boron nitride quasi acts as a scoop wheel for the heat energy due to the good heat conduction.

13.6.3 Output Variables

Grinding wheels wear. Grain and bonding wear occurs. The following types of wear can be differentiated for grain wear:

Pressure softening: This phenomenon can occur with corundum, which does have a melting point of 2,050 °C, but whose strength already drops to a sixth of its compression strength at 1,200 °C compared with room temperature [STA62]. As a consequence of the pressure softening, high friction forces and rounded cutting edges occur, which additionally increases the chip formation temperatures. An unstable condition may be the consequence, which leads to a failure of the grinding wheel. The volume or radius wear is low.

Abrasion: As a consequence of the friction between grain and workpiece, mechanical abrasion occurs (Fig. 13.31). The grain is continuously removed and also produces undesired, because friction and shear force increasing, rounded cutting edge in this case. The volume or radius wear is low.

Splintering: Due to the thermal load and following rapid cool-off, but also due to mechanical load at a sufficient splintering capacity of the abrasive particle, parts

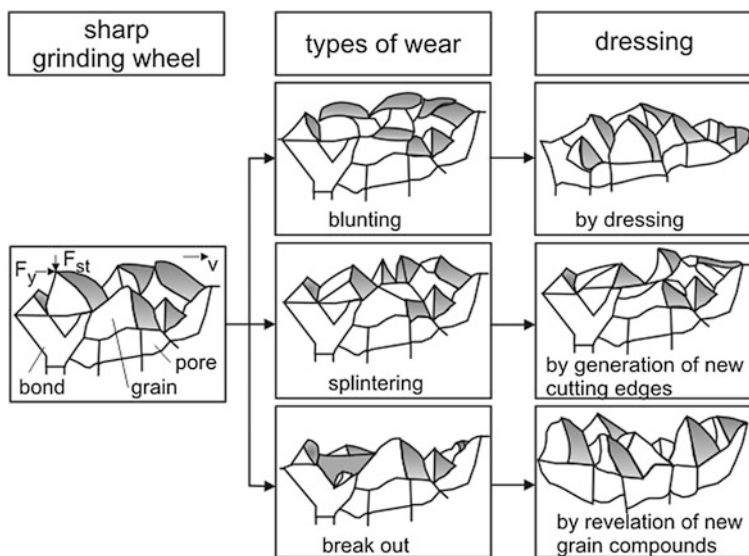


Fig. 13.31 Types of wear and sharpening in the grinding process

of the grains splinter and thus produce new cutting edges. This type of wear is therefore favourable, since the volume and radius wear is actually higher compared with the pressure softening and the abrasive wear, but still sufficiently low and sharp cutting edges develop nevertheless. The capacity of splintering can be marked with the friability test (see Sect. 13.2).

Breaking out: In this type of wear entire grains break out of the compound. The holding force of the bond is not enough, the bond is too soft. Strong volume and radius wear occurs. The grinding wheels do, however, maintain their grindability.

The wear of a grinding wheel is recorded numerically by the volume wear V_s or the radius wear Δr_s . The volume wear is directly included in the grinding ratio or the performance factor.

$$G = \frac{V_w}{V_s} = \frac{Q_w}{Q_s} \quad (13.61)$$

The G-ratio is dependent on the material of the workpiece, the grinding tool, the engagement variables, the conditioning and the grinding fluid among others. It therefore deviates within wide limits. When grinding with corundum on hardened steel 100Cr6 under average conditions and emulsion as grinding fluid, a G-ratio of 80 can be expected. When using CBN and under mineral oil, the G-ratio can be increased to 3,000 and more [GRA87].

In dimension and form precision grinding, the radius wear is mostly more considerable. That is the local abrasion of the grinding wheel after a certain grinding task or grinding time. The average radius wear speed is correlated with the grinding ratio, which results from a volume balance:

$$\frac{\Delta r_s}{\Delta t} = \frac{1}{G} \frac{f_r \cdot v_{ft}}{2\pi r_s} \quad (13.62)$$

Fine machining processes such as grinding generally produce surfaces for their final and usage condition. As explained in Chap. 16 about surface properties, the function properties of components, are fundamentally determined by geometrical and physical properties of their surfaces. Here, it is the question whether and how these properties can be achieved by means of the grinding process and its input variables.

The micro-geometrical surface formation can be described by different parameters such as the roughness parameters R_z and R_a , the bearing contact area ratio and others (see Chap. 16), depending on which function of the surface is essential. Often, the average roughness R_z is specified. In Fig. 13.32, the influences of some input parameters on the surface quality are stated concerning quality. Basically, the surface produced by grinding is connected with the micro-topography of the grinding wheel and the kinematic conditions, which the cutting edges are moved at on the workpiece. A first approximation as a dimension for the surface formation is the cutting thickness resp. the penetration depth of the cutting edges, as modelled in Sect. 13.7.1.

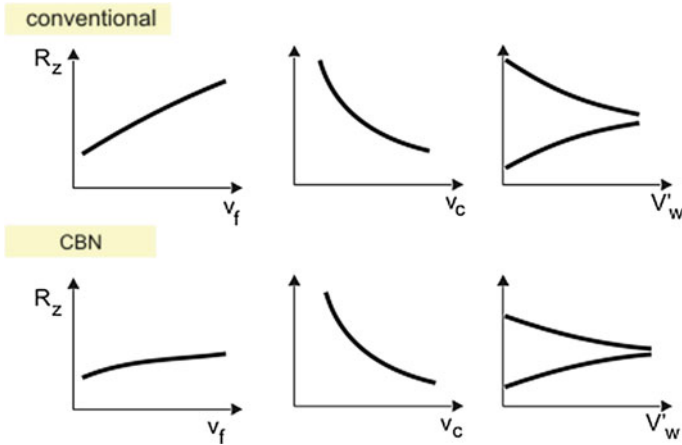


Fig. 13.32 Influence of the adjustment variables on the workpiece roughness

With regard to the wear behaviour Fig. 13.32 differentiates between conventional and super hard grinding materials, at which the same trends can be determined for both, although with CBN, the alterations of the roughness parameters are considerable stretched time-wise [HEU92]. The schematic illustrations show that the roughness increases with increasing feed speed, which can be ascribed to the increase in cutting thickness. For the influence of the cutting speed the corresponding is valid: when it is increased, the cutting thickness decreases. The grinding time resp. the cutting volume V'_w has an ambivalent effect according to the original microtopography of the grinding wheel, as Weinert demonstrated [WEI76] (see also Sect. 13.7.2). With a rough wheel, a smoothing effect shows after an originally higher roughness. Vice versa, with a very smooth wheel, a roughing and thus an increase of the roughness occurs on the workpiece due to wear effects.

Apart from this kinematic approach, the material behaviour is to be considered, namely whether the material tends towards ductile or brittle deformation and separating behaviour under the given process conditions (cutting thickness, temperature distribution). Investigations on one-grain-scratching brittle-hard materials have demonstrated that below a certain scratching normal force, any number of long, tear-free, plastically deformed scratching traces show on the component. At higher scratching normal forces resp. cutting thicknesses, directly after the scratching process load relief tears break open in the area behind the cutting edge due to residual tensile stresses and increasingly lead to brittle material separation (Fig. 13.33). In principle, these conclusions can be transferred to the grinding process, where a large number of abrasive particles is engaged [ROT94]. At this, the size of the average single grain cutting thickness has a decisive influence on the occurring material separation. Lower single grain cutting thicknesses—e.g., produced by using fine-grained grinding wheels—cause a rather ductile material separation, whereas the use of coarse-grained grinding wheels increasingly leads to brittle material separation [LIE98].

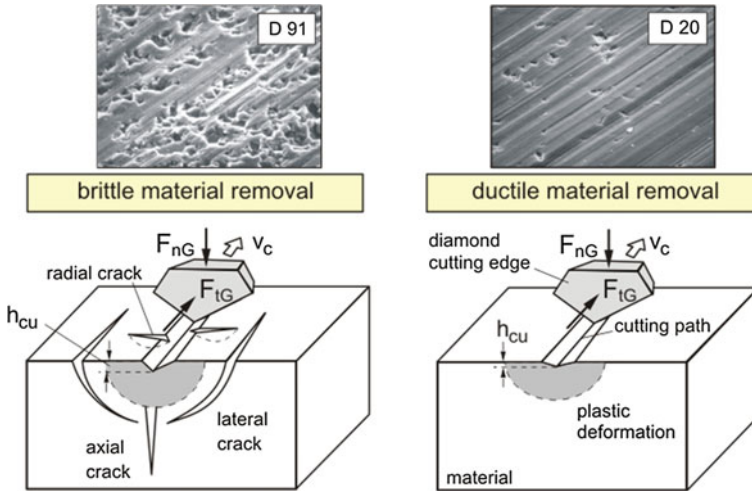


Fig. 13.33 Material separation mechanisms on brittle-hard materials (according to Lawn and Marshall)

The quality of ground components not only depends on the compliance with dimension and form tolerances and a required surface quality, but also on the physical properties of the workpiece surface zone. The physical surface zone properties are determined as the structure condition and the residual stresses in the surface near layers of the machined workpiece [BRI82]. Hardness alterations can also provide information about the structure of the surface zones. High thermal influences can lead to the loss of hardness or—under extreme conditions—even to new hardening zones with underlying soft skin. Such structure alterations significantly deteriorate the usage properties of the components, in addition, steep hardness gradients in connection with surface residual stresses can cause cracks in the component [BRI91] (see Chap. 16).

The superposition of thermal and mechanical effects on the development of residual stresses is explained by *Brinksmeier* by applying residual stresses above the contact area-related grinding power P'_c [BRI91]. The power results from the product of the relative speed between workpiece and grinding wheel and the tangential force F_t . It is referred to the contact surface formed by the engagement width a_p and geometrical contact length l_g .

$$P'_c = \frac{F_t \cdot (v_s \pm v_{ft})}{a_p \cdot l_g} \text{ (W/mm}^2\text{)} + \text{down grinding} - \text{up grinding} \quad (13.63)$$

If the workpiece speed is considerably lower than the grinding wheel speed, the obtained grinding power can be calculated with a good approximation as follows:

$$P'_c = \frac{F_t \cdot v_c}{a_p \cdot l_g} \text{ (W/mm}^2\text{)} \quad (13.64)$$

At very low grinding power, at first only thermally-conditioned residual stresses by means of external friction are to be expected. Plastic deformations caused by mechanical load lead to the development of residual compressive stresses. The temperatures, which rise with increasing grinding power, reduce the residual compressive stresses maximally induced by mechanical effect and, at the same time, lead to a continuously growing dominance of the terminally-conditioned residual tensile stresses. The thermal and mechanical influences overlap in a highly non-linear way so that a simple superposition is inadmissible and the illustration can only be schematic. A lower thermal load of the component leads to a more favourable course of the resulting residual stresses. This effect can be obtained by exchanging the grinding material or cutting liquid or by reducing the cutting speed or the material removal rate [BRI91].

Heuer [HEU92] demonstrates the limits of this model notion. An increase of the tangential feed speed at a constant cutting speed can lead to higher contact surface related grinding powers at a parallel lower residual stress level. *Karpuschewski* therefore considers the heat penetration time and defines a path energy (energy per unit path) as the effect referring to a cutting volume unit and describes the resulting residual stress condition as follows (k : transfer coefficient) [KAR95]:

$$\sigma_{||} = k \cdot \frac{e_c \cdot a_c}{l_c} \text{ (MPA)} \quad (13.65)$$

Another approach for the description of the energies converted in the grinding process and their effects on the residual stresses remaining within the component is proposed by *Lierse* [LIE98]. He applies observations from the welding and laser technology, at which the contact time on the surface is directly considered for the calculation of a contact area-related energy and uses the parameter

$$E_c'' = P_c'' \cdot t_k = P_c'' \cdot \frac{l_g}{v_{ft}} = \frac{F_t \cdot v_c}{a_p \cdot v_{ft}} \text{ (J/mm}^2\text{)} \quad (13.66)$$

during his investigations on mechanic and thermal effects in grinding of technical ceramics.

The thermal workpiece damage in grinding machining is influenced by the settings of the adjustment and system variables. Not only the primary process variables influence the thermo-physical processes while grinding. Also variables, which influence the grinding wheel topography decisively and thus also the described elementary processes during cutting, act on the development of thermal damages [BRI91]. This is also detectable for the used cutting fluids and their adjustment variables [GRA87, HEU92].

Basically it can be determined that any change in the contact zone between grinding wheel and workpiece affects the developing surface zone influence. Each one of these factors influences either the heat produced by cutting or the occurring forces resp. the heat distribution and thus causes a different influence, which can be determined by the developing residual stresses [BRI91]. For the layout of a

grinding process, it is necessary to avoid residual tensile stresses so as not to influence the functional behaviour of the components negatively (see Chap. 14).

In the following, the influence of important adjustment variables of the grinding process on the residual stress development in the machined workpiece will be described. At this, exclusively residual stresses parallel to the grinding direction will be consulted, since these mostly show bigger amounts in the direction of residual tensile stresses and are therefore considered more critical for the component behaviour [HAU80]. In Fig. 13.34, the residual stresses at the workpiece surface are illustrated for different related material removal rates via the cutting speed and the residual stress depth curves for different speed ratios. In the case of both large related material removal rates illustrated, an increase in the cutting speed leads to a drop of the measured residual stresses. For the low set material removal rate, residual compressive stresses exist for all conditions. The formerly discussed reduction of the cutting thickness and thus of the grinding forces at an increase of the cutting speed leads to a reduction of the residual stresses remaining on the workpiece surface for high related material removal rates. Although the cutting power necessary for cutting increases together with the increase of the cutting speed, the higher thermal power apparently does not have an effect on the residual stresses in the considered area.

The thermal and mechanical influence on the component material due to the grinding is not only limited to the immediate surface. According to the type and extent of the load, it has a varying depth effect [TÖN65]. For the evaluation of a grinding process, an analysis of this effect is of special interest, since higher residual stresses might exist below the surface, which means a strong damage of the component. For the interpretation of grinding processes it is necessary to

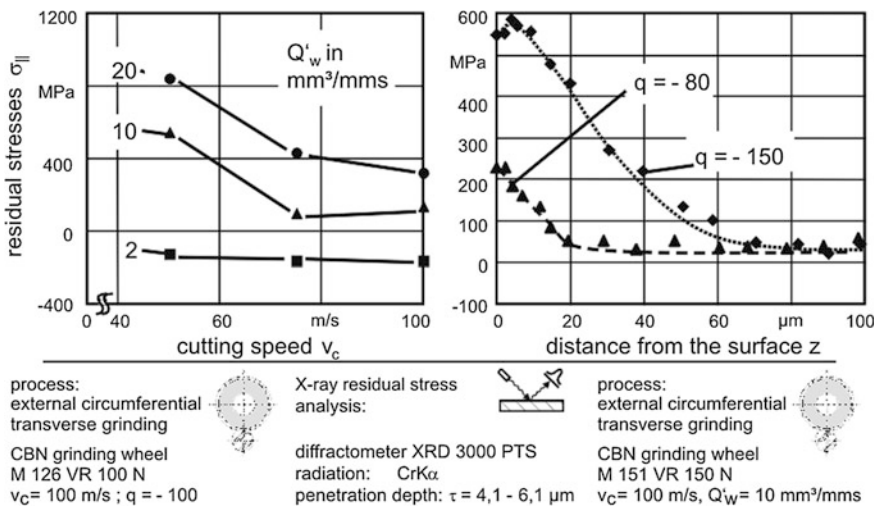


Fig. 13.34 Influence of the cutting and workpiece speed on the workpiece residual stresses of hardened components

possess knowledge of the depth effect of the adjustment variables. The influence of different speed conditions at a constant material removal rate can be gathered from the right part of Fig. 13.34. A higher speed ratio is achieved by reducing the workpiece rpm at the same cutting speed. As a consequence, the residence time of the heat produced by cutting is shorter than in the case of low speed conditions. The effect is clearly visible in the picture. The longer heat effective time leads to higher residual compressive stresses with a higher depth effect in the workpiece [CZE99].

The residual stress depth courses of different related material removal rates are illustrated in Fig. 13.35. At a low material removal rate of $Q'_w = 2 \text{ mm}^3/\text{mms}$, residual compressive stresses occur at the surface. The depth effects of these mainly mechanically-conditioned residual stresses are but very low and amount to approx. $15 \mu\text{m}$. The stress course shows a high gradient until the surface zone influenced by the compressive stress and then adopts the residual stress parameters of the basic compound. The hardness depth course and the grinding pattern of this sample also correspond to that of the undamaged basic compound.

At an increase of the related material removal rates to $Q'_w = 10 \text{ mm}^3/\text{mms}$, the influence of the thermal load prevails compared with the mechanical load component. Only residual tensile stresses in the material are measured. The residual stress course drops from about 200 MPa residual tensile stresses at the surface about linearly to the condition of the basic compounds. The higher temperature introduced into the workpiece at this material removal rate leads to residual tensile stresses at the workpiece surface with a depth effect of $20 \mu\text{m}$. In the micrograph, some annealing texture is recognisable at the workpiece edge and the measured hardness variables in the edge zone are lower than that of the undamaged original texture.

By means of an additional increase of the heat generated in the grinding process by a material removal rate of $Q'_w = 20 \text{ mm}^3/\text{mms}$, the heat effective depths and the maximum values of the residual tensile stresses increase considerably.

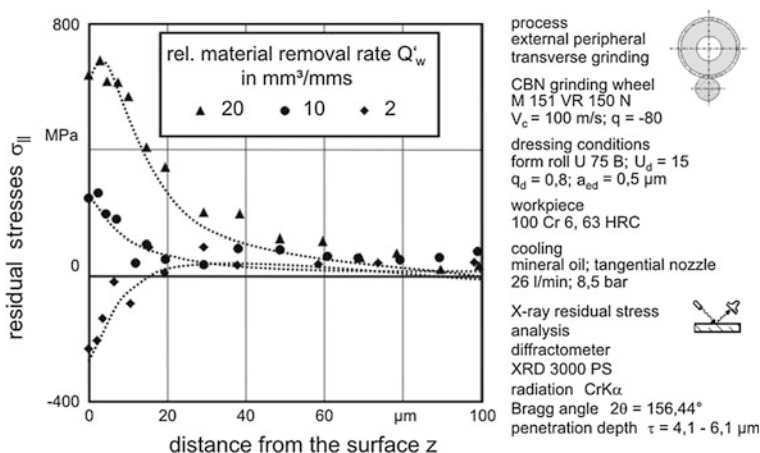


Fig. 13.35 Influence of the related material removal rate on the workpiece residual stresses

The radial spreading of the annealing texture rises analogically to the heat development. Due to the temperature effect, an annealing of the hardened texture occurs, which loses hardness because of the temperature-conditioned texture transformation. The temperature produced by the grinding process reaches values, which lead to the development of rehardening zones. An increase in hardness due to the rehardening is not detectable in the hardness course, since this zone is limited to few μm of depth. A measurement of the material hardness in this small area is not feasible.

13.7 Conditioning of Grinding Tools

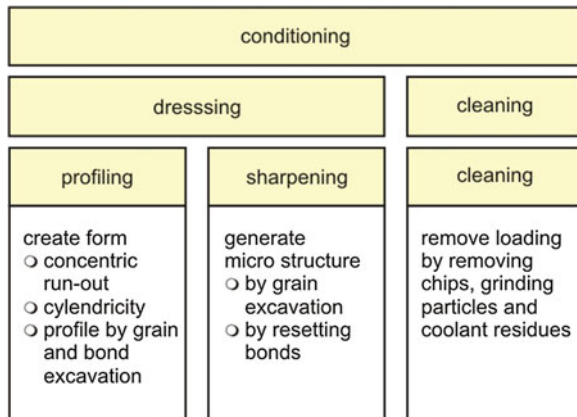
13.7.1 Basics

Wear by splintering or break out of particles or wear caused by bonding erosion leads to the resharpening of grinding tools. This effect may be desired for rough grinding so as to avoid a conditioning of the tool. However, in finishing and fine grinding, conditioning is generally indispensable (E. Saljé: “If you cannot condition, you might as well not even start grinding”). The conditioning can serve three purposes (Fig. 13.36) [SPU89].

Profiling: This is about the restoration or new generation of a grinding wheel contour. If the cylindricity or the concentricity get lost or waves develop on the active grinding surface due to the wear of a grinding wheel, profiling becomes necessary, i.e., in this case a cylindric surface is generated. By profiling, even non-cylindric tool shapes can be generated for profile grinding. Profiling acts macro-geometrically.

Sharpening: If grinding tools are no longer suitable for grinding due to rounded cutting edges or loading (clogging of the chip spaces), sharpening can generate a new layer of particles or cutting edges. Sharpening acts micro-geometrically.

Fig. 13.36 Conditioning of grinding wheels (according to G. Spur)



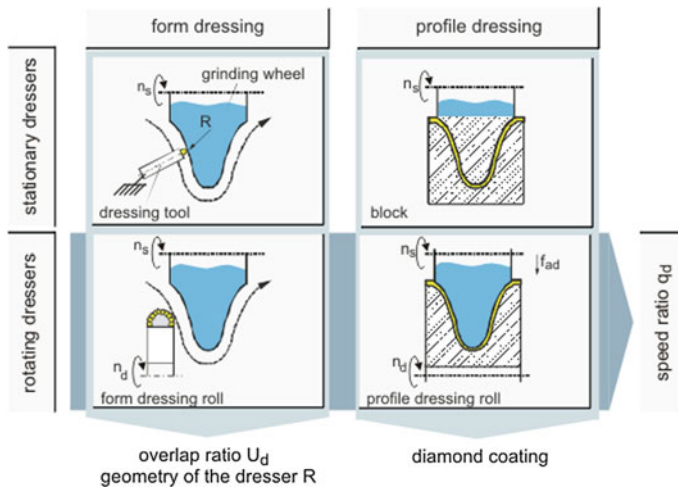


Fig. 13.37 Dressing process (according to Dr. Kaiser GmbH, Celle)

Cleaning: Cleaning removes residue consisting of workpiece and tool material or cutting liquid deposits. Cleaning does not alter the topography of the grinding tool; neither the particles nor the bonding are removed.

Profiling and sharpening together are also called dressing. Since in finishing or fine grinding the chip formation all the resulting effective parameters depend decisively on the dressing, i.e., the type and the adjustment parameters of this process, a grinding process can never be regarded by itself but must always be seen as a combination of conditioning/dressing and grinding.

Figure 13.37 illustrates dressing processes, which are distinguishable according to their kinematic resp. form generation [KAI09].

Grinding wheels can be dressed with rotatory and non-rotatory, fixed tools (Fig. 13.37). A second aspect of order is the type of shape generation. We distinguish form dressing, i.e., the controlled operation of the dressing tool, and profile dressing, at which the dressing tool receives the contour of the profile by copying.

Dressing tools can be handled with one or several cutting edges (consisting of one or several particles) (Fig. 13.38). The illustration shows the typical application of the Diaform process, at which the profile of the grinding wheel is generated by the controlled dressing of single diamonds.

The cutting elements consist of artificial or natural diamonds and are cased in a metal matrix. These diamonds can be coarse, form-cut or exist in another geometrically defined condition. They can be arranged in a stochastic distribution or according to a defined pattern on cylinder-, board- or slice-shaped carriers.

Form rolls are rotating dressers studded with diamonds at the circumference (Fig. 13.39). They are bi- or triaxially controlled so as to generate the wheel profile. Due to their multi-studding with diamonds, their durability is considerably higher than that of a single diamond. An additional advantage is that they are

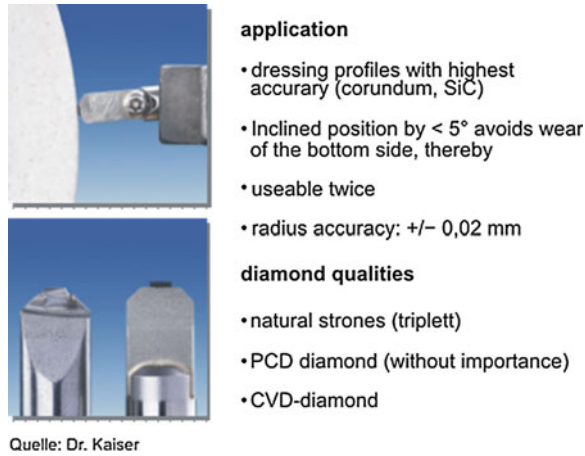


Fig. 13.38 Single particle dressers (works photo Dr. Kaiser GmbH, Celle)

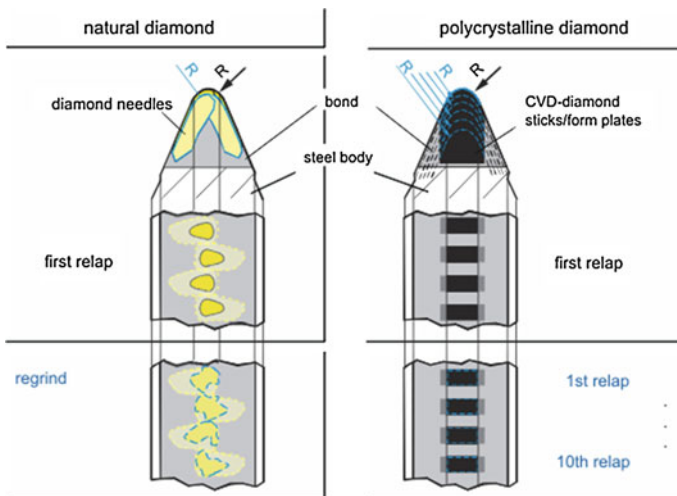


Fig. 13.39 Form rolls with set natural and poly-crystalline diamonds (works photo Dr. Kaiser GmbH, Celle)

largely independent from the profile to be generated. Therefore, they are suitable for small and medium-sized series. For large series, rotating profile tools, diamond profile rolls are used (Fig. 13.40). They bear the contour of the wheel profile. Due to the mostly necessary high-precision machining of such profile rolls and because of the entirely circumferential diamondization they are expensive, but do have a high durability and permit short dressing times, since only a short radial infeed is required.

Fig. 13.40 Profile roll with workpiece (works photo Dr. Kaiser GmbH, Celle)



Further differentiating factors for dressing tools are the deployed bonding systems (electro-plating or sintering bonds), the possibilities of diamondization (stochastic distribution by spreading, regular distribution by hand setting and one- or multi-layer tools) and the number of diamonds on the dresser in carat per cubic millimeter determined by the coating density. The properties of dressing tools, the influences of the adjustment parameters during dressing and practical deployment recommendations are clearly compiled by Minke [MIN99].

Basically, dressing corresponds to turning (Fig. 13.41). With the dressing feed f_{ad} and the intervention width a_{pd} , an overlapping ratio U_d can be defined as

$$U_d = \frac{a_{pd}}{f_{ad}} \tag{13.67}$$

The engagement width follows from

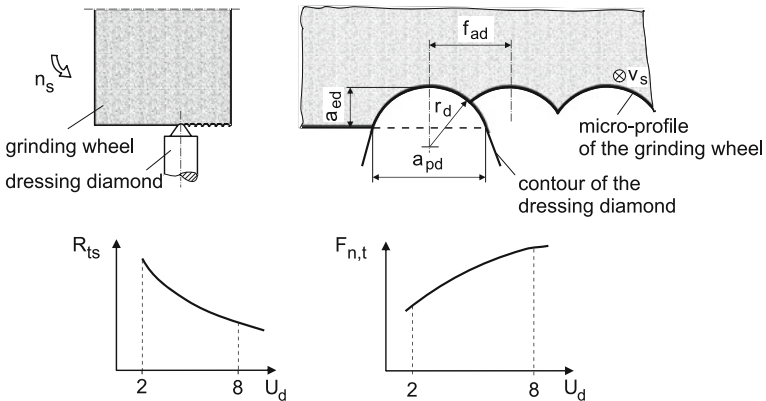


Fig. 13.41 Dressing with single diamonds

$$a_{pd} = 2 \cdot (2 \cdot r_d \cdot a_{ed} - a_{ed}^2)^{1/2} \quad (13.68)$$

and the dressing feed with the grinding wheel rotary frequency n_s at

$$f_{ad} = \frac{v_{fad}}{n_s}. \quad (13.69)$$

Common settings when dressing vitrified bonded grinding wheels are [MAG08]:

$$f_{ad} \leq 0.2 \text{ mm}, a_{ed} = 10 \mu\text{m} \div 30 \mu\text{m} \quad (13.70)$$

The effective parameters can be influenced in large areas with the degree of overlapping (overlap ratio) (Fig. 13.38), since the effective roughness of the active grinding surface and thus the number of active cutting edges of the grinding tool are strongly altered. The effective roughness R_{ts} is used to describe the cutting edge space topography of a grinding wheel. To determine this parameter, a test workpiece with fixed parameters is machined with the grinding wheel. The maximum roughness measured on the test workpiece produce the effective roughness of the grinding wheel [SCH68]. The effective roughness R_{ts} of the grinding wheel is

$$R_{ts} = \frac{f_{ad}^2}{8 \cdot r_d} \quad (13.71)$$

A higher degree of overlapping generates more active cutting edges with lower roughnesses on the workpiece. The forces and required power rise.

13.7.2 Conditioning of Conventional Grinding

Conventional grinding tools can generally be profiled and sharpened at the same time by the dressing tools shown in Fig. 13.37. The influence of the set conditions continuously gets lost with increasing grinding duration. The active cutting space of the grinding wheel changes due the occurring wear. The connected effects on the effective roughness of the grinding wheel at differently related material removal rates and dressing conditions for a fixed dresser are illustrated in Fig. 13.42. Depending on the initial effective roughness $R_{t,s0}$ of the grinding wheel caused by the dressing, with increasing grinding time, the grinding wheel tends towards a stationary roughness, which is independent from the dressing conditions. The upper part of the picture shows that at a constant roughness of the grinding wheel, with deployment time, different final roughnesses develop due to a wear-conditioned alteration of the cutting area. Vice versa, the lower part of the picture shows that, with deployment time, the initial roughness is altered and tends towards a stationary value. The cutting area of the grinding wheel quasi loses its memory [WEI76]. For the practical use in serial production it is of interest that a

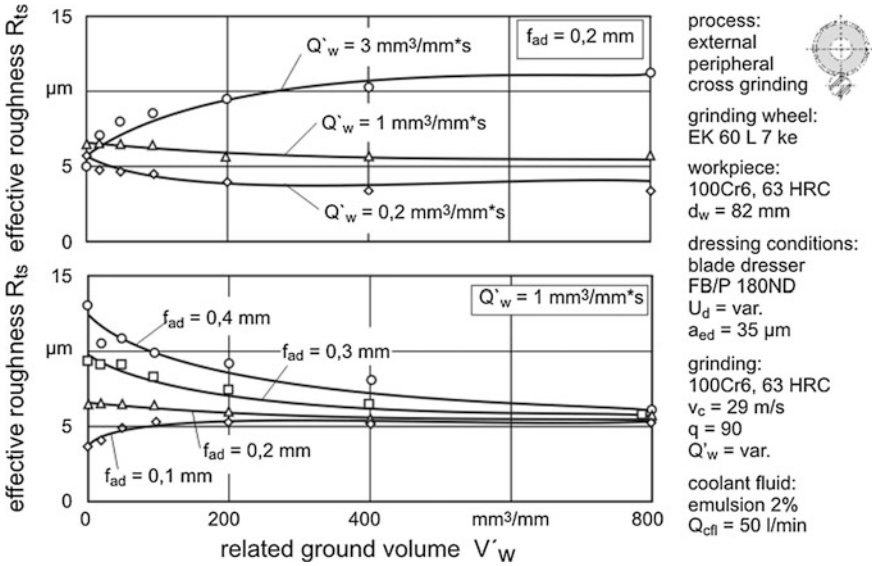


Fig. 13.42 Effective roughness depending on the related cutting volume for different adjustment parameters (according to K. Weinert)

steady grinding result can be obtained by means of the dressing strategy by hitting the stationary roughness already when dressing. On the other hand, very different roughnesses can be achieved in small batch production with the same wheel (grit size) due to the dressing [VER79].

The dressing of conventional grinding wheels with rotating tools is frequently used to condition profile wheels. At this, it is possible to work with a diamond studded dressing wheel analogue to the dressing with a single-grain diamond, at which the wheel has to be path-controlled in at least two axis or the profile to be generated contained in a diamond profile roll. The latter process is generally deployed in large serial production due to the high costs for the profile roll. Figure 13.43 illustrates the dependence of the initial effective roughnesses $R_{t,s0}$ of the grinding wheel profile achievable when dressing with profile rolls depending on the two parameters dressing speed ratio and radial dressing feed per rotation of the grinding wheel.

During the dressing process, the diamonds of the roll move in relation to the grinding wheel on cycloidal paths. At this, the shape of the curves depends on the speed ratio. If the diamond grains penetrate more steeply into the grinding wheel, the roughness of the grinding wheel increases. In same direction ($q_d > 0$), strongly bent paths develop in the area of the contact point, whereas the paths are elongated in the counter direction ($q_d < 0$). Analogue to these bends, greater effective roughnesses appear in the counter direction than in the same direction [SCH68]. With rising parameters for the radial dressing feed, the initial effective roughness also increases, whereas the roughness course maintains its basic tendency above

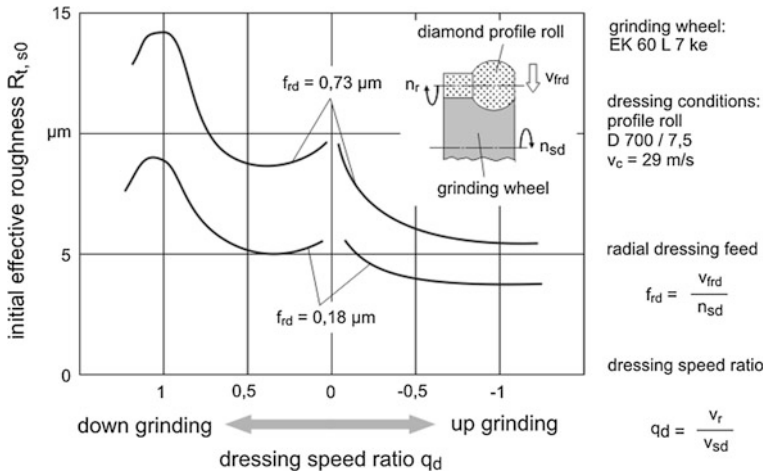


Fig. 13.43 Influence of the dressing conditions on the initial effective roughness in case of diamond profile rolls (according to Schmitt)

the feed speed ratio. In the case of the dressing speed ratio $q_d = 1$, a rolling-off (crushing) takes place between the grinding wheel and the diamond roll. At this, the abrasive particles and the bonding at the circumference of the grinding wheel are crushed and the initial roughness reaches a maximum parameter. In contrast, at the ratio $q_d = 0$, the diamonds of the roll cause pronounced marks, which only cover each other slightly in axial direction. A high waviness appears in axial direction, which is the cause for the roughness increase [SCH73].

13.7.3 Conditioning of Super Hard Grinding Wheels

While profiling and dressing is carried out in one step with conventional grinding materials, super hard grinding wheels frequently require consecutively operated processes, because generally a sufficient exposure of abrasive particles concerning the bonding level of the grinding wheel cannot be achieved due to the profiling process [TÖN79].

The processes for profiling are partitioned into profiling tools, which can either contain diamonds or not (Fig. 13.44) [FRI99]. For the profiling of linear profiles, profiling with silicon carbide (SiC) roll is a common and economic process. The relative speed between profiling roll and grinding causes a mechanical abrasion. At this, the drive of the SiC roll occurs either by friction of the effective partners and is decelerated by means of a centrifugal force brake or the profiling unit possesses its own drive. In crushing, a steel or hard metal roll is deployed as a form or profile tool. The crushing roll is then pressed against the grinding wheel axially parallel and carried along by friction, at which no relative speed v_{rel} should occur between

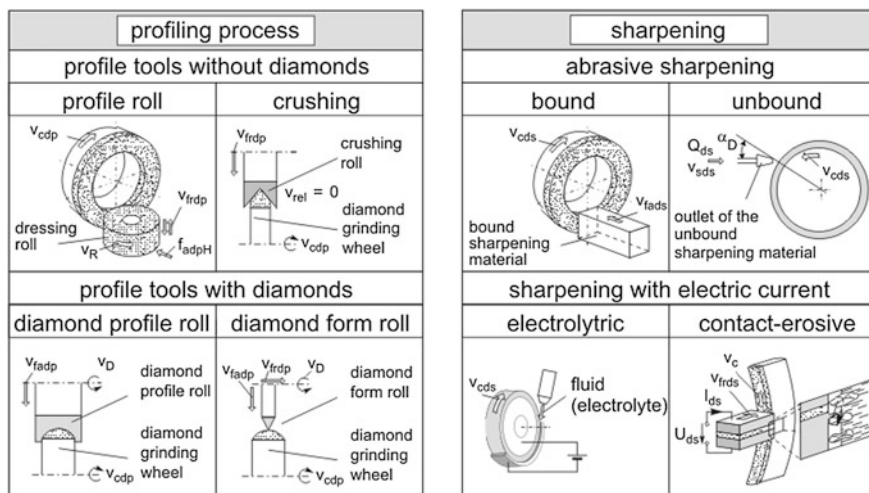


Fig. 13.44 Profiling and dressing processes for super hard grinding wheels

the effective partners. Vitrified or especially crushable (sufficiently brittle) metal bondings are necessary for this process. The use of tools containing diamonds allows a profile-representing (diamond profile roll) as well as a path-controlled (diamond form roll) profiling. Since the contact with the grinding wheel bonding reduces the durability of diamond dressing tools, it is generally recommendable to sharpen the grinding layer at the same time [TÖN75]. Point-crushing is a process, which is based on the engagement conditions of dressing with a form roll and the effective mechanisms of crushing. At this, the abrasive wear on the dressing tool is reduced by directing the relative speed between the effective partners towards zero or at least to a minimum.

Nowadays, rotating diamond dressing tools are increasingly used for the dressing of grinding wheels with vitrified bonding. The deployment of fixed dressing tools is irrelevant for super hard grinding wheels (especially diamond) due to the high wear. The dressing processes for super hard grinding wheels can be differentiated into abrasive processes and processes, which are based on the effect of electric current (Fig. 13.44).

The functional principle of dressing with a dressing block, also called block dressing, is based on the use of a bar-shaped dressing tool made of corundum or silicon carbide in vitrified or synthetic resin bonds. At this, the bonding material is set back due to the abrasive effect of the dressing material and the outermost abrasive particles are exposed.

In the so-called blast dressing process, a blasting material made of loose corundum or silicon carbide grain is blast onto the grinding surface with a bearing liquid (generally cutting liquid). At this, the targeted grain exposure occurs via the type and amount of dressing material as well as through the effective angle of the abrasive jet [UHL93].

Apart from the abrasive processes, dressing with electrolyte is becoming increasingly important for the dressing of very fine-grained diamond grinding wheels. For in-process dressing, it is called ELID-grinding [TIO90, OHM95]. The basic principle is based on the anodic ablation of bonding material in an electrolytic reaction. The grinding wheel, which is charged with a direct current via a brush system, represents the anode in this process. The gap between anode and cathode is filled with an electrolytic liquid and by means of the applied high-frequency pulsed operating current, electro-chemical ablation of the bonding material in the grinding layer takes place.

Another process based on the effect of electric current is contact erosion or electric erosion. The basic requirement for the deployment of dressing technology is an electrically-conductive bonding material. An electrode of conductive material, which is cut by the embedded grains, is fed to the grinding layer. Due to the applied stress, an electric field extends between the electrode and the grinding layer [FAL98], at which field distortions occur due to the cut electrode particles. Field exaggerations develop, which allow for a spark discharge between the electrode and the bonding material of the grinding wheels and, at this, cause a thermal ablation of the bonding material [FRI99].

Considering the timely order, we can differentiate between pre- and in-process dressing, i.e., the dressing takes place at the same time as the grinding process. The effects of the in-process dressing by means of a dressing block are illustrated in Fig. 13.45 in the machining of ceramic. The dressing process without the deployment of in-process dressing technology is characterised by increasing dressing forces, which can be attributed to the effective wear mechanisms such as clogging and grain blunting.

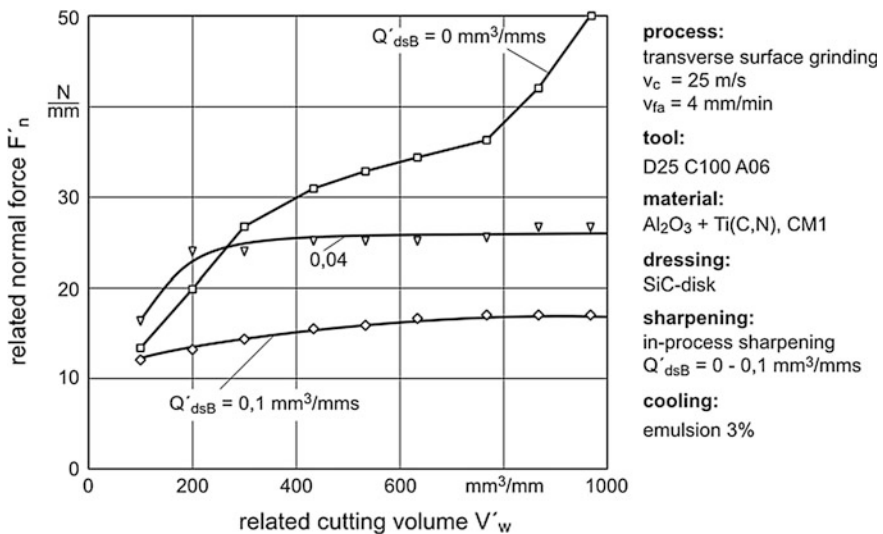


Fig. 13.45 Influence of the block dressing material removal rates Q_{dsB} on the process course

The use of in-process block dressing can minimise the influences of the wear mechanisms. Depending on the selected block dressing material removal rate Q_{dsB} , stationary dressing force courses develop after an infeed phase. An increase of Q_{dsB} and thus an increase of the dressing intensity lead to a reduction of the dressing force level.

13.8 Grinding Costs

Grinding is a “twin process”, i.e., apart from the actual grinding process, the dressing also has to be considered regarding the costs.

The grinding costs per unit are then

$$K_F = K_{mach} + K_T + K_d \quad (13.72)$$

with

K_{mach} machine costs incl. wages (space costs)

K_T costs of grinding tool per piece

K_d costs for dressing calculated per piece.

The machine costs result from the machine time rate plus labour costs [TÖN95] (space costs per time unit k_{sp}) and the total time $t_{tot.} = t_h + t_n$ from main and secondary time [DEN10]

$$K_{mach} = k_{sp} \times (t_h + t_n) \quad (13.73)$$

The main time/operating time t_h can be detected via the radial feed speed (in plunge grinding) and the oversize or from the volume to be ground V_w and the material removal rate Q_w . Subsequently, the wheel volume worn during the grinding process V_s results from the grinding ratio $G = V_w/V_s$ defined above

$$K_T = V_s \times k_s \quad (13.74)$$

with the wheel costs per volume unit k_s . Then the dressing costs K_d are added. These are

$$K_d = (k_{pl} \times t_{tot,d} + V_{s,d} \times k_d)/n + K_{T,d}/n \quad (13.75)$$

with the total dressing time $t_{tot,d}$, the wheel volume lost by dressing $V_{s,d}$, and the dressing material worn due to the dressing $K_{T,d}$. To collect the proportion falling upon one piece, we must divide by the quantity n , that means by the number of pieces up to the next dressing cycle.

Example: Plunge grinding of a shaft of tempered steel 42CrMoV4 with diameter $d = 30$ mm, grinding width $a_p = 20$ mm and grinding oversize $w = 0.25$ mm at a tolerance width of $10 \mu\text{m}$. Grinding is carried out with corundum ($k_s = \text{Euro } 100 \cdot 10^{-6}/\text{mm}^3$, $G = 40$) and, due to the required accuracy,

in a two-step operation (roughing at $v_{fr} = 1.5$ mm/min, finishing at $v_{fr} = 0.25$ mm/min) The wheel life quantity up to the dressing is to be 15 pieces.

Together with practical data, the following costs result per workpiece:

$K_F = 4.10$ € with the portions: $K_{mach}/K_F = 0.90$, $K_T/K_F = 0.08$, $K_d/K_F = 0.02$.

If the same task is machined with a super hard grinding wheel on CBN basis, the cost for the tool rises to approx. 15 %, the grinding time and thus the machine-dependent costs K_{mach} decrease, possibly over-proportionally less.

13.9 Questions

1. Name processes, which cut with undetermined cutting edges.
2. Classify the processes according to their separating mechanisms and the effective motion.
3. Do you see limitations for the path bonding during the grinding process? How do you explain the energy bonding in the blast cutting process?
4. Which grinding processes do you know? Name the corresponding motions of tool and workpiece.
5. Deduce the equivalent cutting thickness h_{eq} from the continuity condition.
6. Indicate the equivalent diameter for different grinding processes.
7. Which components is a grinding wheel composed of? What tasks do they have?
8. Which grinding materials do you know? Organise them according to their hardness.
9. Which deployment areas do you assign to the grinding materials?
10. What does the friability index mean? Which material properties does it characterise?
11. How is the friability index determined?
12. Which kinds of corundum grinding materials do you know? How are they structured and what effect is achievable with them?
13. Characterise the possible crystal shapes of the super hard grinding materials. What does the index 111 mean? And what about 100?
14. How is the grain size of a grinding material specified and how is it determined?
15. What is meant with the hardness of a grinding wheel? How can it be influenced?
16. How can the hardness of a grinding wheel be determined?
17. Which types of bonding do you know?
18. How can the wear of a grinding wheel be defined?
19. How can the average radius wear of a wheel be calculated from the G parameter (grinding ratio)?
20. Which loads are dominant in the case of fast-running grinding wheels? Where is the maximum load?

21. What basic equations does one need to determine the dominant load of a grinding wheel by calculation?
22. How are the blasting speed and the permitted operating speed connected?
23. What possibilities do you see to increase the bursting speed resp. the permitted work speed?
24. What advantage does a holeless grinding wheel have (theoretically)?
25. Which types of wear occur at the grinding wheel?
26. Characterise the grinding process in the sense of the system technology (black-box).
27. Name the characteristics for the description of grinding processes.
28. What is the purpose of the equivalent radius?
29. What is not considered by the approximate calculation for the geometric contact length?
30. How do the kinematic and the geometric contact length differ?
31. How can the average cutting thickness in the grinding process be deduced considering the micro-topography of the grinding wheel?
32. Give an estimate as to how the energy removal from the grinding zone adjusts with different grinding materials.
33. Which methods for temperature measurement in the grinding process do you know?
34. What does the term conditioning of grinding wheels include? Name the tasks of the single process steps.
35. Divide the dressing processes and name typical dressing tools.
36. Which dressing processes do you apply for small, medium and large series?
37. What effect do you achieve by dressing in the same or counter direction?
38. How is the degree of overlapping defined in the dressing process; how and when does it affect the roughness at the workpiece and the forces in the grinding process?
39. Name dressing processes and subdivide them according to their effective principle.
40. Indicate the most important terms for the cost calculation in the grinding process.

References

- [ANSB7418] American National Standard B 7418–1965: Ball Mill Test of Friability of Abrasive Grains
- [ARG00] Argyropoulos, G.: Rundscheifen mit Schleifbändern, Schleiftechnik im Wettbewerb [External grinding by abrasive belts, grinding technology in competition]. 2. Schleiftechnisches Kolloquium, November 2000, Bremen
- [BRI82] Brinksmeier, E.: Randzonenanalyse geschliffener Werkstücke [Surface zone analysis of ground workpieces]. Dr.-Ing. Diss. Universität Hannover 1982
- [BRI91] Brinksmeier, E.: Prozess- und Werkstückqualität in der Feinbearbeitung [Process- and workpiece-quality in fine finishing]. Habilitationsschrift, Universität Hannover (1991)

- [BRU98] Brunner, G.: Schleifen mit mikrokristallinen Aluminiumoxid Schleifkorn [Grinding by micro-crystalline alumina grains]. Dr.-Ing. Diss. Universität Hannover (1998)
- [BUN55] Bundy, F.P., Hall, H.T., Strong, H.M., Wentorf, R.F.: Man-made diamonds. *Nature* **176**, S.55 (1955)
- [BÜT68] Büttner, A.: Das Schleifen sprödharter Werkstoffe mit Diamant-Topfscheiben [The grinding of brittle materials by diamond cup wheels]. Dr.-Ing. Diss. Universität Hannover (1968)
- [CHO86] Choi, H.Z.: Beitrag zur Ursachenanalyse der Randzonenbeeinflussung beim Schleifen [Contribution to cause analysis of surface integrity in grinding]. Dr.-Ing. Diss. Universität Hannover (1986)
- [COL81] Colleselli, K.: Konventionelle Schleifmittel und Bindungen zur Herstellung von Schleifkörpern [Conventional abrasives and bonds to manufacture grinding wheels]. *Jahrbuch Schleifen, Honen, Läppen und Polieren*, 50. Ausgabe, S. 207–211 (1981)
- [CZE99] Czenkusch, C.: Technologische Untersuchungen und Prozessmodelle zum Rundschleifen [Technological investigations and process models for external grinding]. Dr.-Ing. Diss. Universität Hannover (1999)
- [DEN03] Denkena, B., Becker, J.C., Catoni, F.: Characterisation of vitrified bonded grinding wheels. ISAAT, Bristol, 18–20 Nov (2003)
- [DEN10] Denkena, B.: Konstruktion, Gestaltung und Herstellung von Produkten II. Vorlesungsmanuskript [Design, configuration and manufacturing of products II, lecture manuscript]. Universität. Hannover (2010)
- [DIN8589-0] Fertigungsverfahren Spanen—Teil 0: Allgemeines; Einordnung, Unterteilung, Begriffe/Manufacturing processes chip removal—Part 0: General; classification, subdivision, terms and definitions. Hrsg. Beuth Verlag (2003)
- [DIN ISO8486-1] Schleifkörper aus gebundenem Schleifmittel—Bestimmung und Bezeichnung von Korngrößenverteilung—Teil 1: Makrokörnungen F4 bis F220/Bonded abrasives—Determination and designation of grain size distribution—Part 1: Macrogrits F4 to F220. Hrsg. Beuth Verlag (1997)
- [DIN ISO 525] Schleifkörper aus gebundenem Schleifmittel - Allgemeine Anforderungen/Bonded abrasive products - General requirements. Hrsg. Beuth Verlag (2000)
- [DOW72] Dow Whitney, E.: Thermodynamic properties of abrasive materials. In: *Proceedings of International Grinding Conference*, Pittsburg (1972)
- [FAL98] Falkenberg, Y.: Elektroerosives Schärfen von Bornitrid Schleifscheiben [Electro-erosive dressing BN grinding wheels]. Dr.-Ing. Diss. Universität Hannover (1998)
- [FRI02] Friemuth, T.: Herstellung spanender Werkzeuge [Production of cutting tools]. Habilitation, Universität Hannover (2002)
- [FRI99] Friemuth, T.: Schleifen hartstoffverstärkter Werkzeuge [Grinding of hard particle reinforced tools]. Dr.-Ing. Diss. Universität Hannover (1999)
- [GRA87] Grabner, T.: Leistungspotential keramisch gebundener CBN-Schleifscheiben [Power potential of CBN grinding wheels]. Dr.-Ing. Diss. Universität Hannover (1987)
- [GRE58] Greiner, K.: Festigkeitsuntersuchungen an Klebeverbindungen zwischen Schleif- und Tragkörper [Investigation of strength at glued connections between wheel and carrying body]. Dr.-Ing. Diss. TH Hannover (1958)
- [HAU80] Hauk, V.; Krug, W.K.; Vaessen, G; Weisshaupt; H.: Der Eigendehnungs-/Eigenspannungszustand nach Schleifbeanspruchung [the residual strain/residual stress state after grinding loadst]. *HTM* **35**(3), S. 61–62 (1980)
- [HAH63] Hahn, R.S.: On the nature of the grinding process. In: *Proceedings Third International MTDR Conference*, Sept. 1962, Oxford, S.129–154 (1963)

- [HAL60] Hall, H.T.: Ultra high pressure temperature analysis. The belt. Rev. Sci. Inst. 31, 125, (1960)
- [HEU92] Heuer, W: Außenrundscheifen mit kleinen CBN-Scheifscheiben [External grinding with small wheels]. Dr.-Ing. Diss. Universität Hannover (1992)
- [KAI75] Kaiser, M.: Schleifen von Hartmetallen [Grinding of cemented carbides]. Dr.-Ing. Diss. TU Hannover 1975, München: Techn. Verlag Resch (1975)
- [KAI09] Dr. Kaiser GmbH: Company booklet. Celle (2009)
- [KAR95] Karpuschewski, B.: Mikromagnetische Randzonenanalyse geschliffener einsatzgehärteter Bauteile [Micro-magnetic analysis of surface zones of ground case hardened components]. Dr.-Ing. Diss. Universität Hannover (1995)
- [KAR01] Karpuschewski, B.: Sensoren zur Prozessüberwachung beim Spanen [Sensors for process monitoring in cutting]. Habilitation, Universität Hannover (2001)
- [KAS69] Kassen, G.: Beschreibung der elementaren Kinematik des Schleifvorganges [Description of the elementary kinematics of the grinding process]. Dr.-Ing. Diss. RWTH Aachen (1969)
- [KEL80] Kelker, H.(Hrsg.): Ullmanns Encyklopedie der technischen Chemie [Encyclopedia of technical chemistry]. 4. neubearbeitete und erweiterte Auflage, Band 5 Analysen und Messverfahren. Verlag Chemie, Weinheim (1980)
- [KLO02] Klocke, F., Merbecks, T.: Charakterisierung von keramisch gebundenen CBN-Scheifscheiben [Characterization of vitrified bond CBN grinding wheels]. IDR 36 Nr. 3, S. 242–251 (2002)
- [KLO86] Klocke, M.: Einfluss des Gefüges von Edelkorund Schleifscheiben auf ihre Werkstoffkennwerte und das Schleifverhalten [Influence of the structure of aluminum oxide grinding wheels on their material parameters and their grinding behavior]. Dr.-Ing. Diss. TU Berlin (1986)
- [KUR27] Kurrein, M.: Die Bearbeitbarkeit der Metalle im Zusammenhang mit der Festigkeitsprüfung [Machinability of metals regarding the strength test]. Werkstatttechnik 21, S.612–621 (1927)
- [LIE98] Lierse, T.: Mechanische und thermische Wirkungen beim Schleifen keramischer Werkstoffe [Mechanical and thermal effects in grinding of ceramic materials]. Dr.-Ing. Diss. Universität Hannover (1998)
- [LOR75] Lortz, W.: Schleifscheibentopographie und Spanbildungsmechanismen beim Schleifen [Grinding wheel topography and chip formation mechanisms in grinding]. Dr.-Ing. Diss. RWTH Aachen (1975)
- [MAH00] Mahoney, M.: Höhere Zerspanleistung durch neue Schleifscheibenstrukturen [Higher material removal rates by new grinding wheel structures]. Schleiftechnik im Wettbewerb, 2. Schleiftechnisches Kolloquium, November 2000, Bremen
- [MAG08] Malkin, S., Guo, C.: Grinding technology. Industrial Press, New York (2008)
- [MAR01] Marzenell, C.: Verzahnungshonen mit Diamantwerkzeugen [Gear honing with diamond tools]. Dr.-Ing. Diss. Universität Hannover (2001)
- [MIN99] Minke, E.: Handbuch zur Abrichttechnik [Handbook of dressing technology]. Eisligen, Druck und Verlag E. Dischner
- [MÜL01] Müller, N.: Ermittlung des Einsatzverhaltens von Sol-Gel-Korund Schleifscheiben [Determination of the application behavior of sol-gel corborundum grinding wheels]. Dr.-Ing. Diss. RWTH Aachen (2001)
- [OHM95] Ohmori, H.: Ultraprecision grinding of optical materials and components applying ELID (Elektrolytic In-Process Dressing). SPIE 2576, S. 26–45 (1995)
- [PAD93] Padberg, H.-J.: Entwicklung anwendungsorientierter Bindungs-Systeme für Schleifwerkzeuge [Development of application related bond systems for

- grinding tools]. Jahrbuch Schleifen, Honen, Läppen und Polieren, 57. Ausgabe, S. 196–211 (1993)
- [PAU94] Paul, T.: Konzept für ein schleiftechnologisches Informationssystem [Concept for a grinding technological information system]. Dr.-Ing. Diss. Universität Hannover (1994)
- [PEK57] Peklenik, J.: Ermittlung von geometrischen und physikalischen Kenngrößen [Determination of geometric and physical characteristics]. Dr.-Ing. Diss. RWTH Aachen (1957)
- [PET68] Peters, J., Snoeys, R., Decnent, A.: Sonic testing of grinding. In: Proceedings of 9th International Machine Tool Design and Research Conference, S.1113 (1968)
- [RAM78] Ramdohr, P.; Strunz, H.: Klockmanns Lehrbuch der Mineralogie [Textbook of mineralogy]. Ferdinand Enke Verlag, Stuttgart (1978)
- [REI56] Reichenbach, G.S., Mayer, J.E., Shaw, M.C., et al.: The role of chip thickness in grinding. Trans. ASME **78**, S.847–859 (1956)
- [ROT94] Roth, P.: Abtrennmechanismen beim Schleifen von Aluminiumoxidkeramik [Cutting mechanisms in grinding of aluminum oxide]. Dr.-Ing. Diss. Universität Hannover (1994)
- [ROW93] Rowe, W.B. et al.: The effect of deformation on the contact area in grinding. Ann. CIRP **42**(1), S.409–412 (1993)
- [SAL82] Salmang, H.; Scholze H.: Keramik [Ceramics]. Springer Verlag 6. Aufl. (1982)
- [SAL91] Saljé, E.: Begriffe der Schleif- und Konditioniertechnik. Essen, Vulkan Verlag (1991)
- [SCH68] Schmitt, R.: Abrichten von Scheifscheiben mit diamantbestückten Rollen [Dressing of grinding wheels by bediamonded rolls]. Dr. -Ing. Diss. TU Braunschweig (1968)
- [SCH73] Scheidemann, H.: Einfluss der durch Abrichten mit zylindrischen und profilierten Diamantrollen erzeugten Schleifscheiben-Schneidfläche auf den Schleifvorgang [Influence of the grinding wheel cutting face, generated by cylindric and profiled diamond rolls]. Dr.-Ing. Diss. TU Braunschweig (1973)
- [SIM88] Simpfendörfer, D.: Entwicklung und Verifizierung eines Prozessmodells beim Planparallelläppen [Development and verification of a process model in double plate face lapping]. Dr.-Ing. Diss. TU Berlin (1988)
- [SPU89] Spur, G.: Keramikbearbeitung [Machining of ceramics]. München: Carl Hanser Verlag (1989)
- [STA62] Stade, G.: Technologie des Schleifens [Technology of grinding]. München, Carl Hanser Verlag (1962)
- [STA02] Stabenow, R.; Bruhn, J.; Golla, B. J.: Mikrokristalline Sinterkeramik in Schleifkörpern [Micro-cristalline sintered ceramic in grinding wheels]. 10. Internationales Braunschweiger Feinbearbeitungskolloquium, Braunschweig (2002)
- [TIO90] Tio, T.-H.: Pendelschleifen nicht oxidischer Keramiken [Reciprocating grinding of non-oxidi ceramics]. Dr.-Ing. Diss. TU Berlin (1990)
- [TÖN65] Tönshoff, H.K.: Eigenspannungen und plastische Verformungen im Werkstück durch spanende Bearbeitungsverfahren [Residual stresses and plastic deformations in the workpiece by cutting and abrasive processes]. Dr.-Ing. Diss. TH Hannover (1965)
- [TÖN75] Tönshoff, H.K.; Kaiser, M.: Profilieren und Abrichten von Diamant- und Bornitrid-Schleifscheiben [Profiling and dressing of diamond and boron nitride grinding wheels]. wt-Z.ind.Fertig. 65(1975)4, S. 179–183, (1975)
- [TÖN79] Tönshoff, H.K., Geisweid, G.: Profiling of diamond and boron nitride wheels. Ann. CIRP **28**, 1 (1979)

- [TÖN92] Tönshoff, H.K. et al.: Modelling and simulation of grinding process. *Ann. CIRP* **41**(2) S.677–688 (1992)
- [TÖN95] Tönshoff, H.K.: *Werkzeugmaschinen- Grundlagen* [Machine tools—fundamentals]. Springer (1995)
- [TRI76] Triemel, J.: Untersuchungen zum Stirnschleifen von Schnellarbeitsstählen mit Bornitridwerkzeugen [Investigations of face grinding of high speed steels by boron nitride tools]. Dr.-Ing. Diss. Universität Hannover (1976)
- [UHL87] Uhlmann, E; Stark, C.: Potentiale von Schleifwerkzeugen mit mikrokristalliner Aluminiumoxidkörnung [Potentials of grinding tools with micro-cristalline aluminum oxide grains]. *Jahrbuch Schleifen, Honen, Läppen und Polieren* **58**, S. 281–309 (1987)
- [UHL93] Uhlmann, E.: Tiefschleifen hochfester keramischer Werkstoffe [Creep grinding of high strength ceramic materials]. Dr.-Ing. Diss. TU Berlin (1993)
- [VER79] Verkerk, J., Pekelharing, A.J.: The influence of the dressing operation on productivity in precision grinding. *Ann. CIRP* **28**, 2 (1979)
- [VOL00] Vollstädt, H.; List, E.; Recht, H.: Methoden und Geräte zur Qualitätsbestimmung von Industriediamanten [Methods and devices to determine the quality of industrial diamonds]. *Proceedings of 4. IFW-Steinseminar*, 4–6.7.2000, Seite 43–52
- [WEI76] Weinert, K.: Die zeitliche Änderung des Schleifscheibenzustandes beim Außenrund-Einstechschleifens [The temporal alteration of the grinding wheel state in external grinding]. Dr.-Ing. Diss. TU Braunschweig (1976)
- [WER71] Werner, G.: Kinematik und Mechanik des Schleifprozesses [Kinematic and mechanics of the grinding process]. Dr.-Ing. Diss. RWTH Aachen (1971)
- [WOB91] Wobker, H.-G.: Schleifen keramischer Werkstoffe [Grinding of ceramic materials]. Dr.-Ing. Diss. Universität Hannover (1991)

Chapter 14

Gear Grinding

14.1 Introduction

The hard finishing of gears with involute flanks is examined here as an example for the finishing of highly-loaded complex surfaces. Gears are among the most important machine elements in engineering and vehicle construction. They are produced in several steps. Soft machining, which includes turning, hobbing or gear shaping processes, is followed by a heat treatment because the specific loads of gears are increased due to space and mass reduction and so the hardness and strength of the functional surfaces have to be increased. The hardness distortions resulting from the heat treatment as well as the required surface zone and surface properties lead to the fact that the hardening process is followed by a finishing, mostly a grinding process (Fig. 14.1).

The quality of a tooth is mainly determined by the generation of the involute flank. In batch production, hard finishing processes are becoming increasingly important for the completion of the gear. The reasons for this are

- apart from the higher specific load and the increased requirements concerning strength,
- the rising significance of a reduced noise emission by the gear as well as,
- the enhancement of near-net-shape technologies by means of forming and primary shaping (e.g., casting) processes [BEH97].

Among others, the most frequent forms of damage to gears are surface damages of the tooth flank, such as gray spots or pit marks. They develop over a longer period of time and can generally be attributed to material fatigue. At this, material particles break out of the tooth flank. With an increasing damage to the surface, cracks can occur resulting in a tooth breakage. The so-called fatigue fracture develops as a consequence of repetitive changing loads. At this, a slight crack appears at the point with the highest load (mostly the tooth root), which grows with continued load up to the point where the remaining rest cross section is no longer able to transfer the load [DIN3979]. Tooth breakages often lead to a total gear failure and may be connected with enormous costs.

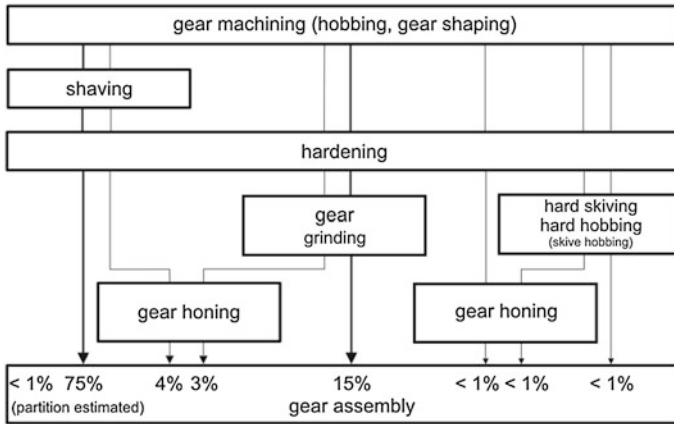


Fig. 14.1 Production sequences of gear production in large batch production (according to Bausch)

The described damage developments can be influenced by grinding in a targeted way. Investigations have shown that high residual compressive stresses and low roughness values in the entire tooth gap as well as large bending radii in the tooth root range have a positive effect on the fatigue life of the gears. Production-conditioned damages to the gear, which are often accompanied by residual tensile stresses and crack development in the surface zone of the tooth gap, can be avoided by a precise process design [STE04, SCH07, HER08, BRE08, KAG02].

When designing the grinding processes, the points of maximum material removal rates have to be observed, since the material removal rate directly affects the important output parameters of the process in gear grinding, too. At a rising material removal rate, the roughness R_z decreases. This is to be attributed to increased wear and a blunting of the abrasive particles. Accordingly, the grinding power also increases. The converted energy per removed volume and thus the temperature in the surface zone of the tooth flank rises with the smoothing of the micro-topography of the grinding wheel. The consequence is generally a reduction of residual compressive stresses as illustrated in Fig. 14.2 as an example for discontinuous profile grinding. At a further increase of the material removal rate, the abrasive particles splinter and break out, which leads to an increased roughness. This in turn, is accompanied by an alteration of the grinding wheel profile and leads to geometrical deviations on the workpiece.

After it has become possible to considerably reduce engine noises in a vehicle by means of primary and secondary noise reduction measures, gear noises are now in the foreground. Customer demands concerning comfort, force the tooth manufacturers to further increase the gear quality. This can be reached with the grinding process (Fig. 14.3) [SCH94]. Apart from the reduction of deviations and wavinesses along the involute, the targeted generation of tooth flank modifications bears a special significance. The established corrections include convexities in

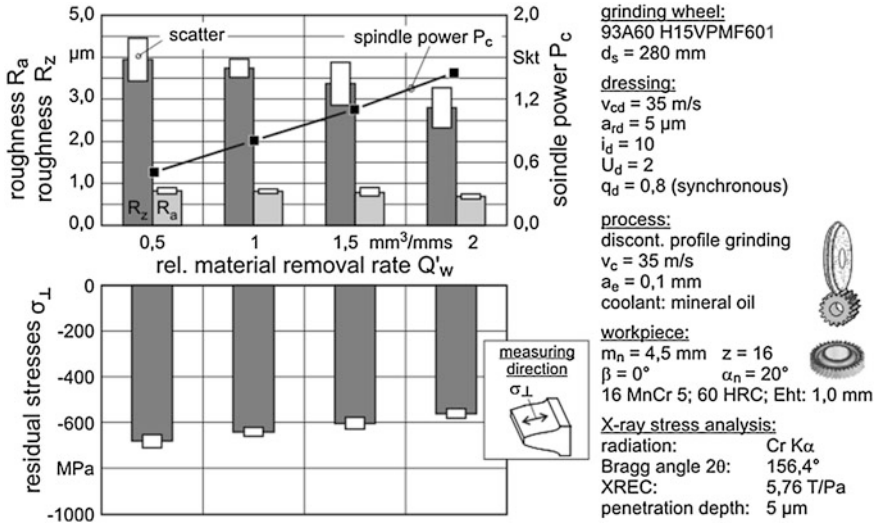
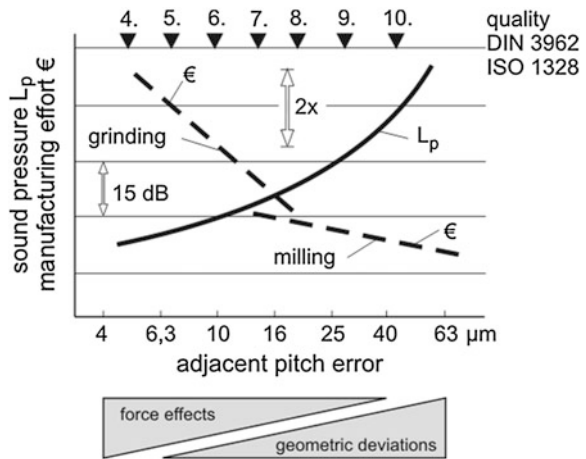


Fig. 14.2 Influence of the related material removal rate on the roughnesses and residual stresses in discontinuous profile grinding

Fig. 14.3 Production effort and noise emission [SCH94]



height and width direction of the tooth flank as well as upper edge chamfering and tooth root relief-cutting (protuberance). They are generated by targeted alterations of the tool profile as well as the machining kinematic.

In connection with the noise emission, the micro-structure of the tooth flank also gains a high significance. While the surface roughness is primarily influenced by the specification of the grinding wheel (grain, bonding), the arrangement of the grinding grooves is to be attributed to the process-innate kinematic. For example, the grinding groove profile typical for crossed helical grinding is ascribed an especially beneficial noise behavior. In industrial practice, strategies have been

developed to interrupt the continuous grinding grooves in continuous generating grinding and thus achieve a reduction of the operating noises.

Near net shape forging (precision forging) allows the production of tooth raw parts, which no longer require any soft machining of the gear because the tooth gaps are already preformed with sufficient precision. They are heat-treated and then hard machined immediately [DEN03]. Chapter 15 deals with the design of the process chain for the gear production as well as the advantages of precision forging in detail.

The processes for the hard finishing of gears can be divided into profile and generation grinding processes. In profile grinding, the desired gear geometry is the negative of the tool profile, while in generating grinding, the target geometry is generated by a kinematic linking of tool and workpiece motion [TÜR02, NEW91]. Each one of these process groups in turn can be subdivided into continuous and discontinuous processes. On the generating grinding side, there is the discontinuous profile grinding with dish grinding wheels, the continuous profile grinding with cylindrical grinding worms as well as the gear honing. On the profile grinding side, there is the very widely spread discontinuous profile grinding and the continuous profile grinding with globoidal grinding worms. Figure 14.4 shows the classification of hard finishing processes for gears according to [DIN8589].

This chapter concentrates on the discontinuous profile grinding, the continuous generating grinding with cylindrical grinding worms as well as the continuous crossed helical grinding with grinding rings due to the broad application of these processes in industrial practice. Fundamental process characteristics of these processes are contrasted at the end of this chapter (Fig. 14.18).

First, however, some basic correlations of involute gears have to be clarified. The involute of a spur-toothed wheel develops by rolling a tangential line at the

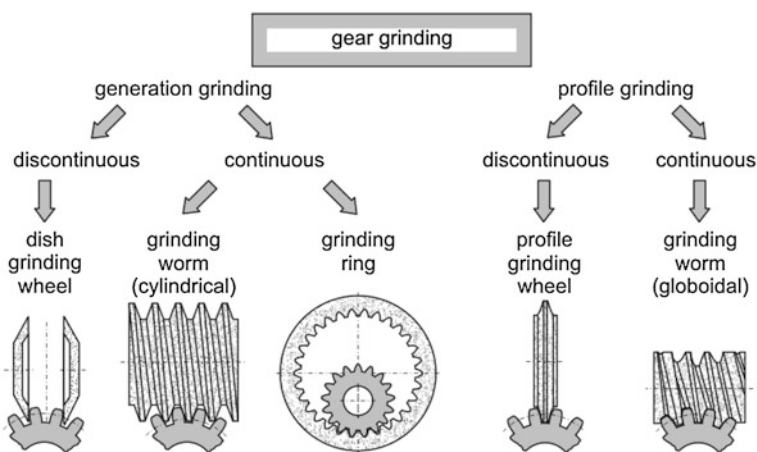


Fig. 14.4 Classification of tooth flank grinding processes according to [DIN8589]

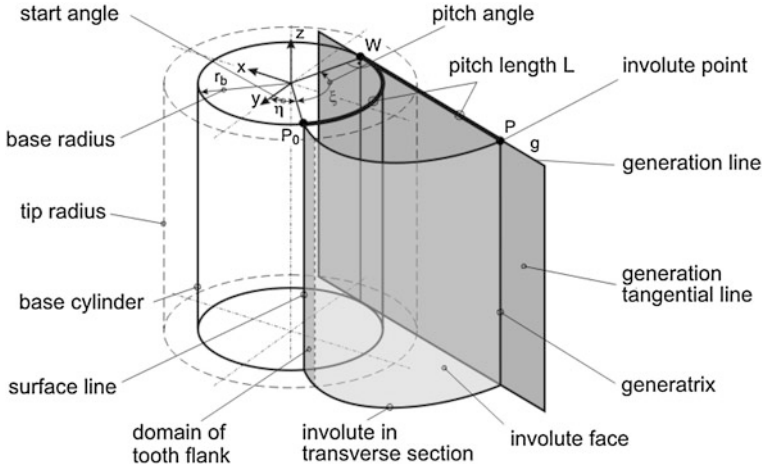


Fig. 14.5 Base cylinder with involute face and generatrix (according to [DIN3960])

base circle of the gear. The parallel shifting of the involute in direction \$z\$ generates an involute face (Fig. 14.5).

With the aid of the operating parameter \$\tau\$ in direction \$z\$, this face can be described by

$$\vec{E}(\xi\tau) = r_b \cdot \begin{pmatrix} \sin(\xi + \eta) - \xi \cdot \cos(\xi + \eta) \\ \cos(\xi + \eta) + \xi \cdot \sin(\xi + \eta) \\ \tau \end{pmatrix} \quad (14.1)$$

The range used by the tooth flank is limited by the root and tip radius. Thus, the following applies:

$$\sqrt{\left(\frac{r_{Ff}}{r_b}\right)^2 - 1} \leq \xi \leq \sqrt{\left(\frac{r_{Fa}}{r_b}\right)^2 - 1}; \quad 0 \leq \tau \leq \left(\frac{b}{r_b}\right) \quad (14.2)$$

with

- \$r_{Ff}\$ root radius
- \$r_{Fa}\$ tip radius
- \$r_b\$ base radius
- \$b\$ tooth width.

Corresponding relations can be provided for helical toothed gears, if it is considered that a generatrix on the tangential plane is not inclined parallel to the wheel axis but by the helix angle \$\beta\$. This caused the generation of the tooth flanks by involute helicoids [LOO59, TÜR02].

Gear ratio, force and moment transmission as well as running smoothness are of central significance when designing the gear. Thus, sizing and calculation of the

gears are primarily carried out via the determination of the tooth number z , the normal module m_n , the normal pressure angle α_n as well as the helix angle β . These variables are standardized and form the core of the tooth calculation, which is not explained in more detail at this point [DIN3960].

When machining helical gears with the copying process, it must be observed that the pitch diameter and the base diameter are mathematically related to the base data mentioned above. For example, the alteration of the pitch diameter at a constant tooth number and normal module leads to an alteration of the helix angle. The curvature conditions along the tooth flank directly depend on the base circular radius, which in turn can be influenced by an alteration of the tooth number of the gear, for example [DIN3960, DIN8000]. It is to be attributed to this fact that the involute of a gear with few teeth is strongly curved, whereas that of a gear with many teeth appears almost straight at otherwise constant gear base data. The helical gears include cylindrical gears as well as worm and hollow gears. The consequences of the above-mentioned observations for each corresponding hard finishing process are also explained in the following sections.

14.2 Discontinuous Profile Grinding

In discontinuous profile grinding both flanks are mostly machined simultaneously with correspondingly profiled tools. For this, vitrified grinding wheels with melting or sintering corundum, boron nitride as well as galvanically coated boron nitride grinding wheels are employed.

The grinding wheel is placed in the helix angle β corresponding to the gear axis. At first, the infeed occurs radially, then axially so as to grind the tooth flanks above the gear width (Fig. 14.6).

In helical gearing, the axial motion along z_w and the turning motion of the wheel around z_w have to be kinematically linked for this purpose. Nonproductive times accumulate during the run-in and run-out of the tool from the tooth gap, for the indexing of the gear in the next gap and for the return into the original position. Therefore, the process is time-consuming compared with continuous processes. Thus, a lower productivity results for profile grinding. On the other hand, with an exact design of the wheel profiles [TÜRO2] high gear qualities of up to quality 1 according to [DIN3961, DIN3962, ISO1328] can be achieved [WOB95]. With this process, the tooth root can be machined in a process-safe manner, which influences the fatigue life of the gear positively [KLK00, KÖN94].

The related material removal rate Q'_w is calculated from the difference of the effective wheel profile and the raw part profile. From this, an average value above the involute results at

$$Q'_w = a_e \cdot v_f \quad (14.3)$$

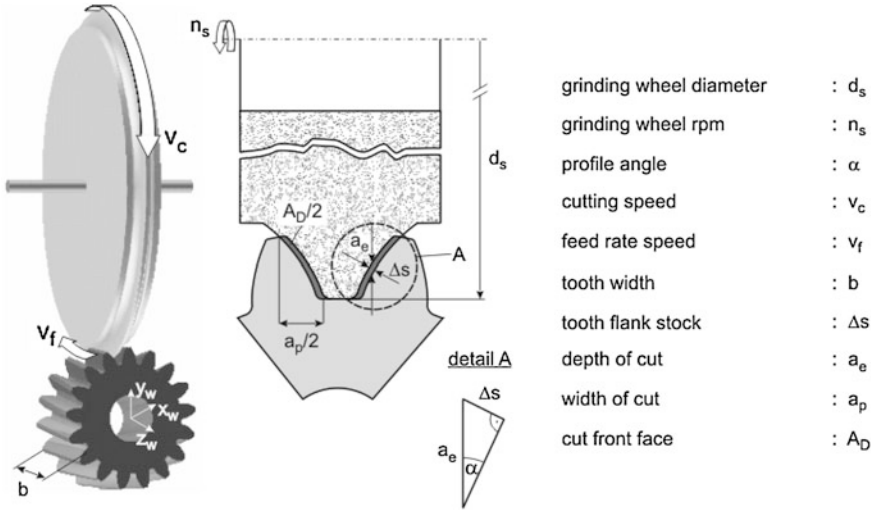


Fig. 14.6 Profile grinding of gears

In fact, depending on stock a_e above the profile, Q'_w can differ from the average value considerably. Figure 14.7 illustrates the fluctuating related material removal rates Q'_w for normal and radial equidistant stocks Δs and a_e . One can recognize that at a normal equidistant stock, high depth of cut values occur especially in the range of the tooth root, which leads to high material removal rates via Eq. 14.3. This is to be considered in the profile grinding of the gears pre-toothed by hobbing.

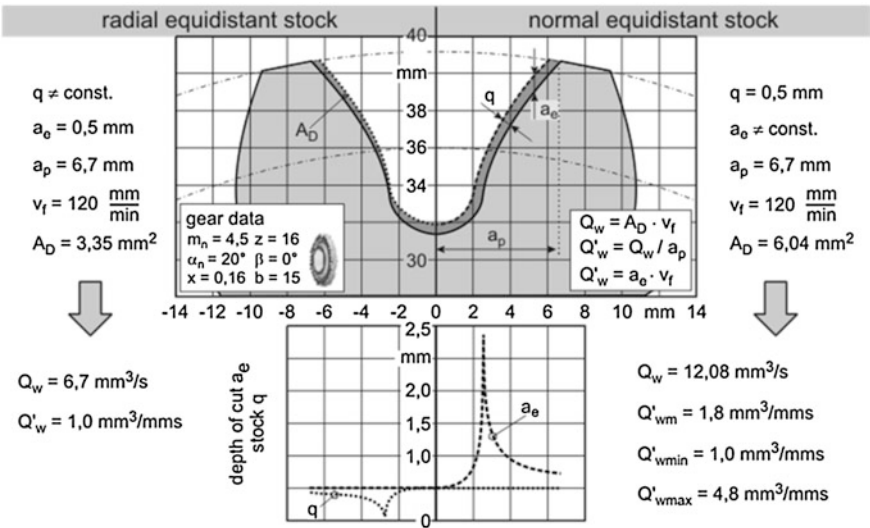


Fig. 14.7 Related material removal rate Q'_w for different stock distributions

A special characteristic of profile grinding is the continuous machining of a tooth gap at relatively large contact lengths compared with generating processes. This condition benefits the heat flux in the workpiece and makes the process prone to grinding burn effects.

As explained in the previous chapter, grinding is a combined process composed of conditioning and the actual grinding process. Profile grinding wheels are also dressed for the application preparation. For this, the tool is to be profiled in such a manner that the face determined by Eq. 14.1 develops. For helical gears it has to be taken into consideration that the helix angle β and the spatial engagement of the tool cause a profile distortion, which has to be provided when dressing [TÜR02]. The grinding wheel profile is directly dependent on the gear data. Workpieces with different tooth numbers or helix angles can therefore only be produced with the same tool profile with quality loss. The manufacturing of high-quality gears thus requires differently profiled tools. Concerning the tool supply and storage costs, this bears a disadvantage for galvanically coated grinding wheels. In contrast, the corundum grinding wheels, which are optionally dressable due to the line dressing, have proven to be very flexible.

Figure 14.8 demonstrates the kinematic of the path-controlled dressing of a profile grinding wheel. The right and left profile sides of the gap are advantageously profiled in two contour strings. Therefore, both parts can be dressed concordantly either by pushing or pulling, which avoids different forces between the effective partners. The pulling cutting is preferable [TÜR02]. At this, the conditioning is carried out by means of a rotating dressing tool, which is furnished with special diamond sticks at the circumferential outer edges [LIE02].

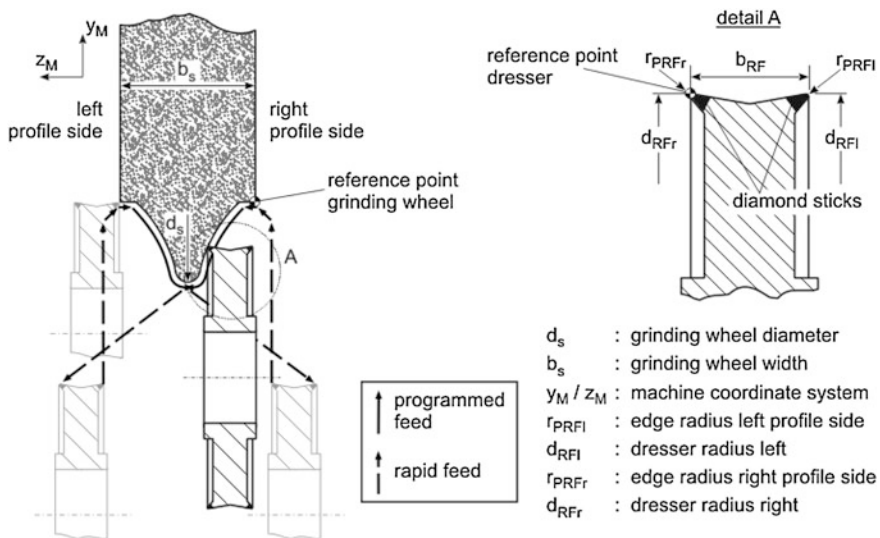


Fig. 14.8 Path-controlled dressing of profile grinding wheels

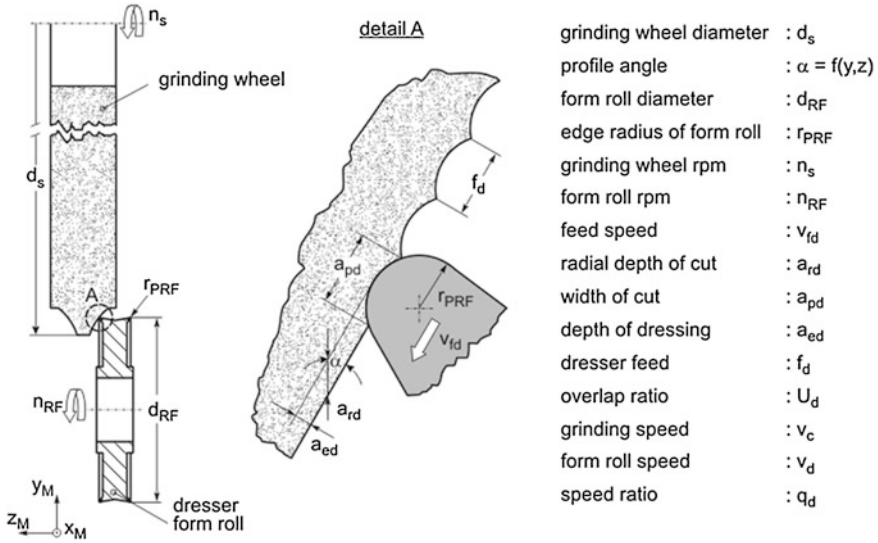


Fig. 14.9 Dressing of profiles

Apart from the macro-geometrical profile generation of the grinding wheels it is the target of the dressing process to adjust the micro-topography to the case of application. The dressing result with a powered form roll is determined by the roll geometry, the type of diamond as well as their allocation and also fundamentally by the manipulated variables overlap ratio U_d , effective dressing depth of cut a_{ed} and speed ratio q_d . The significance of these variables in the dressing of profiles is illustrated in Fig. 14.9.

As previously mentioned, the overlap ratio is the relation between the width of cut of the dresser a_{pd} to the dressing feed f_d . This dimensionless variable is a measurement as to how close to each other the different lanes of the feed spiral generated during the dressing are located. Thus, a smoother wheel surface develops at a high overlap ratio compared with a low one. While the overlap ratio and the effective depth of cut a_{ed} acting normally to the surface remain constant in the dressing of linear profiles, these variables change depending on the profile angle α in the dressing of curved profiles. With the variables defined in Fig. 14.9 the overlap ratio results at

$$U_d = \frac{v_c \cdot \sqrt{2 \cdot a_{rd} \cdot r_{PRF} \cdot \sin \alpha - a_{rd}^2 \cdot \sin^2 \alpha}}{v_{fd} \cdot \pi \cdot d_s} \quad (14.4)$$

The course of the overlap ratio U_d and the effective depth of cut a_{ed} over the grinding wheel profile are exemplarily illustrated in Fig. 14.10. Due to the reasons mentioned, the roughness at the gear decreases with an increasing overlap ratio, whereas the grinding power increases noticeably.

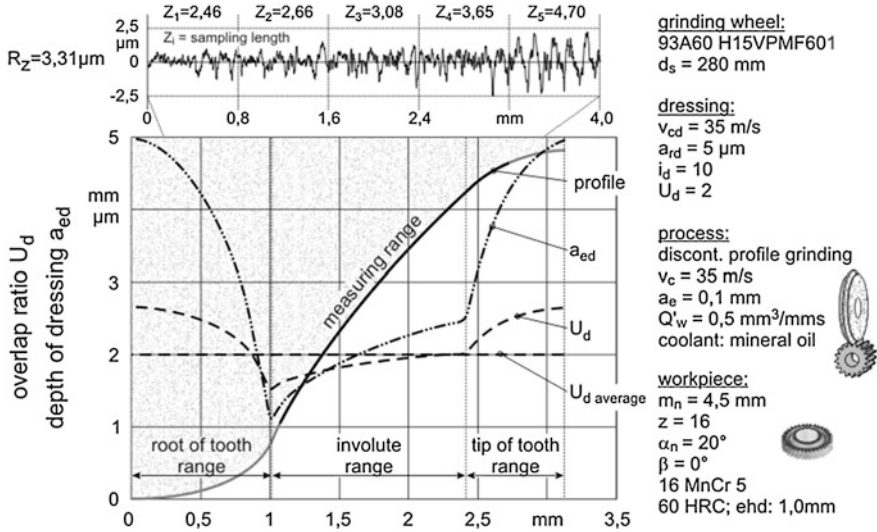


Fig. 14.10 Influence of the overlap ratio and the depth of dressing on the roughness

14.3 Continuous Generating Grinding with Grinding Worms

Continuous generating grinding works with a cylindrical grinding worm, which can be approximate by a gear rack profile in its normal section. The worm depends on module m and pressure angle α of the gear. It is therefore applicable for gears of the same module and pressure angle independent from the helix angle. Worms are used in ceramic bonding with fused corundum, sintering corundum or CBN as a grinding material as well as in galvanic bonding with CBN allocation. As galvanically coated grinding worms, worm sets of roughing and finishing worms are often used to achieve high removal rates and high surface qualities at the same time. High gear qualities can be reached in continuous generating grinding. Pitch and concentricity errors are small due to the continuous process. Continuous generating grinding is preferred in the batch production of medium-sized and large batches of workpieces up to module 5 mm. The machining of gears up to module 10 mm, however, is currently already feasible.

When machining the gear, the grinding worm is pivoted opposite the workpiece axis by the angle $\varphi = \beta - \gamma_0$ (γ_0 : helix angle of the worm) (Fig. 14.11). The tool and workpiece axes are linked to each other so that the tooth and the worm rotate in a constant rotation speed ratio. The flank stock is removed by means of a radial depth of cut. For the machining of the tooth width, the grinding worm or the gear carries out an axial (differential process, Pfauter-process) or a feed motion in the direction of the tooth helix (Grant-process).

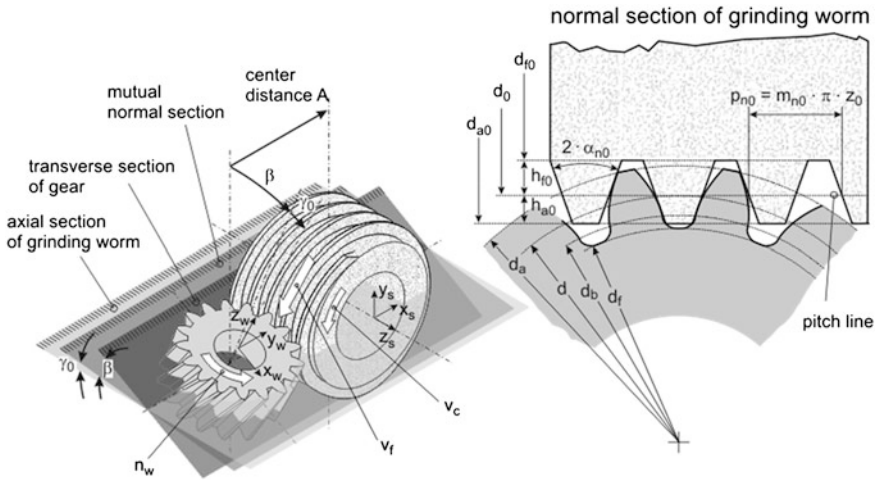


Fig. 14.11 Kinematic of generating grinding (differential process)

Due to the generating kinematic, the tooth flank stock on the right and left tooth flanks are removed in a different way to each other. One gear flank is machined with a worm flank, which generates from the tooth tip to the tooth root, whereas the stock on the opposite flank is abraded simultaneously from the tooth root to the tooth tip. Due to the continuous process, tool approaches and idle times are omitted. The stock is removed in fine strips per workpiece revolution. This leads to the process-typical waviness along the flank line. The resulting generating feed therefore occurs along the profile line and not in the direction of the tooth width. While the workpiece tooth is out of engagement and revolves, no material removal takes place. The interrupted gap machining resulting from this enables a better cooling of the workpiece compared with discontinuous profile grinding.

In continuous generating grinding, several right and left tooth flanks are always in engagement. At this, altering engagement conditions and a varying number of engagements on the right and left tooth flanks occur. The consequences are periodical force deviations between tool and gear. Figure 14.11 illustrates the kinematic and the geometrical contact relations between grinding worm and gear.

The average related material removal rate can be calculated from the geometrical variables and the feed speed. It is

$$Q'_{wm} = \frac{v_f \cdot z \cdot a_e \cdot \sin \alpha_n \cdot \cos \beta \cdot (d_a^2 - d_{FF}^2)}{2 \cdot d_b \cdot l_p \cdot \cos \gamma_0} \quad (14.5)$$

with

- v_f feed speed
- z teeth number of the gear
- a_e work engagement
- α_n normal pressure angle

- β helix angle of the gear
 d_a tip diameter
 d_{FF} root diameter
 d_b Base diameter
 l_p Profile formation length
 γ_0 helix angle of the grinding worm.

The profile formation length l_p results from the distance of the engagement points in the normal section of the grinding worm [TÜR02]. This is however, only a value averaged over the entire grinding process, i.e., the summarized material removal rate of all engagement points. The locally related material removal rate Q'_{wl} , which regards the material removal rate existing at a point of the tooth flank, differs strongly from it. It is calculated as follows

$$Q'_{wl} = \frac{2 \cdot \sin \alpha_n \cdot \Delta s \cdot v_f \cdot \pi \cdot \sqrt{d_y^2 - d_b^2}}{d_0 \cdot \sqrt{1 - \frac{(2 \cdot \Delta s \cdot \sin \alpha_n - d_0)^2}{d_0^2}}} \quad (14.6)$$

with

- Δs tooth flank stock
 d_y diameter of the contact point
 d_0 pitch circle diameter of the grinding worm.

At this, the running variable above the radial extension of the flank is given by the diameter of the contact point d_y . Figure 14.12 shows an example of the courses of averaged and locally-related material removal rates. The courses of Q'_{wl} make it clear that at an increase of the averaged material removal rate Q'_{wm} via an increase of the depth of cut Δs , the corresponding maximum related material removal rate Q'_{wl} rises considerably more weakly than at an increase of the feed speed v_f . Furthermore, the difference between both variables can be recognized. For example, the locally related material removal rate Q'_{wl} can be higher at the tooth tip by factor 2.5 than the averaged related material removal rate Q'_{wm} .

A higher material removal rate in the workpiece tip range leads to deviations in the workpiece profile and can be interpreted as an indicator for a stronger profile loss, especially in the root range of the grinding worm. Investigations on the influence of the number of worm threads on the tool wear and residual stresses in the workpiece have shown that the profile loss can be observed especially in the case of multi-thread worms. At the same time, multi-thread tools show better residual stress results [STI09].

Technological characteristic values, such as the geometrical contact length or the single grain chip thickness, have already established themselves in process design for other hard finishing processes, i.e., surface or external grinding. A description of these characteristic values for continuous generating grinding occurs with [STI09]

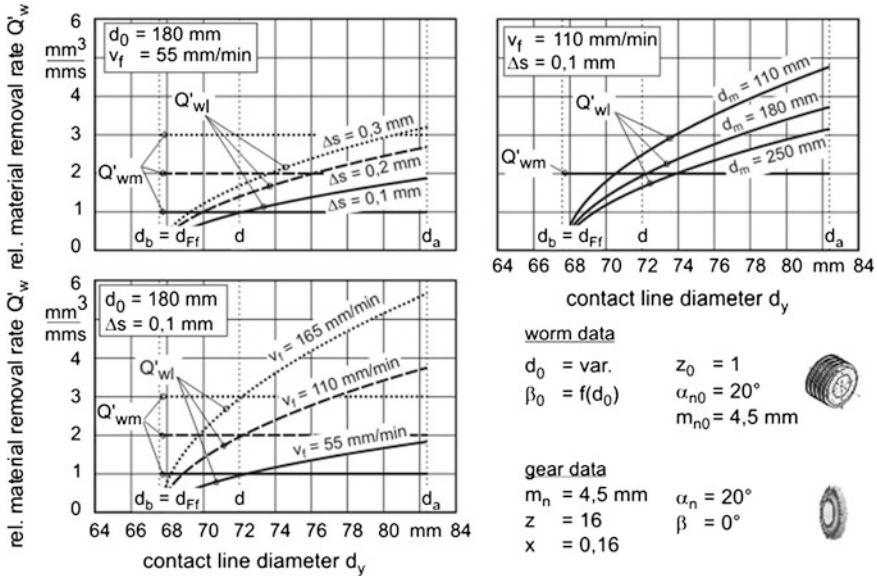


Fig. 14.12 Averaged and locally-related material removal rate in generation grinding

on the basis of empirically detected data. Thus, the geometrical, maximum contact length is determined by

$$l_{g,max} = \sqrt[4]{\Delta s} \cdot \left(\sqrt{f} + 0.4 \cdot \sqrt[4]{d_{a0}} + 0.2 \cdot \sqrt{m_n} - 0.0025 \cdot (\beta + 2)^2 \right) \quad (14.7)$$

and the single grain chip thickness by

$$h_{cu,max} = 0.14 \cdot f^{0.25} \cdot \Delta s^{0.15} \cdot z_0^{0.5} \cdot d_{a0}^{-0.5} \cdot m_n^{0.25} \cdot z^{-0.25} \quad (14.8)$$

At this, the index 0 characterizes a tool related variable, while f stands for the feed per workpiece revolution.

Copying processes are mainly used for the dressing of grinding worms. For this, the tool profile of a diamond profile roll is derived from the grinding worm geometry. The dressing tool is placed at a helix angle and lead along the worm, while the latter turns. This process corresponds to a thread grinding process. The geometrical relations are illustrated in a simplified manner in Fig. 14.13.

Attention should be paid to the fact that the profile of the rotating dressing tool does not correspond to the gap profile in the normal section of the worm. In fact, one has to consider that the contact line between dressing tool and grinding worm is not representable in a plane. Similar to the grinding of gears with profile grinding wheels, an alteration of the worm data also leads to alterations of the required dressing tool profile in this case. These alterations can occur during the process adjustment to a different number of threads of the grinding worm as well as following the dressing related diameter alteration of the grinding wheels. In industrial

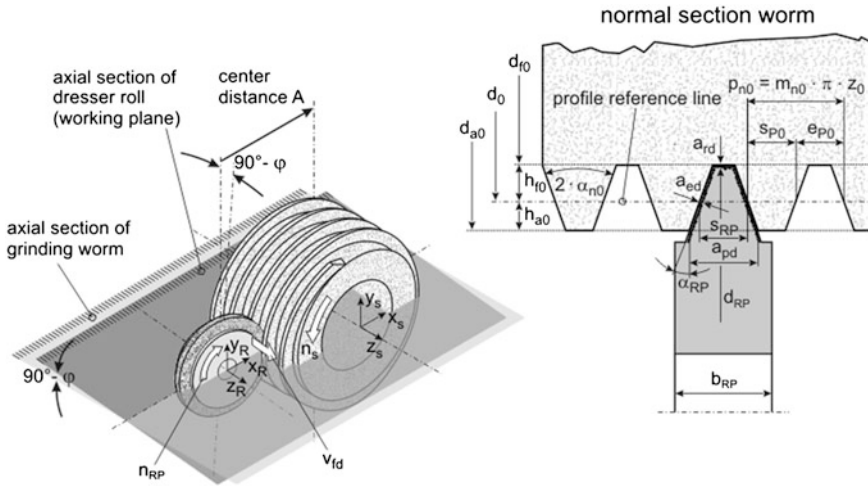


Fig. 14.13 Dressing of a grinding worm

practice, the flanks of the dressing tools are produced with a radius so that approximated worm flanks are generated when dressing an involute surface. A mathematical illustration of the dressing profile, which also considers possible machine axes compositions, was developed by [TÜR02]. Line dressing strategies offer more flexibility in the profile generation. However, due to the merely punctual contact they are accompanied by longer dressing cycles and therefore, are less attractive from an economic point of view.

14.4 Continuous Crossed Helical Grinding

In continuous crossed helical grinding, the effective partners are positioned like a worm gear with crossed (skew) axes. The process is mathematically similar to tooth shaving (Fig. 14.14) [BAU94]. However, grinding tools are used here. At this, the tool is mostly an internal toothed ring for reasons of beneficial contact ratios. In practice, this process is also called gear honing, pitch honing, shave grinding or also coroning (brand name of KAPP). It is, however not a honing process in the sense of [DIN8589]. In fact, it is a grinding process. Within the gear grinding processes, it can be classified as continuous generating grinding (see Fig. 14.14) [SCH99].

Tool and gear roll off at the pitch cylinders. The axis crossing angle causes an axial motion of the grinding wheel opposite the gear. This produces a cutting motion on the pitch circle. As is generally known above and below the pitch circle, at every tooth matching and in this case a “sliding”, i.e., cutting motion takes place, which superposes the axial motion as a resulting cutting speed, depending

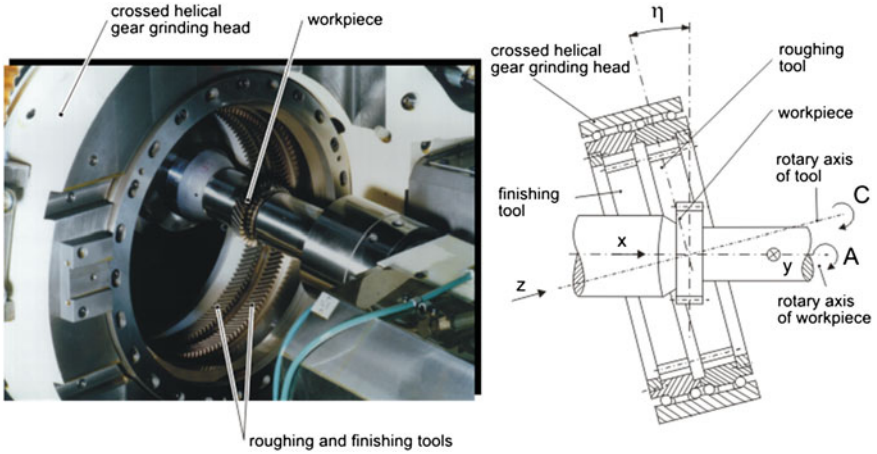


Fig. 14.14 Principle of crossed helical grinding (source Kapp GmbH)

on the contact point and whether it is an arriving or a departing flank (Fig. 14.15). At this, the axial cutting speed component is v_{ax} with the axis crossing angle δ (Fig. 14.15 bottom)

$$v_{ax} = \frac{\sin\delta}{\cos\beta} v_s \tag{14.9}$$

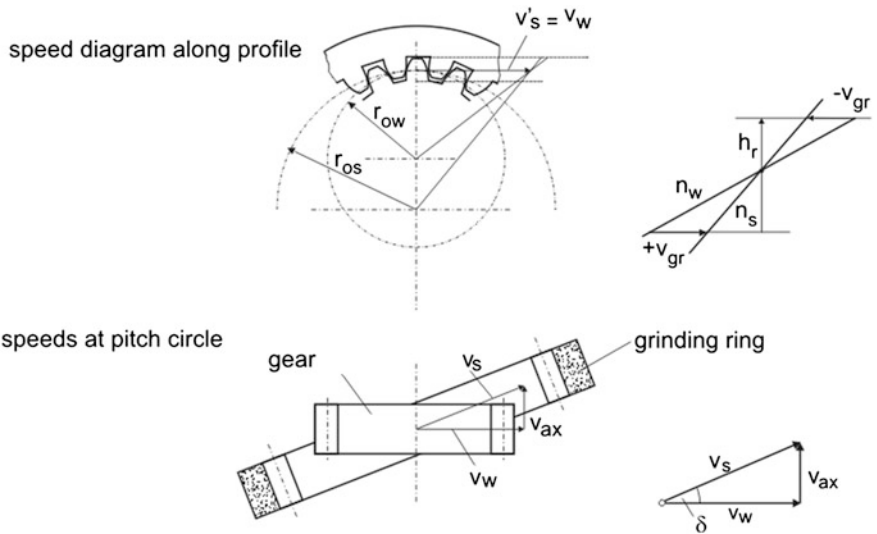


Fig. 14.15 Speed plans in crossed helical grinding

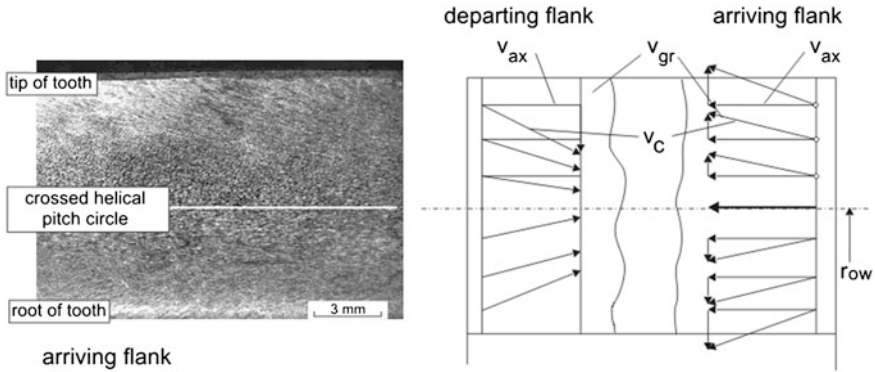


Fig. 14.16 Cutting speeds and grinding grooves in crossed helical grinding

From Fig. 14.15 (top) it can be deduced that the radial speed over the distance from the pitch circle h_r , the angular speed of the gear ω_w and the teeth number ratio z_s/z_w can be determined.

$$v_{gr} = \pm h_r \cdot \omega_w \left(1 + \frac{1}{z_s/z_w} \right) \tag{14.10}$$

Thus, the resulting cutting speeds illustrated in Fig. 14.16 result from the involute of the gear, in fact, differing according to arriving and departing flanks. Consequently the typical grinding groove profile for this kind of “finishing results.” Various sources [KOC83, BAU93, STA96, WRI97, AMI99] ascribe an especially beneficial noise behavior to this surface structure. Due to the considerable efforts to reduce the running noise, crossed helical grinding has become considerably more important lately.

The cutting speeds are far below those usual in grinding. The motion resulting from the kinematic of the crossed helical grinding gear is superposed by a second motion in the form of a linear oscillation in the direction of the workpiece axis in many cases. Its purpose is to further reduce the tooth flank roughness. The tooth flank removal enabled by crossed helical grinding is currently set at 0.1 mm by the leading machine and tool producers. The increase of the removal values can be attributed to a new drive and machine concept, which permit higher rpm and thus higher cutting speeds.

The tools are internally toothed rings of different grinding materials. Diamond rings need not be dressed and can be deployed economically especially in large batch production. However, dressable rings of aluminum oxide are mainly used for workpiece hardnesses below HRC 63, silicon carbide for workpiece hardnesses above HRC 63 or micro-crystalline aluminum oxide in usual grain sizes of 80–100 μm . The usual bonding types are artificial resin compounds and vitrified bonds, the latter showing a higher degree of stiffness but with a greater tendency to tool wear. To unite the positive properties of both types of bonding artificial resin-ceramic-mix bondings have been developed. For the dressing of the grinding ring,

diamond dressing gears are deployed whose geometry is identical to that of the gears to be machined. The dressing gears represent steel cores galvanically coated with a single layer of diamond grains. The axis distance between tool and workpiece is increased as a consequence of the grinding ring wear after each dressing process. At this, the axis crossing angle is to be updated so as to compensate the alteration of the pitch diameter. According to the current state-of-the-art, dressing intervals of up to 400 workpieces and total tool life quantities of 60,000 gears can be realized.

It is interesting that diamond grinding wheels can also be used for this process when machining steel. The process is known with the brand name “coroning” [NN00]. This possibility results from the fact that, only a very low grinding speed develops between tool and workpiece. A strong chemical wear only occurs at a higher temperature level due to the affinity between diamond and steel. Therefore, the high degree of hardness of the diamond can be put to beneficial use at low process temperatures in this case.

The typical mechanical and very low thermic load of the gear surface in the process leads to the fact that an especially beneficial residual stress condition can be achieved in the subsurface of the tooth flanks, whereas deeper lying layers are barely influenced. This is illustrated in Fig. 14.17 by means of several residual stress-depth courses.

The surface roughness of the tooth flanks after grinding is also relevant for the component life time. Therefore, the system and manipulated variables of the process were varied in tests, resulting in different component topographies. The test gears of the HD1 series showed the lowest roughness with values around $R_z = 2 \mu\text{m}$. The low flank roughness was achieved by using a fine grain size. In addition, an oscillating tool motion was superposed to the machining process. The highest flank roughnesses of up to $R_z = 4.1 \mu\text{m}$ occurred with the HD3 series. At this, a rougher grain size and no oscillation motion were deployed [MAR01].

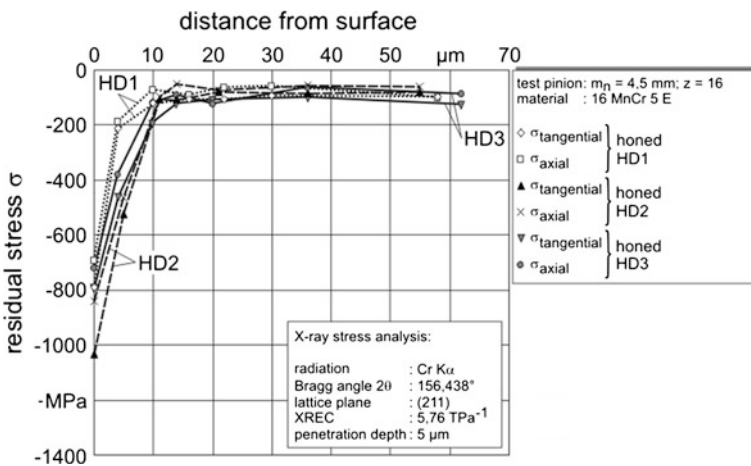


Fig. 14.17 Residual stress-depth courses in crossed helical grinding

	discontinuous profile grinding	continuous generating grinding	continuous crossed helical grinding
	copying	generating	
contact	total gap	convex-convex	convex-concave
contact times	long	short	short
kinematic	axial feed, few strokes, discont. radial infeed, positioning	generating feed, cont. change of gap, discont. depth of cut, few strokes	radial-axial sliding motion, cont. change of gap, cont. radial infeed, many generating movements
grinding speed	high	high	low
grinding burn	dangerous	less dangerous	no danger
residual stresses	process dependent	process dependent	generally compressive
topography (stimulation)	less beneficial	medium	especially beneficial
productivity	rather low	high	medium
flexibility	high	limited	limited
advantages if	larger workpieces, small number of teeth, internal gearing, geometric modifications	smaller workpieces, large number of teeth, batch production	smaller workpieces, small run-out distance, batch production

Fig. 14.18 Comparison of the introduced hard finishing processes

In Fig. 14.18, the essential characteristics of the processes introduced in this chapter have been opposed for a better overview.

14.5 Questions

1. Name some process chains in gear machining.
2. Which hard finishing processes for involute surfaces do you know?
3. Which motions have to be kinematically linked (straight gearing, helical gearing) in the profile grinding of gears?

4. Which values achieves the average related material removal rate in profile grinding? What is it averaged by?
5. Which motions have to be coordinated in path-controlled dressing?
6. What technological significance does the overlap ratio have in dressing?
7. Which motions have to be linked in continuous generating grinding (straight gearing, helical gearing)?
8. What significance do the medium and the locally related material removal rate have in generating grinding? What is the former averaged by?
9. How can grinding worms be dressed?
10. What is crossed helical grinding? Why does the term “gear honing” not apply?
11. What speed components does the (local) cutting speed consist of?
12. Where is the radial speed positive, where is it negative (choice of algebraic sign with the radius)?

References

- [AMI99] Amini, N., Westberg, H., Klocke, F., Köllner, T.: An experimental study on the effect of power honing on gear surface topography. *Gear Technol.* **16**(1), 11–18 (1999)
- [BAU93] Bausch, T.: Honen (Schabschleifen) von Verzahnungen [Honing (shaving) of gears]. In: Salje, E., Westkämpfer, E. (Hrsg.): *Jahrbuch Schleifen, Honen, Läppen und Polieren*, 57. S. 228–248. Ausgabe, Vulkan-Verlag, Essen (1993)
- [BAU94] Bausch, T.: Verfahren und Maschinen zum Wälzhonen (Schabschleifen) [Processes and machines for generating honing (shaving)]. In: *Moderne Zahnradfertigung*, 2. S. 514–563. Auflage, expert Verlag, Renningen-Malmsheim, (1994)
- [BEH97] Behrens, B.-A.: Entwicklung eines automatisierten Präzisionsschmiedeprozesses mit integrierter Qualitätsprüfung [Development of an automated forging process with integrated quality check]. Dr.-Ing. Dissertation, Universität Hannover, (1997)
- [BRE08] Bretl, N.: Zahnfußbruch mit Rissausgang unterhalb der Oberfläche an einseitgehärteten Zahnrädern [Tooth root fracture with crack initiation at case hardened gears]. Abschlussbericht FVA-Forschungsvorhaben Nr. 293II, FVA-Heft 851, Forschungsvereinigung Antriebstechnik e. V., Frankfurt am Main, (2008)
- [DEN03] Denkena, B., Becker, J.C., Stimpel, F: Grübchentragsfähigkeit einseitgehärteter Verzahnungen [Pitting load capacity of case hardened gears]. *Jahrbuch Schleifen, Honen, Läppen und Polieren*, 61. Ausgabe, Vulkan-Verlag, Essen, (2003)
- [DIN3960] N.N.: DIN3960 Begriffe und Bestimmungsgrößen für Stirnräder (Zylinderräder) und Stirnradpaare (Zylinderpaare) mit Evolventenverzahnung/Definitions, parameters and equations for involute cylindrical gears and gear pairs. Hrsg. Deutsches Institut für Normung, Beuth Verlag GmbH, Berlin, (1987)
- [DIN3961] N.N.: DIN3961 Toleranzen für Stirnradverzahnungen, Grundlagen/Tolerances for cylindrical gear teeth; bases. Hrsg. Deutsches Institut für Normung, Beuth Verlag GmbH, Berlin, (1978)
- [DIN3962] N.N.: DIN3962-1 Toleranzen für Stirnradverzahnungen. Toleranzen für Abweichungen einzelner Bestimmungsgrößen/Tolerances for cylindrical gear teeth; tolerances for deviations of individual parameters. Hrsg. Deutsches Institut für Normung, Beuth Verlag GmbH, Berlin, (1978)

- [DIN3979] N.N.: DIN3979 Zahnschäden an Zahnradgetrieben, Bezeichnung, Merkmale, Ursachen/Tooth damage on gear trains; designation, characteristics, causes. Hrsg. Deutsches Institut für Normung, Beuth Verlag GmbH, Berlin, (1979)
- [DIN8000] N.N.: DIN8000 Bestimmungsgrößen und Fehler an Wälzfräsern für Stirnräder mit Evolventenverzahnung, Grundbegriffe/Design dimensions and errors of hobs for involute spur gears; fundatmental terms. Hrsg. Deutsches Institut für Normung, Beuth Verlag GmbH, Berlin, (1962)
- [DIN8589] N.N.: DIN8589-0 Fertigungsverfahren Spanen; Einordnung, Unterteilung, Begriffe/ Manufacturing processes chip removal—Part 0: General classification, subdivision, terms and definitions. Hrsg. Deutsches Institut für Normung, Beuth Verlag GmbH, Berlin, (2003)
- [ISO1328] N.N.: ISO1328-1 (1995), ISO1328-2 (1997) Cylindrical gears—ISO system of accuracy. International Standard Organisation (1995, 1997)
- [HER08] Hergesell, M.: Einfluss der Graufleckigkeit auf die Grübchentrugfähigkeit einsatzgehärteter Zahnräder [Influence of the micro-pitting (gray staining) on the pitting load capacity of case hardened gears]. Abschlußbericht FVA-Forschungsvorhaben Nr. 459, FVA-Heft 844, Forschungsvereinigung Antriebstechnik e. V., Frankfurt am Main, (2008)
- [KAG02] Kage, R.: Begrenzungskriterien für die Maximalbelastung bei Verzahnungen [Limiting criteria for the maximum load capacity of gears]. Abschlußbericht FVA-Forschungsvorhaben Nr. 246II, FVA-Heft 670, Forschungsvereinigung Antriebstechnik e. V., Frankfurt am Main, (2002)
- [KLK00] Klocke, F., Kempa, B., Schenk, T.: Zahnfußtragfähigkeitssteigerung durch optimiertes Schleifen der Zahnfußrundung [Increase of tooth root load capacity by optimized grinding of the tooth root rounding]. Abschlußbericht FVA-Forschungsvorhaben Nr. 306, FVA-Heft 619, Forschungsvereinigung Antriebstechnik e. V., Frankfurt am Main, (2000)
- [KOC83] Koch, R.: Zahnradhonen—ein konkurrenzfähiges Feinbearbeitungsverfahren [Gear honing—a competitive finishing process]. VDI-Z 125 Nr. 17, S. 657–660 (1983)
- [KÖN94] König, W., Knöppel, D.: Feinbearbeitung gehärteter Zylinderräder mit unterschiedlichen Verfahren [Finishing of hardened cylindric gears by different processes]. Abschlussbericht FVA-Forschungsvorhaben Nr. 180/I+II, FVA-Heft 433, Forschungsvereinigung Antriebstechnik e.V., Frankfurt am Main, (1994)
- [LIE02] Lierse, T., Kaiser, M.: Dressing of grinding wheels for gearwheels. IDR (Industrial Diamond Review), S. 273–281 4/2002
- [LOO59] Looman, J.: Das Abrichten von profilierten Schleifscheiben zum Schleifen von schrägverzahnnten Stirnrädern [Dressing of profiled grinding wheels to grind helical gears]. Dr.-Ing. Dissertation, TU München, (1959)
- [MAR01] Marzenell, C.: Verzahnungshonen mit Diamantwerkzeugen [Gear honing with diamond tools]. Dr.-Ing. Dissertation, Universität Hannover, (2001)
- [NEW91] Newman, R.: Hard finishing by conventional generating and form grinding. Gear Technol. 3/4, 36–41 (1991)
- [NN00] N.N.: Verzahnungsbearbeitung, Profilbearbeitung, Fertigungsprogramm [Gear machining, profiling, production program]. Firmenschrift, Kapp GmbH, Coburg, (2000)
- [SCH94] Schriefer, H.: Hartfeinbearbeitungsverfahren mit zahnradförmigen Werkzeugen [Hard finishing processes by gear shaped tools]. In: Moderne Zahnradfertigung, 2. S. 323–350. Auflage, expert Verlag, Renningen-Malmsheim, (1994)
- [SCH99] Schneider, C.: Schleifen mit niedriger Schnittgeschwindigkeit und veränderlicher Wirkrichtung [Grinding with low cutting speeds and variable effective direction]. Dr.-Ing. Dissertation, Universität Bremen, (1999)

- [SCH07] Schwienbacher, S.; Wolter, B.: Ermittlung und Charakterisierung von Randzonenkennwerten und -Eigenschaften und deren Einfluss auf die Flankentragfähigkeit einsatzgehärteter, geschliffener Zahnräder [Determination and characterization of surface values and surface properties and their influence on the flank load capacity of case hardened ground gears]. Abschlussbericht FVA-Forschungsvorhaben Nr. 453I, FVA-Heft 830, Forschungsvereinigung Antriebstechnik e.V., Frankfurt am Main, (2007)
- [STA96] Stark, C., Konstantinidis, D.: Feinbearbeitung von Zahnrädern mit profilierten Honringen [Finishing of gears with profiled honing rings]. VDI-Z 138 Nr. 6, S. 66–92 (1996)
- [STE04] Stenico, A.; Krug, T.: Eigenspannungseinfluss auf die Zahnfußtragfähigkeit kleinmoduliger Zahnräder [Influence of residual stresses on the tooth root load capacity of small module gears]. Abschlussbericht FVA-Forschungsvorhaben Nr. 369/I+II, FVA-Heft 745, Forschungsvereinigung Antriebstechnik e.V., Frankfurt am Main, (2004)
- [STI09] Stimpel, F.: Technologische Kenngrößen für das Kontinuierliche Wälzschleifen von Evolventenverzahnungen [Technological characteristics in continuous generating grinding of involute gears]. Dr.-Ing. Dissertation, Leibniz Universität Hannover, (2009)
- [TÜR02] Türich, A.: Werkzeug-Profilherzeugung für das Verzahnungsschleifen [Generating of tool profiles for gear grinding]. Dr.-Ing. Dissertation, Universität Hannover, (2002)
- [WOB95] Wobker, H.-G., Brunner, G.: Hartfeinbearbeitung präzisionsgeschmiedeter Zahnräder [Hard finishing of precision forged gears]. Technica Nr. 20, S. 16–23 (1995)
- [WRI97] Wright, N.W., Schiefer, H.: Basic honing and advanced free-form honing. Gear Technol. 7/8, 26–33 (1997)

Chapter 15

Process Layout and Integration into the Process Chain

A process, such as the manufacturing of a component by cutting or abrasive machining is system-technically defined as the transformation of input variables of a system into corresponding output variables in the sense of system engineering. At this, the transformation represents a development relative to the reference criterion “time”. The cutting process is already described as a system in [Sect. 1.4](#).

This chapter begins with explaining definitions and correlations around the term “process chains”. On that basis, the theoretical basics of process and process chain layout are described by means of simple examples. [Section 15.5](#) “process monitoring” demonstrates ways to monitor the process quality and take influence on the machining process.

15.1 Basics of Process Chain Layout

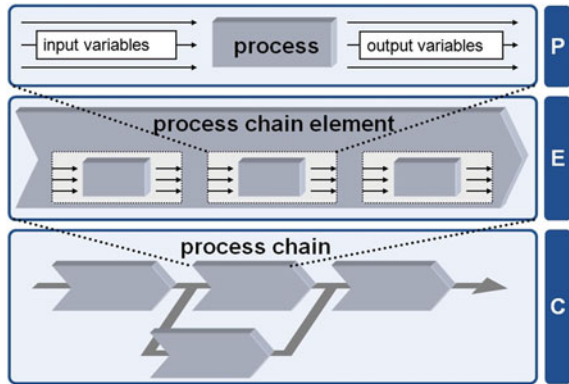
To understand the approach in process chain layout, it is initially necessary to delimit the terms “process”, “process chain element” and “process chain” contentwise. The PEC model shown in [Fig. 15.1](#) gives an overview of the terms used in the following.

The PEC model is divided into three levels. At this, the *process (P)* represents the smallest and thus indivisible unit of a process chain. Input and output variables are part of a process. A manufacturing operation such as, for example the generation of a hole with a tool, is called a process.

The *process chain element (E)* is defined as a sequential line up of single processes. A parallel configuration of processes to a process chain element is not permissible. The term process element is also used as a synonym for the term process chain element. For example, a process element is the workpiece machining on a machine, such as the grinding of all the main and pin bearings of a crank shaft.

If more than one process element is necessary to manufacture a product, their line-up is called *process chain (C)*. The single process elements are either put into

Fig. 15.1 Definition of the term process by the PEC model



sequential or parallel order or a mix of both. Thus, a process chain can be defined as an orderly line up of process elements with the target of transferring certain transformation objects from an input condition to a corresponding output condition. In the sense of production technology, transformation objects are raw or half-finished parts, but in general, they can also be other material and immaterial objects such as energies, information or services.

15.1.1 Technological Interfaces

For the layout of a process chain, it is important to know about the hand-over variables between the process elements. At the same time, the hand-over variables represent output and input variables of two subsequent process elements (n) and ($n + 1$). Some examples for hand-over variables of production-oriented processes are:

- measurements and oversize,
- surface structure or
- temperature of a component.

The totality of the hand-over variables between two process elements is the hand-over condition. In production-oriented systems, this condition is called *technological interface*. Figure 15.2 illustrates technological interfaces between process element ($n - 1$) and process element (n), as well as between process element (n) and process element ($n + 1$).

Process elements are displayed in a timely correlation. Per process element, the process time t_n incurs. Technological interfaces, however, can only be assigned to one point of time. A corresponding time interval does not exist. The total of all sequential processes of a process chain makes up the total time t_{tot} .

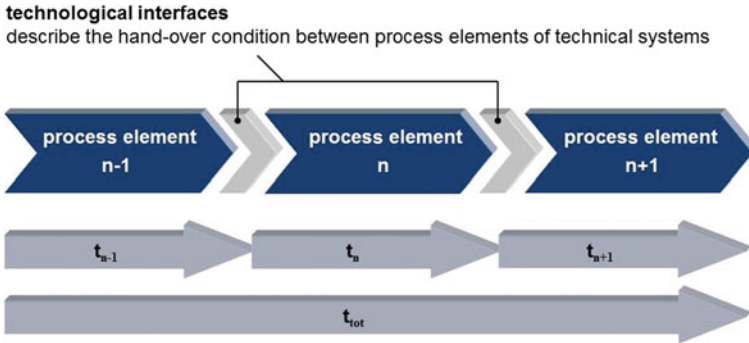


Fig. 15.2 Technological interfaces within a process chain

15.1.2 Process Chain Layout

Improved cutting material, more efficient and more accurate machines as well as increased requirements towards a cost-efficient, rapid and environmentally sound manufacturing contribute to the fact that cutting processes have further developed to a high degree. Especially the processes of hard finishing with geometrically defined cutting edge can be named here as examples. They can make a considerable contribution for the shortening of process chains and thus to the reduction of processing times and to the reduction of production costs.

To optimise existing process chains by using new technologies or to configure new process chains optimally, a process chain layout is carried out. The tasks to be passed through for this purpose are subdivided into two steps, which depend on each other [BRA08]. At the beginning of the process chain layout, the processes are identified, which allow the generation of the product in their order, which is to be determined. This step is called *process chain design*. Based on this, it is possible to configure the process parameters and technological interfaces.

The target of the process chain design is to identify suitable processes so as to allow a most efficient production. The assessment factors are, for example, economically-logistic target variables such as processing times, work cycle times and machining costs. Complex process chains, however, rapidly let the production planner reach his limits due to the high number of design variants. This problem can be confronted with the use of process chain simulation. The technological basis of a process chain simulation are the locally optimised single processes such as sawing, turning/milling, hardening or finishing. The result of a simulation cycle gives an indication concerning the profitability of the reviewed process chain. Rationalisation potential for the process chain can be exploited by redesigning.

The development of new process chains as a medium to improve the profitability and quality must not only be applied on single work or production steps, it must be targeted at the total optimum [TÖN07]. The *ASI method* represented in Fig. 15.3 offers support for the implementation of a holistic process chain layout.

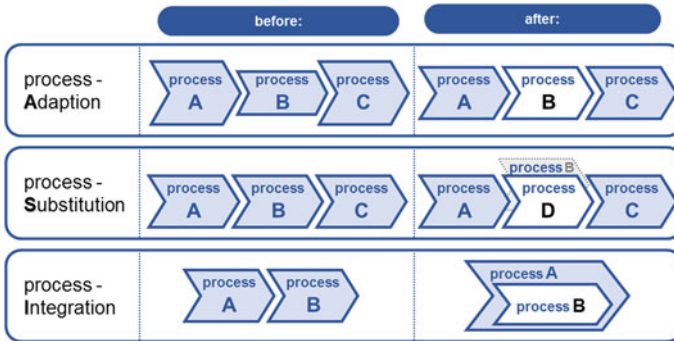


Fig. 15.3 ASI method for process chain design

The basis is the redesign of production-oriented process chains by adaption, substitution and/or integration of single production steps.

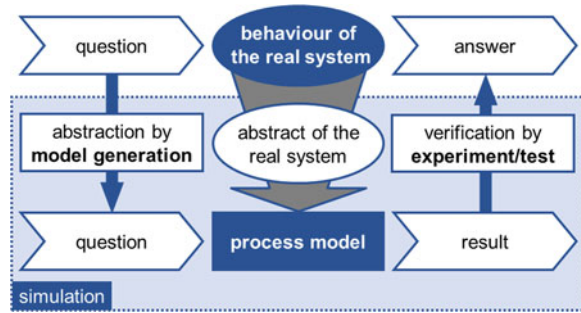
Adaption is the adjustment of two subsequent processes, e.g., the production of raw parts by forging and the following cutting. In the figure, process B is adapted to processes A and C. In the development of tools and tool machines or as a reaction to altered cost structures, the *substitution* of a production process can be sensible. One example for such a substitution is the substitution of a grinding process by hard turning. In Fig. 15.3, process B is substituted by the further developed process D. The *integration* of manufacturing steps shortens the operation sequence. This is often connected with direct process-conditioned cost savings or indirect cost savings based on shortened through-put times and reduced controlling effort. A current example for this is the complete machining of components by integration of different manufacturing processes on a multi-axial turning machine or a machining centre. In the illustration, process B is integrated into the course of production step A.

15.2 Process Model Generation

In technology, the term model stands for an image of reality. The VDI guideline 3633 defines model as a simplified reproduction of a system [VDI3633]. In this context, simplified reproduction means the reduction to only those characteristics relevant for the modelling target. Here, model generation is to be all the necessary steps for the generation of a model.

The analysis of complex technical processes such as cutting processes requires the set-up of process models. For this purpose, all single process steps are abstracted first so as to achieve a reduction of the complexity and a concentration on the main characteristics. Toenshoff defines the term “*process model*” as an abstract presentation of a process, which serves to link up the causes and effects

Fig. 15.4 Model generation to predict the behaviour of a real system



with each other [TÖP92]. The target of the process model generation is to understand the correlations and interactions within a process better as well as being able to predict resp. optimise future process results. The application of process models is often called “simulation”.

The process model depicts the correlations between input and output variables of a process. It thus describes the static and dynamic behaviour of a process. Figure 15.4 clarifies the correlations between real process and process model. During the model generation, an abstraction of the initial question takes place to begin with. It is fed into the process model. The application of the model supplies an outlook of the behaviour of the real system. Before using the process model, its functioning has to be verified using known input and output variables.

The generation of process models can occur in different ways, depending on the application and the information at hand. Toenshoff and Paul distinguish between three types of process models [TÖP92]:

- heuristic models, which can be obtained by means of the sophisticated description of know-how,
- physical/empiric models, which rely on physical, mathematical basics and
- information-oriented data models.

Figure 15.5 illustrates the mutual relations between these types of models.

Heuristic models depict know-how, e.g., the process understanding of a machine operator in production. For instance, the experienced operator of a CNC turning machine is often able to draw conclusions for the layout of the machining process from process noises or the shape of the generated chips. This knowledge, however, often gets lost with a change of workplace. On the other hand, the filing and guarantee of a permanent availability of know-how, e.g., from the manufacturing area are of great importance for the success of a company. The supply and maintenance of such knowledge is referred to as knowledge-management. The modelling of know-how occurs by means of simple production rules (if/then relations), class or object structures (ER or UML diagrams) [OES98] or by means of fuzzy quantities (fuzzy logic) [PAU94].

Technological dependencies, for example as between cutting force F_c and cutting power P_c (Sect. 5.1), can be illustrated in mathematical algorithms.

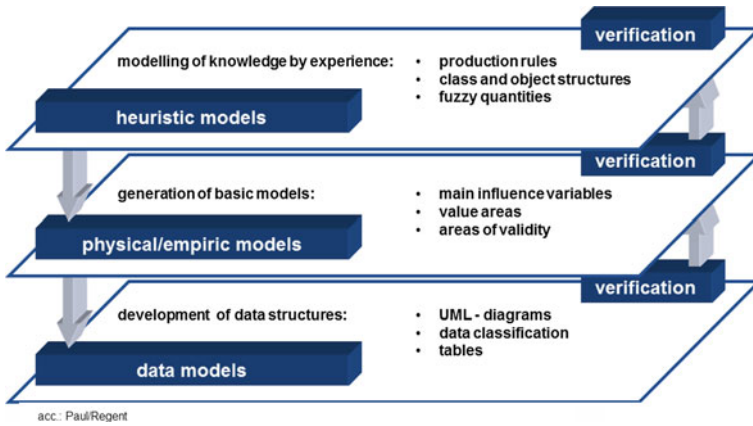


Fig. 15.5 Levels of model generation

The thus resulting process models are determined as *physical or empiric models*—depending on their type of retrieval [PRO77]. While physical process models are based on physical laws, empiric process models are detected by means of measurements in the process experimentally (Fig. 15.6).

For the generation of physical process models, relevant physical processes are selected and transformed into a qualitatively model, based on the target of the process. The mathematical representation of the model—the physical process model—is detected on the basis of physical laws. It represents the quantitative dependencies between technological input and output variables, the correlation between adjustment variables and work result, for example. Empiric process models are, as mentioned before, determined by measurements in the process

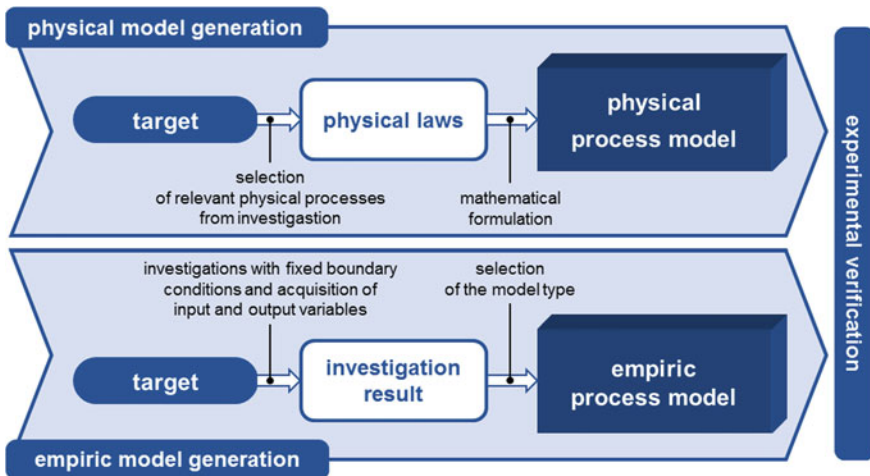


Fig. 15.6 Physical and empiric process model generation

experimentally. For example, in the cutting technology, grinding tests are carried out, at which relevant input and output variables are to be recorded. The test results are evaluated, a type of model is selected (correlation function), the coefficients determined and the empiric process model verified by means of further tests. The benefit of physical process models is a process-independent process understanding and the connected simple transferability to altered machining conditions. For cutting processes, however, a purely physical model generation is unrealistic because the existing physical laws are not sufficient and therefore have to be completed by experimental investigations empirically.

Apart from the heuristic and physical/empiric models, Fig. 15.5 illustrates *data models* as the third level of process model generation. Data structures are determined in data models so as to ensure a holistic description of the entire relevant production-oriented information. Data modelling includes the development of an object-oriented relationship model in the form of class diagrams. These can also be illustrated as sequence, condition or activity diagrams for further use [OES98]. The data models are deposited, i.e., filed in relational, object-relational or purely object-oriented data banks.

15.3 Process Layout Using the Example of “Hard Finishing”

The result of a cutting process is determined by the input, process and output variables. The setting of these variables, considering the mutual dependencies is called process layout. The starting point of a process layout is the determination of target variables. These target variables represent specifications for the result variables generated by the machining process. Generally, we distinguish between quality-relevant, economic and ecological targets of a machining process.

The quality of a cutting process is judged according to the resulting component quality. For this, characteristics are macro-geometry, micro-geometry and surface zone influence. Figure 15.7 shows the quality characteristics of an external grinding process in an exemplary way. Analogically, the relevant characteristics are assigned for the economic and ecological targets. In the design process or production planning, component-specific target values or target intervals are detected for the single characteristics of a process. These targets are illustrated in Fig. 15.8 for an external grinding process in an exemplary way.

In the following, the approach to the layout of machining processes is explained by means of the above described external grinding process. The difficulty of a process layout is the weighting of the target variables compared with each other. What is for example, the significance of the ecological targets of the machining which are the quality-determining ones? A proven and tested method to determine these weightings is the *target tree process*. In design methodology it is applied to carry out an evaluation of different concept variants [ZAN70]. For the layout of the

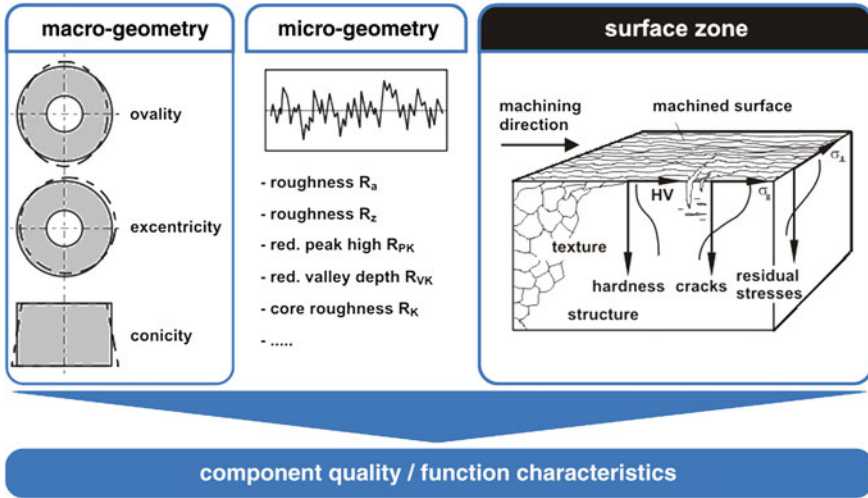


Fig. 15.7 Quality characteristics in external grinding

	characteristic	specification/target variable	set value(example)
quality	macro-geometry	diameter d_W	$40 \pm_{0,000}^{0,010}$ mm
		workpiece width b_W	$20 \pm_{0,000}^{0,015}$ mm
	micro-geometry	roughness R_a	$\leq 0,5 \mu\text{m}$
		roughness R_z	$\leq 6,3 \mu\text{m}$
surface zone influence	residual stress state σ_{II}	≤ 0 MPa	
	workpiece hardness (Rockwell)	≥ 60 HRC	
economy	times	cutting time t_C	≤ 10 s
		workpiece time t_e	≤ 30 s
costs	grinding cost per piece K_e	≤ 5 €	
ecology	environment. compatibility	cutting fluid quantity Q_{dcc}	≤ 10 l/min
		type of cutting fluid	virgin oil
energy consumption	grinding power P_C	≤ 10 kW	

Fig. 15.8 Exemplary target variables for external grinding

exemplary grinding process it is used to calculate the mutually corresponding priorities from the weightings of the single target variables.

Figure 15.9 illustrates a target tree for the above mentioned target variables. This one is subdivided into four levels. The target function to be determined is located on the first level. The second level organises the target variables in the group's quality, economy and ecology. A detailing in partial groups is shown on the third level and the targets variables themselves on the fourth level. Weightings

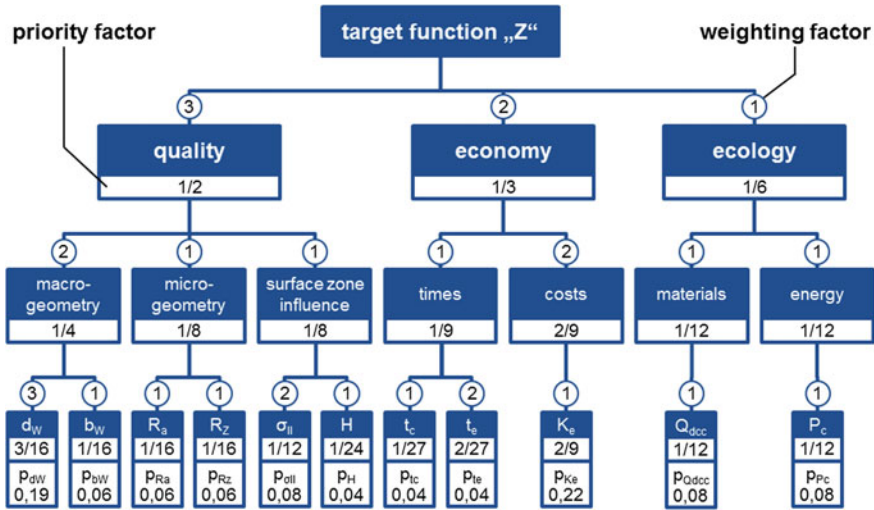


Fig. 15.9 Determination of priority factors according to the target tree process

are assigned to each branch of the target tree. The weight of the group quality amounts to 3 in this example, the group economy is weighted with 2 and the group ecology with 1. In practice, this means that for the grinding process to be designed, the quality of the manufactured components is exactly 3 times as important as the ecological target variables. The weightings are carried out the same way on the lower levels.

Priority factors are determined from the *weighting factors* for each element of the target tree. For this purpose, the weighting factors of a level are added to begin with. For the second level, this adds up to $3 + 2 + 1 = 6$. A *priority factor* is represented as a fractional rational number. The sum of the priorities is in the denominator of this fraction, the priority of the element concerned in the numerator. So the priority factor for the quality amounts to $3/6$, which equals $1/2$. In the lower levels the priorities are determined in a similar way. However, the determined single priorities of the third and fourth level additionally have to be multiplied with the priority of the group located above. The sum of the priorities of a level is generated as a test. It should always be 1.

After having defined the priorities of all target variables, the *target function* for the layout of the machining process is compiled (Eq. 15.1). In target function Z , the standardised variables for the target variable \bar{x}_i enter apart from the priority factors p_{xi} .

$$Z = \sum_{i=1}^n (1 - p_{xi} \cdot |\bar{x}_i|) \tag{15.1}$$

The standardisation is necessary so as to be able to compare the target variables with each other independently from their different values and dimensions. As a

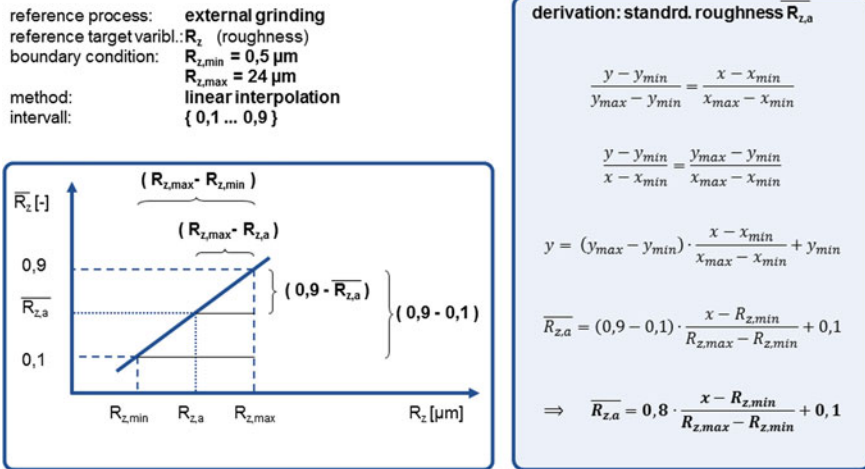


Fig. 15.10 Standardisation of the target function for the roughness R_z

standardisation interval, the variable area (0.1–0.9) is selected. The approach to the standardisation is clarified in the example in Fig. 15.10:

After the standardisation of all target variables these can be either positive ($x > 0$) or negative ($x < 0$). A uniform orientation is necessary, however, to ensure the comparability. Thus, Eq. 15.1 generates the value of the standardised variables.

In addition, in Eq. 15.1 it must be observed which values of the standardised target variables \bar{x}_i lead to an improvement of the target function Z . If evaluations criteria are mainly used as in the example from Fig. 15.8, which have an advantageous effect for smaller values, (example: roughness or costs), the standardised and weighted target variables are to be subtracted from 1. If, on the contrary, evaluation criteria are considered which have an advantageous effect for higher values (example: efficiency factor), the term $p_{xi}|x_i|$ from Eq. 15.1 is not to be subtracted from 1. The result of the target function is called evaluation code Z . The machining result is better, the higher Z .

In the so-generated target function, technological models (so-called basic model) are introduced to describe the target variables. For example, the following model is used for the roughness R_z illustrated in Fig. 15.10 [CZE00]:

$$R_z = c_0 \cdot v_{ft}^{c_1} \cdot f_r^{c_2} \cdot v_c^{c_3} [\mu m] \tag{15.2}$$

The constants and exponents c_0 to c_3 required to determine the roughness R_z are model-specific values and can adopt different variables according to the combination of workpiece, tool and machine.

15.4 Process Chain Layout Using the Example “Gear Production”

In practice, cutting machining processes cannot be regarded alone. Generally, the machining occurs in several subsequent partial steps as so-called multi-step process conduct. This multi-step process conduct (example: roughing and finishing a function area) represents the layout of a process chain element according to the PEC model. The layout of different process chain elements to each other is called process chain layout. The target of a *multi-step process conduct* is a preferably high correlation of the machining result with previously determined target variables. For example, a high material removal rate in the roughing process allows a more rapid material removal. In contrast, high surface qualities as well as dimension and shape accuracies are achieved with a lower material removal rate and consequently lower finishing forces.

The following example (Fig. 15.11) demonstrates the effects of two-step grinding on the workpiece surface zone. Generally, the surface zone state is characterised by residual stress course, hardness and structure condition. It is very significant for highly-loaded components. A faultless functional behaviour of the components is only achievable by reaching certain quality targets. At this, it is especially important to avoid residual tensile stresses in the surface zone of the terminated components, so as to counteract crack formation among other. Figure 15.11 shows how critical residual tensile stresses caused by grinding can be avoided for an external plunge grinding process by means of multi-step machining.

The high material removal rate of roughing causes a relatively high thermal influence in the workpiece surface zone. The resulting residual tensile stresses can

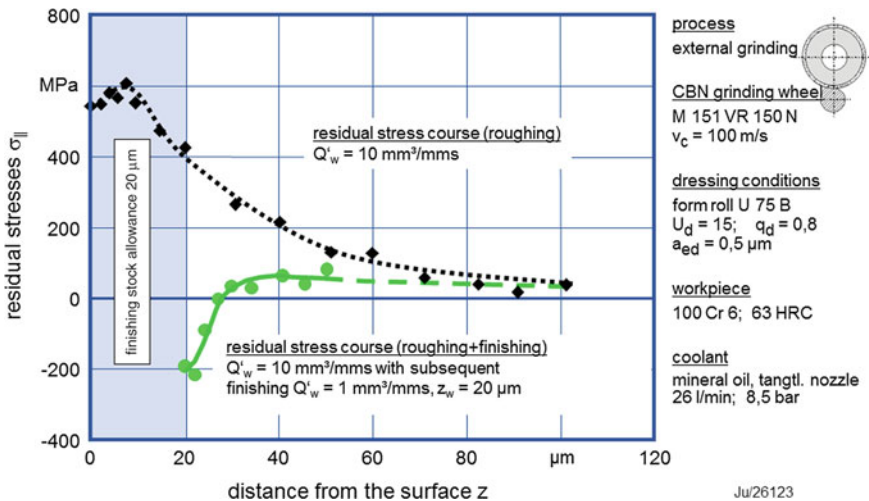


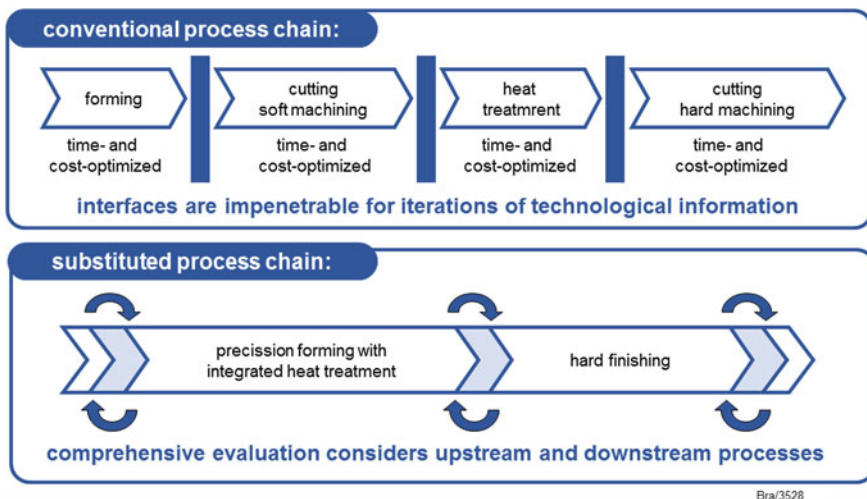
Fig. 15.11 Residual stress course at multi-step process conduct

be removed by adapting the oversize in the finishing process. In addition, a mainly mechanical influence of the workpiece surface occurs due to the low material removal rate in the finishing process. This causes residual compressive stresses, which mostly balance the residual tensile stresses remaining in the deeper layers of the workpiece surface and often has a positive effect on the component fatigue life.

Complex technical components, e.g., gears, are generated by different manufacturing processes. They develop complex process chains consisting of different process chain elements such as forming, cutting and hardening. A process chain layout is carried out so as to obtain an optimum result from such process chains. In the following paragraph the necessary process for this purpose will be explained using the example of a gear production.

The top of Fig. 15.12 illustrates a conventional process chain for the manufacturing of gears for automobile transmissions. The single process chain elements are locally optimised concerning time and costs. The interfaces of the process elements are impenetrable for an iterative information flow towards the layout of the process chain.

The bottom part of Fig. 15.12 shows a further developed process chain where the generation of raw parts, cutting soft machining and heat treatment have been substituted by precision forging with integrated heat treatment. The background of substitution is the intention to exploit the economic advantages of forging, which occur at high lot sizes. In addition, the integrated heat treatment supersedes the repeated heating before hardening, which considerably reduces the energy need of the process chain. The process chain layout and optimisation takes place considering economic-logistic targets and technological interactions between the process chain elements. At this, the approach is according to the “method for the



Bra/3528

Fig. 15.12 Process chain design by substitution and integration of single processes

positioning of technological interfaces” (design of technological interfaces—DTI-method) [BRA08, DEB03].

During the process chain layout, two questions have to be answered as a matter of principle:

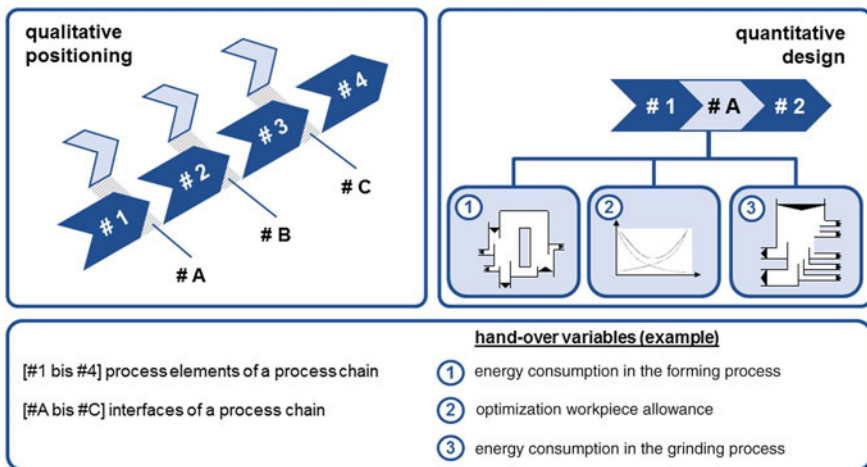
1. Where in the process chain do technological interfaces occur?
2. What level are technological hand-over parameters planned at?

The answer to the first question occurs during the process chain design. As tools for this, a process chain simulation with subsequent application of the ASI method is described in Sect. 15.1. In connection with the DTI method, this first phase of the process chain optimisation is called “qualitative positioning” (see below). The problem of the second question can be illustrated for the exemplary process chain for the manufacturing of gears as follows:

- Generation of a high component quality by means of precision forging and a resulting lower effort for the hard finishing or
- Generation of a lower component quality by means of precision forging at a higher effort in hard finishing.

The target is to determine an optimum between these two layout variants. For this purpose, the technological hand-over values at the interfaces of the process chain have to be analysed and quantitatively configured. The DTI method describes this phase as “quantitative positioning”. The necessary approach is explained below. The following Fig. 15.13 illustrates a schematic image of the approach when positioning technological interfaces.

Target of the *qualitative positioning* of technological interfaces is the process chain design using suitable manufacturing technologies. At this, an increase in the



Bra/32914

Fig. 15.13 Qualitative and quantitative positioning of technological interfaces

productivity and profitability is always aspired. This is achieved, e.g., by reducing the production steps and the technological interfaces within the process chain. The reduction of the number of production steps aims for a decrease of the throughput time and thus of the manufacturing costs. In addition, a reduction of the interfaces decreases the computing time for the layout of the hand-over variables to the technological interfaces.

To carry out the qualitative positioning, an analysis of the production steps and cycles required for production is carried out. Based on this, manufacturing processes which allow a preferably efficient component production are identified. An evaluation of the single production processes acts in accordance with the degree of added value, for example. So during the process chain design, attention must be paid to combine processes with a low degree of added value with ones that considerably increase the workpiece value (→process integration). As tools for the subsequent process chain design, the ASI method (see above) or methods of process substitution, process combination, process elimination and process exchange recommended by Koenig [KÖN87] are used. The result is different process chain variants based on alternative manufacturing processes.

Figure 15.14 illustrates different technological variants for the design of the process chain for the production of gears with high accuracy requirements. In all three variants demonstrated, the input material is a rod-shaped semi-finished product.

The *quantitative layout* of technological interfaces describes the dimensioning of the technological hand-over values between the single process steps. The process models for all process elements are determined based on physical and empiric models (see above). The next step is the definition of the prevailing boundary

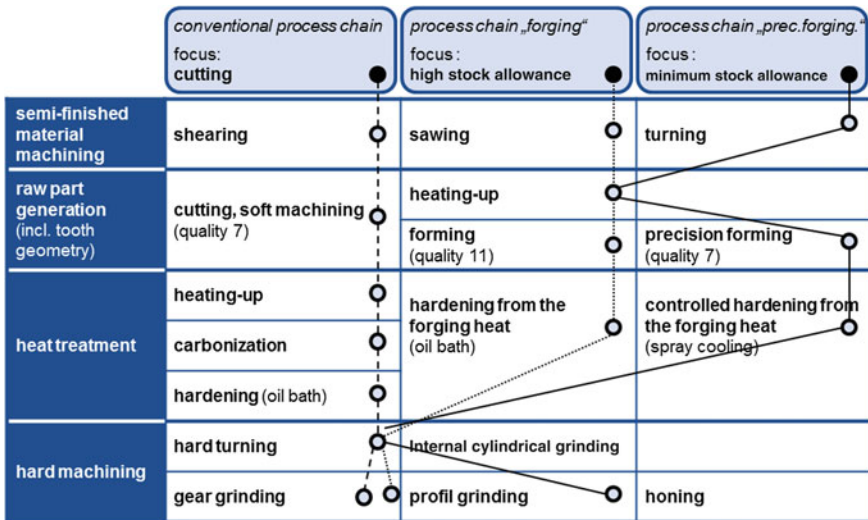


Fig. 15.14 Alternative process chains for the manufacturing of gears

conditions for each production process. The resulting functions (specific process model) are merged to target functions for the layout of single technological variables. The determination of the target functions and the identification of weightings for each target variable occur according to the target tree process (Sect. 15.3).

First, the detected target functions for the single production steps are weighted and then merged to a total target function. The calculation of the target function produces the degree of layout of the process chain under the given boundary conditions. Varying the boundary conditions for the process chain (e.g., cycle time) or for single processes (e.g., amount of cutting fluid) can influence the layout result of the process chain positively or negatively. The determination of the basic conditions and the weights of the target variables depend decisively on the know-how of the planner.

Process chains consisting of few subsequent process steps can easily take the planner to his limits, if the process chain is to be designed holistically at an optimum. Not only the multiple process parameters of all production processes, also the mutual correlations seem to make a layout based on the cognitive tasks of the planner impossible. The linkage of the single process models of the entire process chain for an optimum determination of the interfaces do not allow the deterministic identification of a solution in an acceptable period, not even with modern data processing systems. Therefore, one must resort to heuristic solution methods (e.g., genetic algorithms) or methods such as “design of experiments” DoE [DEH09]. At this, the use of simulation systems allows an automated application of the test plans and under stochastic conditions, finding a sufficiently good solution for an optimum dimensioning of the technological interfaces.

In the following, an example for the layout of a technological interface is explained. For this purpose, the process chain for the production of highly-loaded gears for automobile transmissions by means of precision forging is consulted [DER07]. In this new process no soft machining of the gearing takes place. Between the process elements precision forming and hard machining, research has shown that the workpiece oversize and its alteration in serial production are the main hand-over variables between the process steps. It has decisive influence on the economic targets, i.e., the production costs of the gears. To demonstrate these correlations, Fig. 15.15 illustrates the different wear behaviour of the forging dies and the grinding wheel.

The left side of the image shows a forging process. At each press stroke, the dies flare due to wear—the generated components become bigger in the course of time. If a tight diameter tolerance of the forged part has been determined (oversize tolerance), only few components can be manufactured with one set of dies. The image on the right shows a grinding process. The used grinding tool wears during the grinding process. The bigger the absolute forging oversize at this (planned machining oversize plus oversize tolerance of the forging process) has been set, the higher the grinding wheel wear per generated component. This is due to the increased workpiece volume, which has to be removed by grinding in the case of a worn set of dies. It becomes clear that the grinding oversize itself has little effect

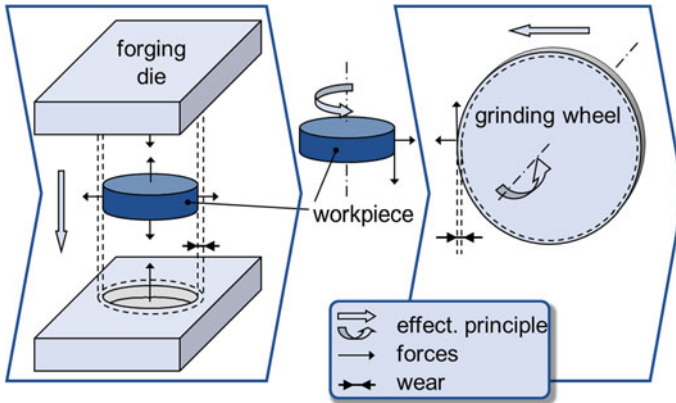


Fig. 15.15 Wear effect during the forming and grinding process

on the layout of the forging process. In fact, it is the oversize increase of the generated half-finished parts caused by the wear of the forging dies, that has a negative effect on the following production steps.

Figure 15.16 illustrates the qualitative courses of the process costs depending on the oversize increase for a precision forming process and a multi-step hard finishing process. The target of the comparison of both curve progressions is the determination of a value for the optimum oversize increase Δa_{opt} .

The life time of a forming tool can be prolonged to be a high oversize tolerance. If in contrast, only a very low oversize tolerance is permitted, the process costs for the precision forming process will rise due to lower tool life. For hard finishing, on the other hand, an increase of the process costs occurs due to the increased

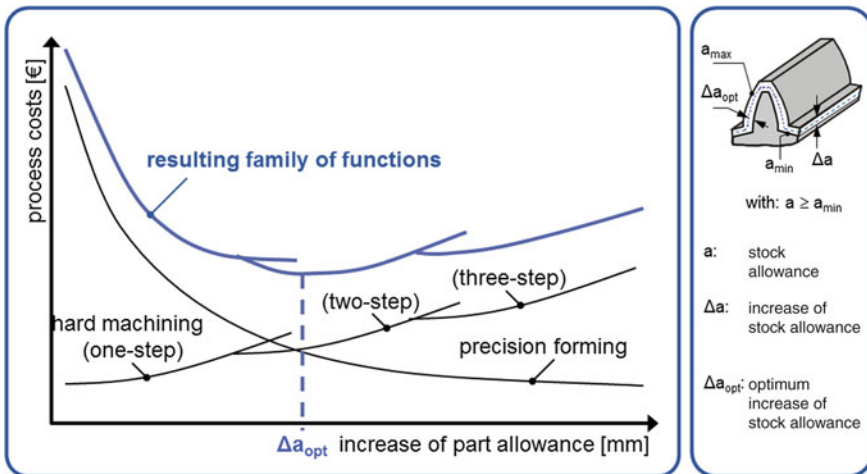


Fig. 15.16 Technological correlations between forming and hard machining

workpiece oversize after forging, since a higher Δa is accompanied by an increased oversize a and the process time increases as well as the tool wear. The discontinuous course of the cost function illustrated in image 15.16 results from the multi-step structure (roughing/finishing) of the grinding process.

15.5 Process Monitoring

The process monitoring represents an important task within the framework of manufacturing, so as to achieve the target variables determined in the process and process chain layout. In its course, input, process and result variables are analysed and compared with each other. This is how, on the one hand, the basis for an active intervention in the process via controlling mechanisms and, on the other hand, the basis for the development, evaluation or verification of empiric process models is generated (Sect. 15.2). The *process monitoring* represents the testing of defined process characteristics and parameters. In Fig. 15.17, the qualitative test (*perception*) and quantitative test (*measurement*) are distinguished.

A direct perception, for example, is taste of a medium. The appearance, on the other hand, is only perceived indirectly via reflected light. The evaluation of these perceptions is based on implicit, i.e., unstructured know-how. A measurement, however, complies with explicit, i.e., structured and documented knowledge. At this, the compilation of a length by means of a comparative normal represents a direct measurement. Temperatures (e.g., in a thermometer) are deduced from the length expansion of a comparative normal. It is therefore an indirect measurement.

In production technology, especially in cutting, the measurable variables are differentiated after the time of their development. Variables which occur during a process, are called process variables. Variables which exist as a permanent result at the end of a process, are called result variables or output variables (Fig. 15.18).

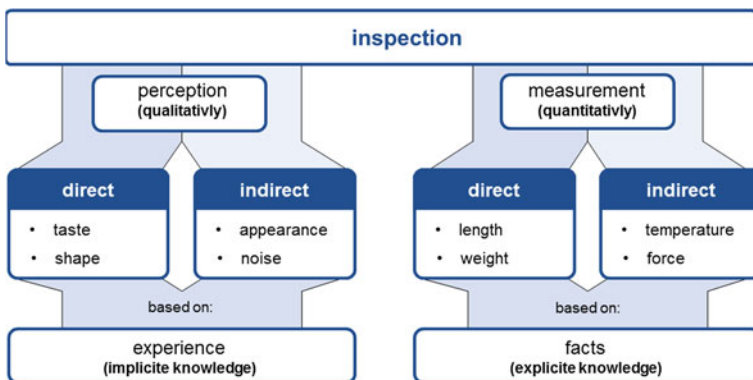


Fig. 15.17 Testing as a basis of process monitoring

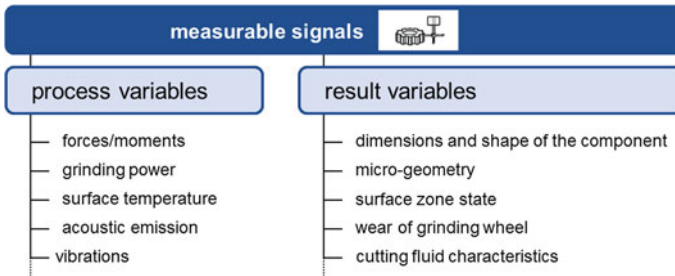


Fig. 15.18 Signals and variables on process monitoring in the cutting process

Further information on this topic is delivered by Toenshoff [TÖI01] and Karpuschewski [KAR01].

A comparison of the measured process and result variables with the corresponding target variables generally provide deviations from the set values. So disturbances are affecting the process. According to whether the deviations resulting from the disturbances are within a determined tolerance, a regulatory intervention in the process will become necessary. The causes for such an intervention can be of *stochastic* origin, e.g., temperature alterations, but also *systematic* alterations of the boundary conditions, e.g., grinding wheel wear during the grinding process.

Figure 15.19 introduces different quality control loops. The target of quality control is the reduction of the mentioned disturbances variables on the resulting component quality. The control loops are differentiated according to the type of the underlying measurement variables (process variables or result variables) and the time delay of the intervention in in-process, process-near and superior control. For the execution of the quality control, a process layout takes place first. For this purpose, the primary (e.g., cutting speed) and secondary manipulated variables (e.g., cutting force) have to be determined. As input information for this, existing process models and process data, as contained for example in a quality information system [TÖC96] are used.

During a machining process, process signals such as forces, powers or sound emission can be recorded by sensing. These process signals allow the gaining of process variables by means of data reduction and parameter generation. They can be deployed for an *in-process control*. The adaptive control (AC) for the grinding process can be mentioned as an example [TÖF02].

The in-process quality control occurs on the basis of process variables. In the process-near and superior quality control, result variables are considered additionally. The target of the *process-near quality control* is to balance a lack of process quality as quickly as possible. In a best case, this can be regulated from component to component. A *superior quality regulation* acts during the entire production period of a component. This kind of control is carried out, for example, by collecting process data about different components and production lots. The underlying process data are updated with these data and a new process layout and

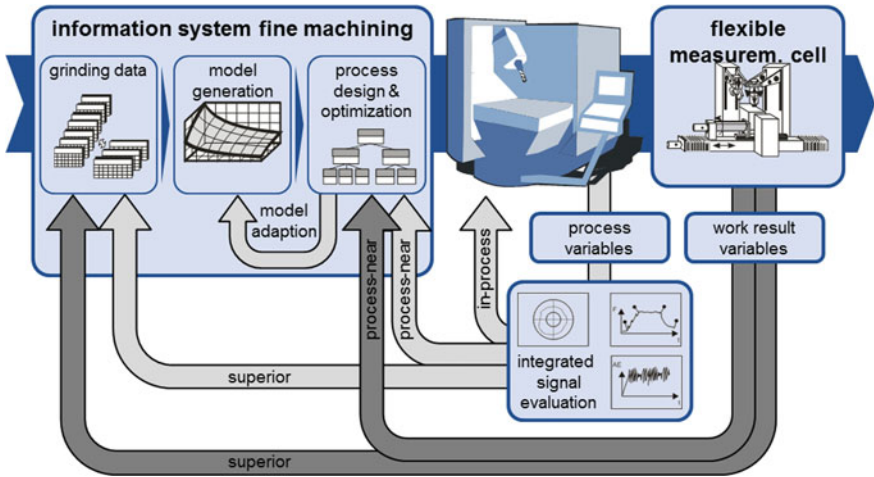


Fig. 15.19 Quality control loops for grinding processes

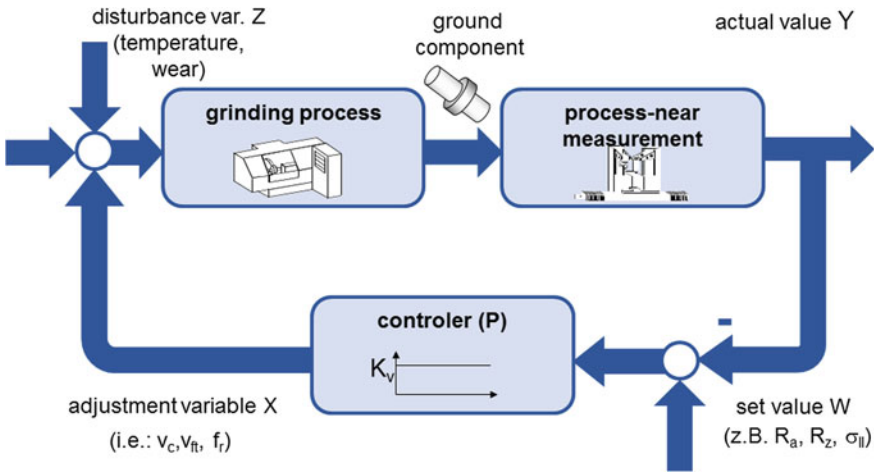


Fig. 15.20 Control loop for the process-near regulation of external plunge grinding

optimisation takes place. The statistical process control SPC can be mentioned as an example.

Systematic disturbance variables (e.g., grinding wheel wear), as illustrated in Fig. 15.20, are detected and balanced by control loops.

The core element of the illustrated control loop is the process-near quality check, for example in a flexible measuring cell immediately after machining. Target variables of machining such as roughness or the residual stress state of the component represent the target variables in the represented control loop. These are compared with the result variables (actual values) detected in the measuring cell.

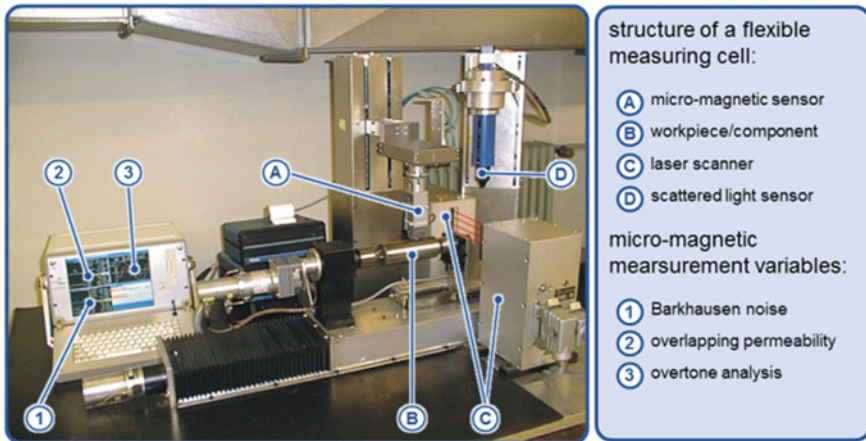


Fig. 15.21 Layout of a flexible measuring cell for process-near measurement

Via the determined offset, an altered adjustment variable is defined for the next component [CZE00]. In addition, the framework of a process-near control offers the possibility of carrying out a component-specific optimisation of the process chain of the subsequent machining steps. Based on the process models, which have already been used for the process chain layout, the technological interfaces of the following processes can again be configured at an optimum while considering correlations. This is necessary because distributions can lead to component-specific result variables, which differ from the previously considered optimum value determined for the entire process chain, after every machining process. At this, it has to be ensured that a layout of all technological interfaces can be configured individually for each component without causing a delay of the component production. The current methods do not allow this sufficiently yet.

In the illustrated flexible measuring cell (Fig. 15.21), micro-magnetic, laser and scatter light sensors are deployed. The micro-magnetic sensor analyses machining-conditioned alterations in the component surface zone. These are detected by the so-called Barkhausen noise (volatile alteration of the magnetisation), the overlapping permeability (reversible alteration of the magnetisation) and the harmonic analysis (Fourier analysis of the magnet field) [KAR01]. In addition, the measuring cell contains a laser scanner for the compilation of macroscopic quality characteristics (component geometry, concentric runout) and a scatter light sensor for the touch-free registration of the micro-geometries (roughness). The results of the component checking in a flexible measuring cell represent result variables, which are deployed in the process-near or superior quality control (Fig. 15.19).

In summary, the course of a process monitoring in principle can be described as follows. Based on a functional process, an entity (detector) compiles and maps all arising problems. According to whether the underlying data basis consists of explicit knowledge (facts) or implicit knowledge (experience), different analysis processes (measurement or perception) are deployed. Once the problem is phrased,

different strategies for problem solving resp. for optimisation are applied depending on the underlying data basis (explicit/implicit). The target of the process monitoring is to regain control over the process, which is problem-afflicted due to a malfunction. If this succeeds lastingly, it becomes necessary to consider setting the process limits more tightly. This means a permanent improvement of the process quality (reduction of the standard deviation σ).

15.6 Questions

1. Explain the term process chain element using the PEC model.
2. Name the transformation variables concerning the function structure of a technical product.
3. What is meant with a technological interface?
4. What connection is there between a real process (system) and a process model?
5. Name three typical model generation levels.
6. How do physical and empiric process models differ?
7. Delimit the input, process and output variables of a cutting -process against each other.
8. What is meant with the quality criteria of a cutting process?
9. Under which three aspects can cutting processes be configured resp. evaluated?
10. Name a simple method for the determination of the target function of a grinding process.
11. What is the difficulty in detecting the priority codes of a target function?
12. Draw the radial stress course of a shaft under bending and explain why residual tensile stresses can have a negative effect in the surface zone.
13. What process chain designing measures is the ASI method based on?
14. How do conventional and process-comprehensive process chain layouts differ?
15. According to the method introduced here, the process chain layout can be divided into two sections. What are they?
16. What is meant with qualitative positioning of technological interfaces?
17. Why is a quantitative layout of the technological interfaces additionally necessary after the process chain design?
18. Testing as a basis of process monitoring occurs according to two different methods. Name them.
19. Does the surface zone condition of a component represent a process or a result variable?
20. Distinguish the stochastic and systematic errors of a grinding process.
21. What does the difference between in-process control and process-near quality control consist in?

References

- [BRA08] Brandes, A.: Positionierung technologischer Schnittstellen—Beitrag zur ganzheitlichen Auslegung fertigungstechnischer Prozessketten [Positioning of technological interfaces—contribution to an integrated layout of production process chains] Dr.-Ing. Diss. Leibniz Universität Hannover. PZH Verlag, (2008)
- [CZE00] Czenkusch, C.: Technologische Untersuchungen und Prozessmodelle zum Rundschleifen [Technological investigations and process models in external grinding]. Dr.-Ing. Diss. Universität Hannover. Fortschrittsbericht VDI Reihe 2 Nr. 530. VDI-Verlag, (2000)
- [DEB03] Denkena, B., Brandes, A., Apitz, R.: Designing integrated process chains. *Mach. Eng.* 3, 63–65 (2003) ISSN 1642-6568
- [DEH09] Denkena, B., Henjes, J., Henning, H.: Holistic process chain optimisation based on simulation of technological interfaces. 3rd international conference on changeable, agile, reconfigurable and virtual production (CARV 2009), Munich, October 5th–7th, pp. 867–876, (2009)
- [DER07] Denkena, B., Rabinovitch, A., Henning, H.: Holistic optimisation of manufacturing process chains based on dimensioning technological interfaces. 4th international conference on digital enterprise technology (DET 2007), Bath, September 19th–21th, pp. 322–330, (2007)
- [KAR01] Karpuschewski, B.: Sensoren zur Prozessüberwachung beim Spanen [Sensors to monitor cutting processes]. Habilitationsschrift Universität Hannover. Fortschrittsbericht VDI Reihe 2 Nr. 581. VDI-Verlag, (2001)
- [KÖN87] König, W.: Strategien zur Optimierung der Fertigungsfolgen. Tagungsband “Harte Werkstoffe richtig bearbeiten” [Strategies to optimize the production sequences], VDI-Tagung, Stuttgart, February (1987)
- [OES98] Oestereich, B.: Objektorientierte Softwareentwicklung: Analyse und Design mit der Unified Modelling Language [Object oriented software development: Analysis and design by the unified modelling language]. 4. Aktualisierte Auflage, ISBN 3-486-24787-5, Oldenbourg-Verlag, (1998)
- [PAU94] Paul, T.: Konzept für ein Schleiftechnologisches Informationssystem [Concept for a grinding technological informationsystem]. Dr.-Ing. Diss. Universität Hannover. Fortschritts Bericht VDI Reihe 2 Nr. 313. VDI-Verlag, (1994)
- [PRO77] Profos, P.: Modellbildung und ihre Bedeutung in der Regelungstechnik [Modeling and its significance in control technology]. *VDI Berichte* 276, 5–12 (1977)
- [TÖC96] Tönshoff, H.K., Czenkusch, C.: Informationssystem zur prozessintegrierten Qualitätssicherung beim Schleifen [Information system for the process oriented quality control in grinding]. Proceedings of 7th international DAAAM symposium, Vienna, Austria, pp. 443–444, 17–19th October 1996
- [TÖF02] Tönshoff, H.K., Friemuth, T., Becker, J.C.: Process monitoring in grinding. *CIRP Ann.* 51(2), 551–571 (2002)
- [TÖI01] Tönshoff, H.K., Inasaki, I.: Sensors in manufacturing. Wiley-Vch Verlag GmbH, Germany (2001). [TÖI01]. ISBN 3-527-29558-5
- [TÖN07] Tönshoff, H.K.: Übersicht über die Fertigungsverfahren [Review of the manufacturing processes]. *Dubbel—Taschenbuch für den Maschinenbau*, 22. Auflage, Springer, Berlin, (2007) ISBN 978-3-540-49714-1
- [TÖP92] Tönshoff, H.K.; Perters, J., Inasaki, I., Paul, T.: Modelling and simulation of grinding processes. *Ann. CIRP* 41(12), 59–64 (1992)

- [VDI3633] N.N.: VDI3633 Blatt 1 Simulation von Logistik-, Materialfluß- und Produktionssystemen [Simulation of logistic, material flow and production systems]. Verein deutscher Ingenieure. Beuth Verlag, (2000)
- [ZAN70] Zangenmeister, C.: Nutzwertanalyse in der Systemtechnik [Analysis of the utility value in systems technology]. Wittmansche Buchhandlung (1970)

Chapter 16

Surface and Subsurface Properties

Cutting processes are employed to generate functional components. Finally, the surface and subsurface properties of the components are decisive for the functioning and durability. It is not always possible to draw a sharp line between surface and subsurface as shown by the definition of the terms. In a general sense, the surface describes the outer limitation of a body. In mathematics, the surface determines the mass of all the boundary points of a body. In science, the surface is the limit between two media. In production technology, a further specification of the term becomes necessary. The [DIN 4760] differentiates between various definitions:

- **Real surface:** surface, which separates the object from the medium it is surrounded by (exception: the inner surface of porous materials)
- **Nominal surface:** measurably collected, approximated image of the real surface of a shape element. Different measuring processes can produce different real surfaces
- **Geometrical surface:** ideal surface, whose desired size is defined by the drawing and/or other technical documents.

However, in the analysis of surfaces it is not always sensible to assume a thickness of zero. When characterizing certain surface properties, thicknesses of approx. 1 nm to approx. 10 μm (10^{-9} to 10^{-5} m) are regarded. This means that a surface can consist of a single atom layer (mono layer) or of 10,000 mono layers. In addition, within this thickness the surface is not necessarily homogeneous. The chemical composition and structure as well as physical properties often manifest differences. For the analyst the surface must always be the area, which is decisive for the required property.

The subsurface is the volume area of the material, whose properties were altered by the machining process. The consequence of the application of this definition is that, strictly speaking, statements about “surface residual stresses” or “surface hardness” are impossible because the determination of these variables always also requires information from the surface-near subsurface. According to the definitions mentioned here, surface properties can only be geometrical

properties. However, as the definition of the surface shows, surface and subsurface often fade into each other seamlessly [BRE11].

By far, not all connections between cutting processes and the functional properties of a component are known yet. However, it has proved itself to differentiate between surface and subsurface properties of a component. These properties can be described and measured by variables. The designer of a component can stipulate such variables. The production technician has to know which process and which input variables of the process allow the achievement of the required surface and subsurface properties.

16.1 Surface Properties




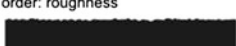
The component surface is the part which makes contact with the surrounding medium, a further component or the observer's view. Not only the requirements concerning technical components are diverse, even certain parts of the surface of one single component can fulfill different tasks. For example, we can differentiate between surfaces without technical function such as visible or reverse surfaces (internal sides), surfaces with technical function for clogging, adhering or joining or surfaces with different technical functions and occurring friction. Based on the loads, in [DIN 4764] technical surfaces in engineering and in precision engineering are divided into three groups, only taking the mechanical load as a basis:

- surfaces with no or low mechanical load
- stress-loaded surfaces mostly without relative motion to the counter surface
- friction-loaded surfaces with relative motion to the counter surface.

The micro geometry of the surface is mainly responsible for the component behavior during mechanical loads of different types. Thus, the production process of a certain component surface has to ensure that a certain micro geometry, in the form of roughness, is not surpassed or underrun. Functional surfaces such as visible, clogging, adhering or planing surfaces for example, have to manifest the lowest possible roughnesses. Substrate surfaces, on the other hand, require a process-dependent minimum roughness so as to enable the layer adherence.

The requirements concerning surface roughness have to be fulfilled by suitable cutting processes. One single process is not always able to generate the surfaces in the required quality. If nothing else due to economic considerations, two processes of the same cutting method often have to be carried out one after the other (roughing, finishing). In some cases, the cutting process alone is not enough to obtain the required surface quality so that a second, different process has to be connected in series (e.g., drilling and rubbing, milling and roller burnishing).

However, if cutting processes are planned to fulfill the roughness requirements towards the component, it has to be taken into account that in practice, the nominal surface differs from the geometrical surface by shape deviations of different orders. These are defined in [DIN 4760] and proven with examples (Fig. 16.1) [BRE11].

shape deviation (as profile section with vertical exaggeration)	examples for the type of deviation	examples for the cause
1st order: form deviation 	straightness, flatness, roundness deviation etc.	error in the guideways of the machine tool, machine or of workpiece deflection, incorrect clamping of workpiece, hardening distortion, wear
2nd order: waviness 	waves (according to DIN 4761)	off-center clamping, form or concentric deviation of a milling cutter, machine or tool vibrations
3rd order: roughness 	grooves (according to DIN 4761)	cutting edge shape, feed or depth of cut of the tool
4th order: roughness 	grooves scales lumps (according to DIN4761)	process of chip formation (discontinuous chip, segmented chip, built-up edge), material deformation during shot peening, boss at galvanic treatment
5th order: roughness annotation : can not be visually represented in a simple way	texture	processes of crystallization, surface alteration by chemical reaction (e.g. by etching), corrosion processes
6th order: annotation : can not be visually represented in a simple way	structure of the material	

the shown shape deviations of 1st to 4 th order interfere with each other as a rule to the real surface

example: 

Fig. 16.1 Order, examples and causes for shape deviations [DIN 4760]

Cutting processes which show a distinctive cutting direction, consistently cause aligned, groovy surfaces. Non-groovy surfaces are generated by spark eroding, pressure shot peening, forming or primary shaping (casting), for example. Aligned surfaces generally manifest higher roughnesses transversely to the cutting direction than in the cutting direction.

16.1.1 Determination of Surface Properties

The most frequently encountered roughness characteristics in the area of cutting technology are the arithmetic mean roughness R_a , the average surface roughness R_z and the maximum scallop height R_{max} . The arithmetic mean roughness R_a can quantify gradual alterations of the surface as caused by tool wear. Peaks and grooves however, cannot be differentiated, neither can different profile shapes. If R_a is used as a surface characteristic, the character of the roughness should also be known from other tests. R_a is regarded as a robust variable, since it only shows light reactions to single disturbances. In principle, R_a can be determined with all kinds of stylus instruments. The results of single metering points only scatter to a rather low degree, since the determination of R_a is based on a strong averaging [VOL05]. R_a describes the average deviation of the profile from the centerline (Fig. 16.2). The calculative determination takes place according to [DIN 4768]:

$$R_a = \frac{1}{l_n} \int_0^{l_n} |z(x)| dx \tag{16.1}$$

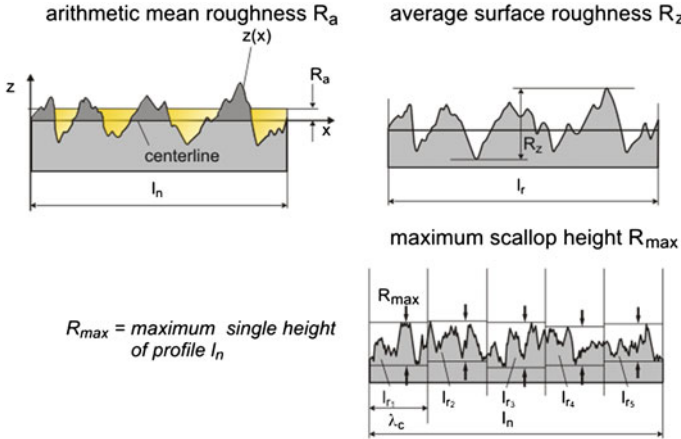


Fig. 16.2 Some important roughness characteristics [VOL05]

with:

- l_n analyzed part of the metering distance
- z distance of the roughness profile from the centerline within the metering distance

The two surface characteristics average surface roughness R_z and maximum scallop height R_{max} are frequently used together. In this combination, single outliers can be detected: if R_{max} is considerably higher than R_z , this means that the measured profile section contains a single especially high peak. A measurement at another place on the specimen can clarify whether it is actually a single outlier.

To determine R_z and R_{max} , the measured surface profile with the selected cutoff wave length λ_c , which delimits roughness and waviness from each other is filtered. The metering distance l_n is generally determined so that it can be divided into five equal sections l_r , each with the length of the cutoff wave length λ_c . The maximum height value z_i is taken from each section and the arithmetic average generated from these values (Fig. 16.2). Thus, R_z results from:

$$R_z = \frac{1}{5} \sum_{i=1}^5 z_i \tag{16.2}$$

R_{max} is the largest distance from the highest peak to the deepest groove within a metering segment. The highest roughness value within the metering segments 1–5 is defined as R_{max} (Fig 16.2) [VOL05].

The measurement process for micro-geometrical characteristics of a surface can act with or without direct contact. Basically, three measuring principles are distinguished:

- tactile methods
- optical methods
- scanning probe microscopic methods.

The classical measuring processes all place a profile section into the surface, so they are two-dimensional processes. Nowadays, by scanning the surface with a point sensor or also by using two-dimensional sensors, it is possible to determine the roughness of surfaces within justifiable time periods. It is therefore necessary to differentiate between two- and three-dimensional processes [BRE11]. Even today, most roughness profiles are still registered with mechanical styluses, transformed into electrical signals, pre-processed (filtered) and passed off in the defined measurement variables or as a profile diagram. Due to depiction reasons, the profile diagrams are mostly recorded in a strongly exaggerated way (e.g., at the ratio of 100:1). So, they can be the reason for misinterpretations. Figure 16.3 shows typical profile diagrams for turning and grinding in exaggerated and straightened (1:1) illustration.

On the one hand, the micro geometry of the newly generated surface by the cutting process is determined by the cutting edge geometry, on the other hand it can be considerably influenced by the variation of machining parameters. In the turning process, i.e., the shape of the tool is reproduced in the surface so that the feed is the most important roughness determining parameter. For example, if the cutting edge radius r_e and the feed f are known, it is possible to determine the roughness depth R_{th} which a turning process would generate on the surface of a non-deformable material by machining on an ideally stiff machine tool according to:

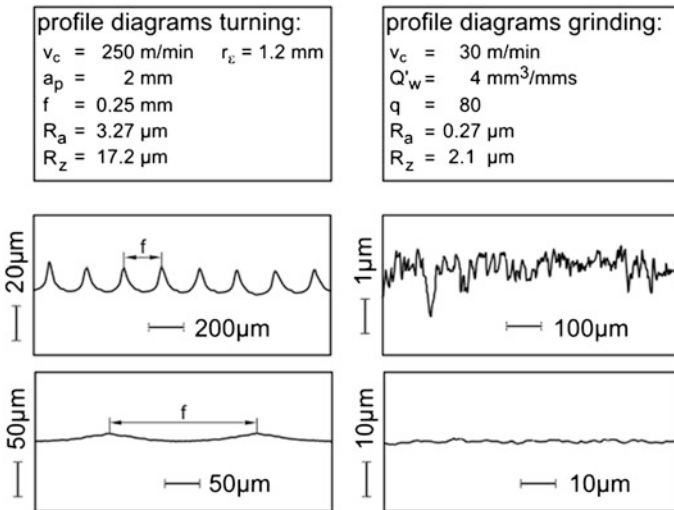


Fig. 16.3 Workpiece profile diagrams for turning and grinding

$$R_{th} = r_\varepsilon - \sqrt{r_\varepsilon^2 - \frac{f^2}{4}} \quad (16.3)$$

For applications in practice, the expression has been simplified as follows:

$$R_{th} \approx \frac{f^2}{8r_\varepsilon} \quad (16.4)$$

with:

R_{th} theoretical roughness depth

r_ε cutting edge radius

f feed

So, the thus determined theoretical surface roughness R_{th} increases quadratically with the feed and decreases linearly with an increased cutting edge radius [PAU08, BAU34]. The effect of the elastic material deformation, which shows in the system-dependent minimum cutting thickness h_{min} among others and gains influence with a decreasing feed, is considered in an extended surface roughness formula [BRA61, BRE11].

$$R_{th} = \frac{f^2}{8r_\varepsilon} + \frac{h_{min}}{2} \cdot \left[1 + \frac{r_\varepsilon \cdot h_{min}}{f^2} \right] \quad (16.5)$$

The theoretical surface roughness can be regarded as a lower limit for R_z . Because, due to the vibrations between tool and workpiece, the generation of built-up edges and the wear-conditioned alteration of the cutting edge, additional roughness proportions arise which superimpose R_{th} . For the fishing process, the surface rate \dot{A}_w (generated surface per time unit) applies:

$$\dot{A}_w = f \cdot v_c \quad (16.6)$$

$$\dot{A}_w = v_c \cdot \sqrt{8 \cdot r_\varepsilon \cdot R_{th}} \quad (16.7)$$

At a specified surface roughness, the surface rate thus depends on the cutting speed and the edge radius. The cutting speed is delimited by wear (see Chap. 6). The edge radius cannot be optionally increased either, because with r_ε the friction between the effective partners increases and thus also wear, and because chatter occurs and the process becomes unstable with a greater length of the secondary cutting edge [NED75]. These are also the limits for wiper-finish turning (broad finishing), which achieves a high cutting rate with a high feed and a low tool cutting edge angle of the main or secondary cutting edge, if the system stiffness is large enough (Fig. 16.4).

These questions are highly up-to-date in the development of special broad-tool turning or milling tools, which are equipped with broad-tool or drag cutting edges—also called wipers.

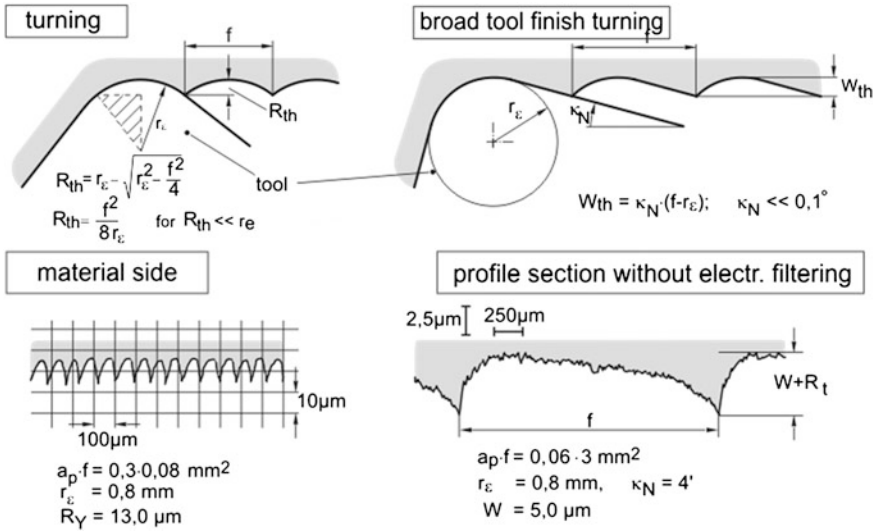


Fig. 16.4 Shape deviations during turning and broad-tool finish turning (wiper finish turning)

16.2 Subsurface Properties

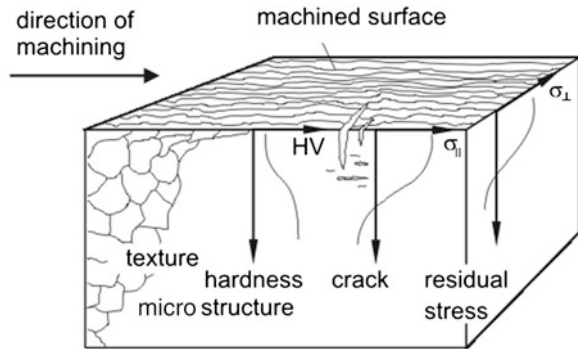
Not only the surface but also the subsurface is exposed to multiple loads in the usage phase of the component. At this, the mechanical loads are the most obvious. An overload of the component can mean the end of its life time or the reduction of its life cycle. Apart from the mechanical loads, the thermal loads are also decisive for the component life cycle. In action many components are exposed to high frictions, which can lead to their warming. At this, high temperatures can be reached (e.g., for cutting tools) so that the component in action may have totally different properties than at room temperature.

Apart from the mechanical and thermal loads, many components are also exposed to chemical attacks. Because of this, the material combinations of the components in action can cause corrosion or diffusion, which can lead to the alteration of component properties. During the course of the aspired life cycle, the properties of the subsurface are only allowed to change due to load to such an extent that the functioning of the component is ensured [BRE11].

In the case of components machined by cutting, the following subsurface properties illustrated in Fig. 16.5 can be measured or detected:

- microstructure alterations
- plastic deformations
- hardness alterations
- residual stresses
- textures
- cracks.

Fig. 16.5 Subsurface properties after cutting [BRI91]



16.2.1 Determination of Subsurface Properties

Microstructure alterations can be proved by means of metallographic polished sections. Grinding, polishing and suitable etchings show the fine structure of the subsurface and allow the recognition of crystallite transformations. This method is also suitable to determine *plastic deformations* as a consequence of cutting. The deformation of the crystals (Fig. 16.12) serves as an indicator. However, due to their irregular shape the resolution of the degree of the plastic deformations and their penetration depth is low. Thus, the line process has proved itself at which a test body is divided and line structures are applied on its dividing plane. The deformation can be quantitatively determined from the curving of these lines after machining.

Hardness alterations due to cutting only occur in thin layers of but some 1/100 mm. The hardness gradients can also be very steep. Therefore, these subsurface alterations can only be proved by means of micro or low load hardness tests [TÖN80]. In principle, testing is possible normally to the machined surface or in a cutting plane vertical to it. In any case, the test surface has to be treated with electro polishing, so as to eliminate preparation influences.

The sloping process was developed to assimilate a course of the hardness alteration above the penetration depth (Fig. 16.6). At this, the surface generated by cutting is cut at a soft (e.g., 1:200) slope on which the hardness is measured. The influence of underlying layers of different hardnesses can be corrected.

For special investigations, for example hardness courses in segmented chips [TÖN05], ultra micro hardness determinations with very low test loads (e.g., $F = 0.016 \text{ N}$) are carried out. The resulting small indentations allow high local resolution in hardness determination.

Residual stresses can be determined using an indirect or direct method. In both cases, the strains are measured and the stresses calculated accordingly. The indirect method, also called spring-back method separates small parts or layers from the stress-afflicted test body and measures the deformation of the remaining body by means of strain gauges or optical interference (Fig. 16.7) [TÖN65]. With algorithms of elasto-mechanics, the surface forces resp. stresses are counted back,

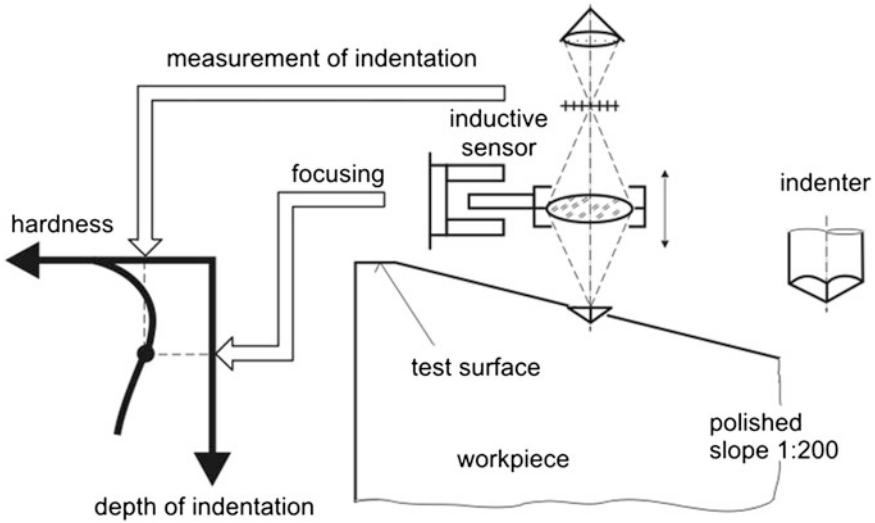


Fig. 16.6 Measurement of hardness courses at slope material removal

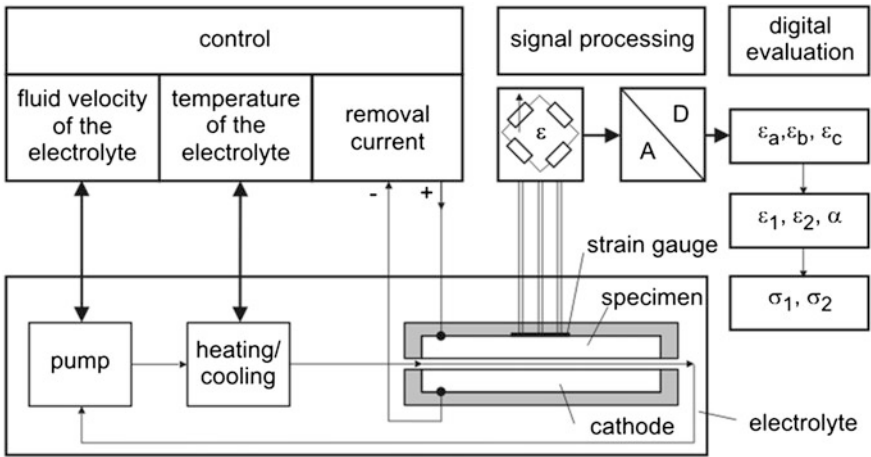


Fig. 16.7 Indirect stress analysis after the rebound process

which must have reigned in the separated part or layer and whose release caused the measured deformation of the remaining body. This process is called an indirect method due to the “detour” via the spring-back of the remaining body. Only residual stresses with macroscopic distribution (residual stresses 1st order) can be detected.

In the case of the direct method, the lattice strains in the crystallites of a material which are caused by residual stresses, are determined. This can be done

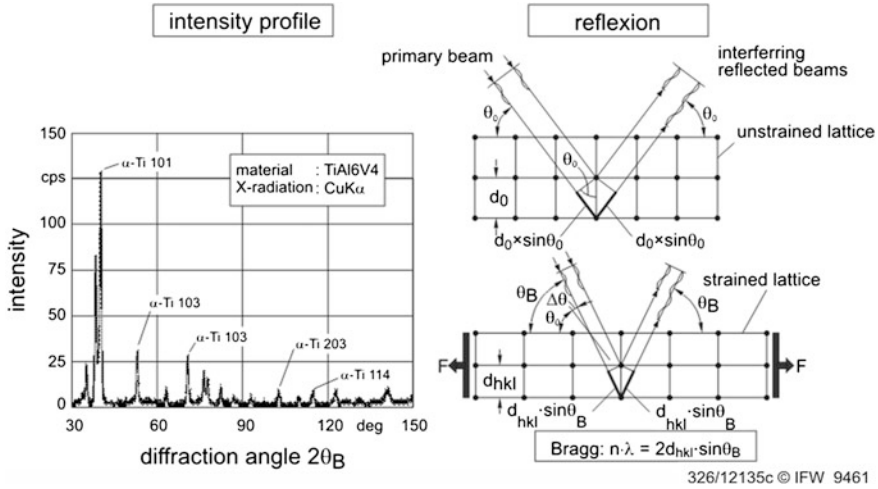


Fig. 16.8 X-ray diffraction

by using X-ray diffraction. Other processes use electro-magnetic effects or ultrasonic sound. The X-ray method employs a diffractometer, which records the intensity distribution of the diffracted ray (Fig. 16.8).

So as to determine stresses in the direction of interest parallel to the specimen surface it is necessary to determine the lattice strains depending on the inclination angle ψ of the lattice planes to the surface normal (Fig. 16.9). From an X-ray elasticity constant $1/2s_2$ (XEC) ($1/2s_2 = (1 + \nu)/E$; with $\nu =$ Poisson's ratio, $E =$ elasticity module), which is material-dependent and the slope of a connecting straight line $\varepsilon_{(\varphi,\psi)}$ above $\sin^2\psi$, the stress in direction φ results at

$$\sigma_\varphi = \frac{1}{1/2s_2} \cdot \frac{d\varepsilon}{d(\sin^2\psi)} \tag{16.8}$$

The borehole method occupies a leading position with the processes for the determination of residual stress, which do not work non-destructively. At this, users often call it a “part destroying” process, because the relatively small drilling is not supposed to influence the properties of some component negatively. The fact is however, that the process does not work non-destructively.

The borehole method is being applied since the 1930s [MAT33]. The principle of this process is based on the measurement of residual stress-conditioned deformations in the environment of an inserted blind hole. It is therefore an indirect measuring process. Generally, the measurement of the deformations takes place using a deformation gauge rosette, especially designed for this process. These measuring gauges consist of three strain measuring slats twisted by 45° towards each other located radially to the drilling, which are positioned centrally to the so-called drilling circle.

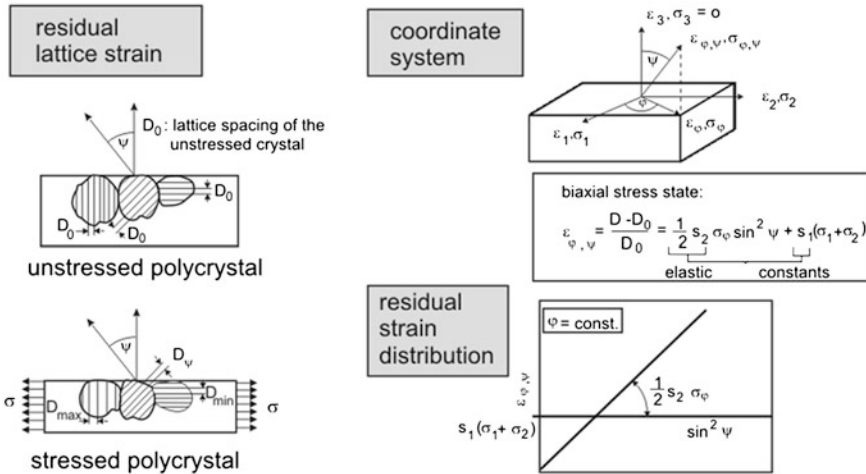


Fig. 16.9 Principle illustration of the X-ray stress analysis

When inserting the drilling step by step, a new residual stress balance occurs after each step so that it becomes possible to determine the residual stress depth courses when applying suitable evaluation processes. Various processes for the generation of blind holes were examined, because if possible, no new residual stresses should be induced into the workpiece during drilling and the borehole should ideally have a cylindrical shape. The most suitable and therefore most widely spread drilling process nowadays is the so-called high speed drilling technique. At this, the material removal takes place by means of a cemented carbide face milling cutter, which is powered by a compressed air turbine with up to 300,000 revolutions per minute. This should lead to a negligible induction of new residual stresses due to the drilling process [SCH96].

Texture is a property of poly-crystalline materials and thus of most metallic materials, many synthetics, ceramic material and of stones. Texture (crystallographic texture) describes the arrangement of the single crystallites towards each other and a workpiece coordinate system, which orients itself mostly by the surface or a determined direction of the workpiece. At the existence of random textures, the material properties behave in a quasi-isotropic manner, whereas oriented textures result in an anisotropic material behavior. Figure 16.10 schematically illustrates a random texture in the upper part and an oriented texture with a preferred direction. Such preferred directions are called orientations or texture components and described with the indices $(hkl)[uvw]$. At this, (hkl) describes the crystallographic surface, which is adjusted parallel to the specimen surface and $[uvw]$ describes the crystallographic direction, which is adjusted parallel to a determined direction, e.g., the rolling direction for sheet metal. In the case of the longitudinal turning of steel, certain analogies to a rolling texture have been detected [PLÖ02].

The determination of textures generally takes place by means of diffraction experiments using electrons, neutrons or X-rays. Intensity measurements at different azimuth and pole distance angles are carried out on low-indexed diffraction peaks. The measured intensities are then projected into the equator plane via a stereographic projection where they show certain intensity patterns at the existence of an oriented texture. This type of illustration is called pole figure. By means of extensive arithmetic operations, the orientation distribution function ODF can be determined based on the measured pole figures. Another possibility for the determination of crystallographic textures is the evaluation of the information from the diffraction experiments with back scattered electrons (EBSD). Compared with the X-ray texture determination, this is a relatively new technique. An advantage of electron diffraction experiments over X-ray diffractometry is the high local resolution.

Cracks can be proven with different methods, the most important of which will be briefly introduced in the following. The possibility of proof is limited for each method. Position, geometry and orientation of the cracks have to be considered for the choice of a suitable method.

Just like the light and scanning electron microscopic methods, the color penetration test is limited to such cracks which have a connection to the surface. The process is based on the capillary effect towards liquids. The liquid which is colored or furnished with fluorescent materials and has penetrated into the cracks, is extracted with acceleration by a contrast medium and thus makes the cracks visible.

The crack test with magnetic powder is exclusively applicable to ferromagnetic workpieces, because a magnetization of the specimen has to be carried out. The basis of this method is the magnetic leakage flux measurement. The workpiece is

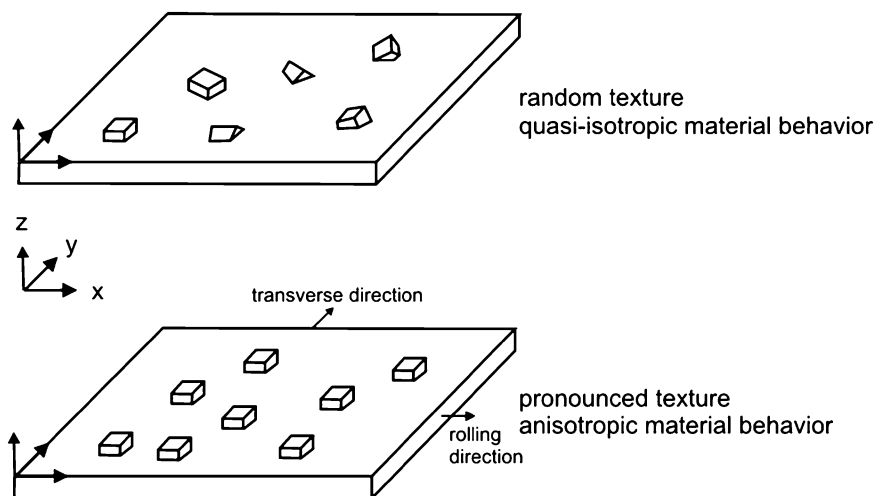


Fig. 16.10 Schematic illustration of random (*top*) and cube texture (*bottom*) [BUN69]

magnetized so that the magnetic flux lines run parallel to the surface. In a magnetically badly-conductive area, e.g., a crack, the lines split up into those which lead into the material, those which flow through the material separation and finally those which are crowded out of the surface and bypass the flaw in the air. The latter are called magnetic leakage flux [BRI91]. At this point, there is an increased addition of particles of magnetic powder which is applied to the specimen for the detection of cracks [TÖN87] (Fig. 16.11).

The ultrasonic sound methods applied for the workpiece testing are based on correlations of the material with irradiated acoustic waves [BRI91]. Different testing procedures have been developed, the impulse echo method being the most important [SCH92]. It allows the proof of cracks even far below the surface. For the examination of metals, testing frequencies between 0.5 and 10 MHz are mostly used, since this allows the bundling and adjustment of higher frequencies and smaller defects are more easily detected. The impulse echo method makes use of the reflection of acoustic waves at boundary surfaces, such as can be found in cracks.

Eddy current methods are also applied for the detection of defects (cracks, cavities, pores). An inductor flown through by high-frequency alternating current generates eddy currents in the electrically-conductive specimen. Defects in the workpiece lead to an alteration of the eddy current distribution and thus of the magnetic field, which overlaps the generating inductor field. The resulting magnetic field is measured. It contains information about material defects [ROO05].

For some years, induction and conduction-thermographic processes have been successfully employed which are capable of detecting even hidden cracks. The

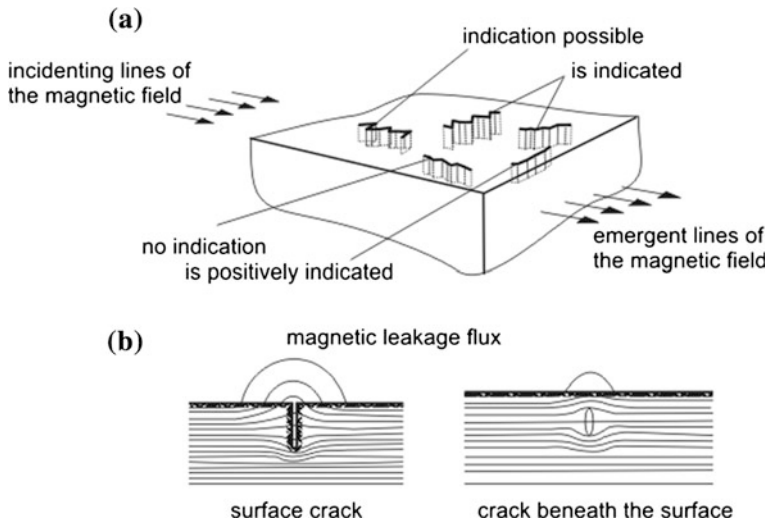


Fig. 16.11 Magnetic powder method for crack testing [BRI91]. **a** Orientation of crack. **b** Location of crack

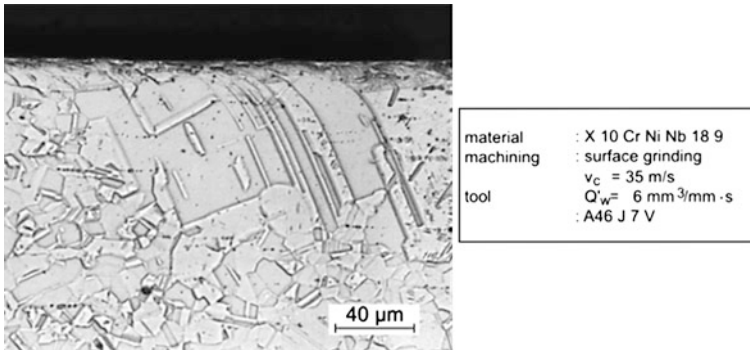


Fig. 16.12 Structure after grinding

component is selectively heated via an electro-magnetic stimulation. Disturbances of the electric conductivity as caused by cracks alter the thermal image locally. This condition is documented by a high-resolution thermography-camera [VRA08, KRE05].

16.2.2 Effects of Cutting Processes

Subsurface influences can have mechanical or thermal causes, often a combination of both. Mechanical influences result from the penetrations of one or several cutting wedges and the connected plastic deformations in the subsurface of the workpiece. As explained in Chap. 2 for the cutting with geometrically defined cutting edge, the deformation preliminary zone and the secondary shearing zone before the flank face, penetrate the zones below the newly developing surface of a component and generate permanent deformations. Quite similar processes occur during grinding (Chap. 13), only the dimensions of the mechanically-influenced areas are smaller.

The *plastic deformations* of the subsurface mainly develop due to shear deformation as a consequence of shearing before the cutting wedge and friction between the flank face and the material. These deformations are clearly recognizable in crystalline-structured materials due to the grain deformations (Fig. 16.12).

The alterations of grain shape and orientation can also be made visible by measuring the pole figures for texture determination. In longitudinal turning of steel C45 (SAE 1045) it was shown that cutting produces a texture similar to rolling, but with an orientation of the crystallites tipped towards the surface [PLÖ02] (Fig. 16.13).

The line method allows the quantitative registration of the deformations (Fig. 16.14). The impact depth is at 40–80 μm . The deformation is direction-

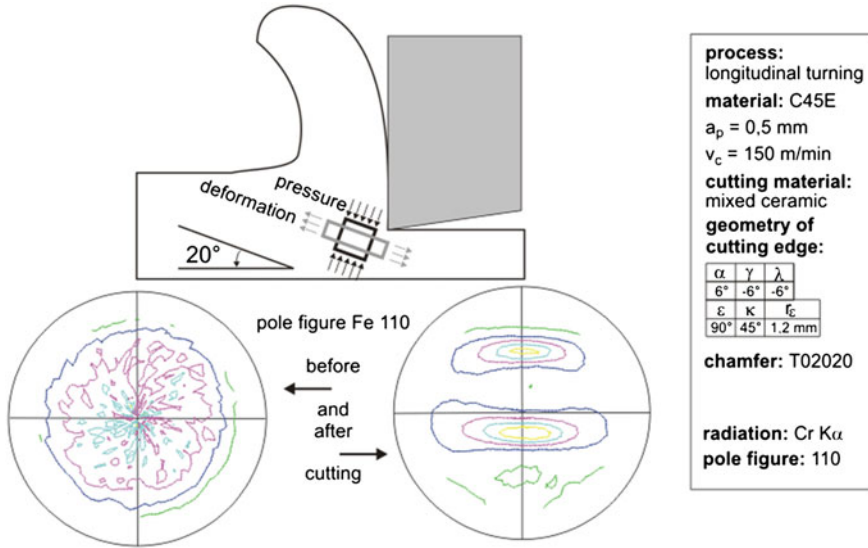


Fig. 16.13 Alteration of the texture by cutting

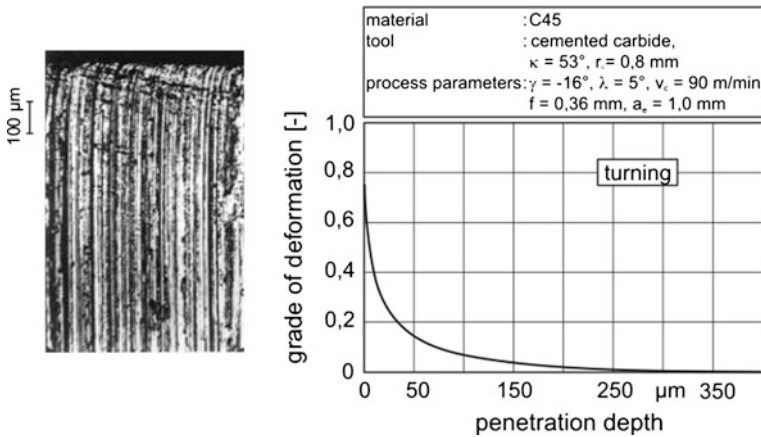
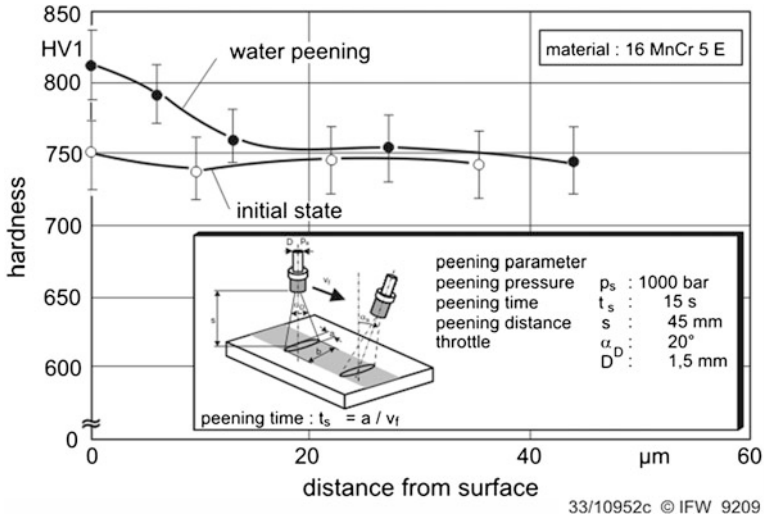


Fig. 16.14 Deformation of the edge layer by turning (line method)

dependent and is determined by the cutting direction. The material is strongly stretched as a consequence of the mechanical influence.

The plastic deformation is also accompanied by *strain hardening*, which causes an increase in hardness just as a consequence of mechanical influence. In cutting, generally mechanical and thermal influences act at the same time, therefore this strain hardening cannot be proven in an isolated manner. In the case with a high pressure water jet the situation is different. The hardness increase on a case-hardened material consisting of the microstructure components martensite and—retained



33/10952c © IFW 9209

Fig. 16.15 Hardness increase in the subsurface by water peening

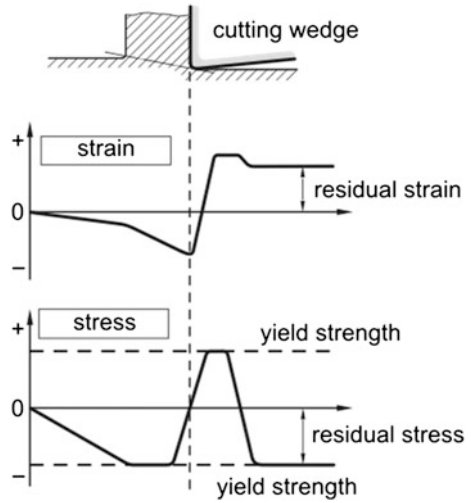
austenite illustrated in Fig. 16.15 can therefore be attributed entirely to the mechanical effect. In this case there is no mentionable heating only the mechanical influence. A hardness increase due to strain hardening and stress-induced transformation of the retained austenite into martensite in the subsurface has been proven [TÖN95].

Due to the subsurface deformation, residual stress sources [TÖN65] in the surface-near layers of a component are induced which generate *residual stresses* in the entire component for equilibrium reasons. In the surface itself only a biaxial stress condition can arise. Normal and shearing stresses normal to the surface disappear. The principal stress directions depend on the cutting direction. In peripheral grinding they coincide with the grinding direction to reasons of symmetry. The same also applies to orthogonal or quasi-orthogonal cutting. However, generally the principal stress directions do not coincide with the cutting direction.

Due to mechanical influence, residual compressive stresses occur in cutting direction as a consequence of the plastic strains in the surface-near layers. Figure 16.16 shows a model for the development mechanism. The course of the elastic and plastic strains and the stresses in cutting direction are displayed. When the cutting wedge advances, first elastic and then plastic compressions occur. Immediately after the tool contact, elastic and plastic strains occur which partly spring back. The stress course first shows compressive and then tensile stresses under load. They rise up to the yield strength. Residual compressive stresses remain after load relief. The permanently stretched layers are quasi too long and have to be compressed by the residual stresses, so as to create the material coherence.

Thermal influences result from the power conversion into heat (Chap. 5). The workpiece subsurfaces are heated strongly for a short time. A quick cooling off

Fig. 16.16 Residual stress development by mechanical influence



occurs due to self-quenching of the material and heat abstraction via the cutting liquid. This temperature course can be connected to structure alterations, hardness increases by secondary quenching and also annealing effects, i.e., hardness decreases. Figure 16.17 shows a hardness course of a ground bearing steel 100Cr6 (SAE 52100). The influenced zone is recognizable. At the hardness course, the new hardening zone also becomes clear. The hardness courses as illustrated in Fig. 16.17 were registered according to two different analysis methods: one according to the previously explained slope method (marked with slope material removal) and one by hardness indentations on a surface normal to the ground

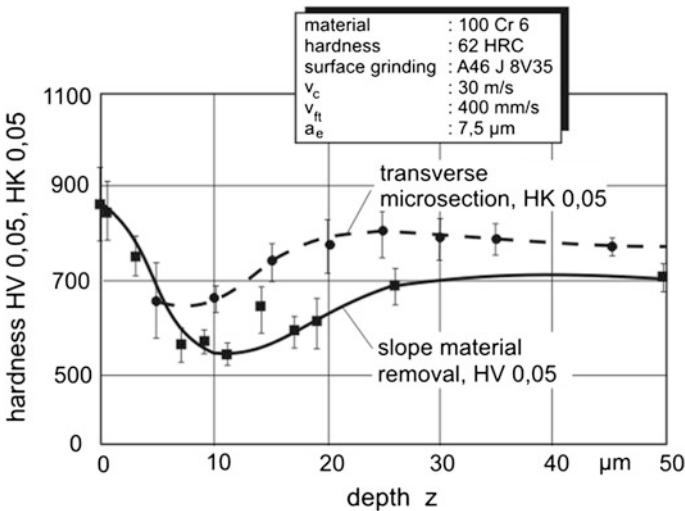
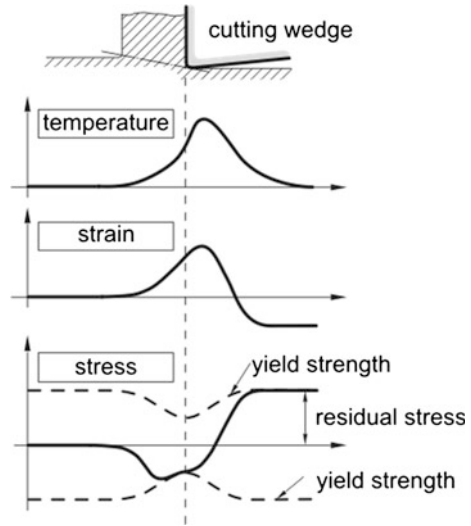


Fig. 16.17 Hardness alterations by grinding

Fig. 16.18 Residual stress development by thermal influence



surface (marked with transverse micro section). With the slope method, it is possible to measure directly until the surface.

The thermal effect of cutting also causes typical *residual stresses*. The subsurface layers stretch when the temperature rises. Thermal compressive stresses occur whose effect causes the subsurface layers to deform plastically at reduced yield strength. They are compressed. After cooling down to room temperature, the shortened subsurface layers are quasi too short and have to be lengthened by means of residual tensile stresses, so as to fit into the material coherence (Fig. 16.18). This effect of thermal deformation can be superimposed by a contrary process, if materials with low transformation temperatures and a volume increase with transformation from high to low temperatures are machined. Carbon steel with 12 % nickel, for example, deforms from austenite to ferrite (A_3 point) at 330 °C. As a consequence of the rapid self-quenching, residual compressive stresses occur which are called residual phase transition stresses.

Since mechanical and thermal influences act simultaneously in cutting, they superimpose each other in a high-grade non-linear way. A simple superposition is not admissible. A formal superposition can, however, give indications concerning the thermal and mechanical situation in the chip formation zone. Figure 16.19 shows residual stress courses in components machined by surface grinding with corundum and CBN wheels. The strong deviations can be attributed to the different heat flow referred to in Chap. 13.

Due to its high heat conductivity, CBN is able to dissipate essential parts of the energy transformed into heat via the grinding wheel; whereas in grinding with Al_2O_3 , whose heat conductivity is several times lower than that of CBN, considerably larger parts of the transformed energy enter the component and produce higher temperatures (compare Chap. 13).

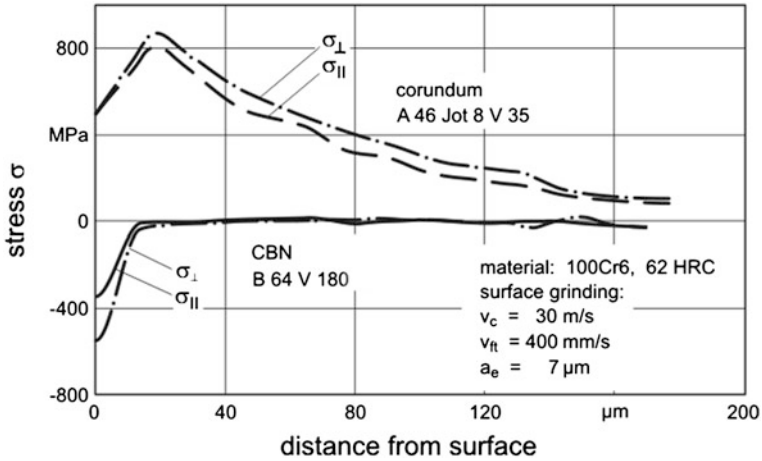


Fig. 16.19 Residual stresses and grinding material

Figure 16.20 demonstrates that the level of the surface-near residual stresses strongly depends on the material removal rate (volume rate) and thus on the cutting power fed in total. Finishing conditions cause residual compressive stresses or only low residual tensile stresses. The tensile stress level rises at a high material removal rate, until overheating of the component surface occurs, causing cracks or structure deformations which in turn cause lower stresses.

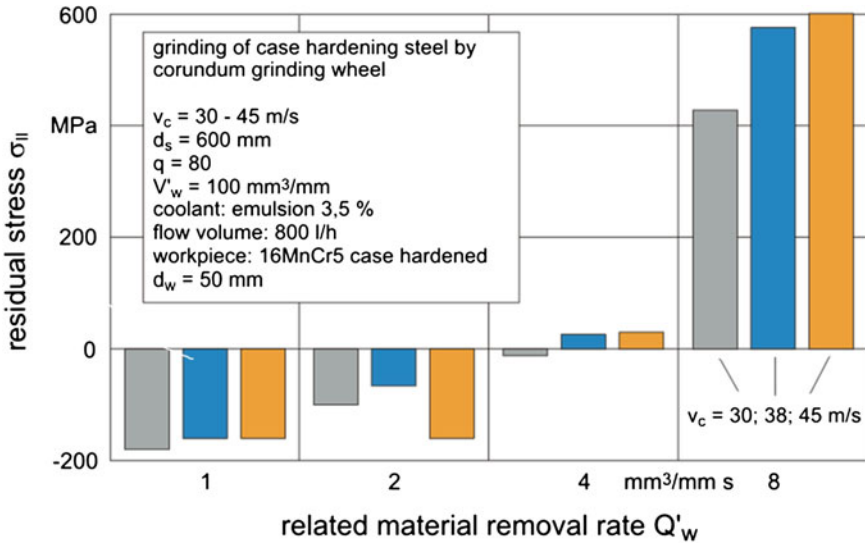
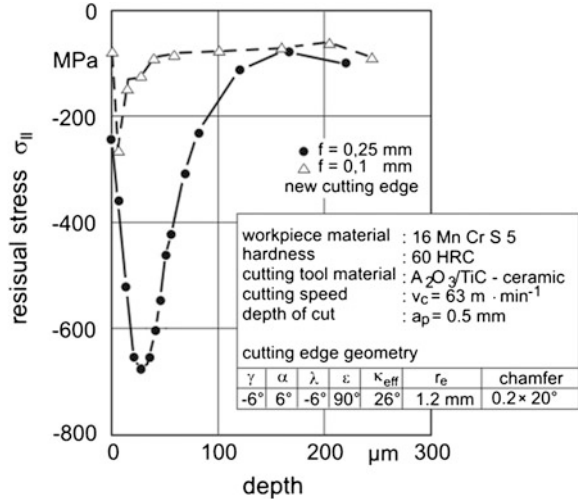


Fig. 16.20 Residual stresses depending on cutting speed and related material removal rate in grinding

Fig. 16.21 Residual stress depth course after turning



Cutting with geometrically-defined cutting edges generally generates unsymmetrical residual stress conditions, i.e., main stress directions no longer correspond to the motion directions of cutting. Residual stresses, which are produced by means of a heat treatment process, for example, are dominantly overlapped by a cutting process such as milling.

Figure 16.21 shows residual stresses in hard turned workpieces of case-hardened steel 16MnCrS5 (SAE 5115). After machining with new cutting edges, low residual compressive stresses exist in the surface of the workpiece. Below, a compressive stress maximum develops. A higher feed and the connected higher mechanical loads cause the residual compressive stresses to rise considerably and the maximum shifts to greater depths.

16.3 Questions

- Explain the most important roughness values according to DIN EN ISO 4287.
- Why is R_a lower than R_z concerning its value?
- Which surface parameter considers “horizontal” characteristics?
- What are the limits of broad tool finish turning?
- Name the connection between theoretical roughness depth R_{th} and feed in turning.
- Which physical subsurface alterations do you know?
- How can the subsurface alterations be measured?
- Where do you see limitations of the direct and indirect methods for the measurement of residual stress?
- What is the purpose of the $\sin^2\psi$ method?
- Name models for the development of residual stresses (case study).

References

- [BAU34] Bauer, M. H.: Messen der Oberflächengüte [Measuring of surface quality]. *Maschinenbau—Der Betrieb* **13**(3–4), 81–83 (1934)
- [BRA61] Brammertz, P.-H.: Die Entstehung der Oberflächenrauheit beim Feindreihen [The generation of surface roughness in finishing]. *Industrie Anzeiger* **83**(2), 25–32 (1961)
- [BRE11] Breidenstein, B.: Oberflächen und Randzonen hoch belasteter Bauteile [Surfaces and subsurface zones of highly loaded components]. Habilitationsschrift Leibniz Universität Hannover (2011)
- [BRI91] Brinksmeier, E.: Prozess- und Werkstückqualität in der Feinbearbeitung [Process and workpiece-quality in finishing]. Habilitationsschrift Universität Hannover (1991)
- [BUN69] Bunge, H. J.: Mathematische Methoden der Texturanalyse [Mathematical methods of the texture analysis]. Akademie-Verlag, Berlin (1969)
- [DIN 4760] Gestaltabweichungen; Begriffe, Ordnungssystem/Form deviations; concepts; classification system (1982)
- [DIN 4764] Oberflächen an Teilen für Maschinenbau und Feinwerktechnik/Surfaces of components used in mechanical engineering and light engineering; terminology according to stress conditions (1982)
- [DIN 4768] Ermittlung der Rauheitskenngößen Ra, Rz, Rmax mit elektrischen Tastschnittgeräten; Begriffe, Messbedingungen/Determination of values of surface roughness parameters Ra, Rz, Rmax using electrical contact (stylus) instruments; concepts and measuring conditions (1990)
- [KRE05] Kreissig, U.: Rissprüfung—in einer Sekunde zum Ergebnis [Crack test—in one second to the result]. Report MTU Aero Engines, Sommer/Herbst, S. 24–25 (2005)
- [MAT33] Mathar, J.: Ermittlung von Eigenspannungen durch Messung von Bohrloch-Verformungen [Determination of residual stresses by measuring of borehole deformations]. *Archiv für Eisenhüttenwesen* **6**, 277–281 (1933)
- [NED75] Nedeß, C.: Breitschlichtdrehen. Dr.-Ing. Diss. Univ. Hannover [Broad tool finish turning], München: Technischer Verlag Resch (1975)
- [PAU08] Paucksch, E.; Holsten, S.; Linß, M.; Tikal, F.: Zerspantechnik—Prozesse, Werkzeuge, Technologien [Cutting technology—processes, tools, techniques]. 12. Auflage, Vieweg und Teubner Verlag, GWV Fachverlage Wiesbaden (2008)
- [PLÖ02] Plöger, J. M.: Randzonenbeeinflussung beim Hochgeschwindigkeitsdrehen [Subsurface influencing in high speed turning]. Dr.-Ing. Diss. Universität Hannover (2002)
- [ROO05] Roos, E.; Maile, K.: Werkstoffkunde für Ingenieure [Material science for engineers]. 2. Auflage, Springer Verlag, Berlin, Heidelberg (2005)
- [SCH92] Schlengermann, U.: Ultraschall-Werkstoffprüfung—Das Krautkrämer Taschenbuch [Ultrasonic material testing—the Krautkraemer handbook]. Vulkan-Verlag, Essen (1992)
- [SCH96] Schwarz, T.: Beitrag zur Eigenspannungsermittlung an isotropen, anisotropen sowie inhomogenen, schichtweise aufgebauten Werkstoffen mittels Bohrlochmethode und Ringkernverfahren [Contribution to the determination of residual stresses at isotropic, anisotropic and inhomogenous layerwise constructed materials by the borehole method and ring core method]. Dr.-Ing. Diss. Universität Stuttgart (1996)

- [TÖN65] Tönshoff, H. K.: Eigenspannungen und plastische Verformungen im Werkstück durch spanende Bearbeitung [Residual stresses and plastic deformations at the workpiece through cutting and abrasive processes]. Dr.-Ing. Diss. Univ. Hannover (1965)
- [TÖN80] Tönshoff, H. K.; Brinksmeier, E.: Determination of mechanical and thermal influences on machined surfaces by microhardness and Residual Stress Analysis. *Ann. CIRP* **29**(2), 519–530 (1980)
- [TÖN87] Tönshoff, H. K.; Brinksmeier, E.; Hetz, F.: Detection of microcracks. *Ann CIRP* **36** 2, 545–552 (1987)
- [TÖN95] Tönshoff, H. K.; Wobker, H.-G.; Kroos, F.: Improving surface integrity of finished surfaces of case hardened steel by water peening. International Symposium for Electromachining, I SEM-XI, 17–20 Apr 1995, CH-Lausanne
- [TÖN05] Tönshoff, H. K., Denkena, B.; Ben Amor, R.; Ostendorf, A.; Stein, J.; Hollmann, C.; Kuhlmann, A.: Spanbildung und Temperaturen beim Spanen mit hohen Geschwindigkeiten [Chip formation and temperatures in cutting with high speeds]. In: Tönshoff, H. K.; Hollmann, F. (Hrsg.): Hochgeschwindigkeitsspanen metallischer Werkstoffe. Wiley-VCH Verlag (2005)
- [VOL05] Volk, R.: Rauheitsmessung—Theorie und Praxis [Measurement of roughness—theory and practice]. Beuth Verlag, Berlin (2005)
- [VRA08] Vrana, J.: Grundlagen und Anwendungen der aktiven Thermographie mit elektromagnetischer Anregung [Basics and applications of the active thermography by electromagnetic excitation]. Dr.-Ing. Diss. Universität Saarbrücken (2008)

Chapter 17

Cooling Lubrication

Tool wear is a consequence of mechanic, thermal and chemical loads. These loads can be reduced by feeding suitable cooling lubricating fluids. This may reduce tool wear. In addition, the heat removal from the chip formation zone can influence the surface integrity of the workpiece beneficially. The force and power requirement for the cutting process can be reduced and increase surface quality achieved by reducing friction and adhesion between tool and workpiece [BRI04a, BRI95]. These are beneficial effects among all four criteria of the cutting process (see Sect. 1.4). On the other hand, cooling lubricating systems produce considerable costs, at which disposal costs are becoming increasingly significant. Cooling lubrication also has to be considered critically under workplace and environmental aspects. The right choice and layout of cooling lubricating processes and systems is therefore primarily a manufacturing problem.

17.1 Requirements

The requirements concerning cooling lubricating systems can be divided into primary and secondary functions [BAR78, ZWI79]. Main functions are:

- *Cooling* Heat removal from the tool, the workpiece and the machine.
- *Lubricating* Reduction of the friction between tool and material and reduction of the forces and powers, reduction of adhesion tendency between cutting and workpiece material.

The requirements concerning the two main functions depend on the cutting process to a high degree. Figure 17.1 provides a schematic overview, at which in each single case further criteria can be important.

There is interdependency between the two main functions: The reduction of the power transformed into heat by means of good lubrication directly affects the cooling function, less heat has to be conducted. Inversely, a stronger coolant in the

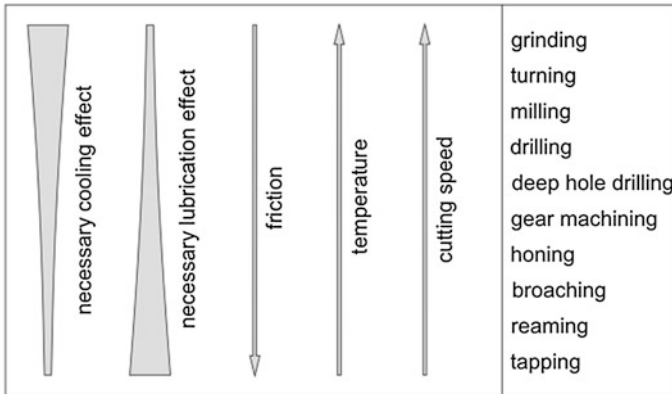


Fig. 17.1 Requirements on cooling lubricants and their dependence on the requirements on the machining process on cooling lubricating fluids

chip formation zone can lead to an increase of the yield strength of the materials and thus to an increase of the force and power requirements.

Apart from this, cooling lubricating fluids (CLFs) can take over various additional functions which lead to further requirements. Additional functions and the necessary properties are:

- Transport of the chips and bonding of cutting particles:

In some processes such as drilling and deep drilling, chips have to be transported away from the cutting zone, at which liquids are often used for cooling. CLFs are also often used for the removal of chips and cutting particles from the work space of a machine. Grinding wheels are often cleaned by high pressures of CLF above 10 bar.

- Surface protection of the workpieces:

Cutting generates new surfaces on the workpiece, which do not possess any passivating protective layers at the beginning. Such surfaces are chemically highly active and can react in undesired ways according to the medium. For this, liquid CLFs have to be sufficiently alkaline (pH value >7 , if possible, pH = 8–9.5) so as to prevent corrosion.

- Human compatibility:

In general, skin contact of the machine operator with the CLF is inevitable even if the working space of the machine is well capsuled. Therefore, the media has to be skin tolerable. The alkalinity should not surpass the value pH = 9.5. Steams and gases which escape from the working space, have to be tested on their harmfulness and suctioned safely.

- Protection of the machine parts:

It has to be ensured that liquid CLFs do not corrode any machine components, such as coats of paint, sealing, scrapers or covers of synthetic material.

- Ageing durability:

Liquid CLFs should be chemically and physically stable and not change due to environmental influences. They should be durable. This characteristic is in direct competition with biological degradability.

- Biological degradability:

The disposal of CLFs containing carbon hydride, additionally with different additives, is difficult. Therefore, biologically degradable CLF are preferred. At this, however, it must be considered that lubricating media (lubricating oils or greases) escape at the machine tools and thus load the liquid media [HOW91].

17.2 Cooling Lubricating Fluids

According to the aggregate condition, the media which possess cooling, lubricating or combined effects can be differentiated into:

- mono-phase media such as gases and fluids and
- bi-phasic media such as solid body suspensions and fluid-gas mixtures.

Liquid cooling lubricating fluids (CLFs) have the greater practical significance. They can be divided into not water-mixable (mineral oils) and water-mixable CLFs (Fig. 17.2). The code letters are shown in Table 17.1. The DIN51385 classify three groups of additionally regarding the water-mixed CLFs SEW as an own group. However, this classification is technologically not sensible but is rather oriented towards the CLF trade. For practice it is sensible to classify the two groups SN and SE as shown in Fig. 17.2.

17.2.1 Not Water-Mixable Cooling Lubricating Fluids

Due to the high pressure between material and tool, a hydro-dynamic lubrication effect cannot occur during cutting. Therefore, separation layers are used to reduce the friction.

The basic oils for not water-mixable CLFs are mainly mineral oils. The use of oils is, however, linked with special efforts:

- The machines have to be capsuled against the escape of oil, oil mist and oil vapor.
- The machines have to be equipped with a suctioning installation for the removal of oil mist.
- Workpieces generally have to be degreased after machining.

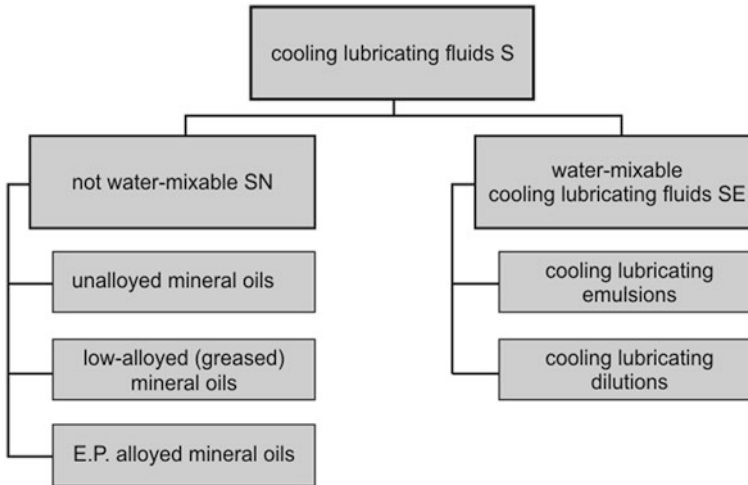


Fig. 17.2 Cooling lubricating fluids for cutting

As a principle, mineral oils with and without friction-reducing and/or EP (Extreme Pressure) additives are differentiated, at which they are additionally subdivided into chemically active and inactive additives (see Table 17.1).

In principle, mineral oils show a high lubricating and corrosion-protective effect but a relatively low cooling effect. The dependence of the properties on the types of mineral oil is illustrated in Table 17.2. Since mineral oils are sterile they can generally do without corrosion inhibitors and preservation. A negative effect is however, the foaming behavior so that foam inhibitors are usually added.

The optimum viscosity of the CLFs is determined by effects in the opposite direction: It should be large enough to ensure a good adhesion and low oil mist generation, but it should also be kept low with regard to a better cooling effect because thinner oils flow to the cutting zone more easily. At the same pumping power, a larger oil quantity is fed and the penetration in capillaries is facilitated. The durability of not water-mixable CLFs is generally high. It strongly depends on the maintenance of the circulating system and the cleaning of the oils. It is a precondition that no polluting external oil, e.g., from lubricating or hydraulic oil circulations, can penetrate. Such leakage oils are totally mixable with the CLFs, so they cannot be removed from the CLFs in the circulating facilities. Therefore, the circulating facilities have to be protected from such leakage oils.

Table 17.3 illustrates thermo-physical characteristic values of a mineral oil used in cutting compared with water.

Table 17.1 Significance of the code letters for cooling lubricating fluids [DIN 5 1385 and DIN 5 1520]

Code letter	Significance	Definition
S	Cooling lubricating fluid	Material, which is used in the cutting and partially in the forming of material for cooling and lubricating
SN	Not water-mixable cooling lubricating fluid	Cooling lubricating fluid, which is not mixed with water for use
SNO	Without friction-reducing and/or EP additives	
SNP	With friction-reducing additives	
SNPA	With EP additives, chemically inactive	
SNPB	With EP additives, chemically active	
SNPC	With friction-reducing and EP additives, chemically inactive	
SNPD	With friction-reducing and EP additives, chemically active	
SE	Water-mixable cooling lubricating fluid	Cooling lubricating fluid, which is mixed with water before use
SEM	Emulsifiable cooling lubricating fluid	Water-mixable cooling lubricating material, which can form the discontinuous phase of an emulsion oil in water
SES	Water soluble cooling lubricating fluid	Cooling lubricating fluid, which produces solutions when mixed with water
SEW	Water-mixed cooling lubricating fluid	Cooling lubricating material mixed with water
SEMW	Cooling lubricating emulsion	Emulsifiable cooling lubricating fluid mixed with water
SESW	Cooling lubricating dilution	Water soluble cooling lubricating fluid mixed with water

17.2.2 Water-Mixable Cooling Lubricating Fluids

Due to their higher heat capacity, their heat conductivity and their vaporization heat water-mixable CLFs show better cooling effects than mineral oils. Water-mixable CLFs can be deployed for almost all machining on steel, cast iron and aluminum alloys. Approximately 90 % of the production facilities are operated with water-mixed CLFs [ZWI79].

We differentiate between emulsifiable and water soluble CLFs.

17.2.2.1 Emulsifiable Cooling Lubricating Fluids

This group denominates water-mixable CLFs capable of generating the discontinuous phase of an oil-in-water emulsion. In emulsions, one fluid (here mineral oil or ester as the lubrication carrier) is dispersed in another (here water), i. e.

Table 17.2 Properties of mineral oil types

Properties	Oil types		
	Paraffinic	Naphthenic	Aromatic
Density	Low	Medium	High
Viscosity-temperature behavior	Good	Medium	Bad
Viscosity index	High	Medium	Low
Low temperature behavior	Bad	Good	Good
Solidification point	High	Low	Low
Vaporization behaviour	Good	Medium	Bad
Flashing point	High	Medium	Low
Oxidation stability	Good	Good	Bad
Ageing products	Acids	Condensation products	Slurry
Thermostability	Medium	Good	High
Radiation resistance	Medium	Good	High
Wettability	Medium	Good	High
Dispersing power	Medium	Good	High
Solvability of additives	Medium	Good	High
Compatibility/elastomer	Good	Good	Bad
Toxicity	Low	Medium	High

Table 17.3 Thermo-physical values: oil–water (40 °C, 1.013 bar)

	Mineral oil	Water
Kinematic viscosity (mm ² /s)	9.5	0.66
Density (g/cm ³)	0.85	0.99
Heat conductivity (W/mK)	0.13	0.63
Vaporization heat (J/g)	200*	2250
Specific heat capacity (J/gK)	1.95	4.2

*dependent on distillation fraction

distributed in form of drops. In the thermodynamic sense, a cooling lubricating emulsion is a metastable system, which returns to a condition of low energy even in the case of MQL disturbances. Thus, for the dispersion of oil in water, energy has to be fed which corresponds to the surface energy of the droplets to be generated [GOT53]. This can occur by means of strong agitation, which however, only creates an unstable system. Stable emulsions can be generated by feeding surface active agents (emulsifiers). Emulsifiers considerably reduce the surface energy. They mainly recharge at the boundary surfaces and thus generate a film around the oil droplets, which prevents them from being merged. The type and amount of emulsifiers is determined by the size of the oil droplets. We differentiate between coarse (low emulsifier content) and fine-particle emulsions. In practice, the cooling lubricating emulsions are sometimes incorrectly called “cutting oils”.

Coarse-particle emulsions have a droplet size of approx. 9 µm, for fine-particle emulsions it is 5 µm and less. The latter have an opalizing to still transparent

appearance. Due to their high degree of dispersion (MQL droplets, high surface energy) they are less wettable to workpieces than coarse-particle emulsions. On the other hand, they are generally more stable. Therefore, they are deployed where high lifetimes are necessary. The precondition for a long use of this emulsion type is, however, that they are kept clean even with longer operating times, by effective filter facilities resp. separators [ZWI73].

Fine-particle emulsions have a higher tendency to foaming than coarse-particle emulsions. The latter can precipitate air better and faster due to the bigger droplets. In addition, their cooling and lubrication effect is stronger than that of fine-particle emulsions [ROE95].

The lubrication effect of emulsions is mainly determined by the oil proportion. It is also decisive for the corrosion protection of the workpieces, the tools and the machine tool. The minimum concentration is therefore 2 %. A rising oil proportion improves the anti-corrosive protection and the lubricating proportion. The following has to be considered for an optimum adjustment of the oil content [ZWI79, JAC88]:

- The oil content has to be high enough to ensure sufficient lubrication.
- The emulsion should have a high water proportion for a high cooling effect.
- The costs of the emulsion increase with a higher oil proportion.

The durability of cooling lubricating emulsions also depends on the hardness of the water used. A high content of hardness components can lead to reactions with the anionic emulsifiers. At this, the water soluble calcium and magnesium compounds of the hardness components are converted into insoluble compounds. They fall out as lime soaps. The consequence is a segregation of emulsifiers and linked to this, a destabilization of the emulsion [LIN86, GÜN84].

Emulsions are sensitive to infestation with micro-organisms, e.g., aerobic and anaerobic bacteria and fungi. Of these, especially the anaerobic bacteria are disturbing, because they act under air exclusion and generate hydrogen sulfides and thus the so-called “Monday morning odor”. In addition, emulsifiers are degraded by micro-organisms. The consequences are oil precipitations, decrease of the pH value and decrease of the anti-corrosive protection. Effective media against the infestation with micro-organisms are bactericides and fungicides, which are often already contained in the concentrate. However, too high concentrations can lead to skin diseases.

During use the concentration and the droplet size of emulsions can change due to the drag-out of oil and emulsifiers by the chips. Therefore, it should be monitored continuously. An alteration of the concentration can be determined optically by measuring the refraction index in a refractometer. The refraction index depends concordantly on the density of the mixture and the droplet size. In many cases, a more exact determination of the concentration by means of a titration process is necessary due to the increasing droplet size. The durability of emulsions can be extended by additivating with biocides, surface-active agents and stabilizers and by targeted monitoring and maintenance measures [KNO86].

The disposal of emulsions is expensive. For reasons of environmental protection, oil and water have to be separated for disposal.

17.2.2.2 Water Soluble Cooling Lubricating Fluids

Cooling lubricating fluids which result in water-mixed solutions, are called cooling lubricating dilutions. The contents are solute in water or even more finely spread than in fine-particle emulsions. These fluids are generally more stable. They contain only little (or no) amounts of mineral oil. Their advantages are the strong cleaning and cooling effect as well as the good stability and transparency. Aqueous solutions are generally saline solutions. They are among others, loaded with organic corrosion protection substances against corrosion infestation of the machine parts and workpieces and surface-active agents so as to improve the wetting capacity. Furthermore, cooling lubricating dilutions may contain surface-active substances (EP additives) [BAR81]. Polymer (e.g., on the basis of polyvalent alcohols and polyglycol), ester and similar materials are used as organic ingredients. The lubrication effect and pressure stability is improved with a higher content of these materials. Due to their synthetic production these solutions are also called synthetic CLFs.

17.2.3 Additivation of Cooling Lubricating Fluids

Feeding additives can alter the properties of CLFs considerably. Additives are synthetic compounds or their mixtures. The latter permit property combinations as “multi-purpose additives” [VAM84, ROE95].

To increase the lubrication effect of CLFs they are fed additives, which can develop adsorption and reaction layers. EP (extreme pressure) additives are supposed to prevent welding and fretting under high pressures and temperatures. Mostly they are fatty acid or chlorine, sulfur and phosphor compounds which generate reaction layers from metal soaps resp. chlorides, sulfides and phosphides on metal surfaces. These chemically active materials cause an increase of the friction coefficient at low temperatures, because the reaction layers are still solid. Above a certain temperature, the layers macerate and thus reduce the friction coefficient. The layers of the metal soaps resp. salts break down after having surpassed the melting point [BAR81, LAN73]. Figure 17.3 illustrates the effective areas of the different reaction products.

The EP additives generally contain not just one active element. Combinations of several effective substances are often used. When selecting the additives one has to consider that they can also mutually influence each other in their effect. If and which additives are used depends on the type of load. The more difficult the cutting conditions, the higher-alloyed CLFs are deployed.

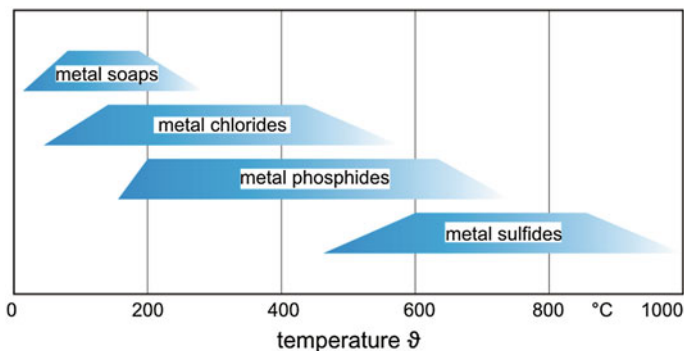


Fig. 17.3 Effective areas of the reaction products of cooling lubricating fluid additives

The concentration of the EP additives is critical. A too low content reduces the separating effect and a too high content increases the tool wear (wear lubrication) [ROE95]. The additives are consumed by reacting with the metal surface. Their concentration in the basic oil decreases.

Chloric additives (e.g., chloroparaffins) have lower reaction temperatures, high pressure resistance and are almost universally deployable. Therefore, they were frequently used in the past. However, environmental requirements and the connected disposal difficulties have led to the fact that meanwhile chloric cooling lubricating materials are hardly being deployed. Chlorinated fluids are treated as hazardous waste [HÖR87]. Meanwhile, combinations of other additives with comparable results are being used.

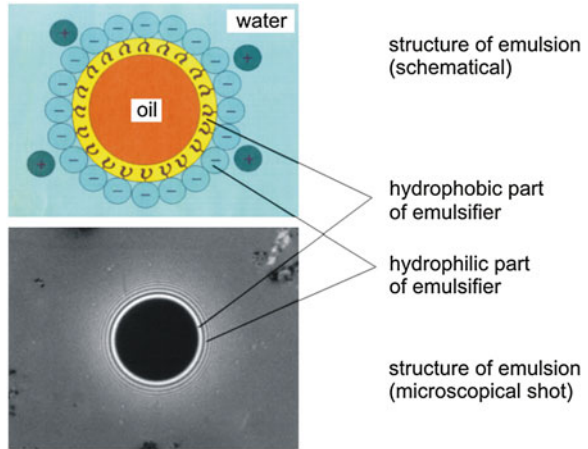
Oil-in-water emulsions are stabilized by adding *emulsifiers*. Emulsifiers reduce the surface energy of the water. They thus determine the distribution and size of the oil drops in the water and their durability. The effect is based on the fact that the oil drops are enclosed by a soap coat (Fig. 17.4). By this means, stabilization and an adhesive effect (polar orientation) are achieved on the effective partners [ROE95]. We differentiate between anion and cation active as well as not ionogenic emulsifiers [ZWI79, BAR81, MÜL87].

Corrosion inhibitors are deployed to improve the corrosion protection of the machined workpiece. They are used to develop covering layer against the penetration of water and air [BAR81]. Amine salts, sulfonates and benzotriazoles are deployed for this purpose.

The lubrication effect of oils is negatively influenced by a development of foam. In addition, their oxidation is encouraged by a more intensive mixing with air. *Foam inhibitor* or anti foam products are used to prevent the generation of foam. These are higher fatty alcohols and silicon oils. However, silicon oils are difficult to wash off so that they can have a disturbing effect on the final treatment of the machined parts (e.g., varnishing, enamelling) [ZWI79].

Adhesive agents serve to improve the adhesive capacity of CLFs on workpieces. They have a positive effect on the cooling lubrication by increasing the viscosity of

Fig. 17.4 Structure of an emulsion



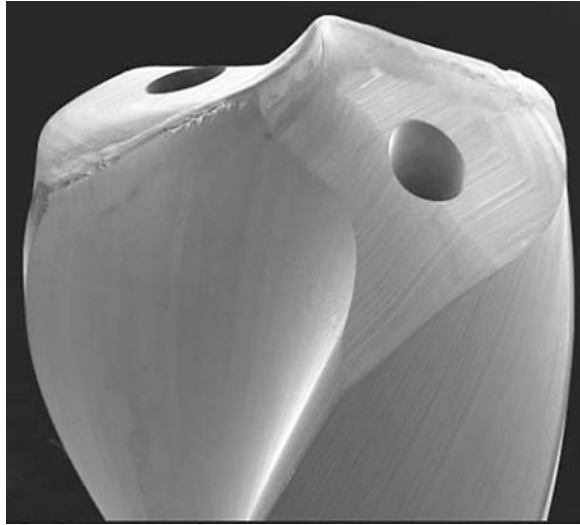
the CLFs at the boundary layer to the material [ZWI79]. Polymeric hydrocarbons such as polymethacrylates and polyisobutylenes are used as adhesive agents.

Conservation agents are biocides. They are meant to protect the CLF from infestation with micro-organisms. Bacteria, fungi and yeasts can use water-mixed CLFs as nutrient media and decompose the ingredients of the CLFs biochemically by means of their metabolism. Thus, they have a disadvantageous effect on the cooling lubricating properties and den hygienic status of the CLFs (toxins can develop as metabolic products). Formaldehyde releasing fluids or mercury compounds can be added as suitable conservation agents [BAR81]. Such emulsions have to be continuously monitored to prevent skin damages and waste water problems.

17.3 Use of Cooling Lubricating Fluids in Geometrically Determined Cutting

Cooling lubricating fluids (CLF) cause additional costs and can burden the operator, the environment and parts of the machine [SCH04]. Due to the costs and disposal problems, CLF have to be deployed in an economically and ecologically sensible way since they are indispensable for a series of processes. The recycling of used CLF is being worked on increasingly [ÖST03]. The cost and environmental situation has led to the development of the minimum quantity lubrication (MQL) which has facilitated the reduction of the CLF consumption [WEI99]. In MQL we basically differentiate between the external feed of CLF via spray throttles (generation of aerosols) and internal feed via channels introduced into the tool [AUR06, STÄ04, LOI04]. Figure 17.5 shows the exit openings of the cooling channels of a twist drill. The minimum quantity lubrication represents a compromise between ecology, work hygiene, business economics as well as machining

Fig. 17.5 Scanning electron micrographs of the exit openings of the cooling channels of a twist drill, tool diameter = 8 mm



quality, productivity and effectiveness compared with dry machining. Since these lubricating fluids evaporate more quickly due to their large surface, it is also important to use substances with no health threat.

The use of biologically degradable lubricating fluids such as synthetic esters is being researched so as to do without environmentally burdening cooling lubrication systems in production. When using synthetic ester in external longitudinal turning processes, the lack of additives leads to a different weighting of the wear mechanisms. Novel PVD coatings are being developed to compensate this and nevertheless achieve an optimum separation of the effective partners in the tribological contact. Multi-Layer coatings $\text{TiAlN}/\gamma\text{-Al}_2\text{O}_3$ increase the lifetime of the tool and improve the tool wear pattern while turning X5CrNi18-10 and 42CrMo4V. In the case of the material 42CrMo4V, it might even be possible to machine without cooling lubrication [KLO04]. In the case of Inconel 718, drilling processes with multi-layer TiAlN coatings, TiN/TiAlN layers in nano-composite design as well as TiAlN with a WC/C covering layer of the tools are being carried out. Compared with the use of cooling lubricating emulsion (6 %) a significant lifetime gain of the tools was achieved with synthetic ester [KLO06a].

In micro-milling, oil based CLFs show better results compared with water based ones. Minimum quantity lubrication can also ensure the chip removal from the working area. The viscosity of the CLF has to be low enough to reach the working area. However, it must not be too low to allow the development of a lubricating film. This shows that the cooling lubricating conditions always have to be designed process-specifically for an optimum effect in cutting processes [KLO06b].

For example, in spite of a reduction of the use of CLF, an almost continuous drilling quality can be achieved when drilling C45E steel [WEI97]. Considerably

reduced drilling moment and feed force values are possible, especially in minimum quantity lubrication. This underlines the significance of the targeted and process adapted use of CLF. The deployment of emulsion reduces the diameter deviations compared with other CLF concepts. Concerning the roundness deviations and the surface roughness, the minimum quantity lubrication is a very good alternative. The machining of holes with a L/D ratio of above 2 with a reduced use of CLF is only possible with the support of chip removal, e.g., by means of compressed air supply, because otherwise plastic deformations of the hole wall can occur as a consequence of the interaction with the chip.

New findings for steel machining, which are meanwhile already in industrial application, resulted from the influencing of the chip form in turning by ultra-high pressure coolant, for example [DAH05]. Mixing a 2-component CLF directly at the machine tool has been successfully substituted by using a CLF with sulfur additive [BAU05]. Investigations in the cutting of stainless steel have shown that an exact adjustment of the machining parameter and the use of a MQL lead to better machining results [DEV05]. A beneficial lubricating effect of silver nanoparticles in a PVD tool coating has also been proven [ALB07].

Methods for the deployment of solid lubricating fluids have been successfully tested. In the turning of hardened steel, tools were used which had been prepared with molybdenum disulfide MoS_2 by means of eroded cavities in the rake resp. flank face (diameter $D \approx 200 \mu\text{m}$) [JIA09]. The lubricating fluid is directly fed into the process zone via this channel. The process forces and the tool wear are considerably influenced by the use of these tools. A lubricating cavity on the flank face causes a lower flank face wear of the tool, compared with the unprepared cutting edge. A cavity on the rake face leads to a significant reduction of the process forces and the friction coefficient. The cause for this is the development of a MoS_2 lubricating film between tool and workpiece resp. chip. This underlines that the targeted supply of cooling and lubricating materials can cause a significant improvement of the tool use behavior.

High pressure cooling lubricating systems have been analyzed concerning their effectiveness [SHA09]. In such systems, the CLF is specifically supplied into the contact zone between workpiece and tool so that a fluid pressure develops between the friction partners. Experimental cutting investigations in the turning of the material TiAl6V4, which is difficult to cut, have demonstrated that this achieves a better cooling and lubricating effect. This causes a significant reduction of the built-up edge development and the diffusion wear of the tool, as well as an improvement of the surface roughness and the chip breakage and finally an extension of the tool lifetime. Similar significant effects are obtained with MQL lubrication resp. oil mist with the use of compressed air in turning. At this, the process temperature is reduced, which in turn allows the increase of the cutting speed. In this case, dominant adjustment variables are the type of oil mist generation as well as the orientation of the supply throttles [TAK06].

17.4 Use of Cooling Lubricating Fluid in Grinding

Cooling lubricating is of special significance for grinding. The comparatively large contact area between grinding wheel and workpiece makes the supply of the cooling lubricating fluid (CLF) into the grinding gap difficult. The specific energy in grinding—that is the required energy per cut volume—is relatively high (compare Chap. 4). This is due to large friction proportions and very small cutting thicknesses in grinding. Also in this case, the supplied energy is almost completely transformed into heat. High temperatures develop in the grinding gap, which damage the surface zone of the workpiece (Chap. 13) and can cause an increased wear of the grinding tools and a clogging of the active grinding space.

The type and composition of the CLF as well as the cleaning and processing of the CLFs, influence the cooling and lubricating effect in the contact zone. The supply of CLFs with degrees of freedom such as throttle design, nozzle position, size of the supply volume flow and CLF pressure provide the edge conditions concerning if and how much CLF can reach the contact zone.

Different throttles for different grinding tasks have been developed to achieve a high effect. Those most widely spread in practice are the flooding throttles. At this, we differentiate between free jet throttles and throttles without free jet. There are free jet throttles with rigid tube systems and with segmented pipe systems. The advantages of free jet throttles are their simple installation and handling. In addition, they are relatively well-priced. A disadvantage is that mostly the air film cushion around the grinding wheel cannot be overcome with these throttles. To ensure the wetting of the grinding wheel with CLF it is possible to use air cushion fenders, which can weaken the wall flux of the air, the so-called air coat [BRÜ96]. The benefit of air cushion fenders becomes especially noticeable in high speed grinding [OKU93, INA98]. Figure 17.6 clearly illustrates that an air coat is generated in front of the working area.

Mostly the relatively high CLF volume flow does not achieve the optimum cleaning effect. In addition, the position of the throttle cannot be adjusted in a way to be reproduced when using segmented pipe systems.

Throttles without free jets, the so-called shoe throttles, offer some advantages. They are able to break through the air cushion. Their better cooling effect causes less damage to the subsurface integrity zones of the component. The CLF flow and pressure are lower than with free jet throttles, the effectiveness can even be increased by means of leading elements. However, the installation of shoe throttles requires considerably more effort than with free jet throttle. Shoe throttles should not be used for strongly wearing grinding wheels or complex grinding wheel geometries.

Considerably less CLF is required by not flooding throttles, which include point and needle jet throttles as well as spray throttles. Point and needle jet throttles can be individually adapted to the profile of the grinding wheel. They then provide a steadily directed jet with low loss volume flow. However, a higher pump power is necessary and the installation is linked to the profile of the grinding wheel. The spray throttles, which supply the CLF to the working area in a finely sprayed

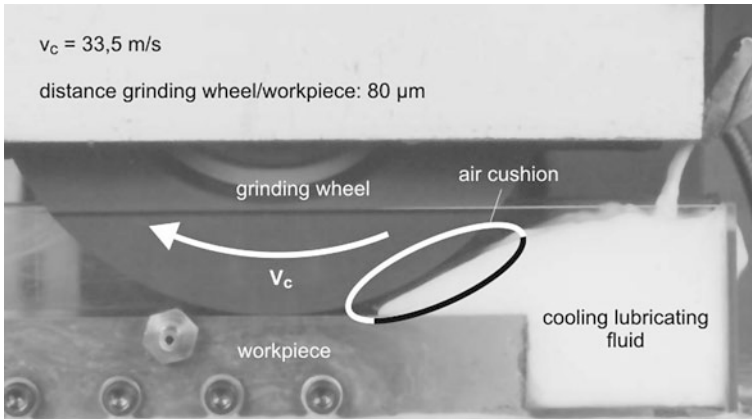


Fig. 17.6 Influence of the air cushion on the cooling lubricating fluid wetting of the grinding wheel [EBB00]

condition, require very little CLF because they lubricate via an aerosol of CLF and air (MQL). Problems caused by the jointly rotating air cushion and the low chip removal have to be considered. Spray throttles are only conditionally deployable for grinding processes, since the cooling effect is often not sufficient.

Further solutions, e.g., an internal coolant at which the CLF flows out through the wheel or segmented grinding wheels, are still exceptions.

The advantages and disadvantages of different cooling lubricating fluid supply throttles have been summarized in Table 17.4 as an overview.

The attempt of covering the requirement of cooling and lubricating fluids by an excessive supply of CLF before the engagement zone is useless. The maximum volume flow, which flows through a grinding gap is geometrically limited. Excessive amounts are thrown back by the grinding wheel [MAL92].

Higher volume rates have further disadvantages. Rising forces between tool and workpiece and an increase of the necessary spindle power are the consequences of an increased offer of CLF [BRI93, TRE95, BRÜ96]. Here, pressure generating,

Table 17.4 Cooling lubricating fluid supply systems in comparison

CLF supply	Advantage	Disadvantage
Rigid tube	Inexpensive system	Throttle form mostly not optimum
Segment pipe	Very flexible	Throttle position not reproducible
Shoe throttle	Very good cooling effect	Adaptation to the grinding wheel necessary
Point jet throttle	High cooling lubricating fluid speed	Low cooling effect
Needle throttle	Adaptable to grinding wheel profile	High pump power necessary
Spray throttle (MQL)	Very low cooling lubricating fluid consumption	Low cooling effect
Internal coolant	Good cooling effect	Spindle with cooling lubricating fluid bore necessary

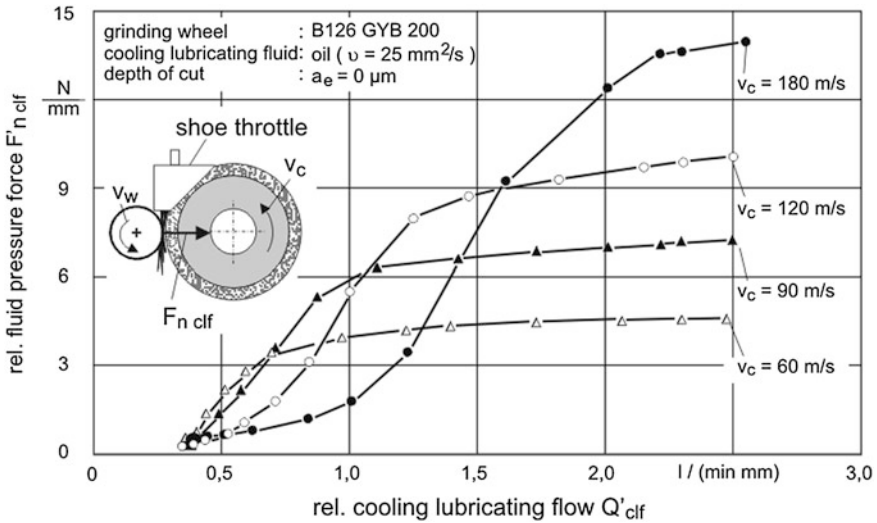


Fig. 17.7 Impact of the cooling lubricating fluid volume flow with the cutting speed depending on the fluid pressure force [TRE95]

hydrodynamic effects are active and have an impact in the contact zone. Figure 17.7 illustrates the effect of the volume rates on the normal force, which develops due to the fluid pressures for different cutting speeds in external plunge grinding. The forces were measured during spark-out, i. e., a radial feed motion did not take place. It can be detected that stationary values for the fluid pressure forces can be achieved independently from the cutting speed. The fluid pressure force rises strongly with the CLF volume flow. The thus resulting normal force is added to the force resulting from the process. Especially in high speed grinding it is therefore impossible to reach a grinding force reduction [TRE95]. This strong action of force can lead to deformations of the workpiece and negative influences on the dimensional and form accuracy.

The necessary spindle power is also strongly increased with the increased volume rate of the CLF. At this, the drag effect of fluid has an impact by means of the grinding wheel rotation. The loss power conditioned by this can amount to 80 % of the total power [BRI93, KLO97, TAW90] (Fig. 17.8).

17.4.1 Methods to Determine the Cooling Lubricating Fluid Effect in Grinding

To analyze the effect of the cooling lubrication in grinding, different laboratory methods were developed by Brinksmeier and co-workers (Fig. 17.8). For this purpose, the pressure in the grinding gap, the amount of the CLFs transported

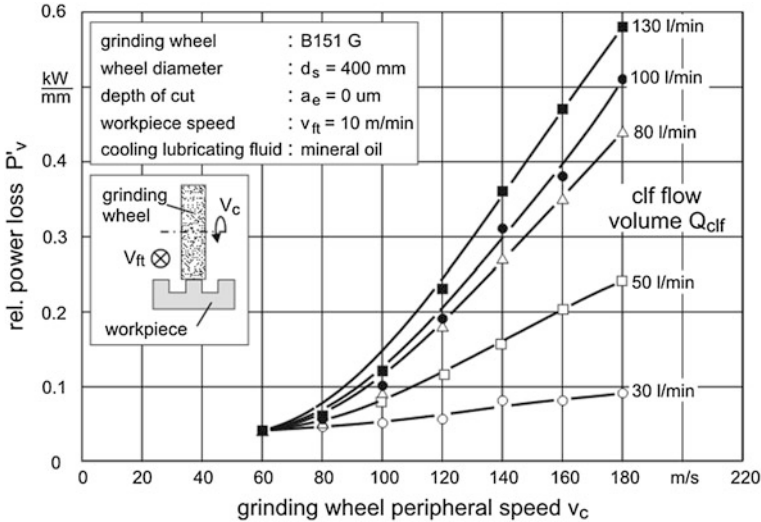


Fig. 17.8 Influence of the grinding wheel circumferential speed and the cooling lubricating fluid volume flow of the loss power [BRI93]

through the contact zone and the cooling effect are measured. The flux within the CLF throttles is made visible in a suitable manner.

A sensor is mounted in the workpiece in one or several measurement bores for pressure measurement. Pressure profiles can be recorded by using several sensors along the generatrix of the grinding wheel. The time and location profile is recognizable when over grinding the sensor row (see Fig. 17.9, top left). An integration of the pressures above the contact surface allows the determination of the normal force, which is caused by the fluid pressure [HEI99].

The upper right illustration in Fig. 17.9 shows the measuring setup behind the grinding gap in surface grinding, with which the CLF can be captured. The cooling effect can be determined with a very ingenious method (Fig. 17.9, bottom left). The workpiece is ground-in with the grinding wheel. The workpiece is heated up by a constant heat source and the temperature in the workpiece is measured via thermocouples. These thermocouples show the cooling effect at different supplies of CLF [BRI04b].

Figure 17.9, bottom right, illustrates the possibility of flux visualization with the aid of a light-intersection process. The flow distribution can be followed by means of encased tracer particles. This is how back flow or flow detachments in the throttle, which affect the effectiveness of the CLF supply, can be detected. It is also possible to examine the interface between grinding wheel and throttle in more detail in this manner. Air bubbles which lower the cooling effect in the contact zone and have been introduced by the rotating grinding wheel, can be observed like this [HEI99].

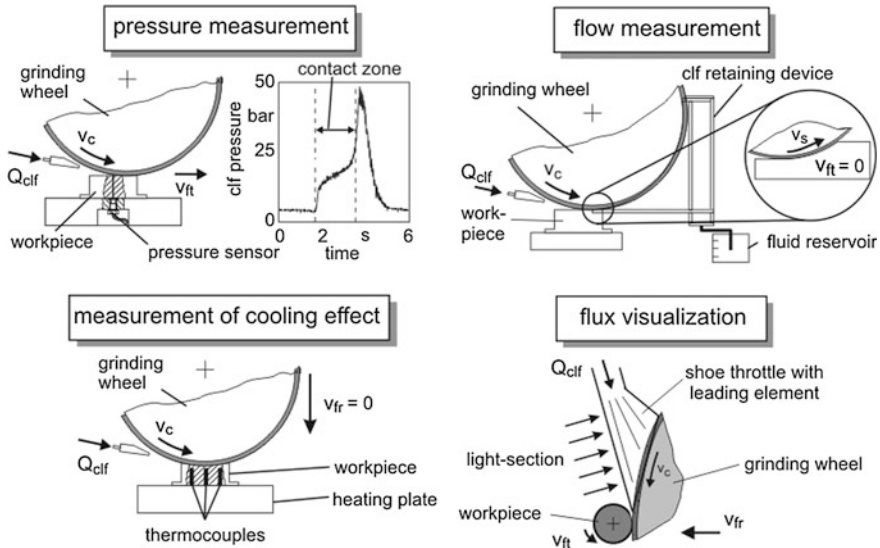


Fig. 17.9 Laboratory methods for the examination of the cooling lubricating fluid effect in grinding [HEI99, BRI01, BRI04b]

17.4.2 Applications and Effects

Generally liquid CLFs are used in grinding so as to avoid damages in the surface zone of the workpiece (see Chap. 13). Mineral oils, emulsions and dilutions are deployed. They differ considerably concerning their effect. Figure 17.10 illustrates the influence of unalloyed mineral oil and of 5 % emulsion on the radial wear in external plunge grinding. The tests were carried out with CBN grinding wheels. Similar results have been obtained using corundum grinding wheels. The assumption that CBN grinding materials wear due to hydrolytic processes does not seem sustainable. In fact, the major influence can be explained with the strong bonding wear, which occurs due to stronger friction between chip and bonding in the case of water-mixed CLFs and leads to a premature release of the grains. This is also confirmed by the roughness shown in the image. Emulsions cause considerably higher roughnesses, because grains constantly break out and therefore lower grain numbers lead to higher averaged cutting thicknesses per cutting edge [HEU92].

The noticeably improved lubrication effect of oil compared with emulsions also shows in the level of the grinding forces (Fig. 17.11). The friction is reduced, at the same time however the number of active cutting edges is higher. The typical force course results from these influences running in opposite directions. The increased forces which occur during the initial phase of the grinding are linked with a resetting of the bonding level and a break out of the loosened grinding and filling grains. This leads to the fact that the number of active grains drops strongly,

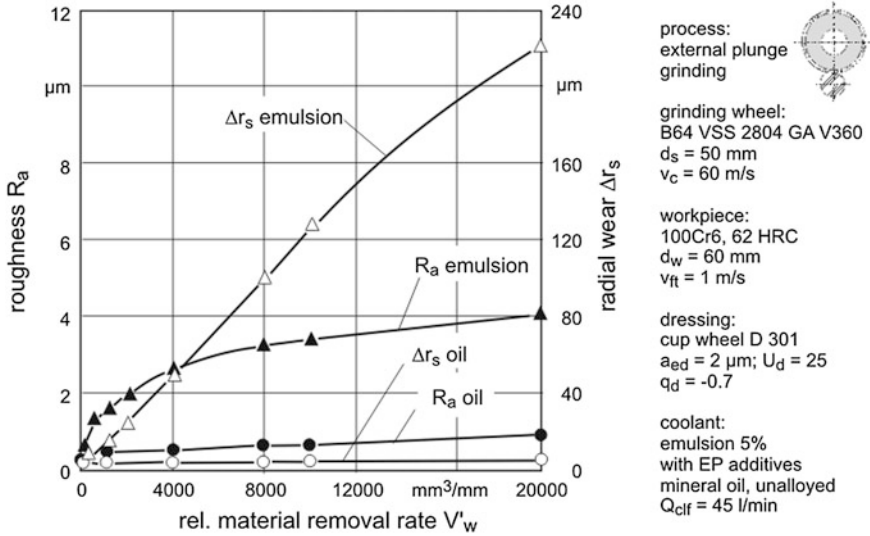


Fig. 17.10 Influence of the types of cooling lubricating fluids on the grinding process [HEU92]

above all in the case of emulsion coolant. As a consequence the grinding forces decrease, especially at the beginning. The strong bonding wear linked with emulsion coolant causes a stationary condition, at which a considerably lower number of active grains exist than with oil coolant. Therefore, lower normal forces

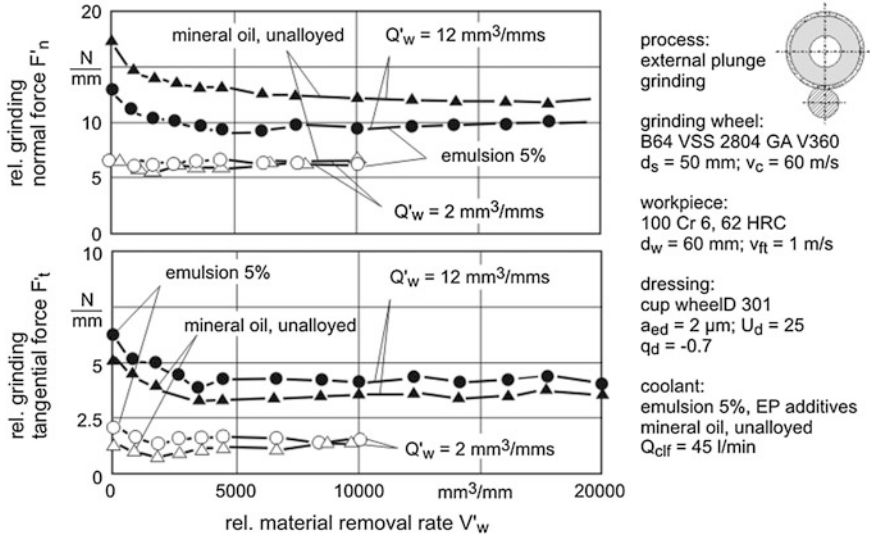


Fig. 17.11 Influence of the cooling lubricating fluid types on the grinding process forces [HEU92]

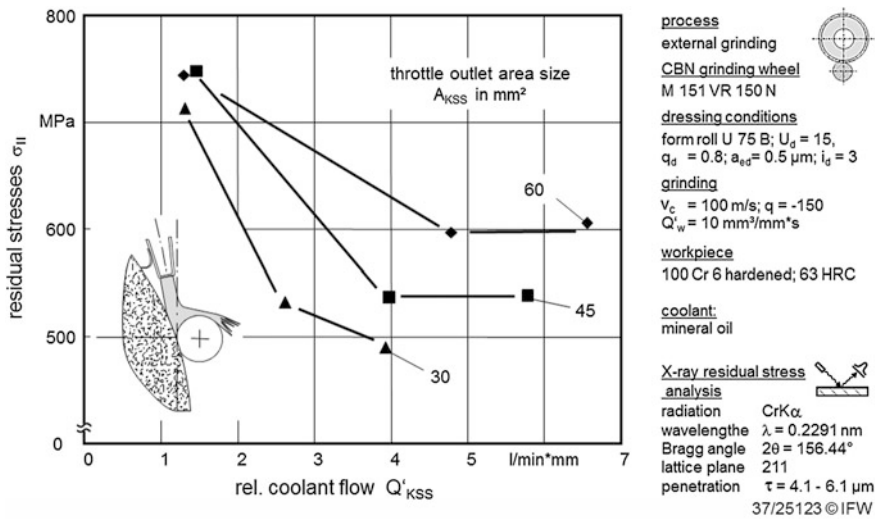


Fig. 17.12 Residual stresses at the workpiece surface for different throttle cross sections and flows [CZE99]

occur than when using oil. However, the better lubricating properties of oil lead to a lower friction ratio so that with oil, there are lower tangential forces despite a higher number of active cutting edges than with emulsion [HEU92].

In the following, the influence of different throttle geometries will be illustrated by means of tests concerning CBN external plunge grinding with three tangential

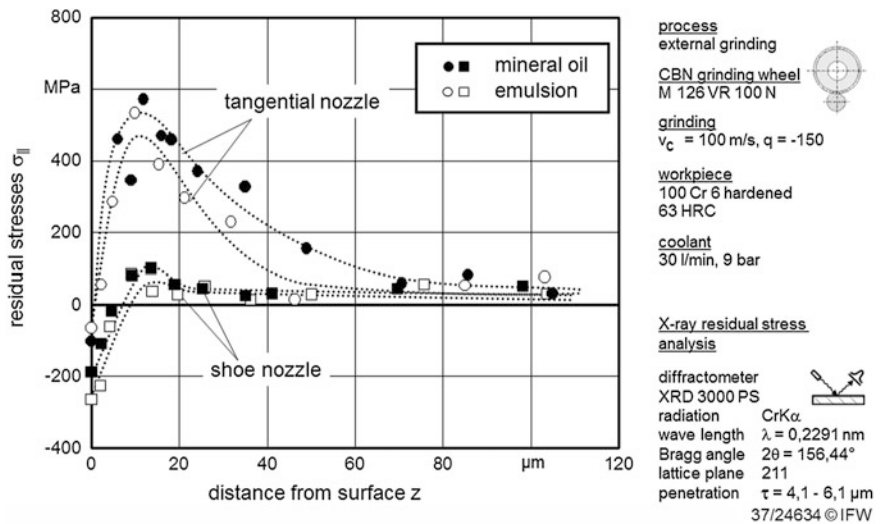


Fig. 17.13 Influence of cooling lubricating fluid and throttle type on the residual stress depth course [CZE99]

throttles and with an exit cross section of 30, 45 and 60 mm². For the evaluation of the cooling effect, surface residual stresses are measured depending on the amount of CLF Q'_{KSS} (Fig. 17.12). At a given throttle cross section, the jet speed increases with the flow. Apparently greater jet speeds improve the adhesion of the CLF to the grinding wheel and the surrounding air cushion is overcome more easily. Larger proportions of the total amount of supplied CLF reach the contact zone [CZE99], the thermal load of the workpiece is lower. This is linked with the reduction of residual tensile stresses which—as explained in Chap. 13—is typical for thermal influence.

A comparison of the influence of tangential and shoe throttles on the distribution of residual stresses at the workpiece surface is illustrated in Fig. 17.13. Using shoe throttles apparently facilitates a more effective supply of the CLF into the contact zone between grinding wheel and workpiece, which improves the cooling and lubricating effect. Under otherwise identical adjustment conditions, a thermal influence can be almost completely eliminated with the shoe throttle. Residual compressive stresses occur which suggest dominant, mechanical sub surface effects.

Minimum quantity lubrication (MQL) or pure dry machining allow a drastic reduction of the amount of CLF in grinding or it is possible to do without CLF altogether. These conditions were compared with conventional flooding cooling lubrication, so to investigate the influence of the MQL and dry machining in internal grinding with micro-crystalline aluminum oxide. MQL reduced the amount of CLF from $Q_{KSS} = 11$ l/min to $Q_{KSS} = 0.4$ l/min. For MQL, a synthetic ester was deployed, in conventional flooding it was an unalloyed mineral oil.

With increasing grinding time resp. increasing cutting volume dry machining leads to a strong increase of the process forces (Fig. 17.14). Already after a related cutting volume of $V'_w = 160$ mm³/mm, that corresponds to a grinding time of less than 3 min, the test had to be discontinued due to the clogging of the active grinding space. In flooding cooling lubrication, the force rise at first but then remain constant. It is interesting that the force level with MQL is fundamentally minimal. The reasons for this are the lack of a hydrodynamic force effect and the better lubricating effect of the used ester compared with mineral oil [BRU98].

The grinding wheel wear with MQL is between that of flooding cooling lubricating and that of dry machining (Fig. 17.15). This is to be attributed to the reduced resp. missing cooling effect. A higher wear occurs due to the increased thermal load of grinding grain and bonding. The workpiece roughnesses achievable with MQL are only slightly above those after grinding with flooding cooling lubrication. The roughness values after dry grinding are considerably higher.

Apart from the micro-geometric development of the surface, the influence of the MQL and dry machining on the workpiece surface zone was analyzed and compared with conventional cooling lubrication. Figure 17.16 illustrates structure micrographs of the workpiece surface zone, transverse to the machining direction and the surface residual stresses parallel to the grinding direction depending on the cutting volume resp. on the grinding time. In dry machining, thermal damages in

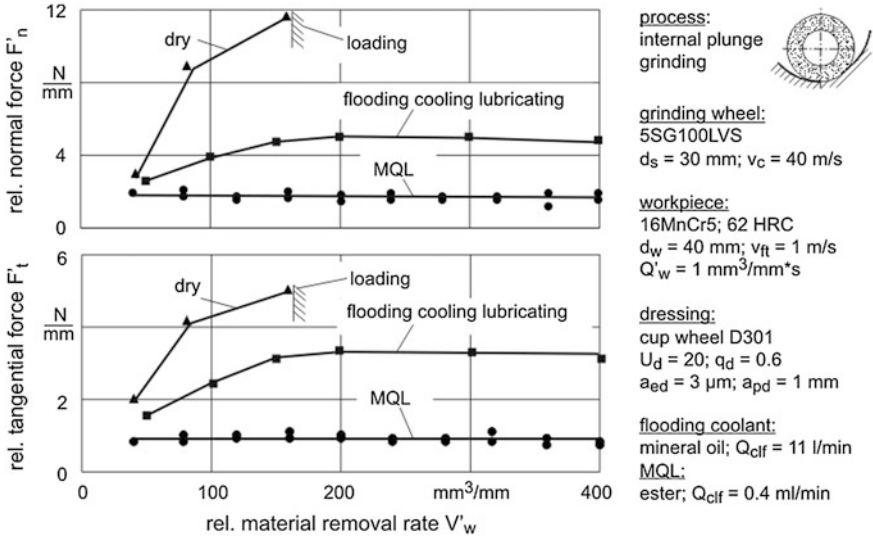


Fig. 17.14 Grinding forces depending on the amount of cooling lubricating fluid [BRU98]

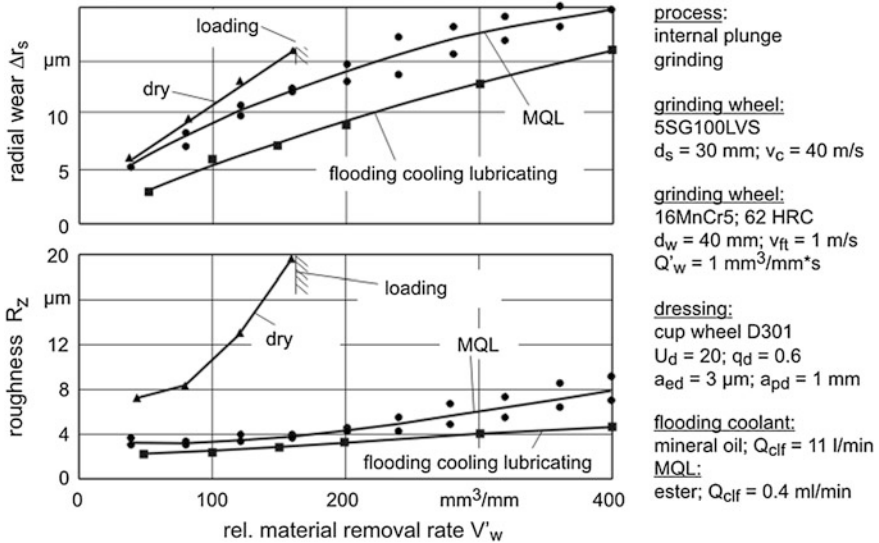


Fig. 17.15 Radial wear and workpiece roughness depending on the amount of cooling lubricating fluid [BRU98]

the form of annealing and new hardening zones occurred (development of white layers). Residual stress measurements showed that the surface values for the dry machining are offset by more than 100 MPa in the direction of the residual tensile stresses compared with the other two conditions. The surface residual stress values

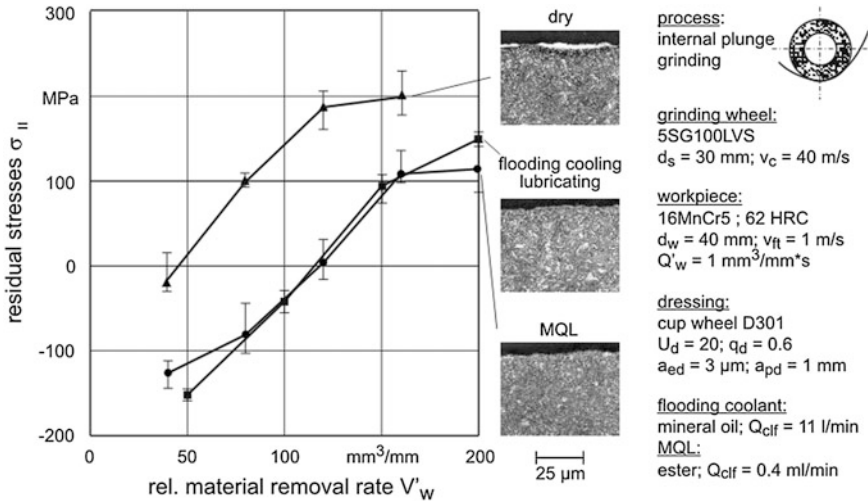


Fig. 17.16 Structure and residual stresses of the workpiece surface zone [BRU98]

with MQL and flooding cooling lubrication cannot be significantly differentiated from one another. Even tests with an increased material removal rate of $Q'_w = 2.5 \text{ mm}^3/\text{mms}$ showed no damages to the workpiece structure.

It can thus be determined that by using a minimum quantity lubrication, lower process forces are achieved compared with a conventional flooding cooling lubrication. The grinding wheel wear and the workpiece roughness are marginally above the comparative values. The surface zone influence corresponds to the flooding cooling lubrication. In internal grinding without liquid CLF it was only possible to work with low material removal rates over a limited grinding time resp. cutting volume. However, dry grinding is economically possible in a process combination of hard turning and grinding (see Chap. 11).

17.5 Questions

1. Which main requirements concerning cooling lubricating fluids do you know? Name and explain them.
2. What are the additional functions of cooling lubricating fluids?
3. Which cooling lubricating fluid substances do you know concerning their aggregate condition?
4. Classify the liquid cooling lubricating fluids.
5. What advantages does the use of emulsions offer compared with not water-mixed cooling lubricating fluids?

6. Why is the measurement of the refractometer value necessary when using cooling lubricating emulsions and what does it mean?
7. The use of oils is linked with considerable effort in industry. Name factors to be considered when using oils.
8. What sub-categories are the not water-mixed cooling lubricating fluids in [DIN 51520](#) divided into?
9. What are EP additives?
10. What are the tasks of preserving agents as additives for cooling lubricating fluids and what must be observed during their loading?
11. Following the maxim “a lot helps a lot”, why can the cooling lubricating fluid supply (which can be observed often in practice), not apply?
12. What methods for the optimization of cooling lubricating fluid supplies in grinding do you know?
13. Name the possibilities to reduce the deployment of cooling lubricating substance and evaluate them concerning their influence on the productivity in grinding.
14. What basic conditions seem to be necessary to facilitate dry machining with internal grinding?

References

- [ALB07] Alberdi, A. et al.: High seizure resistant TiN-Ag nanocomposite coatings. In: Proceedings of the 6th International Conference the Coatings, Oct 25–26, pp. 171–177. Hannover, Germany (2007)
- [AUR06] Aurich, J.C., Sudermann, H., Hellmann, D.H., Roclowski, H.: Interne Schleifölfzufuhr beim Hochleistungsschleifen. Entwicklung eines Grundkörperprototyps mit internen, strömungsdynamisch ausgelegten Schleifölkanälen [Internal grinding oil supply in high power grinding. Development of a base body prototype with internal flow mechanically designed grinding oil pipes]. *wt Werkstatttechnik online* 96 (2006) 11/12, S. 810–813
- [BAR78] Bartz, W.J.: Wirtschaftliches Zerspanen durch Kühlschmierstoff [Economically cutting with cooling lubrication fluids]. *wt-Z. ind. Fert.* 68(8), 471–475 und 10, 621–624 (1978)
- [BAR81] Bartolomé, E., et al.: Ullmanns Enzyklopädie der technischen Chemie [Ullmann's encyclopedia of technical chemistry]. Weinheim: Verlag Chemie 20 1981 S. 617–633
- [BAU05] Baumgärtner, R.: Trends bei Kühlschmierstoffen aus Anwendersicht [Trends in cooling lubrication fluids from application view]. In: Das 15. Dt. Kühlschmierstoffforum, 8./9. Dezember, Bad Nauheim S 73–95 (2005)
- [BRI93] Brinksmeier, E., Minke, E.: High-performance surface grinding: the influence of coolant on the abrasive process. *Annals of the CIRP* 42(1), 367–370 (1993)
- [BRI95] Brinksmeier, E., Heinzl, C.: Aufgaben und Auswahl der Kühlschmierstoffe [Tasks and choice of cooling lubrication fluid]. DIF-Tagung, Deutsches Industrieforum für Technologie, 10, 1–32 (1995)

- [BRI01] Brinksmeier, E., et al.: Auswirkung unterschiedlicher Kühlschmierstoff-Zuführbedingungen auf die Randzoneeigenstressungen beim Schleifen [Effects of various cooling lubrication fluids supply on the surface residual stresses]. Schleifen, Honen, Läppen und Polieren, 60. Ausgabe, Vulkan-Verlag Essen (2001)
- [BRI04a] Brinksmeier, E., Lucca, D.A., Walter, A.: Chemical aspects of machining processes. CIRP Ann. 53(2), 685–699 (2004)
- [BRI04b] Brinksmeier, E., Wittmann, M.: Methode zur Bewertung der Kühlwirkung des Kühlschmierstoff-Zufuhrsystems beim Schleifen [Evaluation method of the cooling effect of cooling lubrication fluid supply systems in grinding]. In: Proceedings of the 14th International Colloq. Tribology: Tribology and Lubrication Engineering, Tech. Akademie Esslingen, Esslingen, Jan 2004
- [BRU98] Brunner, G.: Schleifen mit mikrokristallinem Aluminiumoxid [Grinding with micro-crystalline aluminum oxide]. Dr.-Ing. Dissertation, Universität Hannover (1998)
- [BRÜ96] Brücher, T.: Kühlschmierung beim Schleifen keramischer Werkstoffe [Cooling lubrication in grinding of ceramic materials]. Dr.-Ing. Dissertation, TU Berlin (1996)
- [CZE99] Czenkusch, C.: Technologische Untersuchungen und Prozessmodelle zum Rundschleifen [Technological investigations and process models in external grinding]. Dr.-Ing. Dissertation, Universität Hannover (1999)
- [DAH05] Dahman, P.: High pressure jet assistance in steel turning. Thesis Chalmers University of Technology, Gothenburg (2005)
- [DEV05] Deville-Cavellin, C., et al.: Improving the Machinability of Stainless Steels. Luxembourg. Office for Official Publications of the European Communities, EUR; 21801: Technical steel research: steel products and applications for building, construction and industry, Contract no. 7210-PR/237, ISBN: 92-79-00057-8 (2005)
- [DIN 51385] DIN 51385: Schmierstoffe, Kühlschmierstoffe, Begriffe/Lubricants; metal working fluids; terms (1991)
- [DIN 51520] DIN 51520: Schmierstoffe—Kühlschmierstoffe—Nichtwassermischbare Kühlschmierstoffe SN; Mindestanforderungen (Entwurf)/Lubricants—Metal working fluids—Straight cutting oils (non aqueous fluids) SN; specifications (2008)
- [EBB00] Ebbrell, S., et al.: The effects of cutting fluid application methods on the grinding process. Int. J. Mach. Tools Manuf. 40, 209–223 (2000)
- [GOT53] Gottwein, K., Reichel, W.: Kühlschmierer [Cooling lubricating]. Carl Hanser Verlag München (1953)
- [GÜN84] Günther, F., Pocklington, J.: Der pH-Wert von wassergemischten Kühlschmierstoffen [The pH-value of watermixed cooling lubrication fluid]. Tribologie und Schmiertechnik 31(1), 36–42 (1984)
- [HEI99] Heinzl, C.: Methoden zur Untersuchung und Optimierung der Kühlschmierung beim Schleifen [Method to investigate and optimize the cooling lubricating in grinding]. Dr.-Ing. Dissertation, Universität Bremen (1999)
- [HEU92] Heuer, W.: Außenrundschleifen mit kleinen keramisch gebundenen CBN-Schleifscheiben [External grinding with small grinding wheels]. Dr.-Ing. Dissertation, Universität Hannover (1992)
- [HÖR87] Hörner, D.: Erfahrungen mit chlorfreien Kühlschmierstoffen [Experiences with chlorine-free cooling lubrication fluids]. VDI-Z 9, 14–15 (1987)
- [HOW91] Howes, T.D., Tönshoff, H.K., Heuer, W., Howes, T.: Environmental aspects of grinding fluids. Ann. CIRP 40(2), 623–630 (1991)

- [INA98] Inasaki, I.: Fluid Film in the Grinding Arc of Contact. January-CIRP Meeting, Paris, 27–31 Jan 1998
- [JAC88] Jacobs, P.: Stabile wassermischbare Kühlschmierstoffe für die Aluminiumbearbeitung [Stable water mixable cooling lubrication fluids in machining of aluminum]. TZ für Metallbearbeitung 5, 77–78 (1988)
- [JIA09] Jianxing, D., Welong, S., Hui, Z.: Design, fabrication and properties of a self-lubricated tool in dry cutting. Int. J. Mach. Tools Manuf. 49, 66–72 (2009)
- [KLO97] Klocke, F., Beck, T.: Zufuhrsysteme für den anforderungsgerechten Kühlschmierstoffeinsatz [Supply systems for cooling lubrication systems meeting the requirements]. Schleiftechnik im Wettbewerb, Schleiftechnisches Kolloquium, Aachen, 9./10. Oktober 1997, Düsseldorf, VDI-Verlag (1997)
- [KLO04] Klocke, F., Maßmann, T., Grams, J.: Grundlagenuntersuchungen zum Einsatz umweltverträglicher Tribosysteme beim Zerspanen und in der Kaltumformung [Basic investigations of the application of environmentally compatible tribosystems]. Materialwissenschaft und Werkstofftechnik 35(2004) 10/11, S. 901–909
- [KLO06a] Klocke, F., Gerschwiler, K., Fritsch, R., Lung, D.: PVD-coated tools and native ester: an advanced system for environmental friendly machining. Surf. Coat. Technol. 201, 4389–4394 (2006)
- [KLO06b] Klocke, F., Arntz, K., Bodenhausen, J., Avila-Robinson, A.: Influence of cutting fluids on the performance of the micro milling process of tool steel. In: 8th Annual General Meeting of the European Society for Precision Engineering and Nanotechnology, Euspen, 6, 220–223 (2006)
- [KNO86] Knobloch, H.: Kühlen und Schmierer [Cooling and lubricating]. Maschinenmarkt 91, 54–59 (1986)
- [LAN73] Landov, E. N.: A tapping test for evaluation cutting fluids. Lubr. Eng. 30(1), 5–9 (1973)
- [LIN86] Lingmann, H., Ölscher, H.-P.: Kühlschmierstoff—ein Garant für wirtschaftliche Fertigung [Cooling lubrication—a guarantor for economic production]. TZ für Metallbearbeitung 4, 13–16 (1986)
- [LOI04] Loichinger, A.: Analyse und Optimierung der Kühlschmierstoff-Versorgung von rotierenden Werkzeugen [Analysis and optimization of the cooling lubrication supply of rotating tools]. Dr.-Ing. Dissertation, Universität Dortmund (2004)
- [MAL92] Malkin, S., Engineer, F., Guo, C.: Experimental measurement of fluid flow through the grinding zone. ASME J. Eng. Ind. 114, 61–66 (1992)
- [MÜL87] Müller, J.: Profil festlegen [Profile determining]. Maschinenmarkt 93, 44–45 (1987)
- [ÖST03] Österholm, L. H., et al.: Recycling of rolling oil emulsions: towards an economic and sustainable process; final report, Luxembourg: Office for Official Publications of the European Communities, EUR; 20625: Technical steel research—analytical techniques for processes, products and environment, Contract no 7210-PR/098, ISBN: 92-894-5152-1, 2003
- [OKU93] Okuyama, S., Nakamura, Y., Kawamura, S.: Cooling action of grinding fluid in shallow grinding. Int. J. Mach. Tools Manufact. 33(1), 13–23 (1993)
- [ROE95] Roethel, J.: Kühlschmierung bei der Zerspanung von Aluminiumlegierungen [Cooling lubricating in cutting of aluminum alloys]. Dr.-Ing. Dissertation, Universität Hannover (1995)
- [SCH04] Schepers, A.: Einsatzmöglichkeiten wiedergewonnener Kühlschmierstoffe und Feststoffe aus Schleifschlämmen [Application possibilities of recycled cooling lubrication fluid and solid materials from grinding slurry]. Dr.-Ing. Dissertation Universität Bremen (2004)

- [SHA09] Sharma, V.S., Dogra, M., Suri, N.M.: Cooling techniques for improved productivity in turning. *Int. J. Mach. Tools Manuf.* 49, 435–453 (2009)
- [STÄ04] Stäbler, D.: Minimalmengenschmierung für die Zerspanung—Aerosolerzeugung, -transport, -abscheidung und Arbeitssicherheit [Minimum quantity lubrication for cutting processes—generation, transport, segregation and safety at work of aerosol]. Dr.-Ing. Dissertation, Universität Stuttgart (2004)
- [TAK06] Takashi, U., Hosokawa, A., Yamada, K.: Effect of oil mist on tool temperature in cutting. *J. Manuf. Sci. Eng.* 128, 130–135 (2006)
- [TRE95] Treffert, C.: Hochgeschwindigkeitsschleifen mit galvanisch gebundenen CBN-Schleifscheiben [High speed grinding with galvanic bonded CBN grinding wheels]. Dr.-Ing. Dissertation, RWTH Aachen (1995)
- [TAW90] Tawakoli, T.: Hochleistungs-Flachschleifen: Technologie, Verfahrensplanung und wirtschaftlicher Einsatz [High power surface grinding: technology, process planning and economical application]. Dr.-Ing. Dissertation, Universität Bremen (1990)
- [VAM84] Vamos, E.: Neue Versuche zur Wirkungsweise von EP-Additiven in Kühlschmierstoffen [New experiments on the effects of EP-additives in cooling lubrication fluids]. *Tribologie-Schmier-technik* 4, 190–196 (1984)
- [WEI97] Weinert, K., Schulte K., Thamke, D.: Bohren von Stahl mit Wendeschneidplatten-Bohrern. Neue Kühlschmierstoffkonzepte für die umweltverträgliche Stahlbearbeitung [Drilling of steel with insert drills. New cooling lubrication concepts for the environmentally compatible machining of steel]. *Werkstattstechnik—wt* vol. 87 (1997) 9/10, S. 475–478
- [WEI99] Weinert, K.: Trockenbearbeitung und Minimalmengenkühlschmierung [Dry Machining and Minimum Quantity Lubrication]. Springer (1999)
- [ZWI73] Zwingmann, G.: Wassermischbare KSS [Water mixable cooling lubricating fluids]. *Industrie-Anzeiger* 95(108), 2554–2558 (1973)
- [ZWI79] Zwingmann, G.: Kühlschmierstoffe für die spanende Metallbearbeitung [Cooling lubrication fluids for cutting metals]. *Werkstatt und Betrieb* 112(6), 409–414 (1979)

Chapter 18

Appendix

18.1 Solution to the Exercise for Chap. 3, Question 9

1. The curving radius of the chip is:

$$R_0 = \frac{t_1^2 + b_1^2}{2 \cdot t_1} = 1.82 \text{ mm}$$

The strain ε_r of the curved chip results at

$$\varepsilon_r = \frac{\Delta l}{l} = \frac{h' \varphi}{2(R_0 - h') \cdot \varphi} = 0.05 = 5 \%$$

at which the chip thickness $h' = 0.158 \text{ mm}$ is calculated from the chip thickness compression $\lambda_h = \frac{h'}{h}$ with the relationships $\frac{h}{h_0} = \sin \phi$ and $\frac{h'}{h_0} = \cos(\phi - \gamma)$.

Since the fracture strain of the chip amounts to $\varepsilon_b = 7.1 \%$, the chip does not break under the given conditions.

2. The strain inside the chip has to be larger than the fracture strain. This can be achieved by increasing the chip thickness respectively the feed.

$$h \geq \frac{2\varepsilon_b \cdot R_0}{\lambda_h \cdot (2\varepsilon_b + 1)} = 0.143 \text{ mm}$$

18.2 Solution to the Exercise for Chap. 4, Question 26

Equations 4.44, 4.49, 4.53–4.55 are necessary for the solution. Figure 4.13 implies $\rho = \arctan \mu = 11.3^\circ$ and with Eq. 4.44 $\phi = 36.4^\circ$.

Equations 4.49 and 4.53 imply the tangential force

$$\Rightarrow F_{T\phi} = 260.9 \text{ N.}$$

With Eq. 4.54 the resulting force determines

$$\Rightarrow F_z = 304.7 \text{ N.}$$

The cutting force results from Eq. 4.55 with ϕ and F_z

$$\Rightarrow F_c = 291.1 \text{ N.}$$

18.3 Solution to the Exercise for Chap. 5, Question 17

1. The speed diagram (Fig. 2.12) of the shear plane model implies 2.10. With the addition theorem λ_h results at

$$\lambda_h = \frac{\cos \gamma}{\tan \phi} + \sin \gamma, \text{ this implies: } \phi = \arctg \left[\frac{\cos \gamma}{\lambda_h - \sin \gamma} \right].$$

$$\Rightarrow \phi_{konv.} = 35.1^\circ$$

$$\Rightarrow \phi_{HSC} = 16.5^\circ.$$

Equation 5.12 allows the determination of the ratio $\frac{k_{M,HSC}}{k_{M,konv.}} = 9.5$.

2. Speed influence: $\frac{v_{c,HSC}^2}{v_{c,konv.}^2} = 11.1$

$$\text{Shear angle influence: } \frac{\cos^2(\phi_{konv.} - \gamma)}{\cos^2(\phi_{HSC} - \gamma)} = 0.85.$$

This allows the derivation that the influence of the shear angle is low concerning the cutting speed increase.

3. The yield criterion of Tresca (Eq. 4.5) implies:

$$k_{f,konv.} = 77.5 \text{ MPa and } k_{f,HSC} = 73.5 \text{ MPa.}$$

The specific shearing energy can be determined with Eq. 5.3 and with Eq. 5.11 the specific deviation energy. The following relations result from this:

$$\frac{k_{M,konv.}}{k_{\phi,konv.}} = 0.055;$$

i.e. the proportion of the energy from the change of material flow corresponds to 5.5 % of the forming energy.

$$\frac{k_{M,HSC}}{k_{\phi,HSC}} = 0.295;$$

i.e. the HSC machining increases the proportion of the energy from the change of material flow in relation to the forming energy to 29.5 %.

18.4 Solution to the Exercise for Chap. 6, Question 25

The Taylor equation is: $C = v_c \cdot T^{-(1/k)}$.

An optimization of the piece production time concerning the optimum lifetime delivers the equation:

$$v_{cT_{opt}} = C \cdot [t_{wz}(-k - 1)]^{1/k}.$$

The determination of k and C for $VB = 0.2$ mm (see given data) result at:

$$\begin{aligned} v_{c1} &= 14 \text{ m/min} & T_{14} &= 110 \text{ min} \\ v_{c2} &= 35 \text{ m/min} & T_{35} &= 11 \text{ min.} \end{aligned}$$

The Taylor exponent k results from the gradient of the Taylor straight line:

$$k = \frac{\ln 110 - \ln 11}{\ln 14 - \ln 35} = -2.513.$$

The Taylor equation generates the minute cutting speed:

$$C = v_{c1} \cdot T_{14}^{-(1/k)} = 14 \text{ m/min} \cdot 110^{-(1/-2.513)} = 90.9 \text{ m/min.}$$

The time optimum cutting speed thus results at:

$$v_{cT_{opt}} = 90.9 \text{ m/min} \cdot [6 \cdot (2.513 - 1)]^{1/-2.513} = 37.8 \text{ m/min.}$$